UNIVERSITÉ DE STRASBOURG

ÉCOLE DOCTORALE DES SCIENCES DE LA VIE ET DE LA SANTÉ

UPR 9002 – ARCHITECTURE ET RÉACTIVITÉ DE L'ARN

THÈSE présentée par :

Morgane BALDACCINI

soutenue le : **21 Septembre 2023**

pour obtenir le grade de : **Docteur de l'université de Strasbourg**

Discipline/ Spécialité : Aspects moléculaires et cellulaires de la biologie

Rôle du domaine hélicase de la protéine Dicer humaine lors de l'infection virale

Role of human Dicer helicase domain upon viral infection

THÈSE dirigée par :

Mr PFEFFER Sébastien Directeur de recherche, CNRS, Université de Strasbourg

RAPPORTEURS :

Mme ETIENNE Lucie Directrice de recherche, CNRS, CIRI, ENS, Lyon

Mr Van RIJ Ronald Professeur, Centre médical de l'Université de Radboud, Pays-Bas

---

AUTRES MEMBRES DU JURY :

Mme MEIGNIN Carine Professeure, CNRS, Université de Strasbourg

Mr MAILLARD Pierre Directeur de recherche, Université de Londres Queen Mary, Angleterre

Acknowledgements

I would like to thank first my thesis jury members Lucie Etienne, Pierre Maillard, Carine Meignin and Ronald Van Rij for accepting to evaluate my thesis work and to come to Strasbourg to discuss about it in person. I want also to address a special thanks to the two latter for accepting to be a part of my thesis progress committee throughout my 4 years of thesis.

Je ne sais même pas par où commencer tant j'ai de personnes à remercier pour m'avoir soutenue tout au long de ma thèse. Tout d'abord, j'aimerais sincèrement remercier Sébastien qui a été mon directeur de thèse pendant ces 4 années mais aussi celui qui a cru en moi dès les premiers jours de mon stage de Master. Je ne saurai comment te remercier d'avoir accepté de m'intégrer à ton équipe. Je te remercie pour ta confiance envers moi et tes très nombreux conseils. Quoi qu'il arrivait, lorsque je pensais que j'allais droit dans le mur tu avais toujours le mot pour me rassurer et trouver un côté positif à n'importe quel résultat. Tu as été pour moi un mentor (mon premier sans aucun doute) avec lequel je pouvais discuter de sciences et surtout sur qui je pouvais me reposer en cas de doute, même au niveau de la suite de ma carrière. Et c'est d'autant plus vrai que tu as été celui qui m'a permis de me décider quant à mon avenir en faisant le choix de faire un post-doc. Là encore j'ai eu tout ton soutien. Merci pour tout, d'avoir cru en moi et de continuer à le faire.

Comment ne pas remercier celui qui fut en quelque sorte mon maître Jedi dans mon périple en master, Dr. Thomas Montavon. Tu as été celui qui, on peut le dire, m'a appris comment survivre en milieu hostile, dans un laboratoire qui travaille sur l'ARN. J'ai pu grâce à toi découvrir Dicer et la vie de chercheur. Je pense que si j'ai pu m'en sortir en thèse c'est parce que j'ai été très bien formée en master. Ce fut un réel plaisir de pouvoir publier avec toi sur Dicer, bouclant un travail qu'on a fait ensemble.

Et viens ensuite le moment à accorder à l'équipe, et quelle équipe ! Je crois ne pas me tromper en disant que je suis la doctorante la plus chanceuse d'avoir travaillé avec et côtoyé tant d'étudiants et de chercheurs brillants qui ont toujours été là pour me soutenir. À commencer par Erika qui est celle qui continue à me faire croire que la place des femmes dans la recherche n'est plus à prouver tant elle est inspirante en alliant ses vies de chercheuse et

mère de famille. Merci pour tes conseils toujours très pertinents. Évidemment, merci à toi ma maman de labo, Mélanie. Je n'ai même pas les mots pour te dire à quel point sans toi ma vie au laboratoire aurait été bien différente. Nos discussions me manqueront tout comme je suis persuadée que ma tour de pise de western blot te manquera. Tu es celle qui m'a toujours aidée, scientifiquement et personnellement. Tu me rassurais à tout moment lors de mes (nombreux, très nombreux) moments de doute. Tu resteras celle qui m'a montré qu'avoir confiance en soi et que se jeter dans le grand bain des nouvelles expériences est toujours bénéfique, quelle que soit l'issue. Que dire de l'équipe de post-docs et doctorants que j'ai côtoyée. À commencer par les « anciens » qui sont désormais en train de vivre leur vie d'après. J'aimerais remercier le trio Antoine, Olivier P. et Olivier T. qui ont été des piliers pour moi dès le master et avec qui j'ai eu le privilège de partager le bureau. Antoine et Olivier P., comment vous dire que sans vous je n'aurais même pas été acceptée en thèse. Non seulement vous m'avez soutenue mais vous m'avez littéralement harcelée de questions pour l'oral de master afin que je sois la meilleure. Olivier T. tu as été celui qui me soutenait quoi qu'il arrivait et qui me permettait d'oublier un peu le labo quand j'avais besoin de faire un break (au passage, je n'ai qu'une chose à dire : aller l'OM !). Merci à tous les trois pour cette incroyable ambiance dans le bureau. Merci également à Paula de m'avoir appris tant de choses sur les virus alors que je n'y connaissais absolument rien et d'avoir été là quand j'avais besoin d'oublier un peu le labo. Très chère Monika, qui pense toujours avoir tout raté alors qu'elle est sans aucun doute la femme la plus brillante et la plus généreuse que je connaisse. Tu es un modèle pour moi et également celle qui me grondait quand je passais trop de temps au labo (tu secondais très bien Mélanie dans son rôle de maman). Ce fut un plaisir de te côtoyer tout au long de ta thèse et aussi de la mienne. J'aimerais remercier aussi le petit bulot stagiaire alias Pauline que j'ai connue au tout début de ma thèse et qui a été la première sans aucun doute à me re-motiver quand je m'apitoyais sur mon sort. Qu'est-ce que j'ai pu rire avec les mêmes, le karaoké au labo ou animal crossing. Tu as été là pendant une période toute particulière de ma thèse où sans ton soutien durant l'été de ma première année, tout se serait sans doute passé autrement.

Passons désormais aux petits nouveaux à commencer par les deux meilleurs stagiaires qu'on puisse avoir. Thomas, désormais doctorant un étage plus bas, qui a été mon premier vrai stagiaire et qui a fait preuve de patience à mon égard car il en faut pour me supporter.

On dit souvent que les stagiaires apprennent tout de leur maître de stage, je dirai que c'est en partie faux. Les maîtres de stage en apprennent tout autant de leur stagiaire et ça a été mon cas. J'ai appris à faire confiance et à faire preuve de patience et de pédagogie grâce à toi. Tu as été un brillant stagiaire qui je le sais est un brillant doctorant et sera un brillant docteur. Mélissa, on peut dire que ta venue en tant que stagiaire a été totalement due au hasard. Comme quoi le bouche à oreille fonctionne très bien car je n'ai pas été déçue que tu sois ma stagiaire. Tu as été particulièrement intéressée, rigoureuse et attentive. Ça a été un plaisir tant scientifiquement qu'humainement, car il faut le dire ta présence est comme un rayon de soleil. Ta bonne humeur, ta générosité et ta capacité à être attentive aux autres ont été une véritable bouffée d'oxygène dans une période de stress extrême pour moi. Et pour couronner le tout, tu as fini par travailler dans le même labo que Thomas (je vais finir par demander des intérêts à force de fournir tous leurs étudiants d'ailleurs). Mes deux autres stagiaires (je plaisante évidemment), Yasmine et Léa, sont aussi sans aucun doute parmi celles qui ont été un soutien quotidien. Yasmine, même si ta thèse n'a pas suivi le chemin que tu désirais, moi qui te connais depuis le début je peux facilement te dire que tu as tout de même été une doctorante passionnée et persévérante. Ta bonne humeur, les longues discussions de science, de sujets du quotidien, de ChatGPT ou de prix Nobel étaient à chaque fois des moments de partage toujours bienvenus. Avoir eu la chance de te former au début de ta thèse a aussi été un plaisir et j'admire toujours autant la passion que tu peux mettre dans tout ce que tu décides de faire. Léa, ma dernière stagiaire et pas des moindres, tu as sans doute été la clé pour me décider. À quoi ? Eh bien tout simplement à continuer. Je ne trouve pas de mots plus forts que soutien quand il s'agit de décrire ce que tu m'as apporté en si peu de temps. Tu fais preuve d'un esprit scientifique incroyable et ça a toujours été un plaisir de discuter de sciences avec toi. Merci de m'avoir aidée à la fin de ce long périple qu'a été ma thèse et de m'avoir appris que les qPCR c'est trop bien (non c'est faux je n'arrive toujours pas à le croire). Floriane, ou la personne avec qui j'ai passé le plus de temps au P3. Ça a été un plaisir de travailler avec toi et de partager de nombreuses discussions (dont beaucoup de potins). Benoit, alias Benny, qui est le post-doc le plus décontracté de France et l'un des plus incroyables quand il s'agit de sciences. On peut le dire, depuis ton arrivée au labo, on ne s'ennuie pas, on découvre la gastronomie mondiale avec une mention spéciale pour les insectes en biscuits apéritifs. Merci pour ta bonne humeur et tes conseils sur la vie d' « adulte » d'après-thèse. Merci également à Lisanne et Peter pour leurs précieux conseils de fin de thèse qui m'ont permis de sortir la

tête de l'eau (en fait plutôt des analyses bio-informatiques). En parlant de bio-informatique, je dois remercier particulièrement Béatrice qui même si elle croulait sous le travail a été toujours là pour m'aider avec mes millions de données de séquençage. Je te remercie aussi pour ta patience lors des explications et pour ta disponibilité à chaque instant.

Merci à celles et ceux qui ont, à un moment croisé, ma route ou tout simplement avec qui j'ai discuté et qui m'ont apporté à leur façon l'aide pour garder le moral tout au long du marathon de la thèse qui s'est révélé être un voyage inattendu.

Et c'est aussi à ce moment que je dois remercier les trois plus importants soutiens que j'ai pu avoir durant ma thèse. Claire, ma petite filleule de master, que j'ai eu la chance de côtoyer en dehors et au labo. Tu es une brillante scientifique et une amie sincère sans qui mes journées et mes week-ends passés au labo auraient été bien tristes. Que ça soit pour parler de science, juste pour rigoler ou pour tester n'importe quel type de nourriture, je trouvais toujours en toi quelqu'un sur qui je pouvais compter. Comme on le dit souvent, les autres doctorants sont là pour nous écouter nous plaindre et me concernant tu as su faire preuve d'une écoute attentive et patiente. Ma très chère Janine, comment dire, c'était « plutôt pas mal » de vivre cette thèse avec toi. Tu es tellement gentille, à l'écoute et ouverte d'esprit. On aura organisé tellement d'événements ensemble que je ne les compte même plus. Plus important, quand je n'allais pas bien, tu étais là et quand j'allais bien, tu étais là aussi, c'est ce qui me fait dire qu'au-delà d'une aventure scientifique, la thèse aura été une incroyable aventure humaine. Merci pour ce soutien incomparable (surtout les matins, tôt très, trop tôt quand il fallait être au labo). Enfin, et on le dit bien, la meilleure pour la fin. Ça aura commencé avec un rapport de la mort et ça sera fini par une belle amitié. Charline, tu m'auras supportée alors que j'ai un caractère absolument insupportable quand je fais ma tête de mule. Je t'aurais vu grandir en tant que scientifique et je suis tellement fière de toi. Tu es une femme forte, persévérante et inspirante. Je ne compte même plus le nombre de fois où tu m'as rassurée ou soutenue. Merci pour toutes ces discussions et ces moments passés ensemble au labo et en dehors.

Par la suite, j'aimerais remercier Pascale Romby de m'avoir accueillie dans son unité et de m'avoir permis d'évoluer scientifiquement dans un cadre de travail idéal. Évidemment,

merci à toutes celles et tous ceux avec qui j'ai discuté ou travaillé dans l'institut et qui ont contribué à mon épanouissement scientifique et personnel.

Merci également à mes amis que j'ai eu la chance de rencontrer avant ma thèse, en arrivant à Strasbourg et qui ont malgré tout été assez courageux pour continuer à me supporter pendant celle-ci : Romane, Clara, Mélanie et Andreas.

Enfin, merci à ma famille pour leur soutien exceptionnel tout au long de ma thèse. Je dois remercier un petit être qui depuis ma deuxième année de licence est mon pilier émotionnel et mon coloc (enfin j'habite plutôt chez lui apparemment) : mon lapin, Yoda. Petit bonhomme, tu portes le nom d'un grand maître Jedi et c'est donc pour ça que je ne doutais pas une seconde que tu serais celui qui me motiverait le plus à continuer en étant sans le vouloir mon psychologue (certes, pas très bavard). P.S. : je te remercie pour tous les « A » de l'introduction du papier, que tu auras écrits avec amour (et avec l'aide de beaucoup de galettes).

J'aimerais accorder les dernières lignes de ces remerciements à celle qui est la raison même de ma présence en Sciences, ma mère. Maman, qui aurait cru que j'en arriverai là aujourd'hui si ce n'est toi. Je m'estime tellement chanceuse de t'avoir comme mère, je ne m'imaginais même pas en arriver là sans toi. Si je devais citer un modèle dans ma vie, ça serait sans aucune hésitation toi. Ta force m'a permis d'avancer. Quand je t'appelais au bord des larmes, tu étais là pour me remonter le moral et me motiver mieux que quiconque aurait pu le faire. Tu m'écoutais parler de ma thèse alors que tu n'y comprenais rien du tout mais tu arriverais toujours à m'approuver dans ce que je faisais. Alors comme un merci ne suffit pas à te montrer ma reconnaissance, je préfère finir sur cette phrase : tu m'as permis de garder les pieds sur Terre pour mieux viser les étoiles. Et à ce moment-même j'ai la tête dans les étoiles car je suis parvenue à faire ce que je t'avais promis de faire depuis que je suis toute petite : avoir un travail et une vie dans lesquels je m'épanouis complètement.

Table of contents

Abbreviations

ADAR1: adenosine deaminase acting on RNA

AGO: Argonaute

ATP/GTP: adenosine/guanosine triphosphate

cGAS: cyclic GMP-AMP synthase

CHIKV: Chikungunya virus

DENV: Dengue virus

DLP: downstream loop

dsRBP: dsRNA binding protein

dsRNA/ssRNA: double-/single-stranded RNA

EEEV, VEEV, WEEV: Eastern/Venezuelan/Western equine encephalomyelitis virus

eIF2α: eukaryotic translation initiation factor 2α

EV71: Enterovirus 71

GCN2: general control nonderepressible-2

HIV-1: human immunodeficiency virus 1

HRI: heme-regulated inhibitor

IAV: Influenza A virus

IAV: Influenza A virus

IFN-I: type I interferon response

IkB: inhibitor of kB

IKK: IkB-kinase complex

IRF: interferon regulatory factor

ISG: interferon-stimulated gene

ISGF3: IFN-stimulated gene factor 3

ISRE: IFN-stimulated regulatory elements

JAK-STAT: Janus kinase – Signal transducers and activators of transcription

MAVS: mitochondrial antiviral-signaling

MDA5: melanoma differentiation-associated protein 5

miRNA/pri-/pre-: micro-RNA/primary/precursor

NES: nuclear export signal

NF-kB: nuclear factor kB

NLS: nuclear localization signal

nsP: non-structural protein

OAS: 2’-5’-oligoadenylate synthetase

ORF: open reading frame

PACT: protein activator of dsRNA-activated protein kinase

PAMP: pathogen-associated molecular pattern

PERK: protein kinase R-like endoplasmic reticulum kinase

PKR: dsRNA-activated protein kinase

PRR: pattern recognition receptor

RIG-I: retinoic acid-inducible gene I

RISC: RNA-induced silencing complex

RLR: RIG-I-like receptor

RNAi: RNA interference

SARS-CoV-2: Severe Acute Respiratory Syndrome Coronavirus 2

SFV: Semliki forest virus

SINV: Sindbis virus

TAR RNA: tat-responsive region RNA

TLR: toll-like receptor

TRBP: TAR-RNA binding protein

UTR: untranslated region

VSV: Vesicular stomatitis virus

List of figures

List of Annexes

Introduction

French summary

A. La réponse immunitaire

Les organismes cellulaires ont développé rapidement au cours de l'évolution une gamme variée de réponses immunitaires pour se défendre contre les éléments étrangers. Les éléments transposables ont été décrits comme les ancêtres des virus à ADN (Krupovic and Koonin, 2015). Un mécanisme développé pour bloquer les éléments génétiques envahissants est l'utilisation d'ARN antisens qui constitue une réponse immunitaire chez les organismes unicellulaires. Ce système guidé par l'ARN a évolué avec l'ajout de protéines ayant une activité enzymatique : c'est ce qu'on appelle le système de restriction. C'est par exemple la base du célèbre système CRISPR-Cas9 chez les bactéries, qui peut cibler spécifiquement des acides nucléiques étrangers mais aussi maintenir des éléments d'acides nucléiques étrangers intégrés dans le génome de l'hôte en tant que "mémoire immunitaire" (Barrangou et al., 2007; Jinek et al., 2012). Chez les organismes eucaryotes, on peut distinguer trois couches de systèmes de défense contre les pathogènes : l'immunité intrinsèque (apparentée à un système de restriction), l'immunité innée et l'immunité adaptative. Le système immunitaire adaptatif repose sur une mémoire immunitaire chez les vertébrés et sur la production d'anticorps spécifiques contre un pathogène. Cela implique l'activité de deux types de cellules, les lymphocytes B et T, mais aussi l'expression d'un modèle spécifique de gènes pour produire les anticorps adaptés. Les anticorps peuvent reconnaître spécifiquement un agent pathogène afin d'induire sa dégradation par d'autres acteurs immunitaires. Parmi les voies liées à l'immunité innée, on peut citer l'ARNi antiviral, qui a été bien décrit chez les plantes et les invertébrés, et dont l'importance dans les cellules des vertébrés est encore débattue. Chez les chordés, l'immunité innée est basée sur la reconnaissance d'éléments étrangers (acides nucléiques, protéines) appelés pathogen-associated molecular patterns (PAMPs) par des récepteurs cellulaires, les pattern recognition receptors (PRRs). Les PRRs déclenchent une cascade de signalisation transcriptionnelle conduisant à l'expression de cytokines pour inhiber l'infection (tenOever, 2016).

Parmi les cytokines, les interleukines et les interférons sont les plus représentés dans les cellules de mammifères. Dans de nombreux cas où l'ARNi antiviral est décrit comme inefficace contre une infection, la réponse interféron (IFN) l'emporte expliquant en partie l'incompatibilité entre les deux voies (Maillard et al., 2016). L'IFN a été découvert en 1957 avec l'étude de

l'interférence virale contre le virus de la grippe (Isaacs and Lindenmann, 1957). Depuis, 10 cytokines interféron différentes ont été découvertes. La dérégulation de cette réponse ne modifie pas seulement l'immunité contre les pathogènes, mais peut également conduire à des pathologies humaines appelées interféronopathies (Mogensen, 2019). L'IFN et l'ARNi partagent des facteurs de détection communs liés aux hélicases DExD/H-Box capables de reconnaître l'ARN (Fairman-Williams et al., 2010), respectivement les récepteurs RIG-I-like (RLRs) et une endoribonucléase de type III nommée Dicer.

B. Dicer et la voie des microARN (miARN)

L'un des principaux rôles de Dicer est la biogenèse des microARN (miARN), qui sont des régulateurs clés de l'expression des gènes. Le premier rapport sur un ARN régulateur court est issu d'une étude réalisée chez Caenorhabditis elegans dans les années 1990 (Lee et al., 1993; Reinhart et al., 2000). Ces petits ARN, dont on a découvert par la suite qu'ils existaient chez d'autres animaux et qu'ils étaient appelés miARN, présentent une complémentarité imparfaite avec leurs cibles, ce qui implique une activité dépendant de l'inhibition de la traduction (Lau et al., 2001; Lee and Ambros, 2001; Olsen and Ambros, 1999).

La voie des miARN a été largement caractérisée. Un transcrit d'ARN polymérase II (polII) dérivé d'un ARNm primaire (pri-miARN) est reconnu par la ribonucléase de type III DROSHA (Lee et al., 2004). DROSHA, aidée par son principal partenaire d'interaction DGCR8, clive le pri-miRNA en un précurseur-miARN (pré-miARN) à boucle de 60 nt (Lee et al., 2003). Le pré-ARNm est ensuite exporté vers le cytosol par un mécanisme actif ARN-GTP/Exportine 5 (Yi et al., 2003). Une fois dans le cytoplasme, le pré-miRNA est transformé, de manière indépendante de l'ATP, en un duplex miRNA de 22 nt de long par Dicer, aidé par son principal cofacteur, la TAR-RNA Binding Protein (TRBP) (Chendrimada et al., 2005). Un brin du duplex est incorporé dans une protéine effectrice de la famille Argonaute (AGO) (Hammond et al., 2001) pour former le complexe de silencing induit par l'ARN (RISC). Cette opération nécessite l'aide de protéines chaperonnes (Iwasaki et al., 2010). Le petit ARN sert de guide au RISC pour l'amener à ses ARNm cibles complémentaires. Chez l'animal, cela se traduit dans la plupart des cas par une inhibition de la traduction, qui nécessite l'interaction des protéines AGO avec la protéine adaptatrice TNRC6B (Meister et al., 2005). Dans de rares cas,

c'est-à-dire lorsqu'il y a une complémentarité parfaite entre l'ARN guide et l'ARN cible, l'ARN cible peut être clivé par le RISC (Yekta et al., 2004).

Avant d'être impliquée dans la voie des miARN, Dicer a été identifiée comme l'enzyme responsable de l'ARNi et a été nommée d'après sa capacité à digérer les ARNdb en petits ARN (siARN) (Bernstein et al., 2001).

La protéine Dicer est très conservée au cours de l'évolution et se compose de 3 principales parties : une partie régulatrice et fixatrice de l'ARN, le domaine hélicase ; un cœur catalytique, les domaines RNaseIII ; et des domaines supplémentaires de fixation de l'ARN, les domaines PAZ, DUF283 et dsRBD terminal. Le domaine hélicase est l'élément régulateur de l'activité de la protéine Dicer. Dans un premier temps, ce domaine hélicase DExD/H-Box est incapable d'hydrolyser l'ATP et présente un effet auto-inhibiteur sur le traitement des ARNdb longs chez l'homme (Ma et al., 2008; Zhang et al., 2002). Il a été démontré que la perte de l'hydrolyse de l'ATP est corrélée à une perte de l'activité de clivage des longs ARNdb : en examinant la phylogénie des Dicer, un lien clair entre ces deux aspects est apparu puisque le Dicer ancestral a conservé ces deux caractéristiques (Aderounmu et al., 2023). Ainsi, des changements dans le domaine hélicase pourraient modifier sa capacité à lier l'ARNdb et à hydrolyser l'ATP, ce qui souligne l'importance de ce domaine dans l'activité du Dicer.

De plus, le domaine hélicase de Dicer semble être une plaque tournante pour les interactions, principalement en relation avec son rôle dans la biogenèse des miARN. Dicer interagit avec l'hélicase A DExH/-Box RNA ou DHX9, qui est capable de dérouler à la fois l'ARN et l'ADN dans le noyau et le cytosol. DHX9 est impliquée dans le chargement du RISC, ce qui permet une meilleure association entre le siRNA et AGO2 (Robb and Rana, 2007).

Dicer interagit également directement avec la protéine ADAR1 (Adenosine Deaminase Acting on RNA 1) dans le contexte du traitement des miARN. Il a été démontré qu'ADAR1 augmente le taux de traitement de Dicer et favorise le chargement des miARN sur AGO2 (Ota et al., 2013). Pendant longtemps, ADAR1 a été considéré comme un antagoniste de la voie de l'ARNi, car l'édition A-to-I inhibe le traitement correct des ARNm pri ou modifie les cibles des ARNm (Kawahara et al., 2007b, 2007a). Cependant, lorsque Dicer interagit avec ADAR1, la désaminase induit des changements de conformation de Dicer et améliore le traitement des précurseurs de miARN, l'assemblage du RISC et le chargement des miARN, tout comme

TRBP. Là encore, cette interaction est médiée en partie par le domaine hélicase de Dicer (Ota et al., 2013).

Enfin, une autre dsRBP homologue à TRBP, la protéine activatrice de la protéine kinase activée par l'ARNdb (PACT), est un partenaire bien connu du domaine hélicase de Dicer. PACT a été décrit pour la première fois à la fin des années 1990 pour son rôle d'activateur de la protéine kinase activée par l'ARNdb (PKR). Dans ce cas, PACT interagit avec la PKR et active son activité kinase normalement induite par l'ARNdb (Patel and Sen, 1998). Toutefois, PACT et TRBP jouent un rôle différent in vitro dans le traitement de Dicer. Dicer associé à PACT révèle des différences de spécificité de substrat par rapport à Dicer avec TRBP, car le premier induit une diminution de la transformation de l'ARNdb par Dicer (Lee et al., 2013). Cependant, in vivo, Dicer a besoin de l'hétérodimère PACT/TRBP pour traiter l'ARNdb, ce qui indique la régulation complexe de ce complexe (Kok et al., 2007). Cette interaction est médiée par les deux premiers dsRBD de PACT et de TRBP, laissant leur troisième dsRBD libre pour les interactions avec Dicer.

C. La réponse interféron (IFN)

Dans les cellules de mammifères, la réponse immunitaire contre les virus est basée principalement sur la réponse IFN. La réponse IFN peut être déclenchée par différents types d'agents pathogènes : bactéries, parasites, virus et champignons. L'IFN est un système en deux étapes, qui implique d'abord l'expression des cytokines IFN, suivie de leur action à la fois autocrine et paracrine. Elles agissent en se liant à des récepteurs cellulaires pour induire la transcription des gènes stimulés par l'IFN (ISG), qui sont les effecteurs cellulaires directs. Ce système permet à l'organisme de mettre en place une réponse immunitaire globale grâce à la transmission du signal. Les deux principaux IFN communément impliqués dans la réponse immunitaire sont les interférons de type I et de type III (IFN-I et IFN-III). Ces deux réponses sont associées à des cytokines et des récepteurs cellulaires différents. Lors d'une infection par un virus à ARN ou à ADN, l'IFN-I est décrit comme la réponse la plus large et est prédominant dans les cellules immunitaires. L'IFN-III se trouve principalement dans les cellules épithéliales (McNab et al., 2015).

L'IFN-I est déclenché par différentes classes de PRR : les récepteurs Toll-like (TLR) associés à la membrane, les récepteurs cytosoliques RIG-I-like (RLR) et les récepteurs d'ADN, tels que la GMP-AMP synthase cyclique cytosolique (cGAS). Leur activation entraîne la phosphorylation par TBK1 de facteurs de transcription spécifiques, tels que les facteurs de régulation de l'interféron (IRF) 3 et 7. Cette phosphorylation permet leur translocation nucléaire (Mogensen, 2019). Ils agissent en tant qu'homo- ou hétéro-dimères et peuvent être associés à d'autres facteurs de transcription, y compris NF-kB. IRF3 et 7 induisent la transcription de l'IFN α et ß, les deux groupes de cytokines de l'IFN-I (Honda and Taniguchi, 2006).

Les cytokines produites peuvent alors agir de façon paracrine et autocrine se fixant à leur récepteur cellulaire, IFNAR. La fixation entraîne le déclenchement d'une cascade de signalisation moléculaire qui active la translocation nucléaire de facteurs de transcription, principalement STAT1 et STAT2 qui sont capables d'activer l'expression de centaines de gènes stimulés par l'IFN (ISGs) (Ivashkiv and Donlin, 2014).

Parmi les ISGs, une kinase activée par l'ARNdb, appelée protéine kinase R (PKR) est un des premiers acteurs de la réponse immunitaire face aux virus. PKR est capable de reconnaître l'ARNdb qui va entraîner son activation via son homodimérisation (Lemaire et al., 2008). La forme dimérique fixe l'ATP permettant l'autophosphorylation du dimère qui est alors stablement actif. PKR peut phosphoryler divers substrats. Ainsi, PKR a été longtemps liée à la régulation du cycle cellulaire via la phosphorylation de p53 (Cuddihy et al., 1999; Yoon et al., 2009). Mais son rôle principal demeure la phosphorylation du facteur eucaryotique d'initiation de la traduction eIF2α. Une fois phosphorylé, p-eIF2α ne peut plus initier la traduction notamment à cause d'une incapacité à réaliser le transport de l'ARNt initiateur. Ainsi, PKR permet le blocage de la traduction cellulaire (Krishnamoorthy et al., 2001).

Cependant, outre son rôle de kinase, PKR a aussi été liée à l'initiation de la réponse IFN dans les cellules humaines. Ainsi, PKR est souvent retrouvée au niveau des granules de stress formés par G3BP1 permettant alors le déclenchement de la réponse IFN-I (Onomoto et al., 2012). En outre, PKR a aussi été associée à l'activation de la voie NF-kB responsable de l'expression de gènes pro-inflammatoires et de l'immunité et cela sans besoin nécessaire de son activité catalytique (M. C. Bonnet et al., 2000).

Néanmoins, PKR reste un acteur très régulé dans la cellule, notamment par certains cofacteurs lors de conditions de stress. Ainsi, deux cofacteurs précédemment associés à Dicer,

TRBP et PACT, ont des rôles antagonistes sur l'activité de PKR. PACT est un activateur de PKR, capable d'interagir avec sa partie N-terminale dans le but d'activer sa fonction de kinase lors de stress (Ito et al., 1999; Ruvolo et al., 2001). A l'inverse, l'interaction de PKR avec TRBP empêche cette dernière de reconnaître et d'être activée par de longs ARNdb lors de la mitose (Kim et al., 2014).

D. Le virus de Sindbis, modèle des alphavirus

Les alphavirus sont un genre au sein de la famille des *Togaviridae* qui est composé de virus possédant un génome à ARN simple brin positif. Ce genre contient notamment les virus du Chikungunya ou la rivière Ross. Ils sont enveloppés et possèdent un cycle exclusivement cytoplasmique. Leur génome est coiffé en 5' et polyadénylé en 3' et possède deux cadres de lecture, le premier encodant les protéines non-structurales impliquées dans la réplication et le second, transcrit à partir d'un promoteur subgénomique, encodant les protéines structurales nécessaires à la production des virions (Frolov et al., 2001).

Le virus de Sindbis (SINV) possède un cycle viral qui dure entre 4 et 6h et pendant lequel, lors de la réplication de l'ARN génomique, de l'ARNdb apparaît dans le cytoplasme. Cet ARNdb est un signal de danger dans la cellule eucaryote et est le principal élément étranger détecté par le système immunitaire. Ainsi, MDA5 et RIG-I, deux RLRs, sont capables de détecter la présence de SINV dans le cytoplasme (Akhrymuk et al., 2016).

Le rôle de Dicer dans la réponse antivirale contre les alphavirus a été étudié. Des petits ARN interférents (siARN) dérivés du virus et produits par Dicer ont été détectés dans des cellules somatiques infectées par le SINV (Zhang et al., 2021). En revanche, d'autres études portant sur des cellules HEK293 infectées par le virus SINV n'ont pas pu mettre en évidence l'accumulation de siARN, ce qui va à l'encontre d'un rôle antiviral de l'ARNi (Donaszi-Ivanov et al., 2013; Girardi et al., 2013). Le fait que les cellules humaines HEK293 déficientes en Dicer ne présentent pas d'infection accrue par le SINV renforce cette hypothèse (Bogerd et al., 2014). Enfin, un autre produit de Dicer peut participer à la modulation de l'infection : les miARN se sont révélés être des acteurs clés en contrôlant soit l'expression des gènes cellulaires, soit directement le génome viral (revue dans (Girardi et al., 2018)). En effet, un criblage à haut débit

a montré que le miARN cellulaire neuronal, miR-124, peut augmenter la réplication du SINV et du CHIKV dans les cellules somatiques humaines (López et al., 2020).

E. Étude du rôle de Dicer dans l'immunité antivirale humaine

Le rôle de Dicer pendant l'infection virale des cellules de mammifères reste un sujet de recherche débattu. Il a été démontré que Dicer est proviral dans certains cas. En effet, deux éléments limitent l'activité de Dicer dans les cellules humaines et sont incompatibles avec l'ARNi antiviral. Premièrement, le domaine de l'hélicase Dicer humaine présente des caractéristiques uniques qui rendent Dicer moins processif. Les trois sous-domaines (HEL1, HEL2i et HEL2) sont des freins majeurs à l'activité de traitement de Dicer sur les ARNdb longs. En outre, le Dicer humain n'a pas besoin d'ATP pour traiter le pré-miRNA ou l'ARNdb. Un autre problème majeur pour l'activité antivirale de Dicer est l'existence dans les cellules humaines d'une autre réponse immunitaire, la réponse IFN-I. Dans de nombreux cas, l'activité antivirale de Dicer a été évaluée lorsque cette réponse était perturbée. De plus, Dicer partage de nombreux facteurs avec cette réponse comme ADAR1, LGP2 ou PACT. Si Dicer joue un rôle dans la réponse antivirale, il ne peut être complètement séparé de son interaction avec l'IFN-I. Cependant, ce type d'interaction reste peu étudié. Puisque le domaine hélicase de Dicer représente une plaque tournante pour l'effet d'auto-inhibition et pour les partenaires cellulaires potentiels, les études se concentrent sur son rôle précis.

L'objectif principal de ce projet était d'étudier le rôle central du domaine hélicase de Dicer humain lors d'une infection virale.

L'hypothèse était que les fonctions antivirales de Dicer sont limitées par l'existence de l'IFN-I et que sa position atypique à l'interface de l'ARNi et de l'IFN-I le rend moins enclin à être antiviral. Le projet s'est d'abord concentré sur l'alphavirus modèle, le SINV. Ce virus +ssRNA a déjà été utilisé pour étudier le rôle de Dicer lors de l'infection et est capable de générer un intermédiaire de réplication d'ARNdb qui constitue le principal substrat de Dicer. Une version modifiée de SINV a été utilisée pour faciliter le suivi de l'infection : SINV-GFP exprime la GFP à partir d'une duplication du promoteur sous-génomique.

Pour étudier le rôle de Dicer lors d'une infection virale dans le contexte de l'interaction entre les deux réponses, nous avons établi l'interactome de Dicer humain lors d'une infection par SINV-GFP. De nombreux partenaires enrichis par l'infection ont été attribués à des acteurs de la réponse IFN-I tels que la désaminase ADAR1, l'hélicase ARN DHX9, la dsRBP PACT et la kinase PKR.

Les objectifs de cette thèse, regroupés dans les deux chapitres suivants, étaient :

a- La caractérisation et la validation des partenaires de Dicer enrichis lors de l'infection par SINV-GFP. L'étude s'est concentrée sur l'interaction entre Dicer et la kinase PKR. Les rôles du domaine hélicase dans cette interaction et dans la régulation de l'infection ont été étudiés. Un mutant spécifique de Dicer, supprimé des deux premières parties du domaine de l'hélicase, N1 Dicer, a été étudié. Le rôle de la kinase PKR a également été étudié dans le contexte du Dicer N1.

b- La caractérisation du rôle des différents sous-domaines du domaine hélicase de Dicer lors de l'infection par SINV-GFP et leur lien possible avec l'activité de la PKR. A nouveau, les différents mutants d'hélicase et leurs homologues mutants catalytiques ont été exprimés en présence et en absence de PKR. Parallèlement, le Dicer N1 a également été étudié pour son rôle potentiel dans la voie antivirale de l'ARNi en utilisant le séquençage de petits ARN et un mutant catalytique, N1-CM. Afin de déterminer l'implication de la réponse IFN dans le rôle de N1 Dicer lors de l'infection par SINV-GFP, un séquençage de l'ARN total a été réalisé. L'activité transcriptionnelle de l'IFN a été validée à l'aide de cibles génétiques spécifiques et de l'activation du principal facteur de transcription à l'origine de la réponse immunitaire. Le mécanisme sous-jacent à l'activité transcriptionnelle de l'IFN a été étudié plus en détail, mettant en évidence un rôle déterminant de la PKR. Ceci a été rendu possible par l'utilisation de lignées cellulaires invalidées pour l'expression de la PKR et exprimant soit WT soit N1 Dicer ainsi que par la complémentation de ces lignées cellulaires avec des mutants de la PKR. Ensuite, l'étude de l'activité du Dicer N1 a été élargie à d'autres virus de différents groupes : l'alphavirus SFV, l'entérovirus EV71, le rhabdovirus VSV (exprimant la protéine GFP dans son génome, appelé VSV-GFP) et le coronavirus SARS-CoV-2.

F. Principaux résultats et discussion

À la lumière de la récente pandémie de COVID-19, le besoin de comprendre les dynamiques hôtes-virus s'est retrouvé au centre des études menées afin de développer des traitements antiviraux et des vaccins. Mise à part le SARS-CoV-2, beaucoup de virus demeurent une menace permanente pour la santé. Parmi eux, les alphavirus sont responsables de plusieurs centaines de morts par an dans le monde. En plus d'être maintenus dans des animaux sauvages vertébrés, ces virus peuvent parfois infecter des hôtes humains. Chez les Hommes et les animaux, les virus, en tant que parasites intracellulaires dépendant de la machinerie cellulaire de l'hôte, font face au système immunitaire inné qui repose principalement sur la réponse IFN-I chez les mammifères. De plus, de par leur réplication dans les vecteurs invertébrés, les alphavirus font face au système immunitaire des arthropodes qui est principalement basé sur la voix ARNi.

Ces deux réponses immunitaires permettent de contrôler l'infection et d'éliminer les virus, ce qui les rendrait redondant ; ainsi, il a été proposé qu'elles sont mutuellement exclusives. De ce fait, l'ARNi reposant sur l'endoribonucléase de type III Dicer-2 a été décrite comme la réponse immunitaire principale contre les virus chez les moustiques (Campbell et al., 2008; Myles et al., 2008). Chez les mammifères, l'IFN-I a été étudiée pour la suppression de l'infection virale de façons locale et globale. Ceci est dû au fait que ce système basé sur des cytokines permet la signalisation immunitaire à travers tout le corps en plus d'une action dans la cellule infectée elle-même (Carpentier and Morrison, 2018; Schoggins et al., 2011).

Cependant, chez les moustiques, une balance finement régulée entre ARNi et d'autres voies de signalisation immunitaires déclenchées par le système Toll-Imd existe (Lee et al., 2019). La question demeure sur l'existence de ces deux voies en parallèle chez les mammifères. De façon intéressante, la principale fonction conservée de Dicer est dans la voie de biogenèse des miARN. Contrairement aux insectes, les mammifères expriment seulement un gène pour Dicer qui est dédié au clivage des miARN, et ils n'expriment pas de second Dicer spécialisé dans l'ARNi (Aderounmu et al., 2023). Le rôle lié à l'immunité du Dicer humain a été le sujet d'un intense débat pendant plusieurs années. Il y a eu plusieurs études, même récemment, qui ont proposé qu'une réponse ARNi antivirale efficace pourrait être détectée dans les cellules somatiques de souris et humaines, comme lors de l'infection avec des alphavirus tels que le SFV (Adiliaghdam et al., 2020; Kong et al., 2023; Li et al., 2013; Yang Li et al., 2016). D'autres groupes ont échoué à détecter des activités antivirales liées à Dicer dans les cellules somatiques,

sauf dans certains cas en l'absence d'une voie IFN-I fonctionnelle (Girardi et al., 2013; Maillard et al., 2016, 2013; Schuster et al., 2019).

Le projet de thèse présenté ici se concentre sur les interactions qui pourraient moduler le rôle joué par Dicer humain lors de l'infection virale. Dicer a déjà été décrit comme un centre d'interaction entre l'ARNi et l'IFN-I. Nous avons émis l'hypothèse que ces interactions pourraient avoir un effet négatif sur la fonctionnalité de Dicer dans la défense antivirale. Ainsi, en réalisant l'étude de l'interactome de Dicer lors de l'infection par SINV, nous avons découvert des co-facteurs de Dicer qui étaient spécifiquement enrichis lors de l'infection. Les mêmes partenaires étaient aussi retrouvés avec un autre alphavirus, le SFV. De façon intéressante, plusieurs d'entre eux étaient déjà liés à la réponse immunitaire : la kinase PKR, la déaminase ADAR1, l'hélicase DHX9 et la dsRBP PACT. Ces interactions ont été confirmées dans deux types cellulaires, les cellules embryonnaires humaines de rein HEK293T et les cellules humaines de carcinome colorectal HCT116. Pour aller plus loin, j'ai développé la technique de complémentation de fluorescence bimoléculaire basée sur la Vénus (BiFC) pour visualiser la localisation exacte de l'interaction dans les cellules, ce qui a permis de confirmer que toutes les interactions impliquant Dicer étaient localisées dans le cytoplasme.

Comme le domaine hélicase de Dicer est essentiel à la fois pour moduler directement sa processivité et comme plateforme pour les interactions avec ses co-facteurs connues, je me suis demandée si ce domaine était aussi impliqué dans la médiation de ces interactions. Même si la plupart d'entre elles était partiellement dépendante de l'ARN, j'ai aussi pu montrer que deux mutants tronqués du domaine hélicase N1 et N3, délétés respectivement des deux premières parties et de l'intégralité du domaine hélicase, perdaient complètement les interactions lors de l'infection. Inversement, le domaine hélicase seul était toujours capable d'interagir avec tous les partenaires testés. Ainsi, le domaine hélicase de Dicer est important pour maintenir plusieurs interactions avec des partenaires qui sont impliqués dans la réponse IFN-I dans les cellules humains lors de l'infection par SINV.

Ensuite, nous avons regardé en détail la fonctionnalité du domaine hélicase. Dans les cellules exprimant Dicer N1 et Dicer N3, nous avons observé un fort phénotype antiviral contre les alphavirus SINV et SFV. Ceci était corrélé avec une forte baisse des ARN génomiques et subgénomiques de SINV, indiquant un défaut dans la réplication virale dans ces cellules. Au contraire, les cellules exprimant seulement le domaine hélicase étaient infectées autant, si ce n'est même mieux, que celles exprimant le Dicer WT.

J'ai décidé d'approfondir nos recherches sur la fonctionnalité du domaine hélicase de Dicer en me focalisant sur l'activité antivirale de Dicer N1. Dicer N1 a déjà été décrit comme étant plus processif contre les ARN db synthétiques (Kennedy et al., 2015). De plus, quelques papiers décrivent que déléter une partie du domaine hélicase de Dicer est suffisant pour induire un phénotype dépendant de l'ARNi, qui peut être antiviral chez l'Homme (Flemr et al., 2013; Poirier et al., 2021). En utilisant trois méthodes différentes, j'ai été capable d'écarter tout implication de l'ARNi dans le phénotype antiviral. En effet, en absence d'AGO2 ou en rendant Dicer N1 catalytiquement inactif, nous observons toujours une diminution de l'infection par SINV dans les cellules exprimant Dicer N1. En addition, le séquençage des petits ARN a révélé qu'il n'y avait pas d'accumulation accrue de siARN spécifiques à SINV dans les cellules exprimant Dicer N1 comparées à celles exprimant Dicer WT. Cependant, quand nous avons regardé les autres mutants du domaine hélicase, délétés individuellement de chacun des sous-domaines, nous avons observé que le phénotype était dépendant de l'activité catalytique de Dicer.

En plus d'être fonctionnellement différents, les mutants du domaine hélicase pourraient aussi présenter une différence dans les partenaires d'interaction. Ainsi, le domaine HEL2i est déjà connu pour être impliqué dans la médiation des interactions avec TRBP et PACT (Daniels et al., 2009; Yoontae Lee et al., 2006). Comme énoncé précédemment, Dicer N1 ne peut plus interagir avec PKR, le meilleur résultat de l'interactome de Dicer WT dans les cellules infectées. Ainsi, j'ai décidé d'étudier la fonctionnalité de cette interaction en utilisant les cellules NoDiceΔPKR complémentées avec les différents mutants du domaine hélicase. La présence de PKR dans ces cellules étaient nécessaire pour maintenir le phénotype antiviral dans tous les cas. En effet, même pour les mutants dont l'activité antivirale était dépendante de l'ARNi, quand l'expression de PKR était invalidée, le phénotype antiviral n'était plus détecté. Une hypothèse concernant les mutants du domaine hélicase pourrait être que PKR est impliquée dans la liaison à l'ARN db par Dicer et/ou le clivage lors de l'infection, soit à cause de la liaison directe soit car PKR pourrait aussi amener et/ou séquestrer d'autres protéines qui pourraient moduler l'activité de Dicer. Il faudrait également tenir compte de la cinétique d'infection et du fait que le délai de la réponse pourrait être différents entre les deux réponses cellulaires (ARNi et IFN-I). Nous pouvons imaginer que comme les deux réponses dépendent de la même molécule de signal, l'ARN db, elles doivent rivaliser pour la liaison à cette molécule. Cependant, une différence majeure entre elles est que tous les composants de l'ARNi sont déjà exprimés et prêts à détecter et agir contre l'ARN db, alors que la réponse transcriptionnelle

induite par l'IFN-I peut prendre plus de temps pour entrer en jeu. Donc, après 24h d'infection, l'IFN a le temps de se mettre en place alors que dans les temps précoces (6h), l'ARNi pourrait jouer un rôle antiviral. Mais qu'en est-il du rôle joué par PKR dans ce scénario ? PKR peut détecter l'ARN db tôt lors de l'infection et bloquer la traduction cellulaire. En addition, SINV est majoritairement insensible à l'inhibition de la traduction comme il utilise un mécanisme alternatif de l'initiation (Ventoso et al., 2006). Ceci signifie que PKR doit être impliquée dans une voie différente que celle canonique de phosphorylation d'eIF2α.

Dans les cellules exprimant Dicer N1, comme PKR est libre de son interaction avec Dicer, je me suis demandée si cela pouvait augmenter son activité kinase. Cependant, cela ne semble pas être le cas car lorsque je marque la forme active phosphorylée de PKR, je vois une diminution de l'activation de PKR. Ceci pourrait être dû à une infection moins efficace avec moins d'accumulation d'ARN db. J'ai confirmé plus en détail le fait que la capacité de dimérisation et l'activité canonique de kinase de PKR n'étaient pas nécessaires à l'activité antivirale observée pour Dicer N1. Pour ce faire, j'ai stablement co-exprimé les mutants de PKR avec Dicer N1. Les formes sauvages et mutantes de PKR ont pu complémenter l'absence de PKR et restaurer l'effet antiviral de Dicer N1 contre SINV.

PKR peut également jouer un rôle antiviral grâce à une activité de signalisation moléculaire. PKR a été liée à l'induction de la réponse IFN-I en permettant l'activation des IRFs, STATs ou NF-kB lors d'infections virales (Marion C. Bonnet et al., 2000; Pflugheber et al., 2002; Wong et al., 1997). De plus, dans les cellules exprimant Dicer N1, comme l'ARNi n'était pas la cause de la baisse de l'infection par SINV, la seule autre voie antivirale restante était la réponse IFN-I. De ce fait, j'ai réalisé le séquençage de l'ARN total dans les cellules exprimant soit Dicer WT soit Dicer N1 infectées ou non avec SINV. Comme attendu lors de l'infection par SINV dans les cellules exprimant Dicer WT, un blocage transcriptionnel a été observé. Inversement, ce blocage n'a pas été détecté dans les cellules exprimant Dicer N1. En examinant les cellules N1 mock, nous avons pu identifier les gènes différentiellement exprimés (DEGs) par rapport aux cellules WT mock. Plusieurs DEGs dans les cellules N1 mock ou N1 infectées avec SINV ont été retrouvés liés aux GO terms « Réponse interféron » et « Réponse inflammatoire ». Ceci suggérait que dans les cellules N1 mock, les gènes liés à l'immunité étaient déjà exprimés à un niveau basal permettant alors aux cellules exprimant Dicer N1 de mieux faire face à l'infection. De façon intéressante, ils étaient contrôlés par des facteurs de transcription liés à l'immunité. Parmi eux, les gènes régulés par NF-kB et STAT2 étaient

fortement représentés dans les cellules exprimant Dicer N1 comparées à celles exprimant Dicer WT. L'enrichissement de l'expression de ces gènes pourrait être expliqué par deux mécanismes. Le premier est la régulation post-transcriptionnelle par les miARNs. Par exemple, les miARNs sont bien connus pour contrôler l'expression de nombreux facteurs reliés à la voie NF-kB. Ceci ne peut pas être écarté considérant le fait que Dicer N1 n'interagit plus à la fois avec TRBP et PACT qui sont partiellement responsables de la précision de clivage du pre-miARN (Kok et al., 2007). De plus, de récentes structures de Dicer renforcent le fait que le domaine hélicase est essentiel pour le bon placement et la précision de clivage des pre-miARNs (Zapletal et al., 2022). Dicer N1 est alors plus prompt à générer des mirtrons qui ne seraient plus capable de reconnaître efficacement leurs cibles menant à une dérégulation de l'expression. Malheureusement, l'analyse de l'accumulation des mirtrons dans les cellules exprimant Dicer N1 n'a pas encore été réalisée. Ceci serait informatif pour de futures études sur l'effet de la délétion du domaine hélicase sur la maturation des miARNs dans les cellules exprimant Dicer N1. Le second mécanisme de régulation est un contrôle transcriptionnel des cibles immunitaires. La réponse IFN-I est une voie hautement régulée avec plusieurs couches de régulation mais la principale est la phosphorylation et la translocation nucléaire des facteurs de transcription liés à l'immunité. Dicer a déjà été lié chez les plantes et les insectes à une induction de la réponse immunitaire transcriptionnelle (Deddouche et al., 2008; Nielsen et al., 2023). Dans ces cas, le domaine hélicase n'a pas été directement impliqué et le besoin d'autres facteurs dans la cascade d'activation a été évoqué, même si ils n'ont pas été identifiés. Nous pouvons également émettre l'hypothèse qu'un rôle nucléaire de Dicer pourrait être impliqué, comme il a été décrit dans le cas de la réduction des éléments ARN db endogènes délétères (Burger et al., 2017). Mais aucun rôle d'activateur transcriptionnel n'a été décrit.

Comme nous avons montré que l'activité kinase de PKR n'était pas nécessaire à l'activité de Dicer N1, et qu'il est connu que c'est aussi le cas pour son rôle dans l'activation de NF-kB (Marion C. Bonnet et al., 2000), j'ai décidé finalement d'étudier plus en détails l'implication de cette voie. De façon surprenante, bloquer la voie NF-kB avec une drogue spécifique, BAY 11-7082, dans les cellules exprimant Dicer WT ne changeait pas l'issue de l'infection. Cependant, faire la même chose dans les cellules exprimant Dicer N1 a réverté l'effet antiviral montrant une forte corrélation entre l'activation de NF-kB et le phénotype antiviral. Malheureusement, j'ai observé que le BAY 11-7082 induisait rapidement l'apoptose dans les cellules traitées, nous empêchant d'augmenter la concentration de drogue pour observer un blocage complet de l'activité de NF-kB. Ainsi, nous devrions considérer la

réalisation d'une invalidation de l'expression transitoire ou définitive de NF-kB pour confirmer son implication. De plus, je n'ai pas testé la dépendance du phénotype antiviral de Dicer N1 pour les autres facteurs tels que STAT1, STAT2 ou IRF3. En effet, les cibles de ces facteurs de transcription étaient significativement enrichies dans les cellules mock exprimant Dicer N1, nous laissant penser qu'il pourrait y avoir plusieurs couches de régulation impliquées. En particulier, parmi les cibles de STAT2, plusieurs membres de la voie d'ISGylation étaient fortement enrichis, comme par exemple ISG15 et OAS3. Tous les deux sont connus pour jouer un fort rôle antiviral contre des alphavirus et sont donc de bons candidats pour expliquer l'activité antivirale contre SINV (Bréhin et al., 2009; Lenschow et al., 2007; Yize Li et al., 2016). Pour mieux comprendre le mécanisme sous-jacent, nous pourrions imaginer la réalisation d'un crible d'inactivation de cibles à petite échelle comme nous avons désormais des gènes cibles candidats qui sont enrichis dans les cellules exprimant Dicer N1.

PKR est l'acteur central dans l'activation immunitaire transcriptionnelle. Cependant, la façon dont PKR est liée à l'activation transcriptionnelle reste à être déterminée. Il y a toujours un manque de connaissances concernant les partenaires de PKR lors de conditions de stress ou d'infections virales. Dans des cas spécifiques, comme l'induction de NF-kB, PKR a été montrée en interaction directe avec le complexe de kinases IKK (Bonnet et al., 2006). Nous pouvons émettre l'hypothèse que dans les cellules Dicer N1, PKR a des partenaires spécifiques qui permettent l'activation transcriptionnelle de gènes en aval. Pour aller plus loin, nous pourrions mener l'études des partenaires de PKR dans les cellules exprimant soit Dicer WT soit Dicer N1 an conditions mock et infectées pour relier les différences de partenaires avec la modulation de l'activation transcriptionnelle. Nous pouvons aussi proposer que la libération de partenaires spécifiques dûe à la délétion du domaine hélicase de Dicer pourrait moduler l'interactome de PKR et donc sa fonction. Deux dsRBPs, des co-facteurs connus de PKR et Dicer, sont de premier intérêt : TRBP et PACT. Ils possèdent des propriétés antagonistes sur la fonction de PKR. En effet, tandis que PACT est un activateur de PKR grâce à une interaction directe, TRBP se comporte comme un inhibiteur de PKR soit par interaction directe soit par la séquestration de PACT (Chukwurah and Patel, 2018; Farabaugh et al., 2020; Gupta et al., 2003). Le lien entre les formes libres de TRBP, PACT et PKR ainsi que l'activité antivirale de Dicer N1 devrait être étudié à la lumière de ces interactions.

Malheureusement, je n'ai pas eu le temps d'aller plus loin dans l'étude de la fonctionnalité de l'interactome de Dicer lors de l'infection. Certains de ses partenaires au cours de l'infection tels qu'ADAR1, PACT ou DHX9 sont aussi liés à la voie des miARN, effaçant

encore une fois la frontière entre les voies des miRNA et de l'IFN-I. comme nous avons également vu que Dicer N1 ne peut plus interagir avec ces partenaires, nous pouvons envisager qu'ils jouent un rôle dans la réponse immunitaire différentielle des cellules exprimant Dicer N1. Pour étudier ces partenaires, nous devrions aussi prendre en compte leur rôle potentiel dans les voies miARN et siARN. Par exemple, ADAR1 peut bloquer la potentielle voie antivirale par son activité d'édition des miARN (Uhl et al., 2023). De plus, ADAR1 est aussi lié à la limitation de la réponse inflammatoire principalement par l'édition d'ARNdb soit exogènes soit endogènes empêchant alors leur reconnaissance par PKR ou MDA5 (Chung et al., 2018; Pujantell et al., 2017). Il serait intéressant de voir si dans les cellules exprimant Dicer N1, la fonctionnalité d'ADAR1 est dérégulée. J'ai mentionné le rôle de DHX9 dans la voie des miARN, mais elle est aussi connue pour sa possible localisation nucléaire qui est liée à l'activation de STAT1 ou NF-kB (Liu et al., 2021; Ren et al., 2023). Finalement, PACT, aussi connu pour réguler la précision de Dicer dans le clivage et le chargement de pre-miARN, est lui-même lié à la signalisation immunitaire en tant que potentiel activateur de RIG-I lors de l'infection virale (Kok et al., 2011). En résumé, il est clair que le domaine hélicase de Dicer rassemble tous ces potentiels partenaires pro- ou anti-viraux, maintenant un équilibre inflammatoire. L'étude de la localisation précise de PACT ou DHX9 dans les cellules exprimant Dicer N1 pourrait aussi mettre en lumière le mécanisme cellulaire en jeu.

La question demeure comment le domaine hélicase de Dicer est physiquement lié à la réponse immunitaire te à tous ces partenaires. En regardant les autres partenaires de Dicer, j'ai trouvé EDC4 (du complexe de décoiffage) et WDR48 (du complexe de dé-ubiquitination) souvent trouvés dans les P-bodies et les granules de stress, et liés respectivement à la stabilité de l'ARNm et des protéines. La localisation de Dicer devrait aussi être explorée en regard de ses interactions spécifiques avec ces deux composants. Dicer a déjà été lié à une localisation potentielle dans les P-bodies (Much et al., 2016). Des études plus approfondies doivent se concentrer sur l'effet de la délétion du domaine hélicase sur la relocalisation de Dicer dans d'autres compartiments à cause de la perte de partenaires impliqués dans la localisation. D'un autre côté, nous devrions à nouveau nous intéresser au rôle potentiel d'EDC4 ou de WDR48 à séquestrer le complexe entier avec Dicer dans des granules, renforçant l'hypothèse d'un blocage éventuel de l'activité antivirale ARNi de Dicer par des partenaires protéiques. Il est important de noter qu'EDC4 et WDR48 sont également impliqués dans la régulation des vois de signalisation immunitaires, liant encore Dicer avec la régulation de la réponse IFN-I (Han et al., 2021; Mikuda et al., 2018; Xing et al., 2023).

Finalement, en regardant d'autres virus j'espérais obtenir plus d'informations sur le mécanisme antiviral de Dicer N1. J'ai pu généraliser le phénotype à d'autres virus à ARN simple brin de polarité positive tels que le SFV ou l'EV71 mais pas pour des virus à ARN simple brin de polarité négative comme le VSV. Il semble donc qu'une molécule d'ARN double brin accessible (ce qui n'est pas le cas pour les cellules infectées par le VSV) soit nécessaire pour permettre l'effet antiviral du Dicer N1. De façon surprenante, le phénotype antiviral n'a pas pu être observé lors de l'infection par le SARS-CoV-2. Cependant, le Dicer AviD (ΔHEL2i) possédait un effet antiviral contre ce virus qui était dépendant de l'ARNi (Poirier et al., 2021). Dans notre cas, Dicer N1 ne semble pas jouer de rôle dans l'ARNi antiviral mais plutôt une réponse liée à l'immunité. En faisant le lien entre toutes ces observations, j'ai émis l'hypothèse que la réponse pro-inflammatoire dans les cellules exprimant Dicer N1 pouvait devenir provirale dans le cas de l'infection par le SARS-CoV-2. En effet, la voie NF-kB a été extensivement montrée comme étant importante pour le SARS-CoV-2 pour créer un environnement pro-inflammatoire dans le but de mieux infecter les cellules humaines, ceci étant utilisé désormais comme un marqueur diagnostique (Li et al., 2021; Nilsson-Payant et al., 2021; Su et al., 2021). Ceci pourrait donc expliquer le phénotype inversé. Nous devrions donc regarder l'issue de l'infection lorsque la voie NF-kB est bloquée avec l'inhibiteur BAY. Il a déjà été montré que dans d'autres types cellulaires, ceci avait un effet positif sur l'infection par le SARS-CoV-2 (Nilsson-Payant et al., 2021).

Ainsi, le travail de thèse présenté ici permet d'ajouter une nouvelle pièce dans le puzzle de l'interaction entre ARNi et réponse IFN-I dans les cellules humaines, soulignant le rôle du domaine hélicase de Dicer dans la maintenance d'un état immunitaire plus faible. Le réseau complexe de partenaires autour du domaine hélicase joue un rôle crucial dans la modulation de la réponse immunitaire contre les alphavirus et les entérovirus. De plus, j'ai pu souligner un nouveau rôle non-canonique du domaine hélicase de Dicer dans le blocage de la réponse transcriptionnelle immunitaire induite par un de ses principaux partenaires lors de l'infection, PKR. Ce travail donne plus d'informations sur l'exclusivité mutuelle entre deux voies immunitaires conservées dans les cellules humaines.

CHAPTER 1: Cellular immunity, a tale of RNAs

A. The eukaryotic DExD-Box helicases-based immunity

Cellular organisms developed rapidly upon evolution a diverse range of immune responses to defend themselves against foreign elements. Transposable elements were described as the ancestors of DNA viruses (Krupovic and Koonin, 2015). A mechanism developed to block invading genetic elements is the use of antisense RNAs that stands as an immune response in unicellular organism. This RNA-guided system evolved with the addition of proteins carrying enzymatic activity: this is called the restriction system. It is for example the basis of the well-known CRISPR-Cas9 system in bacteria, which can target specifically foreign nucleic acids but also keep foreign nucleic acid elements integrated in the host genome as an "immune memory" (Barrangou et al., 2007; Jinek et al., 2012). In eukaryotic organisms, one can recognize three layers of defense systems against pathogens: the intrinsic immunity (akin to a restriction system), the innate immunity and the adaptative immunity. The adaptative immune system relies on an immune memory in vertebrates and on the production of specific antibodies against a pathogen. This involves the activity of two cell types, the B and T lymphocytes, but also the expression of a specific pattern of genes to produce the adapted antibodies. The antibodies can recognize specifically one pathogen to induce its degradation by other immune actors. Among innate immunity-related pathways, we can cite antiviral RNAi, which has been well-described in plants and invertebrates, and whose importance in vertebrate cells is still debated. In chordates, innate immunity is based on the recognition of foreign elements (nucleic acids, proteins) called pathogen-associated molecular patterns (PAMPs) by cellular receptors, the pattern recognition receptors (PRRs). PRRs trigger a transcriptional signaling cascade leading to the expression of cytokines to inhibit the infection (tenOever, 2016).

Among the cytokines, the interleukins and interferons are the most depicted in mammalian cells. In many cases where antiviral RNAi is described as inefficient against an infection, the interferon response (IFN) prevailed explaining partially the incompatibility between the two pathways (Maillard et al., 2016). IFN was discovered in 1957 with the study of viral interference against Influenza virus (Isaacs and Lindenmann, 1957). Since then, 10 different interferon cytokines have been discovered. Dysregulation of this response not only

changes the immunity against pathogens but can also lead to human pathologies called Interferonopathies (Mogensen, 2019). IFN and RNAi are sharing common sensing factors related to the DExD/H-Box helicases able to recognize RNA (Fairman-Williams et al., 2010), respectively the RIG-I-like receptors (RLRs) and a type III endoribonuclease named Dicer.

1. Untangling the roles of RNA helicases in antiviral immunity

The following part describes the roles of DExD-Box helicases in antiviral immunity in eukaryotic cells, especially in mammalian cells. The aim is to put the light on the specificities and the similarities between helicases from two innate immune pathways: RNAi and the IFN response. The manuscript was published in PLOS Pathogens and can be found below.

PLOS PATHOGENS

REVIEW

Untangling the roles of RNA helicases in antiviral innate immunity

Morgane Baldaccini, Sébastien Pfeffer

Université de Strasbourg, Architecture et Réactivité de l'ARN, Institut de Biologie Moléculaire et Cellulaire du CNRS, Strasbourg, France

* s.pfeffer@ibmc-cnrs.unistra.fr

Abstract

One of the first layers of protection that metazoans put in place to defend themselves against viruses rely on the use of proteins containing DExD/H-box helicase domains. These members of the duplex RNA–activated ATPase (DRA) family act as sensors of double-stranded RNA (dsRNA) molecules, a universal marker of viral infections. DRAs can be classified into 2 subgroups based on their mode of action: They can either act directly on the dsRNA, or they can trigger a signaling cascade. In the first group, the type III ribonuclease Dicer plays a key role to activate the antiviral RNA interference (RNAi) pathway by cleaving the viral dsRNA into small interfering RNAs (siRNAs). This represents the main innate antiviral immune mechanism in arthropods and nematodes. Even though Dicer is present and functional in mammals, the second group of DRAs, containing the RIG-I-like RNA helicases, appears to have functionally replaced RNAi and activate type I interferon (IFN) response upon dsRNA sensing. However, recent findings tend to blur the frontier between these 2 mechanisms, thereby highlighting the crucial and diverse roles played by RNA helicases in antiviral innate immunity. Here, we will review our current knowledge of the importance of these key proteins in viral infection, with a special focus on the interplay between the 2 main types of response that are activated by dsRNA.

Citation: Baldaccini M, Pfeffer S (2021) Untangling the roles of RNA helicases in antiviral innate immunity. PLoS Pathog 17(12): e1010072. https://doi.org/10.1371/journal.ppat.1010072

Editor: Tom C. Hobman, University of Alberta, CANADA

Published: December 9, 2021

Funding: Our work is funded by European Research Council (ERC-CoG-647455 RegulRNA, to SP) and Agence Nationale de la Recherche through the Interdisciplinary Thematic Institute IMCBio, part of the ITI 2021-2028 program of the University of Strasbourg, CNRS and Inserm (ANR-10-IDEX-0002 and ANR-17-EURE-0023, to SP). The funders had no role in study design, data collection and analysis, decision to publish, or preparation of the manuscript.

Competing interests: The authors have declared that no competing interests exist.

Introduction

To ward off viral infections, cells rely on a large variety of mechanisms that have been refined throughout evolution. During the initial response to an infection, the defense put in place will mainly consist in detecting the invading pathogen via the sensing of specific molecular patterns, which, in turn, will either trigger a signaling cascade or act directly on the detected molecule to hamper its function and/or degrade it. Different danger signals exist, but the presence of a foreign nucleic acid in the cell is one of the most prominent. Thus, the accumulation of DNA in the cytoplasm of eukaryotic cells, or of aberrant RNA molecules that do not possess the hallmarks of cellular RNAs, will immediately result in the onset of an innate immune response. Among the molecular features that are commonly associated with these pathogenic RNAs we can cite the presence of a 5′ triphosphate instead of a 5′ cap or of a double-stranded structure. In fact, double-stranded RNA (dsRNA) accumulates in cells infected by almost all viruses. While for RNA viruses, dsRNA is either generated during replication or by base

pairing of single-stranded RNA regions within the genome, it can originate from convergent transcription for DNA viruses [1]. Therefore, dsRNA is a potent pathogen-associated molecular pattern (PAMP), which is recognized by both cytosolic and membranous receptors named pattern recognition receptors (PRRs). Upon dsRNA sensing, PRRs act in 2 different ways: either directly as effector molecules or indirectly as signal transducers. These receptors can be grouped into 3 different families: the Toll-like receptors (TLRs), the cytosolic NOD-like receptors (NLRs), and the cytosolic RIG-I-like receptors (RLRs) [2], which will be the subject of this review.

RLRs belong to a class of helicase-containing proteins able to sense nucleic acid to induce an antiviral response. They use ATP to bind to and/or unwind nucleic acids, thereby altering ribonucleoprotein complexes. Structural and sequence features that have been observed in archaea, bacteria, and eukaryotic cells allowed to classify RNA helicases into different superfamilies (SFs) [3]. Only SF1 and SF2 include helicases containing 2 bacterial RecA-like fold domains. The DExD/H-box helicase proteins family we are interested in are found within the SF2 subgroup [3]. This family is composed of RNA helicases involved in all aspects of RNA metabolism but also in antiviral defense [4,5]. These proteins can either unwind RNA upon ATP binding and hydrolysis or clamp around RNA to act as a platform to recruit other proteins [6].

Within the DExD/H-box helicases family, the subgroup of duplex RNA–activated ATPases (DRAs) is composed of SF2 helicases activated by dsRNA [7]. DRAs share the same activation mechanism: upon dsRNA binding, they undergo conformational changes to become catalytically active [8]. However, due to significant differences in their protein domain organization and their functions [6,8], we can distinguish signaling DRAs (sDRAs) and catalytic DRAs (cDRAs). These proteins include RLRs and Dicer proteins, which share a similar helicase domain [7,8] and participate in 2 main antiviral pathways, namely the RNA interference (RNAi) and the type I interferon (IFN) response. Here, we will focus on metazoan DRAs and more specifically on the 3 mammalian RLRs (RIG-I, MDA5, and LGP2), the mammalian Dicer, the 2 *Drosophila melanogaster* Dicers (dmDicer-1 and dmDicer-2), the *Caenorhabditis elegans* Dicer (ceDicer), and the 3 *C. elegans* Dicer-related helicases (DRH-1 to 3) [7]. We will discuss the role of DRAs as direct effectors of the antiviral response, before reviewing their roles as signaling molecules. Finally, we will elaborate on the noncanonical roles played by DRAs during viral infection in the light of recently published data and will comment on the possible crosstalk that can exist between pathways.

RNA helicases as direct effectors of the antiviral response

The best example of helicases acting directly on viral dsRNA upon sensing is without any doubt the case of Dicer proteins, which are the primary effectors of antiviral RNAi. This ancestral defense mechanism is the main antiviral system in nematodes and insects [9,10], while in mammals, this role is fulfilled by type I IFN response [11]. However, as we will see later, RNAi has been shown to play a role in the fight against viruses in mammalian cells, and an IFN-like antiviral response in invertebrates has been described [12–15], further blurring the boundaries between these 2 major innate immunity mechanisms.

With the notable exception of *Saccharomyces cerevirisiae* [16], Dicer is conserved in most eukaryotes. This enzyme is involved in the microRNA (miRNA) pathway and in RNAi through the generation of small interfering RNA (siRNA) [17]. The origin of Dicer functional diversity can be found in early branching metazoans [18]. Some organisms, such as *Drosophila melanogaster*, present a duplication of the *dicer* gene, thus splitting the proto-function in 2. One protein (dmDicer-1) is involved in the miRNA pathway, whereas the other one

(dmDicer-2) is responsible of both exogenous and endogenous long dsRNA processing [9]. Phylogenetically, dmDicer-2 is closer to the common ancestral RNase III than dmDicer-1 [18]. Conversely, the nematode *Caenorhabditis elegans* genome encodes one single Dicer (ceDicer), which is very similar to the proto-Dicer as it carries both functions in miRNA and siRNA pathways [19]. Similarly, only one Dicer (hsDicer), involved in the miRNA pathway, is present in humans [20]. The capacity of hsDicer to perform efficient antiviral RNAi is still a matter of debate [14,21].

All these Dicer proteins share a similar organization in different domains, some of which are conserved with the bacterial RNase III [22] (Fig 1A). From the N-terminal part, there is a DExD/H-Box helicase split into 3 subdomains HEL1, HEL2i, and HEL2. Then, there is a domain of unknown function DUF283, which was computationally predicted [23] and recently structurally defined [22] as a dsRNA-binding domain (dsRBD). It is followed by an -helix connector, Piwi–Argonaute–Zwille (PAZ) and Platform domains involved in the recognition of RNA with 3′-overhanging extremities [24]. Finally, toward the carboxyl-terminal part, there are a conserved tandem RNase III domain (IIIa and IIIb) that forms an intramolecular dimer to cleave RNA substrates [25] and a dsRBD able to bind the minor groove of dsRNA [26,27]. One hypothesis is that the helicase domain is involved in auto-inhibiting the proper function of Dicer. In *Drosophila*, the 2 Dicers differ by their helicase domain [28]. As opposed to dmDicer-2, dmDicer-1 contains only a truncated version of the helicase with just a HELICc motif (Fig 1A). By alignment of metazoans helicases, it can be observed that dmDicer-1 is the least conserved among them with divergences in the ATP-binding and in the intramolecular interaction motives [29]. Conversely, the helicase domain of dmDicer-2 is more conserved and is involved in its processivity as it hydrolyzes the ATP necessary for its translocation along the dsRNA [29]. The ceDicer also hydrolyzes ATP to translocate, whereas the hsDicer protein does not require ATP hydrolysis and seems to be closer to dmDicer-1 helicase [19,22]. As such, the helicase domain has an auto-inhibitory effect on hsDicer activity [30]. In addition, it is involved in the recruitment of regulatory co-factors such as TAR RNA-binding protein (TRBP), protein activator of the interferon-induced protein kinase (PACT), and ATP-dependent RNA Helicase A (DHX9) [31–34].

Recently, the determination of the 3D structure of hsDicer allowed novel features of its helicase domain to be uncovered. Cryo-electron microscopy revealed that hsDicer adopts an L-shaped structure where the helicase domain is located in the shorter arm [22,35,36] (Fig 1B). The 3 subdomains of the DExD/H-box helicase form a C-shaped structure in which HEL1 is at the junction between the 2 parts of the "L" and interacts with DUF283 and RNaseIIIb. HEL2 is at the center of the "C-shaped" structure, while HEL2i is at the arm tip and is involved in mediating the interaction with TRBP [31,32]. Finally, an -helix connects HEL1 and HEL2 forming a pincer-like motif with a flexible HEL1 that can easily move around substrates (Fig 1B). Interestingly, dmDicer-2 cryo-electron microscopy structure resembles the hsDicer "L-shaped" structure [37].

In both *C. elegans* and *D. melanogaster*, Dicer proteins are involved in antiviral RNAi. Despite several differences in the RNAi pathway of the 2 organisms, the key steps are conserved (Fig 2). In the worm, Dicer is involved in viral siRNA production that, in turn, causes a decrease in viral load [10,38]. ceDicer triggers RNAi against vesicular stomatitis virus (VSV) [10,38]. These results were later confirmed with the Orsay virus (OrV), which is a natural pathogen of *C. elegans* [39–41]. The viral dsRNA is recognized by a complex composed of ceDicer, the RNA helicase DRH-1, and the Argonaute protein RDE-1 [42–44]. The latter is not efficient in RNA silencing, even though it can target specific RNAs. However, silencing can be amplified by secondary siRNAs, or 22G-RNAs, which are generated by an RNA-dependent RNA polymerase RRF-1 and another RNA helicase, DRH-3 [45–47]. In somatic cells, these

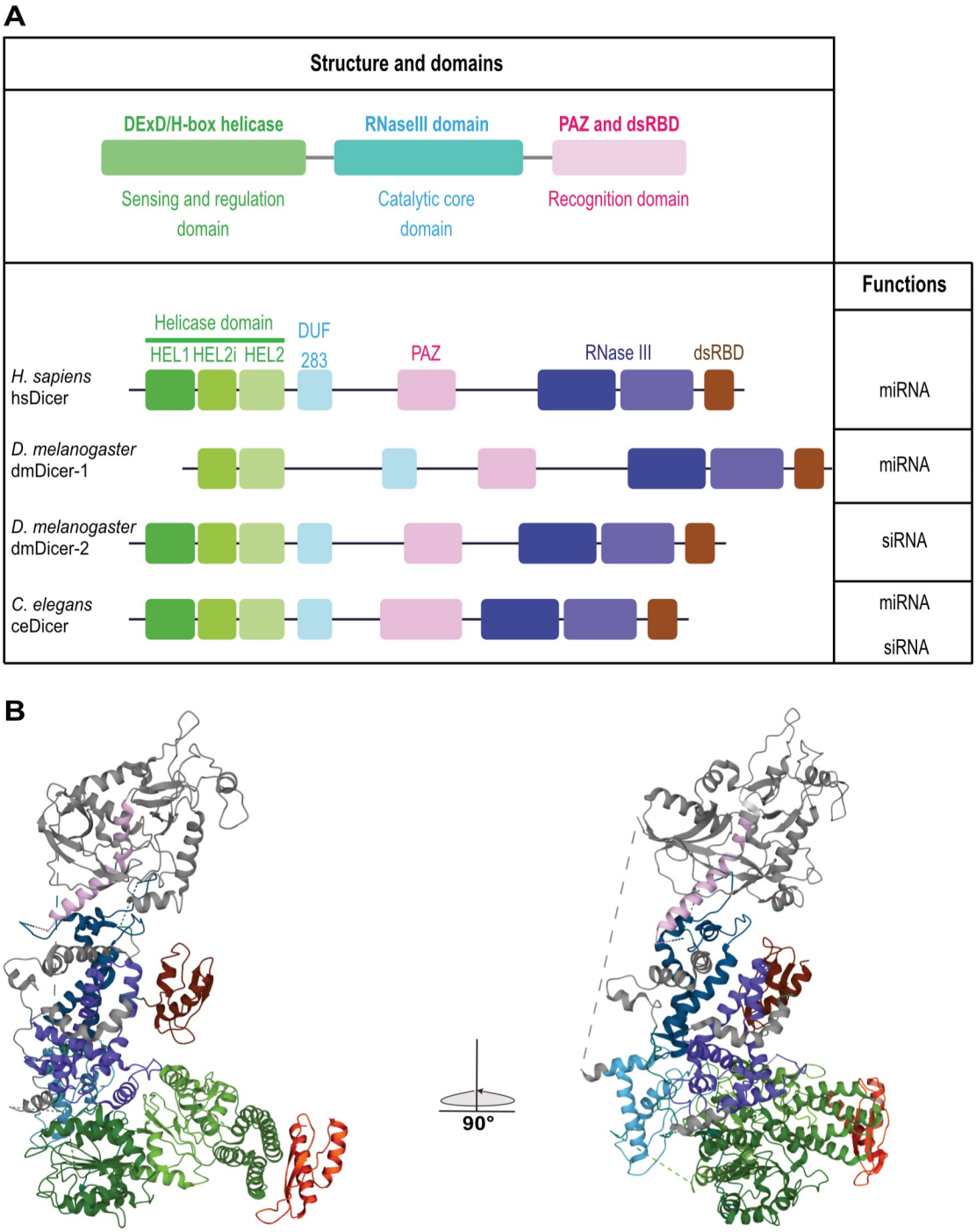

Fig 1. Domains organization and functions of Dicer proteins in metazoans. (A) Dicer carries a DExD/H-box helicase, which is divided into 3 subdomains: HEL1, HEL2i, and HEL2. The domain of unknown function (DUF283) is regulating pre-miRNA binding and the PAZ domain is involved in the recognition of the 3′-overhanged extremities. The catalytic core is composed of 2 RNase III domains that each processes one strand of the duplex. Finally, the terminal dsRBD is involved in the binding of the dsRNA minor groove. **(B)** Position of the different domains in the tridimensional structure of human Dicer in complex with TRBP determined by cryo-EM [22]. The color code used for the domains is the same as in A. TRBP is in orange (adapted from PDB structure n˚5ZAK). cryo-EM, cryo-electron microscopy; dsRBD, dsRNA-binding domain; miRNA, microRNA; PAZ, Piwi–Argonaute–Zwille; siRNA, small interfering RNA; TRBP, TAR RNA-binding protein.

https://doi.org/10.1371/journal.ppat.1010072.g001

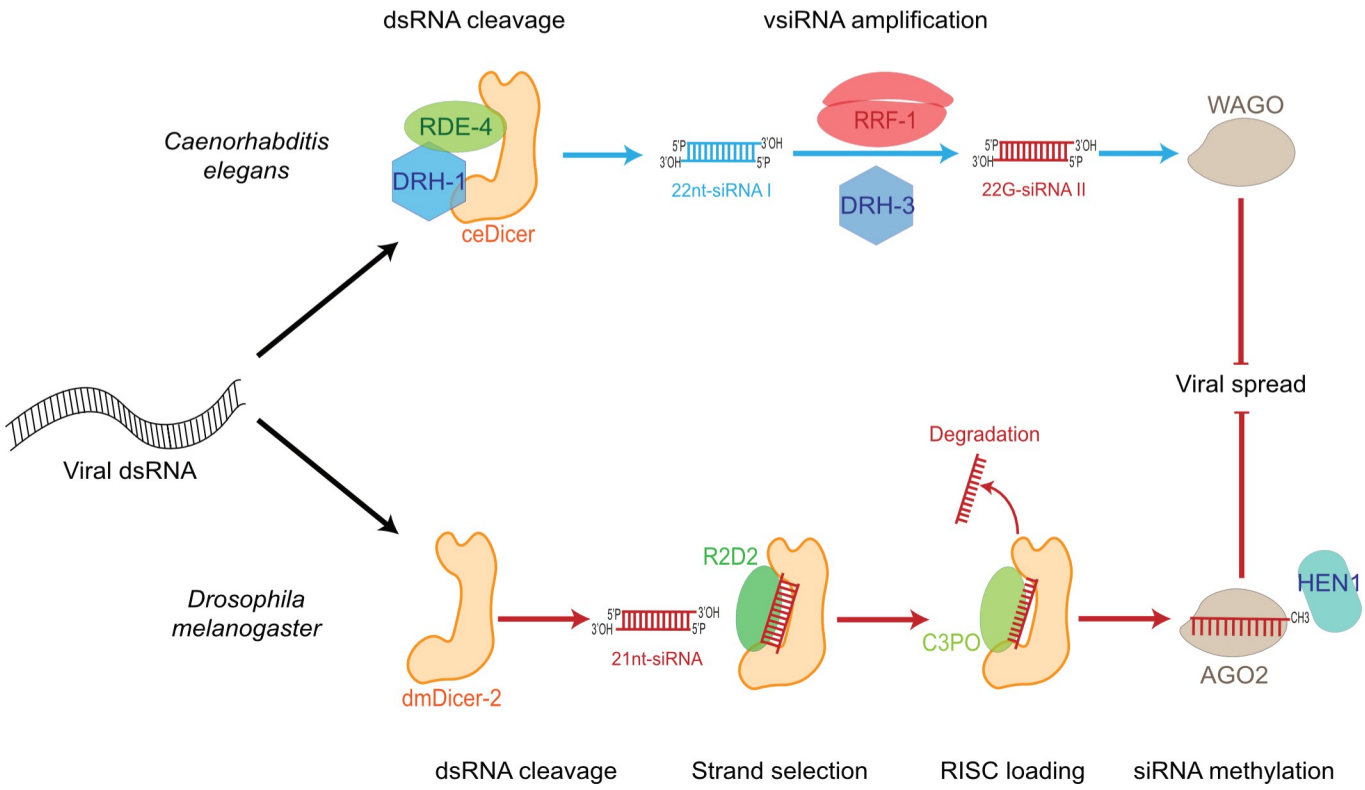

Fig 2. Antiviral RNAi pathways in *Caenorhabditis elegans* and *Drosophila melanogaster*. Upon viral infection, dsRNA triggers RNAi after its recognition by Dicer. In *C. elegans*, Dicer helped by the dsRBP RDE-4 and another DExD/H-box helicase, DRH-1, recognizes the dsRNA and processes it into primary 22 nt siRNA duplexes. These duplexes serve as a template for the generation of secondary 22G-siRNA by the polymerase RRF-1 and a third helicase called DRH-3. They are finally loaded into an Argonaute protein, WAGO. In *D. melanogaster*, Dicer-2 recognizes and cleaves the viral dsRNA into 21nt-siRNA duplexes. Strand selection occurs with the help of the dsRBP R2D2, and the passenger strand is sliced by Ago2 before being degraded by the nuclease C3PO. The guide strand is then 2′-O-methylated at the 3′ end by HEN1 to be stabilized. For both worms and flies, the loaded Argonaute protein can then cleave viral complementary sequences, resulting in the antiviral state. dsRNA, double-stranded RNA; RNAi, RNA interference; siRNA, small interfering RNA; vsiRNA, virus-derived small interfering RNA.

https://doi.org/10.1371/journal.ppat.1010072.g002

secondary siRNAs are then loaded in another Argonaute protein, WAGO [46,48]. This amplification system is common to all siRNA pathways in *C. elegans* and allows to increase both the siRNA pool and targeted sequences on RNAs [44]. A point mutation in ceDicer helicase domain dramatically decreases virus-derived small interfering RNA (vsiRNA) and endogenous small interfering RNA (endosiRNA) production but has no consequences on exosiRNA production [49–51]. Moreover, this helicase domain is essential for siRNA production from internal regions of blunt-ended dsRNA [52].

In the fly *D. melanogaster*, dmDicer-2 is involved in the recognition and cleavage of endogenous dsRNA, exogenous dsRNA, and viral dsRNA [15]. Since dmDicer-2 is not an essential gene, it could be inactivated to show that RNAi is indeed a defense mechanism against many (+) ssRNA viruses such as Flock house virus (FHV), *Drosophila* C virus (DCV), Cricket paralysis virus, and Sindbis virus (SINV) [53–57]. In the viral dsRNA maturation process, the D isoform of the Loquacious protein (Loqs-PD) is dispensable, whereas R2D2 is required for vsiRNA loading into Ago2 [58]. In vitro, dmDicer-2 was shown to act independently from other factors to process long dsRNA thanks to its helicase domain [59]. The generated siRNA duplexes are then transferred from dmDicer-2 to another dsRBP, R2D2, to bring the duplexes to Ago2 and allow the formation of a pre-RISC complex. To be active, Ago2 cleaves the passenger strand, which is then degraded by the C3PO nuclease [60]. The guide strand is 2′-O-

methylated at its 3′ terminal nucleotide to be stabilized and guides Ago2 to target RNAs, which are sliced and degraded [15]. The helicase domain in dmDicer-2 is multifunctional allowing substrate recognition, cleavage efficiency, and discrimination of dsRNA extremities. How can dmDicer-2 discriminate between viral dsRNA and other dsRNA molecules? One hypothesis is that viral dsRNA carries specific structures recognized by Dicer, similar to what happens with mammalian RLRs. Indeed, the helicase domain of dmDicer-2 is necessary for antiviral RNAi and permits the recognition of noncanonical extremities on dsRNA [51]. This domain can be found in 2 states, one of them allowing it to widen its range of recognizable dsRNA extremities following conformational change induced by ATP binding [61].

RNA helicases with signaling antiviral activities

As opposed to the situation in arthropods and nematodes, the main antiviral response in mammals is based on type I IFN. At the heart of this pathway are 3 cytosolic nucleic acid sensors called RLRs. Retinoic acid–inducible gene I (RIG-I or DDX58) recognizes 5′ di- or triphosphorylated dsRNA or ssRNA [62,63]. Melanoma differentiation–associated gene 5 (MDA5 or Helicard or IFIH1) recognizes long dsRNA [62,63]. Laboratory of genetics and physiology 2 (LGP2 or DHX58) modulates the functions of the 2 other RLRs instead of acting as a signal transducer (reviewed in [64]). RIG-I and MDA5 are composed of 4 domains (Fig 3) [65,66]: 2 N-terminal caspase activation and recruitment domains (CARDs), a central DExD/H-box helicase domain, and a pincer domain that connects the helicase to the regulatory carboxyl-terminal domain (CTD). The latter is essential for the recognition of the RNA substrate and autoinhibition of the protein when not RNA-bound. LGP2 is highly similar to RIG-I and MDA5 except it does not have CARD domains (Fig 3). Phylogenetic studies between all

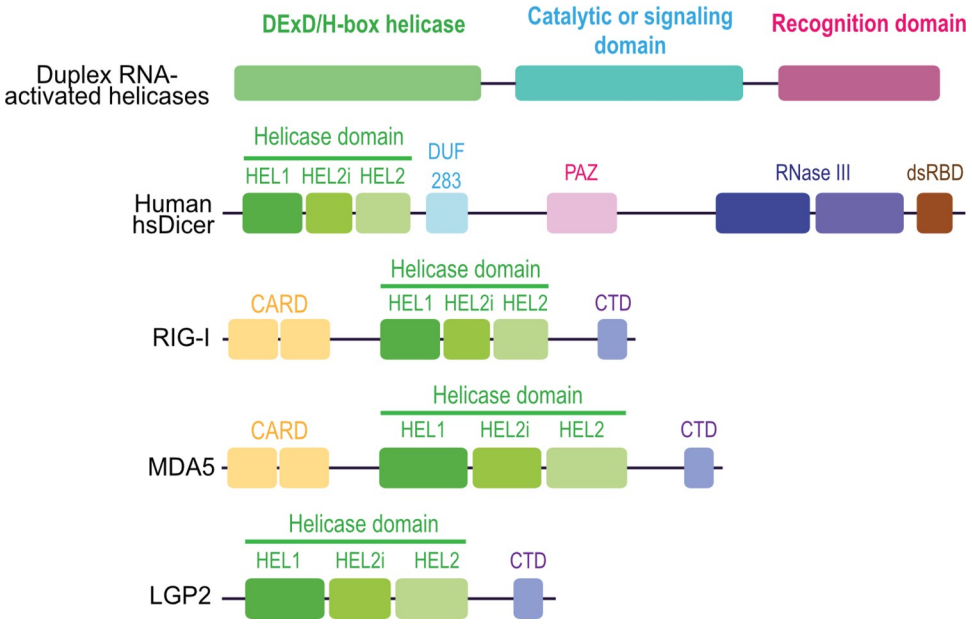

Fig 3. Domains organization of RLRs. RLRs are directly involved in the IFN-I response upon viral infection. RIG-I and MDA5 can activate the mitochondrial adaptor protein MAVS via their N-terminal CARD domains. Their central DExD/H-box helicase domain shares the same organization as the Dicer one and, together with the CTD, is involved in dsRNA recognition. LGP2 lacks the signaling CARD domains but possesses the whole helicase domain and the CTD. CARD, caspase activation and recruitment domain; CTD, carboxyl-terminal domain; IFN, interferon; MAVS, mitochondrial antiviral signaling adaptator; MDA5, melanoma differentiation–associated gene 5; RIG-I, retinoic acid–inducible gene I; RLR, RIG-I-like receptor; LGP2, laboratory of genetics and physiology 2.

https://doi.org/10.1371/journal.ppat.1010072.g003

known PRRs show that the helicase domain of Dicer and RLRs are close in terms of sequence and structure [67]. Both belong to SF2 helicases and share some specificities that put them in the subclass of DRAs.

Like Dicer, RIG-I has a C-shaped DExD/H-box helicase domain composed of 3 subdomains: HEL1, HEL2i, and HEL2. HEL1 and HEL2 form the core helicase with dsRNA binding and ATPase functions. A flexible linker (HEL2i) with an autoregulatory role links these 2 domains [68]. The helicase and the CTD are involved in dsRNA and 5′ PPP-RNA recognition required for CARD-mediated signaling [68]. The CTD (also called repressor domain) together with the helicase domain form a ring around dsRNA adopting a compact conformation that, in absence of RNA substrates, is flexible and extended [68]. RIG-I can translocate along dsRNA (like dmDicer-2) but, as all helicases in the DRAs subclass, it cannot unwind the duplexes [69]. Under physiological conditions, RIG-I persists in the cytosol in an auto-inhibitory closed state where the tandem CARD domains are in head-to-tail conformation and directly interact with HEL2i to form an inactive structure [70]. dsRNA binding leads to a conformational change and to the stabilization of RIG-I clamp around dsRNA [71,72]. An activation model was proposed where dsRNA first binds the CTD, which then brings together several dsRNA molecules near the helicase domain. This increased dsRNA concentration permits the cooperative fixation of dsRNA and ATP on the helicase, thereby freeing the CARD domains that mask the dsRBD and the K63 polyubiquitination site [70] (Fig 4). ATP hydrolysis enhances RIG-I dissociation from dsRNA [66].

Although RIG-I and MDA5 share structural similarities, MDA5 is not activated by opening a closed conformation between its CARD and HEL2i domains. After dsRNA recognition in the cytosol, several MDA5 molecules gather and form helicoidal filaments along the dsRNA to coalesce into an active fibrillar form [73] (Fig 4). The formation of this MDA5 polar helix is allowed by cooperative assembly of their CTD. The contacts between filaments are supposedly mediated by HEL2i and CTD. ATP is involved in the disassembly of MDA5 oligomers, regulating dsRNA binding affinities in a concentration-dependent manner [73,74].

LGP2 lacks CARD in the N-terminal part, but it has a CTD and a DEAD/H-box helicase domain, which is highly conserved, showing a great selection pressure to maintain this domain [75]. Interestingly, LGP2 is a perfect chimera of the 2 other RLRs, with its helicase domain closer to the MDA5 one, while its CTD is closer to the RIG-I one. It can act both as an activator of MDA5 and an inhibitor of RIG-I [76]. Similar to MDA5, LGP2 can form helicoidal-like filaments in the cytosol [76]. Crystal structure obtained from chicken LGP2 indicates that it can adopt 2 conformations that are partially or fully closed [76]. These conformations are guided by ATP binding and hydrolysis and directed by the HEL2 helicase subdomain that is flexible and can orient its CTD [76]. The LGP2 structure after ATP hydrolysis is similar to the one adopted by RIG-I after activation [76].

Upon dsRNA recognition, both RIG-I and MDA5 interact with CARD-like domains of the mitochondrial antiviral signaling adaptator (MAVS) [77,78] (Fig 4). MAVS then activates a signal transduction cascade in 2 ways. On one hand, it interacts with TBK1 (TANK-binding kinase 1) and IKK (IkB kinase), which will phosphorylate and induce translocation of a complex of transcription factors, IRF3 and IRF7 (IFN regulatory factor 3 and 7), which will activate IFN-I genes expression [77,78]. On the other hand, MAVS activates the NF-kB pathway leading to nuclear translocation of this transcription factor that induces expression of antiviral cytokines [77,78]. Through a molecular cascade involving the Janus kinase Signal transducer and activator of transcription (JAK-STAT) pathway, these cytokines finally activate hundreds of ISGs to prevent viral spreading [78–80].

Despite their similarities, RIG-I and MDA5 have nonredundant recognition capacities upon viral infection. Since they are activated by different substrates, they are not necessarily

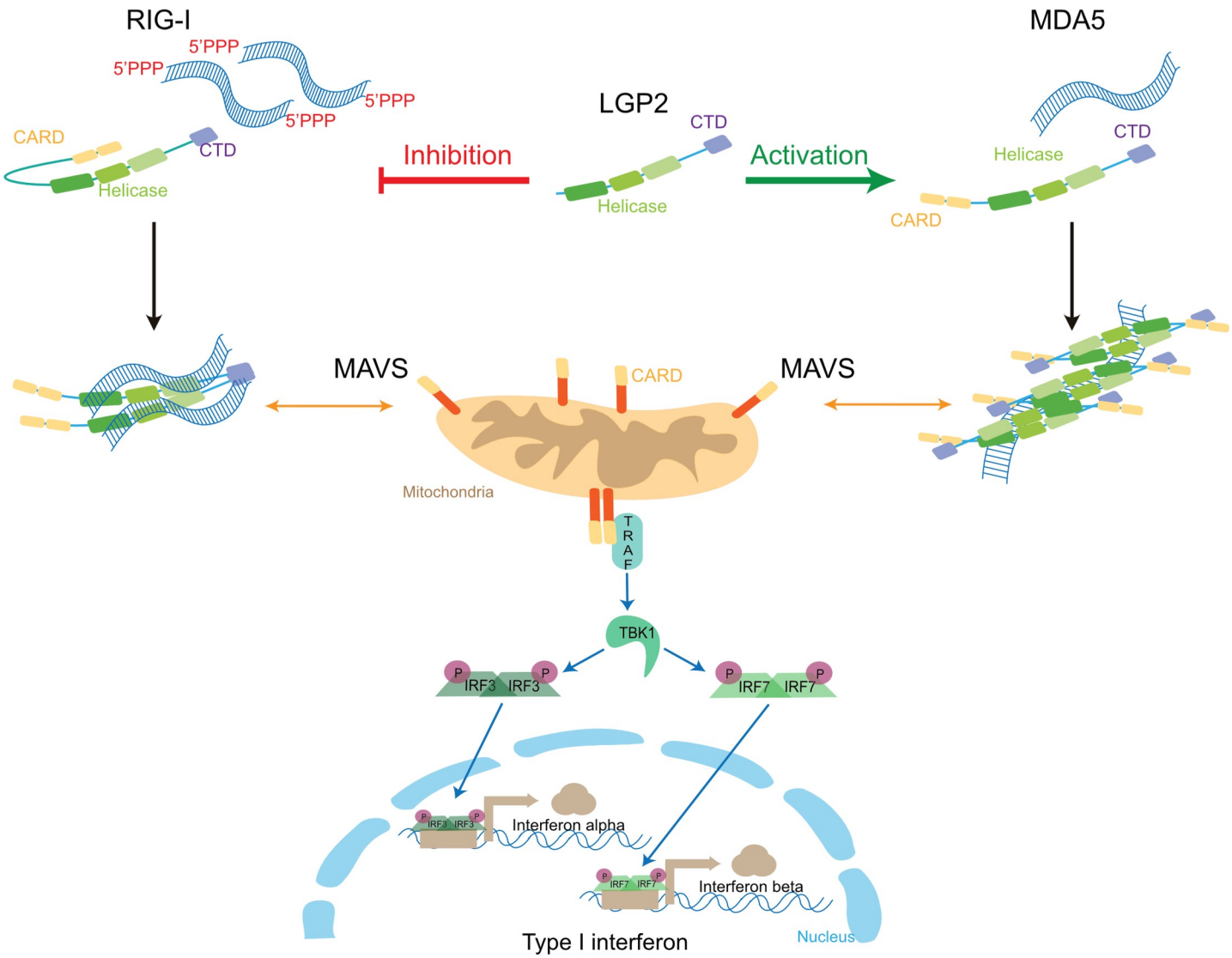

Fig 4. Mode of action of RLRs upon viral infection. Both dsRNA replication intermediates and 5′ terminal motifs can be recognized by cytosolic RLRs. RIG-I detects 5′ di- or tri-phosphorylated dsRNA via its CTD and helicase domains whereas MDA5 recognizes long dsRNA structures. Upon dsRNA binding, RIG-I opens and homodimerizes to mediate interactions with MAVS CARD domains at the surface of mitochondria. By contrast, MDA5 constantly shifts between open and close conformations and when it is activated, it polymerizes along the dsRNA forming helicoidal filament to expose its CARD domains and activate MAVS. Once activated, MAVS aggregates and triggers a signaling cascade through the TRAF protein that activates the TBK1 kinase. The latter then phosphorylates the cytosolic transcription factors, IRF3 and IRF7, thereby allowing their dimerization and their translocation into the nucleus where they activate the transcription of IFN-I genes. CARD, caspase activation and recruitment domain; CTD, carboxyl-terminal domain; dsRNA, double-stranded RNA; IFN, interferon; MAVS, mitochondrial antiviral signaling adaptator; MDA5, melanoma differentiation–associated gene 5; RIG-I, retinoic acid–inducible gene I; RLR, RIG-I-like receptor.

https://doi.org/10.1371/journal.ppat.1010072.g004

induced by the same viruses [63,66,81,82]. Blunt-ended dsRNA, 5′di or tri P, uncapped or 2′O-unmethylated 5′ extremities are RIG-I substrates. It is activated by rhabdoviruses (VSV), paramyxoviruses, orthomyxoviruses, filoviruses (Ebola), Epstein–Barr virus (EBV), hepatitis C virus (HCV), Japanese encephalitis virus, Zika virus (ZIKV), and Dengue virus (DENV) [66]. Interestingly, host RNAs can also be recognized as PAMPs by RIG-I [66]. For instance, upon infection by DNA viruses, such as Herpes simplex virus type I (HSV-1) and Kaposi sarcoma–associated herpesvirus (KSHV), host-encoded small noncoding RNAs can be recognized by RIG-I [83,84]. Rather, MDA5 is involved in the recognition of the dsRNA replication

intermediate of picornaviruses [85]. MDA5 is also able to detect dsRNA from HCV, norovirus, encephalomyocarditis virus (EMCV), hepatitis B virus (HBV), herpes simplex virus, avian Influenza virus H5N1, and hepatitis D virus [86–92]. In some cases, such as infection with flaviviruses and reoviruses, both RIG-I and MDA5 seem to be recruited to trigger an IFN-I response [82].

Noncanonical and interdependent actions of RNA helicases

In addition to performing the abovementioned activities, RNA helicases can also function in an uncommon manner. Thus, RLRs can have direct antiviral activities and Dicer proteins can exert signaling functions. In addition, such as in the case of mammalian Dicer, their role in antiviral RNAi may depend on additional factors as indicated below.

There are at least 2 dmDicer-2–dependent pathways that do not rely on its canonical catalytic activity. First, both in *Drosophila* and mosquitoes, studies on persistent viral infection by RNA viruses led to the discovery of a new viral genomic element in host-infected cells [93,94]. After vsiRNA biogenesis, a transposon-encoded cellular retrotranscriptase can amplify and convert viral RNA into DNA (vDNA) [93]. In both insects, vDNA was retrieved either in linear or in circular forms (cvDNA). cvDNA are homologous to defective viral genome (DVG) and can amplify the RNAi response in insects (Fig 5A, right part). Those cvDNA are sufficient to trigger biogenesis of new siRNAs targeting the viral genome. Although the molecular mechanism has not been elucidated, vDNA synthesis is entirely dependent on dmDicer-2 DEAD-Box helicase domain, which would make it an insect RLR [93]. Indeed, this is reminiscent of the situation in mammalian cells, where DVGs are recognized by cytosolic RLRs and trigger IFN-I responses against arboviruses [95,96]. Second, dmDicer-2 helicase domain is also involved in another aspect of an IFN-like pathway, namely the capacity to induce cytokine production after detection of PAMPs. Although there is no equivalent to mammalian IFN /ß cytokines in *Drosophila*, its genome encodes for a cysteine-rich protein named Vago, which may be considered as a cytokine-like element [67]. Upon DCV infection, Vago expression is increased and exerts antiviral effects against DCV in a manner depending on dmDicer-2 DEAD-Box helicase integrity (Fig 5A, left part). Vago expression is totally independent of other RNAi pathway members, but when dmDicer-2 helicase domain is mutated, Vago expression is dramatically decreased [67]. However, to date, a little is known regarding the pathway involved upon Vago induction by dmDicer-2 or its role in other viral infections.

The relevance of RNAi as an antiviral defense mechanism in mammals is still a matter of debate, and many reports have tried to answer the issue pertaining to the evolution of Dicer antiviral activity in metazoans [9,14,17,97]. VsiRNAs were found to be functional and to reduce viral load in a sequence-dependent fashion in undifferentiated mouse embryonic stem cells (ESCs) (Fig 5B) and somatic cells [98–100]. In oocytes, ESCs and generally, undifferentiated cells, IFN-I is not set up yet to avoid inflammatory response and apoptosis during development [101–103]. In MAVS- or IFNAR-deficient mouse somatic cells, sequence-specific hsDicer- and Ago2-dependent siRNAs are detected when cells are transfected with an exogenous long dsRNA [104]. Moreover, AGO4 was recently showed to be involved in antiviral RNAi against influenza A virus (IAV), VSV, and EMCV in mouse macrophages [105]. It seems also that viral suppressors of RNAi (VSRs) prevent Dicer from playing an antiviral role. Indeed, in mammalian cells, a decrease in viral replication was observed with flaviviruses deleted from their VSR [106].

On the other hand, other experiments on the detection of vsiRNA were not conclusive enough to validate a functional antiviral RNAi. Indeed, hsDicer is less processive than *Drosophila* dmDicer-2 to generate siRNAs from long-dsRNA [107,108]. This could explain the

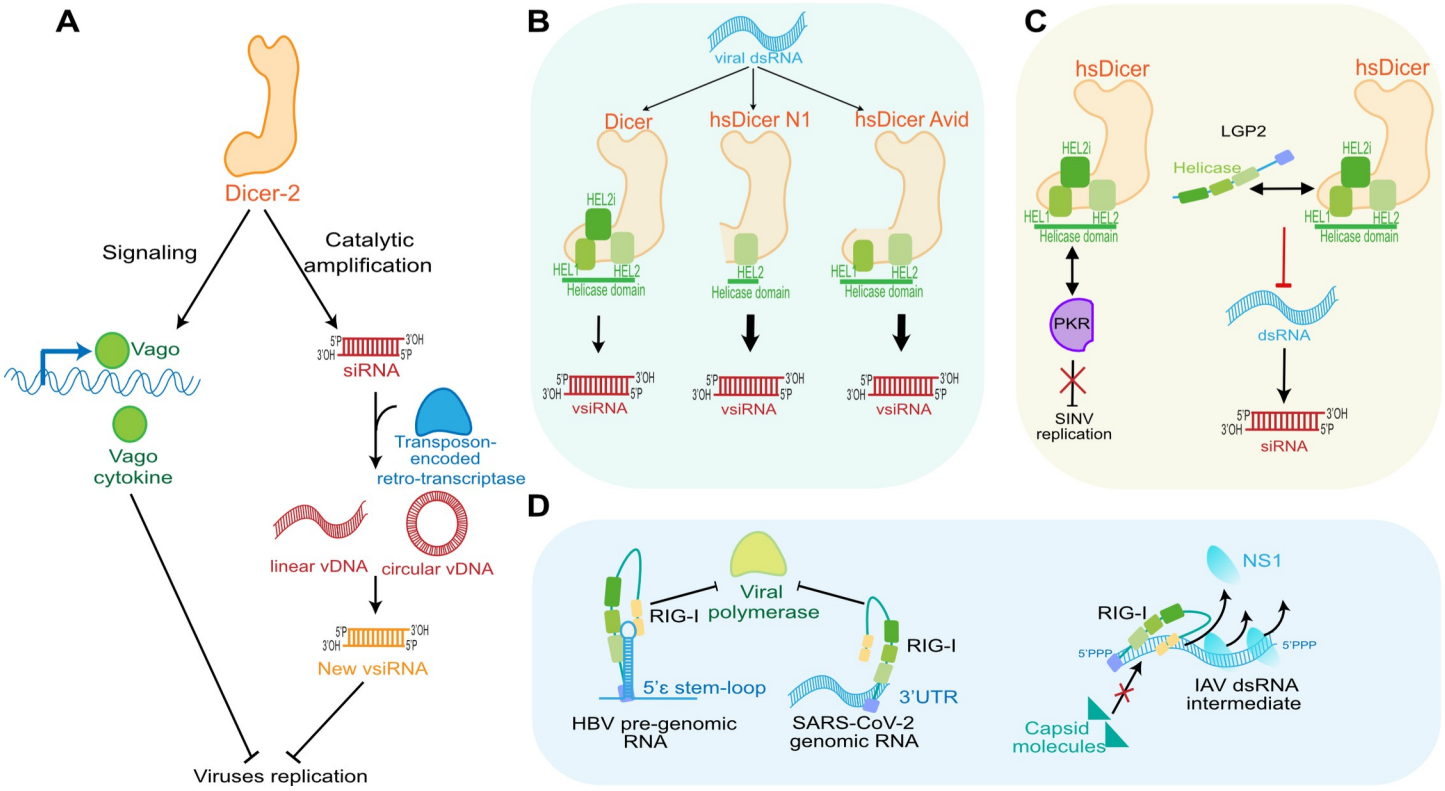

Fig 5. Noncanonical functions of helicases during viral infection. (A) In insects, Dicer-2 is involved in 2 antiviral pathways in addition to its canonical role in RNAi. First, its helicase domain is necessary to induce the transcription of Vago, a *Drosophila* cytokine. Vago inhibits viral replication through a yet to be defined mechanism. Second, in *Drosophila* and mosquitoes, Dicer-2-generated siRNAs can be used by a transposon-encoded retrotranscriptase to generate both linear and circular vDNA molecules. These vDNA can be a source of new vsiRNA duplexes, thereby amplifying the antiviral signal in the cell. **(B)** In the case of mammalian Dicer, its involvement in direct catalytic antiviral pathways remains debated. During viral infection of undifferentiated ESCs, Dicer is responsible for the production of vsiRNAs functionally involved in the blocking of viral replication. Artificial generation of a helicase-truncated form of Dicer (N1) allows to uncover antiviral RNAi functions in differentiated cells as well. The recent discovery in human ES cells of a naturally occurring isoform of Dicer called Avid, which lacks the HEL2i domain, provides some support to the existence of antiviral RNAi in humans. **(C)** In human cells, Dicer is also at the center of many interactions, which could modulate either its own or the interacting protein functions. For instance, human Dicer interacts with PKR via its helicase domain and modulates its function during SINV infection. LGP2 is also interacting with the Dicer helicase domain and inhibits Dicer catalytic activity. **(D)** In mammalian cells, RLRs can be involved in steric obstruction of viral dsRNA. Thus, RIG-I can block the binding and catalytic action of viral proteins (polymerase or capsid) or displace them (NS1), thereby allowing recognition of the dsRNA by other antiviral proteins. dsRNA, double-stranded RNA; ESC, embryonic stem cell; HBV, hepatitis B virus; IAV, influenza A virus; PKR, protein kinase R; RLR, RIG-I-like receptor; RNAi, RNA interference; SARS-CoV-2, Severe Acute Respiratory Syndrome Coronavirus 2; SINV, Sindbis virus; siRNA, small interfering RNA; vDNA, viral DNA.

https://doi.org/10.1371/journal.ppat.1010072.g005

difficulty to detect vsiRNA in mammalian somatic cells infected with several viruses [109]. In agreement with this hypothesis, in IFN-I–deficient human cells that express the regular Dicer protein, no vsiRNA was detected when infected by SINV, Yellow fever virus (YFV), or EMCV [110]. Besides, when hsDicer is genetically invalidated, no replication increase could be observed for many RNA viruses [111].

Explanations on this defective RNAi pathway in mammals are now centered on the helicase domain of Dicer. First, as opposed to dmDicer-2, hsDicer is not processive due to the fact that it cannot hydrolyze ATP [30,59,108,112,113]. Dicer helicase domain appears to limit its functionality. Indeed, *in vitro* studies on hsDicer revealed that siRNA production is performed less efficiently than pre-miRNA to miRNA maturation [30,114]. Accordingly, in human somatic cells, only the artificial expression of a helicase-truncated form of human Dicer, named Dicer-N1, could produce functional siRNA from IAV genome with a moderate antiviral effect [115] (Fig 5B). This helicase deletion was inspired from the specific case of murine oocytes, which express a truncated version of Dicer, Dicer^{O}, due to an insertion of a retrotransposon in the 5′

part of the Dicer gene [116]. The part of the helicase domain missing in Dicer^{O} is the same one that was deleted in Dicer-N1, and indeed the shorter mouse Dicer lacking part of its helicase domain has enhanced capacities in term of siRNA production from endogenous and exogenous hairpin [116]. However, the role of Dicer^{O} in antiviral defense has not been explored to date. Interestingly enough, another Dicer isoform has been recently identified in human stem cells. It also presents a deletion in its helicase domain; more precisely, it lacks the HEL2i subdomain. This splicing isoform, which has been coined Avid (for antiviral Dicer) shows enhanced antiviral RNAi properties against several RNA viruses including ZIKV and the Severe Acute Respiratory Syndrome Coronavirus 2 (SARS-CoV-2) (Fig 5B) [117].

Another possible and nonmutually exclusive explanation for the inhibition of Dicer-dependent RNAi in mammalian cells could be its interaction with a protein with repressive activity. Such a protein could be LGP2, which was shown to associate with Dicer to inhibit dsRNA cleavage (Fig 5C, right) [118]. One hypothesis to explain this observation is that there is a need to prevent dsRNA degradation by Dicer and preserve it for sensing by other DRAs, thereby suggesting a competition for substrate binding. This may be the main reason why there seems to be a crosstalk between RNAi and IFN-I. As LGP2 is similarly involved in MDA5 oligomerization enhancement, LGP2 might also bring dsRNA substrate to MDA5. Interestingly, the helicase domain of LGP2 interacts with Dicer and several other proteins involved in antiviral defense pathways including TRBP, PACT, and the dsRNA-activated protein kinase R (PKR) [118].

Finally, Dicer itself might be involved in modulating the activity of other key antiviral proteins. Dicer is already known to be involved in several interactions with cofactors via its helicase domain. Thus, 2 proteins that are known for their interaction with PKR interact with Dicer during miRNA biogenesis: TRBP and PACT [33,119]. Upon HIV-I infection, TRBP appears to bind the TAR RNA to inhibit PKR activation, thereby preventing an efficient antiviral response. PACT, another dsRNA-binding protein, is also an activator of PKR upon stress except when it interacts with TRBP [120–122]. Recently, our laboratory showed that Dicer is part of a complex involving not only TRBP and PACT but also PKR. The direct interaction of Dicer with PKR was specifically observed in cells infected with SINV and had a negative effect on PKR antiviral activity (Fig 5C, left) [123]. Another indication of the crosstalk between Dicer and PKR was reported in mouse ESCs, where Dicer represses the IFN response as well as PKR activity upon dsRNA transfection [124]. As mentioned before, Dicer could interact with ISGs but its role in the IFN-I response is not clear yet. Thus, other ISGs such as the deaminase ADAR1 or the RNA helicase DHX9 are part of the RISC assembly complex [125,126] but are also found specifically enriched within a Dicer-containing complex upon SINV infection [123]. This indicates that the helicase domain of Dicer could be involved in modulating the IFN response by acting as a central interaction platform during viral infection.

RLRs as well can be involved in IFN-independent antiviral functions (Fig 5D). Upon HBV infection, RIG-I recognizes the 5′ extremities of pre-genomic RNA and interferes with the retrotranscriptase activity [127]. Upon IAV infection, RIG-I competes with capsid molecules for the genomic RNA. Besides, both RIG-I and MDA5 can, in an ATP-dependent fashion, displace viral proteins from dsRNA including IAV NS1 [128]. Thus, this helicase-dependent activity promotes dsRNA recognition by other antiviral proteins including PKR to enhance the antiviral response [129]. Recently, RIG-I was also shown to be involved in an IFN-I independent regulation of SARS-CoV-2 infection. It recognizes the 3′ untranslated region of the SARS-CoV-2 RNA genome via the helicase domain, but not the CTD, and does not activate MAVS-dependent pathways. Rather, it seems to prevent the viral RdRp from initiating replication [130].

Conclusions

DExD/H-box helicases are increasingly being recognized as key components of the innate antiviral response in eukaryotes. Although they all share as a core component a helicase domain able to bind dsRNA, they diverge into 2 main families characterized by their structural organization and their mode of action. Indeed, they can act either in a catalytic mode, or by triggering an antiviral signaling cascade, ultimately leading to an immune response. Here, we mainly focused on a subset of these RNA helicases, which either participate in RNAi or in IFN-I response. However, the boundary between the 2 types of response has become blurred in the past years, while there is more and more evidence that they are rather interconnected. Although Dicer is retrieved in almost all metazoans, its exact contribution to antiviral responses varies from one organism to another. Dicer has a clearly defined catalytic activity against long dsRNA in *Drosophila* and *C. elegans* but appears to be more limited in mammalian cells. In the latter case, this restriction seems to be mediated by the helicase domain, since its complete or partial deletion results in a more potent antiviral activity. The recent discovery of a naturally occurring splicing isoform of Dicer in stem cells, lacking the Hel2i helical subdomain, is exciting and will likely reignite the interest in the field. In addition, Dicer could have other roles during viral infection independent on dsRNA processing into siRNAs, such as the regulation of antiviral proteins like PKR. So, we clearly do not have yet a complete picture of its importance in different contexts. The tight regulation of mammalian Dicer activity is similar to what can be observed for RIG-I and MDA5, which are both regulated by posttranslational modifications or by the binding of proteins that can activate or inhibit their recognition as well as their catalytic activities [66]. Even when the situation seems to be simple at first glance, such as antiviral RNAi in *C. elegans*, other RNA helicases (DRH-1 to 3) were shown to be essential to maintain a robust response and help Dicer to function properly. It goes without saying that since helicases are the main immunity receptors, viruses developed counter mechanisms to block dsRNA recognition or their catalytic function [131], an interesting aspect that would require a review of its own.

In addition to the few helicases we discussed in this review, there is a large variety of other DExD/H helicases that can be involved in antiviral defense (see [132] for a recent review). In some cases, these proteins contribute to the RLRs function, but they also have the capacity to function independently of the IFN response. Some of these helicases can also have a proviral role in specific cases [133], an aspect that we did not develop here for the sake of brevity. It would be especially interesting to decipher the full involvement of these RNA helicases in modulating Dicer activity during viral infection either by modulating its ability to interact with dsRNA or its processivity. Our recent determination of the Dicer interactome upon SINV infection provides hints that this might be the case, but we need to expand the field of investigation by looking into different cell types as well as viruses. Only then will we be able to fully grasp the importance of RNA helicases in the cellular response to viral infections.

Acknowledgments

We would like to thank members of the laboratory for discussion and Erika Girardi for her critical reading of the manuscript.

References

1. Weber F, Wagner V, Rasmussen SB, Hartmann R, Paludan SR. Double-Stranded RNA Is Produced by Positive-Strand RNA Viruses and DNA Viruses but Not in Detectable Amounts by Negative-Strand RNA Viruses. J Virol. 2006; 80:5059–5064. https://doi.org/10.1128/JVI.80.10.5059-5064.2006 PMID: 16641297

2. Pichlmair A, Reis e Sousa C. Innate recognition of viruses. Immunity. 2007; 27:370–383. https://doi.org/10.1016/j.immuni.2007.08.012 PMID: 17892846
3. Fairman-Williams ME, Guenther U-P, Jankowsky E. SF1 and SF2 helicases: family matters. Curr Opin Struct Biol. 2010; 20:313–324. https://doi.org/10.1016/j.sbi.2010.03.011 PMID: 20456941
4. Ahmad S, Hur S. Helicases in Antiviral Immunity: Dual Properties as Sensors and Effectors. Trends Biochem Sci. 2015; 40:576–585. https://doi.org/10.1016/j.tibs.2015.08.001 PMID: 26410598
5. Jarmoskaite I, Russell R. DEAD-box proteins as RNA helicases and chaperones. Wiley Interdiscip Rev RNA. 2011; 2:135–152. https://doi.org/10.1002/wrna.50 PMID: 21297876
6. Linder P, Jankowsky E. From unwinding to clamping—the DEAD box RNA helicase family. Nat Rev Mol Cell Biol. 2011; 12:505–516. https://doi.org/10.1038/nrm3154 PMID: 21779027
7. Luo D, Kohlway A, Pyle AM. Duplex RNA activated ATPases (DRAs). RNA Biol. 2013; 10:111–120. https://doi.org/10.4161/rna.22706 PMID: 23228901
8. Paro S, Imler J-L, Meignin C. Sensing viral RNAs by Dicer/RIG-I like ATPases across species. Curr Opin Immunol. 2015; 32:106–113. https://doi.org/10.1016/j.coi.2015.01.009 PMID: 25658360
9. Kemp C, Imler J-L. Antiviral immunity in drosophila. Curr Opin Immunol. 2009; 21:3–9. https://doi.org/10.1016/j.coi.2009.01.007 PMID: 19223163
10. Schott DH, Cureton DK, Whelan SP, Hunter CP. An antiviral role for the RNA interference machinery in Caenorhabditis elegans. Proc Natl Acad Sci U S A. 2005; 102:18420–4. Available from: http://www.ncbi.nlm.nih.gov/entrez/query.fcgi?cmd=Retrieve&db=PubMed&dopt=Citation&list_uids=16339901. https://doi.org/10.1073/pnas.0507123102 PMID: 16339901
11. Sadler AJ, Williams BRG. Interferon-inducible antiviral effectors. Nat Rev Immunol. 2008; 8:559–568. https://doi.org/10.1038/nri2314 PMID: 18575461
12. Berkhout B. RNAi-mediated antiviral immunity in mammals. Curr Opin Virol. 2018; 32:9–14. https://doi.org/10.1016/j.coviro.2018.07.008 PMID: 30015014
13. Huang B, Zhang L, Du Y, Xu F, Li L, Zhang G. Characterization of the Mollusc RIG-I/MAVS Pathway Reveals an Archaic Antiviral Signalling Framework in Invertebrates. Sci Rep. 2017; 7:1–13. https://doi.org/10.1038/s41598-016-0028-x PMID: 28127051
14. Maillard PV, van der Veen AG, Poirier EZ, e Sousa CR. Slicing and dicing viruses: antiviral RNA interference in mammals. EMBO J. 2019; 38:e100941. https://doi.org/10.15252/embj.2018100941 PMID: 30872283
15. Mussabekova A, Daeffler L, Imler J-L. Innate and intrinsic antiviral immunity in Drosophila. Cell Mol Life Sci. 2017; 74:2039–2054. https://doi.org/10.1007/s00018-017-2453-9 PMID: 28102430
16. Drinnenberg IA, Weinberg DE, Xie KT, Mower JP, Wolfe KH, Fink GR, et al. RNAi in budding yeast. Science. 2009; 326: 544–550. https://doi.org/10.1126/science.1176945 PMID: 19745116
17. tenOever BR. The Evolution of Antiviral Defense Systems. Cell Host Microbe. 2016; 19:142–149. https://doi.org/10.1016/j.chom.2016.01.006 PMID: 26867173
18. de Jong D, Eitel M, Jakob W, Osigus H-J, Hadrys H, DeSalle R, et al. Multiple Dicer Genes in the Early-Diverging Metazoa. Mol Biol Evol. 2009; 26:1333–1340. https://doi.org/10.1093/molbev/msp042 PMID: 19276153
19. Almeida MV, Andrade-Navarro MA, Ketting RF. Function and Evolution of Nematode RNAi Pathways. Non-Coding RNA. 2019; 5:8. https://doi.org/10.3390/ncrna5010008 PMID: 30650636
20. Bartel DP. Metazoan MicroRNAs. Cell. 2018; 173:20–51. https://doi.org/10.1016/j.cell.2018.03.006 PMID: 29570994
21. MacKay CR, Wang JP, Kurt-Jones EA. Dicer's role as an antiviral: still an enigma. Curr Opin Immunol. 2014; 26:49–55. https://doi.org/10.1016/j.coi.2013.10.015 PMID: 24556400
22. Liu Z, Wang J, Cheng H, Ke X, Sun L, Zhang QC, et al. Cryo-EM Structure of Human Dicer and Its Complexes with a Pre-miRNA Substrate. Cell. 2018; 173:1191–1203.e12. https://doi.org/10.1016/j.cell.2018.03.080 PMID: 29706542
23. Dlaki M. DUF283 domain of Dicer proteins has a double-stranded RNA-binding fold. Bioinformatics. 2006; 22:2711–2714. https://doi.org/10.1093/bioinformatics/btl468 PMID: 16954143
24. Tian Y, Simanshu DK, Ma J-B, Park J-E, Heo I, Kim VN, et al. A Phosphate-Binding Pocket within the Platform-PAZ-Connector Helix Cassette of Human Dicer. Mol Cell. 2014; 53:606–616. https://doi.org/10.1016/j.molcel.2014.01.003 PMID: 24486018
25. Zhang H, Kolb FA, Jaskiewicz L, Westhof E, Filipowicz W. Single Processing Center Models for Human Dicer and Bacterial RNase III. Cell. 2004; 118:57–68. https://doi.org/10.1016/j.cell.2004.06.017 PMID: 15242644

26. Kandasamy SK, Zhu L, Fukunaga R. The C-terminal dsRNA-binding domain of Drosophila Dicer-2 is crucial for efficient and high-fidelity production of siRNA and loading of siRNA to Argonaute2. RNA. 2017; 23:1139–1153. https://doi.org/10.1261/rna.059915.116 PMID: 28416567

27. Wostenberg C, Lary JW, Sahu D, Acevedo R, Quarles KA, Cole JL, et al. The role of human Dicer-dsRBD in processing small regulatory RNAs. PLoS ONE. 2012; 7:e51829. https://doi.org/10.1371/journal.pone.0051829 PMID: 23272173

28. Lee YS, Nakahara K, Pham JW, Kim K, He Z, Sontheimer EJ, et al. Distinct Roles for Drosophila Dicer-1 and Dicer-2 in the siRNA/miRNA Silencing Pathways. Cell. 2004; 117:69–81. https://doi.org/10.1016/s0092-8674(04)00261-2 PMID: 15066283

29. Tsutsumi A, Kawamata T, Izumi N, Seitz H, Tomari Y. Recognition of the pre-miRNA structure by Drosophila Dicer-1. Nat Struct Mol Biol. 2011; 18:1153–1158. https://doi.org/10.1038/nsmb.2125 PMID: 21926993

30. Ma E, MacRae IJ, Kirsch JF, Doudna JA. Autoinhibition of Human Dicer by Its Internal Helicase Domain. J Mol Biol. 2008; 380:237–243. https://doi.org/10.1016/j.jmb.2008.05.005 PMID: 18508075

31. Daniels SM, Melendez-Pe a CE, Scarborough RJ, Daher A, Christensen HS, El Far M, et al. Characterization of the TRBP domain required for Dicer interaction and function in RNA interference. BMC Mol Biol. 2009; 10:38. https://doi.org/10.1186/1471-2199-10-38 PMID: 19422693

32. Laraki G, Clerzius G, Daher A, Melendez-Pe a C, Daniels S, Gatignol A. Interactions between the double-stranded RNA-binding proteins TRBP and PACT define the Medipal domain that mediates protein-protein interactions. RNA Biol. 2008; 5:92–103. https://doi.org/10.4161/rna.5.2.6069 PMID: 18421256

33. Lee Y, Hur I, Park SY, Kim YK, Suh MR, Kim VN. The role of PACT in the RNA silencing pathway. EMBO J. 2006; 25:522–32. https://doi.org/10.1038/sj.emboj.7600942 PMID: 16424907

34. Robb GB, Rana TM. RNA helicase A interacts with RISC in human cells and functions in RISC loading. Mol Cell. 2007; 26:523–537. https://doi.org/10.1016/j.molcel.2007.04.016 PMID: 17531811

35. Lau P-W, Guiley KZ, De N, Potter CS, Carragher B, MacRae IJ. The molecular architecture of human Dicer. Nat Struct Mol Biol. 2012; 19:436–440. https://doi.org/10.1038/nsmb.2268 PMID: 22426548

36. Macrae IJ, Li F, Zhou K, Cande WZ, Doudna JA. Structure of Dicer and mechanistic implications for RNAi. Cold Spring Harb Symp Quant Biol. 2006; 71:73–80. https://doi.org/10.1101/sqb.2006.71.042 PMID: 17381283

37. Sinha NK, Iwasa J, Shen PS, Bass BL. Dicer uses distinct modules for recognizing dsRNA termini. Science. 2018; 359:329–334. https://doi.org/10.1126/science.aaq0921 PMID: 29269422

38. Wilkins C, Dishongh R, Moore SC, Whitt MA, Chow M, Machaca K. RNA interference is an antiviral defence mechanism in Caenorhabditis elegans. Nature. 2005; 436: 1044–1047. https://doi.org/10.1038/nature03957 PMID: 16107852

39. Félix M-A, Ashe A, Piffaretti J, Wu G, Nuez I, Bélicard T, et al. Natural and experimental infection of Caenorhabditis nematodes by novel viruses related to nodaviruses. PLoS Biol. 2011; 9:e1000586. https://doi.org/10.1371/journal.pbio.1000586 PMID: 21283608

40. Gammon DB, Ishidate T, Li L, Gu W, Silverman N, Mello CC. The Antiviral RNA Interference Response Provides Resistance to Lethal Arbovirus Infection and Vertical Transmission in Caenorhabditis elegans. Curr Biol. 2017; 27:795–806. https://doi.org/10.1016/j.cub.2017.02.004 PMID: 28262484

41. Sterken MG, Snoek LB, Bosman KJ, Daamen J, Riksen JAG, Bakker J, et al. A heritable antiviral RNAi response limits Orsay virus infection in Caenorhabditis elegans N2. PLoS ONE. 2014; 9: e89760. https://doi.org/10.1371/journal.pone.0089760 PMID: 24587016

42. Parker GS, Eckert DM, Bass BL. RDE-4 preferentially binds long dsRNA and its dimerization is necessary for cleavage of dsRNA to siRNA. RNA N Y N. 2006; 12:807–818. https://doi.org/10.1261/rna.2338706 PMID: 16603715

43. Parrish S, Fire A. Distinct roles for RDE-1 and RDE-4 during RNA interference in Caenorhabditis elegans. RNA N Y N. 2001; 7:1397–1402. PMID: 11680844

44. Zhuang JJ, Hunter CP. RNA interference in Caenorhabditis elegans: uptake, mechanism, and regulation. Parasitology. 2012; 139:560–573. https://doi.org/10.1017/S0031182011001788 PMID: 22075748

45. Ashe A, Bélicard T, Le Pen J, Sarkies P, Frézal L, Lehrbach NJ, et al. A deletion polymorphism in the Caenorhabditis elegans RIG-I homolog disables viral RNA dicing and antiviral immunity. Elife. 2013; 2: e00994. https://doi.org/10.7554/eLife.00994 PMID: 24137537

46. Gu W, Shirayama M, Conte D, Vasale J, Batista PJ, Claycomb JM, et al. Distinct Argonaute-Mediated 22G-RNA Pathways Direct Genome Surveillance in the C. elegans Germline. Mol Cell. 2009; 36:231–244. https://doi.org/10.1016/j.molcel.2009.09.020 PMID: 19800275

47. Pak J, Fire A. Distinct populations of primary and secondary effectors during RNAi in C. elegans. Science. 2007; 315:241–244. https://doi.org/10.1126/science.1132839 PMID: 17124291

48. Yigit E, Batista PJ, Bei Y, Pang KM, Chen C-CG, Tolia NH, et al. Analysis of the C. elegans Argonaute Family Reveals that Distinct Argonautes Act Sequentially during RNAi. Cell. 2006; 127:747–757. https://doi.org/10.1016/j.cell.2006.09.033 PMID: 17110334

49. Pavelec DM, Lachowiec J, Duchaine TF, Smith HE, Kennedy S. Requirement for the ERI/DICER complex in endogenous RNA interference and sperm development in Caenorhabditis elegans. Genetics. 2009; 183:1283–1295. https://doi.org/10.1534/genetics.109.108134 PMID: 19797044

50. Welker NC, Pavelec DM, Nix DA, Duchaine TF, Kennedy S, Bass BL. Dicer's helicase domain is required for accumulation of some, but not all, C. elegans endogenous siRNAs. RNA N Y N. 2010; 16:893–903. https://doi.org/10.1261/rna.2122010 PMID: 20354150

51. Welker NC, Maity TS, Ye X, Aruscavage PJ, Krauchuk AA, Liu Q, et al. Dicer's helicase domain discriminates dsRNA termini to promote an altered reaction mode. Mol Cell. 2011; 41:589–599. https://doi.org/10.1016/j.molcel.2011.02.005 PMID: 21362554

52. Sarkies P, Miska EA. RNAi pathways in the recognition of foreign RNA: antiviral responses and host-parasite interactions in nematodes. Biochem Soc Trans. 2013; 41:876–880. https://doi.org/10.1042/BST20130021 PMID: 23863148

53. Aliyari R, Ding S-W. RNA-based viral immunity initiated by the Dicer family of host immune receptors. Immunol Rev. 2009; 227:176–188. https://doi.org/10.1111/j.1600-065X.2008.00722.x PMID: 19120484

54. Galiana-Arnoux D, Dostert C, Schneemann A, Hoffmann JA, Imler J-L. Essential function in vivo for Dicer-2 in host defense against RNA viruses in drosophila. Nat Immunol. 2006; 7:590–597. https://doi.org/10.1038/ni1335 PMID: 16554838

55. Li H, Li WX, Ding SW. Induction and suppression of RNA silencing by an animal virus. Science. 2002; 296:1319–1321. https://doi.org/10.1126/science.1070948 PMID: 12016316

56. van Rij RP, Saleh M-C, Berry B, Foo C, Houk A, Antoniewski C, et al. The RNA silencing endonuclease Argonaute 2 mediates specific antiviral immunity in Drosophila melanogaster. Genes Dev. 2006; 20:2985–2995. https://doi.org/10.1101/gad.1482006 PMID: 17079687

57. Wang X-H, Aliyari R, Li W-X, Li H-W, Kim K, Carthew R, et al. RNA interference directs innate immunity against viruses in adult Drosophila. Science. 2006; 312:452–454. https://doi.org/10.1126/science.1125694 PMID: 16556799

58. Marques JT, Wang J-P, Wang X, de Oliveira KPV, Gao C, Aguiar ERGR, et al. Functional specialization of the small interfering RNA pathway in response to virus infection. PLoS Pathog. 2013; 9: e1003579. https://doi.org/10.1371/journal.ppat.1003579 PMID: 24009507

59. Cenik ES, Fukunaga R, Lu G, Dutcher R, Wang Y, Tanaka Hall TM, et al. Phosphate and R2D2 restrict the substrate specificity of Dicer-2, an ATP-driven ribonuclease. Mol Cell. 2011; 42: 172–184. https://doi.org/10.1016/j.molcel.2011.03.002 PMID: 21419681

60. Liu Q, Paroo Z. Biochemical principles of small RNA pathways. Annu Rev Biochem. 2010; 79:295–319. https://doi.org/10.1146/annurev.biochem.052208.151733 PMID: 20205586

61. Sinha NK, Trettin KD, Aruscavage PJ, Bass BL. Drosophila dicer-2 cleavage is mediated by helicase- and dsRNA termini-dependent states that are modulated by Loquacious-PD. Mol Cell. 2015; 58:406–417. https://doi.org/10.1016/j.molcel.2015.03.012 PMID: 25891075

62. Brisse M, Ly H. Comparative Structure and Function Analysis of the RIG-I-Like Receptors: RIG-I and MDA5. Front Immunol. 2019; 10:1586. https://doi.org/10.3389/fimmu.2019.01586 PMID: 31379819

63. Kato H, Takeuchi O, Sato S, Yoneyama M, Yamamoto M, Matsui K, et al. Differential roles of MDA5 and RIG-I helicases in the recognition of RNA viruses. Nature. 2006; 441:101–105. https://doi.org/10.1038/nature04734 PMID: 16625202

64. Rodriguez KR, Bruns AM, Horvath CM. MDA5 and LGP2: accomplices and antagonists of antiviral signal transduction. J Virol. 2014; 88:8194–8200. https://doi.org/10.1128/JVI.00640-14 PMID: 24850739

65. Majzoub K, Wrensch F, Baumert TF. The Innate Antiviral Response in Animals: An Evolutionary Perspective from Flagellates to Humans. Viruses. 2019; 11:E758. https://doi.org/10.3390/v11080758 PMID: 31426357

66. Rehwinkel J, Gack MU. RIG-I-like receptors: their regulation and roles in RNA sensing. Nat Rev Immunol. 2020; 20:537–551. https://doi.org/10.1038/s41577-020-0288-3 PMID: 32203325

67. Deddouche S, Matt N, Budd A, Mueller S, Kemp C, Galiana-Arnoux D, et al. The DExD/H-box helicase Dicer-2 mediates the induction of antiviral activity in drosophila. Nat Immunol. 2008; 9:1425–32. https://doi.org/10.1038/ni.1664 PMID: 18953338

68. Jiang F, Ramanathan A, Miller MT, Tang G-Q, Gale M, Patel SS, et al. Structural basis of RNA recognition and activation by innate immune receptor RIG-I. Nature. 2011; 479:423–427. https://doi.org/10.1038/nature10537 PMID: 21947008

69. Myong S, Cui S, Cornish PV, Kirchhofer A, Gack MU, Jung JU, et al. Cytosolic viral sensor RIG-I is a 5'-triphosphate-dependent translocase on double-stranded RNA. Science. 2009; 323:1070–1074. https://doi.org/10.1126/science.1168352 PMID: 19119185

70. Kowalinski E, Lunardi T, McCarthy AA, Louber J, Brunel J, Grigorov B, et al. Structural basis for the activation of innate immune pattern-recognition receptor RIG-I by viral RNA. Cell. 2011; 147: 423–435. https://doi.org/10.1016/j.cell.2011.09.039 PMID: 22000019

71. Saito T, Hirai R, Loo Y-M, Owen D, Johnson CL, Sinha SC, et al. Regulation of innate antiviral defenses through a shared repressor domain in RIG-I and LGP2. Proc Natl Acad Sci U S A. 2007; 104:582–587. https://doi.org/10.1073/pnas.0606699104 PMID: 17190814

72. Yoneyama M, Kikuchi M, Natsukawa T, Shinobu N, Imaizumi T, Miyagishi M, et al. The RNA helicase RIG-I has an essential function in double-stranded RNA-induced innate antiviral responses. Nat Immunol. 2004; 5:730–737. https://doi.org/10.1038/ni1087 PMID: 15208624

73. Berke IC, Yu X, Modis Y, Egelman EH. MDA5 assembles into a polar helical filament on dsRNA. Proc Natl Acad Sci U S A. 2012; 109:18437–18441. https://doi.org/10.1073/pnas.1212186109 PMID: 23090998

74. Berke IC, Modis Y. MDA5 cooperatively forms dimers and ATP-sensitive filaments upon binding double-stranded RNA. EMBO J. 2012; 31:1714–1726. https://doi.org/10.1038/emboj.2012.19 PMID: 22314235

75. Cagliani R, Forni D, Tresoldi C, Pozzoli U, Filippi G, Rainone V, et al. RIG-I-like receptors evolved adaptively in mammals, with parallel evolution at LGP2 and RIG-I. J Mol Biol. 2014; 426:1351–1365. https://doi.org/10.1016/j.jmb.2013.10.040 PMID: 24211720

76. Uchikawa E, Lethier M, Malet H, Brunel J, Gerlier D, Cusack S. Structural Analysis of dsRNA Binding to Anti-viral Pattern Recognition Receptors LGP2 and MDA5. Mol Cell. 2016; 62:586–602. https://doi.org/10.1016/j.molcel.2016.04.021 PMID: 27203181

77. Nan Y, Nan G, Zhang Y-J. Interferon Induction by RNA Viruses and Antagonism by Viral Pathogens. Viruses. 2014; 6:4999–5027. https://doi.org/10.3390/v6124999 PMID: 25514371

78. Schreiber G, Piehler J. The molecular basis for functional plasticity in type I interferon signaling. Trends Immunol. 2015; 36:139–149. https://doi.org/10.1016/j.it.2015.01.002 PMID: 25687684

79. Pestka S, Krause CD, Walter MR. Interferons, interferon-like cytokines, and their receptors. Immunol Rev. 2004; 202:8–32. https://doi.org/10.1111/j.0105-2896.2004.00204.x PMID: 15546383

80. Stark GR, Darnell JE. The JAK-STAT pathway at twenty. Immunity. 2012; 36:503–514. https://doi.org/10.1016/j.immuni.2012.03.013 PMID: 22520844

81. Kato H, Takeuchi O, Mikamo-Satoh E, Hirai R, Kawai T, Matsushita K, et al. Length-dependent recognition of double-stranded ribonucleic acids by retinoic acid-inducible gene-I and melanoma differentiation-associated gene 5. J Exp Med. 2008; 205: 1601–1610. https://doi.org/10.1084/jem.20080091 PMID: 18591409

82. Loo Y-M, Fornek J, Crochet N, Bajwa G, Perwitasari O, Martinez-Sobrido L, et al. Distinct RIG-I and MDA5 signaling by RNA viruses in innate immunity. J Virol. 2008; 82:335–345. https://doi.org/10.1128/JVI.01080-07 PMID: 17942531

83. Chiang JJ, Sparrer KMJ, van Gent M, Lässig C, Huang T, Osterrieder N, et al. Viral unmasking of cellular 5S rRNA pseudogene transcripts induces RIG-I-mediated immunity. Nat Immunol. 2018; 19: 53–62. https://doi.org/10.1038/s41590-017-0005-y PMID: 29180807

84. Zhao Y, Ye X, Dunker W, Song Y, Karijolich J. RIG-I like receptor sensing of host RNAs facilitates the cell-intrinsic immune response to KSHV infection. Nat Commun 2018; 9: 4841. https://doi.org/10.1038/s41467-018-07314-7 PMID: 30451863

85. Dias Junior AG, Sampaio NG, Rehwinkel J. A Balancing Act: MDA5 in Antiviral Immunity and Autoinflammation. Trends Microbiol. 2019; 27:75–85. https://doi.org/10.1016/j.tim.2018.08.007 PMID: 30201512

86. Cao X, Ding Q, Lu J, Tao W, Huang B, Zhao Y, et al. MDA5 plays a critical role in interferon response during hepatitis C virus infection. J Hepatol. 2015; 62:771–778. https://doi.org/10.1016/j.jhep.2014.11.007 PMID: 25463548

87. Dang W, Xu L, Yin Y, Chen S, Wang W, Hakim MS, et al. IRF-1, RIG-I and MDA5 display potent antiviral activities against norovirus coordinately induced by different types of interferons. Antiviral Res. 2018; 155:48–59. https://doi.org/10.1016/j.antiviral.2018.05.004 PMID: 29753657

88. Li L, Fan H, Song Z, Liu X, Bai J, Jiang P. Encephalomyocarditis virus 2C protein antagonizes interferon- signaling pathway through interaction with MDA5. Antiviral Res. 2019; 161:70–84. https://doi.org/10.1016/j.antiviral.2018.10.010 PMID: 30312637

89. Lu H-L, Liao F. Melanoma differentiation-associated gene 5 senses hepatitis B virus and activates innate immune signaling to suppress virus replication. J Immunol. 2013; 191:3264–3276. https://doi.org/10.4049/jimmunol.1300512 PMID: 23926323

90. Melchjorsen J, Rintahaka J, S by S, Horan KA, Poltajainen A, stergaard L, et al. Early innate recognition of herpes simplex virus in human primary macrophages is mediated via the MDA5/MAVS-dependent and MDA5/MAVS/RNA polymerase III-independent pathways. J Virol. 2010; 84:11350–11358. https://doi.org/10.1128/JVI.01106-10 PMID: 20739519

91. Wei L, Cui J, Song Y, Zhang S, Han F, Yuan R, et al. Duck MDA5 functions in innate immunity against H5N1 highly pathogenic avian influenza virus infections. Vet Res. 2014; 45:66. https://doi.org/10.1186/1297-9716-45-66 PMID: 24939427

92. Zhang Z, Filzmayer C, Ni Y, Sültmann H, Mutz P, Hiet M-S, et al. Hepatitis D virus replication is sensed by MDA5 and induces IFN- / responses in hepatocytes. J Hepatol. 2018; 69:25–35. https://doi.org/10.1016/j.jhep.2018.02.021 PMID: 29524530

93. Poirier EZ, Goic B, Tomé-Poderti L, Frangeul L, Boussier J, Gausson V, et al. Dicer-2-Dependent Generation of Viral DNA from Defective Genomes of RNA Viruses Modulates Antiviral Immunity in Insects. Cell Host Microbe. 2018; 23:353–365.e8. https://doi.org/10.1016/j.chom.2018.02.001 PMID: 29503180

94. Tassetto M, Kunitomi M, Whitfield ZJ, Dolan PT, Sánchez-Vargas I, Garcia-Knight M, et al. Control of RNA viruses in mosquito cells through the acquisition of vDNA and endogenous viral elements. Elife. 2019;8. https://doi.org/10.7554/eLife.41244 PMID: 31621580

95. Marriott AC, Dimmock NJ. Defective interfering viruses and their potential as antiviral agents. Rev Med Virol. 2010; 20:51–62. https://doi.org/10.1002/rmv.641 PMID: 20041441

96. Sanchez David RY, Combredet C, Sismeiro O, Dillies M-A, Jagla B, Coppée J-Y, et al. Comparative analysis of viral RNA signatures on different RIG-I-like receptors. Elife. 2016; 5:e11275. https://doi.org/10.7554/eLife.11275 PMID: 27011352

97. Ding S-W. RNA-based antiviral immunity. Nat Rev Immunol. 2010; 10:632–644. https://doi.org/10.1038/nri2824 PMID: 20706278

98. Li Y, Basavappa M, Lu J, Dong S, Cronkite DA, Prior JT, et al. Induction and suppression of antiviral RNA interference by influenza A virus in mammalian cells. Nat Microbiol. 2016; 2:16250. https://doi.org/10.1038/nmicrobiol.2016.250 PMID: 27918527

99. Maillard PV, Ciaudo C, Marchais A, Li Y, Jay F, Ding SW, et al. Antiviral RNA Interference in Mammalian Cells. Science. 2013; 342:235–238. https://doi.org/10.1126/science.1241930 PMID: 24115438

100. Qiu Y, Xu Y, Zhang Y, Zhou H, Deng Y-Q, Li X-F, et al. Human Virus-Derived Small RNAs Can Confer Antiviral Immunity in Mammals. Immunity. 2017; 46:992–1004.e5. https://doi.org/10.1016/j.immuni.2017.05.006 PMID: 28636969

101. Burke DC, Graham CF, Lehman JM. Appearance of interferon inducibility and sensitivity during differentiation of murine teratocarcinoma cells in vitro. Cell. 1978; 13:243–248. https://doi.org/10.1016/0092-8674(78)90193-9 PMID: 627035

102. D'Angelo W, Acharya D, Wang R, Wang J, Gurung C, Chen B, et al. Development of Antiviral Innate Immunity During In Vitro Differentiation of Mouse Embryonic Stem Cells. Stem Cells Dev. 2016; 25:648–659. https://doi.org/10.1089/scd.2015.0377 PMID: 26906411

103. Stein P, Zeng F, Pan H, Schultz RM. Absence of non-specific effects of RNA interference triggered by long double-stranded RNA in mouse oocytes. Dev Biol. 2005; 286:464–471. https://doi.org/10.1016/j.ydbio.2005.08.015 PMID: 16154556

104. Maillard PV, der Veen AGV, Deddouche-Grass S, Rogers NC, Merits A, e Sousa CR. Inactivation of the type I interferon pathway reveals long double-stranded RNA-mediated RNA interference in mammalian cells. EMBO J. 2016; 35: 2505–2518. https://doi.org/10.15252/embj.201695086 PMID: 27815315

105. Adiliaghdam F, Basavappa M, Saunders TL, Harjanto D, Prior JT, Cronkite DA, et al. A Requirement for Argonaute 4 in Mammalian Antiviral Defense. Cell Rep. 2020; 30:1690–1701.e4. https://doi.org/10.1016/j.celrep.2020.01.021 PMID: 32049003

106. Qiu Y, Xu Y-P, Wang M, Miao M, Zhou H, Xu J, et al. Flavivirus induces and antagonizes antiviral RNA interference in both mammals and mosquitoes. Sci Adv. 2020; 6:eaax7989. https://doi.org/10.1126/sciadv.aax7989 PMID: 32076641

107. Girardi E, Lef vre M, Chane-Woon-Ming B, Paro S, Claydon B, Imler J-L, et al. Cross-species comparative analysis of Dicer proteins during Sindbis virus infection. Sci Rep. 2015; 5:10693. https://doi.org/10.1038/srep10693 PMID: 26024431

108. Kennedy EM, Kornepati AVR, Bogerd HP, Cullen BR. Partial reconstitution of the RNAi response in human cells using Drosophila gene products. RNA. 2017; 23:153–160. https://doi.org/10.1261/rna.059345.116 PMID: 27837013

109. Parameswaran P, Sklan E, Wilkins C, Burgon T, Samuel MA, Lu R, et al. Six RNA Viruses and Forty-One Hosts: Viral Small RNAs and Modulation of Small RNA Repertoires in Vertebrate and Invertebrate Systems. PLoS Pathog. 2010; 6:e1000764. https://doi.org/10.1371/journal.ppat.1000764 PMID: 20169186

110. Schuster S, Overheul GJ, Bauer L, van Kuppeveld FJM, van Rij RP. No evidence for viral small RNA production and antiviral function of Argonaute 2 in human cells. Sci Rep. 2019; 9:1–11. https://doi.org/10.1038/s41598-018-37186-2 PMID: 30626917

111. Bogerd HP, Skalsky RL, Kennedy EM, Furuse Y, Whisnant AW, Flores O, et al. Replication of Many Human Viruses Is Refractory to Inhibition by Endogenous Cellular MicroRNAs. J Virol. 2014; 88:8065–8076. https://doi.org/10.1128/JVI.00985-14 PMID: 24807715

112. Provost P, Dishart D, Doucet J, Frendewey D, Samuelsson B, R dmark O. Ribonuclease activity and RNA binding of recombinant human Dicer. EMBO J. 2002; 21:5864–5874. https://doi.org/10.1093/emboj/cdf578 PMID: 12411504

113. Zhang H, Kolb FA, Brondani V, Billy E, Filipowicz W. Human Dicer preferentially cleaves dsRNAs at their termini without a requirement for ATP. EMBO J. 2002; 21:5875–5885. Available from: http://www.ncbi.nlm.nih.gov/htbin-post/Entrez/query?db=m&form=6&dopt=r&uid=12411505. https://doi.org/10.1093/emboj/cdf582 PMID: 12411505

114. Chakravarthy S, Sternberg SH, Kellenberger CA, Doudna JA. Substrate-specific kinetics of Dicer-catalyzed RNA processing. J Mol Biol. 2010; 404:392–402. https://doi.org/10.1016/j.jmb.2010.09.030 PMID: 20932845

115. Kennedy EM, Whisnant AW, Kornepati AVR, Marshall JB, Bogerd HP, Cullen BR. Production of functional small interfering RNAs by an amino-terminal deletion mutant of human Dicer. Proc Natl Acad Sci. 2015; 112:E6945–E6954. https://doi.org/10.1073/pnas.1513421112 PMID: 26621737

116. Flemr M, Malik R, Franke V, Nejepinska J, Sedlacek R, Vlahovicek K, et al. A retrotransposon-driven dicer isoform directs endogenous small interfering RNA production in mouse oocytes. Cell. 2013; 155:807–816. https://doi.org/10.1016/j.cell.2013.10.001 PMID: 24209619

117. Poirier EZ, Buck MD, Chakravarty P, Carvalho J, Frederico B, Cardoso A, et al. An isoform of Dicer protects mammalian stem cells against multiple RNA viruses. Science. 2021; 373:231–236. https://doi.org/10.1126/science.abg2264 PMID: 34244417

118. van der Veen AG, Maillard PV, Schmidt JM, Lee SA, Deddouche-Grass S, Borg A, et al. The RIG-I-like receptor LGP2 inhibits Dicer-dependent processing of long double-stranded RNA and blocks RNA interference in mammalian cells. EMBO J. 2018; 37:e97479. https://doi.org/10.15252/embj.201797479 PMID: 29351913

119. Haase AD, Jaskiewicz L, Zhang H, Laine S, Sack R, Gatignol A, et al. TRBP, a regulator of cellular PKR and HIV-1 virus expression, interacts with Dicer and functions in RNA silencing. EMBO Rep. 2005; 6:961–7. https://doi.org/10.1038/sj.embor.7400509 PMID: 16142218

120. Farabaugh KT, Krokowski D, Guan B-J, Gao Z, Gao X-H, Wu J, et al. PACT-mediated PKR activation acts as a hyperosmotic stress intensity sensor weakening osmoadaptation and enhancing inflammation. O'Riordan MX, Taniguchi T, editors. Elife. 2020; 9:e52241. https://doi.org/10.7554/eLife.52241 PMID: 32175843

121. Li S, Peters GA, Ding K, Zhang X, Qin J, Sen GC. Molecular basis for PKR activation by PACT or dsRNA. Proc Natl Acad Sci. 2006; 103:10005–10010. https://doi.org/10.1073/pnas.0602317103 PMID: 16785445

122. Clerzius G, Shaw E, Daher A, Burugu S, Gélinas J-F, Ear T, et al. The PKR activator, PACT, becomes a PKR inhibitor during HIV-1 replication. Retrovirology. 2013; 10:96. https://doi.org/10.1186/1742-4690-10-96 PMID: 24020926

123. Montavon TC, Baldaccini M, Lef vre M, Girardi E, Chane-Woon-Ming B, Messmer M, et al. Human DICER helicase domain recruits PKR and modulates its antiviral activity. PLoS Pathog. 2021; 17: e1009549. https://doi.org/10.1371/journal.ppat.1009549 PMID: 33984068

124. Gurung C, Fendereski M, Sapkota K, Guo J, Huang F, Guo Y-L. Dicer represses the interferon response and the double-stranded RNA-activated protein kinase pathway in mouse embryonic stem cells. J Biol Chem. 2021; 296:100264. https://doi.org/10.1016/j.jbc.2021.100264 PMID: 33837743

125. Ota H, Sakurai M, Gupta R, Valente L, Wulff B-E, Ariyoshi K, et al. ADAR1 forms a complex with Dicer to promote microRNA processing and RNA-induced gene silencing. Cell. 2013; 153:575–589. https://doi.org/10.1016/j.cell.2013.03.024 PMID: 23622242

126. Fu Q, Yuan YA. Structural insights into RISC assembly facilitated by dsRNA-binding domains of human RNA helicase A (DHX9). Nucleic Acids Res. 2013; 41:3457–3470. https://doi.org/10.1093/nar/gkt042 PMID: 23361462

127. Sato S, Li K, Kameyama T, Hayashi T, Ishida Y, Murakami S, et al. The RNA sensor RIG-I dually functions as an innate sensor and direct antiviral factor for hepatitis B virus. Immunity. 2015; 42:123–132. https://doi.org/10.1016/j.immuni.2014.12.016 PMID: 25557055

128. Weber M, Sediri H, Felgenhauer U, Binzen I, Bänfer S, Jacob R, et al. Influenza virus adaptation PB2-627K modulates nucleocapsid inhibition by the pathogen sensor RIG-I. Cell Host Microbe. 2015; 17:309–319. https://doi.org/10.1016/j.chom.2015.01.005 PMID: 25704008

129. Yao H, Dittmann M, Peisley A, Hoffmann H-H, Gilmore RH, Schmidt T, et al. ATP-dependent effector-like functions of RIG-I-like receptors. Mol Cell. 2015; 58:541–548. https://doi.org/10.1016/j.molcel.2015.03.014 PMID: 25891073

130. Yamada T, Sato S, Sotoyama Y, Orba Y, Sawa H, Yamauchi H, et al. RIG-I triggers a signaling-abortive anti-SARS-CoV-2 defense in human lung cells. Nat Immunol. 2021; 22:820–828. https://doi.org/10.1038/s41590-021-00942-0 PMID: 33976430

131. Onomoto K, Onoguchi K, Yoneyama M. Regulation of RIG-I-like receptor-mediated signaling: interaction between host and viral factors. Cell Mol Immunol. 2021; 18:539–555. https://doi.org/10.1038/s41423-020-00602-7 PMID: 33462384

132. Taschuk F, Cherry S. DEAD-Box Helicases: Sensors, Regulators, and Effectors for Antiviral Defense. Viruses. 2020; 12:E181. https://doi.org/10.3390/v12020181 PMID: 32033386

133. Ranji A, Boris-Lawrie K. RNA helicases: emerging roles in viral replication and the host innate response. RNA Biol. 2010; 7:775–787. https://doi.org/10.4161/rna.7.6.14249 PMID: 21173576

2. Dicer helicase domain: an interacting hub

a. Role of Dicer in gene expression regulation

One of the main roles of Dicer is the biogenesis of microRNAs (miRNAs), which are key regulators of gene expression. The first report of a short regulatory RNA was in a study performed in *Caenorhabditis elegans* in the 1990s. The *lin-4* gene was shown to produce a 22-nt-long non-coding RNAs instead of an mRNA, another instance (Let-7) was published shortly after (Lee et al., 1993; Reinhart et al., 2000). These small RNAs, which were later found to exist in other animals and called miRNAs, have an imperfect complementarity with their targets involving an activity dependent on translation inhibition (Lau et al., 2001; Lee and Ambros, 2001; Olsen and Ambros, 1999).

The miRNA pathway has now been extensively characterized (**Figure 1**). An RNA polymerase II (polII)-derived primary-miRNA (pri-miRNA) transcript is recognized by the type III ribonuclease DROSHA (Lee et al., 2004). DROSHA helped by its main interacting partner DGCR8 cleaves the pri-miRNA into a 60-nt-stem-loop precursor-miRNA (pre-miRNA) (Lee et al., 2003). The pre-miRNA is then exported to the cytosol via an active RNA-GTP/Exportin 5 mechanism (Yi et al., 2003). Once in the cytoplasm, the pre-miRNA is further processed, in an ATP-independent manner, into a 22-nt-long miRNA duplex by Dicer helped by its main co-factor the TAR-RNA Binding Protein (TRBP) (Chendrimada et al., 2005). One strand of the duplex is incorporated into an effector protein of the Argonaute family (AGO) (Hammond et al., 2001) to form the so-called RNA-induced silencing complex (RISC). This required the help of chaperone proteins (Iwasaki et al., 2010). The small RNA acts as a guide for RISC, to bring it to its complementary target mRNAs. In animals, this results in most cases in translation inhibition, which requires the interaction of the AGO proteins with the adaptor protein TNRC6B (Meister et al., 2005). In rare cases, *i.e.* when there is a perfect complementarity between the guide and the target RNA, the target RNA can be cleaved by RISC (Yekta et al., 2004). In mammals, out of the four AGO proteins, only AGO2, and to a lesser extent AGO3, have been shown to possess a slicing activity (Park et al., 2017; Valdmanis et al., 2012).

Before being implicated in the miRNA pathway, Dicer was identified as the enzyme responsible of RNAi and was named after its ability to digest dsRNA into small RNAs (Bernstein et al., 2001).

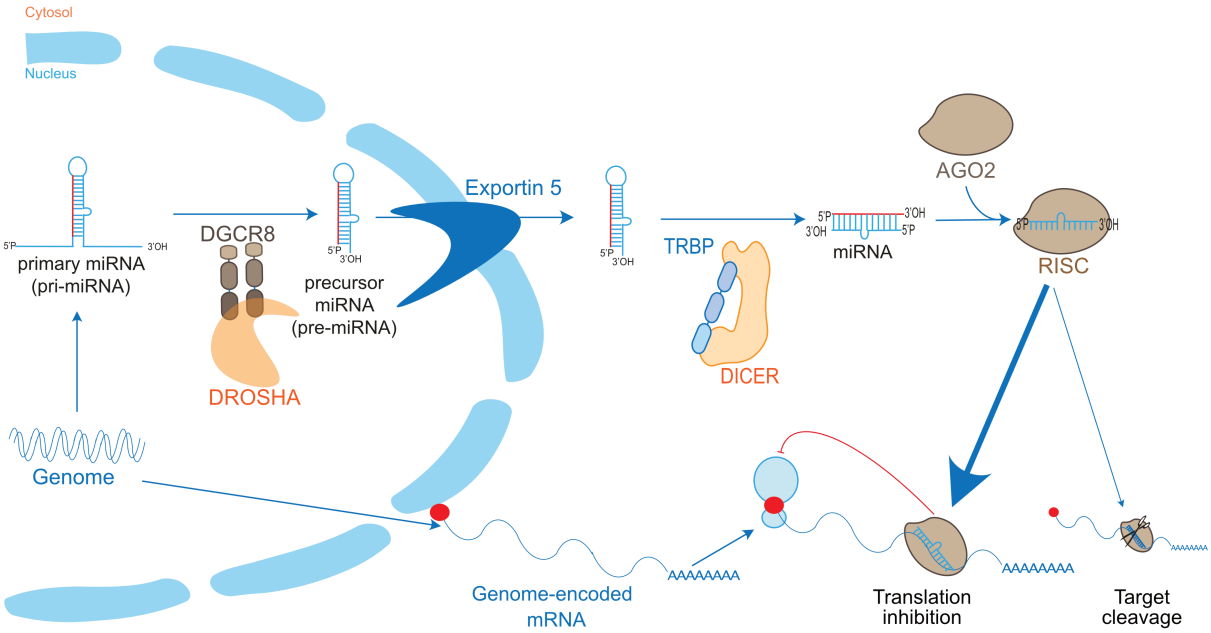

Figure 1 – The microRNA (miRNA) pathway in the gene expression control.

An RNA polymerase II (pol II)-transcribed stem loop called the primary microRNA (pri-miRNA) is processed in the nucleus by the type III ribonuclease DROSHA helped by its cofactor DGCR8. The generated stem loop, called precursor microRNA (pre-miRNA) is exported in the cytosol by the exportin 5 and taken in charge by another type III ribonuclease, Dicer and its cofactor, TRBP. Dicer cleaves out a small 22nt duplex of microRNA (miRNA). The guide strand of the duplex is incorporated into an effector protein of the Argonaute (AGO) family to form the RNA-induced silencing complex (RISC). Guided by the small RNA, RISC can then act upon its target mRNAs and will either cleave them or inhibit their translation.

b. Dicer structure and TRBP function

As mentioned previously, the DExD/H-Box helicase domain of Dicer is unable to hydrolyze ATP and exhibits an auto-inhibitory effect on long dsRNA processing in humans (Ma et al., 2008; Zhang et al., 2002). The loss of ATP hydrolysis has been shown to be correlated to a loss of long dsRNA-cleaving activity: by looking at Dicer phylogeny, a clear link between these two aspects arose since the ancestral Dicer retained these two characteristics (Aderounmu et al.,

2023). Hence, changes in the helicase domain could modify its ability to both bind dsRNA and hydrolyze ATP, underlying the importance of this domain in Dicer activity.

This was further emphasized by the recent solving of the structure of the mouse Dicer and of a mutant, deleted from the first part of the helicase domain, named ΔHEL1 (Zapletal et al., 2022)**(Figure 2)**. The helicase domain keeps Dicer in a closed state allowing the selection of pre-miRNA only. To alleviate this selection, a deletion of part of the helicase domain is required. This perturbs its selectivity but also uncovers an increased cleavage activity against long dsRNAs. Indeed, the ΔHEL1 mutant loses its cleavage precision, which results in the over-accumulation of Dicer-independent miRNA products.

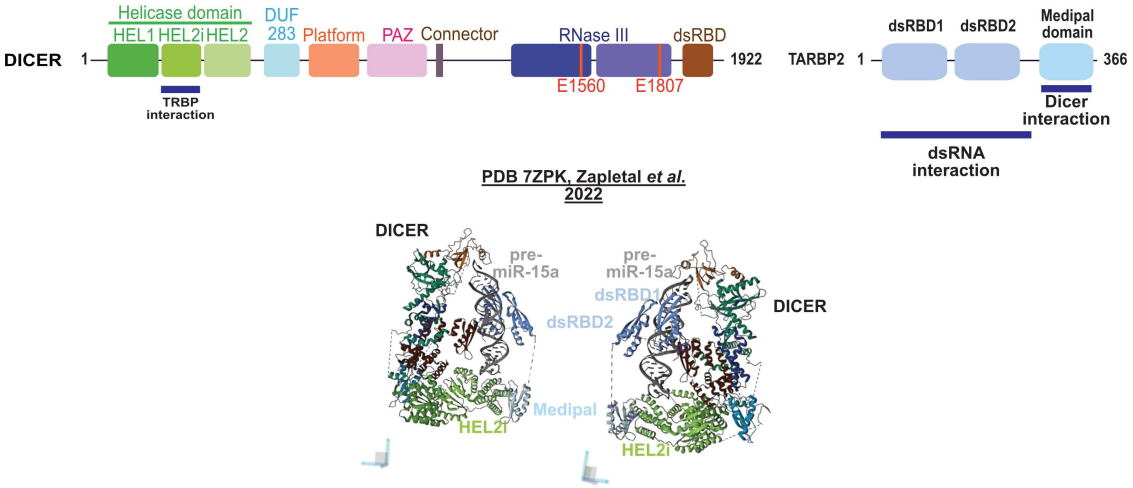

Figure 2 – Dicer structure reveals the importance of the helicase as a functional platform.

Dicer is an L-shaped ribonuclease. At the base of the L, the DExD/H-Box helicase domain is divided in three parts: HEL1, HEL2i and HEL2. In mammals, the helicase domain does not hydrolyze ATP, it binds the pre-miR-15a substrate and is also involved in the interaction with proteins, such as TRBP. The latter is a dsRBP formed of three dsRBDs of which two are involved in the substrate binding and its accommodation in Dicer catalytic site whereas the third one, the Medipal domain, is directly interacting with the HEL2i domain. Dicer DUF283 domain has a dsRBD fold that is supposed to help the loop binding and accommodation in Dicer. At the top of Dicer, the Platform and PAZ domains are responsible for binding the 5' and 3' extremities of the pre-miRNA respectively. The connector links them to the RNAseIII a and b catalytic domains. At their opposite and next to the PAZ domain in the L-shaped structure there is the terminal dsRBD that maintains the substrate in the catalytic core. HEL, helicase; DUF, domain of unknown function; PAZ, Piwi-Argonaute-Zwille; RNase, ribonuclease; dsRBD, dsRNA-binding domain.

Interestingly, the substrate selection and cleavage precision are two functions carried by Dicer's main co-factor, TARBP2 (TRBP) (Haase et al., 2005). TRBP homologs are found in Drosophila with the Loquacious (Loqs) proteins also interacting with DICER1 or DICER2 (Haac et al., 2015). TRBP is an RNA-binding protein composed of three dsRNA-binding domains (dsRBDs) of which the first two display a high affinity for dsRNA (Takahashi et al., 2013; Yamashita et al., 2011) **(Figure 3a)**. It was first discovered in HIV-1 infected cells and named according to its ability to bind to the TAR RNA (Kozak et al., 1995). TRBP was later shown to be associated with Dicer, and to participate in its recruitment to AGO2 in human cells (Chendrimada et al., 2005). TRBP is a central actor ensuring Dicer accuracy in miRNA processing (Fareh et al., 2016; Wilson et al., 2015). It was recently shown that TRBP allows changes in Dicer conformation by binding to its helicase domain, thereby making it competent for pre-miRNA cleavage (Zapletal et al., 2022)**(Figure 2 and 3b)**. The interaction is mediated by the third dsRBD in TRBP called Medipal (MERLIN-Dicer-PACT liaison) domain and the HEL2i domain in Dicer (Daniels et al., 2009). TRBP, separately of its Dicer interaction, is also known to be oncogenic and to promote cell growth. Hence, a nuclear TRBP is able to induce transcripts degradation by promoting introns retention inducing lung cancer pathogenesis (Fish et al., 2019). Independently, its overexpression has also been shown to induce tumorigenesis (Benkirane et al., 1997; Zhong et al., 1999), which explains why it is tightly regulated by the MERLIN protein but also by a transcriptional downregulation in the brain (J. Y. Lee et al., 2006) **(Figure 3c)**.

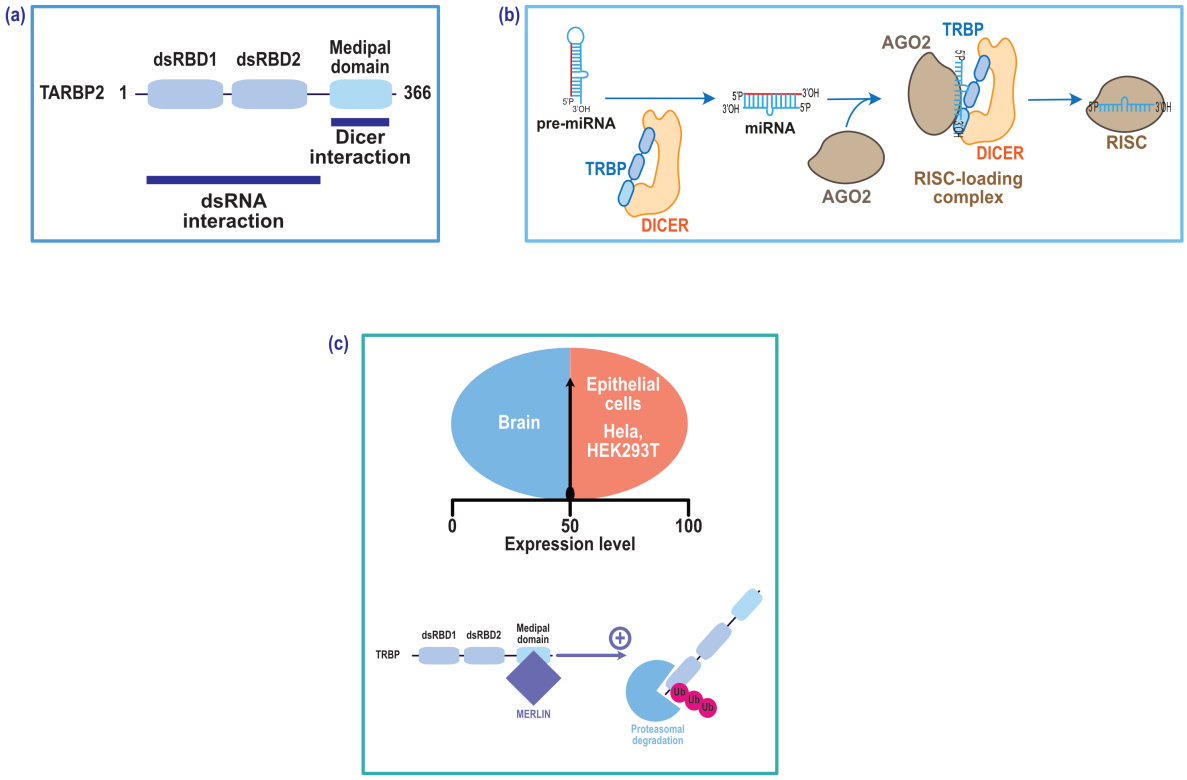

Figure 3 – TARBP2 (TRBP) controls Dicer activity but is also a central regulatory dsRBP.

(a) TARBP2 or TRBP is composed of two canonical dsRBDs at the N-terminal part, which are involved in dsRNA interaction. The last dsRBD, the Medipal domain, slightly differs in structure from the two other and is mediating protein-protein interaction. (b) TRBP acts in the miRNA pathway by directly interacting with Dicer allowing the precise pre-miRNA cleavage and the miRNA loading into AGO. (c) TRBP expression is cell-dependent. Hence, in the brain TRBP expression is transcriptionally downregulated whereas its expression in epithelial cells is increased changing its functions depending on the cell type. Blue: downregulated expression; red: upregulated expression. Another regulation layer is its stability as TRBP is degraded after the binding of the cytoskeletal protein MERLIN on its Medipal domain and recruitment of an ubiquitinoylation complex. dsRBD, dsRNA-binding domain; AGO2, Argonaute 2.

c. Other partners of the helicase domain

Dicer helicase domain appears to be a hub for interactions mainly in relation to its role in miRNA biogenesis. Dicer is interacting with the DExH/-Box RNA helicase A or DHX9, which is able to unwind both RNA and DNA in the nucleus and the cytosol. DHX9 is involved in RISC

loading allowing a better association between siRNA and AGO2 (Robb and Rana, 2007) **(Figure 4a)**. This interaction involves DHX9 dsRBD I and II, which can also bind the miRNA duplex.

Dicer is also directly interacting with the Adenosine Deaminase Acting on RNA 1 (ADAR1) protein in the context of miRNA processing. ADAR1 has been shown to increase Dicer processing rate and to promote miRNA loading onto AGO2 (Ota et al., 2013) **(Figure 4b)**. For a long time, ADAR1 was considered to be an antagonist of the RNAi pathway since A-to-I editing inhibits the correct processing of pri-miRNAs or change miRNA targets (Kawahara et al., 2007b, 2007a) **(Figure 4b)**. However, when Dicer interacts with ADAR1, the deaminase induces Dicer conformational changes and enhances the processing of miRNA precursors, RISC assembly and miRNA loading, just as TRBP. Again, this interaction is mediated partly by Dicer helicase domain (Ota et al., 2013).

Lastly, another dsRBP homologous to TRBP, the protein activator of dsRNA-activated protein kinase (PACT) is a well-characterized partner of Dicer helicase domain. PACT is also composed of three dsRBDs of which the first two mediate dsRNA interactions and the third is used for protein-protein interaction **(Figure 4c)**. PACT was first described in the late 1990s for its role of activator of the dsRNA-activated protein kinase (PKR). In that case, PACT interacts with PKR and activate its kinase activity normally induced by dsRNA (Patel and Sen, 1998). PACT also interacts *via* its third dsRBD with Dicer helicase domain, and can also be found in a complex with AGO2 and TRBP (Y. Lee et al., 2006) **(Figure 4c)**. However, PACT and TRBP show a differential role *in vitro* on Dicer processing. Dicer associated with PACT reveals differences in substrate specificity compared to Dicer with TRBP, as the former induces a decrease of dsRNA processing by Dicer (Lee et al., 2013). However, in vivo, Dicer needs the PACT/TRBP heterodimer to process dsRNA indicating the complicated regulation of this complex (Kok et al., 2007) **(Figure 4c)**. This interaction is mediated by the first two dsRBDs of PACT and of TRBP, letting their third dsRBD free for Dicer interactions.

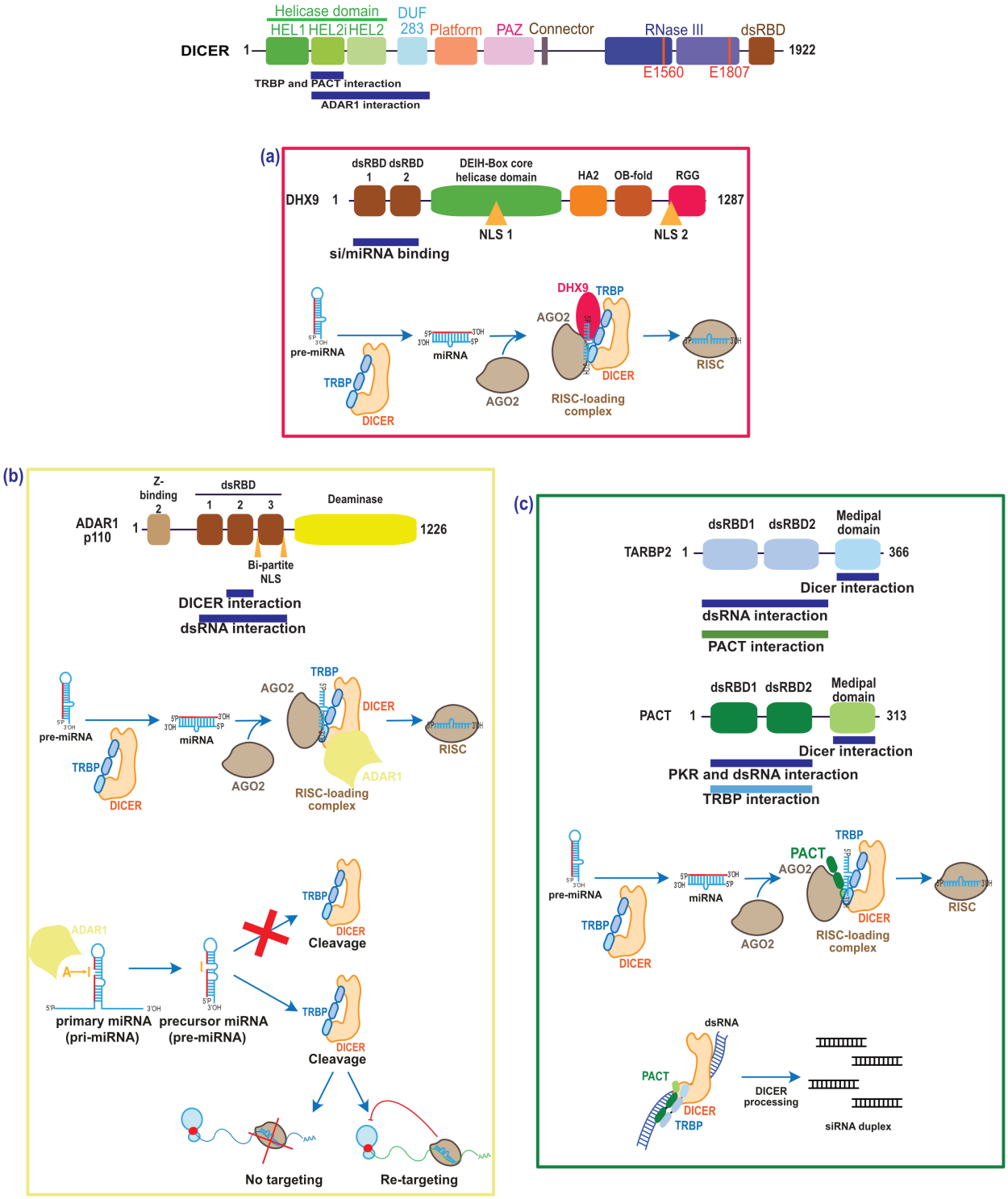

Figure 4 – Dicer is an interaction hub for many dsRNA-binding proteins (dsRBPs).

(a) The DExH Box RNA helicase A (DHX9) carries a core helicase domain and two N-terminal dsRBDs allowing the binding of si- or miRNA to favor their loading into AGO2. dsRBD, dsRNA-binding domain; NLS, nuclear localization signal; HA2, helicase-associated domain 2; OB-fold, oligonucleotide/oligosaccharide-binding fold; RGG-box, Glycine-rich. (b) The adenosine deaminase acting on RNA 1 (ADAR1) is composed of a Z-RNA binding domain, 3

dsRNA-binding domains (dsRBDs) and the deaminase domain. The constitutive p110 isoform of ADAR1 directly interacts with Dicer increasing its processing rate and helping the miRNA loading into AGO2. ADAR1 also uses its adenosine deaminase activity to modulate processing of pre-miRNA or to change the repertoire of target mRNAs. (c) The protein activator of dsRNA-activated protein kinase (PACT) is structurally homologous to TRBP with its two canonical αßßα dsRBD in N-ter and the C-ter Medipal domain. Thanks to the Medipal, PACT associates with the RISC-loading complex formed by AGO2, Dicer and TRBP and help for the mi- and si-RNA loading. Besides, PACT can heterodimerize with TRBP and both are interacting with Dicer increasing its processing activity on dsRNA.

B. Interferon responses

1. The type I interferon response

IFN response can be triggered by different types of pathogens: bacteria, parasites, viruses and fungi. IFN is a two-step system, which involves first the expression of IFN cytokines followed by their action in both an autocrine and paracrine fashion. They act by binding to cellular receptors to induce the transcription of IFN stimulated genes (ISGs), which are the direct cellular effectors. This system allows the organism to mount a global immune response thanks to the signal transmission. The two main IFN commonly involved in the immune response are the type I and type III interferon (IFN-I and IFN-III). These two responses have different associated cytokines and cellular receptors. Upon infection with an RNA or DNA virus, IFN-I is described as the broader response and is predominant in immune cells. IFN-III is mostly found in epithelial cells (McNab et al., 2015).

IFN-I is triggered by different classes of PRRs: the membrane-associated Toll-like receptors (TLRs) , the cytosolic RIG-I-like receptors (RLRs) and DNA sensors, such as the cytosolic cyclic GMP-AMP synthase (cGAS). Their activation leads to the phosphorylation by TBK1 of specific transcription factors, such as interferon regulatory factor (IRF) 3 and 7 **(Figure 5)**. This phosphorylation allows their nuclear translocation (Mogensen, 2019). They act as homo- or hetero-dimers and can be found associated with other transcription factors including NF-kB. IRF3 and 7 induce the transcription of IFN α and ß, the two groups of IFN-I cytokines. IRF3 is only responsible for IFN ß production whereas IRF7 can elicit both IFN α and ß (Honda and Taniguchi, 2006).

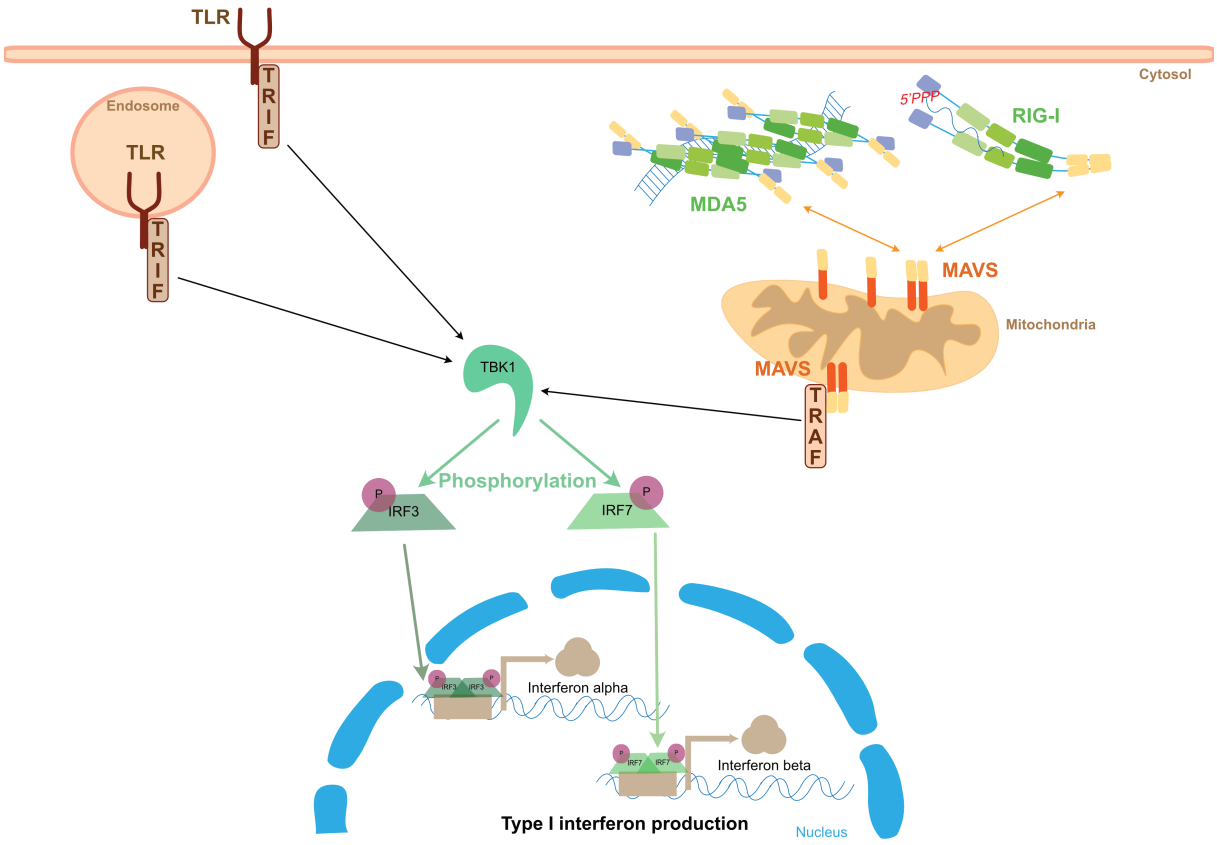

Figure 5 – The type I interferon response (IFN-I) is triggered by the detection of foreign elements by cellular receptors.

Foreign pathogen-associated molecular patterns (PAMPs) are recognized by cellular pattern recognition receptors (PRRs) such as toll-like receptors (TLRs) and RIG-I-like receptors (RLRs). Via the adaptor protein TRIF (TIR-domain-containing adapter-inducing interferon-ß) TLRs trigger the activation of the TBK1 kinase (TANK-binding kinase 1) that phosphorylates IRF3 and IRF7 (interferon regulatory factors) transcription factors. These will then translocate to the nucleus to activate transcription of interferon α and ß cytokines genes. The RLRs MDA5 (melanoma differentiation-associated protein 5) and RIG-I (retinoic acid-inducible gene I) recognizes long dsRNA and 5' triphosphorylated-single-stranded RNA respectively. Once activated, they interact with the mitochondria-associated MAVS (mitochondrial antiviral-signaling) adapter protein via their CARDS (caspase activation and recruitment domains) domain. MAVS agglomerates at the mitochondria membrane and activates the adaptor protein TRAF (TNF receptor associated factors) that will then activate the TBK1 kinase, resulting in IFN production as previously described.

Once produced, IFN-I cytokines will bind to membrane-associated receptors, IFNAR1 and IFNAR2, on their extracellular part. IFNAR binding activates the JAK-STAT pathway (Janus kinase – Signal transducers and activators of transcription) **(Figure 6)**. The JAK family is

composed of four members: JAK 1, 2, 3 and tyrosine kinase 2 (TYK2). STAT proteins are transcription factors that once phosphorylated on a key tyrosine residue, can homo- or hetero-dimerize and translocate in the nucleus to activate transcription of ISGs. The STAT family is composed of 7 transcription factors: STAT1, 2, 3, 4, 5A, 5B and 6. STAT1, 2, 3 and 6 are involved in the direct regulation of the immune response, whereas STAT4, 5A and 5B are linked to the development of immune cells. JAK1 and TYK2 are associated to IFNAR and phosphorylate STAT1 and 2 that are cytosolic **(Figure 6)**. Once phosphorylated they can homo- or hetero-dimerize, the latter happening with IRF9. Together with the two phosphorylated STATs, IRF9 forms the IFN-stimulated gene factor 3 (ISGF3) complex that will bind IFN-stimulated regulatory elements (ISRE) in the ISGs promoter sequence. This in turn leads to the expression of hundreds of ISGs composed of direct cellular effectors but also STATs and IRFs transcription factors themselves (Awasthi et al., 2021). Among the ISGs, several proteins have direct effects on the foreign nucleic acids and proteins. Given its key role in regulating gene expression, IFN-I must be tightly regulated to prevent unwanted effect due to a spurious activation. This explains why transcriptional repressors can also be found among the induced genes. When rightfully activated however, apoptosis can be an outcome of the IFN-I activation to control the infection (Ivashkiv and Donlin, 2014).

Among all the factors that are linked to IFN-I activation in response to RNA virus infection, two are of special interest for this work: the dsRNA-activated protein kinase (PKR) (see Chapter 2) and the 2'-5'-oligoadenylate synthetase (OAS)/RNaseL pathway **(Figure 6)**. In the latter case, IFN-I-dependent induction is restricted to the OAS family, whereas RNaseL is constitutively expressed (Rusch et al., 2000). It is however activated by the recognition of 2'-5'-linked oligoadenylate nucleotides (2-5A) synthetized by the OAS proteins **(Figure 6)**. The 2-5A nucleotides induce dimerization of RNaseL, which is then able to cleave every RNA molecule in the cell, resulting ultimately in cell death (Choi et al., 2015; Rusch et al., 2000).

Some OAS genes can bear antiviral activities that are independent from RNaseL. Four OAS genes are described: OAS1, OAS2, OAS3 can all activate RNaseL to different extent and can be activated differentially depending on the virus (Henrik Gad et al., 2012; Lin et al., 2009). OAS-like protein (OASL) binds dsRNA but does not synthetize 2-5A. Nonetheless, it possesses antiviral activity against several RNA viruses and is able to directly activate the RIG-I pathway (Marques et al., 2008; Zhu et al., 2014).

Mutations in OAS genes are linked to viral infection or disease susceptibility. Hence, in humans, a simple mutation in the OASL gene increases the symptoms severity of flavivirus infections (Yakub et al., 2005). More recently, a single mutation in the OAS1 gene was linked to protection against SARS-CoV-2 in patients (Wickenhagen et al., 2021). Likewise, inborn errors in OAS or RNaseL genes were linked to severe disease in SARS-CoV-2 patients with an enhanced inflammatory response (Lee et al., 2022).

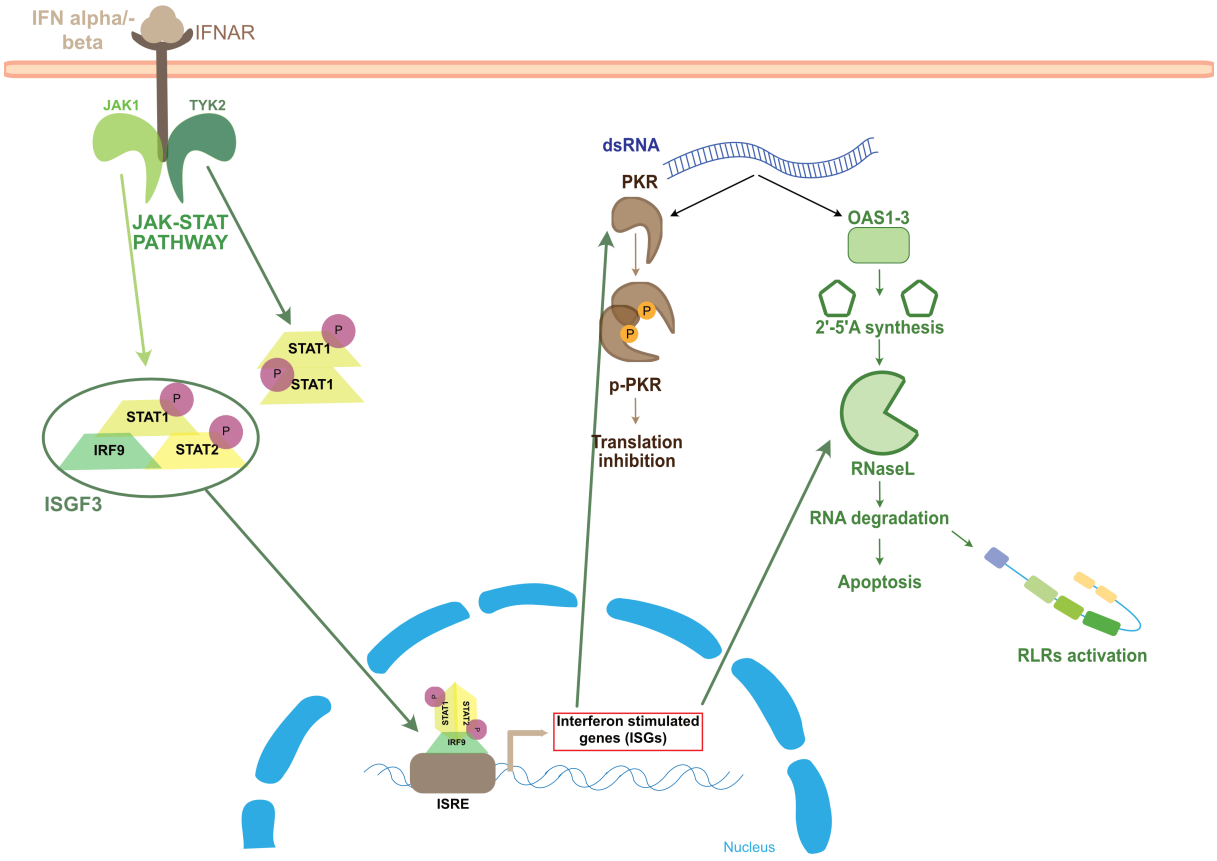

Figure 6 – IFN-I involves a transcriptional cascade leading to the expression of hundreds of cellular antiviral effectors.

The interferon α and ß cytokines bind the IFNAR allowing the activation of the JAK/STAT pathway. JAK1 (janus kinase 1) and TYK2 (tyrosine kinase 2) phosphorylate STAT1 and 2 leading to their homodimerization or heterotrimerization with IRF9 to form the ISGF3 complex (interferon-stimulated gene factor 3). The complexes then translocate to the nucleus to activate ISGs by binding to the ISRE (interferon-sensitive response element). Among the activated ISGs are the dsRNA-activated protein kinase (PKR) and the ribonuclease L (RNaseL). The activated PKR autophosphorylates and inhibits cellular translation. RNaseL is activated by the binding of 2'-5'-linked oligoadenylate nucleotides (2'-5'A) produced by OAS1-3 (oligoadenylate synthetase). RNaseL degrades RNA in a non-specific way ultimately leading to apoptosis.

2. The NF-kB pathway

The nuclear factor-kB (NF-kB) transcription factor family is part of an immune pathway commonly induced by the different PRRs. It contains 5 members: NF-kB1 (p50), NF-kB2 (p52), RELA (p65), RELB and c-Rel, which can form hetero- or homo-dimers to bind the kB promoting sequence of immune and inflammatory genes. RELA, RELB and c-REL are transcriptional activators whereas the two others are repressors that derive from longer precursor. The two main dimers responsible for the immune signaling is composed of the ubiquitously expressed RELA/p50 or RELA/p52 (Li and Verma, 2002). When in the cytosol, NF-kB proteins are maintained in an inactive form by a protein inhibitor of the IkB family (α, ß or ε). Their interaction is mediated by the ankyrin domains in each partner. IkB binding to NF-kB masks one of the two nuclear localization domains (NLS). However, the second NLS allows the complex to shuttle in the nucleus where the nuclear export signal (NES) contained in IkB initiates the cytoplasmic return. This balance guarantees the inactivation of NF-kB transactivation activity (Birbach et al., 2002; Huang et al., 2000). Only IkBß can mask both of the NLSs, thereby inhibiting this shuttle movement. IkBα is the main inhibitor of RELA associated dimers.

The NF-kB pathway is activated by multiple signals depending on RLRs, TLRs, cGAS sensors, Tumor necrosis factor (TNF) or interleukins (IL-1) **(Figure 7)**. In the canonical TLRs activation, the adaptor protein MYD88 recruits and activate IRAK (IL-1-receptor-associated kinase). IRAK interacts with the TRAF adaptor (TNF-receptor-associated factor 6), and the complex relays the signal through another kinase complex, TAK1 (TGFß-activated kinase 1) and its two accessory proteins, TAB1 and 2 (TAK-1-binding proteins). This in turn activates the IkB-kinase complex (IKK). This complex is composed of two kinases, IKK1 and 2 (or α and ß) and the regulatory subunit IKKγ/NEMO (NF-kB essential modulator). The IKK complex is at the center of all signaling pathways able to activate NF-kB and can phosphorylate all the IkB (Li and Verma, 2002). Upon phosphorylation, IkBα is ubiquitylated by the ß-TRCP E3 protein and sent to the 26S proteasome for degradation (Karin and Ben-Neriah, 2000) **(Figure 7)**. NFkB dimers are then released and translocate in the nucleus to activate their targets.

A last regulation step for NF-kB activity is direct phosphorylation **(Figure 7)**. For instance, p65 has been shown to be highly phosphorylated at different residues to display its

transactivation functions. Hence, phosphorylation of S276 by PKA catalytic subunit (PKAc), S529 by casein kinase II (CKII) or S529 and S536 by IKK2 are necessary for p65 activity (Sakurai et al., 1999; Wang et al., 2000; Zhong et al., 1998). To avoid uncontrolled inflammatory responses, the NF-kB pathway is self-regulated thanks to feedback loop involving activation of the IkBα gene (*NFKBIA*) by RELA (Gao et al., 2005). This ensures the production of inhibitors that will control the availability of NF-kB in the nucleus.

The NF-kB pathway plays an essential role to control the balance between the antiviral immune response and an over-activation of the inflammation response leading to cell death. Hence, this pathway has been frequently linked to auto-immune diseases but also to infection severity (Liu et al., 2017; Santoro et al., 2003). Upon viral infection, the common features activated by the NF-kB pathway are cell survival, cell proliferation but also the inflammatory and immune actors (Oeckinghaus and Ghosh, 2009).

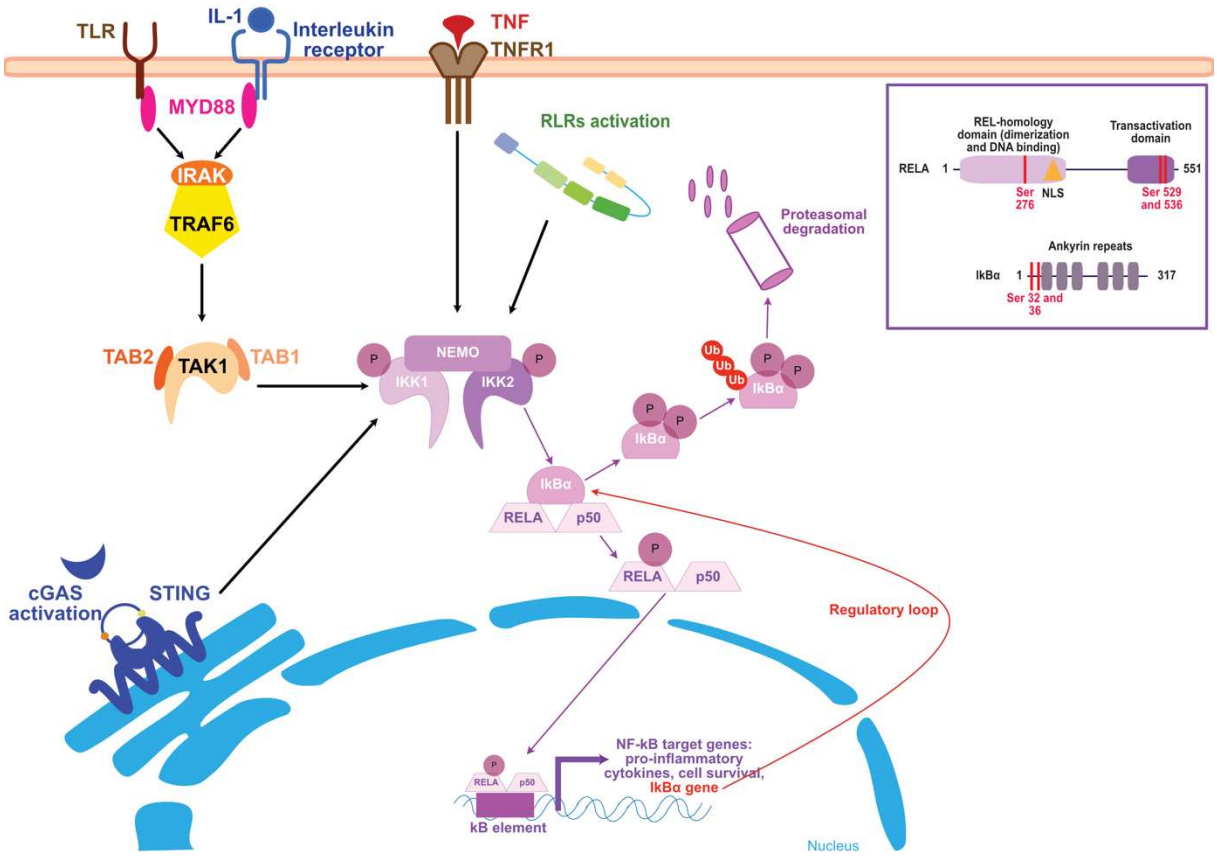

Figure 7 – The Nuclear factor-kB (NF-kB) pathway is another way to trigger IFN-I response.

Toll-like receptors (TLR), interleukin (IL) receptor and Tumor necrosis factor receptor (TNFR) as well as RLRs activate the NF-kB pathway. TLR and IL receptor signal to the MYD88 adapter (myeloid differentiation primary

response 88) that activates IRAK (IL-1-receptor-associated kinase) and allow its interaction with TRAF6 (TNF-receptor-associated factor 6). The signal is relayed by TAK1 (TGFß-activated kinase 1) and its two accessory proteins TAB1 and 2 (TAK-1-binding proteins), which activate the IKK complex (IKK1 and 2 and NEMO (NF-kB essential modulator)). IKK phosphorylates the cytosolic NF-kB inhibitor IkBα leading to its ubiquitylation and proteasomal degradation. The released NF-kB dimer RELA/p50 undergoes further phosphorylation before being translocated to the nucleus to activate the expression of pro-inflammatory genes. In a regulatory loop, IkBα expression is induced by NF-kB members. RELA possesses one NLS (nuclear localization signal), one phospho-site in its DNA-binding domain, and two in its C-ter transactivation domain. The inhibitor IkBα is composed of 6 Ankyrin repeats and two N-ter phospho-sites.

CHAPTER 2: PKR, a central IFN-I-induced kinase

A. Discovery and structure

PKR is one of the four eIF2α kinases (EIF2AK), the other ones being general control nonderepressible-2 (GCN-2), protein kinase R-like endoplasmic reticulum kinase (PERK), heme-regulated inhibitor (HRI). HRI was first discovered in reticulocytes and is activated upon heme-deprivation (Han et al., 2001) **(Figure 8)**. PERK is a component of the endoplasmic reticulum-linked stress response and is activated upon unfolded proteins detection. PERK is also crucial in the pancreatic homeostasis (Harding et al., 2001). GCN-2 was discovered in yeast where it is a stimulator of *GCN4* mRNA translation. It is activated by amino-acids starvation (Hinnebusch, 1993).

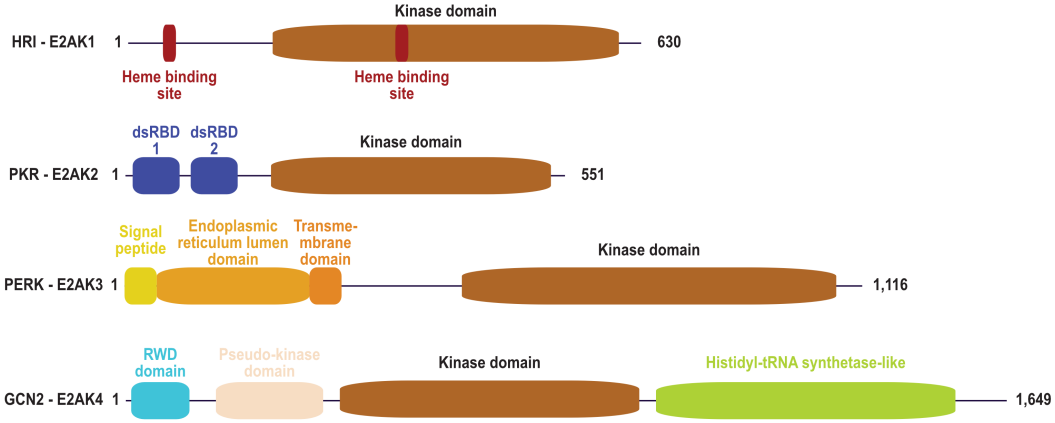

Figure 8 – The eIF2α kinases (EIF2AK) family.

All members of the family contain an ATP-dependent kinase domain and a stimulus-binding domain. HRI (heme-regulated inhibitor) is composed of two heme binding sites and one kinase domain. PKR has two dsRBDs (dsRNA-binding domains) and a kinase domain. In addition to its kinase domain, PERK (protein kinase R-like endoplasmic reticulum kinase) contains three domains linked to its endoplasmic reticulum (ER) localization: a signal peptide, an ER lumen domain and a transmembrane domain. GCN2 (general control nonderepressible-2) displays a kinase and a pseudokinase domain surrounded by a N-ter RWD domain (RING finger-WD repeat) and a histidyl-tRNA synthetase-like domain to sense the nutrients deprivation.

PKR (EIF2AK2) was discovered as an ISG in human and mouse cells, where it was coined respectively p68 and p65 based on its molecular weight (Galabru and Hovanessian, 1987). Its activity depends on the detection of a dsRNA molecule (Lemaire et al., 2008). It can auto-phosphorylate and phosphorylate the eukaryotic translation initiation factor eIF2α (Samuel, 1979; Samuel et al., 1984). The latter is directly responsible for translation arrest and cell growth defects in yeast. PKR activation was then detected upon viral infection in mouse and human cells and shown to display an antiviral activity (Meurs et al., 1992). PKR was further characterized as serine-threonine kinase activated by dsRNA upon viral infection (Sadler and Williams, 2007). PKR mode of action is now well-described **(Figure 9)**. It is composed of two dsRBDs in N-ter and a kinase domain in C-ter. Upon recognition of a minimal 30-bp-dsRNA by the first dsRBD, PKR mononers accumulate on the substrate leading to their interaction (Lemaire et al., 2008). PKR homodimerizes via a region between residues 244 and 296 of the kinase domain (Dar et al., 2005). Hence, the mutant K296R deprived of ATP-binding and phosphate transfer activity (Katze et al., 1991) can no longer homodimerize (Dey et al., 2005). Afterward, the active part of the kinase domain is structurally rearranged to allow the auto-phosphorylation of residues T446 (Dey et al., 2014) and T451 (Romano et al., 1998). This results in a stable and fully functional dimer ready to engage its substrates. The phosphorylation of eIF2α depends on T487, a critical residue in the catalytic site of PKR (Dey et al., 2005).

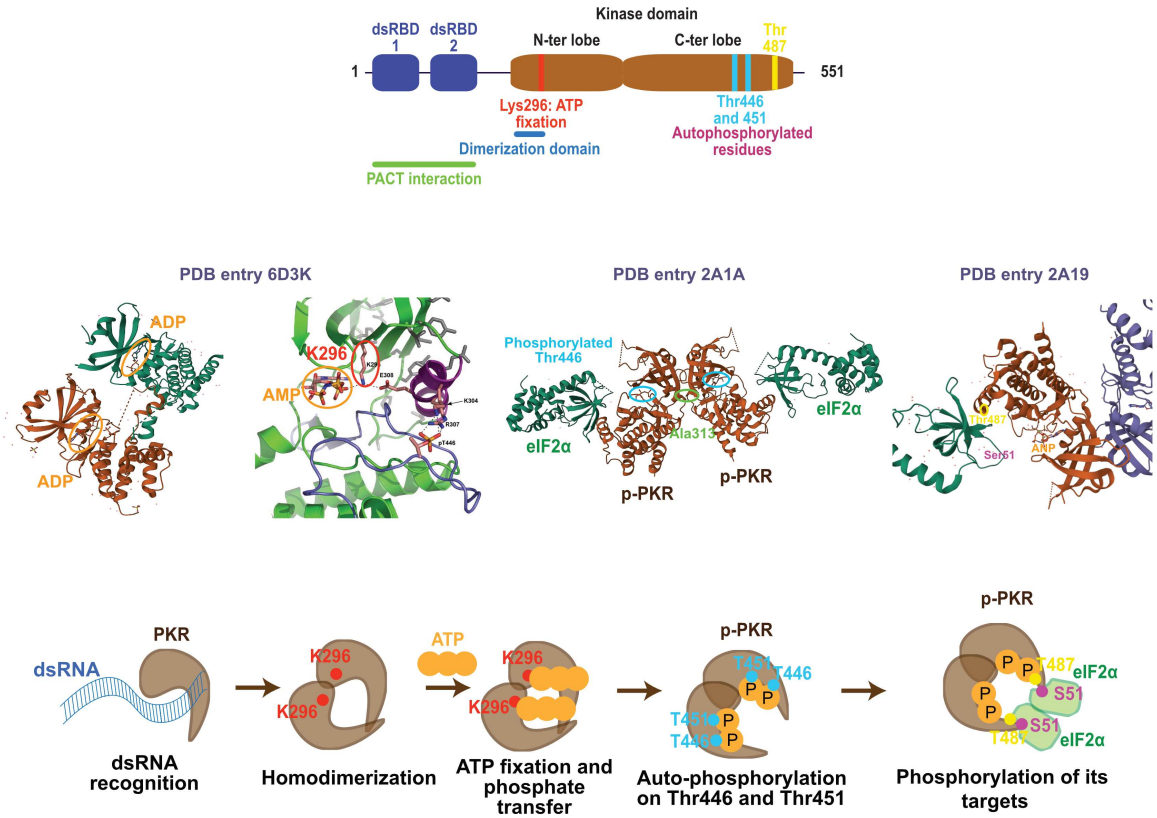

Figure 9 – Mechanism of dsRNA activation and phosphorylation activity of PKR.

PKR dimerizes following its binding of dsRNA. The structural rearrangement allows the opening of the ATP fixation site in the N-ter lobe of the kinase domain. One residue, K296, binds ATP and will transfer first one phosphate on residue T446 in the C-ter lobe of the kinase domain. This is followed by a second phosphorylation on residue T451, which definitely stabilizes the dimer and opens the catalytic site. T487 is one of the catalytic residues that will allow the phosphorylation of eIF2α on S51. As PKR functions as a dimer, 2 molecules of eIF2α can be phosphorylated at the same time. AMP, adenosine monophosphate; ADP, adenosine diphosphate; ATP, adenosine triphosphate; p-PKR, phospho-PKR. Structures PDB: 6D3K, 2A1A and 2A19.

PKR is retrieved in many mammals and paralogous kinases are found in frog, fish and chicken (Rothenburg et al., 2009). Interestingly, the kinase domains of PKR evolved more rapidly than the ones in the other EIF2AKs, indicating that it is under selection pressure. Indeed, positive mutation selection events in the kinase domain are directly linked to the targeting of PKR by viruses. In addition, a recent study on bats PKR show that they are the ones that undergo the most positive selection events, compared to other mammalian PKRs.

Besides, an *EIF2AK2* gene duplication is present in *Myotis* species, suggesting a diversification of bats PKR in the antiviral response. (Jacquet et al., 2022).

B. A cellular hub

1. A kinase with multiple targets

PKR kinase activity is mainly directed to eIF2α phosphorylation, resulting in translation inhibition. eIF2α is one of the three subunits of eIF2 involved in the binding of Met-tRNAi^{Met} by the 40S ribosomal subunit to form the 43S scanning complex. Once the initial AUG is recognized, eIF2 drops the charged tRNA on the Met initiation codon thanks to GTP hydrolysis by the eIF5 GTPase. eIF2-GDP has no affinity for the initiator tRNA and needs GDP recycling into GTP. This is done by the guanine exchange factor eIF2B. eIF2-GTP is then able to initiate again the cap-dependent translation (Liu et al., 2020). However, if the α regulatory subunit of eIF2 is phosphorylated (p-eIF2α), its affinity for eIF2B increases thereby sequestering eIF2B in cells (Krishnamoorthy et al., 2001). As a result, cap-dependent translation is inhibited since eIF2B levels are much lower than eIF2 levels in cells. Thereby, since viruses rely on the host translation machinery, inhibiting translation is an antiviral mechanism.

PKR is also a central kinase tightly regulating the cell cycle progression. It is activated by cellular dsRNAs formed by Alu repeats during mitosis. Its kinase activity plays a role in the c-Jun N-terminal kinase activation regulating cell cycle actors (Kim et al., 2014a) **(Figure 10a)**. In the same way, during cell cycle or upon stress, mitochondrial and nuclear dsRNAs can bind to PKR and regulate its activity (Kim et al., 2018). This explains why PKR has been linked to the p53 pathway and to cancer progression. PKR phosphorylates p53 regulating its transcriptional activity. In return, upon genotoxic stress, p53 induces PKR expression favoring eIF2α phosphorylation and leads to apoptosis, partly explaining p53 tumor-suppressor activity (Cuddihy et al., 1999; Yoon et al., 2009).

PKR is also able to phosphorylate other substrates such as the DNA/RNA helicase DHX9 upon poly(I:C) transfection **(Figure 10b)**. When phosphorylated, DHX9 is no longer able to bind dsRNA. Phosphorylated DHX9 loses its ability to activate HIV-1 LTR transactivation. Thereby, PKR kinase activity reduces HIV-1 infection in a eIF2α-independent way (Sadler et al., 2009).

Another downstream effect of eIF2α phosphorylation is the upregulation of ATF4, a major player in integrated stress response (ISR) and neurodegenerative disorders. Indeed, ATF4 mRNA is translated when p-eIF2α levels are high by a cap-independent translation mechanism. In a mouse Alzheimer's disease model, the blocking of PKR by a chemical inhibitor rescue the memory deficit at early stages of the pathology (Segev et al., 2015) **(Figure 10c)**. Another aspect of ISR is the formation of stress granules. Stress granules are composed of mRNA in translational pause due for instance to the phosphorylation of eIF2α. Stress granules are formed upon viral infection and can be driven by phosphorylation of eIF2α or by the direct binding of an inactive PKR with a stress-granule component, G3BP1 (Onomoto et al., 2014; Reineke and Lloyd, 2014).

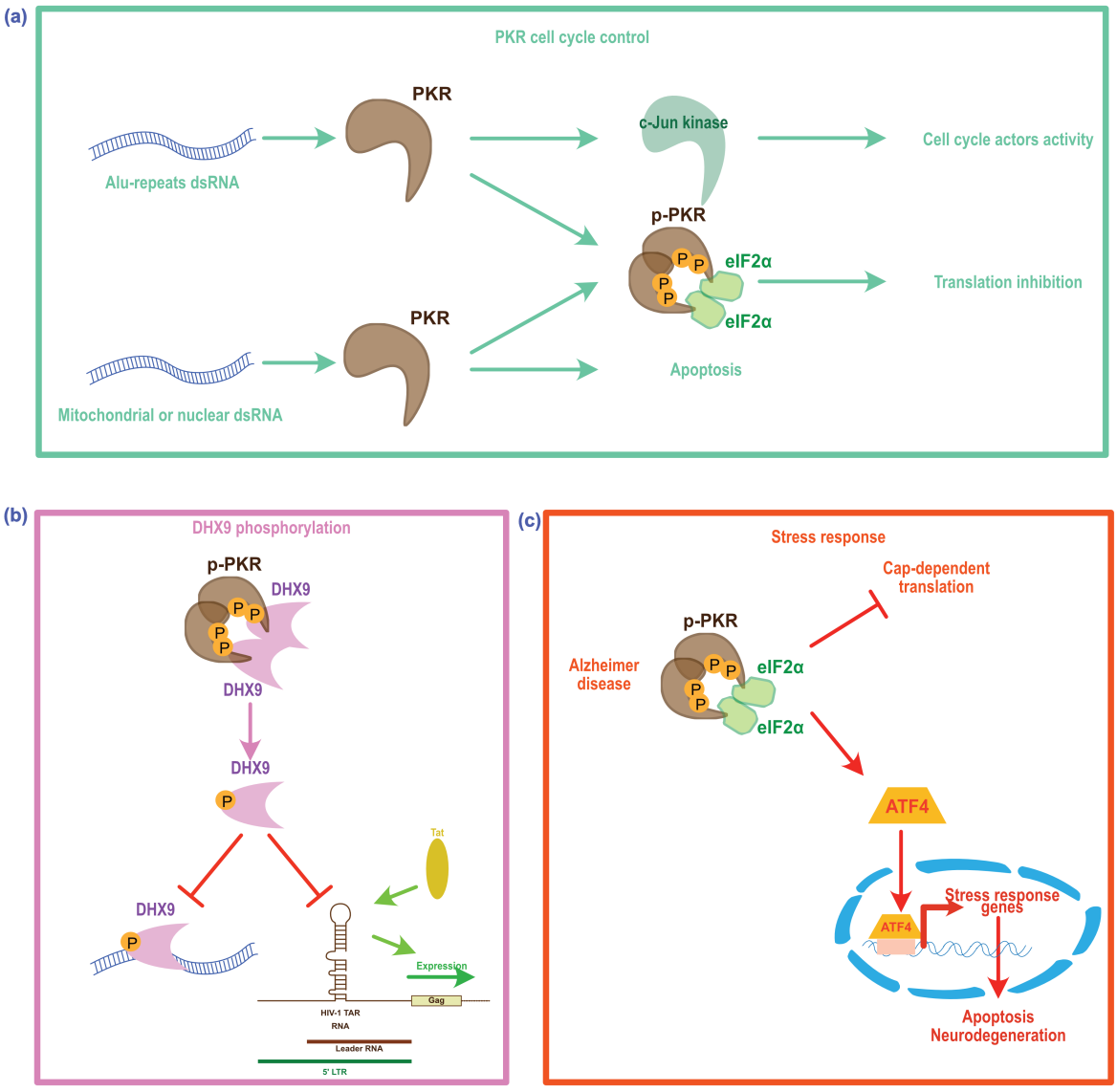

Figure 10 – PKR kinase activity involves other features than translation inhibition.

(a) During the cell cycle, PKR is activated by endogenous nuclear or mitochondrial dsRNAs. Besides blocking translation initiation, it can also activate the c-Jun kinase to regulate cell cycle. (b) PKR can phosphorylate DHX9, which affects its dsRNA- and HIV-1 TAR RNA-binding capacity, which results in a drop of HIV-1 mRNA activation. (c) Upon stress, for example in Alzheimer disease, phosphorylation of eIF2α by PKR results in the cap-independent translation of stress factors such as the transcription factor ATF4 that will induce the expression of stress-related genes.

2. Interferon signaling

One of the main functions of stress granules is to modulate IFN signaling and the induction of ISGs expression **(Figure 11a)**. Upon infection with and NS1-deficient Influenza A virus, stress granules are formed and contain both PKR and RIG-I cytosolic receptor. Deletion of PKR inhibits IFN signaling but also stress granules formation. At the same time, deletion of the stress granules component G3BP1 downregulates PKR activity on eIF2α. PKR may be involved in RIG-I activation upon IAV infection (Onomoto et al., 2012). Another RLR-related role of PKR is its involvement in MDA5-signal transduction upon Vaccinia virus infection (Pham et al., 2016). PKR is able to trigger IRF3 nuclear translocation to activate IFN-I expression in a MAVS-dependent manner **(Figure 11b)**. MAVS also interacts and stimulates PKR activation and eIF2α phosphorylation upon dsRNA detection thus promoting the formation of stress granules (Zhang et al., 2014). Lastly, upon Vaccinia virus infection, MAVS is required to activate PKR-dependent IRF3 activation to restrict viral infection (Zhang and Samuel, 2008).

PKR was also found in complex with STAT1 and in response to IFN or dsRNA, PKR dissociates from STAT1 to allow the expression of ISGs. This transcriptional regulation does not depend on PKR catalytic activity and is even increased when a kinase-deficient PKR is expressed (A. H.-T. Wong et al., 1997). Upon measles virus infection, PKR activity is essential to activate the MAPK pathway leading to IFN response (Taghavi and Samuel, 2012).

Interestingly, PKR also plays a role in IFN ß production in two different ways. First, upon infection with viruses such as Semliki forest virus or encephalomyocarditis virus (EMCV), PKR stabilizes the integrity of newly synthetized IFN ß mRNAs (Schulz et al., 2010). PKR is also able to induce the transcription of IFN ß mRNA. Upon measles virus infection or synthetic dsRNA

transfection, eIF2α phosphorylation by PKR results in a decrease of IKBα, the NF-kB inhibitor, and an increase of the NF-kB transcriptional response (McAllister et al., 2012) **(Figure 11c)**.

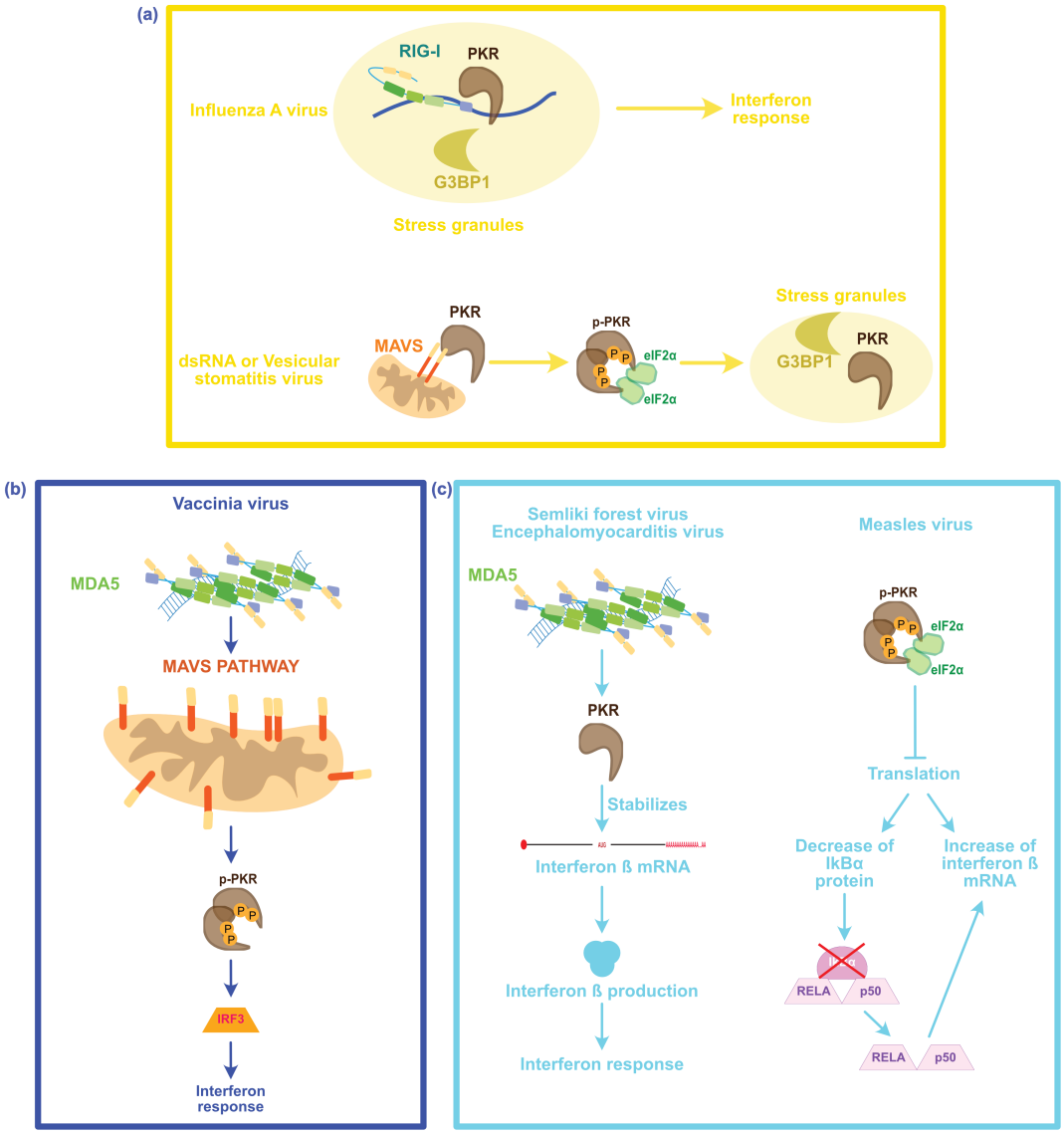

Figure 11 – PKR is involved in the immune signaling activation.

(a) Upon Influenza A virus infection, RIG-I is activated and is relocalized in stress granules formed by PKR and G3BP1. These stress granules are known to be component of the IFN-I signaling cascade. It is also the case upon vesicular stomatitis virus infection where this time, the interaction between activated MAVS and PKR triggers PKR activity on eIF2α necessary to form the G3BP1-induced stress granules. (b) PKR has also direct functions in the IFN-I transcriptional activation. Upon vaccinia virus infection, the MDA5-MAVS activation leads to the activation of PKR that is responsible for IRF3 activation and nuclear translocation enabling the IFN-I response. (c) Finally, PKR can also control IFN ß production by stabilizing its mRNA in the cytosol after MDA5 activation by Semliki forest virus and encephalomyocarditis virus. During measles virus infection, PKR induces translation

inhibition that results in a decrease of protein accumulation of the inhibitor IkBα thereby freeing RELA that will transcriptionally activate IFN ß.

The link between PKR and NF-kB is now firmly established and different activation mechanisms have been described. The first occurrence of this link was the realization that the NF-kB pathway was activated in several cell lines treated with dsRNA. PKR was shown *in vitro* to phosphorylate IkB leading to p65 activation (Kumar et al., 1994) **(Figure 12a)**. However, other activation pathways that depend or not on PKR catalytic activity have been reported. Thus, PKR and its mutant K296R, which cannot phosphorylate but still binds RNA, were found interacting with the IKK complex **(Figure 12a)**. This enhances the kinase activity of the complex and in the end, the NF-kB binding activity (Ishii et al., 2001). Other have shown that PKR interaction with the kinase IKKß is sufficient to activate the IKK complex, with no requirement for an active kinase activity (M. C. Bonnet et al., 2000). PKR has also been associated with a regulatory action upstream of the IKK complex (Gil et al., 2000). These disparities on the involvement of PKR catalytic activity in NF-kB activation highlight subtle differences depending on the type of stress or cells considered.

NF-kB induction by PKR was further associated with many cellular events including apoptosis, IRF1 induction, macrophages activation, metabolism defects (hyperosmotic stress), cancer progression and viral infection (Farabaugh et al., 2017; Gil et al., 1999; Kirchhoff et al., 1999; Li et al., 2001; Maggi et al., 2000; Zhu et al., 2021). Unexpectedly, in some cases, the PKR transcriptional inducer activity can lead to an inflammatory state that will promote viral infection. Thus, in HIV-1 infected cells, Tat protein activate the PKR-dependent NF-kB pathway to enhance Tat transactivation activity (Demarchi et al., 1999). PKR-dependent pro-viral effect also happens upon Zika virus infection, where the virus-mediated inhibition of mitophagy activates PKR and its capacity to induce the expression of pro-inflammatory cytokines in an eIF2α-phosphorylation independent manner (Ponia et al., 2021) **(Figure 12b)**.

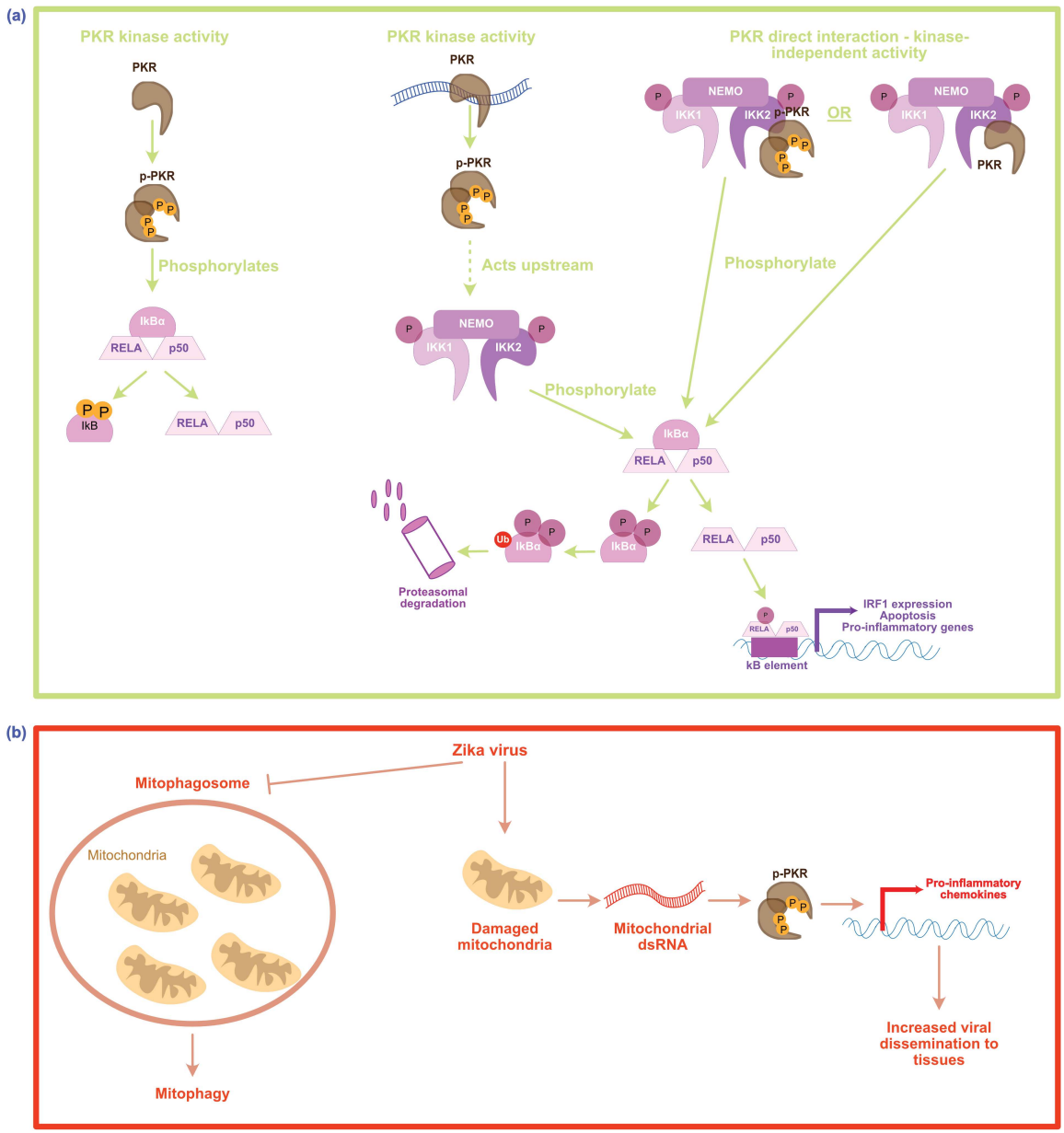

Figure 12 – PKR acts as a NF-kB inducer to mount the pro-inflammatory response.

(a) In vitro, PKR activity was shown to be essential for the phosphorylation of IkBα allowing the NF-kB transcriptional response. However, in vivo, even though PKR kinase activity is required, it seems to be acting upstream of the activation of the IKK kinases complex. In another case, PKR catalytic activity was not required for IkBα phosphorylation by IKK complex but its interaction with IKK2 is essential to activate the NF-kB response and the expression of pro-inflammatory genes. (b) The immune transcriptional activation by PKR is hijacked by Zika virus that uses the inhibition of mitophagy to activate PKR and the expression of pro-inflammatory cytokines. These cytokines display a pro-viral role and help the viral dissemination in the body.

3. Viral evasion and PKR inhibition

Given its implication in antiviral defense mechanisms, it is no surprise that many have developed counter-measures against PKR activity. Many strategies have been reported such as direct inhibition of PKR RNA-binding, pseudo-substrate formation, dsRNA masking, PKR degradation or cap-independent translation mechanisms (Cesaro and Michiels, 2021) **(Figure 13)**.

Poxviruses K3L protein is well-studied for its eIF2α mimicry. This allows the viral protein to bind the kinase pocket in PKR and to block the interaction with eIF2α (Dar et al., 2005; Kawagishi-Kobayashi et al., 1997) **(Figure 13a)**. Vaccinia virus encodes another PKR inhibitor, E3L, which sequesters dsRNA. A similar strategy is adopted by HIV-1, which sequesters PKR via its 23bp Tat-responsive region RNA (TAR). It is not long enough to activate PKR as 30 bp are required to attract two PKR monomers leading to their activation (Gunnery et al., 1990). The foot-and-mouth disease picornavirus is restricted by PKR but uses an efficient countermeasure to avoid PKR antiviral activity: the 3C protease is able to induce its lysosomal degradation (Li et al., 2017).

To overcome translation inhibition by PKR some viruses developed a genomic feature enabling cap-independent translation **(Figure 13b)**. For instance, Sindbis and Semliki viruses possess a short stem-loop at the beginning of their subgenomic RNA, which directly attracts the ribosome without requirement of the initiation complex (Carrasco et al., 2018; Ventoso et al., 2006).

Conversely, some viruses, like hepatitis C virus, activate PKR to induce the translation inhibition of IFN cytokines, thus indirectly down-regulating the immune signaling (Arnaud et al., 2010).

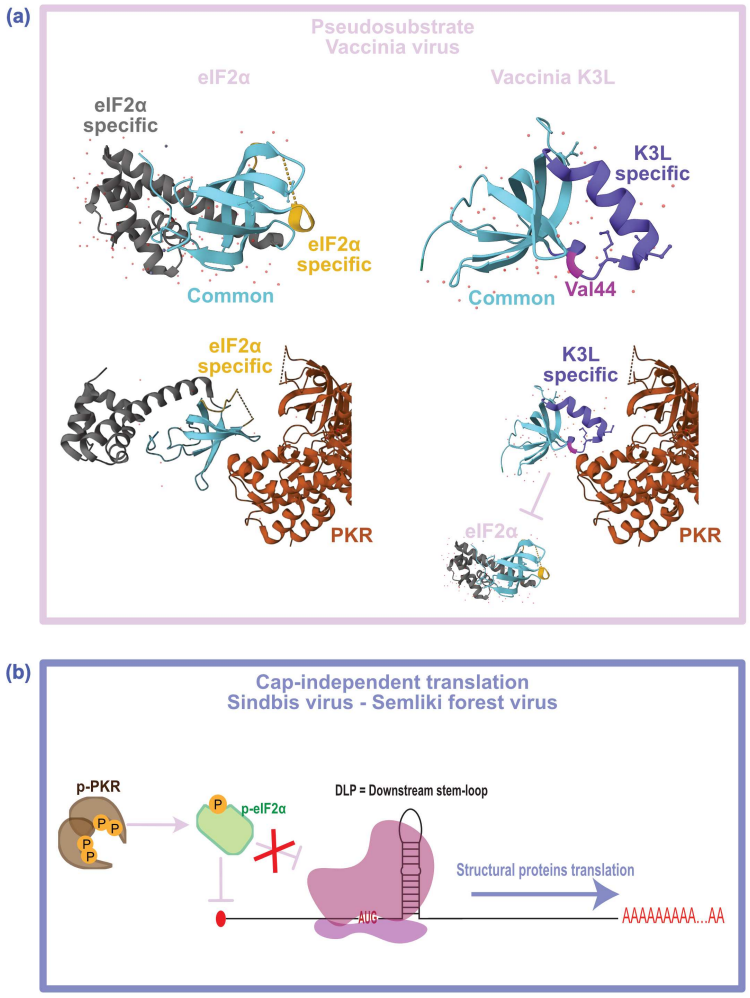

Figure 13 – PKR functions are inhibited by viruses via different mechanisms.

(a) Vaccinia virus adopts a pseudo-substrate strategy to counteract PKR. Its K3L protein shares a strong homology with eIF2α competing for PKR binding in its catalytic pocket. Thus, eIF2α phosphorylation by PKR is abrogated. PDB structure: eIF2α, 1KL9; PKR + eIF2α, 2A1A; K3L, 1LVZ. (b) Sindbis virus and Semliki forest alphaviruses use a cap-independent translation mechanism to express their structural proteins. A stem-loop, called DLP (downstream stem-loop), directly attract the 80S ribosome.

4. PKR partners

PKR activity can be directly controlled by the binding of cellular factors, such as for instance NF-90, Hsp90 or the ribosomal protein L18 (Donzé et al., 2001; Kumar et al., 1999; Wen et al., 2014). Two dsRBPs, which are also partners of Dicer, have opposite effects on PKR activity. First, PACT is known to be in most cases a PKR activator even in the absence of dsRNA binding. PACT was discovered as an interactant of PKR in a yeast two-hybrid screen using the inactive PKR K296R as a bait. This interaction occurs between the two first dsRBDs of PACT and PKR dsRBDs (Patel and Sen, 1998). The third dsRBD in PACT, also known as the Medipal domain is structurally different from the two others, lacks the amino-acids necessary for dsRNA binding, and is involved in the direct activation of PKR (Peters et al., 2001) **(Figure 14)**. The Medipal domain interacts with the beginning of PKR kinase domain near the ATP binding site, therefore allowing its opening to free the K296 and T446 residues (Li et al., 2006).

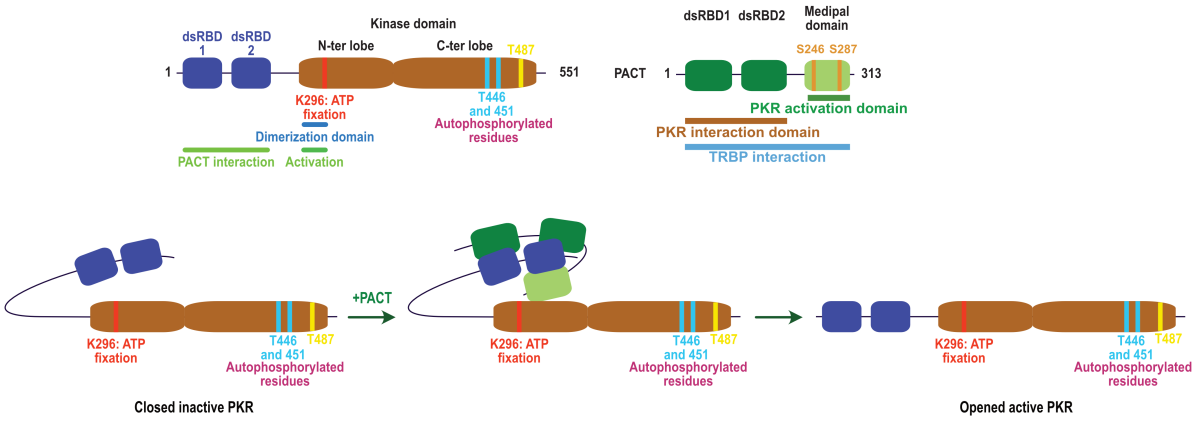

Figure 14 – PACT binding to PKR releases its kinase domain.

PKR and PACT interact *via* their first two dsRBDs. In a latent state, PKR is in a close conformation hiding the dimerization and ATP fixation sites. PACT fixation to the PKR dsRBDs allows its Medipal domain to open the N-ter lobe of PKR kinase domain, which releases the dimerization site and K296 to activate PKR. Two phospho-sites are found in the Medipal domain, S246 is constitutively phosphorylated and S287 is phosphorylated upon stress.

PACT is involved in the induction of PKR-dependent apoptosis in stressed cells (Peters et al., 2001). Of note, PACT also plays many other roles as the direct activation of RIG-I-mediated signaling upon infection (Kok et al., 2011). Cell treatment with diverse stress agents

such as arsenite, thapsigargin, ceramide, hydrogen peroxide or even IL-3 deprivation induces PKR in mouse cells (Ito et al., 1999; Ruvolo et al., 2001). Overexpression of PACT can also by itself activate PKR without any external stimuli (Ito et al., 1999; Patel et al., 2000). Upon tunicamycin-induced ER stress, PACT is also able to activate PKR and its role in the unfolded protein response pathway (Singh et al., 2009). The activated PKR induces the expression of the C/EBP homologous protein (CHOP) that will activate the transcription of stress-associated genes **(Figure 15a)**. In all these cases, PKR is activated, autophosphorylates and inhibits cellular translation and cell growth. Upon hyperosmotic stress, PACT induces the PKR-dependent NF-kB/p65 activation leading to an inflammatory state (Farabaugh et al., 2020) **(Figure 15b)**. After PKR activation, PACT dissociates from the phosphorylated PKR (Daher et al., 2009).

The PKR activation by PACT is also tightly regulated. TRBP is able to sequester PACT away from PKR. Upon peroxide or arsenite treatment, the interaction between TRBP and PACT is lost, while the interaction between PACT and PKR increases (Daher et al., 2009). Besides, high TRBP expression levels alleviate PACT-mediated PKR activation without stresses (Daher et al., 2009). Moreover, PACT can be phosphorylated on two serine residues in the Medipal domain, which increases its affinity for PKR dsRBDs (Patel et al., 2000; Peters et al., 2006) **(Figure 15c)**. Under physiological conditions, phospho-S246 PACT is bound to TRBP in the cytosol, therefore not available to interact with PKR. The phosphorylation of S287 residue upon stress dissociates PACT from TRBP, allowing the formation of a PACT homodimer (Singh et al., 2011) **(Figure 15c)**. This homodimer is necessary for PKR activation (Singh and Patel, 2012).

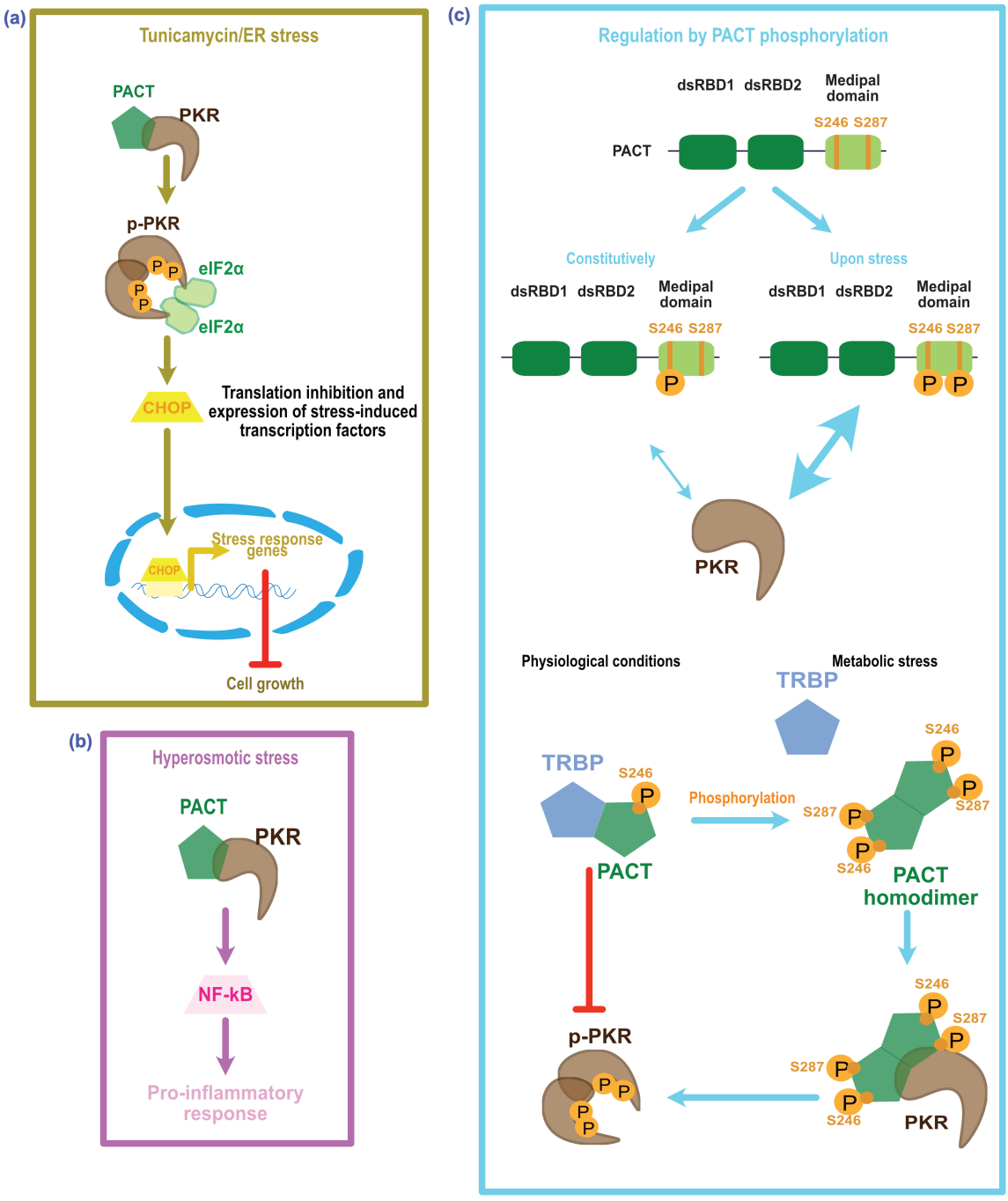

Figure 15 – PACT activates PKR functions upon stresses.

(a) ER stress promotes the PACT/PKR interaction leading to PKR activation and eIF2α phosphorylation. The cap-dependent translation inhibition uncovers the expression of stress-specific transcription factor CHOP (C/EBP homologous protein). (b) Upon hyperosmotic stress, PACT interaction with PKR also promotes its transcriptional induction activity of NF-kB leading to the activation of the pro-inflammatory response. (c) PACT is regulated by two phosphorylations: a constitutive one on S246 and a stress-induced one on S287, which increases PACT

affinity for PKR. The double phosphorylation also induces dissociation of the TRBP/PACT complex and allows PACT to homodimerize and activate PKR.

TRBP can also directly interact with PKR with its first two dsRBDs. On PKR, the same residues are involved in PACT and TRBP interactions (Gupta et al., 2003). The first dsRBDs of PACT, TRBP and PKR share a strong sequence homology explaining the same interacting platform. As opposed to PACT, the Medipal domain of TRBP is involved in PKR inhibition (Gupta et al., 2003) **(Figure 16a)**. In HIV-1 infected cells, TRBP both sequesters PKR and competes with it for the binding of the TAR element thereby promoting HIV-1 infection (Benkirane et al., 1997) **(Figure 16b)**. Similarly to PACT, TRBP is phosphorylated by MAPK/ERK on two key residues, S142 and S152, which reinforces its interaction with PKR (Nakamura et al., 2015), increases its inhibitory effect and enhances cell survival (Chukwurah and Patel, 2018) **(Figure 16c)**. During mitosis and in the presence of long dsRNAs, TRBP is hyperphosphorylated by the JNK kinase and inhibits PKR activity. But this phosphorylation does not alter its interaction with either Dicer or PACT (Kim et al., 2014).

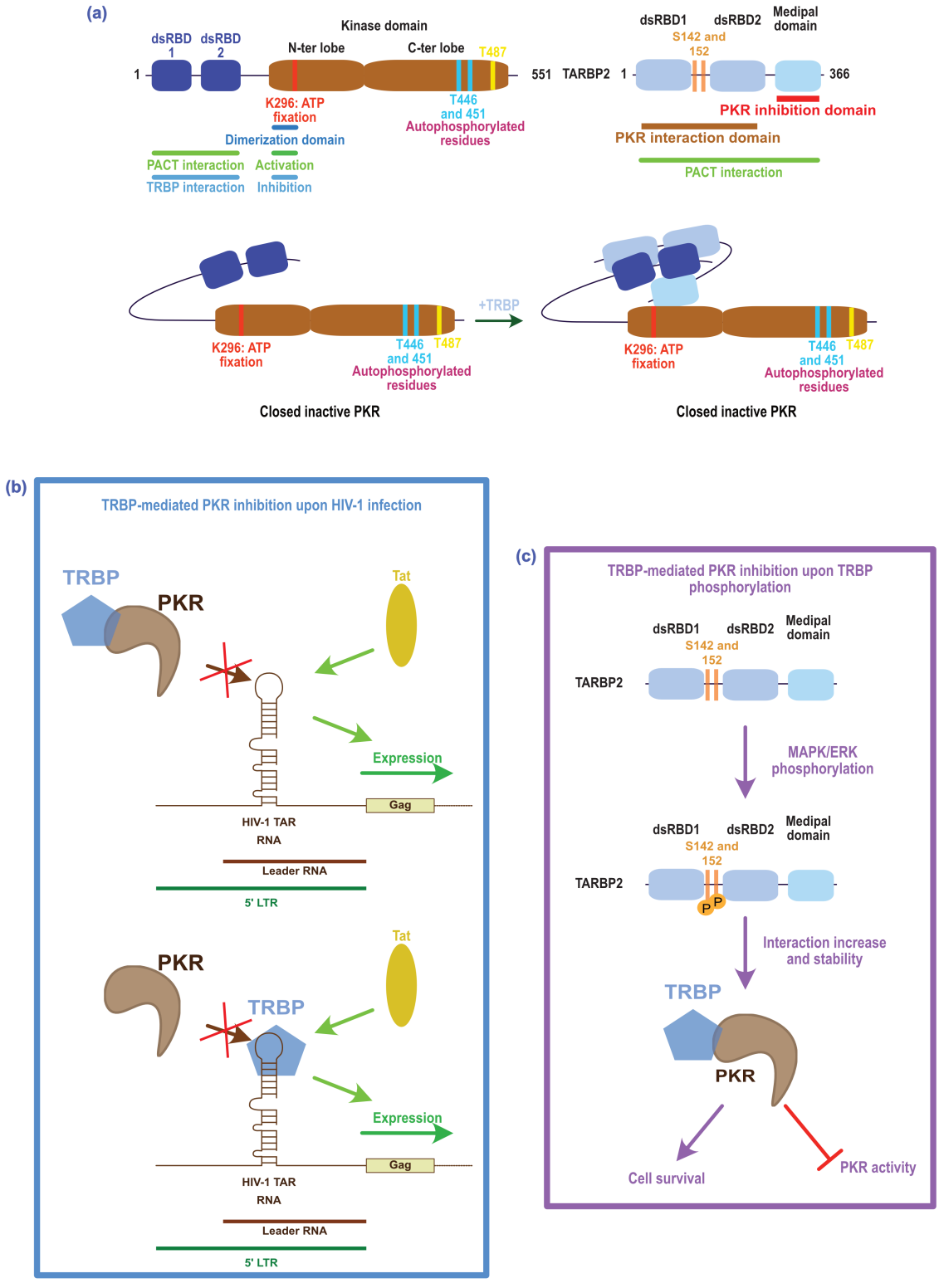

Figure 16 – TRBP inhibits PKR activity.

(a) TRBP competes with PACT for the binding of PKR. Once bound to the first two dsRBDs of PKR, TRBP uses its Medipal domain to block the opening of the dimerization and ATP binding sites in PKR. Since TRBP also interacts

with PACT, exchanges in the interacting complex are responsible for the control of PKR activity. (b) Upon HIV-1 infection, TRBP acts as a pro-viral factor by sequestering PKR and directly binding the TAR RNA. (c) Upon fatty acids accumulation, TRBP is phosphorylated by the MAPK/ERK kinase at S142 and S152, which increases its PKR binding activity and inhibition.

PKR is activated upon HIV-1 infection by the TAR-RNA to block the transactivation (Clerzius et al., 2011). PACT is also retrieved in a multiprotein complex associated with ADAR1 and PKR and acts as a PKR inhibitor of an HIV-1 molecular clone expression in HEK293T cells **(Figure 17a)**. Loss of ADAR1 and PACT, drastically inhibits HIV-1 expression. This time, PACT-mediated PKR inhibition is due to the direct binding of ADAR1 to PACT blocking its activity (Clerzius et al., 2013). Besides, ADAR1 antagonizes PKR activity upon viral infection by editing viral dsRNA masking it from PKR recognition (Pfaller et al., 2011) **(Figure 17b)**. Outside of PACT interaction, ADAR1 also binds directly PKR in vesicular stomatitis virus, HIV-1 and measles virus infected cells, inhibiting its activity and enhancing viral replication (Clerzius et al., 2009; Li et al., 2010; Nie et al., 2007) **(Figure 17b)**.

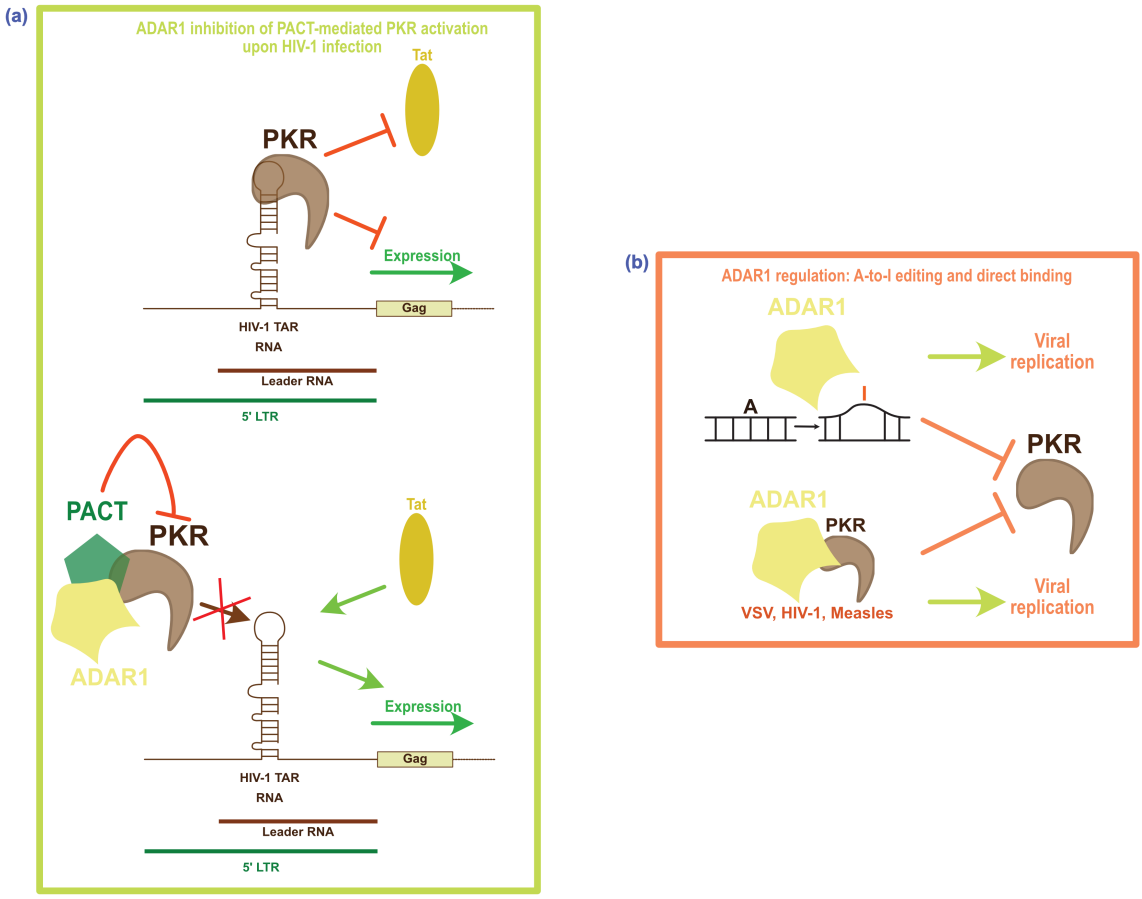

Figure 17 – ADAR1 acts as a pro-viral factor by inhibiting PKR activation.

(a) The deaminase ADAR1 antagonizes PKR upon HIV-1 infection. To do so, ADAR1 binds to the PACT/PKR complex, reverting the PACT-induced PKR activation. (b) ADAR1 activity on dsRNA prevents its recognition by PKR. This mechanism is used by many viruses that hijack ADAR1 to promote their replication. ADAR1 can also directly bind to PKR blocking its activation upon vesicular stomatitis virus (VSV), HIV-1 and measles virus infections.

CHAPTER 3: Human emerging RNA viruses: from alphaviruses to coronaviruses

A. Alphaviruses

1. General information and discovery

Alphavirus is the only genus of the *Togaviridae* family composed of enveloped positive belonging to the group IV of the Baltimore classification (single-stranded RNA (+ssRNA) viruses). Members of this genus have a genome size of 9.7 to 12kb. They infect vertebrate and invertebrate hosts depending on their specific entry receptors. Some of them, called arboviruses (arthropod-borne viruses), are transmitted between invertebrate vectors and vertebrate hosts. They can cause several symptoms in infected animal, especially in humans, including rash, fever, muscle pain, arthritis and in worst cases encephalitis. Alphaviruses are divided into 4 clades according to their E1 and E2 envelope sequences similarities **(Figure 18)**: Semliki forest virus, Eastern equine encephalomyelitis virus, Venezuelan equine encephalomyelitis virus and Western equine encephalomyelitis virus complexes. They are also commonly referred to as Old World and New World viruses, which cause respectively arthritic symptoms and encephalitis (Knipe and Howley, 2013). They are considered as emerging and re-emerging threats as they can still cause epidemic outbreaks with severe human morbidity, as we witness with the Chikungunya virus (CHIKV) since 2004. CHIKV was the first arthritogenic virus identified in the United Republic of Tanzania in 1952 followed by other African and Asian countries (Staples et al., 2009). The virus name is linked to its related symptoms, "*kungunyala*" meaning to walk bent over in Kimakonde language (Bartholomeeusen et al., 2023). Since then, many outbreaks have been reported in urban areas.

Many alphaviruses are found infecting non-human primates, humans and horses and are transmitted via mosquitoes from the *Aedes*, *Culex* or *Anopheles* species depending on their repartition areas. In that case, they are maintained through a sylvatic cycle in "reservoir host" and are transmitted to a vertebrate host where symptoms are detected (Guzmán et al., 2020). Of note, the increasing proliferation of vector insects is linked to climate change (temperature, precipitations), urbanization, demographic concentrations and travels (Guzmán et al., 2020). Other members of the genus do not cycle between arthropods and vertebrate hosts, e.g. the

insect-specific Eilat virus (Nasar et al., 2012) or the salmonid alphaviruses causing pancreas disease in Atlantic salmon (Deperasińska et al., 2018). Interestingly, the discovery of the latest raised the hypothesis of a marine origin for the alphaviruses genus (Forrester et al., 2012).

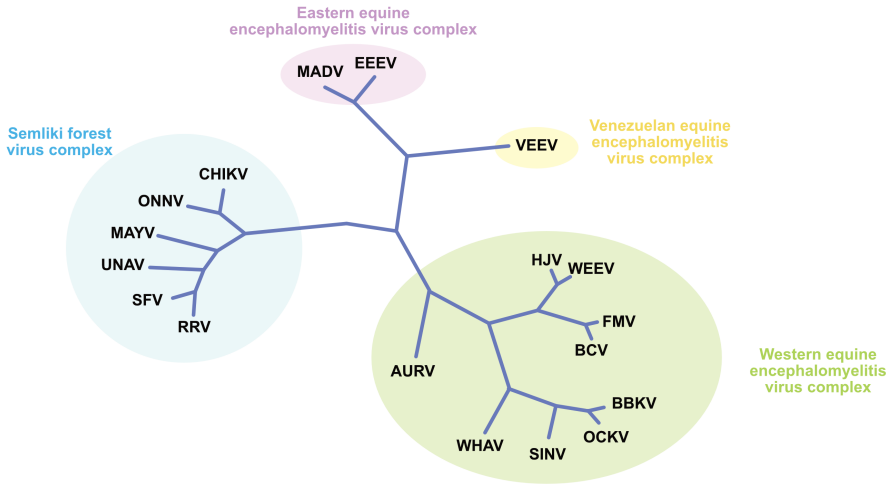

Figure 18 – Phylogeny of Alphaviruses members according to their glycoprotein sequences (E1 and E2).

Adapted from (Zimmerman et al., 2023). The phylogenetic distances are calculated according to the sequence alignment of the E1 and E2 sequences of the different alphaviruses. RRV, Ross river virus; SFV, Semliki forest virus; UNAV, Una virus; MAYV, Mayaro virus; ONNV, O'nyong'nyong virus; CHIKV, Chikungunya virus; MADV, Madariaga virus; EEEV, Eastern equine encephalomyelitis virus; VEEV, Venezuelan equine encephalomyelitis virus; HJV, Highlands J virus; WEEV, Western equine encephalomyelitis virus; FMV, Fort Morgan virus; BCV, Buggy Creek virus; BBKV, Babanki virus; OCKV, Ockelbo virus; SINV, Sindbis virus; WHAV, Whataora virus; AURV, Aura virus.

2. Classification

a. Old world alphaviruses

Members from this group are also referred to as arthritogenic or rheumatoid viruses because of the joints-related symptoms they cause in humans. It includes Barmah Forest, Chikungunya, Ross River, Semliki Forest, O'Nyong-nyong, Mayaro and Sindbis viruses (SINV). They are the cause of recurrent endemic outbreaks as for Chikungunya since 2004 with a spread from Africa to Indian Ocean (Kariuki Njenga et al., 2008; Powers and Logue, 2007). Many cases coming from the East Central South African lineage are reported in almost 40 countries of which Italy and France (Angelini et al., 2008; Delisle et al., 2015). Besides, a new strain emerged from the recent Asian lineage and spread in the Caribbean Sea with an outbreak in 2013 that reached South America (de Oliveira et al., 2021; Van Bortel et al., 2014). Chikungunya is still the most watched and prevalent epidemic-causing arthritogenic alphavirus but other members are often linked to persistent infection in populations with thousands of cases per year. It is the case for Ross River virus causing around 4,000 cases each year in Australia and for Sindbis virus with around a hundred of cases per year in Finland (Laine et al., 2004; Murphy et al., 2020). Chikungunya virus is mainly retrieved in South America, Africa and Pacific areas whereas Ross River virus stays endemic to Australia and SINV to Northern Europe **(Figure 19a)**.

They are naturally amplified through a sylvatic cycle in "reservoir host" such as non-human primates, birds, rodents, bats or kangaroos (for Ross River virus) and will once in while spillover to humans (Guzmán et al., 2020). Once in human, they are propagated in an urban cycle between their final hosts bitten by the same mosquito **(Figure 19b)**. For Chikungunya, Aedes species are predominantly involved in the human transmission with *A. albopictus* and *A. aegypti* being the cause of epidemic outbreaks (Singh and Unni, 2011).

The infection lasts 7 days and usually rapidly triggers the innate immune response (mostly the type I interferon response) (Carpentier and Morrison, 2018). Yet, in some cases, it can evolve in a chronic infection that can last for months. CHIKV RNA was detected in macrophages up to 55 days after infection (Labadie et al., 2010). Alphaviruses have a large range of symptoms due to their tropism infecting fibroblasts (dermal and synovial joints), keratinocytes, endothelial cells, osteoblasts, neurons and macrophages (Suhrbier, 2019). This

leads to the appearance of clinical symptoms in the acute phase: rash, fever, joint and muscle pains and in some cases, a deficiency in the central nervous system and encephalitis (Suhrbier et al., 2012). Alphavirus infections are usually considered as mild with a complete recovery. Mortality is rarely observed, even during the 2004-2011 Chikungunya pandemics and is most often associated with older age or comorbidities (Tandale et al., 2009).

Currently, no vaccine is approved by the FDA but they are under development. The most promising is the live-attenuated VLA1553 against Chikungunya (Roques et al., 2022). The only way to manage infections is by the use of symptoms-related drugs like paracetamol, anti-pyretics and analgesics (WHO, 2023a).

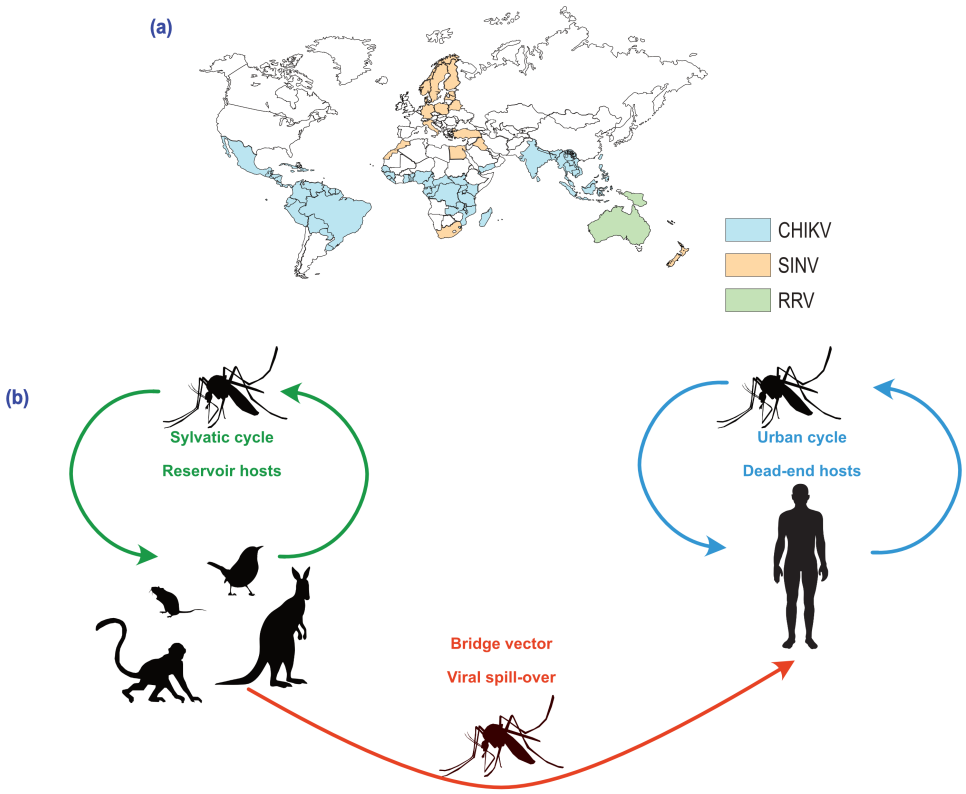

Figure 19 – Worldwide repartition and transmission cycles of three old world alphaviruses.

(a) Repartition of listed cases of three old world alphaviruses on January 2020 adapted from (Baxter and Heise, 2020). CHIKV, Chikungunya virus; SINV, Sindbis virus; RRV, Ross river virus. (b) Representation of transmission cycles. Alphaviruses are maintained in a sylvatic cycle fueled by mosquito bridge vectors. Spill-over infections occur when mosquitoes bite humans. They can then fuel the urban cycle or come back to wild animals to create a new sylvatic reservoir cycle.

b. New world alphaviruses

These are zoonotic viruses are also called encephalitic viruses due to their neurological-linked symptoms onset. They are mainly composed of Western-, Eastern- and Venezuelan equine encephalomyelitis viruses (WEEV, EEEV and VEEV). They were the first alphavirus isolated from horses in California, Virginia, and New Jersey and from a child in Venezuela in the 1930s. They were then found in mosquitoes and in bats. VEEV was detected in a vampire bat in Mexico in 1970 and EEEV was detected last year in neotropical *Myotis* species, raising the concerns that bats could act as viral amplifiers (Correa-Giron et al., 1972; Moreira Marrero et al., 2022) **(Figure 20a)**.

As their name indicates, they are present in Americas: EEEV is found in Eastern North America and Caribbean Seas, VEEV in Mexico and Northern Southern America, WEEV in Canada, Central America and Western and Central United States (Guzmán-Terán et al., 2020) **(Figure 20b)**. Mostly transmitted by mosquitoes from *Culex* and *Culiseta* species (Zacks and Paessler, 2010), they are rarely mortal in humans but EEEV can cause death in up to 90% of infected.

The associated symptoms are flu-like, WEEV and EEEV infections cause fever, headache, muscle pain and malaise. In few cases, this can lead to encephalitis or encephalomyelitis due to hemorrhages in the basal ganglia and thalamus (Reeves et al., 1958) (Deresiewicz et al., 1997). VEEV is the only one that can be transmitted via aerosol causing several laboratory accidents, it is less prone to cause encephalitis in humans and cause flu-like symptoms but can often be associated with neurological sequelae in humans (Johnson and Martin, 1974). After infection, encephalitic viruses replicate in the lymphoid tissues and then reach the central nervous system, through the olfactory pathway. Viral particles can cross and even breach the blood-brain barrier at later infection times (Schäfer et al., 2011). Studies showed that the neuronal axis was the main route for central nervous system infection for VEEV and WEEV (Phillips et al., 2016).

There are currently no FDA-approved vaccines even though the US army developed a live-attenuated vaccine in the sixties and later a formalin-inactivated vaccine to immunize horses and protect laboratory and military personnel from VEEV (Cieslak et al., 2000; Pittman et al., 1996). However, due to their short-term efficiency and high level of secondary effects,

efforts are now focused on the development of new vaccines based on viral vector or DNA strategies (Stromberg et al., 2020).

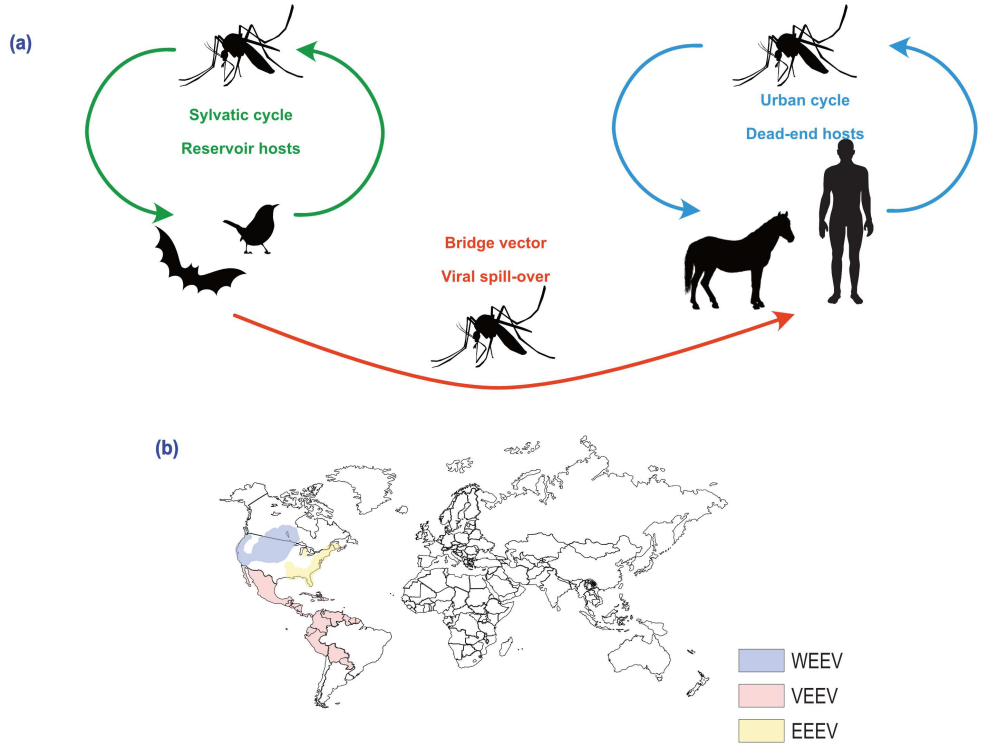

Figure 20 – Transmission cycles and worldwide repartition of three new world alphaviruses.

(a) Representation of transmission cycles of new world alphaviruses. Alphaviruses are maintained in a sylvatic cycle fueled by mosquito bridge vectors. Spill-over can occur through transmission to humans and horses. For horses, this is often fatal. Once in urban areas, mosquitoes can fuel the urban cycle or come back to wild animals to create a new sylvatic reservoir cycle. (b) Repartition of listed cases of three New World Alphaviruses on January 2020 adapted from (Baxter and Heise, 2020). WEEV, Western equine encephalomyelitis virus; VEEV, Venezuelan equine encephalomyelitis virus; EEEV, WEEV, Eastern equine encephalomyelitis virus.

3. Sindbis and Semliki viruses

Sindbis virus (SINV) was isolated from *Culex* mosquitoes in 1952 in the village of Sindbis near Cairo (Laine et al., 2004). The first human cases were observed in 1961 in Uganda ("Facts about Sindbis fever," ECDC, Europa 2017). SINV is widespread and was detected for the first time in

Europe in ticks in Italy in 1975 (Gresíková et al., 1978). Few years later, it was isolated from Russian and Norwegian mosquitoes leading to the conclusion that at least 3 SINV strains emerged from Europe, Middle East and Africa (Norder et al., 1996). SINV strains are phylogenetically closer to New World alphaviruses (Powers et al., 2001). Birds (fieldfare, redwing, capercaillie) are the main reservoir host and spill-over to other vertebrate hosts, mainly in Northern Europe, is mediated by *Aedes, Culiseta* and *Culex* mosquitoes (Brummer-Korvenkontio et al., 2002).

SINV is linked to three diseases described by their symptoms linked to rash, fever and arthritis: Ockelbo disease (Sweden), Pogosta disease (Finland) and Karelian fever (Russia), but these symptoms are usually mild compared to other alphaviruses (Laine et al., 2004). In some cases, it can also cause muscle pain and headache. In general, most infections are asymptomatic and no fatal infections were reported by ECDC ("Facts about Sindbis fever," 2017).

Semliki Forest virus (SFV) is another old world alphavirus, mainly found in Africa and transmitted by mosquitoes. SFV was first isolated from *Aedes abnormalis* mosquito in the Semliki forest in Uganda in 1942 (Smithburn and Haddow, 1944). SFV is considered as mildly pathogenic in humans causing fever, myalgia and arthritis (Mathiot et al., 1990). However, neurological related symptoms are close to the one observed with New World alphaviruses. SFV causes specifical neurological symptoms reaching oligodendrocytes and is mostly studied in encephalitis models in mice (Baxter and Heise, 2020). SFV is related to the same clinical onset as the other arthritogenic alphaviruses.

4. Structure, viral genome and viral cycle

a. Structure and genome

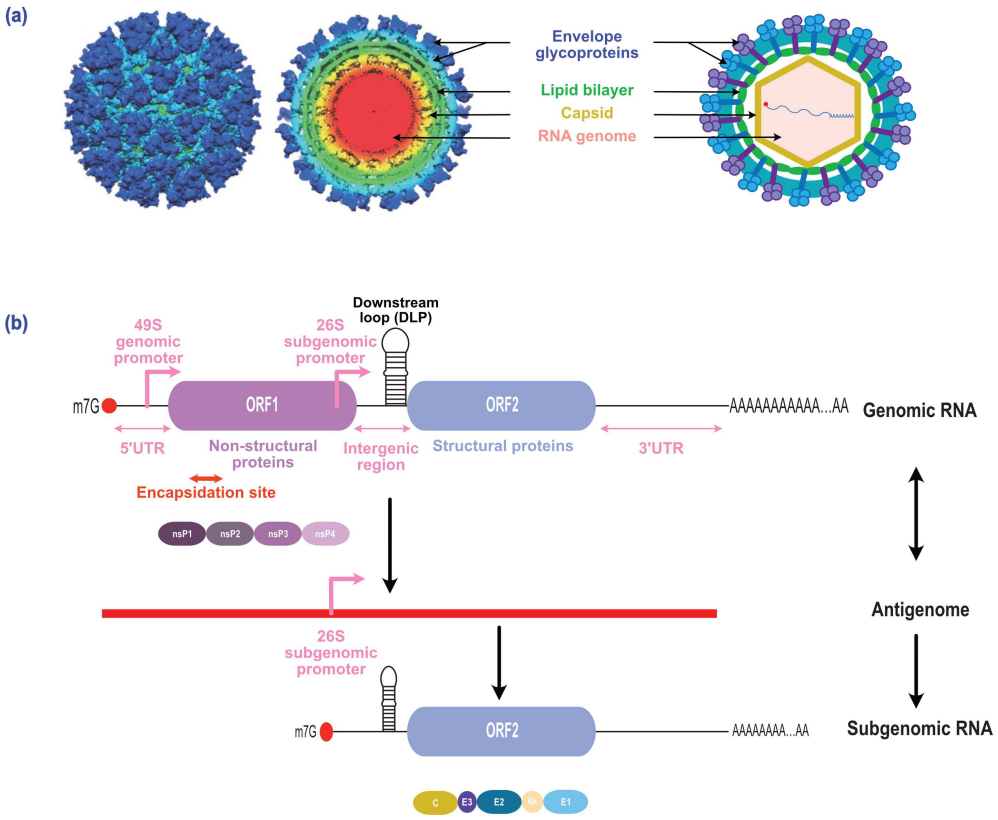

Figure 21 – Particle and genome structure of SINV.

(a) SINV particle structure as determined by Cryo-EM. The enveloped spherical particle is composed from outside to inside of envelope glycoproteins (blue), lipid bilayer coming from host cells (green), capsid (yellow) and the RNA genome (red). (b) The +ssRNA genome of about 11 kb capped is polyadenylated and encodes two ORFs (open reading frames) surrounded by a 5' and 3'UTR (untranslated region) and separated by an intergenic region. The genomic 49S RNA is translated into the non-structural proteins from the ORF1 and replicated into a negative antigenome from which the 26S subgenomic promoter allows the expression of the structural proteins from the ORF2. Although it is capped, ORF2 translation is cap-independent thanks to the DLP (downstream loop). nsP2 is a protease, nsP1 the capping enzyme and nsP4 the RNA-dependent RNA polymerase. m7G, 7-methylguanosine; nsP1 to 4, non-structural proteins 1 to 4; C, capsid; E1 to E3, envelope protein 1 to 3.

The family name "*Togaviridae*" came from the particular morphology of the particle observed in electron microscopy and that looks like a Roman cloak ("*toga*" in Latin). They are enveloped spherical viruses with 240 capsid monomers forming a T=4 icosahedral symmetry. The virion is about 60-70nm in diameter and composed of the structural proteins protecting the 10 to 12kb genomic RNA in the capsid **(Figure 21a)**. The envelope is composed of E1/E2 glycoproteins heterodimers organized in trimers and a host-derived lipid bilayer membrane (Strauss and Strauss, 1994).

The genome is composed of two open reading frames (ORFs) and 3 untranslated elements: 5' and 3'-untranslated regions (UTR) and an intergenic element **(Figure 21b)**. The genome is polyadenylated and capped 5' with a type 0 cap (N7mGpp) by the viral non-structural protein nsP1. Overall, alphaviruses genomic RNA looks like a cellular messenger RNA allowing its rapid translation after cell entry (Strauss and Strauss, 1994). The 5'UTR ranges from 27 to 85nt and is structurally essential for the replication as it contains the promoter, translation and evasion from the innate immune response (Hyde et al., 2015). The 3'UTR, 87 to 723nt-long, is also essential for replication as the replication of the positive strand 3'UTR uncovers a promoter element in the generated minus strand. 5' and 3' UTR are also interacting together to initiate replication and promoter elements for the positive and minus strand are different (Frolov et al., 2001). Replication is also enhanced by two stem-loop structures in the nsP1 coding region (Frolov et al., 2001). Between the two ORFs stands another stem-loop structure called the downstream loop (DLP) essential to escape the host translational shutoff and which allows the translation of the second ORF (Ventoso et al., 2006). Chikungunya virus presents a specific 3'UTR including a succession of direct repeats with lineage-specificities and may be due to a fitness adaptation allowing a better replication in mosquitoes cells and increasing its host range (Chen et al., 2013).

The first ORF encodes the non-structural proteins nsP1 to nsP4, which form the replication complex early in the infection cycle **(Figure 21b)**. The second ORF, translated later after the first rounds of replication, includes the structural proteins, the capsid, the envelope glycoproteins E1 to E3 and the 6k protein, which is essential for the formation of functional viral particle. The second ORF is translated from the 26S subgenomic RNA in a capped-independent manner. The DLP structure (as IRES for other viruses) directly binds the 40S ribosomal subunit to start translation **(Figure 21b)**. Interestingly, there is no identical PKR-

dependent translation shut-off in invertebrate cells, making this DLP dispensable for SINV replication in insect cells. This supports an evolutionary pressure on DLP selection in alphaviruses genome to overcome the translational shut-off, allowing them to infect vertebrate cells (Ventoso, 2012).

b. Virus attachment and entry

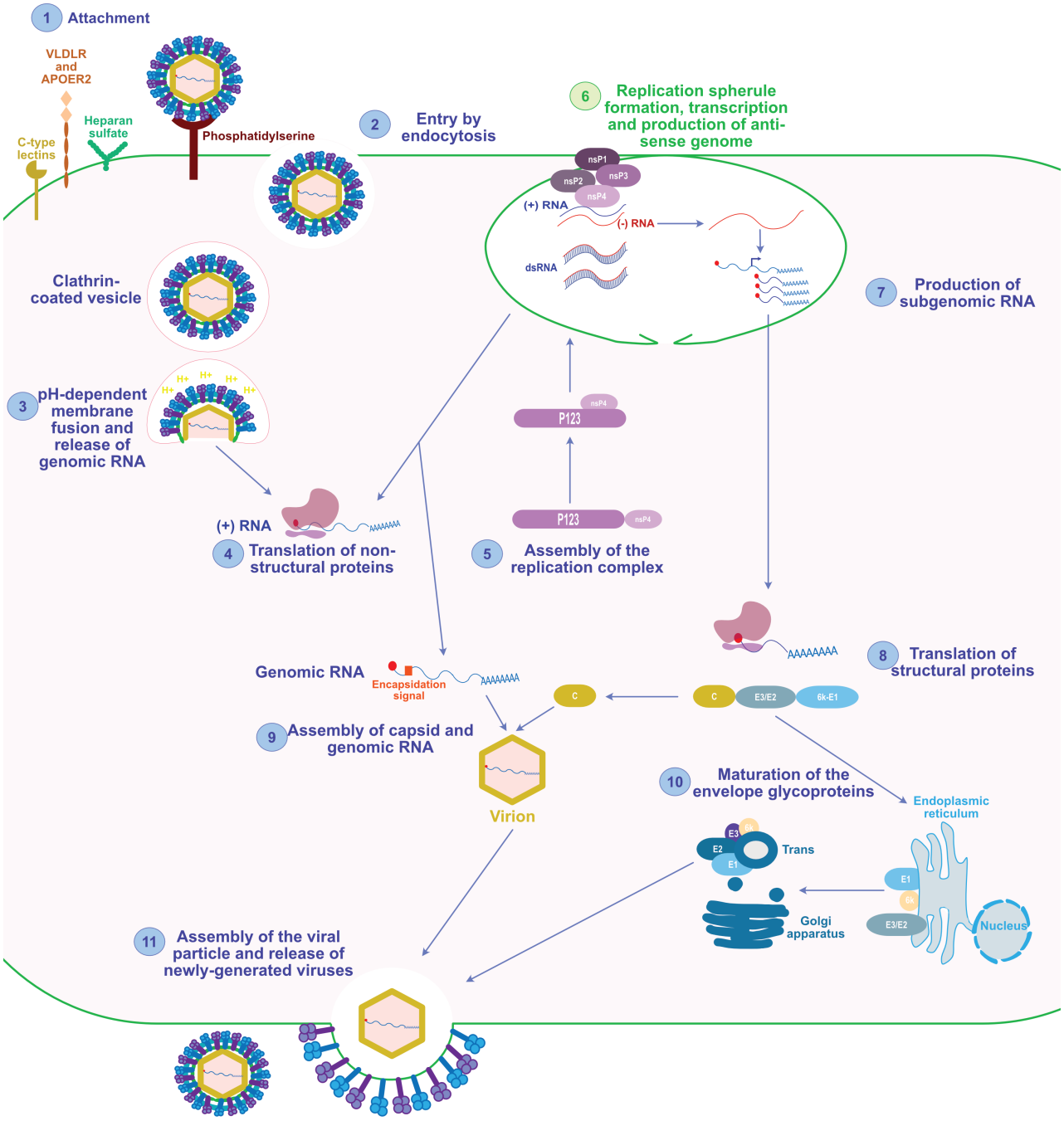

Figure 22 – Alphaviruses infection cycle.

The first step is the binding of the viral particle via the E1/E2 glycoproteins to its receptors: C-type lectins, VLDLR, APOER2, Heparan sulfate or phosphatidylserine (1). The viral particle enters via clathrin-dependent endocytosis and its genome is released in the cytosol after an acidification-dependent fusion of the viral and the vesicle membranes (2 and 3). Once in the cytosol the genomic RNA is directly translated to produce the non-structural proteins further proteolytically matured by nsP2 (4). The assembled replication complex migrates to the cell membrane forming a replication spherule where genome, antigenome and subgenome are produced (5 and 6). The antigenome unveils the subgenomic promoter allowing the production of the structural proteins in a cap-independent way (7 and 8). Capsid proteins associate with the genomic RNA via the encapsidation site in the nsp1-nsP2 sequence (9). Meanwhile, the glycoproteins and the 6k/TF protein are further matured and modified via the endoplasmic reticulum-Golgi apparatus pathway to reach the host membrane where they assemble (10). The nucleocapsid reaches the neo-envelope and buds out of the host cell (11).

The search for a specific alphaviruses receptor in vertebrate cells is a complex endeavor since alphaviruses infect a large range of hosts and cell types. A family of receptors found in both mammals and mosquitoes was shown to be involved in SFV entry partially explaining the adaptation to the different hosts. Indeed, the very low-density lipoprotein receptor (VLDR) and apolipoprotein E receptor 2 (ApoER2) can interact with the dimers E1/E2 from the envelope of SFV, SINV and EEEV allowing their internalization **(Figure 22 – 1)**. Their insect and worm orthologs are also functional for viral entry (Clark et al., 2022). Other vertebrate specific cellular receptors were also discovered, explaining the cell type range of alphaviruses. The most common is the heparan sulfate, a glycosaminoglycan interacting with E1/E2 upon Chikungunya, SINV or EEEV infection (Byrnes and Griffin, 1998; Gardner et al., 2011; Silva et al., 2014). Mutating the heparan binding site in the E1/E2 of EEEV restrains its cell tropism (Gardner et al., 2011). However, for instance upon SINV infection, heparan sulfate depletion was not sufficient to completely block the entry highlighting the existence of other receptors (Byrnes and Griffin, 1998). Another glycan-containing broad receptor is the C-type lectin, of which DC-SIGN (dendritic cell-specific intercellular adhesion molecule-3-grabbing non-integrin) and L-SIGN (liver/lymph node-specific intracellular adhesion molecule-3-grabbing non-integrin) are known as entry receptors for SINV and are preferred by viruses produced in arthropod vectors (Klimstra et al., 2003) **(Figure 22 – 1)**. Phosphatidylserine receptors, such as TIM-1, are also suspected to play a role in alphaviruses entry and promote attachment but

this seems to be cell-dependent (Kirui et al., 2021). Other receptors are suspected to participate in alphaviruses attachment to mammalian cells: the laminin receptor or NRAMP2 for SINV, CD147 for Chikungunya, class I major histocompatibility complex (MHC-I) for SFV or MXRA8 that is common for many arthritogenic alphaviruses (reviewed in (Kim and Diamond, 2022)).

The viral particle enters the cell *via* clathrin-dependent endocytosis **(Figure 22 – 2)**. The lower endosomal pH allows the disruption of E1 and E2 interaction, uncovering the E1 fusogenic activity. E1 induces the fusion of the viral and host membranes, freeing the nucleocapsid in the cytosol (Leung et al., 2011) **(Figure 22 – 3 and 4)**. The nucleocapsid interacts with the ribosomes to be disassembled revealing the genomic RNA.

c. Non-structural proteins production

Translation of ORF1 into polyproteins nsP123 or nsP1234 happens from the genomic RNA in a cap-dependent manner**(Figure 22 – 4)**. The expression of nsP4 depends on the readthrough of an opal STOP codon and thus, it accumulates to lower levels than the other nsPs (Myles et al., 2006; Strauss et al., 1983). The polyprotein then, undergoes a self-proteolytic cleavage led by nsP2 on nsP4 first **(Figure 22 – 5)**. nsP4 in complex with the polyprotein P123 is then able to initiate the replication of genomic RNA through the synthesis of a negative strand. nsP1 is then cleaved from the polyprotein forming a complex nsP1-nsP23-nsP4 switching the replication to positive-sense RNA. Finally, at a later stage, nsP2 and nsP3 are cleaved apart and the whole replication complex is formed of individual nsPs (Utt et al., 2014). All the replication cycle takes place in the cytosol, mainly at the cellular membrane where structural rearrangement allow the formation of replication spherules connected to the cytoplasm by a bottleneck structure (Pietilä et al., 2018) **(Figure 22 – 6)**. Upon replication, a highly immunogenic double-stranded RNA intermediate is formed and is hidden in these complexes to limit triggering of the immune response **(Figure 22 – 6)**.

The nsP1 protein is constituted of a methyltransferase and guanylyltransferase domain that directs the addition of the methyl-7-guanine at the 5’ extremity of newly generated genomic and subgenomic RNAs (Ahola and Karlin, 2015). Right after this domain, there is an

amphipathic helix and a palmitoylation motif that confer a membrane-anchoring function to nsP1 (Laakkonen et al., 1996; Lampio et al., 2000). nsP1 is also necessary for the minus strand synthesis although its precise mode of action is not fully understood yet (Lulla et al., 2006).

The nsP2 protein is composed of two domains that are essential for alphaviruses replication. At the N-terminal part, is the NTPase/RNA triphosphatase domain (RTPase) carrying a helicase function that unwinds RNA structures formed upon replication (Gomez de Cedrón et al., 1999). The RTPase activity is essential to remove the γ-phosphate at the 5' extremities of newly synthetized genomic and subgenomic RNAs, and allow nsP1-mediated capping (Vasiljeva et al., 2000). The C-terminal part of nsP2 is a protease domain that acts in *cis* and in *trans* on the non-structural polyprotein (Lulla et al., 2006). Early in the infection nsP2 preferentially acts in *cis* whereas upon increased concentrations of nsP2 in the cytosol, it can act in *trans* (de Groot et al., 1990). Finally, nsP2 is also associated with an increased subgenomic RNA synthesis by directly binding to the subgenomic promoter (Suopanki et al., 1998).

The nsP3 protein is composed of three domains: the macrodomain, the alphaviruses unique domain (AUD) and the hypervariable domain (HVD). nsP3 is essential for RNA synthesis, more precisely for the minus-strand and subgenome synthesis (LaStarza et al., 1994). The AUD domain, an ADP-ribosylhydrolase enzyme, is also essential for structural protein expression (Gao et al., 2019). Besides, the HVD is associated with the formation of replication complex at the host membrane favored by the direct interaction between G3BP proteins from stress granules and the HVD. It is also true for their insect-homolog *Rasputin* that acts in the same way with nsP3, conveying another adaptation to cover a large host spectrum (Fros et al., 2015, 2012).

The nsP4 protein carries the RNA-dependent RNA polymerase activity (Hahn et al., 1989). The construction of chimeras between nsP4 proteins in alphaviruses allowed to highlight its importance in template selectivity (Lello et al., 2021).

d. Viral particles formation and release

The synthesis of the minus-strand RNA uncovers the subgenomic promoter, composed of 19nt upstream and 2nt downstream the beginning of the 26S subgenomic RNA (Levis et al., 1990; Miller and Koev, 2000) **(Figure 22 – 7)**. This subgenomic RNA is translated into the structural polyprotein composed of the capsid, the 6k and TF proteins and the E1-E2-E3 glycoproteins **(Figure 22 – 8)**.

The capsid protein thanks to its serine protease activity is the first cleaved from the polyprotein. After its release, the capsid directly interacts with the 49S genomic RNA, more precisely on the encapsidation site overlapping the nsP1 and nsP2 sequences, to form nucleocapsid particles (Kim et al., 2011) **(Figure 22 – 9)**. A recent study uncovered multiple binding sites on the genomic RNA, which increase the packaging selectivity (R. S. Brown et al., 2020).

After its production, the structural polyprotein goes to the endoplasmic reticulum thanks to the signal peptide located in E3 **(Figure 22 – 10)**. Cellular signalases cleave out the 6k protein, E1 and the precursor E2/E3 (Garoff et al., 1978). The glycoproteins then follow the endoplasmic reticulum/Golgi apparatus pathway to be glycosylated and palmitoylated (Ryan et al., 1998). E1 and E2/E3 precursor heterodimerize and E2 is cleaved out by the furin protease in the *trans*-Golgi (Zhang et al., 2003). The glycoproteins complex is finally embedded in the host cell membrane thanks to a transmembrane helix in E2 and E1 (Strauss and Strauss, 1994). E2 interacts directly with the nucleocapsid with its C-terminal part and with the host receptors thanks to its N-terminal domain (Byrnes and Griffin, 1998; Lopez et al., 1994). Heterodimers assemble into a spike-like structure with the help of E3 (Lobigs et al., 1990). E3 is also responsible for the spike transport to the cell membrane (Parrott et al., 2009). Lastly, the 6k gene encodes two different proteins thanks to a ribosomal frameshift: the 6k protein and the transframe protein (TF) (Firth et al., 2008). The 6k protein is essential for E1 translocation in the endoplasmic reticulum. If TF is translated, no E1 glycoprotein is produced (Firth et al., 2008). TF may function as a virulence factor and 6k as a viroporin allowing the viral release (Dey et al., 2019; Ramsey and Mukhopadhyay, 2017). TF protein is incorporated into viral particles and has been described to antagonize the IFN-I response (Rogers et al., 2020).

The 6k protein also helps particle assembly by mediating interactions between E2 and the capsid and enhancing budding (Gaedigk-Nitschko and Schlesinger, 1991). Once the glycoproteins are embedded in the membrane, the released viral particle is coated by the surrounding membrane-derived lipids to form the envelope **(Figure 22 – 11)**.

5. Alphavirus and immune response

SINV, SFV and Chikungunya viruses are often used to study the innate immune response in human cells in particular the suppression of type I interferon response and host cell translational shut-off (Breakwell et al., 2007; Carpentier and Morrison, 2018; Fros and Pijlman, 2016; Sanz et al., 2015). Studies on IFNAR1-deficient mice highlighted that type I interferon response is the main immune response against alphaviruses (Ryman et al., 2000). Innate sensing occurs through different sensors such as TLR3, which was proposed to restrict Chikungunya infection in mice (Her et al., 2015). However, this is not the case for SINV since TLR3-deficient mice do not show exacerbated neurological inflammation upon infection (Esen et al., 2012). RLRs are also key immune sensors of alphaviruses infection. Both RIG-I and MDA5 are acting in this recognition within the first hours of infection (Akhrymuk et al., 2016). Using non cytopathic mutants of VEEV and SINV, it was shown that type I interferon is induced in NIH 3T3 cells and that at least one of the RLRs is sufficient to mount an efficient immune response, which worked better if both of them are functional. Surprisingly, CHIKV and SFV are less sensitive to RLR detection than VEEV and SINV, showing once again differences in the same genus (Akhrymuk et al., 2016). MAVS-deficient NIH 3T3 cells are unable to mount an efficient IFN-I response against CHIKV (Schilte et al., 2010). Alphavirus pathogenesis is also influenced by the activation of NOD-like receptors (NLRs) that are less studied but seem to be proviral. Indeed, patients infected by CHIKV expressed elevated levels of NLRP3 and pro-inflammatory cytokines in blood, and these were shown to be proviral in a mouse model (Chen et al., 2017).

Few ISGs have been characterized upon alphaviruses infection. Infection of mouse and human primary fibroblasts by SINV, SFV and CHIKV activates PKR (Barry et al., 2009; Ventoso et al., 2006; White et al., 2011) **(Figure 23a)**. In the case of CHIKV, this is also accompanied by

the blocking or IRF3-mediated transcriptional response (White et al., 2011) **(Figure 23a)**. However, PKR activation does not necessarily result in the decrease of viral load since no drop of infectivity was detected upon SINV and SFV infection in PKR-deficient mice (Barry et al., 2009). This can be explained by the presence of the downstream loop (DLP) at the beginning of the 26S subgenomic mRNA, which allows the translation of structural proteins in an eIF2α-independent manner (Ventoso et al., 2006) **(Figure 23a)**. Interestingly, another eIF2α-kinase, GCN2, normally activated by amino-acid deprivation, is also activated by alphaviruses infection (Berlanga et al., 2006). GCN2 recognizes a bipartite sequence at the beginning of SINV genomic RNA, overlapping the encapsidation signal. As a result GCN2-deficient mouse fibroblasts are more susceptible to SINV infection (Berlanga et al., 2006).

The RNaseL pathway was also showed to be involved in the immune response. RNaseL and OAS genes are ISGs that act against SINV **(Figure 23b)**. OAS3 overexpression in Hela cells blocks SINV and SFV replication in an RNaseL-independent manner (Bréhin et al., 2009). Nevertheless, this cannot be generalized since in A549 cells, OAS3, but not OAS1 or 2, is essential for RNaseL activation upon SINV infection (Bréhin et al., 2009; Yize Li et al., 2016). In addition, RNaseL activity was involved in SINV genome cleavage in HEK293 and Vero cells (Girardi et al., 2013)**(Figure 23b)**.

Interferon-stimulated gene 15 (ISG15), a ubiquitin homolog, also plays a key role in alphaviruses immunity. ISG15-deficient mouse are more susceptible to SINV (Lenschow et al., 2007). Its action mechanism is not completely understood but seems to be independent from its ubiquitin-like activity. Indeed, in mice lacking the ISG15 E1 ubiquitin enzyme, UbE1L, there is no dramatic increase in CHIKV infection. Conversely, in the absence of ISG15, CHIKV-infected mice show an enhanced inflammatory response, pointing out a non-canonical role for ISG15 in immunomodulation (Werneke et al., 2011).

The role of Dicer in the antiviral response against alphaviruses has also been studied. Virus-derived siRNAs produced by Dicer have been detected in somatic cells infected with SINV **(Figure 23c)**. This was reverted by the ectopic expression of the viral suppressor of RNAi (VSR), B2, or of the RLR LGP2 (Y. Zhang et al., 2021). Conversely, other studies of SINV-infected HEK293 cells, could not find evidence of vsiRNAs accumulation, in contrast with an antiviral role of RNAi (Donaszi-Ivanov et al., 2013; Girardi et al., 2013) **(Figure 23c)**. The fact that

HEK293 Dicer-deficient human cells do not show an increased infection by SINV and VEEV reinforces this hypothesis (Bogerd et al., 2014) **(Figure 23c)**. Finally, another Dicer product can participate in the modulation of infection: miRNAs have been shown to be key players by either controlling cellular gene expression or directly the viral genome (reviewed in (Girardi et al., 2018)). Indeed, a high-throughput screen showed that the neuronal cellular miRNA, miR-124, can increase SINV and CHIKV replication in human somatic cells (López et al., 2020) **(Figure 23c)**.

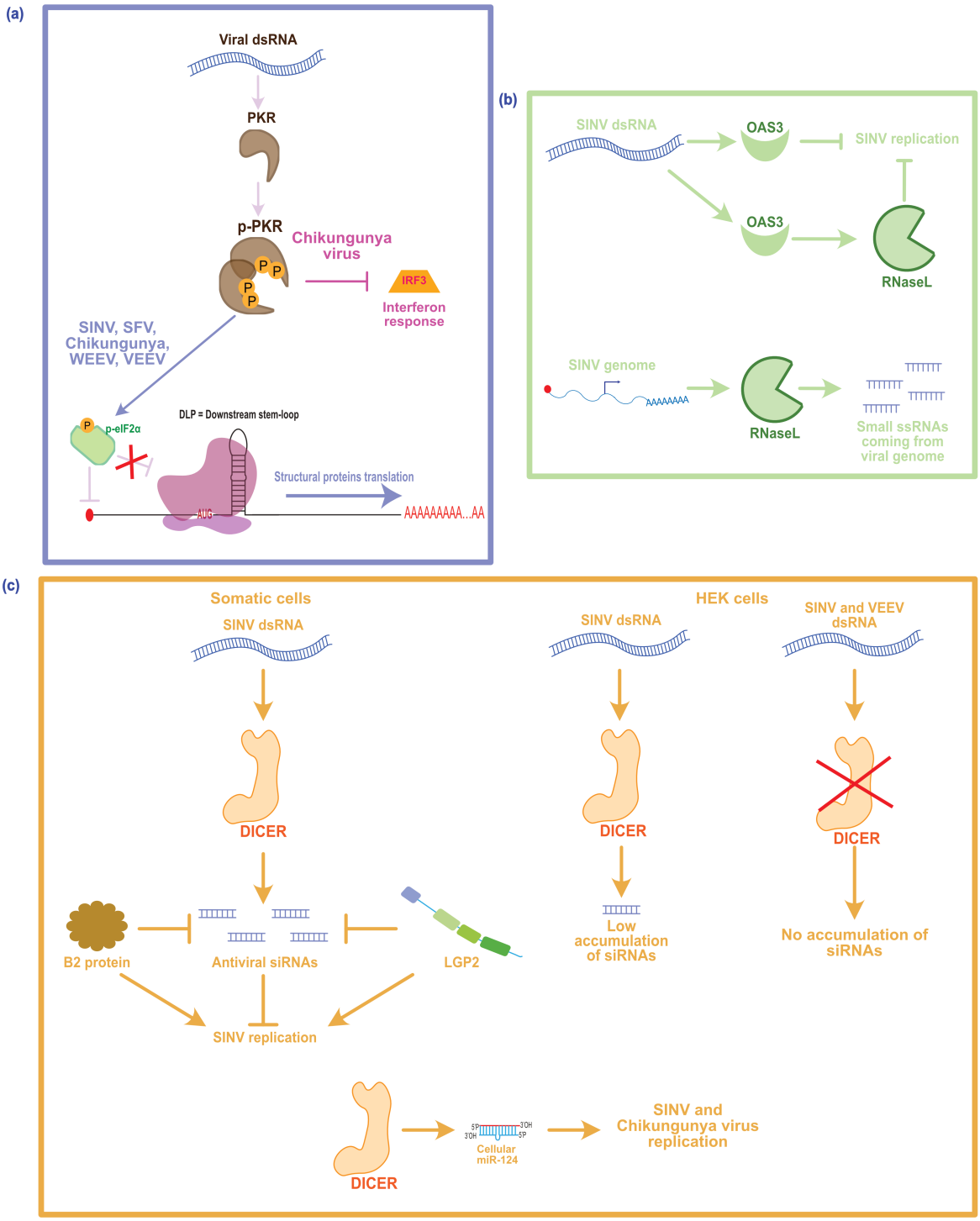

Figure 23 – Immune response to alphaviruses.

(a) Alphaviruses dsRNA is the main PAMP recognized by immune sensors. Hence, viral dsRNA is recognized by PKR that is then activated to block the cap-dependent translation, which is bypassed by the DLP (downstream loop). In addition, CHIKV diverts the activated PKR to block the IRF3-transcriptional induction, thereby dampening the immune response. (b) SINV dsRNA is recognized by OAS3 that can directly block SINV replication or activate RNaseL to block the infection. Upon SINV infection, RNaseL cleaves the viral RNA into small RNAs participating in

the antiviral defense. (c) In some reports, Dicer can recognize and cleave SINV dsRNA into small interfering RNAs (siRNAs) duplexes in somatic cells. Conversely, in HEK293T cells, Dicer cannot produce siRNAs. Accordingly, the absence of Dicer has no effect on SINV replication. However, SINV can hijack cellular miRNAs such as miR-124 to promote its replication.

6. Suppression of the immune response by alphaviruses

Several alphaviruses proteins have been shown to counteract the immune response by different mechanisms.

a. nsP1

SINV genome includes neurovirulence determinants that are located in nsP1 sequence (Suthar et al., 2005). Interestingly, one particular residue in this position is involved in the regulation of IFN-I. Mutating this residue in SINV (T538I) results in an increased IRF-3 activation. This mechanism is conserved in Ross River virus. The mechanism is not fully understood but it may involve nsP1 role in capping and/or remodeling viral RNA structure, mostly of the 26S subgenomic RNA (Cruz et al., 2010) **(Figure 24a)**. Another nsP1 antagonist function is linked to its palmitoylation modification. Indeed, upon CHIKV infection, nsP1 is interacting with STING blocking signal transduction and allowing nsP1 stabilization and palmitoylation (Webb et al., 2020) **(Figure 24a)**. This palmitoylation is also essential for the replication of some alphaviruses such as SFV (Žusinaite et al., 2007).

b. nsP2

The nsP2 protein is the main host response regulator. It directly participates in host transcriptional shut-off for CHIKV, SFV and SINV. Even though it participates mainly in the viral replication complex, a large fraction of nsP2 is found in the nucleus. Suppressing the nuclear localization of SFV nsP2 significantly improved the IFN-I response in mouse cells. This could indicate that the IFN-I suppression activity occurs after nuclear translocation of immune transcription factors (Breakwell et al., 2007). However, CHIKV nsP2 can also act by blocking

STAT1 phosphorylation and nuclear translocation **(Figure 24b)**. This can be reverted by a single point mutation, which restores the JAK-STAT signaling and renders the virus non-cytopathic (Fros et al., 2010). SINV nsP2 is also responsible for degradation of the catalytic sub-unit of the host RNA polymerase II (RPB1), inhibiting the immune transcriptional response **(Figure 24b)**. RPB1 degradation occurs through ubiquitin-linked degradation pathway and requires integrity of SAM-dependent methyltransferase-like domains. This degradation happens at early infection stages (Akhrymuk et al., 2012). Mutations of two key residues in the protease domain of nsP2 abrogates this activity and induce a strong IFNß induction in NIH 3T3 cells (Akhrymuk et al., 2018). This allows the development of non-cytopathic SINV strains. nsP2 protein is also involved in host translational shut-off, decreasing translation of ISGs in a PKR-independent manner (Gorchakov et al., 2004) **(Figure 24b)**. nsP2 antagonist activity needs the viral replication and is linked to the release of nuclear proteins. Lastly, CHIKV nsP2 is involved in the suppression of gene expression linked to the unfolded protein response, based on the activation of the PERK kinase upon infection. This inhibits expression of cellular chaperones, degradation and apoptosis effectors (Fros et al., 2015).

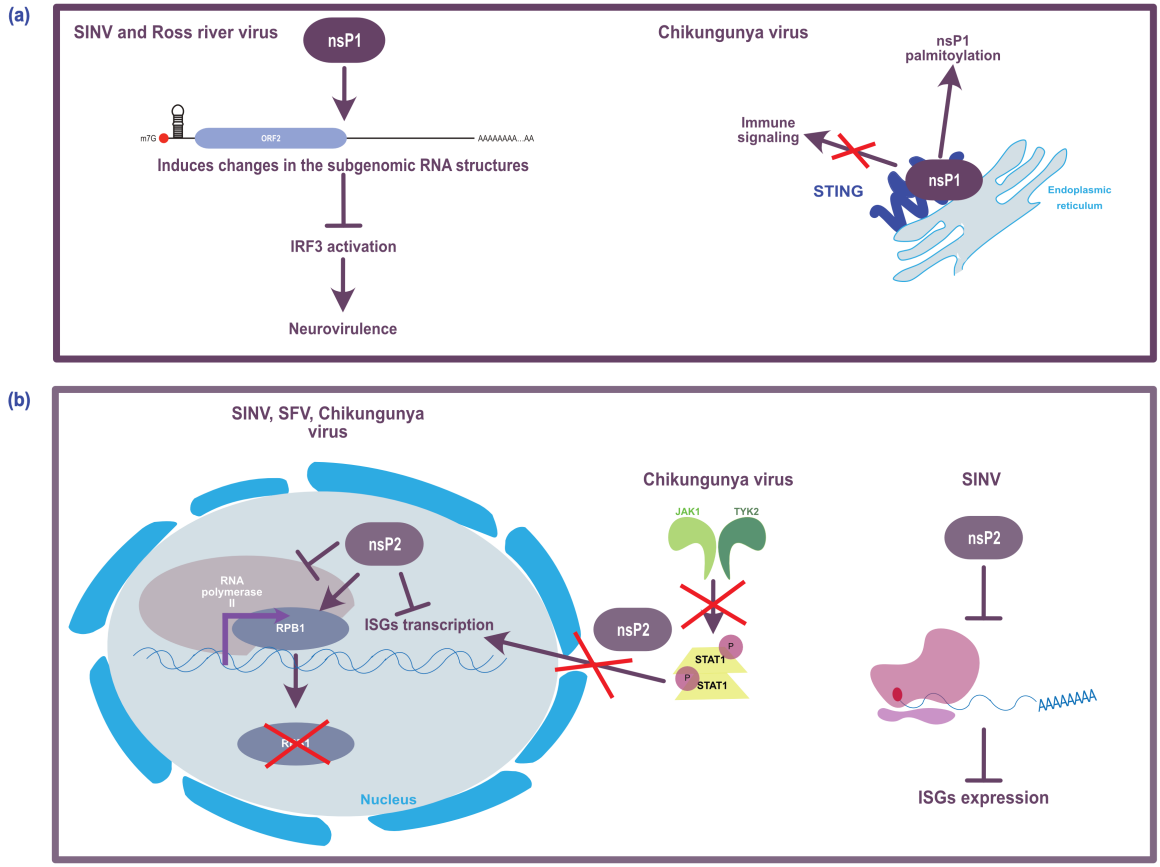

Figure 24 – Alphaviruses nsP1 and nsP2 block the immune response.

(a) nsP1 is a neurovirulent factor able to remodel the subgenomic RNA structure preventing IRF3 activation upon SINV and RRV (Ross river virus) infections. CHIKV nsP1 directly interacts with STING blocking the immune signaling but also allowing a better palmitoylation of nsP1 necessary for its function. (b) nsP2 can block both transcription and translation. Upon SINV, SFV and CHIKV infections, nsP2 induces the degradation of the catalytic RBP1 subunit of the RNA polymerase II blocking ISGs transcription. Besides, CHIKV nsP2 blocks STAT1 phosphorylation and nuclear translocation impeding IFN-I response. SINV nsP2 inhibits translation blocking ISGs expression.

c. nsP3

SINV nsP3 inhibits translation thanks to its mono-ADP-ribosylhydrolase activity (Akhrymuk et al., 2018) **(Figure 25a)**. Besides, nsP3 is considered as an interacting hub for cellular proteins. Hence, nsP3 interacts with G3BP1 protein in human cells (Nowee et al., 2021) **(Figure 25a)**. G3BP1 is a major component of stress granules that are also responsible for translational arrest (White and Lloyd, 2012). Not only stress granules mediate the antiviral response but they also constitute a necessary element for alphaviruses replication (Scholte et al., 2015). These granules are associated with the whole replication complex. It seems also that upon CHIKV infection, nsP3 sequesters G3BP1 from its other cellular partners in non-functional granules, which may prevent its antiviral functions (Fros et al., 2012). Finally, in SINV-infected cells, nsP3 forms membrane-associated complexes around G3BPs, that also contain YBX1, HSC70 and TRBP proteins, favoring viral RNA replication (Gorchakov et al., 2008). Sequestering YBX1 or TRBP may limit their role in the microRNA pathway and favor viral RNA replication since they can bind dsRNA **(Figure 25a)**.

a. Capsid

During the first replication cycle of CHIKV, fibroblasts and immune cells deficient for both cGAS and STING have an increased viral load. Viral capsid was showed to antagonize the cGAS-STING pathway by a rapid autophagy-induced degradation of cGAS leading to cytosolic DNA accumulation **(Figure 25b)**. The capsid protein can also directly block the induction of IFN-I (Webb et al., 2020). In addition, it can also interact with IRAK1 to disrupt its signaling

activity. This interaction happens upon viral entry and is conserved across arthritogenic and encephalitic alphaviruses (Landers et al., 2021). EEEV capsid, similarly to other alphaviruses' nsP2, directly decreases STAT1 expression and is located in the nucleus at early infection stage (Aguilar et al., 2008) **(Figure 25b)**. Apart from disrupting the immune signaling, alphaviruses capsid protein is also able to antagonize direct antiviral effectors. Hence, SFV capsid acts as a VSR by sequestering dsRNA away from Dicer (Qian et al., 2020) **(Figure 25b)**.

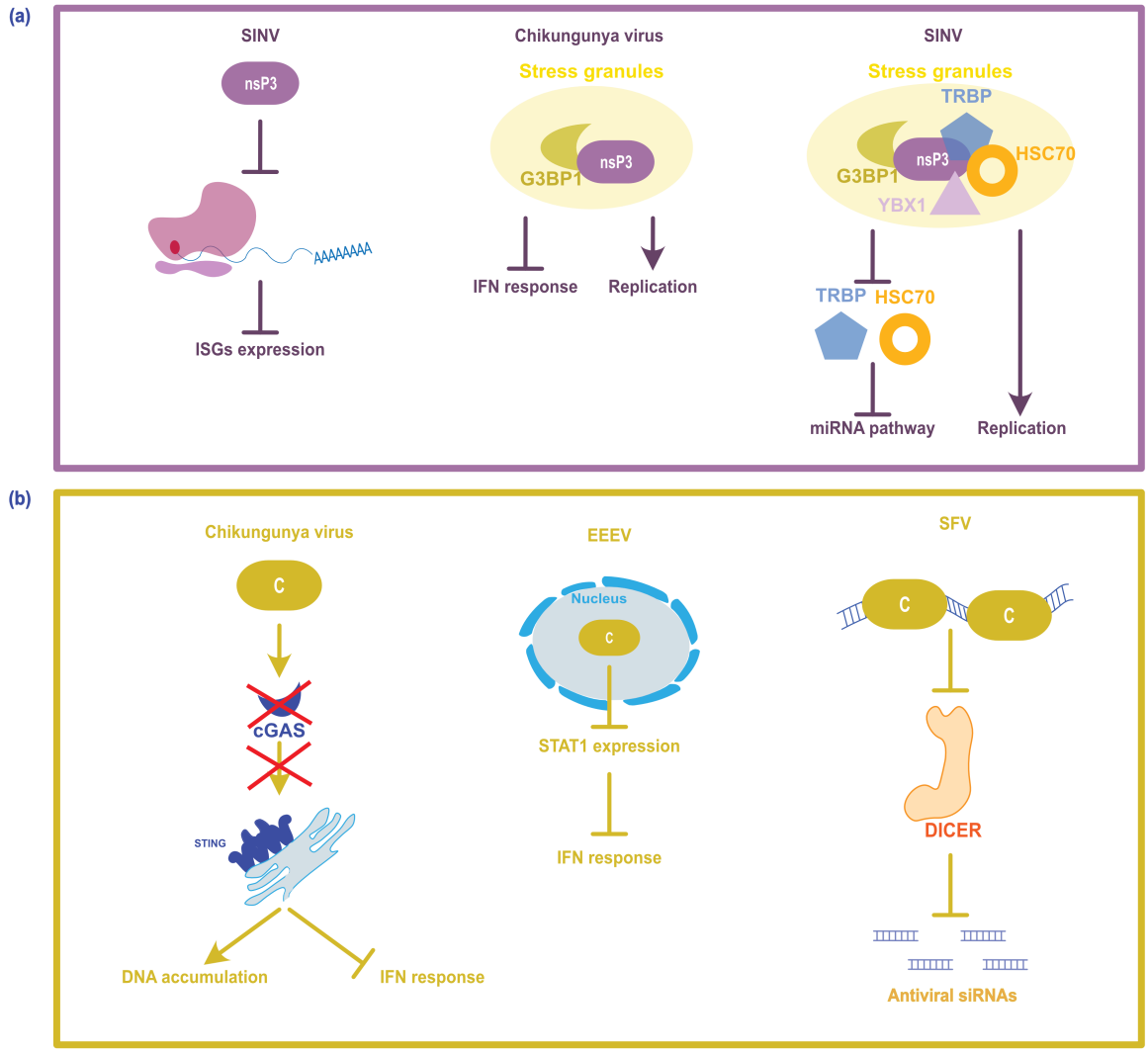

Figure 25 – Alphaviruses nsP3 and capsid proteins antagonize the immune response.

(a) Alphaviruses nsP3 antagonizes translation and is involved in stress granules formation. CHIKV nsP3 drives stress granules formation by interacting with G3BP proteins. However, in this case their formation directly impedes IFN response and promotes viral replication. Likewise, SINV nsP3 forms bigger stress granules containing G3BP proteins but also other unrelated proteins such as YBX1, TRBP or HSC70, which prevent their normal function. (b) The capsid protein is the only structural protein with a major role in IFN antagonism. CHIKV capsid

induces autophagy-mediated degradation of the cytosolic receptor cGAS blocking STING-induction and leading to cytosolic DNA accumulation. EEEV capsid is retrieved in the nucleus where it prevents STAT1 expression. Finally, SFV capsid is described as a VSR as it binds the viral dsRNA impeding Dicer recognition.

B. Enteroviruses

1. History

The enterovirus genus is part of the *Picornaviridae* family, which also includes coxsackieviruses. The genus name comes from the infection route that passes by the gastro-intestinal tract. The first case was reported in New Zealand in 1957 and associated with the hand, foot and mouth disease (HFMD) (Duff, 1968). The virus can be transmitted from person to person via feces or saliva or indirectly by contaminated objects (Omaña-Cepeda et al., 2016). Depending on the serotype, symptoms can range from lung infection to hemorrhagic conjunctivitis and central nervous system failure. Enteroviruses are classified in serotypes and genogroups (A-H). The most frequent enterovirus is the Enterovirus A71 (EV71) named as the 71st detected human serotype. It is a neurotropic virus that affects mainly the brain stem by breaching the blood-brain-barrier or via motor neurons (Ong et al., 2008). EV71-infected patients, mainly children, show aseptic meningitis, rash, HFMD and encephalitis (Nayak et al., 2022). EV71 circulates mostly in Asia, Oceania, Europe and the Americas, causing several epidemics with the first major outbreaks described in 1997 in the Asia-Pacific region (WHO, 2023b). The recent cases were mostly observed in the Asia-Pacific region. Different vaccines passed the phase III of clinical trials and are based on inactivated virus and DNA vaccines focusing mainly on the VP1 protein (Chong et al., 2012). Virus-like particles vaccines are currently under development. Apart from EV71, other enteroviruses are circulating, mainly Enterovirus B and Enterovirus D68 circulating respectively in Africa and North America (D. M. Brown et al., 2020; Nayak et al., 2022).

2. Genomic organization

Enterovirus is a non-enveloped icosahedral T=3 virus with a 20-30nm-diameter size **(Figure 26a)**. The genome is about 7.5kb (Nayak et al., 2022). It is translated in a long polyprotein that can be divided into three parts: P1 for the 4 structural proteins, P2 for 3 non-structural proteins and P3 for 4 non-structural proteins. P2 and P3 form the proteases 2A, 3D and 3C that cleave out the structural proteins **(Figure 26b)**. EV71 capsid is composed of 60 copies of repeated protomers of VP1-2-3-4 and VP1-2-3 are affecting the immune system (Nayak et al., 2022).

The genome is protected by a viral protein VPg at the 5' extremity and is polyadenylated at the 3' **(Figure 26b)**. The 5'UTR bears an IRES for cap-independent translation (Fitzgerald and Semler, 2009). The IRES structure requires specific cellular factors such as the T cell-restricted intracellular antigen 1 (TIA-1) that can also enhance viral replication (Wang et al., 2015).

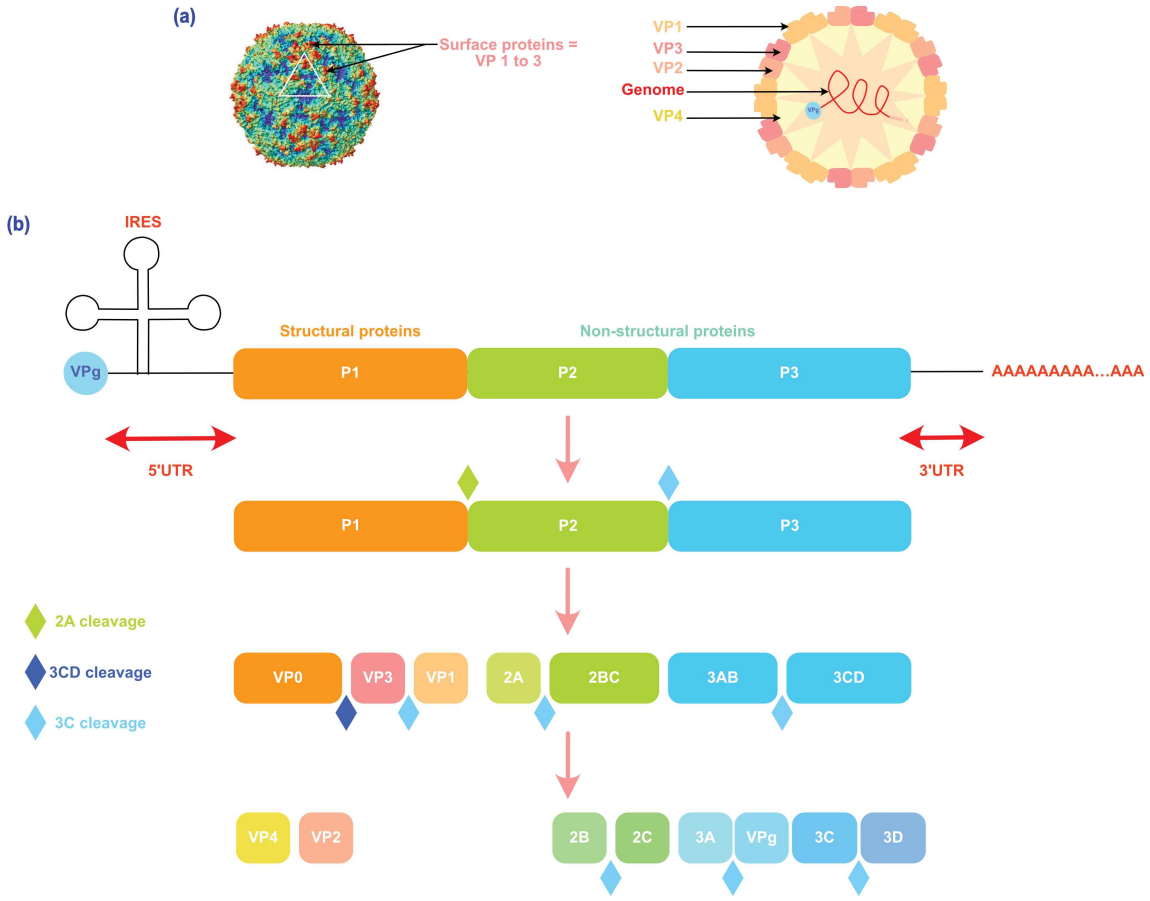

Figure 26 – EV71 viral particle structure and genome organization.

(a) Cryo-EM structure of EV71 at 3Å (adapted from (Baggen et al., 2018)**)**. The non-enveloped icosahedral particle is formed of 3 surface proteins: VP1 (orange), VP2 (light red) and VP3 (pink). VP4 (yellow) constitutes the capsid core protecting the genomic +ssRNA (red). (b) The genomic RNA is protected in 5' by a VPg, polyadenylated and composed of one ORF surrounded by a 5' and a 3'UTR. The translation occurs via an IRES-dependent mechanism. The P1-2-3 polyprotein is cleaved by the viral 2A and 3C proteases. P1 encodes the structural proteins and is further cleaved by the 3CD and 3C proteases into VP0, VP3 and VP1 before a last cleavage to obtain VP4 and VP2. P2 is cleaved twice by the 3C protease to give the 2A, 2B and 2C proteins. P3 is cleaved three times by the 3C protease and gives the 3A, 3C and 3D proteins and the VPg that will bind the 5' extremity of the viral genome.

3. Immune response and viral counter-response

The IFN-I response plays an important role in the immunity against EV71 and directly inhibits EV71 replication (Yi et al., 2011). EV71 is detected by the membrane-associated TLR3, recognizes dsRNA generated upon replication and triggers the IFN-I (Chen et al., 2018). It can also be sensed by TLR7, highly expressed in plasmacytoid dendritic cells, which directly detects the genomic ssRNA and induces the production of pro-inflammatory cytokines via the NF-kB pathway (Luo et al., 2017). Finally, the cytosolic RLR MDA5 is also able to detect dsRNA coming from EV71 replication triggering the MAVS-dependent IFN-I response, especially through the IRF3 activation (Kuo et al., 2013).

EV71 genome expresses two proteases that are directly involved in the suppression of the immune response. Hence, the 2A cysteine protease is involved in the cleavage of MDA5 and MAVS (Feng et al., 2014) and of TLR3 (Chen et al., 2018). 2A also reduces the IFNAR1 receptor protein levels inhibiting the STAT-dependent immune response while IFNß transcription still occurs (Lu et al., 2012). The 3C protease can cleave IRF7 and members of the TAK1/TAB1/TAB2/TAB3 complex involved in the NF-kB response, thereby down-regulating IFN-I transcriptional response(Lei et al., 2014, 2013).

In other cases, the immune evasion is not mediated directly by the viral proteases. Thus, EV71 also induces MDA5 cleavage by the caspase activities (Kuo et al., 2013). Likewise, EV71 blocks the JAK/STAT pathway by inducing the caspase degradation of the karyopherin responsible for the STAT1 nuclear translocation (Wang et al., 2017).

Finally, the non-structural protein 2C can bind to NF-kB/p65 preventing its dimerization with other NF-kB family members and blocking the antiviral response (Du et al., 2015). The 3D polymerase also displays an immune evasion role by interacting with the MDA5 CARDs blocking the MAVS-MDA5 interaction (Kuo et al., 2019).

The IFN-I-induced kinase PKR is rapidly activated during EV71 infection resulting in translational shut-off and stress granules formation, which promotes apoptosis (Zhu et al., 2016). At the same time, PKR can also be degraded by the 3C, which generates a small N-terminal fragment that promotes EV71 replication (Chang et al., 2017).

Dicer can also play a role upon EV71 infection. It has been shown to be involved in antiviral RNAi against EV71 in human cells, and the 3A protein can act as a VSR by sequestering dsRNA (Qiu et al., 2017) **(Figure 27)**. EV71 is also able to affect and hijack cellular miRNA expression. Thus, the expression of miR-146a is transcriptionally increased in infected cells, which results in the down-regulation of IRAK1 and TRAF6. As a result, TLR signaling and the IFN-I response are inhibited and this can be reversed by antisense inhibition of miR-146a (Ho et al., 2014) **(Figure 27)**.

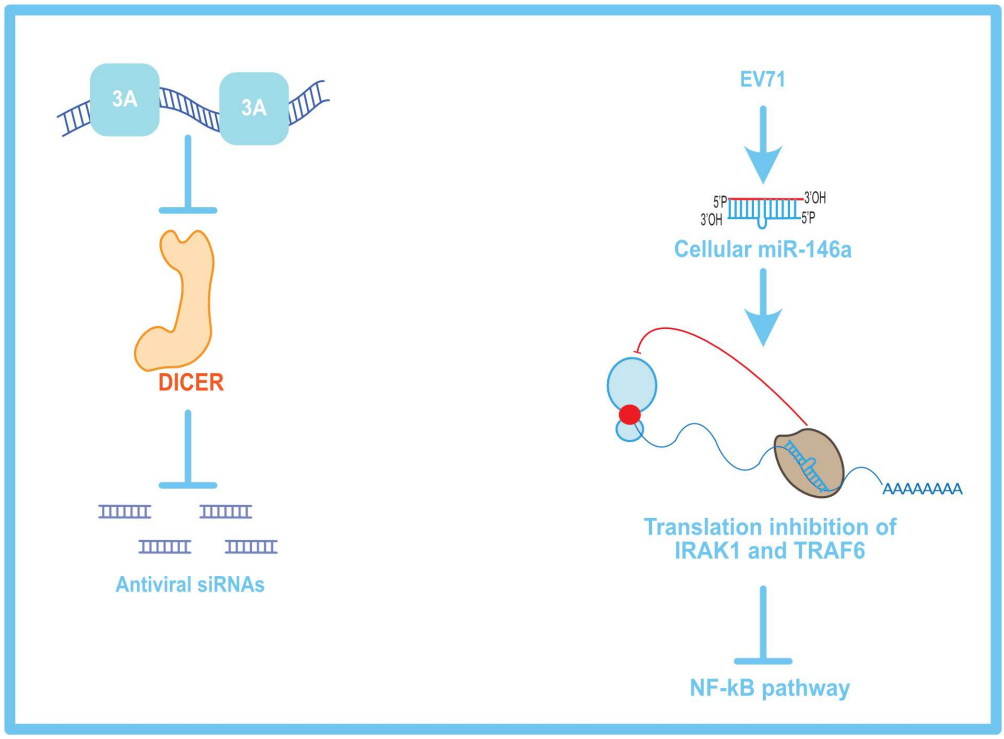

Figure 27 – EV71 and Dicer activity.

(a) Dicer is involved in antiviral RNAi against EV71. The 3A protein acts as a VSR by binding to the viral dsRNA, physically blocking Dicer. (b) EV71 hijacks the miRNA pathway by upregulating the expression of the pri-miR-146a, which targets IRAK1 and TRAF6 involved in the NF-kB triggering pathway.

C. Rhabdoviruses

1. History

Rhabdoviruses family belongs to the *Mononegavirales*, which also contains rabies, Ebola, Nipah and Marburg viruses. The Rhabdoviruses are non-segmented negative ssRNA viruses (-ssRNA) with a broad hosts range: vertebrates, invertebrates, plants, fungi. This family includes two well-studied clades, the lyssaviruses that contain rabies virus and the vesiculoviruses that contains the vesicular stomatitis virus (VSV). VSV is divided into two main serotypes: Indiana (where it was isolated in 1925) and New Jersey (isolated in 1926). The Indiana stain is the one commonly used in laboratories.

The first VSV infection was described in the United States in 1916 in cattle and horses. Nowadays, VSV is almost exclusively retrieved seasonally in the Americas and is enzootic in Central America (Whelan, 2008). VSV does not have a high mortality rate but is linked to animal production loss, with a strong economic impact on the food industry (Rodríguez, 2002). It mostly infects the central nervous system and is transmitted by direct contact, aerosols and arthropod vectors, mostly mosquitoes (*Aedes*), sand flies, black flies and biting midges (Rozo-Lopez et al., 2018; Whelan, 2008). Wild animals such as bats, rodents, bears or coyotes can serve as natural host reservoirs even though the exact transmission cycle is not fully known yet (TESH et al., 1969). Human infections are rare, mainly caused by contact with domesticated animals. The most common symptoms are flu-like and the appearance of vesicular lesions especially in the mouth, the naso-oral mucosa and the coronary bands (Letchworth et al., 1999). One case of viral encephalitis has been described in a child in Panama (Quiroz et al., 1988).

VSV is now used in research for the design of vaccine vectors as its genome is easy to manipulate and its replication rate is high (Bukreyev et al., 2006). Besides, VSV is an oncolytic virus, which can target IFN-I-deficient cancer cells and is often used to develop anti-cancer therapies (Hastie and Grdzelishvili, 2012). Recently, a VSV-based vaccine against Ebola virus was approved (G. Liu et al., 2021).

2. Genomic organization

Rhabdoviruses are enveloped viruses with bullet-shaped particles of 45 to 100nm in diameter **(Figure 28a)**. VSV is about 65 nm in diameter. The envelope comes from the host lipid bilayer and covers the core nucleocapsid (Ge et al., 2010). The genome is 11 kb in length. It is sequentially transcribed into mRNAs coding for the nucleocapsid N, the phosphoprotein P, the matrix protein M, the glycoprotein G and the RNA-dependent RNA polymerase (or large protein) L (Banerjee et al., 1977) **(Figure 28b)**.

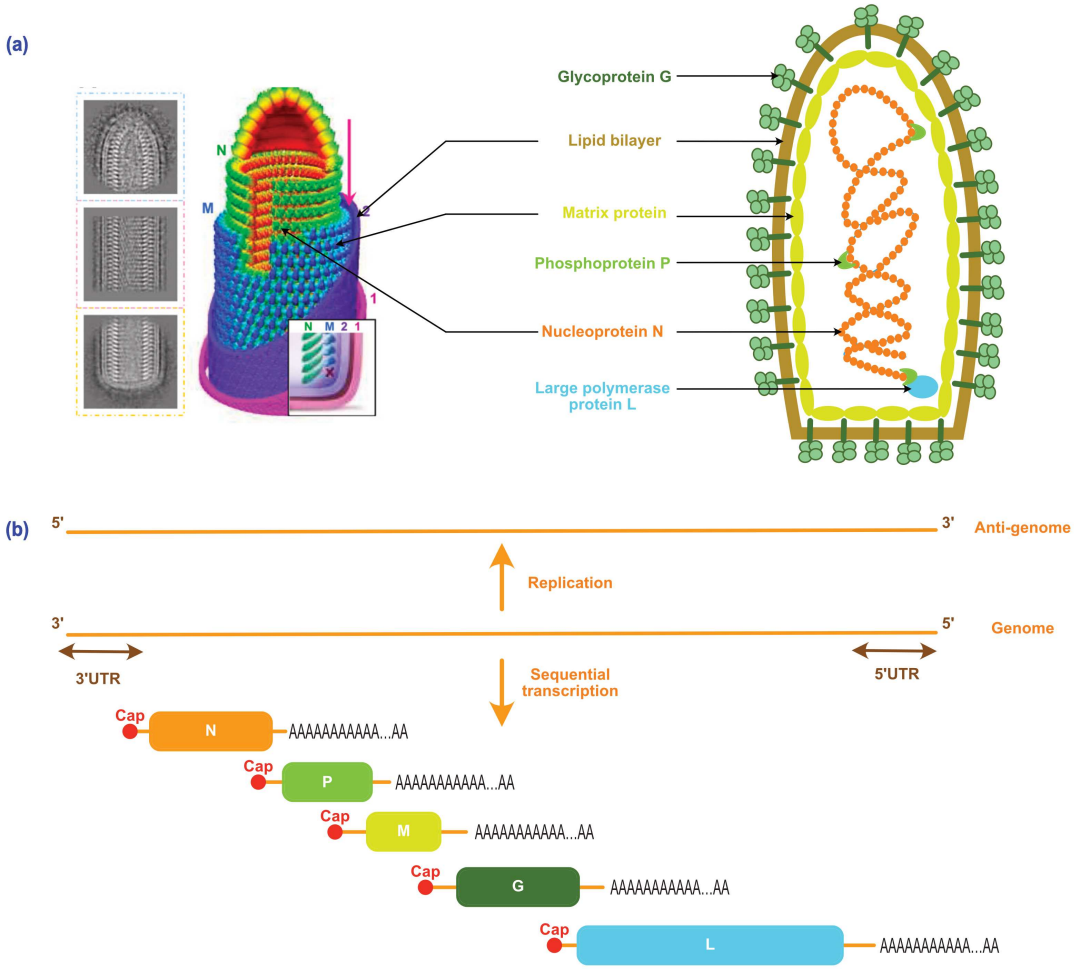

Figure 28 – VSV viral particle structure and genome organization.

(a) Model of the cryo-EM structure at 10.6Å of the bullet-shaped VSV structure. The glycoprotein G (dark green) forms the envelope with the lipid bilayer coming from the host membrane (brown). The matrix protein M (light green) protects the nucleoprotein N molecules (orange) covering the -ssRNA. The large polymerase L (blue) and phosphoproteins P are directly bound to the genomic RNA. (b) The negative single-stranded genomic RNA is flanked by a 3' leader sequence and a 5'trailer sequence. The genome needs to be replicated into the positive sense antigenome to unveil the different ORFs that are sequentially transcribed. Each transcript bears a 5' cap and a 3' polyA tail. L is the RNA-dependent RNA polymerase. N, nucleocapsid; P, phosphoprotein; M, matrix protein; G, glycoprotein.

3. Immune response

Mice are infected in the laboratory by intranasal injection. In that case, VSV causes severe encephalitis and can trigger the IFN-I by several ways (Trottier et al., 2005). VSV G protein can be detected at the cell surface by TLR4 and its ssRNA genome is recognized in the endosome by TLR7 (Georgel et al., 2007; Lund et al., 2004). RIG-I is able to detect the 5' triphosphate on VSV genomic RNA and trigger production of IFN α and ß (Kato et al., 2006) (Linder et al., 2021). Interestingly, VSV infection in microglia induces the expression of the three RLRs, RIG-I, LGP2 and MDA5 (Furr et al., 2008).

VSV induces the NF-kB immune response allowing secretion of IFNα and ß that will activate the JAK1/STAT1 pathway (Kato et al., 2005; Zhang et al., 2010). This pathway is predominant since STAT1-deficient mice die after VSV infection (Durbin et al., 1996). In mouse brain, the absence of IFN-I is compensated by the induction of IFN γ and TNF pathways, through an IRF1-mediated pathway (Mishra et al., 2020).

The infection also induces a weaker inflammatory response and can inhibit the host immune response via its M protein. The latter is the major immune modulator as it can downregulate host gene expression, through direct targeting of TFIID independently from any catalytic activity (Lyles, 2000). Thus, transcription of IFNα, ß and numerous ISGs is down-regulated upon VSV infection (Ferran and Lucas-Lenard, 1997). Besides, M protein inhibits the transport of RNAs from the nucleus to the cytosol by blocking the Ran-GTPase TC4 (Her et al., 1997; Stojdl et al., 2003). M protein is also able to directly block NF-kB activation at later infection stages (Varble et al., 2016).

VSV can also activate PKR. PKR-defective mouse fibroblasts are more susceptible to VSV infection (Durbin et al., 2002; Stojdl et al., 2000). PKR function may occur at the beginning of the infection delaying translation of VSV proteins to let time to IFN-I to set up. Indeed, IFN-I is necessary in cells expressing PKR to mount an efficient antiviral response (Balachandran et al., 2000).

Even though no dsRNA is detected in VSV-infected mammalian cells, Dicer-based antiviral immunity against VSV was shown to be active in Drosophila since deletion of RNAi actors favors VSV infection (Mueller et al., 2010) **(Figure 29)**. In mammalian cells, the immune

response against VSV is restricted to the IFN-I response and does not rely on RNAi, as expression of the Vaccinia VSR VP55 from the VSV genome does not enhance its replication (Backes et al., 2014) **(Figure 29)**. In addition, no VSV replication enhancement was observed in human cells depleted from Dicer (Bogerd et al., 2014). However in mouse cells, Dicer deficiency renders them more susceptible to VSV infection (Otsuka et al., 2007) **(Figure 29)**. This is not linked to a direct targeting of the viral RNA by Dicer, but is due to the targeting of VSV mRNAs by cellular miRNAs (De Cock and Michiels, 2016; Otsuka et al., 2007). For instance, miR-93 and miR-24 can target the P and L mRNAs respectively **(Figure 29)**.

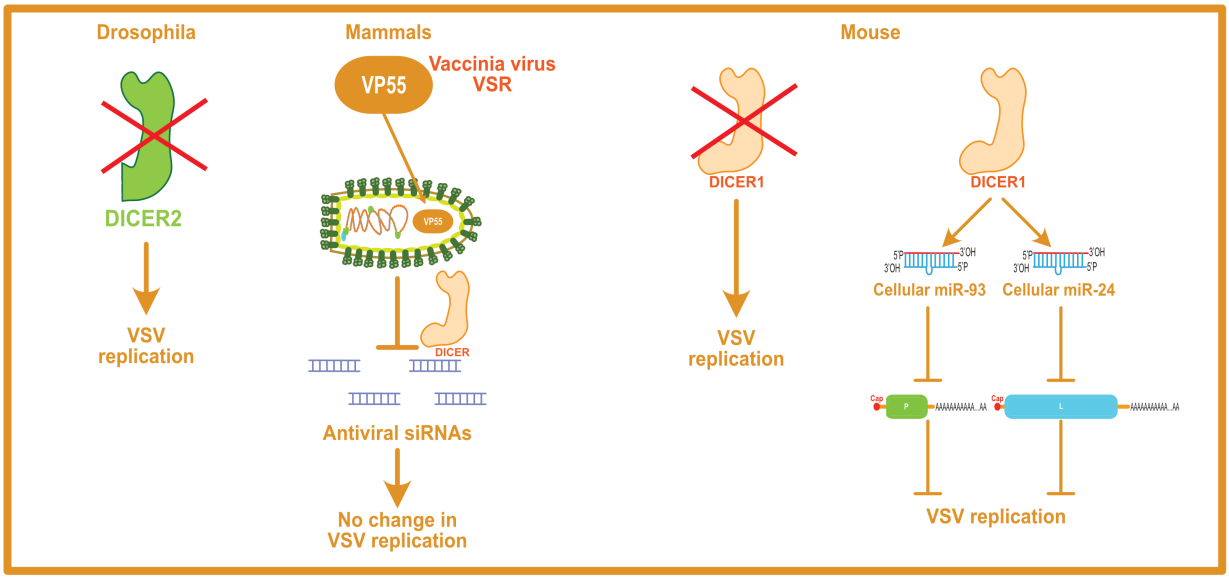

Figure 29 – VSV and the Dicer-dependent immune response.

In Drosophila, the absence of the RNAi-specific DICER2 promotes VSV replication. In mammals, a VSV strain expressing the vaccinia virus VP55 VSR blocks the generation of siRNA duplexes by Dicer but has no effect on VSV replication, ruling out an antiviral role for Dicer. Conversely, the absence of the mouse Dicer promotes VSV replication. This is indirectly linked to two cellular miRNAs, miR-93 and miR-24, which can target two viral mRNAs.

D. Coronaviruses

1. History

Coronaviruses are associated to the subfamily of *Orthocoronavirinae* in the *Coronaviridae* family. They are enveloped +ssRNA viruses known to infect a broad range of vertebrate hosts. Four genera are found in the family, of which *alpha*- and *beta-coronaviruses* are the most prevalent and the ones suspected to directly come from bat reservoirs (Woo et al., 2007). The *Betacoronavirus* includes all the well-known pandemic viruses: Severe Acute Respiratory Syndrome (SARS), Middle East Respiratory Syndrome (MERS) and Severe Acute Respiratory Syndrome Coronavirus 2 (SARS-CoV-2) involved in the COVID-19 disease. The seasonal OC43 respiratory virus is also part of this genus.

The first report of coronavirus infections was in the 1920s in North America in domesticated chickens (Estola, 1970). Human coronaviruses were discovered later, in the 1960s. They were isolated in the United Kingdom and the United States, cultivated in human embryonic trachea or in kidney cells and characterized in laboratories (Hamre and Procknow, 1966; Tyrrell and Bynoe, 1965). SARS-CoV-2 was first detected in Wuhan, China in December 2019 **(Figure 30)**. Since January 2020 and the pandemic outbreak, the virus had spread from China to all continents on March 2020 **(Figure 30)**.

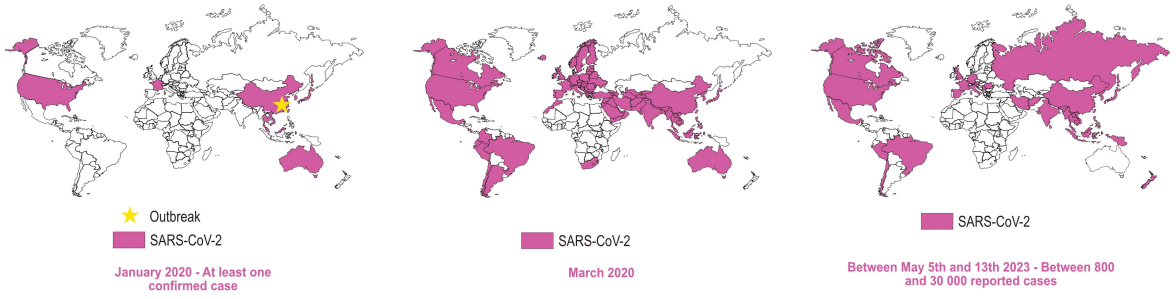

Figure 30 – Repartition of world cases of SARS-CoV-2 infections.

SARS-CoV-2 cases repartition at three different time point. The first one is at the beginning of the epidemic and colored countries are the one with at least one detected case on January 2020. Data from WHO. The second one

is two months later, on March 2020, where lockdowns were systematically applied in all concerned countries. (Data from WHO). The last one is the situation on one week at the beginning of May 2023. The colored countries are the ones where between 800 and 30 000 cases were reported during the week (Data from CDC). The yellow star represents the outbreak location.

SARS-CoV-2 induces flu-like symptoms with fever, cough, headache, fatigue and this can be follows by loss of smell and taste. This can go to severe lung and heart troubles and in worst cases to death caused by lung and multiorgan failures. Since 2019, almost 7 millions of death were accounted for, which is thought to be underestimated (WHO, 2023c). Like other respiratory viruses, SARS-CoV-2 infects preferentially upper respiratory tract cells, pneumocytes and bronchial cells. But it was also detected in intestinal cells, kidney, brain vascular tissues, pancreas and heart (J. Liu et al., 2021).

SARS-CoV-2 infects mammals and is transmitted by aerosols, saliva and direct contact. SARS-CoV-2 is close to the bat coronavirus RaTG13, raising the possibility that bats are the main natural reservoir (Singh and Yi, 2021). This cycle become recently more intricated as domesticated animals or wild animals living near urban areas as deer or racoon dogs were also found to carry this virus (Hale et al., 2022; Jairak et al., 2022). These intermediate hosts are a motif of concerns as they may be at the origin of the appearance of new variants, maintaining the viral circulation **(Figure 31)**.

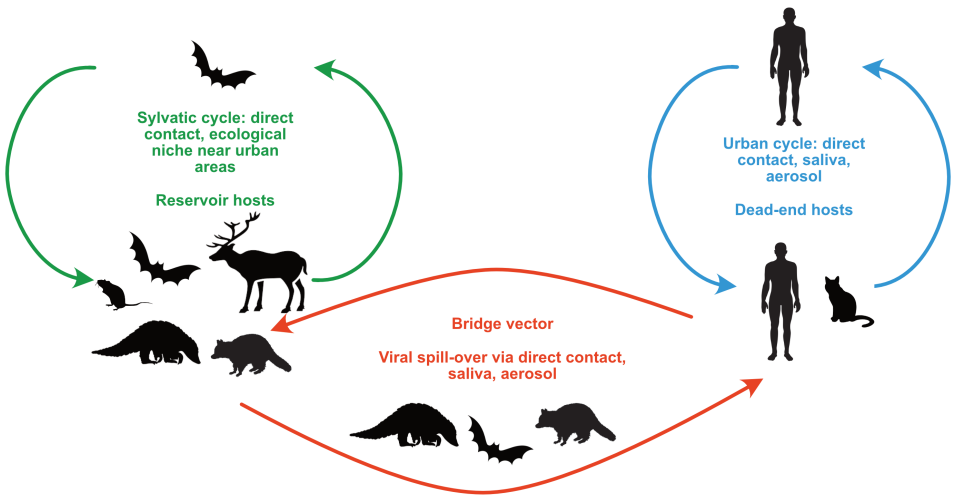

Figure 31 – Transmission cycle of SARS-CoV-2.

Many wild mammals, bats in particular, could act as potential reservoir for the virus. The spill over vectors might be pangolins, racoon dogs or more probably bats. The urban cycle between humans is maintained by the viral propagation by aerosol and direct contacts. Many cases of back transmission to the wild animals are described, often due to the ecological niche, close to the human urban area.

Vaccines were rapidly developed against the first SARS-CoV-2 serotype and allowed the mRNA vaccine technology to be in the spotlight. Pfizer, the first one is used since December 2020 followed by the Moderna one. They are composed of lipid nanoparticles containing a nucleoside-modified mRNA coding for the SARS-CoV-2 spike, a protein directly at the surface of the viral particle (Jackson et al., 2020). As for many vaccines, boosters are recommended to preserve the immunity.

2. Genomic organization and host entry

The name coronavirus came from the Latin "*corona*" meaning crown and refers to the shape of the virion as observed in electron microscopy **(Figure 32a)**. The nucleocapsid has a diameter of 80-120 nm. The genome size ranges from 26 to 32 kb. SARS-CoV-2 genome is about 30kb and encodes 14 ORFs with four structural proteins: spike S, envelope E, membrane M and nucleocapsid N (Singh and Yi, 2021). Each transcript is capped and polyadenylated. The genome also encodes nine accessory proteins (ORF3a, 3b, 6, 7a, 7b, 8, 9, 10, 14) and 16 non-structural proteins **(Figure 32b)**. The first two ORFs, 1a and 1b, are translated into polyproteins further processed by viral proteases to produce nsP1 to 16 (Arya et al., 2021). nsP3 and nsP5 are the proteases, nsP12 is the RNA-dependent RNA polymerase and some nsPs complexes around nsP12 to form the replication complex in membrane-formed compartments called "double-membrane vesicles" (DMV) linked to the endoplasmic reticulum (Arya et al., 2021).

S protein at the surface of the viral particle possesses a receptor-binding domain that will contact directly the host membrane receptor Angiotensin-converting enzyme 2 (ACE2) (Lan et al., 2020).

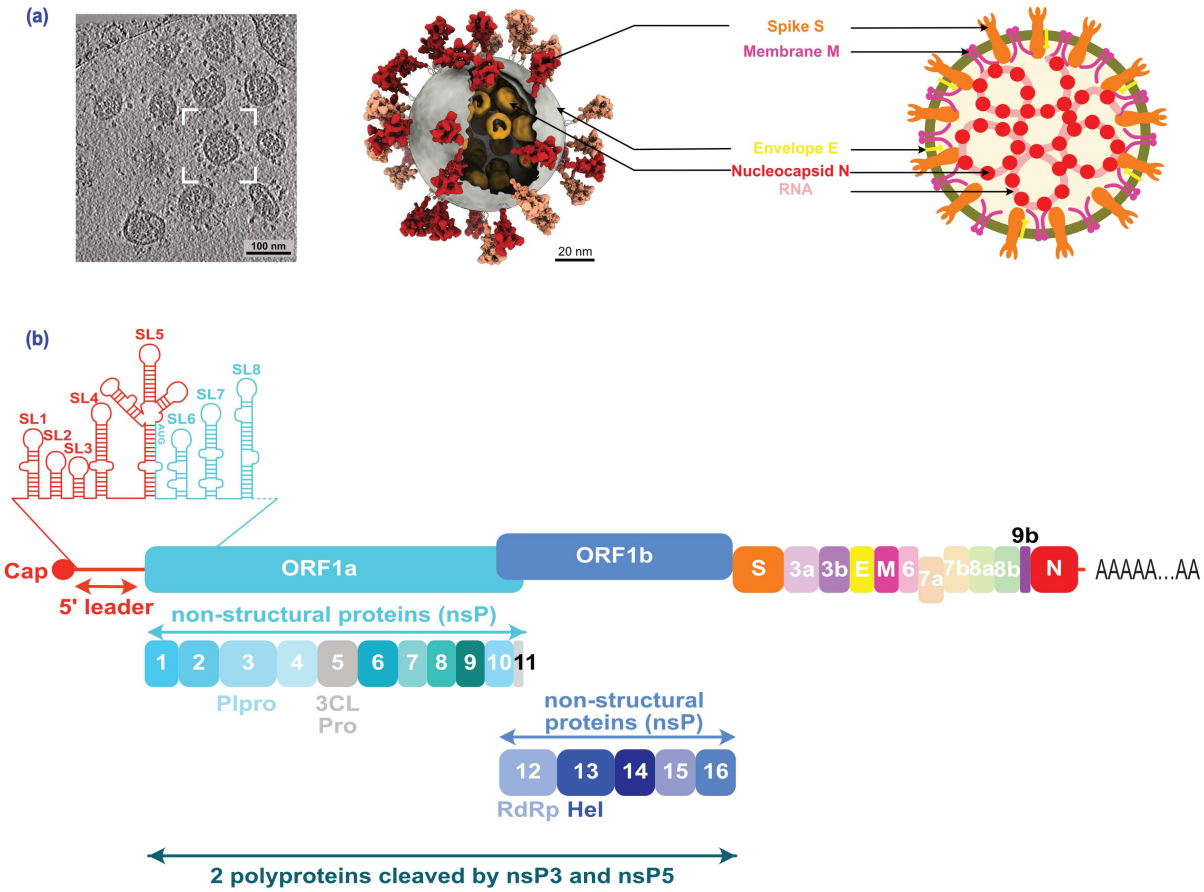

Figure 32 – SARS-CoV-2 viral particle structure and genome organization.

(a) Cryo-EM structure and model of SARS-CoV-2 viral particle at 5Å. Adapted from (Yao et al., 2020). The spike protein S (orange), the membrane protein M (pink) and the envelope protein E (yellow) form the viral envelope and surface glycoproteins. Inside, the nucleocapsid proteins N (dark red) surrounds the positive single-stranded RNA (light red). (b) Genome organization of SARS-CoV-2. The genomic RNA is capped, polyadenylated and composed of two ORF encoding the non-structural proteins, ORF1a and 1b, and 12 ORFs encoding the structural and accessory proteins. The non-structural proteins are translated in polyproteins and cleaved by the action of two viral proteases, nsP3 (Plpro, for papain-like protease) and nsP5 (3CLPro for 3C-like protease). In the 5' leader sequence, SARS-CoV-2 has a structured sequence composed of several stem-loops (SL) able to bypass the translational arrest imposed by the viral nsP1. nsP12 is the RNA-dependent RNA polymerase and nsP13 is a helicase. nsPs assemble into the replication complex.

3. Immune response

COVID-19 disease is known to be characterized in some fatal cases by a “cytokine storm” showing an uncontrolled immune response that aggravates the inflammatory symptoms with a high concentration of cytokines. This is correlated with immune cells dysfunctions in patients (Lee et al., 2020; D. Zhang et al., 2021). The SARS-CoV-2 immune sensing is mainly done by the RLR MDA5, helped by LGP2, that recognizes the dsRNA replication intermediate. In turn, it triggers the IFN-I response led by the activity of IRF3, IRF5 and NF-kB/p65 (Yin et al., 2021). To a lesser extent, TLR3 and TLR7 are also activated upon infection. TLR3 acts on the production of pro-inflammatory cytokines through the IRF3 and NF-kB pathways during the first 24 hours of infection, whereas TLR7 mainly acts at 48 hours of infection via the NF-kB pathway to induce IFN production (Bortolotti et al., 2021). Another dsRNA sensor, OAS1, is also able to detect a dsRNA structure in the 5’UTR of SARS-CoV-2 and to mount an antiviral response based on its property to activate RNaseL (Wickenhagen et al., 2021). The importance of the later has been confirmed by the discovery that inborn mutations in the OAS-RNaseL pathway led to an exacerbated inflammatory response in children upon SARS-CoV-2 infection (Lee et al., 2022). SARS-CoV-2 dsRNA is also able to activate PKR in lung cells even in the absence of IFN induction but without a strong antiviral effect (Y. Li et al., 2021). Moreover, in non-airway related cells, SARS-CoV-2 N protein can inhibit the PKR-induced stress granules formation, promoting viral replication. It seems therefore that, depending on the cell type and the type of immune response, SARS-CoV-2 is keeping a low level of activated PKR to replicate in cells at later infection stages.

The role of Dicer during SARS-CoV-2 infection has been studied as well. First, a helicase-deletion mutant of Dicer called AviD restricts SARS-CoV-2 infection in human cells reinforcing a possible role of Dicer in the antiviral RNAi pathway (Poirier et al., 2021) **(Figure 33a)**. Additionally, SARS-CoV-2 encodes for a miRNA-like small RNA dependent of Dicer processing. This miRNA can modulate the immune response as it targets BATF2 or LAMP3 **(Figure 33b)** (Pawlica et al., 2021; Singh et al., 2022). Moreover, CLEAR-CLIP of AGO-bound miRNAs in SARS-CoV-2-infected human cells uncovered viral RNA-binding sites for cellular miRNAs. Interestingly, they have a limited effect on the viral RNA accumulation itself and on virus production. Instead, this targeting is used to sequester miR-15a away from its cellular targets,

de-repressing the expression of T-cell differentiation and cell death-associated genes (Fossat et al., 2023) **(Figure 33c)**.

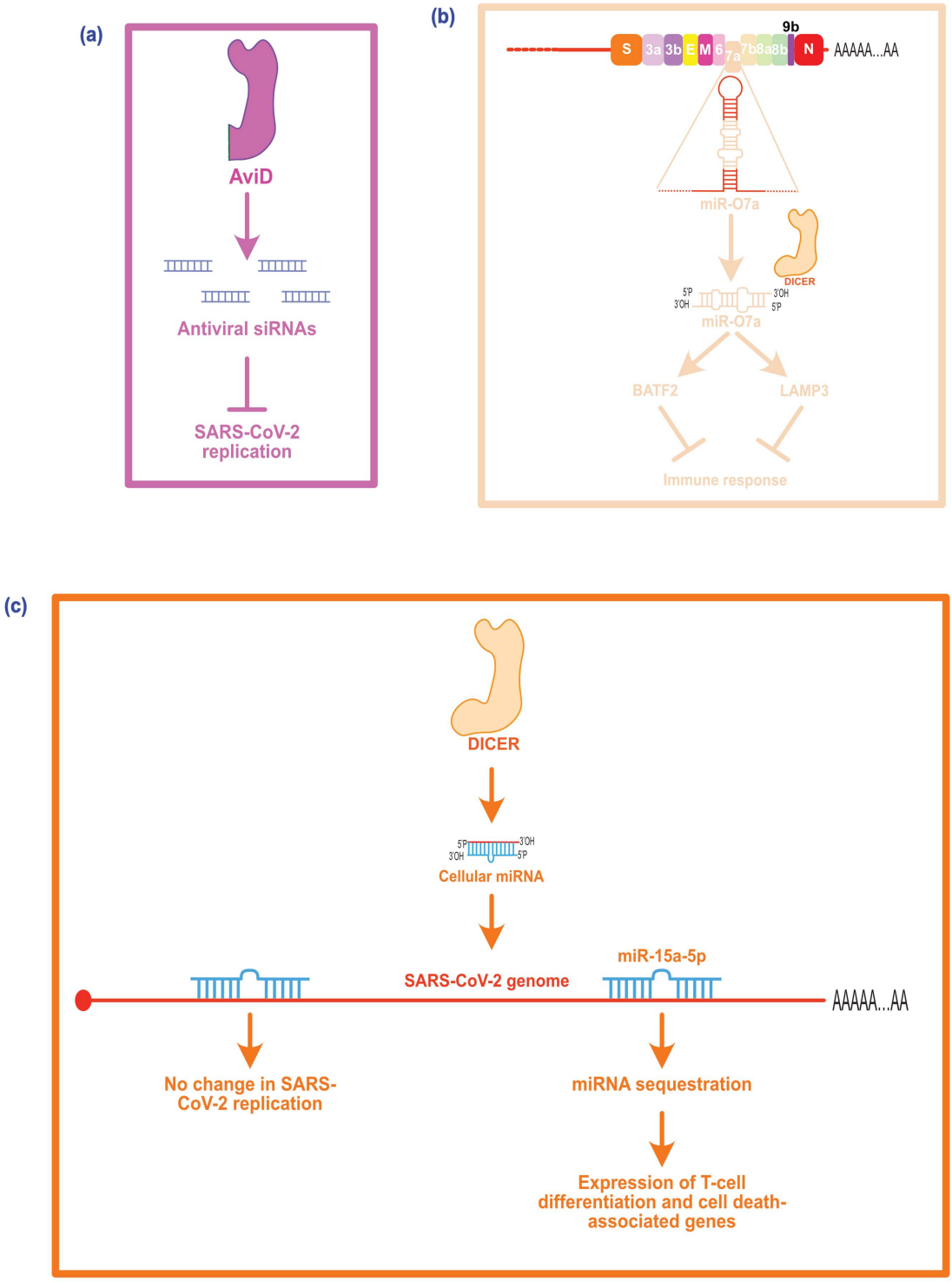

Figure 33 – SARS-CoV-2 and the Dicer-related pathways.

(a) In human cells, a natural Dicer isoform deleted from the HEL2i part of the helicase domain and called AviD (Antiviral Dicer) generates siRNA duplexes from SARS-CoV-2 dsRNA. (b) SARS-CoV-2 encodes a miRNA-like structure in its ORF7a that is matured by Dicer in human cells. The resulting miRNA, miR-O7a, has two main cellular targets involved in the immune response, BATF2 and LAMP3. (c) SARS-CoV-2 disrupts the function of one cellular miRNA, miR15a-5p, by sequestering the miRNA. This has no effect on SARS-CoV-2 replication but rather on cellular gene expression, as the sponge-effect results in the expression of T-cell differentiation and apoptosis-related genes.

An interesting feature of SARS-CoV-2 infection is the balance between excessive and controlled inflammation. Indeed, the pathogenesis rely on both aspects. This explains why in some cases, viral proteins will over-activate the immune response, instead of downregulating it. This is mostly mediated by the activation of the NF-kB pathway. Hence, S, nsP14 and ORF7a proteins all activate the transcription of pro-inflammatory cytokines (T. Li et al., 2021; Olajide et al., 2022; Su et al., 2021). This pattern is often retrieved in severe COVID-19 patients and is beneficial to SARS-CoV-2 replication.

Conversely, SARS-CoV-2 delays, and sometimes attenuates the immune response. Most of the structural, non-structural and accessory proteins are involved in innate immune evasion (Minkoff and tenOever, 2023). **Figure 34** provides a few examples of how SARS-CoV-2 evades immune response. It acts on all the immune sensors and signaling pathways but mostly at the first steps: the recognition and activation of the transcription factors NF-kB, STAT1/2 and IRF3 (Minkoff and tenOever, 2023). SARS-CoV-2 is also able to hide its dsRNA from MDA5, while inducing MDA5 degradation at the same time. nsP1 induces cellular translation shut down (Thoms et al., 2020) and is also involved in the direct blocking of the IFN-I response by preventing IRF3 phosphorylation and degrading TYK2 and STAT2 (Kumar et al., 2021). nsP3 and nsP5 proteases cleave IRF3 (Moustaqil et al., 2021). nsP5 cleaves RIG-I and promotes MAVS degradation (Y. Liu et al., 2021). nsP5 also prevents NF-kB activation by cleaving NEMO and TAB1 involved in the phosphorylation complex of IkBα (Chen et al., 2022) The helicase nsP13 prevents STAT1 phosphorylation by JAK1 (Fung et al., 2022) and blocks TBK1 activity in the NF-kB and IRF3 signaling pathways (Vazquez et al., 2021).

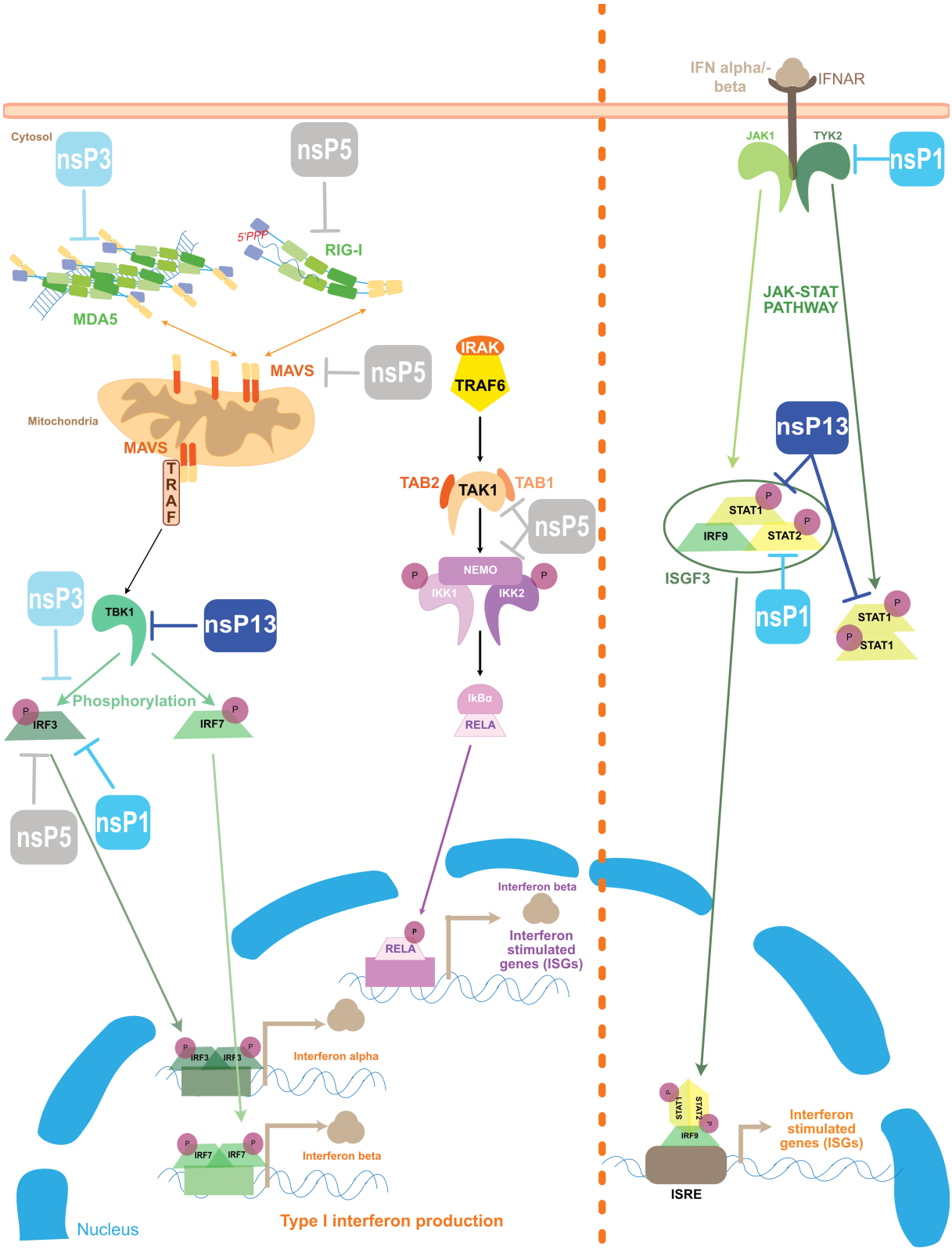

Figure 34 – SARS-CoV-2 possesses many ways to antagonize the immune response.

SARS-CoV-2 because of its numerous non-structural, structural and accessory proteins is well-armed to antagonize the IFN response. See text for details.

Thesis objectives

The role of Dicer during viral infection of mammalian cells remains a debated research topic. Dicer has been shown to be proviral in specific cases. Indeed, two elements restrain Dicer activity in human cells and are incompatible with antiviral RNAi. First, the human Dicer helicase domain has unique features that render Dicer less processive. The three sub-domains (HEL1, HEL2i and HEL2) are major brakes to Dicer processing activity on long dsRNA. Besides, human Dicer does not need ATP to process pre-miRNA or dsRNA. Another major issue for Dicer antiviral activity is the existence in human cells of another immune response, the type I interferon response (IFN-I). In many cases, Dicer antiviral activity was assessed when this response was disrupted. Moreover, Dicer is sharing many factors with this response such as ADAR1, LGP2 or PACT. If Dicer has a role in the antiviral response, it cannot be completely separated from its interplay with IFN-I. However, this kind of interplay stays poorly studied. Since Dicer helicase domain stands as a central hub for the auto-inhibitory effect and for the potential cellular partners, studies are focusing on its precise role.

The main objective of this project was to study the central role of human Dicer helicase domain upon viral infection. The hypothesis was that Dicer antiviral functions are restricted by the existence of IFN-I and its atypic position at the interface on RNAi and IFN-I rendered him less prone to be antiviral. The project first focused on the model alphavirus, SINV. This +ssRNA virus has been already used to study Dicer role upon infection and is able to generate dsRNA replication intermediate that stands as the main Dicer substrate. An engineered version of SINV was used to facilitate the monitoring of the infection: SINV-GFP expresses GFP from a duplication of the subgenomic promoter.

To study Dicer role upon viral infection in the context of the interplay between the two responses, we established the human Dicer interactome upon SINV-GFP infection. Many infection-enriched partners were attributed to be actors of the IFN-I response such as the deaminase ADAR1, the RNA helicase DHX9, the dsRBP PACT and the kinase PKR.

The objectives of this thesis, regrouped in the two following chapters, were:

1- The characterization and the validation of the Dicer partners enriched upon SINV-GFP infection. The study focused on the interaction between Dicer and the top hit in its partners, the kinase PKR. The roles of the helicase domain in this interaction and in the regulation of the infection were investigated. A specific Dicer mutant, deleted from the two first part of the helicase domain, N1 Dicer, was studied. The role of the kinase PKR was also further investigated in the context of the N1 Dicer.

2- The characterization of the role of the different subdomains of Dicer helicase domain upon SINV-GFP infection and their possible link with PKR activity. Once again, the different helicase mutants and their catalytic mutant counterparts were expressed in the presence and the absence of PKR. In parallel, N1 Dicer was also studied for its potential role in the antiviral RNAi pathway using small RNA-sequencing and a catalytic mutant, N1-CM. To determine any involvement of IFN response in N1 Dicer role upon SINV-GFP infection, total RNA-sequencing was performed. IFN transcriptional activity was further validated with both specific gene target and the activation of the main transcription factor leading to the immune response. The mechanism underlying the IFN transcriptional activity was further studied highlighting a determinant role of PKR. This was allowed by the use of cell lines invalidated for PKR expression and expressing either WT or N1 Dicer as well as the complementation of these cell lines with PKR mutants. Then, N1 Dicer activity study was enlarged to other viruses from different groups: the *alphavirus* SFV, the *enterovirus* EV71, the *rhabdovirus* VSV (expressing the GFP protein in its genome, so called VSV-GFP) and the *coronavirus* SARS-CoV-2.

Results

First part

Human Dicer helicase domain recruits PKR and modulates its activity

The following chapter describes the results obtained for the identification of Dicer partners upon SINV infection. Briefly, the manuscript, published in PLOS Pathogens, describes the interactions between Dicer and IFN actors as the kinase PKR. Moreover, the interaction between Dicer and PKR was further investigated, regarding the loss of the interaction between Dicer and PKR with a specific Dicer helicase-deletion mutant called N1 Dicer. Finally, N1 Dicer showing an antiviral activity, I focused on PKR role in this antiviral phenotype.

PLOS PATHOGENS

RESEARCH ARTICLE

Human DICER helicase domain recruits PKR and modulates its antiviral activity

Thomas C. Montavon[1], Morgane Baldaccini[1], Mathieu Lef vre[1], Erika Girardi[1], Béatrice Chane-Woon-Ming[1], Mélanie Messmer[1], Philippe Hammann[2], Johana Chicher[2], Sébastien Pfeffer[1]

1 Université de Strasbourg, CNRS, Architecture et Réactivité de l'ARN, UPR9002, Strasbourg, France, **2** Université de Strasbourg, CNRS, Institut de Biologie Moléculaire et Cellulaire, Plateforme Protéomique Strasbourg–Esplanade, Strasbourg, France

These authors contributed equally to this work.
* s.pfeffer@ibmc-cnrs.unistra.fr

Citation: Montavon TC, Baldaccini M, Lef vre M, Girardi E, Chane-Woon-Ming B, Messmer M, et al. (2021) Human DICER helicase domain recruits PKR and modulates its antiviral activity. PLoS Pathog 17(5): e1009549. https://doi.org/10.1371/journal.ppat.1009549

Editor: Stacy M. Horner, Duke University Medical Center, UNITED STATES

Received: December 2, 2020

Accepted: April 8, 2021

Published: May 13, 2021

Peer Review History: PLOS recognizes the benefits of transparency in the peer review process; therefore, we enable the publication of all of the content of peer review and author responses alongside final, published articles. The editorial history of this article is available here: https://doi.org/10.1371/journal.ppat.1009549

Data Availability Statement: The mass spectrometry proteomics data have been deposited to the ProteomeXchange Consortium via the

Abstract

The antiviral innate immune response mainly involves type I interferon (IFN) in mammalian cells. The contribution of the RNA silencing machinery remains to be established, but several recent studies indicate that the ribonuclease DICER can generate viral siRNAs in specific conditions. It has also been proposed that type I IFN and RNA silencing could be mutually exclusive antiviral responses. In order to decipher the implication of DICER during infection of human cells with alphaviruses such as the Sindbis virus and Semliki forest virus, we determined its interactome by proteomics analysis. We show that DICER specifically interacts with several double-stranded RNA binding proteins and RNA helicases during viral infection. In particular, proteins such as DHX9, ADAR-1 and the protein kinase RNA-activated (PKR) are enriched with DICER in virus-infected cells. We demonstrate that the helicase domain of DICER is essential for this interaction and that its deletion confers antiviral properties to this protein in an RNAi-independent, PKR-dependent, manner.

Author summary

While RNAi has been recognized as an efficient antiviral defense system in organisms such as plants and insects, its physiological importance in mammals remains to be determined. DICER is an enzyme involved in cleaving long double-stranded RNAs and is essential for RNAi induction. Using mass spectrometry analysis, we determined its interactome in human cells and showed that RNA binding proteins such as PKR are specifically enriched upon infection with the Sindbis virus or the Semliki forest virus. We determined that the N terminal helicase domain of the DICER protein acts as a platform to recruit these factors during infection and that its deletion confers an antiviral activity to DICER.

PRIDE partner repository with the dataset identifier PXD019093 and 10.6019/PXD019093.

Funding: This work was funded by the European Research Council (ERC-CoG-647455 RegulRNA) (to SP) and was performed under the framework of the LABEX: ANR-10-LABX-0036_NETRNA (to SP) and ANR-17-EURE-0023 (to SP), which benefits from a funding from the state managed by the French National Research Agency as part of the Investments for the future program. This work has also received funding from the People Programme (Marie Curie Actions) of the European Union's Seventh Framework Program (FP7/2007-2013) under REA grant agreement n° PCOFUND-GA-2013-609102, through the PRESTIGE program coordinated by Campus France (to EG), and from the French Minister for Higher Education, Research and Innovation (to MB). The mass spectrometry instrumentation was funded by the University of Strasbourg, IdEx "Equipement mi-lourd" 2015 (to PH). The funders had no role in the study design, data collection and analysis, decision to publish, or preparation of the manuscript.

Competing interests: The authors have declared that no competing interests exist.

Introduction

In mammalian cells, the main antiviral defense system involves the activation of a signaling cascade relying on production of type I interferon (IFN I). This pathway depends on the recognition of extrinsic signals or pathogen associated molecular patterns (PAMPs) by dedicated host receptors. Double-stranded (ds) RNA, which can originate from viral replication or convergent transcription, is a very potent PAMP and can be sensed in the cell by various proteins among which a specific class of DExD/H-box helicases called RIG-I-like receptors (RLRs) [1]. RLRs comprise RIG-I, MDA5 and LGP2 and transduce viral infection signals to induce expression of IFN I cytokines that act in autocrine and paracrine fashions. These cytokines then trigger the expression of hundreds of interferon-stimulated genes (ISGs) to stop the virus in its tracks [2]. Among those ISGs, dsRNA-activated protein kinase R (PKR) plays an important role in antiviral defense by blocking cellular and viral translation upon direct binding to long dsRNA [3]. PKR is a serine-threonine kinase that dimerizes and auto-phosphorylates upon activation. It then phosphorylates numerous cellular targets among which the translation initiation factor eIF2 , which results in the inhibition of cap-dependent translation [4]. Accordingly, translation of many RNA viruses, including alphaviruses, is inhibited by PKR [5–7]. PKR is also involved in other cellular pathways including apoptosis, autophagy and cell cycle [3,8].

RNAi is another evolutionary conserved pathway triggered by long dsRNA sensing [9]. One key component in this pathway is the type III ribonuclease DICER, which is also essential for micro (mi)RNA biogenesis [10,11]. These small regulatory RNAs are sequentially produced by the two ribonucleases DROSHA and DICER, before being loaded into an Argonaute (AGO) effector protein in order to regulate their target mRNAs [12]. Whatever its substrate, be it long dsRNA or miRNA precursor, DICER relies on interacting with co-factors to be fully functional. In mammalian cells, the TAR-RNA binding protein (TRBP), a dsRNA binding protein (dsRBP), was shown to play a role in the selection of DICER substrates, its stabilization, strand selection and incorporation into AGO2 [13]. The interaction with TRBP is well characterized and depends on the helicase domain of DICER and the third dsRNA binding domain (dsRBD) of TRBP [14]. Another dsRBP, the protein activator of interferon-induced protein kinase R (PACT), was also described as an important cofactor of DICER. Although its function is not fully understood, PACT seems to also participate in miRNA loading and strand selection [15,16] *via* protein-protein interaction between the DICER helicase domain and the third dsRBD of PACT [17].

It is now common knowledge that RNAi is the main antiviral defense system in several phyla such as plants, arthropods and nematodes (reviewed in [18]). However, its exact contribution in the mammalian antiviral response remains unclear [19–21]. Recent studies indicate that a functional antiviral RNAi does exist in mammals in specific cases. An antiviral RNAi response was first detected in undifferentiated mouse embryonic stem cells [22] lacking the IFN response, suggesting that these two pathways could be incompatible. Indeed, in mammalian somatic cells deficient for MAVS or IFNAR, two components of the interferon response, an accumulation of DICER-dependent siRNAs derived from exogenous long dsRNA was detected [23]. In addition, the RLR LGP2 was found interacting with both DICER and TRBP, blocking respectively siRNA production and miRNA maturation [24–26]. Moreover, AGO4 was recently shown to be involved in antiviral RNAi against Influenza A virus (IAV), Vesicular stomatitis virus (VSV) and Encephalomyocarditis virus (EMCV) [27]. Finally, viral suppressors of RNAi (VSRs) have been shown to prevent DICER from playing an antiviral role in mammalian cells [28,29]. Nonetheless, several studies reported no detection of viral siRNAs in mammalian somatic cells infected with several viruses [30–32]. In somatic cells, only a

helicase-truncated form of human DICER could produce siRNAs from IAV genome [33], but it also turned out that these siRNAs cannot confer an antiviral state [34].

Based on these conflicting observations, we decided to study the involvement of DICER during infection of human cells with the Sindbis virus (SINV). SINV is a member of the *Togaviridae* family in the alphavirus genus, which is transmitted by mosquitoes to mammals and can induce arthritogenic as well as encephalitic diseases [35]. It is widely used as a laboratory alphaviruses model as it infects several cell types and replicates to high titers. SINV has a positive stranded RNA genome of about 12 kb, which codes for two polyproteins that give rise to non-structural and structural proteins, including the capsid. Moreover, upon viral replication, a long dsRNA intermediate, which can be sensed by the host antiviral machinery, accumulates. Of note, SINV dsRNA can be cleaved into siRNAs in insects as well as in human cells expressing the Drosophila DICER-2 protein [36]. Nonetheless, although human DICER has the potential to interact with the viral RNA duplex, we did not find evidence that SINV dsRNA could be processed into siRNAs in somatic mammalian cells [30,36]. We thus hypothesized that specific proteins could interfere with DICER during SINV infection by direct interaction and limit its accessibility and/or activity. To address this hypothesis, we generated HEK293T cells expressing a tagged version of human DICER that could be immunoprecipitated in mock or SINV-infected cells in order to perform a proteomic analysis of its interactome. Among the proteins co-immunoprecipitated with DICER and that were specifically enriched upon infection, we identified dsRBPs such as ADAR1, DHX9, PACT and PKR. We further validated the direct interaction between DICER and PKR upon SINV infection. We also demonstrated that the interactions of the endogenous DICER with PKR, PACT and DHX9 could also be detected in SINV-infected, but not mock-infected, HCT116 cells. We dissected the protein domains necessary for this interaction and we found that DICER helicase domain plays a fundamental role as a recruitment platform for PKR but also for other co-factors. Finally, we also show that expression of a helicase-truncated version of DICER has a negative effect on SINV infection. Importantly, this antiviral phenotype is independent of RNAi, but requires the presence of PKR. Our results indicate that DICER interactome is highly dynamic and directly link components of RNAi and IFN pathways in modulating the cellular response to viral infection.

Results

Establishment of a HEK293T cell line expressing FLAG-HA tagged DICER

In order to be able to study the interactome of the human DICER protein during viral infection, we transduced *Dicer* knock-out HEK293T cells (NoDice 2.20) [37] with either a lentiviral construct expressing a FLAG-HA-tagged wild type DICER protein (FHA:DICER WT #4) or a construct without insert as a negative control (FHA:ctrl #1). After monoclonal selection of stably transduced cells, we first characterized one clone of both FHA:DICER WT and of the FHA:ctrl cell lines. We first confirmed that the expression of the tagged version of DICER restored the miRNA biogenesis defect observed in the NoDice cells (S1A Fig). We then monitored the phenotype of these cells during SINV infection by using as a readout of viral infection the modified version of SINV able to express GFP from a duplicated sub-genomic promoter (SINV-GFP) [38]. At 24 hours post-infection (hpi) and a multiplicity of infection (MOI) of 0.02, the GFP fluorescence observed in FHA:DICER WT #4 cells and HEK293T cells was similar. However, the NoDice FHA:ctrl #1 cells displayed a decrease in GFP signal (Fig 1A). Western blot analysis of GFP expression confirmed the observations by epifluorescence microscopy, *i.e.* a significantly lower accumulation of GFP in the absence of the DICER protein (Fig 1B). We therefore wished to confirm the effect of DICER loss on SINV-GFP infection in another NoDice cell line, *i.e.* the NoDice clone 4.25 [39], and in another clone of the NoDice

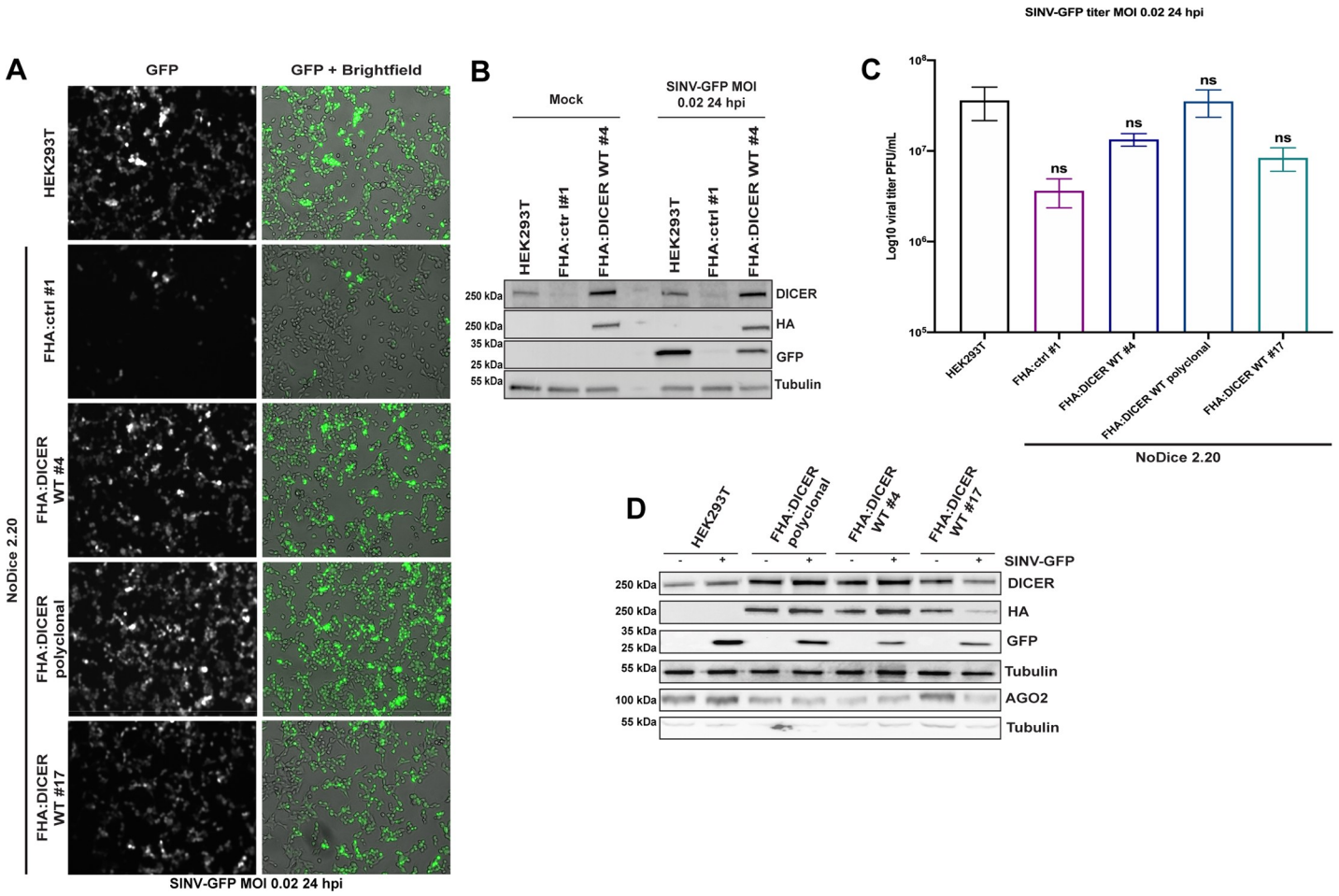

Fig 1. Analysis of SINV infection in HEK293T cells and characterization of FHA:DICER WT cell lines. A. GFP fluorescent microscopy pictures of HEK293T, NoDice FHA:ctrl #1 and FHA:DICER cell lines infected (polyclonal and two clones, #4 and #17) with SINV-GFP at an MOI of 0.02 for 24 h. The left panel corresponds to GFP signal from infected cells and the right panel to a merge picture of GFP signal and brightfield. Pictures were taken with a 5x magnification. hpi: hours post-infection. **B.** Western blot analysis of DICER (DICER and HA) and GFP expression in SINV-GFP-infected HEK293T, NoDice FHA:ctrl #1 and FHA:DICER cell lines shown in A. Gamma-Tubulin was used as loading control. **C.** Mean (+/- SEM) of SINV-GFP viral titers in the same cell lines as in A infected at an MOI of 0.02 for 24 h (n = 3) from plaque assay quantification. ns: non-significant, ordinary one-way ANOVA test with Bonferroni correction. **D.** Western blot analysis of DICER (DICER and HA) and AGO2 expression in HEK293T, NoDice FHA:ctrl #1 and FHA:DICER cell lines. Gamma-Tubulin was used as loading control.

https://doi.org/10.1371/journal.ppat.1009549.g001

2.20 FHA:ctrl cells (NoDice FHA:ctrl #2). We observed a similar decrease of SINV-GFP infection in NoDice 2.20 cells and two independent NoDice FHA:ctrl clones compared to HEK293T cells as shown by GFP microscopy (S1B Fig), by titration of the virus (S1C Fig) and by western blot analysis (S1D Fig). However, the independent NoDice 4.25 *Dicer* knock-out clone appeared mostly unaffected compared to HEK293T cells in term of GFP accumulation and viral titer (S1B, S1C and S1D Fig). This suggests that, despite the observed slight effect on SINV-GFP in NoDice 2.20 cells (Fig 1), DICER proviral effect is not reproductible in an independent clone and therefore could not be generalized.

In order to evaluate whether different expression levels of DICER in a NoDice background could rescue the SINV infection phenotype observed in HEK293T cells, we also infected both the FHA:DICER WT polyclonal and an independent FHA:DICER WT clone (FHA:DICER WT #17) with SINV-GFP (Fig 1A, 1C and 1D). We confirmed that the GFP fluorescence observed by microscopy (Fig 1A), as well as the viral titers and the GFP protein accumulation (Fig 1C and 1D) in all tested FHA:DICER lines were comparable to the ones observed in

HEK293T cells. Moreover, there was no striking difference in AGO2 expression between the FHA:DICER lines (Fig 1D).

Altogether, these results indicate that the FHA-tagged DICER protein can functionally complement the lack of DICER in terms of miRNA biogenesis (S1A Fig) and can therefore be used for proteomics studies. Moreover, because we could not observe significant differences in terms of SINV infection (Fig 1) between the different FHA:DICER clones tested, we decided to select one line, namely FHA:DICER WT #4, for further analysis.

Analysis of DICER interactome during SINV infection by mass spectrometry

Our molecular tool being validated, we then focused on determining the interactome of FHA:DICER during SINV infection. We wanted to look at DICER interactome at an early infection time point to isolate cellular factors that could potentially modulate either DICER accessibility or its effect on viral dsRNA. As SINV replicates quickly upon cellular entry, we chose to set up the infection conditions to a duration of 6 hours at an MOI of 2.

We performed an anti-HA immunoprecipitation experiment (HA IP) coupled to label-free LC-MS/MS analysis in FHA:DICER WT #4 cells either mock-infected or infected for 6 h at an MOI of 2 with SINV-GFP. In parallel, we performed an anti-MYC immunoprecipitation as a negative control (CTL IP). The experiments were performed in technical triplicate in order to have statistically reproducible data for the differential analysis, which was performed using spectral counts. Prior to the detailed analysis of the results, we verified that there was no confounding factor in the experimentation by performing a Principal Component Analysis (PCA). This allowed us to see that the replicates were very homogenous and that the different samples were well separated based on the conditions.

To check the specificity of the HA immunoprecipitation, we first compared the proteins identified in the HA IP with the ones identified in the CTL IP in mock-infected cells. Differential expression analysis allowed us to calculate a fold change and an adjusted p-value for each protein identified and to generate a volcano plot representing the differences between HA and CTL IP samples. Applying a fold change threshold of 2 (abs(LogFC)>1)), an adjusted p-value threshold of 0.05 and a cutoff of at least 5 spectral counts in the most abundant condition, we identified 258 proteins differentially immunoprecipitated between the two conditions out of 1318 proteins (Fig 2A and S1 Table). Among these, 123 proteins were specifically enriched in the HA IP. The most enriched protein was DICER, followed by its known co-factors TRBP and PACT (also known as PRKRA) [13,17]. We were also able to retrieve AGO2, indicating that the RISC loading complex was immunoprecipitated and that proteins retrieved in our HA IP are specific to DICER immunoprecipitation.

We next performed the differential expression analysis of proteins retrieved in the HA IP in SINV-GFP compared to mock-infected cells. Among 1342 proteins, 296 were differentially retrieved between conditions (Fig 2B and S2 Table). Of these, 184 proteins, including viral ones, were at least 2-fold enriched in SINV-GFP-infected cells. GO-term analysis showed a significant enrichment in RNA binding proteins including double-stranded RNA binding proteins and RNA helicases (Fig 2C). We then generated a functional protein association network using STRING on the top 100 proteins enriched in SINV-infected compared to mock-infected cells (Fig 2D). The resulting STRING network confirmed that a limited number of these proteins are known to be interacting with DICER, but that they are all engaged in other complexes (*e.g.* DHX9, DDX18) that could partly explain the presence of some candidates in the mass spectrometry data. In addition, a large number of these proteins are involved in RNA metabolic processes (Fig 2D, in red), or in their regulation (Fig 2D, in blue), while a whole cluster is

A

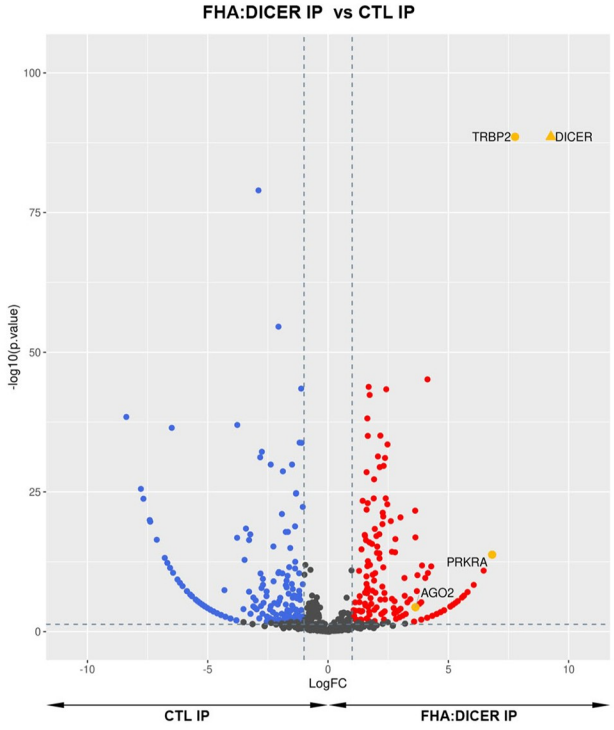

B

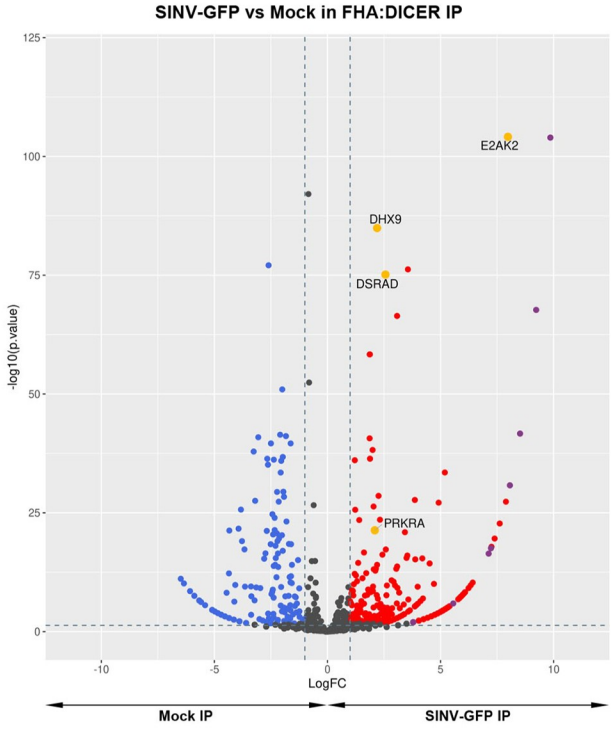

C

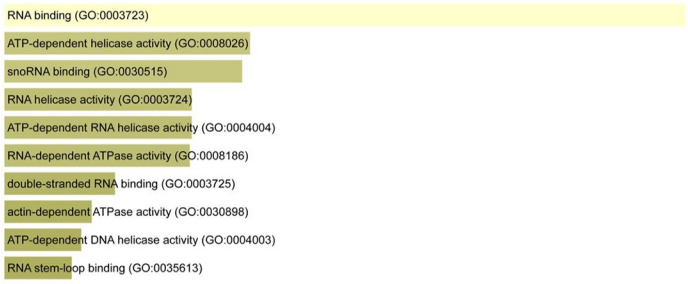

D

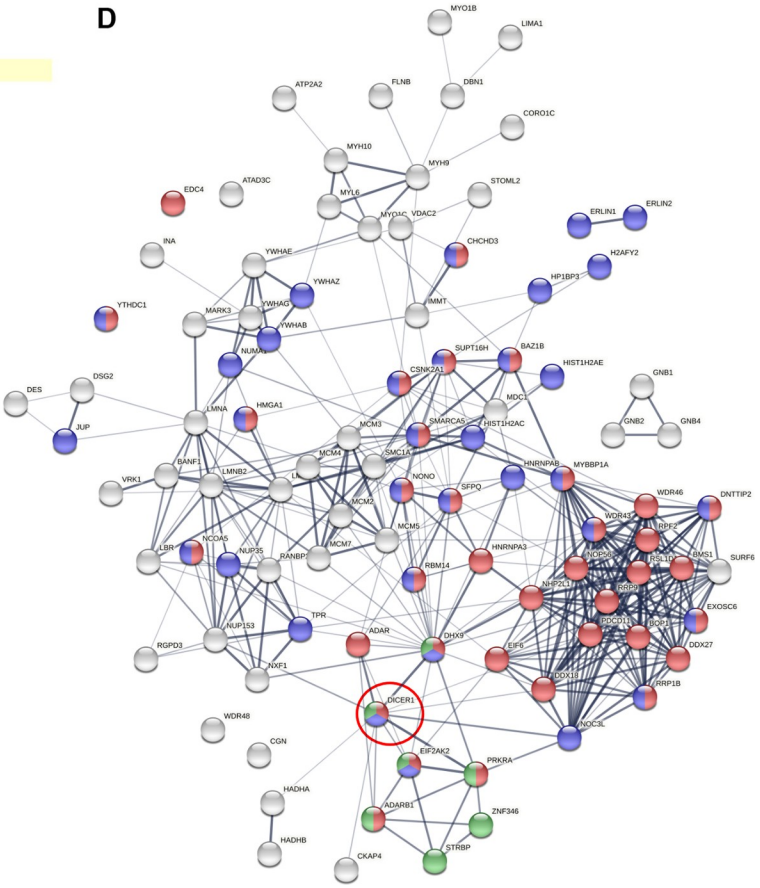

E

Gene name	Mean spectral count		LogFC	Adjusted p-value
	SINV-GFP IP	MOCK IP		
E2AK2 (PKR)	123.3	0.3	7.979	7.316e-102
DSRAD (ADAR-1)	181.3	28.3	2.563	1.421e-73
DHX9	247.3	50	2.194	4.012e-83
PRKRA (PACT)	63.3	13.7	2.093	1.158e-20

Fig 2. LC-MS/MS analysis of DICER interactome during SINV infection. A. Volcano plot for differentially expressed proteins (DEPs) between HA IP and CTL IP in FHA:DICER mock-infected cells. Each protein is marked as a dot; proteins that are significantly up-regulated in HA IP are shown in red, up-regulated proteins in CTL IP are shown in blue, and non-significant proteins are in black. The horizontal line denotes a p-value of 0.05 and the vertical lines the Log2 fold change cutoff (-1 and 1). DICER and its cofactors (TRBP, PACT, AGO2) are highlighted in yellow. **B.** Volcano plot for DEPs between SINV-GFP (MOI of 2, 6 hpi) and mock fractions of HA IP in FHA:DICER cells. Same colour code and thresholds as in A have been applied. Proteins that are discussed in the text are highlighted in yellow and SINV proteins in purple. **C.** Gene Ontology (GO) term enrichment of proteins up-regulated in SINV-GFP fraction of HA IP using Enrichr software [89,90]. The graph displays the GO term hierarchy within the "biological process" branch sorted by p-value ranking computed from the Fisher exact test. The length of each bar represents the significance of that specific term. In addition, the brighter the colour is, the more significant that term is. Viral proteins have been excluded for this analysis. **D.** STRING interaction network of the top 100 proteins enriched in SINV-infected vs. mock-infected cells. Proteins involved in RNA metabolic processes or the regulation thereof are indicated in red and blue respectively, proteins with a known dsRNA binding function are indicated in green. DICER is indicated by a red circle. **E.** Summary of the differential expression analysis of SINV-GFP vs mock fractions from HA IP in FHA:DICER cells. The analysis has been performed using a generalized linear model of a negative-binomial distribution and p-values were corrected for multiple testing using the Benjamini-Hochberg method.

https://doi.org/10.1371/journal.ppat.1009549.g002

composed of dsRNA binding proteins (Fig 2D, in green). Among the RNA binding proteins retrieved, the top and most specific DICER interactor is the interferon-induced, double-stranded (ds) RNA-activated protein kinase PKR (also known as E2AK2), which is enriched more than 250 times in virus-infected cells (Fig 2B and 2E). We were also able to identify the dsRNA-specific adenosine deaminase protein ADAR-1 (also known as DSRAD), as well as PACT, which were enriched 5.9 and 4.2 times respectively in SINV-GFP-infected cells compared to mock-infected cells (Fig 2B and 2E). Among the isolated RNA helicases, we identified the ATP-dependent RNA helicase A protein DHX9, which is implicated in *Alu* element-derived dsRNA regulation and in RISC loading [40,41]. In order to verify if the observed interactions were specific to SINV we performed the same experiments with another virus of the *Togaviridae* family, the Semliki forest virus (SFV). In this analysis, we were able to retrieve ADAR-1, DHX9, PACT and PKR, specifically enriched in SFV-infected samples (S2 Fig and S3 and S4 Tables). These results show that these interactions can be retrieved in *Togaviridae*-infected cells.

Taken together, our data indicate that several proteins interacting with DICER in virus-infected cells are involved in dsRNA sensing and/or interferon-induced antiviral response.

DICER and PKR interact *in vivo* in the cytoplasm during SINV infection

To validate the LC-MS/MS analysis, we performed a co-immunoprecipitation (co-IP) followed by western blot analysis in FHA:DICER WT #4 cells infected with SINV-GFP at an MOI of 2 for 6 h. Whereas TRBP interacted equally well with FHA:DICER in mock and SINV-GFP-infected cells, ADAR-1, PKR, DHX9 and PACT were only retrieved in the HA IP in SINV-GFP-infected cells (Fig 3A). We verified that these interactions could also be observed at a later time post-infection by performing the HA IP in FHA:DICER WT #4 cells infected with SINV-GFP for 24 h at an MOI of 0.02. This indicates that the specific interactions between DICER and ADAR-1, DHX9, PACT or PKR occur at an early stage of the SINV infection and remain stable in time in virus-infected cells (S3A Fig).

In order to verify whether these interactions were mediated by RNA, we performed an anti-HA co-IP experiment on an RNase A/T1 treated total extract from FHA:DICER WT #4 cells infected with SINV-GFP at an MOI of 2 for 6 h. Since the RNase treatment was performed at relatively low salt concentration (140 mM NaCl), RNase A should cleave dsRNA [42,43] and we should therefore assess both ss and dsRNA-dependency in these conditions. We confirmed the efficiency of the RNase treatment by ethidium bromide staining visualisation of total RNA on an agarose gel (S3B Fig). TRBP equally interacted with FHA:DICER, with or without RNase treatment, in mock and SINV-GFP-infected cells (Fig 3B). Instead, the virus-induced interactions between DICER and PKR or PACT upon SINV-GFP infection were almost totally lost in the RNase-treated samples. Upon virus infection, PKR is phosphorylated to be activated and exert its antiviral function [4]. Using an antibody targeting the phosphorylated form of

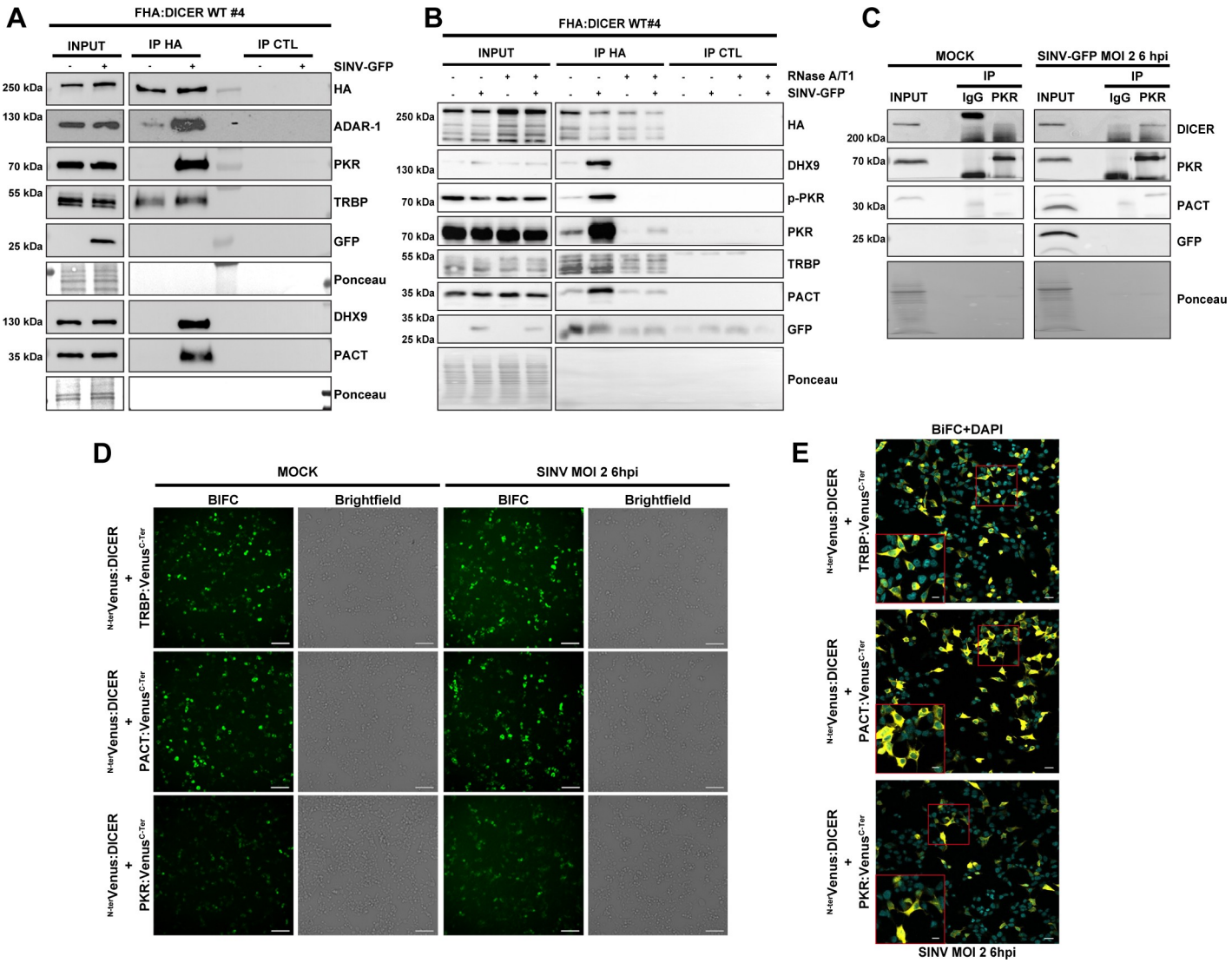

Fig 3. Confirmation of LC-MS/MS analysis by co-IP and BiFC. A. Western blot analysis of HA co-IP in mock or SINV-GFP-infected (MOI of 2, 6 hpi) FHA:DICER WT #4 cells. Proteins associated to FHA:DICER were revealed by using antibodies targeting endogenous ADAR-1, PKR, TRBP, DHX9 or PACT proteins. In parallel, an HA antibody was used to verify the IP efficiency and GFP antibody was used to verify the infection. Ponceau was used as loading control. **B.** Western blot analysis of HA co-IP in mock or SINV-GFP-infected (MOI of 2, 6 hpi) FHA:DICER WT #4 cells. The lysate was treated or not with RNase A/T1. Proteins associated to FHA:DICER were revealed by using antibodies targeting endogenous DHX9, p-PKR, PKR, TRBP, or PACT proteins. In parallel, an HA antibody was used to verify the IP efficiency and GFP antibody was used to verify the infection. Ponceau was used as loading control. **C.** Western blot analysis to validate the interaction of PKR with DICER (upper panel) and PACT (lower panel) in mock or SINV-GFP-infected HEK293T cells (MOI of 2, 6 hpi). Immunoprecipitated proteins obtained from PKR pulldowns were compared to rabbit IgG pulldowns to verify the specificity of the assay. **D.** Interactions between DICER and TRBP, PACT or PKR were visualized by BiFC. Plasmids expressing $^{N\text{-ter}}$Venus:DICER and TRBP:, PACT: or PKR:Venus$^{C\text{-ter}}$ were co-transfected in NoDice PKR cells for 24 h and cells were either infected with SINV at an MOI of 2 for 6 h or not. The different combinations are indicated on the left side. Reconstitution of Venus (BiFC) signal was observed under epifluorescence microscope. For each condition, the left panel corresponds to Venus signal and the right panel to the corresponding brightfield pictures. Scale bar: 100 μm. hpi: hours post-infection. **E.** BiFC experiment on fixed NoDice PKR cells treated as in D. After fixation, cells were stained with DAPI and observed under confocal microscope. Only a merge picture of BiFC and DAPI signals of SINV-infected cells is shown here. A higher magnification of picture showing cytoplasmic localization of the interaction represented by a red square is shown in the bottom left corner. Scale bars: 20 μm and 10 μm.

https://doi.org/10.1371/journal.ppat.1009549.g003

PKR (p-PKR), we looked for p-PKR before and after RNase treatment. The virus-enriched interactions between DICER and p-PKR or DHX9 were completely lost upon RNase treatment. These results therefore indicate that RNA molecules (either single- or double-stranded)

facilitate DICER interaction with DHX9, PACT and PKR and its active form, although the complex may also partially interact in an RNA-independent manner.

Because of the involvement of PKR in antiviral response [44] and the fact that it shares common co-factors with DICER, namely TRBP and PACT [45,46], we decided to focus our analysis on the DICER-PKR interaction. To confirm the biological relevance of this interaction, we first performed a reverse co-IP to immunoprecipitate the endogenous PKR protein in HEK293T cells infected or not with SINV-GFP. While PACT interacted with PKR both in mock and in SINV-GFP-infected cells as expected (Fig 3C), DICER co-immunoprecipitated with the endogenous PKR only in virus-infected cells thereby confirming the specificity of the interaction between the two proteins (Fig 3C).

To further determine whether DICER and PKR could directly interact *in vivo*, we set up a bi-molecular fluorescent complementation assay (BiFC) experiment [47]. To this end, we fused the N- or C-terminal half of the Venus protein ($^{N\text{-}ter}$Venus or $^{C\text{-}ter}$Venus) to DICER and to PKR but also to TRBP and PACT. Since we showed above that an N-terminally tagged DICER was functional, we fused the Venus fragments at the N-terminal end of DICER. For the other three proteins, we fused the Venus fragments at the N- or C-terminus and selected the best combination. To avoid interaction with the endogenous DICER and PKR proteins, we conducted all BiFC experiments in NoDice PKR HEK293T cells [33]. In order to control the BiFC experiments, we chose to exploit the well characterized DICER-TRBP interaction, which is known to occur via the DICER DEAD-box helicase domain [14]. We therefore used the wild-type DICER protein as a positive control and a truncated version of DICER protein lacking part of this helicase domain and called DICER N1 [33] as a negative control (S3C Fig). We first confirmed the expression of the tagged proteins by western blot analysis (S3D Fig) and then, we tested the interactions between DICER and TRBP or PACT or PKR. We co-transfected the Venus constructs for 24 h and then infected cells with SINV or not for 6 h at a MOI of 2. A comparable fluorescent signal was observed both in mock- and SINV-infected cells when $^{N\text{-}ter}$Venus:DICER was co-transfected with either PACT or TRBP fusion construct (Fig 3D). Although we initially expected an increase of the Venus fluorescence in SINV-infected cells, overall we observed a similar signal for the DICER-PKR interaction both in mock- and SINV-infected cells, probably due to the fact that both proteins are transiently overexpressed in this experiment. The same holds true for the DICER-PACT interaction that can also be seen both in mock- and SINV-infected cells.

As a control and to rule out any aspecific interactions between the different proteins tested, we also monitored the DICER-N1-TRBP interaction by BiFC. As expected, no fluorescent signal was observed in cells co-transfected with $^{N\text{-}ter}$Venus:DICER N1 and TRBP:Venus$^{C\text{-}ter}$ (S3E Fig), confirming that DICER helicase domain is required for its interaction with TRBP [14] and validating the specificity of the BiFC approach.

To further confirm that the absence of PKR did not influence the interactions of TRBP or PACT with DICER, we also performed a BiFC analysis in HEK293T cells. After verifying that in this context as well, fusion proteins were expressed as expected (S3F Fig), we observed that the results were similar as in NoDice PKR cells (S3G Fig).

To gain more insight into the subcellular localization of these interactions during SINV infection, we performed the BiFC experiments, fixed the cells and observed them under a confocal microscope. We observed a cytoplasmic fluorescent signal for DICER-TRBP and DICER-PACT interactions (Fig 3E upper and middle panels), which is in agreement with their canonical localization for the maturation of miRNAs [10,48]. Similarly, co-transfection of DICER and PKR led to a strong Venus signal homogeneously distributed in the cytoplasm (Fig 3E lower panel).

Collectively, these results formally confirm that DICER interacts with several RNA helicases and dsRNA-binding proteins in virus-infected cells, among which PKR, and that for the latter this interaction occurs in the cytoplasm.

DICER interactome changes upon SINV infection are not cell-type specific

To further validate our DICER interactome results and generalize them to another biological system, we performed co-IP experiments on the endogenous DICER in a different cell type. To this end, the FLAG-HA-GFP tag was knocked into (KI) the *Dicer* locus in human colon carcinoma cells (HCT116) by CRISPR-Cas9-mediated homologous recombination (S4A, S4B and S4C Fig). A guide RNA (gRNA) targeting the region corresponding to Dicer ATG and a DNA template for homologous recombination bearing the FLAG-HA-GFP sequence surrounded by the upstream and downstream arms of Dicer were used to generate the resulting cell line referred to as HCT116 KI-DICER cells. The expected insertion of the tag in one of the two Dicer alleles was assessed by PCR amplification and Sanger sequencing (S4A, S4B and S4C Fig). In agreement, we could detect two bands for DICER protein by western blot in the HCT116 KI-DICER cells, which confirmed that this cell line is heterozygous (Fig 4A).

We additionally verified the expression of specific DICER-interacting proteins, such as AGO2, PKR or TRBP, in HCT116 KI-DICER cells compared to the parental HCT116 cells and to HEK293T cells (Fig 4A). We also measured the production of mature miRNAs, such as miR-16, by northern blot analysis and confirmed that miRNA expression is maintained in HCT116 KI-DICER cells (Fig 4B). Of note, the GFP inserted at the *Dicer* locus could not be detected by epifluorescence microscopy in the HCT116 KI-DICER cells, which probably reflects the low abundance of the DICER protein.

We then determined whether SINV-GFP infection was comparable in HCT116 cells and HEK293T cells. We infected HCT116, HCT116 KI-DICER and HEK293T cells with SINV-GFP at three different MOI (0.02, 0.1 and 1) and measured GFP fluorescence by microscopy at 24 hpi (Fig 4C). Both HCT116 and HCT116 KI-DICER cells expressed GFP upon infection with SINV-GFP, although with a lower intensity than HEK293T cells. We also verified by western blot analysis the accumulation of GFP and the phosphorylation of both PKR and eIF2 upon SINV-GFP infection of HCT116 KI-DICER and HEK293T cells (S4D Fig) and chose as optimal SINV-GFP condition of infection in HCT116 KI-DICER cells the MOI of 0.1 for 24 h.

To validate the DICER interactions observed in HEK293T FHA:DICER cells, we then performed anti-HA co-IP experiments followed by western blot analysis in HCT116 KI-DICER cells infected or not with SINV-GFP. We successfully retrieved TRBP interacting with DICER in both mock and infected cells, whereas DHX9, PKR (phosphorylated or not) and PACT were only retrieved in the HA IP in infected cells (Fig 4D). These results not only confirm that the endogenous DICER specifically interacts with DHX9, PACT and PKR upon SINV infection, but also that these interactions are not restricted to one specific cell type.

The helicase domain of DICER is required for its interaction with PKR

Even though DICER and PKR are likely brought together by RNA, specific protein domains might be involved in stabilizing the complex. Therefore, we next determined the domain of DICER required for its interaction with PKR. Since its helicase domain was previously shown to be involved in the interaction with TRBP and PACT [14,17], we speculated that it could also be implicated in binding PKR. To test this hypothesis, we cloned several versions of DICER proteins wholly or partly deleted of the helicase domain (Fig 5A DICER N1 and N3). In addition, we also cloned the helicase domain alone (Fig 5A DICER Hel.) and a DICER variant

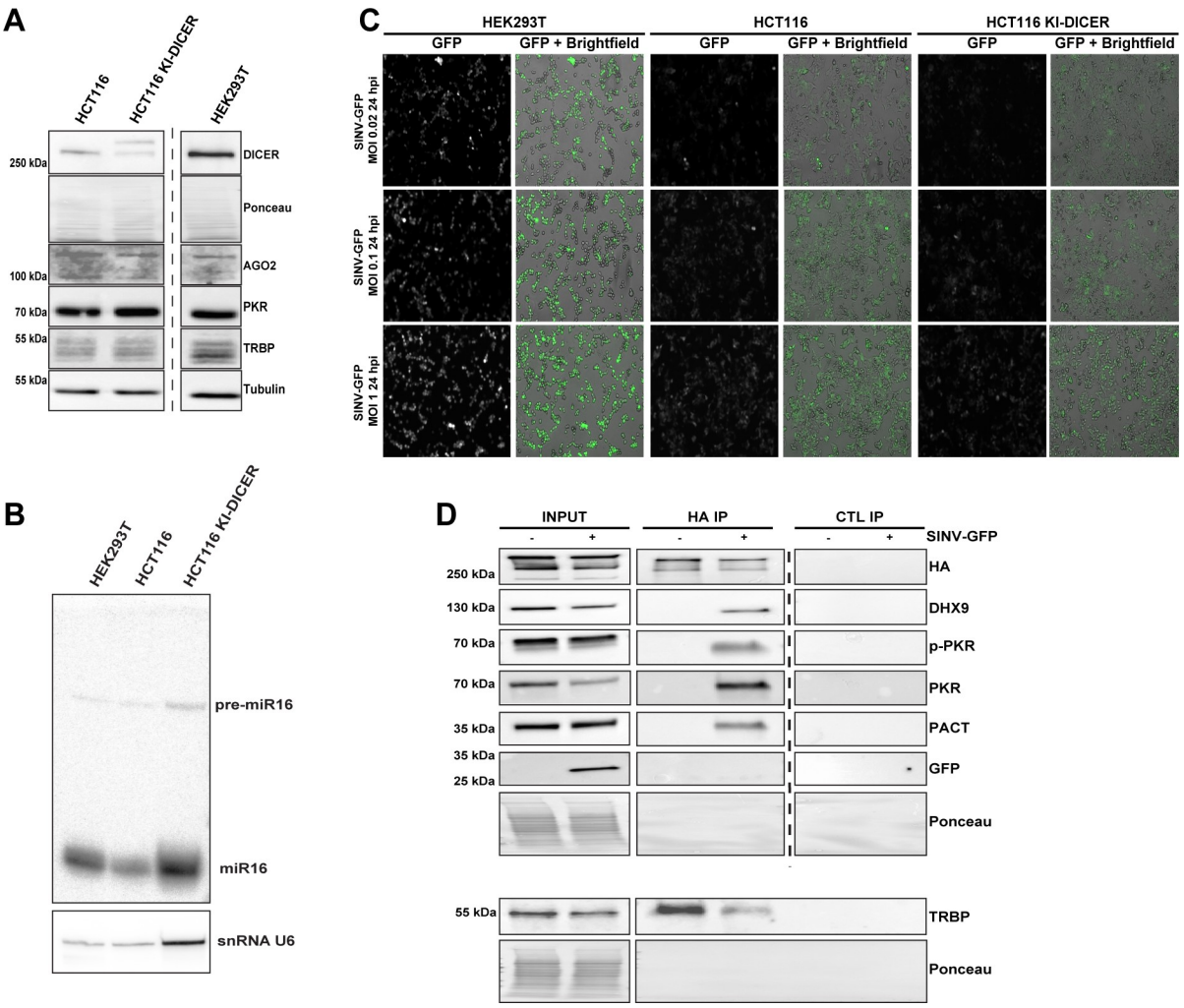

Fig 4. Confirmation of DICER interactome upon SINV infection in HCT116 KI-DICER cells. A. Western blot analysis of DICER, AGO2, PKR and TRBP expression in HEK293T, HCT116 and HCT116 KI-DICER cell lines. Gamma-Tubulin and ponceau were used as loading controls. **B**. GFP fluorescent microscopy pictures of HEK293T, HCT116 and HCT116 KI-DICER cell lines infected with SINV-GFP at an MOI of 0.02, 0.1 and 1 for 24 h. The left panel corresponds to GFP signal from infected cells and the right panel to a merge picture of GFP signal and brightfield. Pictures were taken with a 5x magnification. **C**. miR-16 expression analyzed by northern blot in the same cell lines as in B. Expression of snRNA U6 was used as loading control. **D.** Western blot analysis of HA co-IP in mock or SINV-GFP-infected (MOI of 0.1, 24 hpi) HCT116 KI-DICER cells. Proteins associated to FHA-GFP:DICER were revealed by using antibodies targeting endogenous DHX9, p-PKR, PKR, PACT or TRBP proteins. The TRBP immunoblot was performed by loading the same samples on a separate membrane. In parallel, an HA antibody was used to verify the IP efficiency and GFP antibody was used to verify the infection. Ponceau was used as a loading control.

https://doi.org/10.1371/journal.ppat.1009549.g004

deleted of its C-terminal dsRNA binding domain (Fig 5A DICER dsRBD) since this domain could also be involved in protein-protein interaction [49,50]. We then transfected the different versions of DICER WT and the deletion mutant constructs in NoDice cells. In mock and SINV-GFP infected cells, whole cell extracts were subjected to anti-HA and anti-MYC (CTL) IP. TRBP was retrieved in both conditions with DICER WT, Hel. and dsRBD (Fig 5B and 5C). In mock cells, PACT and PKR were only found weakly interacting with DICER WT (Fig 5B). In SINV-infected cells, we observed that similar to TRBP and to a lesser extent PACT, N1 and N3 mutations strongly reduced the binding of DICER with PKR (Fig 5C lanes 2–3 and 7–8). Importantly, we also noted that the helicase domain alone could bind PKR, TRBP and

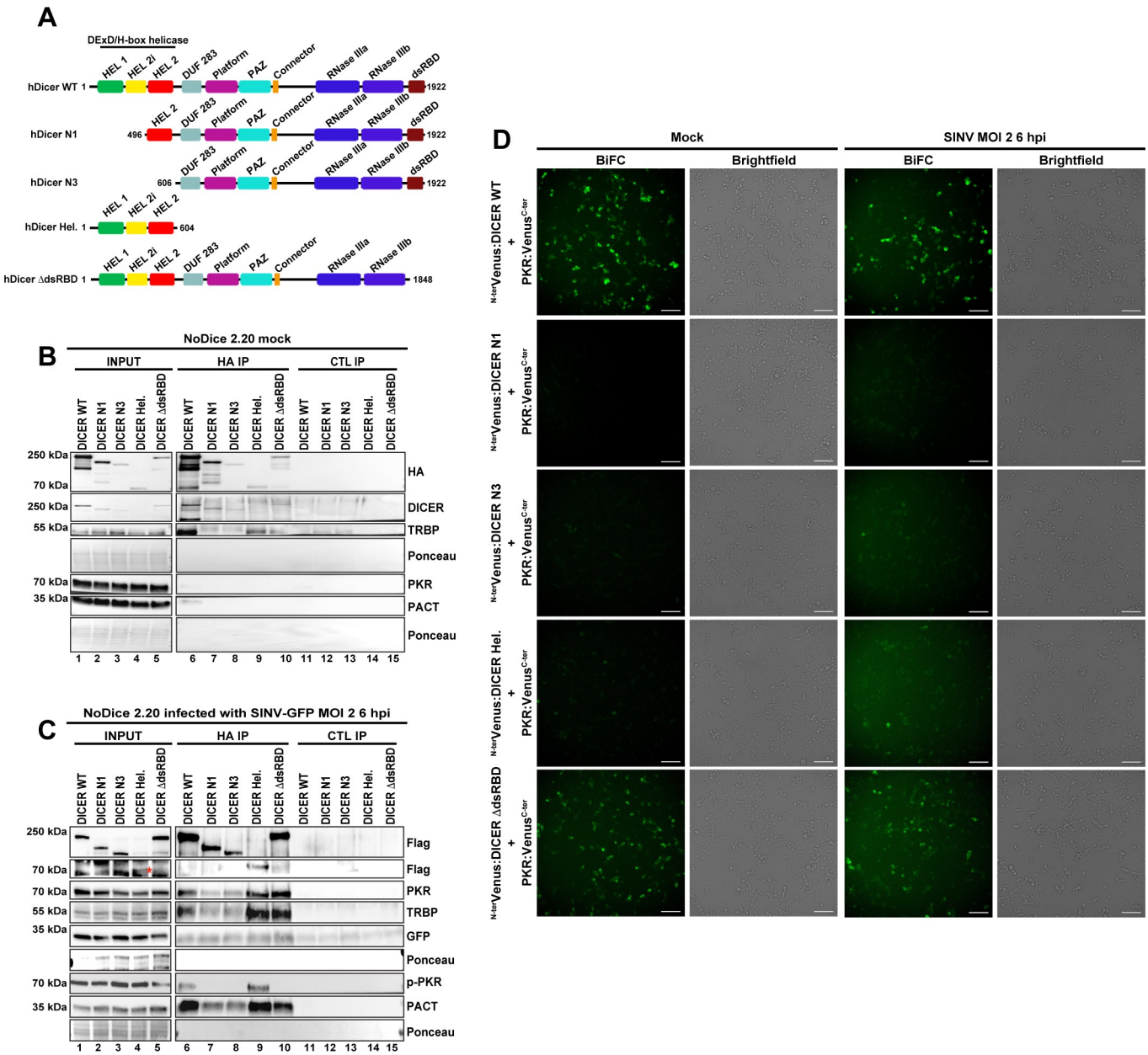

Fig 5. Identification of DICER domains involved in DICER-PKR interaction. A. Schematic representation of Human DICER proteins used in this study. The different conserved domains are shown in colored boxes. DUF283: Domain of Unknown Function; PAZ: PIWI ARGONAUTE ZWILLE domain; dsRBD: dsRNA-binding domain. hDICER WT is the full-length protein. hDICER N1 is deleted of the first N-terminal 495 amino acids. hDICER N3 is wholly deleted of the helicase domain. hDICER Hel. is the whole DICER's helicase domain. hDICER dsRBD is deleted of the C-terminal dsRBD. **B.** Western blot analysis of HA co-IP in mock NoDice 2.20 cells transfected with different versions of FHA:DICER proteins. Efficiency of immunoprecipitation was assessed using anti-HA and anti-DICER antibodies and co-IPs of TRBP, PKR and PACT were examined using appropriate antibodies. Expression of GFP in INPUT fraction was visualized as control of SINV-GFP infection. Ponceau staining of membranes is used as loading control. **C.** Western blot analysis of HA co-IP in NoDice 2.20 cells transfected with different versions of FHA:DICER proteins and infected with SINV-GFP (MOI of 2, 6 hpi). Efficiency of immunoprecipitation was assessed using an anti-Flag antibody and co-IPs of PKR, TRBP, p-PKR and PACT were examined using appropriate antibodies. Expression of GFP in INPUT fraction was visualized as control of SINV-GFP infection. Ponceau staining of membranes is used as loading control. The DICER Hel. band is indicated by a red asterisk. **D.** Plasmids expressing the different versions of DICER proteins fused to the N-terminal part of Venus and PKR:Venus$^{C\text{-}ter}$ plasmid were co-transfected in NoDice PKR cells. Cells were treated as in Fig 3D. The different combinations are noted on the left side. The fluorescent signal was observed using an epifluorescence microscope. For each condition, the left panel corresponds to Venus signal and the right panel to the corresponding brightfield pictures. Scale bar: 100 μm. hpi: hours post-infection.

https://doi.org/10.1371/journal.ppat.1009549.g005

PACT (Fig 5C lanes 4 and 9). Moreover, the deletion of the dsRNA binding domain of DICER did not affect its interaction with TRBP, PACT and PKR (Fig 5C lanes 5 and 10). We also looked for p-PKR in our co-IP (Fig 5C panel p-PKR). We noticed that only WT DICER and its helicase domain were able to interact with p-PKR (Fig 5C lanes 1&6 and 4&9). The fact that DICER dsRBD did not interact with p-PKR (Fig 5C lanes 5&10) is striking but could indicate that the phosphorylation of PKR may induce conformational changes preventing its interaction with some domains of DICER. These results reveal that, like for TRBP and PACT, the helicase domain of DICER is required for DICER-PKR/p-PKR interaction during SINV infection.

In order to confirm these co-IP experiments, we next decided to perform BiFC experiments using the same conditions as previously. In both mock and SINV-infected cells, only the combinations of DICER WT-PKR and DICER dsRBD-PKR showed a strong Venus signal, while neither DICER N1 nor N3 constructs revealed an interaction with PKR (Fig 5D). In contrast, the DICER Hel. construct did not seem to interact with PKR in mock-infected cells but appeared to do so in SINV-infected cells as a faint Venus signal could be observed. These results therefore confirmed the co-IP observations for the DICER-PKR interaction. In addition, we also performed a BiFC experiment using the different DICER constructs with TRBP or PACT. Altogether, the BiFC results mostly fitted with the co-IP experiments for the DICER-TRBP (S5A Fig) and DICER-PACT (S5B Fig) interactions. TRBP indeed did not seem to interact with the DICER N1 and only slightly with the DICER N3. However, PACT interaction was lost with DICER N1, but not with DICER N3 in mock- and SINV-infected cells (S5B Fig third panel). This result may be explained by the fact that DICER interacts with PACT *via* the helicase and DUF domains, whereas only the DICER helicase domain is required for its interaction with TRBP [14,17]. In agreement, the Venus signal observed between the DICER Hel. and PACT seemed weaker than the one we observed with TRBP (S5A and S5B Fig fourth panels).

Taken together these results indicate that DICER interacts with both PKR and its phosphorylated form during SINV infection, and that this interaction requires the helicase domain of DICER.

Functional importance of DICER helicase domain during SINV infection

We then sought to study the functional role of DICER-PKR interaction during viral infection. For this purpose, we decided to use DICER helicase deletion mutants to study SINV infection. To do so, we first generated NoDice HEK293T cells stably expressing FHA-tagged DICER N1 (FHA:DICER N1) by lentiviral transduction. As for the FHA:DICER WT cell line, we first selected a clone expressing the tagged DICER N1 at a level similar to the endogenous DICER protein in HEK293T cells (Fig 6A). DICER N1 protein has been shown to still be able to produce miRNAs [33]. We thus verified by northern blot analysis that DICER N1 is indeed able to process miRNAs similarly to WT DICER in HEK293T and FHA:DICER cells, thereby validating the functionality of the tagged protein (Fig 6B). We next infected HEK293T, FHA:DICER WT #4 and FHA:DICER N1 #6 cells with SINV-GFP and measured virus accumulation by assessing GFP expression by microscopy analysis. Interestingly, the GFP protein level was drastically reduced in FHA:DICER N1 #6 cells compared to FHA:DICER WT #4 and HEK293T cells (Fig 6C). Encouraged by this observation, we decided to infect with SINV-GFP additional DICER deletion mutants, namely N3 and Hel. We generated stable cell lines for these various mutants by lentiviral transduction in the NoDice 2.20 background and infected those cells with SINV-GFP at an MOI of 0.02 for 24 h. We verified by western blot analysis that all selected DICER mutant clones, namely N1 #6, N3 #2.13 and Hel. #2.6, expressed the tagged protein at the expected size and at levels mostly similar to the FHA:DICER WT #4 cell line (Fig 6D, first two panels). We also verified the DICER mutants contribution to the

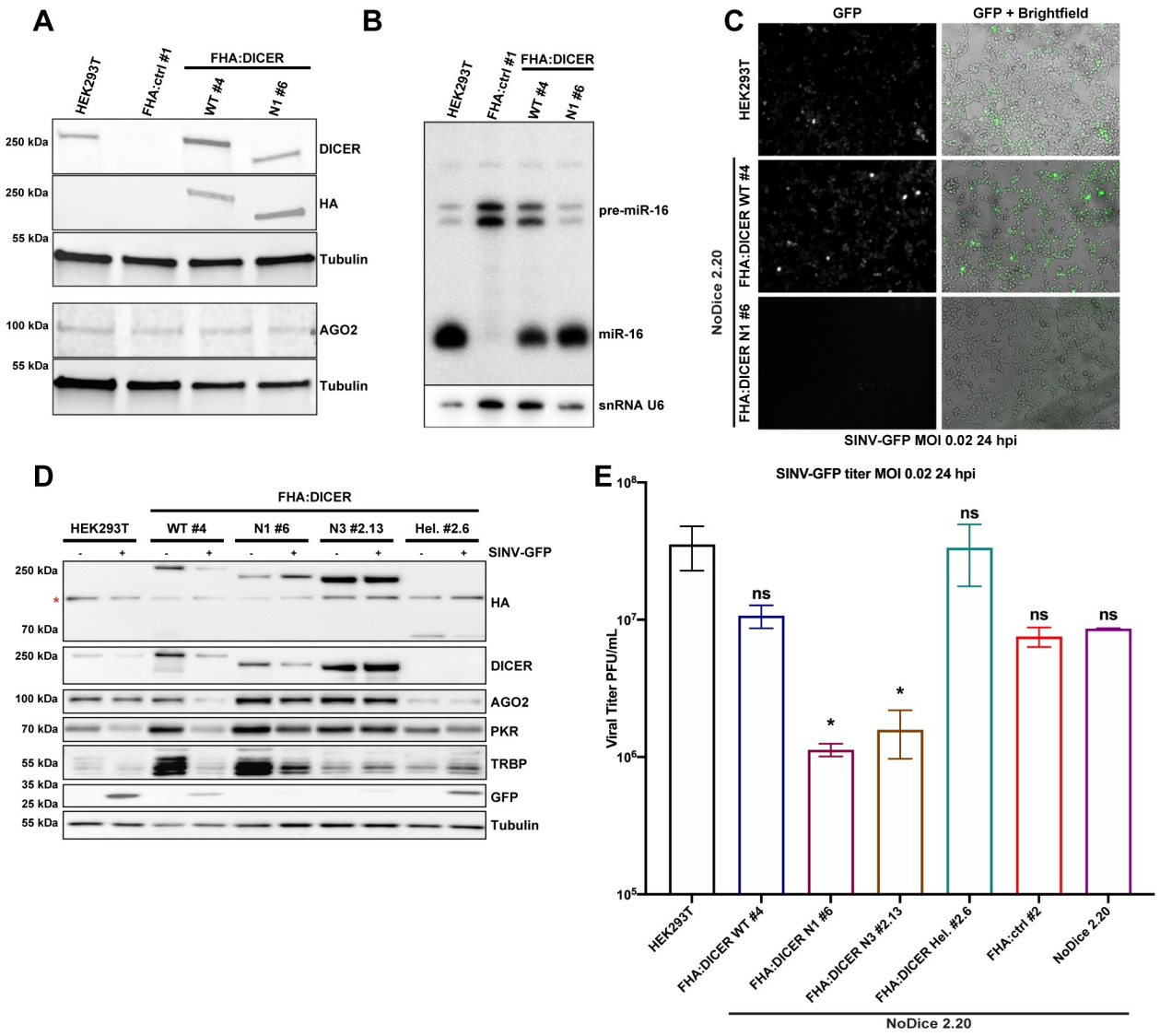

Fig 6. Analysis of the importance of Dicer helicase domain on SINV-GFP infection in FHA:DICER mutant stable cell lines. A. Expression of DICER (DICER, HA), TRBP and AGO2 was analysed by western blot in HEK293T, NoDice FHA:ctrl #1, FHA:DICER WT #4 and FHA:DICER N1 #6 cell lines. Gamma-Tubulin was used as loading control. **B.** Northern blot analysis of miR-16 expression in the same samples as in A. Expression of snRNA U6 was used as loading control. **C.** Representative GFP fluorescent microscopy images of HEK293T, FHA:DICER WT #4 and FHA:DICER N1 #6 cell lines infected with SINV-GFP at an MOI of 0.02 for 24 h. The left panel corresponds to GFP signal and the right panel to a merge picture of GFP signal and brightfield. Pictures were taken with a 5x magnification. hpi: hours post-infection. **D.** Western blot analysis of DICER (DICER and HA), AGO2, PKR, and GFP expression in SINV-GFP-infected cells in the same condition as in C. Gamma-Tubulin was used as loading control. The asterisk correspond to aspecific bands **E.** Mean (+/- SEM) of SINV-GFP viral titers fold change over HEK293T cells in HEK293T, NoDice 2.20, FHA:DICER WT #4 and FHA:DICER mutants cell lines infected at an MOI of 0.02 for 24 h (n = 3) from plaque assay quantification. * $p < 0.05$, ns: non-significant, ordinary one-way ANOVA test with Bonferroni correction.

https://doi.org/10.1371/journal.ppat.1009549.g006

endogenous miRNA biogenesis by performing a northern blot analysis on miR-16 accumulation (S6A Fig).

We additionally verified the impact of these DICER mutants on SINV-GFP infection by measuring the GFP intensity of fluorescence by microscopy (S6B Fig). Our results indicate that GFP accumulation is similar in HEK293T, NoDice 2.20, FHA:DICER WT, Hel. and ctrl cells. However, almost no fluorescence was detected in FHA:DICER N1 #6 and N3 #2.13 cells compared to HEK293T cells (S6B Fig). The reduction of virus-encoded GFP accumulation

and viral production were confirmed by western blot (Fig 6D) and by plaque assay, respectively (Figs 6E and S6C).

Altogether, these results therefore indicate that expressing a helicase truncated version of DICER, which is unable to interact with PKR, appears to confer an antiviral phenotype against SINV infection.

The antiviral phenotype of the helicase-truncated DICER mutants is independent of AGO2

We finally carried out a functional analysis of the helicase-domain-truncated DICER N1 and N3 mutants to investigate the mechanism of the antiviral phenotype. First, to investigate a potential implication of the RNAi pathway, we performed a knock-down of the AGO2 protein prior to the infection of NoDice cells expressing either WT, N1 or N3 FHA:DICER. AGO2 is the main effector protein in RNA silencing pathways [51] and has been previously shown to be a crucial antiviral RNAi factor against Influenza A virus in mouse embryonic fibroblasts (MEFs) [52]. We transfected either control siRNAs, or siRNAs targeting AGO2 for 48 h in NoDice cells stably expressing either an empty vector (FHA:ctrl #2) or WT, N1 or N3 FHA:DICER constructs. Cells were then infected with SINV-GFP at an MOI of 0.02 for 24 h, and virus accumulation was first assessed by looking at GFP expression by microscopy analysis (Fig 7A). In all cell lines, no major difference in GFP fluorescence could be observed when comparing cells transfected with the control siRNA or AGO2-specific siRNAs. We verified the knock-down efficiency by western blot analysis and confirmed the microscopy observation by measuring GFP protein accumulation (Fig 7B). Finally, we measured virus accumulation by plaque assay, and we observed that the antiviral phenotype was clearly visible in FHA:DICER N1 #6 and FHA:DICER N3 #2.13 cell lines but was not complemented upon AGO2 knock-down (Fig 7C).

Altogether, these results indicate that the antiviral phenotype against SINV observed in cells expressing helicase-truncated mutant DICER proteins does not depend on the presence of AGO2, thereby ruling out an involvement of RNAi.

The antiviral phenotype due to the DICER helicase-domain deletion requires PKR

In order to determine the functional role of the PKR-DICER interaction in the antiviral response to SINV, we generated NoDice PKR cells stably expressing either the full length FHA:DICER WT or the helicase deletion mutants FHA:DICER N1 or N3, or the empty vector as a control (FHA:ctrl) by lentiviral transduction. After monoclonal selection of each cell line, we infected them with SINV-GFP at an MOI of 0.02 and assessed virus accumulation by looking at GFP fluorescence by microscopy analysis (Fig 8A). As expected, an increase in GFP fluorescence was observed in NoDice PKR FHA:ctrl cells compared to HEK293T cells at 24 hpi. In contrast we could not observe any difference in GFP fluorescence between NoDice PKR FHA:ctrl cells and those expressing FHA:DICER WT, FHA:DICER N1 or N3 proteins. To verify whether any significant difference in terms of virus accumulation could be observed in NoDice PKR cells expressing WT or helicase truncated DICER proteins, we measured GFP protein levels by western blot analysis (Fig 8B) and virus production by plaque assay (Fig 8C). As opposed to the observations done in NoDice cells expressing PKR (Fig 6), both GFP accumulation and viral titers remained unchanged between NoDice PKR FHA:ctrl cells and those expressing FHA:DICER WT, N1 or N3 constructs. Taken together, these results demonstrate that the antiviral phenotype of helicase-truncated DICER mutants depends on the presence of PKR. Therefore, our data suggest that the helicase domain of DICER sequesters PKR and

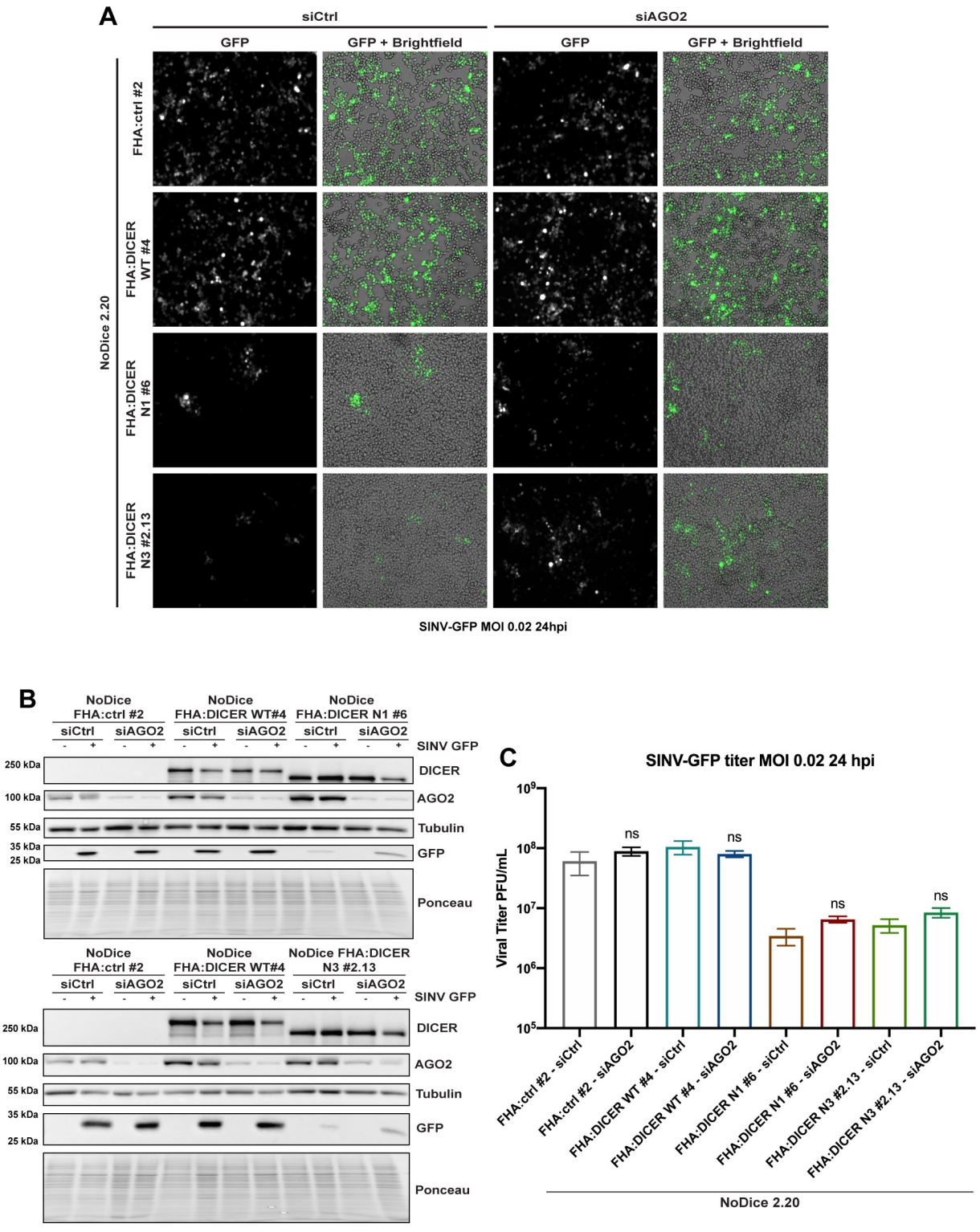

Fig 7. The antiviral effect of helicase-deleted DICER mutants is independent of AGO2. A. GFP fluorescent microscopy pictures of NoDice FHA:ctrl #2, NoDice FHA:DICER WT #4 and NoDice FHA:DICER mutant cell lines treated with two doses of siAGO2 at 20 nM for 48 hours before a 24-hour-SINV-GFP infection at an MOI of 0.02. The left panel corresponds to GFP signal from infected cells and the right panel to a merge picture of GFP signal and brightfield. Pictures were taken with 5x magnification. hpi: hours post-infection. **B.** Western blot analysis of DICER, AGO2 and GFP expression in SINV-GFP-infected NoDice FHA:ctrl #2, NoDice FHA:DICER WT #4 and NoDice FHA:DICER mutant cell lines shown in A. Cells were treated with two doses of siAGO2 at 20 nM for 48 hours before a 24-hour-SINV-GFP infection at an MOI of

0.02. Gamma-Tubulin was used as loading control. **C.** Mean (+/-SEM) of SINV-GFP viral titers in the same cell lines as in A. infected at an MOI of 0.02 for 24 h (n = 3) from plaque assay quantification. ns: non-significant, two-tailed unpaired parametric t-test.

https://doi.org/10.1371/journal.ppat.1009549.g007

when this interaction is lost, the antiviral effect of PKR is exacerbated, thereby explaining the phenotype observed in cells expressing helicase-truncated DICER mutants.

Discussion

The role of DICER in antiviral defense in human cells remains a topic of intense discussion [21,22,53,54]. In particular there have been contradictory reports regarding its capacity to produce siRNAs from viral RNAs [31,37,55,56]. These observations could be due to the fact that several mammalian viruses potentially encode VSR proteins, thereby masking the effect of RNAi [22,28,29,52,57]. Another putative but non-exclusive explanation could be that there is a

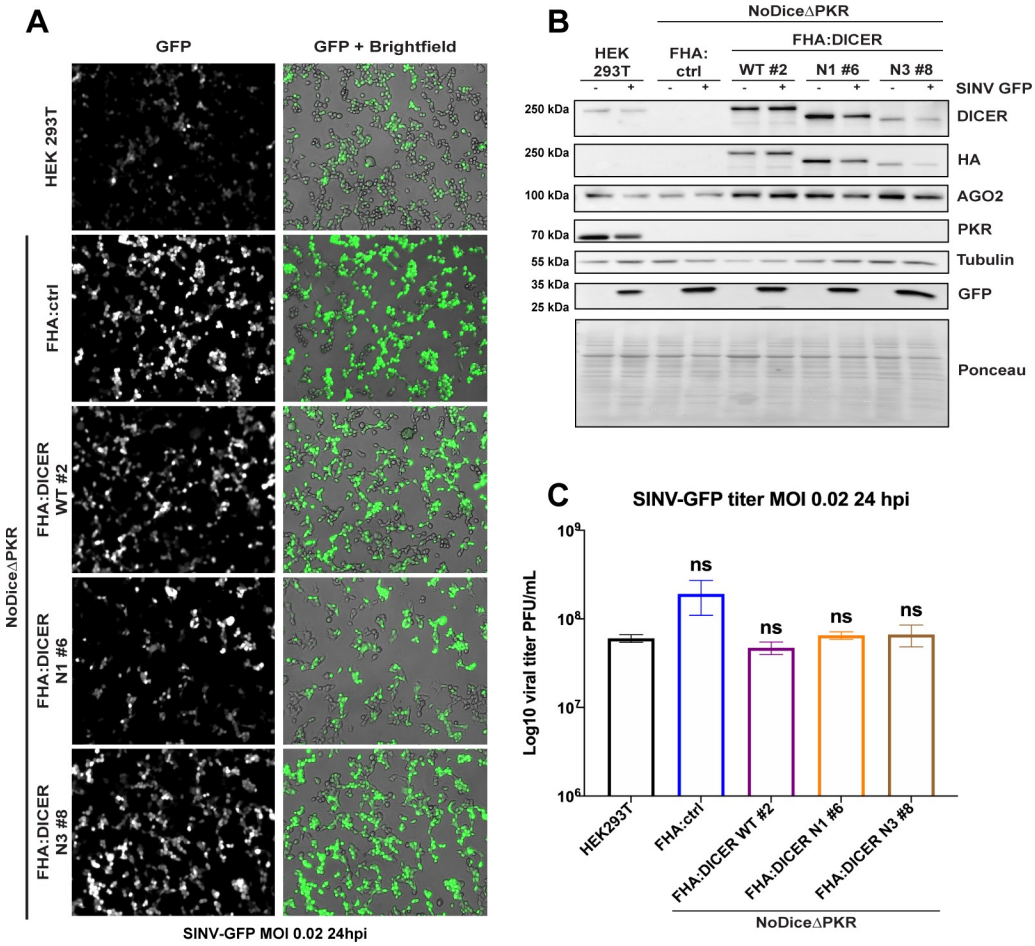

Fig 8. The antiviral effect of helicase-deleted DICER mutants requires PKR. A. GFP fluorescent microscopy pictures of HEK293T, NoDice PKR:ctrl and FHA:DICER mutant cell lines infected with SINV-GFP at an MOI of 0.02 for 24 h. The left panel corresponds to GFP signal from infected cells and the right panel to a merge picture of GFP signal and brightfield. Pictures were taken with 5x magnification. hpi: hours post-infection. **B.** Western blot analysis of DICER (DICER and HA), AGO2, PKR and GFP expression in SINV-GFP-infected HEK293T, NoDice PKR FHA:ctrl and FHA:DICER mutant cell lines shown in A. Gamma-Tubulin was used as loading control. **C.** Mean (+/-SEM) of SINV-GFP viral titers in the same cell lines as in A. infected at an MOI of 0.02 for 24 h (n = 3) from plaque assay quantification. ns: non-significant, ordinary one-way ANOVA test with Bonferroni correction.

https://doi.org/10.1371/journal.ppat.1009549.g008

mutual regulation of type I IFN and RNAi pathways [58,59]. Thus, it has already been shown that PACT can regulate MDA5 and RIG-I during virus infection and therefore the induction of type I IFN response [60,61]. To date, it is not clear whether the activity of the DICER protein as well could be regulated by potential interactors, or inversely whether it could itself modulate the activity of proteins involved in the IFN pathway. To answer this question, we determined the changes in the interactome of human DICER upon SINV and SFV infections. This analysis allowed us to reveal that a lot of proteins associating with DICER during viral infection are dsRNA-binding proteins and RNA helicases. A number of these proteins are known to be involved in antiviral defense pathways, thereby indicating the possible formation of one or several complexes between DICER and these proteins, which are very likely brought together by the accumulation of dsRNA during virus infection.

Among these proteins, we chose to focus on the well-known ISG PKR, which is involved in many cellular pathways such as apoptosis, cellular differentiation, development and antiviral defense [4,8,62,63]. PKR is one of the main actors of the Integrative Stress Response (ISR) in human cells, and its activation or inhibition needs to be tightly regulated in order to have a properly balanced response to stress. Our results indicate that DICER interacts via its helicase domain with PKR in the cytoplasm during SINV infection. The helicase domain of DICER, which is also required for its interaction with TRBP and PACT, belongs to the helicase superfamily 2, which is also found in RLRs such as RIG-I, MDA5 or LGP2 [64,65]. These proteins act as sensors of viral infection and through the activation of proteins such as MAVS, mediate the induction of type I IFN pathway [65]. We hypothesize that even though the human DICER helicase has evolved mainly to act in miRNA/siRNA pathways, it still retained the capacity to act as an RLR. However, as opposed to RIG-I and MDA5, our data suggest that DICER would act more as an inhibitor rather than inducer of the immune response. Therefore, we propose that this domain serves as a platform for the recruitment of different proteins to diversify the functions of DICER.

One such regulatory effect appears to be on the antiviral activity of PKR, as cells expressing a truncated form of DICER unable to interact with PKR become resistant to SINV infection. This is in agreement with previous observations that ectopic expression of the *Drosophila* DICER2 protein in human cells perturbs IFN signaling pathways and antagonizes PKR-mediated antiviral immunity [36]. Although the precise molecular mechanism involved will require further work to be fully deciphered, it seems that the two proteins are likely brought together *via* their interaction with RNA, most probably of viral origin. Indeed, we showed that the co-IP interaction was partially RNase sensitive. However, we confirmed that the interaction is not artificially created during the co-immunoprecipitation procedure, since we could show that DICER and PKR interact in BiFC assay, a technique that favors the detection of direct interactions [47]. Most of the time, the inhibition of PKR activity relies on its inhibition to bind to dsRNA or to auto-phosphorylate. For example, the human tRNA-dihydrouridine synthase 2 (hDus2) binds the first dsRBD of PKR and prevents its activation [66]. TRBP binds dsRNAs but also PKR directly hindering its dimerization. In normal condition, TRBP is also associated with PACT thus preventing PKR activation by PACT [67–70]. Since we showed that DICER can bind the activated phospho-PKR, we hypothesize that this interaction does not result in the inhibition of PKR autophosphorylation. In fact, in condition of infection with a high virus dose, we showed that phospho-PKR levels are similar in cells expressing DICER WT or helicase deletion mutants N1 and N3, but the activated PKR does not associate with these truncated versions of DICER. Therefore, one possibility could be that DICER interaction with PKR prevents the latter from acting upon some of its targets, which remain to be identified, to fine-tune the antiviral response.

As of now, we cannot formally rule out that the effect of DICER on PKR is mediated by other proteins. TRBP and PACT have been shown to regulate PKR activity, the former

normally acting as a repressor and the latter as an activator [46,68,70]. Interestingly, in lymphocytic Jurkat cells infected by HIV-1, PACT can also act as a repressor of PKR [71]. It is thus tempting to speculate that these two proteins participate in the formation of the DICER-PKR complex. However, our results show that this may not necessarily be the case. Indeed, in the BiFC experiment, the DICER N3 mutant still interacted with PACT but not with PKR indicating that PACT binding is not sufficient to confer the association with PKR.

Besides PKR, other proteins were specifically enriched upon viral infection in the DICER IP. These are also interesting candidates to explain the putative regulatory role of DICER. Among these proteins, DHX9 and ADAR-1 are especially intriguing. DHX9, also known as RNA helicase A (RHA), associates with RISC, helping the RISC loading [41]. Moreover, DHX9 is directly involved in removing toxic dsRNAs from the cell to prevent their processing by DICER [40]. It has also been implicated in HIV-1 replication and knockdown of DXH9 leads to the production of less infectious HIV-1 virions [72–74]. Finally, DXH9 interacts with and is phosphorylated by PKR in MEFs. This phosphorylation precludes the association of DHX9 with RNA, thus inhibiting its proviral effect [75]. In light of these observations and ours, we can speculate that the inhibitory effect of DICER on PKR activity could also be linked to DHX9 phosphorylation. ADAR-1 is one of the well-known RNA-editing factors [76]. ADAR-1 is linked to both miRNA biogenesis [77–79] and virus infection. Indeed, ADAR-1 has an antiviral effect against Influenza virus, but most of the time, its depletion leads to a decrease of the viral titer, as was reported for VSV or HIV-1 [80,81]. It has been shown that ADAR-1 and PKR interact directly during HIV-1 infection. This interaction triggers the inhibition of PKR activation, and thus a reduction of eIF2 phosphorylation leading to an increase of virus replication [5,82]. Interestingly, over-expression of ADAR-1 enhances drastically the replication of the alphaviruses Chikungunya virus (CHIKV), and Venezuelan equine encephalitis virus (VEEV) most likely by interfering with the IFN induction [83].

One hypothesis to explain the virus resistance phenotype of the DICER N1 and N3 cell lines could be an increased processivity of these truncated proteins on long dsRNA substrates [33], which would render DICER RNAi proficient. However, our results are not in favor of this hypothesis, since we show that knocking-down AGO2 does not allow to make cells expressing DICER N1 or N3 more sensitive to SINV infection. AGO2 being the only slicer-proficient Argonaute protein expressed at physiological levels in HEK293T cells, we can confidently conclude that the observed phenotype is RNAi-independent.

Finally, we demonstrated that the phenotype of helicase-truncated DICER isoforms depends on PKR expression, because it was completely lost in PKR knockout cell lines. We therefore propose that, at least during infection with SINV, DICER prevents PKR to be fully active by interacting with and potentially sequestrating it. Deciphering the exact molecular mechanism at play will require additional studies in order to get the full picture. Nevertheless, by assessing the interactome of DICER during SINV infection, we have unveiled a new, PKR-dependent, role for the helicase domain of DICER in regulating the cellular response to viral infection.

Material and methods

Plasmids, cloning and mutagenesis

Plasmids used for BiFC experiments were a gift from Dr. Oliver Vugrek from the Ruđer Bošković Institute and described in [47]. The cDNAs of TRBP, PACT and PKR were respectively amplified from (pcDNA-TRBP Addgene #15666) [16], (pcDNA-PACT Addgene #15667) [16], (pSB819-PKR-hum Addgene #20030) [84], and cloned into the four pBiFC vectors by Gateway recombination. DICER N1, N3, Hel. and dsRBD were generated by PCR mutagenesis from

pDONR-DICER described in [36] and cloned into the four pBiFC and pDEST-FHA vectors by Gateway recombination. plenti6 FHA-V5 vector was modified from plenti6-V5 gateway vector (Thermo Fisher Scientific V49610) by Gibson cloning. DICER WT, N1, N3 and Hel. from pDONR plasmids were cloned into plenti6 FHA-V5 by Gateway recombination. All primers used are listed in S5 Table.

Cell lines

HEK293T, HEK293T/NoDice (2.20 and 4.25), and HEK293T/NoDice PKR cell lines were a gift from Pr. Bryan Cullen and described in [33,39]. HCT116 cell line was a gift from Dr. Christian Gaiddon.

Generation of Flag-HA-GFP-DICER knock-in cell line by CRISPR/Cas9

To generate the knock-in cell line, the sequence of Flag-HA-GFP was amplified by PCR from the Flag-HA-GFP plasmid [85]. DNA sequences corresponding to 1 Kb upstream (left homology arm) and downstream (right homology arm) the starting codon (ATG) of DICER gene were amplified from HCT116 cell genomic DNA using primer pairs listed in S5 Table. The three PCR products were gel-purified and cloned into a linearized pUC19 by In-fusion cloning (Clontech) to obtain the template for homologous recombination (LarmDICER-FlagHAGFP-RarmDICER).

Design of the guide RNA targeting the region between Dicer 5'-UTR and its first coding exon for CRISPR/Cas9 mediated knock-in was carried out using the CRISPOR Design Tool [86]. Annealed oligonucleotides corresponding to the gRNA (S5 Table) were cloned into the vector pX459 (Addgene #48139) which also encodes *S. pyogenes* Cas9 with 2A-Puro.

The sequence of the donor plasmid was additionally mutagenized to disrupt the PAM sequence of the right homology arm to avoid its cleavage by the gRNA.

To obtain the knock-in (KI) cell line, 5 x 10^5 HCT116 cells were seeded in a 6 well plate with Dulbecco's modified Eagle medium (DMEM, Gibco, Life Technologies) supplemented with 10% fetal bovine serum (FBS, Clontech) in a humidified atmosphere of 5% CO_2 at 37˚C and transfected after 24 hours with the pX459-gRNADicerNterm-Cas9-2A-Puro plasmid and the Leftarm-FlagHAGFP-RightarmDICER donor plasmids at the ratio of 1 to 1 (6 micrograms plasmids in total) using Lipofectamine 2000 according to the manufacturer's instructions. 24 hours later, puromycin (1 mg/mL) was added to the cells to increase the KI efficiency and genomic DNA was isolated from individual colonies few days later.

The presence of the Flag-HA-GFP tag in frame with hDICER coding sequence was confirmed by sequencing PCR amplicon from KI cell gDNA. Expression of Flag-HA-GFP N-terminal tagged Dicer protein in the KI cells was confirmed by western blot.

Cell culture and transfection

Cells were maintained in Dulbecco's modified Eagle medium (DMEM, Gibco, Life Technologies) supplemented with 10% fetal bovine serum (FBS, Clontech) in a humidified atmosphere of 5% CO_2 at 37˚C. Transfection was performed using Lipofectamine 2000 (Invitrogen, Thermo Fisher Scientific) according to the manufacturer's instructions.

Lentivirus production and generation of stable cell lines

The lentiviral supernatant from single transfer vector was produced by transfecting HEK293T cells (ATCC CRL-3216) with 20 μg of the transfer vector, 15 μg of pMDLg/p RRE and 10 μg of pRSV-Rev packaging plasmids (Addgene #12251 and Addgene #12253) and the pVSV

envelope plasmid (Addgene #8454) using Lipofectamine 2000 reagent (Invitrogen, Thermo Fisher Scientific) according to the manufacturer's protocol. Standard DMEM medium (Gibco, Life Technologies) supplemented with 10% Fetal bovine serum (FBS, Gibco, Life Technologies) and 100 U/mL of penicillin-Streptomycin (Gibco, Life Technologies) were used for growing HEK293T cells and for lentivirus production. One 10 cm plate of HEK293T cells at 70–80% confluency was used for the transfection. The medium was replaced 8 hours post-transfection. After 48 hours the medium containing viral particles was collected and filtered through a 0.45 μm PES filter. The supernatant was directly used for transfection or stored at -80˚C. A 6 well plate of HEK293T/NoDice or HEK293T/NoDice PKR cells at 80% confluency was transduced using 600 μL of lentiviral supernatant either expressing FHA:DICER, N1, N3, Hel. or empty vector, supplemented with 4 ug/mL polybrene (Sigma) for 6 hours. The transduction media was then changed with fresh DMEM for 24 hours and the resistant cell clones were selected for about 6 weeks with blasticidin (15 μg/mL for NoDice or 10 μg/mL for NoDice PKR) and subsequently maintained under blasticidin selection.

Viral stocks, virus infection

Viral stocks of SINV or SINV-GFP were produced as described in [36]. Cells were infected with SINV or SINV-GFP at an MOI of 0.02, 0.1, 1 or 2 and samples were collected at different time points as indicated in the figure legends.

Analysis of viral titer by plaque assay

Vero R cells were seeded in 96-well plates format and were infected with 10-fold serial dilutions infection supernatants for 1 hour. Afterwards, the inoculum was removed, and cells were cultured in 2.5% carboxymethyl cellulose for 72 hours at 37˚C in a humidified atmosphere of 5% CO_2. Plaques were counted manually under the microscope and viral titer was calculated according to the formula: *PFU/mL = #plaques/ (Dilution* Volume of inoculum)*. All data and statistics pertaining to plaque assay analysis can be found in S6 Table.

Western blot analysis

Proteins were extracted from cells and homogenized in 350 μL of lysis buffer (50 mM Tris-HCl pH 7.5, 150 mM NaCl, 5 mM EDTA, 1% Triton X-100, 0.5% SDS and Protease Inhibitor Cocktail (complete Mini; Sigma Aldrich). Proteins were quantified by the Bradford method and 20 to 30 μg of total protein extract were loaded on 4–20% Mini-PROTEAN TGX Precast Gels (Bio-Rad). After transfer onto nitrocellulose membrane, equal loading was verified by Ponceau staining. For PVDF membrane, equal loading was verified by Coomassie staining after transfer and blotting. Membranes were blocked in 5% milk and probed with the following antibodies: anti-hDicer (1:500, F10 Santa Cruz, sc-136979) and anti-hDicer (1:1000, A301-937A, Bethyl), anti-TRBP (1:500, D-5 Santa Cruz, sc-514124), anti-PKR (1:2500, Abcam ab32506), anti-PACT (1:500, Abcam, ab75749), anti-HA (1:10000, Sigma, H9658), anti-DHX9 (1:500, Abcam, ab26271), anti-p-eIF2 (1:1000, Ser-52 Santa Cruz, sc-601670), anti-hADAR-1 (1:500 Santa Cruz, sc-271854) anti-p-PKR (1:1000 Abcam ab81303) anti-GFP (1:10000, Roche, 11814460001) and anti-Tubulin (1:10000, Sigma, T6557). Detection was performed using Chemiluminescent Substrate (Pierce, Thermo Fisher Scientific) and visualized on a Fusion FX imaging system (Vilber).

RNA extraction and northern blot analysis

Total RNA was extracted using Tri-Reagent Solution (Fisher Scientific; MRC, Inc) according to the manufacturer's instructions. Northern blotting was performed on 10 μg of total RNA.

RNA was resolved on a 12% urea-acrylamide gel, transferred onto Hybond-NX membrane (GE Healthcare). RNAs were then chemically cross-linked to the membrane during 90 min at 65˚C using 1-ethyl-3-[3-dimethylaminopropyl]carbodiimide hydrochloride (EDC) (Sigma Aldrich). Membranes were prehybridized for 30 min in PerfectHyb plus (Sigma Aldrich) at 50˚C. Probes consisting of oligodeoxyribonucleotides (see S5 Table) were 5′-end labeled using T4 polynucleotide kinase (Thermo Fisher Scientific) with 25 μCi of [-32P]dATP. The labeled probe was hybridized to the blot overnight at 50˚C. The blot was then washed twice at 50˚C for 20 min (5× SSC/0.1% SDS), followed by an additional wash (1× SSC/0.1% SDS) for 5 min. Northern blots were exposed to phosphorimager plates and scanned using a Bioimager FLA-7000 (Fuji).

Immunoprecipitation

Immunoprecipitation experiments were carried out either on tagged proteins or on endogenous proteins.

Tagged proteins. Cells were harvested, washed twice with ice-cold 1× PBS (Gibco, Life Technologies), and resuspended in 550 μL of lysis buffer (50 mM Tris-HCl pH 7.5, 140 mM NaCl, 1.5 mM $MgCl_2$, 0.1% NP-40), supplemented with Complete-EDTA-free Protease Inhibitor Cocktail (complete Mini; Sigma Aldrich). Cells were lysed by 30 min incubation on ice and debris were removed by 15 min centrifugation at 2000 g and 4˚C. An aliquot of the cleared lysates (50 μL) was kept aside as protein Input. Samples were divided into equal parts (250 μL each) and incubated with 15 μL of magnetic microparticles coated with monoclonal HA or MYC antibodies (MACS purification system, Miltenyi Biotech) at 4˚C for 1 hour under rotation (10 rpm). Samples were passed through μ Columns (MACS purification system, Miltenyi Biotech). The μ Columns were then washed 3 times with 200 μL of lysis buffer and 1 time with 100 μL of washing buffer (20 mM Tris-HCl pH 7.5). To elute the immunoprecipitated proteins, 95˚C pre-warmed 2x Western blot loading buffer (10% glycerol, 4% SDS, 62.5 mM Tris-HCl pH 6.8, 5% (v/v) 2- -mercaptoethanol, Bromophenol Blue) was passed through the μ Columns. Proteins were analyzed by western blotting or by mass spectrometry.

Endogenous proteins. mock or SINV-GFP-infected HEK293T cells (MOI of 2) were lysed 6 hours post-infection using immunoprecipitation buffer (50 mM Tris-HCl [pH 7.5], 150 mM NaCl, 5 mM EDTA, 0.05% SDS, 1% triton) supplemented with Complete-EDTA-free Protease Inhibitor Cocktail (complete Mini; Sigma Aldrich). Lysates were treated for 20 min at 37˚C with 1 μL of DNase I (Thermo Fisher Scientific) using its buffer (10 mM $MgCl_2$, 5 mM $CaCl_2$ and 1 μL of ribolock). Lysates were cleared by centrifugation at 16000 g, 10 min at 4˚C. Supernatants were precleared 1 h at room temperature with magnetic beads blocked with BSA (Thermo Fisher Scientific) to avoid aspecific binding. Lysates were incubated overnight on wheel at 4˚C with immunoprecipitation buffer containing magnetic Protein A DynaBeads (Invitrogen, Thermo Fisher Scientific) conjugated with human PKR antibody (Abcam) or negative control rabbit IgG (Cell signaling, Ozyme). Beads were washed 3 times with immunoprecipitation buffer, 3 times with wash buffer (50 mM Tris-HCl [pH 7.5], 200 mM NaCl, 5 mM EDTA, 0.05% SDS, 1% triton, supplemented with Complete-EDTA-free Protease Inhibitor Cocktail (complete Mini; Sigma Aldrich) and twice with cold PBS 1X (Gibco, Life Technologies). Beads were eluted with 2x western blot loading buffer and incubated for 10 min at 95˚C under agitation. Proteins were analyzed by western blotting.

RNase treatment followed by co-IP

On tagged proteins: Cells were harvested, washed twice with ice-cold 1× PBS (Gibco, Life Technologies), and resuspended in 550 μL of lysis buffer (50 mM Tris-HCl pH 7.5, 140 mM NaCl,

1.5 mM $MgCl_2$, 0.1% NP-40), supplemented with Complete-EDTA-free Protease Inhibitor Cocktail (complete Mini; Sigma Aldrich). Cells were lysed by 30 min incubation on ice and debris were removed by 15 min centrifugation at 2000 g and 4˚C. Lysate was treated or not with RNase A/T1 mix (Thermo Fisher Scientific) and place at 37˚C 30 min. An aliquot of the cleared lysates (25 μL) was kept aside as protein Input and another aliquot (25 μL) was kept to assess RNase treatment efficiency. Co-IP was led as previously described.

Total RNA was extracted using Tri-Reagent Solution (Fisher Scientific; MRC, Inc) according to the manufacturer's instructions. RNA integrity upon treatment was verified on an 1% agarose gel containing ethidium bromide 10 mg/mL (Invitrogen, Thermo Fisher Scientific) and revealed under UV on Gel DocEZ system (Bio-Rad).

siRNA transfection

20 nM of human AGO2 or non-targeting control siRNA (Horizon discovery) were transfected in 130000 NoDice FHA:ctrl #2, NoDice FHA:DICER WT #4, N1 #6 or N3 #2.13 cells using Lipofectamine 2000 transfection reagent (Invitrogen, Thermo Fisher Scientific) according to the manufacturer's instructions. After 24 hours, the cells were again transfected with 20 nM of the same siRNA and incubated overnight. Cells were infected or not with SINV-GFP at an MOI of 0.02 for 24 h. Proteins and supernatants were collected and analyzed by western blotting and plaque assay, respectively.

BiFC assay

Experiments were carried out in two different ways. For non-fixed cells, NoDice PKR or HEK293T cells were seeded at the density of 1.2 x 10^5 cells per well in a 24-well plate. After 16 hours, cells were transfected with equimolar quantities of each plasmid forming BiFC couples. After 24 hours, cells were infected with SINV at an MOI of 2 and pictures were taken 6 hours post-infection using ZOE fluorescent cell imager (Bio-Rad). Proteins were collected with lysis buffer (50 mM Tris-HCl pH 7.5, SDS 0.05%, Triton 1%, 5 mM EDTA, 150 mM NaCl) supplemented with Complete-EDTA-free Protease Inhibitor Cocktail (complete Mini; Sigma Aldrich), and subjected to western blot analysis. For fixed cells, NoDice PKR cells were seeded at the density of 8.10^4 cells per well in 8-well Millicell EZ Slides (Merck Millipore), transfected and infected as described previously. At 6 hours post-infection, cells were fixed with 4% formaldehyde and 0.2% glutaraldehyde for 10 min. Cells were then washed with 1× PBS (Gibco, Life Technologies) and stained with 10 μg/μL DAPI (Invitrogen, Thermo Fisher Scientific) in 1× PBS solution (Invitrogen, Thermo Fisher Scientific) for 5 min. Fixed cells were mounted on a glass slide with Fluoromount-G mounting media (Southern Biotech). Images were acquired using confocal LSM780 (Zeiss) inverted microscope with an argon laser (514x nm) and with ×40 immersion oil objective. All pictures obtained from BiFC experiments were treated using FigureJ software (NIH).

Mass spectrometry analysis

Protein extracts were prepared for mass spectrometry as described in a previous study [87]. Each sample was precipitated with 0.1 M ammonium acetate in 100% methanol, and proteins were resuspended in 50 mM ammonium bicarbonate. After a reduction-alkylation step (dithiothreitol 5 mM–iodoacetamide 10 mM), proteins were digested overnight with sequencing-grade porcine trypsin (1:25, w/w, Promega, Fitchburg, MA, USA). The resulting vacuum-dried peptides were resuspended in water containing 0.1% (v/v) formic acid (solvent A). One sixth of the peptide mixtures were analyzed by nanoLC-MS/MS an Easy-nanoLC-1000 system coupled to a Q-Exactive Plus mass spectrometer (Thermo-Fisher Scientific, USA) operating in

positive mode. Five microliters of each sample were loaded on a C-18 precolumn (75 μm ID × 20 mm nanoViper, 3 μm Acclaim PepMap; Thermo) coupled with the analytical C18 analytical column (75 μm ID × 25 cm nanoViper, 3 μm Acclaim PepMap; Thermo). Peptides were eluted with a 160 min gradient of 0.1% formic acid in acetonitrile at 300 nL/min. The Q-Exactive Plus was operated in data-dependent acquisition mode (DDA) with Xcalibur software (Thermo-Fisher Scientific). Survey MS scans were acquired at a resolution of 70K at 200 m/z (mass range 350–1250), with a maximum injection time of 20 ms and an automatic gain control (AGC) set to 3e6. Up to 10 of the most intense multiply charged ions ($\geq$2) were selected for fragmentation with a maximum injection time of 100 ms, an AGC set at 1e5 and a resolution of 17.5K. A dynamic exclusion time of 20 s was applied during the peak selection process.

Database search and mass-spectrometry data post-processing

Data were searched against a database containing Human and Viruses UniProtKB sequences with a decoy strategy (GFP, Human and Sindbis Virus SwissProt sequences as well as Semliki Forest Virus SwissProt and TrEMBL sequences (releases from January 2017, 40439 sequences)). Peptides were identified with Mascot algorithm (version 2.3, Matrix Science, London, UK) with the following search parameters: carbamidomethylation of cysteine was set as fixed modification; N-terminal protein acetylation, phosphorylation of serine / threonine / tyrosine and oxidation of methionine were set as variable modifications; tryptic specificity with up to three missed cleavages was used. The mass tolerances in MS and MS/MS were set to 10 ppm and 0.02 Da respectively, and the instrument configuration was specified as "ESI--Trap". The resulting .dat Mascot files were then imported into Proline v1.4 package (http://proline.profiproteomics.fr) for post-processing. Proteins were validated with Mascot pretty rank equal to 1, 1% FDR on both peptide spectrum matches (PSM) and protein sets (based on score). The total number of MS/MS fragmentation spectra (Spectral count or SpC) was used for subsequent protein quantification in the different samples. All data have been deposited to the ProteomeXchange Consortium [88].

Exploratory and differential expression analysis of LC-MS/MS data

Mass spectrometry data obtained for each sample were stored in a local MongoDB database and subsequently analyzed through a Shiny Application built upon the R/Bioconductor packages msmsEDA (Gregori J, Sanchez A, Villanueva J (2014). msmsEDA: Exploratory Data Analysis of LC-MS/MS data by spectral counts. R/Bioconductor package version 1.22.0) and msmsTests (Gregori J, Sanchez A, Villanueva J (2013). msmsTests: LC-MS/MS Differential Expression Tests. R/Bioconductor package version 1.22.0). Exploratory data analyses of LC-MS/MS data were thus conducted, and differential expression tests were performed using a negative binomial regression model. The p-values were adjusted with FDR control by the Benjamini-Hochberg method and the following criteria were used to define differentially expressed proteins: an adjusted p-value < 0.05, a minimum of 5 SpC in the most abundant condition, and a minimum fold change of 2 (abs(LogFC) > 1). GO term analysis was performed using the EnrichR web-based tool (http://amp.pharm.mssm.edu/Enrichr). The direct interaction network for proteins enriched in SINV-infected cells was generated using the STRING database (https://string-db.org).

Supporting information

S1 Fig. Analysis of SINV-GFP infection in FHA:DICER cell lines at different MOI and time points. A. miR-16 expression analyzed by northern blot in HEK293T, NoDice FHA:ctrl #1 and FHA:DICER WT #4 cell lines. Expression of snRNA U6 was used as loading control. **B.**

Representative GFP pictures of HEK293T, NoDice 2.20, NoDice 4.25, NoDice FHA:ctrl #1 and NoDice FHA:ctrl #2 cells infected with SINV-GFP at an MOI of 0.02 for 24 h. The left panel corresponds to GFP signal and the right panel to a merge of GFP signal and the corresponding brightfield. Pictures were taken with a 5x magnification. hpi: hours post-infection. **C.** Mean (+/- SEM) of SINV-GFP viral titers in cells infected at an MOI of 0.02 for 24 h (n = 3) from plaque assay quantification. * $p < 0.05$, ns: non-significant, ordinary one-way ANOVA test with Bonferroni correction. **D**. Western blot analysis of DICER, AGO2 and GFP expression in SINV-GFP-infected cells shown in B. Gamma-Tubulin was used as loading control.
(TIF)

S2 Fig. LC-MS/MS analysis of DICER interactome during SFV infection. A. Volcano plot for differentially expressed proteins (DEPs) between HA IP and CTL IP in FHA:DICER mock-infected cells. Each protein is marked as a dot; proteins that are significantly up-regulated in HA IP are shown in red, up-regulated proteins in CTL IP are shown in blue, and non-significant proteins are in black. The horizontal line denotes a p-value of 0.05 and the vertical lines the Log2 fold change cutoff (-1 and 1). DICER and its cofactors (TRBP, PACT, AGO2) are highlighted in yellow. **B.** Left panel: Volcano plot for DEPs between SFV (MOI of 2, 6 hpi) and mock fractions of HA IP in FHA:DICER cells. Same colour code and thresholds as in A were applied. Proteins that are discussed in the text are highlighted in yellow and SFV proteins in purple. **C.** Summary of the differential expression analysis of SFV vs mock fractions from HA IP in FHA:DICER cells. The analysis has been performed using a generalized linear model of a negative-binomial distribution and p-values were corrected for multiple testing using the Benjamini-Hochberg method.
(TIF)

S3 Fig. Confirmation of LC-MS/MS analysis by co-IP and BiFC controls. A. FHA:DICER WT #4 cells were infected with SINV-GFP at an MOI of 0.02 for 24 h and a HA co-IP was performed. Eluted proteins were resolved by western blot and IP efficiency was assessed using an HA antibody. In parallel, co-IPed proteins were visualized using appropriate antibodies. GFP antibody was used to verify the infection and Ponceau staining serves as loading control. **B.** 1% agarose gel analysis of RNA extracted from INPUT of the co-IP in Fig 3B. Ribosomal RNA integrity was compared to a control HEK293T cell line. RNAs were revealed using ethidium bromide under UV. **C.** Schematic representation of Human DICER proteins used for BiFC positive and negative controls. The different conserved domains are shown in colored boxes. DUF283: Domain of Unknown Function; PAZ: PIWI ARGONAUTE ZWILLE domain; dsRBD: dsRNA-binding domain. hDICER WT is the full-length protein. hDICER N1 is deleted of the first N-terminal 495 amino acids. **D.** Expression of BiFC plasmids was assessed by western blot. DICER proteins (WT and N1) and PKR were visualized using antibodies targeting endogenous proteins, whereas TRBP and PACT were detected using GFP antibody. Antibody targeting the SINV coat protein (CP) was used as infection control. Ponceau staining was used as loading control. **E.** Positive and negative BiFC controls on fixed NoDice PKR cells. After co-transfection, cells were infected with SINV at an MOI of 2 for 6 h and fixed. After fixation, cells were stained with DAPI and observed under confocal microscope. Merge pictures of BiFC and DAPI signals of SINV-infected cells are shown. A higher magnification of images showing the interaction represented by a red square is shown in the bottom left corner. Scale bars: 20 μm and 10 μm. **F.** Expression of BiFC plasmids was assessed by western blot. DICER, PKR, TRBP and PACT were detected using GFP antibody. Antibody targeting the SINV coat protein (CP) was used as infection control. Gamma-Tubulin was used as loading control. The asterisk corresponds to an aspecific band. **G.** Interactions between DICER and TRBP, PACT or PKR were visualized by BiFC. Plasmids expressing $^{N\text{-}ter}$Venus:DICER

and TRBP:, PACT: or PKR:Venus$^{C\text{-}ter}$ were co-transfected in HEK293T cells for 24 h and cells were either infected with SINV at an MOI of 2 for 6 h or not. The different combinations are indicated on the left side. Reconstitution of Venus (BiFC) signal was observed under epifluorescence microscope. For each condition, the left panel corresponds to Venus signal and the right panel to the corresponding brightfield pictures. Scale bar: 100 μm.
(TIF)

S4 Fig. Confirmation of DICER interactome upon SINV infection in HCT116 KI-DICER cells. A. Schematic representation of DICER WT and Flag-HA(FHA)-GFP knocked-in (KI) alleles. FHA sequence is in purple, GFP in green, DICER 5'UTR in orange and DICER coding region in yellow. The gRNA used to generate the KI was designed to target the first coding exon of DICER gene. **B.** PCR on genomic DNA extracted from WT and KI cells. **C.** An oligo outside the homologous recombination region and an oligo within the GFP tag were used to verify the presence of a 1040 bp amplicon in HCT116 KI-DICER clone. Sequencing results corresponding to this region are shown. **D.** Western blot analysis of DICER, p-PKR, PKR and p-eIF2 expression in mock or SINVGFP-infected HEK293T and HCT116 KI-DICER cell lines at an MOI of 2 for 6 h or 16 h and 0.02 for 24 h. GFP antibody was used to verify the infection. Ponceau and gamma-Tubulin were used as loading controls.
(TIF)

S5 Fig. Interaction analysis between the different versions of DICER and TRBP or PACT using BiFC assay. NoDice PKR cells were co-transfected for 24 h with plasmids expressing the different versions of DICER proteins fused to the N-terminal part of Venus and either TRBP:Venus$^{C\text{-}ter}$ (**A**) or PACT:Venus$^{C\text{-}ter}$ (**B**). Cells were then infected with SINV at an MOI of 2 for 6 h and Venus signal was observed under epifluorescence microscope. The left panel corresponds to Venus signal and the right panel to the corresponding brightfield picture. Pictures were taken with a 5x magnification. hpi: hours post-infection. Scale bar: 100 μm.
(TIF)

S6 Fig. Analysis of the importance of Dicer helicase domain on SINV-GFP infection in FHA:DICER mutant stable cell lines. A. Northern blot analysis of miR-16 expression in HEK293T, NoDice 2.20, NoDice FHA:ctrl #2, FHA:DICER WT polyclonal, FHA:DICER N1 #6, FHA:DICER Hel. #2.6, and FHA:DICER N3 #2.13. Expression of snRNA U6 was used as loading control. **B.** Representative GFP fluorescent microscopy images of HEK293T, NoDice 2.20, FHA:DICER mutants cell lines infected with SINV-GFP at an MOI of 0.02 for 24 h. The left panel corresponds to GFP signal and the right panel to a merge picture of GFP signal and brightfield. Pictures were taken with a 5x magnification. hpi: hours post-infection. **C**. Mean (+/- SEM) of SINV-GFP viral titers over FHA:DICER WT #4 cells in FHA:DICER N1 #6, FHA:DICER N3 #2.13, NoDice FHA:ctrl #2 and NoDice 2.20 cell lines infected at an MOI of 0.02 for 24 h (n = 3) from plaque assay quantification. *** $p < 0.001$, ns: non-significant, ordinary one-way ANOVA test with Bonferroni correction.
(TIF)

S1 Table. Top 100 proteins that are differentially immunoprecipitated in mock-infected FHA:DICER cells by the HA and Myc (CTL) antibodies. Related to Fig 2.
(XLSX)

S2 Table. Top 100 proteins that are differentially immunoprecipitated with the HA antibody in SINV-infected vs mock-infected FHA:DICER cells. Related to Fig 2.
(XLSX)

S3 Table. Top 100 proteins that are differentially immunoprecipitated in mock-infected FHA:DICER cells by the HA and Myc (CTL) antibodies, in the SFV infection experiment. Related to S2 Fig.
(XLSX)

S4 Table. Top 100 proteins that are differentially immunoprecipitated with the HA antibody in SFV-infected vs mock-infected FHA:DICER cells. Related to S2 Fig.
(XLSX)

S5 Table. List of primers used in this study.
(XLSX)

S6 Table. Data and statistical tests details used in plaque assays shown in Figs 1, 6, 7, 8, S1 and S6.
(XLSX)

Acknowledgments

The authors would like to thank members of the Pfeffer laboratory for discussion, Pr. Bryan Cullen for the kind gift of the HEK293T NoDice and NoDice PKR cell lines and Dr. Oliver Vugrek for the BiFC plasmids.

Author Contributions

Conceptualization: Thomas C. Montavon, Mathieu Lefèvre, Sébastien Pfeffer.

Data curation: Thomas C. Montavon, Philippe Hammann, Johana Chicher.

Formal analysis: Thomas C. Montavon, Morgane Baldaccini, Mathieu Lefèvre, Erika Girardi, Philippe Hammann, Johana Chicher, Sébastien Pfeffer.

Funding acquisition: Sébastien Pfeffer.

Investigation: Morgane Baldaccini, Mathieu Lefèvre, Erika Girardi, Mélanie Messmer.

Methodology: Sébastien Pfeffer.

Project administration: Sébastien Pfeffer.

Software: Béatrice Chane-Woon-Ming.

Supervision: Sébastien Pfeffer.

Validation: Thomas C. Montavon, Morgane Baldaccini, Erika Girardi, Mélanie Messmer.

Visualization: Béatrice Chane-Woon-Ming.

Writing – original draft: Thomas C. Montavon, Morgane Baldaccini, Sébastien Pfeffer.

Writing – review & editing: Thomas C. Montavon, Morgane Baldaccini, Mathieu Lefèvre, Erika Girardi, Béatrice Chane-Woon-Ming, Mélanie Messmer, Sébastien Pfeffer.

References

1. Ivashkiv LB, Donlin LT. Regulation of type I interferon responses. Nat Rev Immunol. 2014; 14:36–49. https://doi.org/10.1038/nri3581 PMID: 24362405
2. Borden EC, Sen GC, Uze G, Silverman RH, Ransohoff RM, Foster GR, et al. Interferons at age 50: past, current and future impact on biomedicine. Nat Rev Drug Discov. 2007; 6:975–990. https://doi.org/10.1038/nrd2422 PMID: 18049472

3. Williams BR. PKR; a sentinel kinase for cellular stress. Oncogene. 1999; 18:6112–6120. https://doi.org/10.1038/sj.onc.1203127 PMID: 10557102

4. Lemaire PA, Anderson E, Lary J, Cole JL. Mechanism of PKR Activation by dsRNA. J Mol Biol. 2008; 381:351–360. https://doi.org/10.1016/j.jmb.2008.05.056 PMID: 18599071

5. Pfaller CK, Li Z, George CX, Samuel CE. Protein kinase PKR and RNA adenosine deaminase ADAR1: new roles for old players as modulators of the interferon response. Curr Opin Immunol. 2011; 23:573–582. https://doi.org/10.1016/j.coi.2011.08.009 PMID: 21924887

6. Fros JJ, Pijlman GP. Alphavirus Infection: Host Cell Shut-Off and Inhibition of Antiviral Responses. Viruses. 2016; 8:166. https://doi.org/10.3390/v8060166 PMID: 27294951

7. Ryman KD, White LJ, Johnston RE, Klimstra WB. Effects of PKR/RNase L-Dependent and Alternative Antiviral Pathways on Alphavirus Replication and Pathogenesis. Viral Immunol. 2002; 15:53–76. https://doi.org/10.1089/088282402317340233 PMID: 11952147

8. Kim Y, Lee JH, Park J-E, Cho J, Yi H, Kim VN. PKR is activated by cellular dsRNAs during mitosis and acts as a mitotic regulator. Genes Dev. 2014; 28:1310–1322. https://doi.org/10.1101/gad.242644.114 PMID: 24939934

9. Meister G, Tuschl T. Mechanisms of gene silencing by double-stranded RNA. Nature. 2004; 431:343–9. https://doi.org/10.1038/nature02873 PMID: 15372041

10. Hutvágner G, McLachlan J, Pasquinelli AE, Balint E, Tuschl T, Zamore PD. A cellular function for the RNA-interference enzyme Dicer in the maturation of the let-7 small temporal RNA. Science. 2001; 293:834–8. https://doi.org/10.1126/science.1062961 PMID: 11452083

11. Wienholds E, Koudijs MJ, Van Eeden FJ, Cuppen E, Plasterk RH. The microRNA-producing enzyme Dicer1 is essential for zebrafish development. Nat Genet. 2003; 217–218. https://doi.org/10.1038/ng1251 PMID: 14528306

12. Bartel DP. Metazoan MicroRNAs. Cell. 2018; 173:20–51. https://doi.org/10.1016/j.cell.2018.03.006 PMID: 29570994

13. Chendrimada TP, Gregory RI, Kumaraswamy E, Norman J, Cooch N, Nishikura K, et al. TRBP recruits the Dicer complex to Ago2 for microRNA processing and gene silencing. Nature. 2005; 436:740–4. https://doi.org/10.1038/nature03868 PMID: 15973356

14. Daniels SM, Melendez-Pe a CE, Scarborough RJ, Daher A, Christensen HS, El Far M, et al. Characterization of the TRBP domain required for dicer interaction and function in RNA interference. BMC Mol Biol. 2009; 10:38. https://doi.org/10.1186/1471-2199-10-38 PMID: 19422693

15. Heyam A, Lagos D, Plevin M. Dissecting the roles of TRBP and PACT in double-stranded RNA recognition and processing of noncoding RNAs. WIREs RNA. 2015; 6:271–289. https://doi.org/10.1002/wrna.1272 PMID: 25630541

16. Kok KH, Ng MH, Ching YP, Jin DY. Human TRBP and PACT Directly Interact with Each Other and Associate with Dicer to Facilitate the Production of Small Interfering RNA. J Biol Chem. 2007; 282:17649–57. https://doi.org/10.1074/jbc.M611768200 PMID: 17452327

17. Lee Y, Hur I, Park SY, Kim YK, Suh MR, Kim VN. The role of PACT in the RNA silencing pathway. Embo J. 2006; 25:522–32. https://doi.org/10.1038/sj.emboj.7600942 PMID: 16424907

18. Guo Z, Li Y, Ding S-W. Small RNA-based antimicrobial immunity. Nat Rev Immunol. 2019; 19:31–44. https://doi.org/10.1038/s41577-018-0071-x PMID: 30301972

19. tenOever BR. The Evolution of Antiviral Defense Systems. Cell Host Microbe. 2016; 19:142–149. https://doi.org/10.1016/j.chom.2016.01.006 PMID: 26867173

20. Cullen BR. Is RNA interference involved in intrinsic antiviral immunity in mammals? Nat Immunol. 2006; 7:563–7. https://doi.org/10.1038/ni1352 PMID: 16715068

21. Maillard PV, van der Veen AG, Poirier EZ, Reis e Sousa C. Slicing and dicing viruses: antiviral RNA interference in mammals. EMBO J. 2019;38. https://doi.org/10.15252/embj.2018100941 PMID: 30872283

22. Maillard PV, Ciaudo C, Marchais A, Li Y, Jay F, Ding SW, et al. Antiviral RNA interference in mammalian cells. Science. 2013; 342:235–238. https://doi.org/10.1126/science.1241930 PMID: 24115438

23. Maillard PV, Veen AGV der, Deddouche-Grass S, Rogers NC, Merits A, Sousa CR e. Inactivation of the type I interferon pathway reveals long double-stranded RNA-mediated RNA interference in mammalian cells. EMBO J. 2016; 35:2505–2518. https://doi.org/10.15252/embj.201695086 PMID: 27815315

24. Takahashi T, Nakano Y, Onomoto K, Murakami F, Komori C, Suzuki Y, et al. LGP2 virus sensor regulates gene expression network mediated by TRBP-bound microRNAs. Nucleic Acids Res. 2018; 46:9134–9147. https://doi.org/10.1093/nar/gky575 PMID: 29939295

25. Takahashi T, Nakano Y, Onomoto K, Yoneyama M, Ui-Tei K. Virus Sensor RIG-I Represses RNA Interference by Interacting with TRBP through LGP2 in Mammalian Cells. Genes. 2018; 9:511. https://doi.org/10.3390/genes9100511 PMID: 30347765

26. van der Veen AG, Maillard PV, Schmidt JM, Lee SA, Deddouche-Grass S, Borg A, et al. The RIG-I-like receptor LGP2 inhibits Dicer-dependent processing of long double-stranded RNA and blocks RNA interference in mammalian cells. EMBO J. 2018; 37:e97479. https://doi.org/10.15252/embj.201797479 PMID: 29351913

27. Adiliaghdam F, Basavappa M, Saunders TL, Harjanto D, Prior JT, Cronkite DA, et al. A Requirement for Argonaute 4 in Mammalian Antiviral Defense. Cell Rep. 2020; 30:1690–1701.e4. https://doi.org/10.1016/j.celrep.2020.01.021 PMID: 32049003

28. Qiu Y, Xu Y, Zhang Y, Zhou H, Deng Y-Q, Li X-F, et al. Human Virus-Derived Small RNAs Can Confer Antiviral Immunity in Mammals. Immunity. 2017; 46:992–1004.e5. https://doi.org/10.1016/j.immuni.2017.05.006 PMID: 28636969

29. Qiu Y, Xu Y-P, Wang M, Miao M, Zhou H, Xu J, et al. Flavivirus induces and antagonizes antiviral RNA interference in both mammals and mosquitoes. Sci Adv. 2020; 6:eaax7989. https://doi.org/10.1126/sciadv.aax7989 PMID: 32076641

30. Girardi E, Chane-Woon-Ming B, Messmer M, Kaukinen P, Pfeffer S. Identification of RNase L-dependent, 3'-end-modified, viral small RNAs in Sindbis virus-infected mammalian cells. mBio. 2013; 4: e00698–00613. https://doi.org/10.1128/mBio.00698-13 PMID: 24255120

31. Parameswaran P, Sklan E, Wilkins C, Burgon T, Samuel MA, Lu R, et al. Six RNA viruses and forty-one hosts: viral small RNAs and modulation of small RNA repertoires in vertebrate and invertebrate systems. PLoS Pathog. 2010; 6:e1000764. https://doi.org/10.1371/journal.ppat.1000764 PMID: 20169186

32. Schuster S, Overheul GJ, Bauer L, van Kuppeveld FJM, van Rij RP. No evidence for viral small RNA production and antiviral function of Argonaute 2 in human cells. Sci Rep. 2019; 9:1–11. https://doi.org/10.1038/s41598-018-37186-2 PMID: 30626917

33. Kennedy EM, Whisnant AW, Kornepati AVR, Marshall JB, Bogerd HP, Cullen BR. Production of functional small interfering RNAs by an amino-terminal deletion mutant of human Dicer. Proc Natl Acad Sci. 2015; 112:E6945–E6954. https://doi.org/10.1073/pnas.1513421112 PMID: 26621737

34. Tsai K, Courtney DG, Kennedy EM, Cullen BR. Influenza A virus-derived siRNAs increase in the absence of NS1 yet fail to inhibit virus replication. RNA N Y N. 2018. https://doi.org/10.1261/rna.066332.118 PMID: 29903832

35. Griffin D. Alphaviruses, p 1023–1067. Fields Virol 5th Ed Lippincott Williams Wilkins Phila PA. 2007.

36. Girardi E, Lef vre M, Chane-Woon-Ming B, Paro S, Claydon B, Imler J-L, et al. Cross-species comparative analysis of Dicer proteins during Sindbis virus infection. Sci Rep. 2015; 5:10693. https://doi.org/10.1038/srep10693 PMID: 26024431

37. Bogerd HP, Skalsky RL, Kennedy EM, Furuse Y, Whisnant AW, Flores O, et al. Replication of many human viruses is refractory to inhibition by endogenous cellular microRNAs. J Virol. 2014; 88:8065–8076. https://doi.org/10.1128/JVI.00985-14 PMID: 24807715

38. López P, Girardi E, Mounce BC, Weiss A, Chane-Woon-Ming B, Messmer M, et al. High-Throughput Fluorescence-Based Screen Identifies the Neuronal MicroRNA miR-124 as a Positive Regulator of Alphavirus Infection. J Virol. 2020; 94. https://doi.org/10.1128/JVI.02145-19 PMID: 32102877

39. Bogerd HP, Whisnant AW, Kennedy EM, Flores O, Cullen BR. Derivation and characterization of Dicer- and microRNA-deficient human cells. RNA. 2014; 20:923–937. https://doi.org/10.1261/rna.044545.114 PMID: 24757167

40. Akta T, Av ar Ilık , Maticzka D, Bhardwaj V, Pessoa Rodrigues C, Mittler G, et al. DHX9 suppresses RNA processing defects originating from the Alu invasion of the human genome. Nature. 2017; 544:115–119. https://doi.org/10.1038/nature21715 PMID: 28355180

41. Robb GB, Rana TM. RNA helicase A interacts with RISC in human cells and functions in RISC loading. Mol Cell. 2007; 26:523–537. https://doi.org/10.1016/j.molcel.2007.04.016 PMID: 17531811

42. Sorrentino S, Naddeo M, Russo A, D'Alessio G. Degradation of double-stranded RNA by human pancreatic ribonuclease: crucial role of noncatalytic basic amino acid residues. Biochemistry. 2003; 42:10182–10190. https://doi.org/10.1021/bi030040q PMID: 12939146

43. Edy VG, Szekely M, Loviny T, Dreyer C. Action of nucleases on double-stranded RNA. Eur J Biochem. 1976; 61:563–572. https://doi.org/10.1111/j.1432-1033.1976.tb10051.x PMID: 813998

44. García MA, Meurs EF, Esteban M. The dsRNA protein kinase PKR: Virus and cell control. Biochimie. 2007; 89:799–811. https://doi.org/10.1016/j.biochi.2007.03.001 PMID: 17451862

45. Haase AD, Jaskiewicz L, Zhang H, Laine S, Sack R, Gatignol A, et al. TRBP, a regulator of cellular PKR and HIV-1 virus expression, interacts with Dicer and functions in RNA silencing. EMBO Rep. 2005; 6:961–7. https://doi.org/10.1038/sj.embor.7400509 PMID: 16142218

46. Patel CV, Handy I, Goldsmith T, Patel RC. PACT, a Stress-modulated Cellular Activator of Interferon-induced Double-stranded RNA-activated Protein Kinase, PKR. J Biol Chem. 2000; 275:37993–37998. https://doi.org/10.1074/jbc.M004762200 PMID: 10988289

47. Lepur A, Kova evi L, Beluži R, Vugrek O. Combining unique multiplex gateway cloning and bimolecular fluorescence complementation (BiFC) for high-throughput screening of protein–protein interactions. J Biomol Screen. 2016; 21:1100–1111. https://doi.org/10.1177/1087057116659438 PMID: 27455993

48. Bernstein E, Caudy AA, Hammond SM, Hannon GJ. Role for a bidentate ribonuclease in the initiation step of RNA interference. Nature. 2001; 409:363–6. https://doi.org/10.1038/35053110 PMID: 11201747

49. Doyle M, Badertscher L, Jaskiewicz L, Güttinger S, Jurado S, Hugenschmidt T, et al. The double-stranded RNA binding domain of human Dicer functions as a nuclear localization signal. RNA N Y N. 2013; 19:1238–1252. https://doi.org/10.1261/rna.039255.113 PMID: 23882114

50. Lambert M, Pépin G, Peralta-Zaragoza O, Matusiak R, Ly S, Landry P, et al. TWEAK Negatively Regulates Human Dicer. Non-Coding RNA. 2016;2. https://doi.org/10.3390/ncrna2040012 PMID: 29657270

51. Meister G, Landthaler M, Patkaniowska A, Dorsett Y, Teng G, Tuschl T. Human Argonaute2 mediates RNA cleavage targeted by miRNAs and siRNAs. Mol Cell. 2004; 15:185–197. https://doi.org/10.1016/j.molcel.2004.07.007 PMID: 15260970

52. Li Y, Basavappa M, Lu J, Dong S, Cronkite DA, Prior JT, et al. Induction and suppression of antiviral RNA interference by influenza A virus in mammalian cells. Nat Microbiol. 2016; 2:16250. https://doi.org/10.1038/nmicrobiol.2016.250 PMID: 27918527

53. Cullen BR, Cherry S, tenOever BR. Is RNA Interference a Physiologically Relevant Innate Antiviral Immune Response in Mammals? Cell Host Microbe. 2013; 14:374–378. https://doi.org/10.1016/j.chom.2013.09.011 PMID: 24139396

54. Cullen BR. RNA Interference in Mammals: The Virus Strikes Back. Immunity. 2017; 46:970–972. https://doi.org/10.1016/j.immuni.2017.05.004 PMID: 28636964

55. Donaszi-Ivanov A, Mohorianu I, Dalmay T, Powell PP. Small RNA Analysis in Sindbis Virus Infected Human HEK293 Cells. Adelman ZN, editor. PLoS ONE. 2013; 8:e84070. https://doi.org/10.1371/journal.pone.0084070 PMID: 24391886

56. Backes S, Langlois RA, Schmid S, Varble A, Shim JV, Sachs D, et al. The Mammalian Response to Virus Infection Is Independent of Small RNA Silencing. Cell Rep. 2014; 8:114–125. https://doi.org/10.1016/j.celrep.2014.05.038 PMID: 24953656

57. Li Y, Lu J, Han Y, Fan X, Ding S-W. RNA interference functions as an antiviral immunity mechanism in mammals. Science. 2013; 342:231–234. https://doi.org/10.1126/science.1241911 PMID: 24115437

58. Berkhout B. RNAi-mediated antiviral immunity in mammals. Curr Opin Virol. 2018; 32:9–14. https://doi.org/10.1016/j.coviro.2018.07.008 PMID: 30015014

59. Takahashi T, Ui-Tei K. Mutual Regulation of RNA Silencing and the IFN Response as an Antiviral Defense System in Mammalian Cells. Int J Mol Sci. 2020; 21:1348. https://doi.org/10.3390/ijms21041348 PMID: 32079277

60. Lui P-Y, Wong L-YR, Ho T-H, Au SWN, Chan C-P, Kok K-H, et al. PACT Facilitates RNA-Induced Activation of MDA5 by Promoting MDA5 Oligomerization. J Immunol. 2017; 199:1846–1855. https://doi.org/10.4049/jimmunol.1601493 PMID: 28760879

61. Kok K-H, Lui P-Y, Ng M-HJ, Siu K-L, Au SWN, Jin D-Y. The Double-Stranded RNA-Binding Protein PACT Functions as a Cellular Activator of RIG-I to Facilitate Innate Antiviral Response. Cell Host Microbe. 2011; 9:299–309. https://doi.org/10.1016/j.chom.2011.03.007 PMID: 21501829

62. Clemens MJ. PKR-a protein kinase regulated by double-stranded RNA. Int J Biochem Cell Biol. 1997; 29:945–9. https://doi.org/10.1016/s1357-2725(96)00169-0 PMID: 9375375

63. Gal-Ben-Ari S, Barrera I, Ehrlich M, Rosenblum K. PKR: A Kinase to Remember. Front Mol Neurosci. 2018; 11:480. https://doi.org/10.3389/fnmol.2018.00480 PMID: 30686999

64. Fairman-Williams ME, Guenther U-P, Jankowsky E. SF1 and SF2 helicases: family matters. Curr Opin Struct Biol. 2010; 20:313–324. https://doi.org/10.1016/j.sbi.2010.03.011 PMID: 20456941

65. Ahmad S, Hur S. Helicases in Antiviral Immunity: Dual Properties as Sensors and Effectors. Trends Biochem Sci. 2015; 40:576–585. https://doi.org/10.1016/j.tibs.2015.08.001 PMID: 26410598

66. Mittelstadt M, Frump A, Khuu T, Fowlkes V, Handy I, Patel CV, et al. Interaction of human tRNA-dihydrouridine synthase-2 with interferon-induced protein kinase PKR. Nucleic Acids Res. 2008; 36:998–1008. https://doi.org/10.1093/nar/gkm1129 PMID: 18096616

67. Park H, Davies MV, Langland JO, Chang HW, Nam YS, Tartaglia J, et al. TAR RNA-binding protein is an inhibitor of the interferon-induced protein kinase PKR. Proc Natl Acad Sci U S A. 1994; 91:4713–4717. https://doi.org/10.1073/pnas.91.11.4713 PMID: 7515177

68. Nakamura T, Kunz RC, Zhang C, Kimura T, Yuan CL, Baccaro B, et al. A Critical Role for PKR Complexes with TRBP in Immunometabolic Regulation and eIF2 Phosphorylation in Obesity. Cell Rep. 2015; 11:295–307. https://doi.org/10.1016/j.celrep.2015.03.021 PMID: 25843719

69. Daher A, Laraki G, Singh M, Melendez-Pe a CE, Bannwarth S, Peters AHFM, et al. TRBP control of PACT-induced phosphorylation of protein kinase R is reversed by stress. Mol Cell Biol. 2009; 29:254–265. https://doi.org/10.1128/MCB.01030-08 PMID: 18936160

70. Singh M, Castillo D, Patel CV, Patel RC. Stress-induced phosphorylation of PACT reduces its interaction with TRBP and leads to PKR activation. Biochemistry. 2011; 50:4550–4560. https://doi.org/10.1021/bi200104h PMID: 21526770

71. Clerzius G, Shaw E, Daher A, Burugu S, Gélinas J-F, Ear T, et al. The PKR activator, PACT, becomes a PKR inhibitor during HIV-1 replication. Retrovirology. 2013; 10:96. https://doi.org/10.1186/1742-4690-10-96 PMID: 24020926

72. Li J, Tang H, Mullen TM, Westberg C, Reddy TR, Rose DW, et al. A role for RNA helicase A in post-transcriptional regulation of HIV type 1. Proc Natl Acad Sci U S A. 1999; 96:709–714. https://doi.org/10.1073/pnas.96.2.709 PMID: 9892698

73. Fujii R, Okamoto M, Aratani S, Oishi T, Ohshima T, Taira K, et al. A Role of RNA Helicase A in cis-Acting Transactivation Response Element-mediated Transcriptional Regulation of Human Immunodeficiency Virus Type 1. J Biol Chem. 2001; 276:5445–5451. https://doi.org/10.1074/jbc.M006892200 PMID: 11096080

74. Roy BB, Hu J, Guo X, Russell RS, Guo F, Kleiman L, et al. Association of RNA helicase a with human immunodeficiency virus type 1 particles. J Biol Chem. 2006; 281:12625–12635. https://doi.org/10.1074/jbc.M510596200 PMID: 16527808

75. Sadler AJ, Latchoumanin O, Hawkes D, Mak J, Williams BRG. An Antiviral Response Directed by PKR Phosphorylation of the RNA Helicase A. Gale M, editor. PLoS Pathog. 2009; 5:e1000311. https://doi.org/10.1371/journal.ppat.1000311 PMID: 19229320

76. Herbert A, Alfken J, Kim YG, Mian IS, Nishikura K, Rich A. A Z-DNA binding domain present in the human editing enzyme, double-stranded RNA adenosine deaminase. Proc Natl Acad Sci U S A. 1997; 94:8421–8426. https://doi.org/10.1073/pnas.94.16.8421 PMID: 9237992

77. Yang W, Chendrimada TP, Wang Q, Higuchi M, Seeburg PH, Shiekhattar R, et al. Modulation of microRNA processing and expression through RNA editing by ADAR deaminases. Nat Struct Mol Biol. 2006; 13:13–21. https://doi.org/10.1038/nsmb1041 PMID: 16369484

78. Iizasa H, Wulff B-E, Alla NR, Maragkakis M, Megraw M, Hatzigeorgiou A, et al. Editing of Epstein-Barr virus-encoded BART6 microRNAs controls their dicer targeting and consequently affects viral latency. J Biol Chem. 2010; 285:33358–33370. https://doi.org/10.1074/jbc.M110.138362 PMID: 20716523

79. Ota H, Sakurai M, Gupta R, Valente L, Wulff B-E, Ariyoshi K, et al. ADAR1 forms a complex with Dicer to promote microRNA processing and RNA-induced gene silencing. Cell. 2013; 153:575–589. https://doi.org/10.1016/j.cell.2013.03.024 PMID: 23622242

80. Samuel CE. Adenosine deaminases acting on RNA (ADARs) are both antiviral and proviral. Virology. 2011; 411:180–193. https://doi.org/10.1016/j.virol.2010.12.004 PMID: 21211811

81. Li Z, Wolff KC, Samuel CE. RNA adenosine deaminase ADAR1 deficiency leads to increased activation of protein kinase PKR and reduced vesicular stomatitis virus growth following interferon treatment. Virology. 2010; 396:316–322. https://doi.org/10.1016/j.virol.2009.10.026 PMID: 19913273

82. Clerzius G, Gélinas J-F, Daher A, Bonnet M, Meurs EF, Gatignol A. ADAR1 interacts with PKR during human immunodeficiency virus infection of lymphocytes and contributes to viral replication. J Virol. 2009; 83:10119–10128. https://doi.org/10.1128/JVI.02457-08 PMID: 19605474

83. Schoggins JW, Wilson SJ, Panis M, Murphy MY, Jones CT, Bieniasz P, et al. A diverse range of gene products are effectors of the type I interferon antiviral response. Nature. 2011; 472:481–485. https://doi.org/10.1038/nature09907 PMID: 21478870

84. Elde NC, Child SJ, Geballe AP, Malik HS. Protein kinase R reveals an evolutionary model for defeating viral mimicry. Nature. 2009; 457:485–489. https://doi.org/10.1038/nature07529 PMID: 19043403

85. Meister G, Landthaler M, Peters L, Chen PY, Urlaub H, Lührmann R, et al. Identification of novel argonaute-associated proteins. Curr Biol CB. 2005; 15:2149–2155. https://doi.org/10.1016/j.cub.2005.10.048 PMID: 16289642

86. Concordet J-P, Haeussler M. CRISPOR: intuitive guide selection for CRISPR/Cas9 genome editing experiments and screens. Nucleic Acids Res. 2018; 46:W242–W245. https://doi.org/10.1093/nar/gky354 PMID: 29762716

87. Chicois C, Scheer H, Garcia S, Zuber H, Mutterer J, Chicher J, et al. The UPF1 interactome reveals interaction networks between RNA degradation and translation repression factors in Arabidopsis. Plant J. 2018; 96:119–132. https://doi.org/10.1111/tpj.14022 PMID: 29983000

88. Perez-Riverol Y, Csordas A, Bai J, Bernal-Llinares M, Hewapathirana S, Kundu DJ, et al. The PRIDE database and related tools and resources in 2019: improving support for quantification data. Nucleic Acids Res. 2019; 47:D442–D450. https://doi.org/10.1093/nar/gky1106 PMID: 30395289

89. Chen EY, Tan CM, Kou Y, Duan Q, Wang Z, Meirelles GV, et al. Enrichr: interactive and collaborative HTML5 gene list enrichment analysis tool. BMC Bioinformatics. 2013; 14:128. https://doi.org/10.1186/1471-2105-14-128 PMID: 23586463

90. Kuleshov MV, Jones MR, Rouillard AD, Fernandez NF, Duan Q, Wang Z, et al. Enrichr: a comprehensive gene set enrichment analysis web server 2016 update. Nucleic Acids Res. 2016; 44:W90–97. https://doi.org/10.1093/nar/gkw377 PMID: 27141961

Figure S1

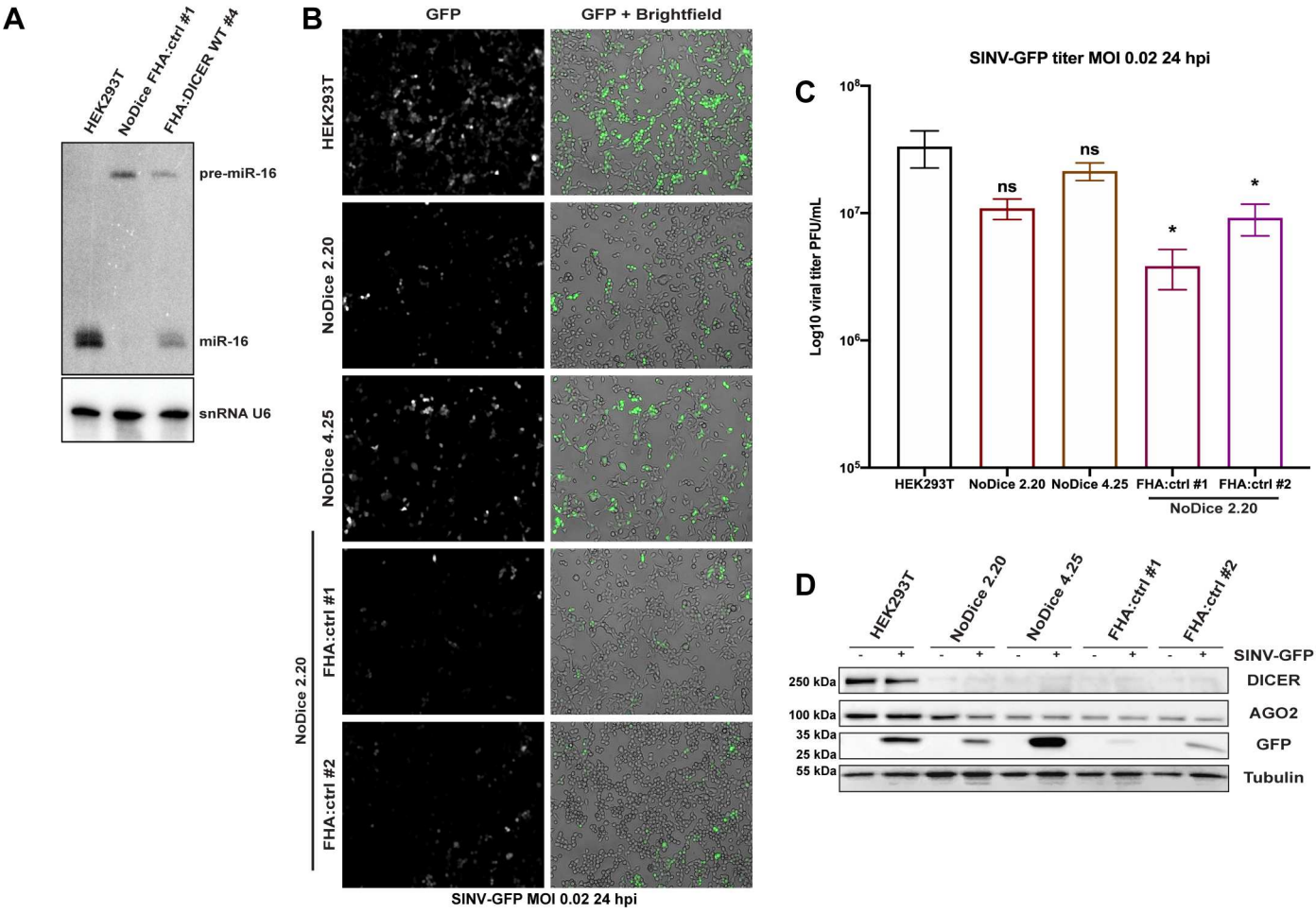
A
HEK293T
NoDice FHA:ctrl #1
FHA:DICER WT #4
pre-miR-16
miR-16
snRNA U6
B
GFP
GFP + Brightfield
HEK293T
NoDice 2.20
NoDice 4.25
NoDice 2.20
FHA:ctrl #1
FHA:ctrl #2
SINV-GFP MOI 0.02 24 hpi
C
SINV-GFP titer MOI 0.02 24 hpi
Log10 viral titer PFU/mL
ns
ns
*
*
HEK293T
NoDice 2.20
NoDice 4.25
FHA:ctrl #1
FHA:ctrl #2
NoDice 2.20
D
HEK293T
NoDice 2.20
NoDice 4.25
FHA:ctrl #1
FHA:ctrl #2
SINV-GFP
250 kDa
DICER
100 kDa
AGO2
35 kDa
25 kDa
GFP
55 kDa
Tubulin

Figure S2

A

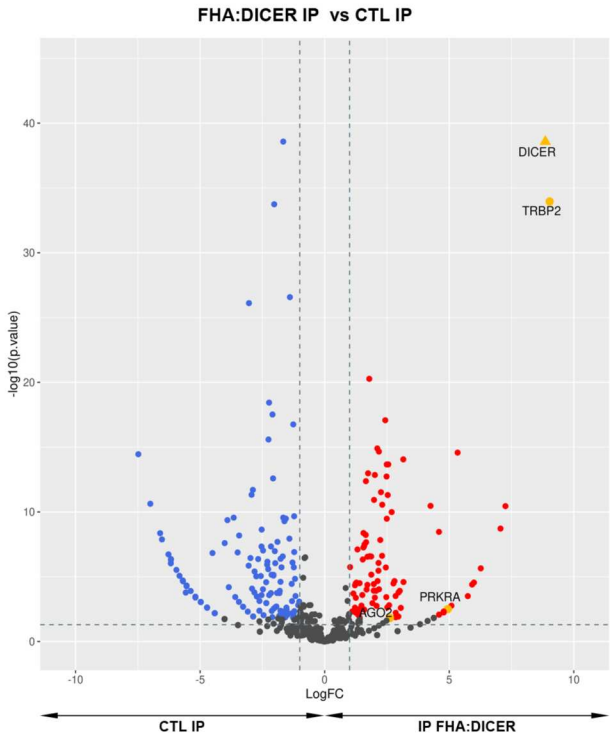

B

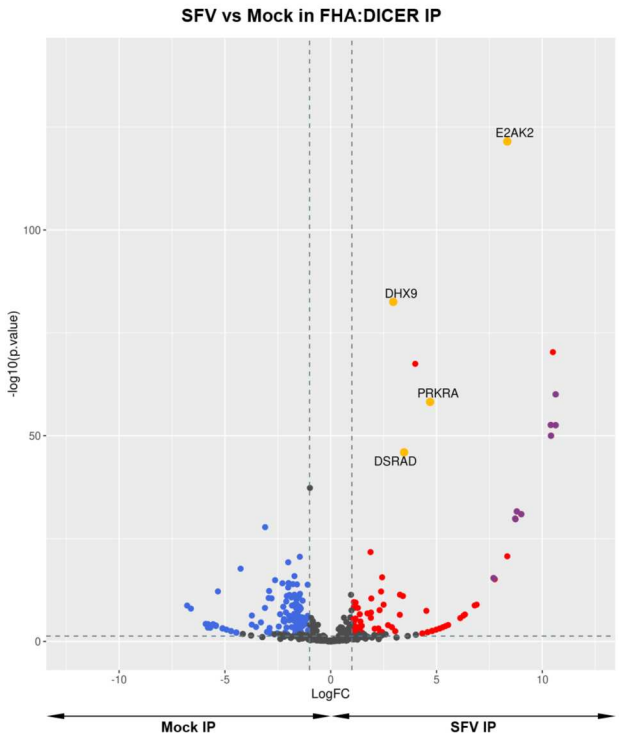

C

Gene name	Mean spectral count		LogFC	Adjusted p-value
	SFV IP	Mock IP		
E2AK2 (PKR)	221	0.5	8.344	2.611e-119
PRKRA (PACT)	131.5	4.5	4.697	8.415e-57
DSRAD (ADAR-1)	268	22	3.466	9.118e-45
DHX9	265	31	2.955	1.245e-80

Figure S3

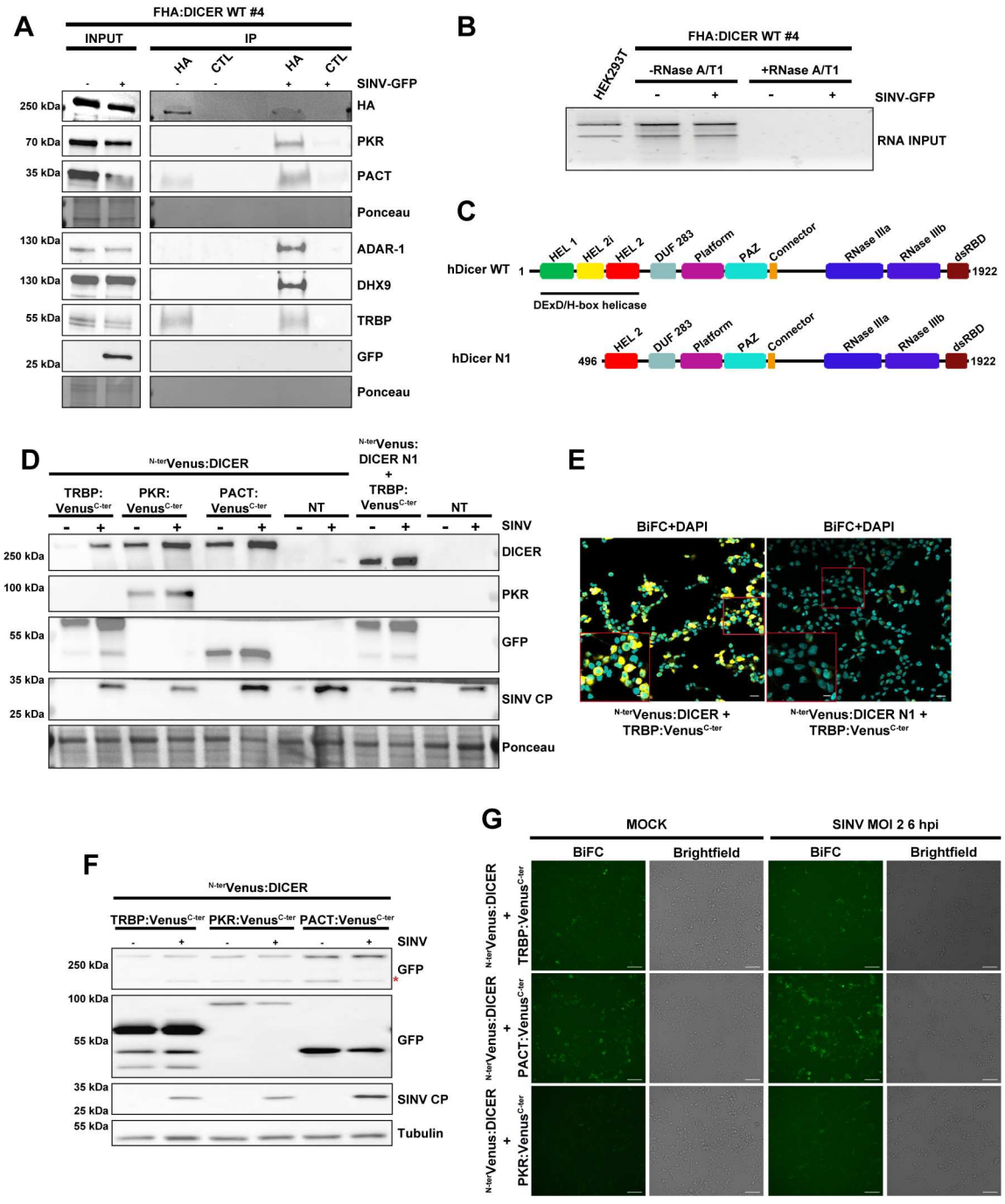
A
FHA:DICER WT #4
INPUT
IP
HA
CTL
HA
CTL
SINV-GFP
250 kDa
HA
70 kDa
PKR
35 kDa
PACT
Ponceau
130 kDa
ADAR-1
130 kDa
DHX9
55 kDa
TRBP
25 kDa
GFP
Ponceau
B
FHA:DICER WT #4
HEK293T
-RNase A/T1
+RNase A/T1
SINV-GFP
RNA INPUT
C
hDicer WT
1
HEL 1
HEL 2i
HEL 2
DUF 283
Platform
PAZ
Connector
RNase IIIa
RNase IIIb
dsRBD
1922
DExD/H-box helicase
hDicer N1
496
HEL 2
DUF 283
Platform
PAZ
Connector
RNase IIIa
RNase IIIb
dsRBD
1922
D
N-terVenus:DICER
N-terVenus: DICER N1 + TRBP: VenusC-ter
TRBP: VenusC-ter
PKR: VenusC-ter
PACT: VenusC-ter
NT
NT
SINV
250 kDa
DICER
100 kDa
PKR
55 kDa
GFP
35 kDa
SINV CP
25 kDa
Ponceau
E
BiFC+DAPI
BiFC+DAPI
N-terVenus:DICER + TRBP:VenusC-ter
N-terVenus:DICER N1 + TRBP:VenusC-ter
F
N-terVenus:DICER
TRBP:VenusC-ter
PKR:VenusC-ter
PACT:VenusC-ter
SINV
250 kDa
GFP
*
100 kDa
55 kDa
GFP
35 kDa
SINV CP
25 kDa
55 kDa
Tubulin
G
MOCK
SINV MOI 2 6 hpi
BiFC
Brightfield
BiFC
Brightfield
N-terVenus:DICER + TRBP:VenusC-ter
N-terVenus:DICER + PACT:VenusC-ter
N-terVenus:DICER + PKR:VenusC-ter

Figure S4

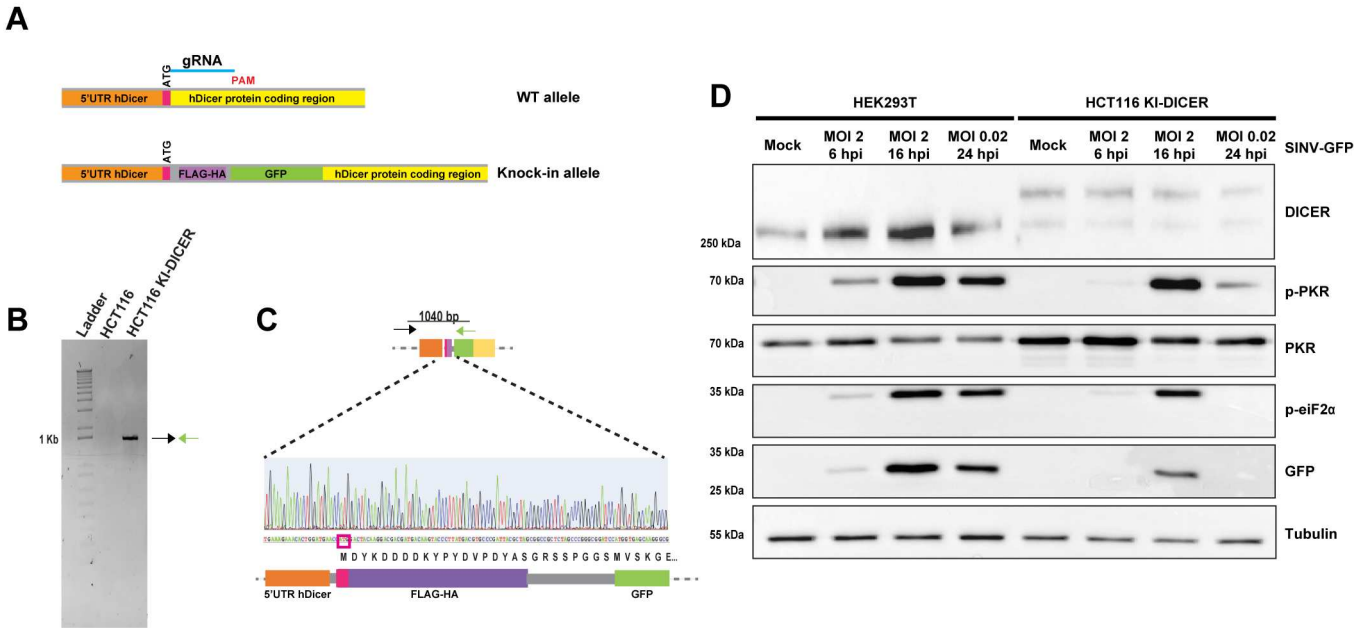
A
gRNA
ATG
PAM
5'UTR hDicer
hDicer protein coding region
WT allele
ATG
5'UTR hDicer
FLAG-HA
GFP
hDicer protein coding region
Knock-in allele
B
Ladder
HCT116
HCT116 KI-DICER
1 Kb
C
1040 bp
M D Y K D D D D K Y P Y D V P D Y A S G R S S P G G S M V S K G E...
5'UTR hDicer
FLAG-HA
GFP
D
HEK293T
HCT116 KI-DICER
Mock
MOI 2 6 hpi
MOI 2 16 hpi
MOI 0.02 24 hpi
Mock
MOI 2 6 hpi
MOI 2 16 hpi
MOI 0.02 24 hpi
SINV-GFP
250 kDa
DICER
70 kDa
p-PKR
70 kDa
PKR
35 kDa
p-eiF2α
35 kDa
GFP
25 kDa
55 kDa
Tubulin

Figure S5

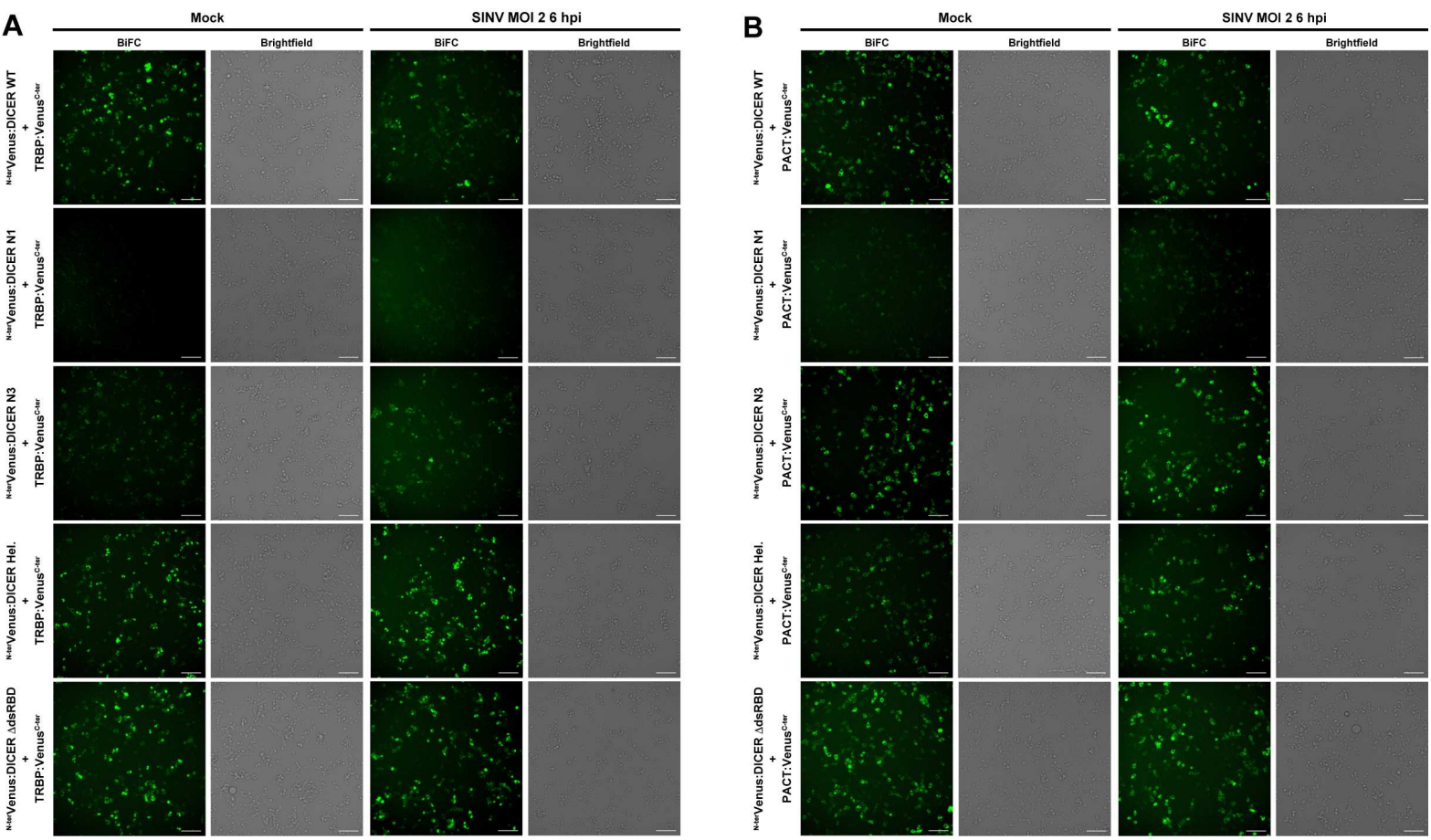
A
Mock
SINV MOI 2 6 hpi
BiFC
Brightfield
BiFC
Brightfield
N-terVenus:DICER WT + TRBP:VenusC-ter
N-terVenus:DICER N1 + TRBP:VenusC-ter
N-terVenus:DICER N3 + TRBP:VenusC-ter
N-terVenus:DICER Hel. + TRBP:VenusC-ter
N-terVenus:DICER ΔdsRBD + TRBP:VenusC-ter
B
Mock
SINV MOI 2 6 hpi
BiFC
Brightfield
BiFC
Brightfield
N-terVenus:DICER WT + PACT:VenusC-ter
N-terVenus:DICER N1 + PACT:VenusC-ter
N-terVenus:DICER N3 + PACT:VenusC-ter
N-terVenus:DICER Hel. + PACT:VenusC-ter
N-terVenus:DICER ΔdsRBD + PACT:VenusC-ter

Figure S6

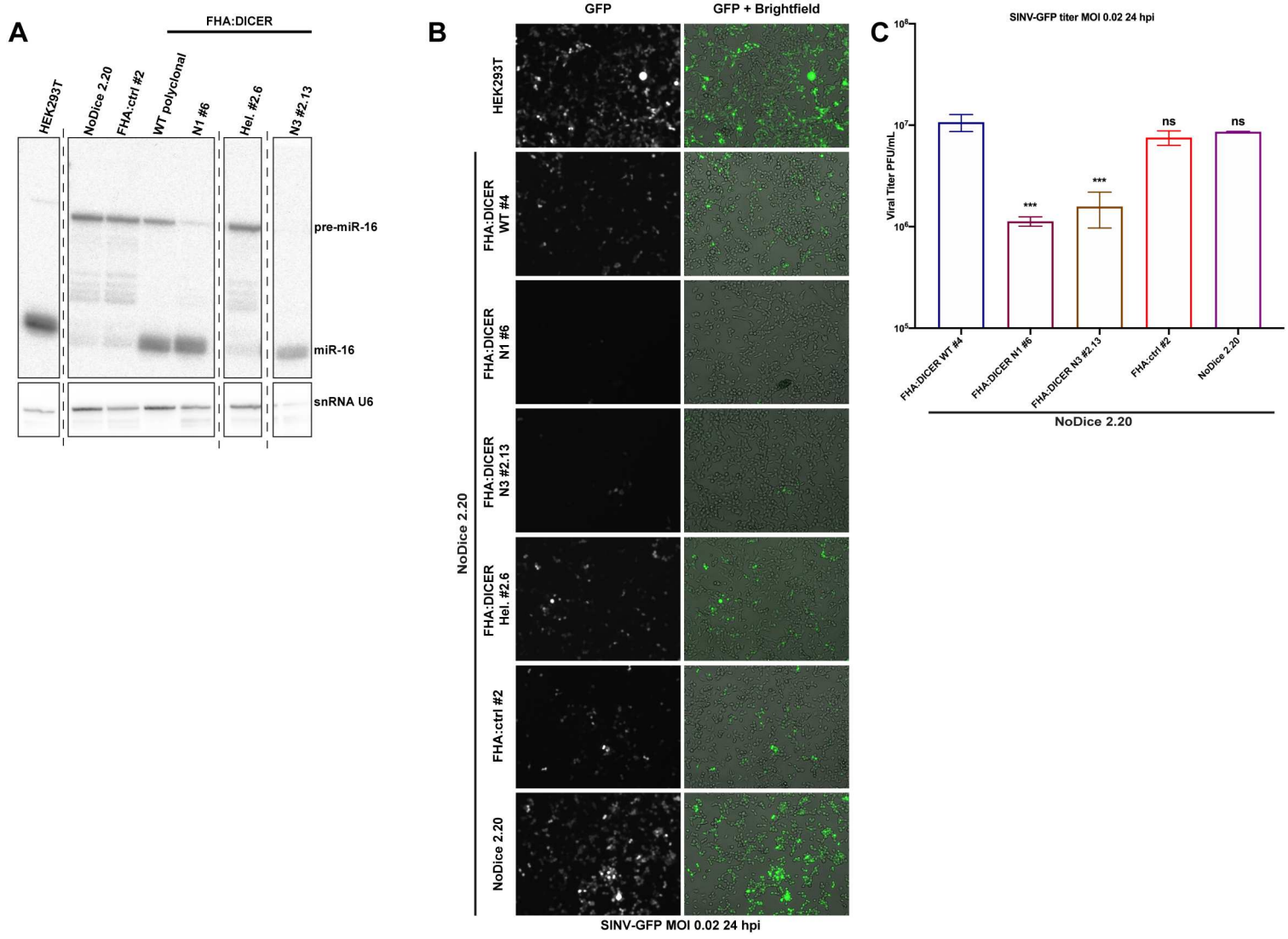
A
FHA:DICER
HEK293T
NoDice 2.20
FHA:ctrl #2
WT polyclonal
N1 #6
Hel. #2.6
N3 #2.13
pre-miR-16
miR-16
snRNA U6
B
GFP
GFP + Brightfield
HEK293T
FHA:DICER WT #4
FHA:DICER N1 #6
FHA:DICER N3 #2.13
FHA:DICER Hel. #2.6
FHA:ctrl #2
NoDice 2.20
NoDice 2.20
SINV-GFP MOI 0.02 24 hpi
C
SINV-GFP titer MOI 0.02 24 hpi
Viral Titer PFU/mL
10^8
10^7
10^6
10^5
***
***
ns
ns
FHA:DICER WT #4
FHA:DICER N1 #6
FHA:DICER N3 #2.13
FHA:ctrl #2
NoDice 2.20
NoDice 2.20

Type	Primer name	
PCR primer for mutagenesis	Forward hDicer mutant truncated from HEL1 and HEL2i (N1)	ACCAATTCAGTCGACATGGAAGCAGA
	Reverse hDicer mutant truncated from HEL1 and HEL2i (N1)	GAATTCTGCTTCCATGTCGACTGAATT
	Forward hDicer mutant truncated from Helicase domain (N3)	GGGAACCAATTCAGTCGACATGGATG
	Reverse hDicer mutant truncated from Helicase domain (N3)	GGAAAACGTCATCATCATCCATGTCGA
	Forward hDicer mutant truncated from terminal dsRBD (ΔdsRBD)	CCACTAATAGAAAAGTTTTCTGCAAA
	Reverse hDicer mutant truncated from terminal dsRBD (ΔdsRBD)	TGGGAACCTGAGGTTGATTATTTGCA
	Forward hDicer mutant helicase domain (Hel)	ACGGTACCGGGGACAAGTTTGTACAA
	Reverse hDicer mutant helicase domain (Hel)	GGGGACCACTTTGTACAAGAAAGCTG
	Forward PKR frameshift allowing C-terminal fusion	GAACGACACACATGTCTAGACCCAGC
	Reverse PKR frameshift allowing C-terminal fusion	CAAGAAAGCTGGGTCTAGACATGTGT
	Forward PACT frameshift allowing C-terminal fusion	GCAGAAAGAAAGCTAAACCCAGCTTT
	Reverse PACT frameshift allowing C-terminal fusion	GTACAAGAAAGCTGGGTTTAGCTTTC
	Forward TRBP frameshift allowing C-terminal fusion	GATCATGGCAGGCAGCAAGCTGAACC
	Reverse TRBP frameshift allowing C-terminal fusion	GAAAGCTGGGTTCAGCTTGCTGCCTG
PCR primer for plasmids construction	Forward TRBP pCDNA amplification to clone into pDONR221 vector	AAAAAGCAGGCTTCATGAGTGAAGAC
	Reverse TRBP pCDNA amplification to clone into pDONR221 vector	AGAAAGCTGGGTTCACTTGCTGCCTGC
	Forward PACT pCDNA amplification to clone into pDONR221 vector	AAAAAGCAGGCTTCATGTCCCAGAGC
	Reverse PACT pCDNA amplification to clone into pDONR221 vector	AGAAAGCTGGGTTTACTTTCTTTCTGC
	Forward PKR pCDNA amplification to clone into pDONR221 vector	AAAAAGCAGGCTTCATGGCTGGTGAT
	Reverse PKR pCDNA amplification to clone into pDONR221 vector	AGAAAGCTGGGTCTAACATGTGTGTC
PCR primer for HCT116 KI-DICER cell line construction	Forward pUC19-LEFT arm DICER	TTTCGGTACCCGGGGATCCACAGTAA
	Reverse LEFT arm DICER	TTTTCATCCAGTGTTTCTTTCATTGC
	Formard LEFT arm DICER_FlagHA	TTTAGAAACACTGGATGAACCATGGA
	Reverse GFP_RIGHT arm DICER	TTTCAAAGCAGGGCTTTTCTTGTACAG
	Forward RIGHT arm DICER	TTTAAAAGCCCTGCTTTGCAACCCC
	Reverse pUC19-RIGHT arm DICER	TTTGACTCTAGAGGATCCCAATTTCCC
	Forward mutagenesis PAM RIGHT arm	GAAAAGCTCTGCTTTGCAACCCCTCAC
	Reverse mutagenesis PAM RIGHT arm	AAAGCAGAGCTTTTCTTGTACAGCTCC
	Forward DICER gRNA	CACCGATGCTGAGGGGTTGCAAAGC
	Reverse DICER gRNA	AAACGCTTTGCAACCCCTCAGCATC

Second part

Canonical and non-canonical contributions of human Dicer helicase domain in antiviral defense

The following chapter describes the results obtained for the investigation on Dicer helicase domain contribution to the innate immune response. This section has been organized as a manuscript that we aim to submit in August. Briefly, the manuscript describes, first, the RNAi contribution to the N1 Dicer antiviral phenotype. Moreover, I investigated the role of the helicase subdomains in the immune response. Finally, I focused on N1 Dicer activity, as it displays an RNAi-independent antiviral phenotype against alphaviruses and an enterovirus. I focused on the transcriptomic analysis of N1 cells, uncovering an upregulation of IFN-related genes controlled by immune transcription factors as STAT2 and NF-kB. Finally, I showed the PKR catalytic-independent role in this antiviral phenotype through the contribution of the NF-kB pathway.

Canonical and non-canonical contributions of human Dicer helicase domain in antiviral defense

Morgane Baldaccini, Léa Gaucherand, Béatrice Chane-Woon-Ming, Mélanie Messmer, Floriane Gucciardi, Sébastien Pfeffer*

Université de Strasbourg, Architecture et Réactivité de l'ARN, Institut de Biologie Moléculaire et Cellulaire du CNRS, 67000 Strasbourg, France

* To whom correspondence should be addressed: s.pfeffer@ibmc-cnrs.unistra.fr

ABSTRACT

In mammals, the co-existence of RNAi and the type I interferon response in somatic cells begs the question of their compatibility and relative contribution during viral infection. Previous studies provided hints that both mitigating co-factors and self-limiting properties of key proteins such as Dicer could explain the apparent inefficiency of antiviral RNAi. Indeed, the helicase domain of human Dicer limits its processing activity and acts as an interaction platform for co-factors that could hinder its function. We studied the involvement of several helicase-truncated mutants of human Dicer in the antiviral response. We show that all deletion mutants display an antiviral phenotype against alphaviruses and an enterovirus. While only one of them, Dicer N1, is antiviral in an RNAi-independent manner, they all require the expression of PKR to be active. To elucidate the mechanism underlying the antiviral phenotype of Dicer N1 expressing cells, we analyzed their transcriptome and found that many genes from the interferon and inflammatory response were upregulated. We could show that these genes appear to be controlled by transcription factors such as STAT-1, STAT-2, and NF-kB. Finally, we demonstrated that blocking the NF-kB pathway in Dicer N1 cells abrogated their antiviral phenotype. Our findings highlight the crosstalk between Dicer, PKR, and the IFN-I pathway, and suggest that human Dicer may have repurposed its helicase domain to prevent basal activation of antiviral and inflammatory pathways.

INTRODUCTION

RNAi is an evolutionary conserved cellular defense mechanism against invading nucleic acids. It is based on the detection and cleavage of a trigger molecule, double-stranded (ds) RNA, by Dicer, a type III ribonuclease. The resulting small interfering (si) RNAs act as guides for effector Argonaute proteins that will act on target RNAs in a sequence specific manner (Meister & Tuschl, 2004). By its nature, RNAi has been shown to be a prominent defense mechanism against viruses in plant and invertebrate organisms (Guo *et al*, 2019; tenOever, 2016), but its exact contribution to the innate antiviral response in mammals remains to be firmly established. Although antiviral RNAi appears to be active in specific conditions, in particular in pluripotent stem cells (Maillard *et al*, 2013), it also seems to be incompatible with other innate immune defense pathways that rely on the type I interferon response (IFN-I). As a result, certain studies have shown that inactivating then IFN-I response allows RNAi to take over. The pattern recognition receptors that are inactivated in these studies are members of the RIG-I like receptors (RLR) family and they are also activated by dsRNA (Ahmad & Hur, 2015; Pichlmair & Reis e Sousa, 2007). However, as opposed to Dicer, they do not act by cleaving dsRNA but rather by inducing a phosphorylation cascade that will ultimately result in the production of the autocrine- and paracrine-acting interferon α and ß cytokines followed by the transcriptional activation of hundreds of interferon stimulated genes (ISGs) (Ivashkiv & Donlin, 2014). Thus, in mammalian somatic cells deficient for MAVS or IFNAR, the production of long-dsRNA-derived siRNAs can be detected and are shown to be dependent on Dicer activity (Maillard *et al*, 2016). Besides, the RLR LGP2 has been shown to be directly interacting with Dicer blocking siRNA production and along with TRBP preventing the correct miRNA maturation (Takahashi *et al*, 2018b, 2018a; van der Veen *et al*, 2018). Thus, in mammalian cells RNAi and IFN-I seem to be functionally mutually exclusive and IFN-I is suggested to tone down Dicer involvement in antiviral RNAi.

One interesting observation is that the N-terminal helicase domain is quite conserved between RLRs and Dicer, which might indicate a functional replacement during evolution (Baldaccini & Pfeffer, 2021). In mammalian Dicer, the helicase domain exerts some molecular constraints that limit Dicer's processivity for cleaving long dsRNA molecules (Ma *et al*, 2008). Accordingly, a synthetic Dicer lacking the first two domains of the helicase, Hel1 and Hel2i, and named Dicer N1 displays better cleavage properties of an artificial dsRNA than the full-length version of Dicer (Kennedy et al., 2015). More recently, a naturally occurring isoform of Dicer, lacking the Hel2i domain, has been identified in human stem cells and showed to possess some antiviral properties in an RNAi-dependent manner (Poirier *et al*, 2021). Similarly, a Hel1-truncated version of Dicer, coined Dicer^{O}, is specifically expressed in mouse oocytes and is better adapted to cleave long dsRNA molecules than pre-miRNAs (Flemr *et al*, 2013). Uncovering the structure of Dicer^{O} isoform revealed that the N-terminal part of the helicase domain plays an important role for the correct positioning of the pre-miRNA and that removing it potentially increases the affinity for longer dsRNA structures (Zapletal *et al*, 2022). On top of having a molecular self-limiting effect, this helicase domain also allows Dicer to interact with proteins that regulate its activity. We have recently shown that during Sindbis virus (SINV) infection the helicase domain of human Dicer specifically interacts with proteins that are involved in the IFN-I response such as PACT, the RNA helicase DHX9, the adenosine deaminase ADAR1 and the dsRNA-activated protein kinase PKR (Montavon *et al*, 2021). In addition, we reported in the same study that the expression of the helicase-truncated Dicer N1 confers a strong antiviral activity against SINV, and that this phenotype is dependent on the presence of PKR. Similarly, another study shows a genetic link between Dicer and PKR in mouse embryonic stem cells and proposes that Dicer can hinder PKR activity in a non-canonical manner (Gurung *et al*, 2021). Dicer thus seems to have an additional antiviral activity linked to PKR that is limited by its helicase domain.

In this study, we sought to uncover the mechanism underlying Dicer N1 antiviral activity. By using HEK293T NoDice cells (Bogerd *et al*, 2014) stably expressing either Dicer WT or N1, we showed that Dicer N1 cells are more resistant than Dicer WT cells to infection with alphaviruses SINV and Semliki forest virus (SFV), and human enterovirus 71 (HEV71). However, this antiviral effect was virus-dependent, as Dicer N1 had no impact on vesicular stomatitis virus (VSV) infection, and we even observed a pro-viral effect of Dicer N1 on SARS-CoV-2 infection. Interestingly, we found that the antiviral effect of Dicer N1 is RNAi-independent, as cells expressing a catalytically inactive Dicer N1 were equally protected against SINV infection. We also tested other helicase-truncated mutants of Dicer and observed that individual deletion of each subdomain (Hel1, Hel2i or Hel2) also conferred an antiviral property to Dicer. However, as opposed to Dicer N1, this phenotype appeared to be partially due to RNAi. Nevertheless, all of the helicase-deletion mutants also required the presence of PKR to maintain their antiviral effect. We thus focused our investigations on the implication of PKR in the phenotype of Dicer N1 and showed that it is required for its antiviral activity independently from its kinase function. Transcriptomic analysis of mock- or SINV-infected cells uncovered that Dicer N1 expressing cells have a higher basal expression of a large subset of genes, including a number that are involved in the antiviral response. We further show that those genes are under the control of transcription factors such as STAT1, STAT2 and NF-kB/p65. Finally, we confirmed the importance of the latter pathway in the phenotype of Dicer N1 cells by alleviating the antiviral effect in cells treated with a chemical inhibitor of NF-kB. Based on these results, we propose that one reason for human Dicer to have maintained a self-limiting helicase domain is to prevent basal activation of antiviral and inflammatory pathways.

RESULTS

Effect of Dicer N1 expression on SINV viral cycle

We previously showed that a partial helicase-deletion mutant of human Dicer expressed in HEK293T NoDice cells presented an antiviral activity against SINV (Montavon *et al*, 2021). We used the two monoclonal cell lines NoDice FHA-Dicer WT #4 and NoDice FHA:Dicer N1 #6 (afterward respectively referred to as Dicer WT and Dicer N1 cells) to better characterize the impact of Dicer WT or Dicer N1 expression on SINV cycle. We used a non-modified SINV strain and two different GFP-expressing strains that either express the fluorescent protein from a duplication of the subgenomic promoter (SINV-GFP) or from a fusion with the capsid protein (SINV-2A-GFP) (Thomas et al., 2003), the latter expressing GFP at higher levels than the former (Supp. Fig. 1A). We infected Dicer WT or Dicer N1 cells with increasing MOIs of all three viruses and measured the accumulation of infectious particles by plaque assay 24 hours post-infection (hpi) (Fig. 1A). For all viruses, we observed a significant antiviral effect at every MOI in cells expressing Dicer N1 compared to cells expressing Dicer WT. The effect was more pronounced in cells infected with the SINV-2A-GFP, which seems to be attenuated at lower MOIs compared to the two other viral strains (Fig. 1A). We also monitored viral protein accumulation as well as PKR activation in cells infected for 24h at an MOI of 0.02. In Dicer N1 cells, both the Capsid and GFP proteins accumulated to lower levels, or even below detection limits for SINV-2A-GFP, compared to Dicer WT cells (Fig. 1B). PKR phosphorylation could be detected to roughly similar levels in Dicer WT and N1 cells infected with SINV or SINV-GFP. However, it was only detectable in Dicer WT cells but not in Dicer N1 cells, infected with the SINV-2A-GFP, which reflected the attenuation of this virus compared to the two others (Fig. 1B). We also monitored double-stranded (ds) RNA accumulation during infection as a proxy for viral replication. We used the dsRNA-specific J2 antibody (Richardson *et al*, 2010) to perform immunostaining of cells infected for 24h at an

MOI of 0.02 with either of the three SINV strains. Compared to Dicer WT cells, dsRNA accumulation decreased in Dicer N1 cells for all three viruses, with a stronger effect for the SINV-2A-GFP virus (Fig. 1C). Finally, to further confirm the impact of Dicer N1 expression on viral replication, we finally measured the accumulation of genomic RNA by RT-qPCR in cells infected with SINV-GFP at an MOI of 0.02 for 24h. In agreement with the previous results, Dicer N1 cells showed a very strong decrease of SINV genomic RNA accumulation compared to Dicer WT cells (Fig. 1D). In parallel, we also performed semi-quantitative strand-specific RT-PCR on the same samples and observed that the anti-genomic viral RNA accumulated to lower levels in Dicer N1 cells than in Dicer WT cells. (Supp. Fig. 1B). Collectively, these data indicate that the antiviral activity of Dicer N1 leads to a defect in SINV viral replication.

Dicer N1 is antiviral against other positive-strand RNA viruses

To see whether the antiviral activity of Dicer N1 could be generalized to other viruses, we infected Dicer WT and Dicer N1 cells with viruses from different families. We first tested another *Togaviridae*, Semliki forest virus (SFV), and observed a lower viral titer in the supernatants of Dicer N1 cells than in Dicer WT cells infected for 24h at an MOI of 1.10^{-4} (Fig. 2A, top panel). In addition, dsRNA accumulation, as assessed by J2 immunostaining, was barely detectable in Dicer N1 cells, whereas it was very high in Dicer WT cells (Fig. 2A, bottom panel). We then infected Dicer WT and N1 cells at an MOI of 0.1 with a (+) RNA virus from the *Picornaviridae* family, human enterovirus 71 (EV71), and measured viral titer in the supernatant by TCID50 at 24 hpi. We observed that the EV71 titer was again lower in Dicer N1 compared to WT cells (Fig. 2B, top panel). J2 immunostaining also confirmed a lower accumulation of dsRNA in Dicer N1 cells compared to WT cells (Fig. 2B, bottom panel). We also tested the effect of Dicer N1 on a single-stranded negative-sense RNA virus from the *Rhabdoviridae* family, *i.e.* vesicular stomatitis virus (VSV). We infected Dicer WT and N1

cells at an MOI of 1.10^{-5} for 24h with an engineered VSV expressing the GFP protein and titrated the virus in the supernatant by plaque assay. We did not detect any significant difference in viral titers between Dicer WT and N1 cells (Fig. 2C, top panel). As previously reported (Weber *et al*, 2006), we were not able to detect dsRNA accumulation by J2 immunostaining, in either Dicer WT or N1 cells infected with VSV-GFP. Since dsRNA is a canonical Dicer substrate upon infection, this result indicates that the absence of dsRNA during VSV infection might prevent the activation and antiviral activity of Dicer N1.

Finally, we infected the two cell lines with the single-stranded positive-sense RNA virus Severe Acute Respiratory Syndrome Coronavirus 2 (SARS-CoV-2). In order to be able to use this virus in the HEK293T cells we work with, we first transduced them with a lentiviral vector expressing human ACE2 (hACE2), which is an essential receptor for SARS-CoV-2 infection (Hoffmann *et al*, 2020). We verified hACE2 expression by western blot with a specific antibody (Fig. 2D). We infected both hACE2-expressing Dicer WT and Dicer N1 cells with SARS-CoV-2 at an MOI of 1.10^{-3} for 48h, and measured viral nucleocapsid expression by western blot analysis. Nucleocapsid expression could be detected in both Dicer WT and N1 cells and seemed to be slightly higher in the latter (Fig. 2E). We also monitored PKR phosphorylation in this experiment and observed a higher signal in Dicer N1 compared to WT cells. Then, we measured viral titer in the supernatant by TCID50 at 48 hpi. We observed that the SARS-CoV-2 titer was higher in Dicer N1 compared to WT cells (Fig. 2F). We also performed J2 immunostaining on SARS-CoV-2 infected cells, and saw that dsRNA was detected equally well in both Dicer WT and N1 cells (Fig. 2G). Finally, we also measured viral RNA accumulation by RT-qPCR, and saw that both ORF1a and Spike RNAs accumulated to higher levels in Dicer N1 than in Dicer WT cells, although the increase was not significant for Spike RNA (Fig. 2H).

Altogether, these last results suggest that Dicer N1 expression can have an antiviral effect for two different (+) RNA viruses (SFV and EV71), but not for a third one (SARS-CoV-2).

This antiviral property does not seem to be active in the case of a (-) RNA virus, VSV, which might be related in this case to the difference in dsRNA accessibility.

RNA interference is not involved in Dicer N1 phenotype

We showed that Dicer N1 expression prevents the accumulation of viral genomic and antigenomic RNA during SINV infection and of dsRNA during SINV, SFV and EV71 infection. Since it was previously shown that Dicer N1 was more active than Dicer WT to cleave an artificial dsRNA into siRNAs (Kennedy et al., 2015), we first hypothesized that the ribonuclease activity of Dicer N1 was responsible for its antiviral activity. To test this hypothesis, we therefore used an affinity-based purification approach (Hauptmann *et al*, 2015) to isolate Ago-associated small RNAs from Dicer WT or N1 cells infected with SINV-GFP at an MOI of 0.02 for 24h and deep-sequenced them. We first mapped the reads to the human and SINV-GFP genomes and observed that the vast majority of small RNAs had a cellular origin (Supp. Fig. 2A). Only 0.2 to 1.2% of sequences could be mapped to the viral genome. Interestingly, the percentage of viral reads was four-to-five-fold lower in Dicer N1 cells than in WT cells. We further analyzed the viral reads and determined their size distribution. Small RNAs mapped to both the genomic and to the antigenomic RNA, with a bias in favor of the former, and showed a peak at 22 nt, consistent with a Dicer-mediated cleavage (Fig. 3A, Supp. Fig. 2B). However, there was no real difference in size distribution or strand origin between Dicer WT and N1 cells. Mapping the small RNAs to the viral genome showed a strong enrichment at the 5' extremity of the genomic RNA in both Dicer WT and N1 cells (Fig. 3B, Supp. Fig. 2C), in agreement with previous reports (Kong *et al*, 2023; Zhang *et al*, 2021). The number of reads that mapped to both strands of the viral RNA was however higher in Dicer WT than in N1 cells. It therefore appears that both Dicer WT and Dicer N1 are competent for the generation of what looks like viral siRNAs that are loaded in Argonaute proteins, but we

205 did not see an increase in their number in Dicer N1 expressing cells. At this stage, we therefore
206 cannot say that the observed antiviral phenotype of Dicer N1 is linked to a stronger RNAi
207 activity.

208 To further confirm that the Dicer N1 phenotype was independent of its role in RNAi, we
209 generated a catalytic-deficient version of Dicer N1 by introducing mutations in both of its
210 RNAse III domains (Fig. 3C). As previously, we used the HEK293T NoDice 2.20 cell line
211 (Bogerd *et al*, 2014) that we transduced with lentiviral vectors expressing a Flag-HA-tagged
212 version of Dicer N1 with mutations in the catalytic domain (N1-CM). We then selected a clone,
213 NoDice FHA:Dicer N1-CM #2.17 (afterwards called Dicer N1-CM), that expressed Dicer at
214 levels similar to the Dicer WT and Dicer N1 cell lines previously generated (Fig. 3D). The
215 levels of PKR and TRBP were mostly similar to the ones in Dicer N1 cells. By blotting AGO2
216 expression in these cell lines, we observed that it was absent in the Dicer N1-CM cells, which
217 is expected for a miRNA-free Argonaute protein and is consistent with previous observations
218 (Gibbings *et al*, 2012). We confirmed the defect in miRNA processing in the Dicer N1-CM
219 cells by measuring miR-16 accumulation by northern blot analysis. As expected, we saw no
220 mature miR-16 form and the accumulation of its precursor in Dicer N1-CM cells (Fig. 3E). We
221 then infected Dicer WT, N1 and N1-CM cells with SINV-GFP at an MOI of 0.02 for 24h and
222 measured the infection rate by western blot analysis and plaque assay. The level of the capsid
223 protein was strongly reduced in both Dicer N1 and Dicer N1-CM cells compared to Dicer WT
224 cells (Fig. 3F). In addition, we could not detect PKR or eIF2α phosphorylation in neither Dicer
225 N1 nor Dicer N1-CM cells. To confirm these observations, we titrated the infectious viral
226 particles in the supernatant and observed a strong and significant decrease of viral titers in both
227 Dicer N1 and Dicer N1-CM compared to Dicer WT cells (Fig. 3G). To rule out any clone-
228 dependent effect, we performed the same experiment in polyclonal cells expressing Dicer WT,
229 N1 or N1-CM. As for the monoclonal cell lines, Dicer N1 and N1-CM cells displayed a drop

in Capsid protein accumulation and an absence of PKR activation compared to Dicer WT cells (Supp. Fig. 2D). Accordingly, the viral titer was strongly reduced in Dicer N1 and N1-CM cells compared to Dicer WT cells (Supp. Fig. 2E). We showed previously that Dicer N1 could no longer interact with the Dicer co-factors TRBP and PACT and with the kinase PKR (Montavon *et al*, 2021). Thus, we verified by co-immunoprecipitation the interaction of Dicer N1-CM with these proteins. The results confirmed that Dicer N1-CM behaved similarly to Dicer N1 regarding the loss of these interactions (Supp. Fig. 2F).

Taken together, these results clearly show that the antiviral phenotype of Dicer N1 does not depend on its catalytic activity, and therefore on RNAi, which is in agreement with our previous observations that the antiviral effect of Dicer N1 did not depend on AGO2 (Montavon *et al*, 2021).

Impact of Dicer helicase subdomain deletions on viral infection

The region deleted in Dicer N1 contains both the Hel1 and Hel2i domains of the helicase, and was designed based on the presence of an alternative initiation codon at this position (Kennedy et al., 2015). Other deletion mutants have been reported in the literature, such as the rodent-specific Dicer^{O}, which is naturally expressed in oocytes (Flemr *et al*, 2013). Similar to Dicer N1, this truncated Dicer was shown to be more potent at generating siRNAs, and was further functionally and structurally studied under the name Dicer ΔHel1 (Zapletal *et al*, 2022). Finally, another Dicer isoform has been recently reported in human embryonic stem cells and was coined antiviral Dicer (AviD) for its RNAi-related antiviral property against different viruses (Poirier *et al*, 2021). This isoform lacks the Hel2i connector domain. To test the behavior of all these deletion mutants during SINV infection, we generated lentiviral constructs expressing a Flag-HA tagged version of Dicer ΔHel1, ΔHel2i and a version lacking the third helicase domain ΔHel2 (Fig. 4A). We used these lentiviral constructs, as well as catalytically inactive version

of them called CM, to generate monoclonal NoDice cell lines. We first verified the correct expression of the Dicer isoforms and checked their impact on AGO2, TRBP, PACT and PKR expression (Supp. Fig. 3A). We also checked that the catalytically inactive versions of the constructs were indeed impaired in miRNA biogenesis by measuring miR-16 expression by northern blot analysis (Supp. Fig. 3B). We then infected cells expressing Dicer WT, ΔHel1, ΔHel2i, ΔHel2 or their catalytically inactive versions (CM) with SINV-GFP at an MOI of 0.02 for 24h and monitored Capsid protein accumulation by western blot analysis. The levels of Capsid were lower in all cell lines expressing helicase truncated versions of Dicer compared to Dicer WT cells, but seemed to go up when the RNAse III activity was mutated, although slightly less so in the case of ΔHel2 (Fig. 4B). To really assess the impact of the expression of these mutants on viral production, we titrated by plaque assay the supernatants of the previous experiment, using Dicer N1 cells as control. We observed that expression of all helicase deletion mutants, Dicer ΔHel1, ΔHel2i and ΔHel2, resulted in a significant drop in viral titer, although slightly less than in Dicer N1 expressing cells, and that this effect was lost in cells expressing the CM versions of the mutants (Fig. 4C). Altogether, these results suggest that deleting any helicase subdomain confers an antiviral activity to human Dicer.

We previously showed that Dicer N1 antiviral phenotype was dependent on the expression of PKR (Montavon *et al*, 2021). We therefore tested the impact of the expression of the various helicase deletion mutants on viral infection in NoDice compared to NoDiceΔPKR cells. We transduced the aforementioned cell lines with Dicer WT, N1, ΔHel1, ΔHel2i and ΔHel2 to generate polyclonal cell lines. We again made sure that these cell lines expressed the different Dicer constructs, that they expressed similar levels of interacting proteins such as AGO2, TRBP and PACT (Supp. Fig. 3C), and that they were also competent for miRNA production (Supp. Fig. 3D). We then infected all those cell lines with SINV-GFP at an MOI of 0.02 for 24h and measured the expression of the Capsid protein by western blot analysis. We

could observe a lower accumulation in NoDice cells transduced with Dicer ΔHel1, ΔHel2 and ΔHel2i compared to cells transduced with Dicer WT (Fig. 4D), although the effect was less evident for cells expressing Dicer ΔHel2. On the contrary, in NoDiceΔPKR cells transduced with Dicer ΔHel1, ΔHel2 and ΔHel2i, we did not observe such a strong decrease in Capsid protein levels. We then determined the viral titers produced upon SINV-GFP infection of NoDice or NoDiceΔPKR cells expressing Dicer WT, N1, ΔHel1, ΔHel2i or ΔHel2. While we confirmed the antiviral effect of the helicase deletion mutants compared to the WT Dicer in NoDice cells, we saw that this effect was completely abrogated in NoDiceΔPKR cells (Fig. 4E). We can therefore conclude that the antiviral phenotype of Dicer N1 can also be observed with smaller deletion mutants lacking individual subdomains of the helicase. However, as opposed to Dicer N1, it seems that in the case of Dicer ΔHel1, ΔHel2i or ΔHel2, this phenotype is dependent on the catalytic activity of Dicer, and thus is likely RNAi-dependent. Yet, the phenotype is also lost in cells that do not express PKR, a property which is also seen with Dicer N1. We thus decided to look more into the role of PKR.

PKR, but not its catalytic activity, is directly involved in the Dicer N1 antiviral phenotype

As shown above, the antiviral phenotype of Dicer helicase mutants seems to be strictly dependent on the expression of PKR. To validate the implication of PKR, we decided to re-express it in NoDiceΔPKR cells to see whether this would complement the antiviral phenotype of Dicer N1. We also designed mutant versions of PKR as indicated in Figure 5A. These mutants are: K296R, which is not able to bind ATP, homodimerize, autophosphorylate or phosphorylate its targets (Dey *et al*, 2005), and T451A, which is still able to form homodimers but loses its ability to autophosphorylate the T451 residue and to phosphorylate its targets (Taylor *et al*, 2001). We first transduced constructs expressing a MYC:CTRL, MYC:PKR WT, MYC:PKR K296R or MYC:PKR T451A in NoDiceΔPKR FHA:Dicer WT cells and infected

them with SINV-GFP at an MOI of 0.02 for 24h. We analyzed the expression of PKR and its phosphorylated form by western blot analysis, which confirmed that all constructs were expressed at high levels, but only WT PKR could be phosphorylated upon SINV infection (Fig. 5B). Interestingly, there was some basal level of phosphorylated PKR in the mock-infected cells expressing WT PKR, which could be due to a higher expression of PKR in transduced cells compared to WT cells. The activation of the MYC:PKR WT construct in the infected condition resulted in an increase in eiF2α phosphorylation compared to the CTRL or mutant PKR constructs. Even in the absence of PKR or in the presence of catalytically inactive version of it, some levels of eiF2α phosphorylation could be detected in the SINV-infected conditions, probably due to the activity of the GCN2 kinase as previously reported (Berlanga *et al*, 2006). In terms of viral capsid accumulation, no real difference could be detected between the different conditions (Fig. 5B). We measured viral particles production by plaque assay in SINV-GFP infected cells, and could not detect any difference between samples (Fig. 5C). This result indicates that in the presence of Dicer WT, expression of a WT or inactive mutant PKR has no significant impact on SINV infection. We then transduced the same MYC:CTRL or PKR constructs as above in NoDiceΔPKR FHA:Dicer N1 cells and performed the same analysis after infection with SINV-GFP. The western blot analysis was consistent with the previous one and confirmed the correct expression of the PKR constructs as well as activation of only the WT PKR version (Fig. 5D). However, we noted a small reduction of Capsid protein accumulation in cells expressing MYC:PKR WT, K296R or T451A compared to the MYC:CTRL condition (Fig. 5D). This was confirmed by the plaque assay analysis that revealed a significant drop in viral titer in NoDiceΔPKR Dicer N1 cells expressing WT or inactive PKR compared to cells expressing the negative control (Fig. 5E). We could thus restore the antiviral phenotype of Dicer N1 by re-expressing PKR in cells where its expression was ablated. Interestingly, this did not require a catalytically active or homodimerization competent PKR since the same

complementation could be observed with two different mutants that were both unable to phosphorylate their substrates. Overall, these results suggest that the antiviral activity of Dicer N1 is linked to PKR, but does not require the canonical activation of PKR through homodimerization and phosphorylation.

Expression of Dicer N1 induces major changes in the transcriptome

To decipher the mechanism behind Dicer N1 antiviral property, we performed total RNAseq analysis on both Dicer WT and Dicer N1 cells either mock-infected, infected with SINV-GFP at an MOI of 2 for 12h or infected with SINV-GFP at an MOI of 0.02 for 24h. We first verified the percentage of viral reads in the libraries and observed that it was higher (about 8-fold for the genomic RNA) in Dicer WT than in Dicer N1 cells (Supp. Fig. 4A). This confirmed the antiviral effect of Dicer N1 at the level of viral replication. Next, we compared the overall profiles of gene expression in the different conditions (Fig. 6A). The analysis identified 5 groups of genes according to their expression patterns. The first group was composed of genes overexpressed in N1 cells compared to WT cells. The second one was composed of genes specifically downregulated in WT cells upon infection, whereas the third one represented genes downregulated upon infection in both cell lines. Finally, the fourth and fifth groups comprised genes that are upregulated in both WT and N1 cells or in WT cells only, respectively. The first two groups were of interest as several genes were upregulated in Dicer N1 cells no matter whether there were infected or not. We then performed a differential gene expression analysis of mRNAs using DEseq2 (Love *et al*, 2014) to determine the impact of the infection on the cell transcriptome. The results confirmed that in Dicer WT cells, infection by SINV resulted in major changes in the expression levels of a large number of mRNAs, which were visible both at 12 and 24 hpi (Fig. 6B, Supp. Fig. 4B). However, in Dicer N1 cells, these changes were substantially more limited at both time points of infection (Fig. 6C, Supp. Fig. 4B), consistent

with the fact that the infection was attenuated in these cells and therefore did not result in a strong cellular response. Strikingly, when we compared the transcriptomes of mock-infected Dicer WT and Dicer N1 cells, we found that there was a large number of up-regulated mRNAs, as well as a smaller number of down-regulated mRNAs (Fig. 6D). It seems therefore that the expression of Dicer N1 results in changes at the transcriptional level, so we set out to examine whether any of these perturbations could explain the phenotype we observed in these cells. To better characterize the phenotypical dynamics underlying differentially expressed genes (DEGs), we looked at gene set enrichment analysis (GSEA) against the Hallmark biological states and processes gene sets (Fig. 6E, Supp. Fig. 4C, D). In Dicer N1 cells, processes linked to interferon alpha and gamma, and to inflammatory and NF-kB responses were significantly enriched (Fig. 6E). Interestingly, the interferon alpha and gamma pathways were already enriched in mock cells, whereas those pathways were not enriched in WT cells upon SINV infection. This was confirmed by the increased number of genes linked to interferon and inflammatory pathways in Dicer N1 cells compared to WT cells, denoting a basal IFN-I signature linked to a subset of genes in N1 cells (Supp. Fig. 4C). Conversely, those pathways were not detected in WT cells upon infection (Supp. Fig. 4D).

Altogether, these results highlight transcriptomic differences in Dicer N1 compared to WT cells in mock and SINV infected cells. Globally, immune-related pathways seem to be enriched in Dicer N1 cells, and this, even in the steady state.

Dicer N1 expression increases the activation of immune-related transcription factors

Given the seemingly increased RNA Pol II transcription in the Dicer N1 cells, we looked for transcription factors that are known to play important roles in innate immunity and analyzed the expression levels of their target genes in the different samples. We retrieved the known targets of NF-kB/p65, STAT1, STAT2, IRF2 and IRF3 and extracted from these lists genes that

were differentially expressed either during infection in Dicer WT or Dicer N1 cells, or between mock-infected Dicer WT and Dicer N1 cells. We then computed the cumulative frequencies of de-regulated transcripts by comparing i) Dicer WT SINV-GFP 24hpi vs. Dicer WT Mock, ii) Dicer N1 SINV-GFP 24hpi vs. Dicer N1 Mock and iii) Dicer N1 Mock vs. Dicer WT Mock. This calculation was done for NF-kB/p65 (Fig. 7A) and STAT2 (Fig. 7B), which were the ones with the greater changes, but also for IRF2 (Supp. Fig. 5A), IRF3 (Supp. Fig. 5B) and STAT1 (Supp. Fig. 5C). The results indicate first that when comparing Dicer WT SINV-infected vs. Mock and Dicer N1 SINV-infected vs. Mock, there were more target genes either up or down-regulated in the Dicer WT cells than in the Dicer N1 cells, which again reflects the lower response of Dicer N1 cells to the infection. Surprisingly, there were significantly more upregulated transcripts when comparing Dicer N1 Mock to Dicer WT Mock than when comparing Dicer WT SINV-infected to Dicer WT Mock conditions (see the red vs. black curves in Fig. 7A, B). A global representation in the form of heatmaps for the same set of genes that are known targets of NF-kB/p65 or STAT2 also allowed to visualize the stronger changes induced by the infection in Dicer WT cells compared to Dicer N1 cells, and that a number of transcripts were more expressed in Dicer N1 Mock than in Dicer WT Mock condition (Fig. 7C, D). We also represented DEseq2 data on volcano plots for NF-kB/p65 and STAT2 for the Dicer WT infected vs mock and Dicer N1 mock vs Dicer WT mock comparisons (Supp. Fig. 5D, E). As seen previously, genes under the control of NF-kB and STAT2 appeared to be more upregulated in Dicer N1 mock cells than in WT cells either mock or SINV-infected.

We validated the increased expression of some selected target genes by RT-qPCR and could confirm that PTGS2, APOBEC3B, MX1, OAS3, and IFIT3 mRNAs were indeed significantly upregulated in mock-infected Dicer N1 compared to Dicer WT cells (Fig. 7E). Conversely, very mild or no expression increase and sometimes a decrease in expression was detected for the selected target genes in Dicer N1 infected compared to mock cells, consistent

with the RNAseq analysis (Supp. Fig. 5F). Besides, the expression decrease observed in WT cells upon infection was expected as SINV blocks RNA Pol II transcription via its nsP2 protein (Akhrymuk *et al*, 2018).

Overall, the transcriptome changes induced by Dicer N1 expression, which we validated for selected transcripts by RT-qPCR, allow us to postulate that these cells are in a pre-activated state that might explain their increased resistance to SINV infection.

The NF-kB pathway is implicated in the antiviral phenotype of Dicer-N1

We showed above that the presence of PKR but not its canonical kinase activity was needed for the Dicer N1 antiviral phenotype. It has been reported that PKR can be involved in activating the immune response in a non-canonical manner. In particular, PKR has been described as an inducer of NF-kB/p65 transcriptional activity independently of its kinase function (Bonnet *et al*, 2000). Since we also found that targets of NF-kB are induced specifically in Dicer N1 cells, we investigated whether this pathway was involved in the antiviral phenotype of these cells. NF-kB/p65 is known to be phosphorylated once IkBα is released from the complex, which results in NF-kB/p65 activation upon translocation into the nucleus (Christian *et al*, 2016; Kanarek & Ben-Neriah, 2012). We looked at the expression and phosphorylation levels of NF-kB/p65 in Dicer WT and N1 cells during a time course of SINV-GFP infection at an MOI of 2 from 3 to 24 hpi (Fig. 8A). In Dicer WT cells, we observed an increase in p65 phosphorylation at 6 hpi, which corresponds to the end of the first replication cycle. However, at 12 hpi the phosphorylation decreased and became undetectable at 24 hpi. In Dicer N1 cells, the level of phosphorylated p65 was already quite elevated in the mock-infected condition and remained high, independently of PKR phosphorylation, until 12 hpi where it slightly decreased until 24 hpi (Fig. 8A). At the same time, we noticed a higher level of NF-kB/p65 protein at both 12 and 24 hpi.

Given the higher activation levels of p65 in Dicer N1 cells, we then decided to block the NF-kB pathway to test its role during SINV infection. To do so, we used the chemical compound BAY 11-7082, which inhibits IkBα phosphorylation by the IKK kinases and thus prevents NF-kB/p65 activation (Pierce *et al*, 1997). We treated Dicer N1 cells with two different concentrations of BAY 11-7082 during 1h. Then, we infected cells with SINV-GFP at an MOI of 0.02 for 24h and evaluated the impact of the drug treatment on the infection efficiency. As shown in Figure 8B (top panel), we observed a decrease in the phosphorylation of p65 in mock-infected cells treated with 5 µM of BAY 11-7082 compound compared to cells treated with DMSO only. Conversely, the level of IkBα was increased in cells treated with the inhibitor compared to the control (Fig. 8B, lower panel). These results indicate that the treatment was effective. We further validated that the inhibitor worked as expected by analyzing the levels of one of the previously validated NF-kB target mRNAs, PTGS2, by RT-qPCR. In Dicer N1 cells treated with 5 µM of BAY 11-7082, the level of this mRNA was significantly reduced compared to the control condition (Fig. 8C). The effect of the NF-kB inhibitor on viral infection could be visualized first by the increased detection of the Capsid protein in SINV-GFP infected cells treated with 5 µM of BAY 11-7082 compared to DMSO-treated cells (Fig. 8B). Finally, we measured the effect of NF-kB inhibition on viral particles production, and observed a significant increase in viral titers in Dicer N1 cells treated with 5µM of BAY compared to the negative control (Fig. 8C). The BAY 11-7082 treatment had no effect on SINV-GFP infection in Dicer WT cells, as assessed by western blot analysis of the Capsid protein and by plaque assay (Supp. Fig. 6A, B). Overall, these results indicated that by blocking the NF-kB/p65 pathway with BAY 11-7082, the antiviral activity of Dicer N1 could be reverted, suggesting that the antiviral activity of Dicer N1 is partially mediated through the NF-kB/p65 pathway.

DISCUSSION

In this study, we examined the role played by Dicer during viral infection in human cells. We specifically focused on the importance of its helicase domain, as it is known to play important roles in modulating its activity. Indeed, some of the deletion mutants that we used in our analysis, such as Dicer N1, Dicer ΔHel1 or Dicer ΔHel2i have been reported to display an increased RNAi activity either directed against artificial dsRNA substrate or specific viruses (Kennedy et al., 2015; Poirier et al., 2021; Zapletal et al., 2022). Our results confirmed that helicase-truncated Dicer proteins displayed an antiviral phenotype against some, but not all, viruses. While we observed that the catalytic activity of Dicer was involved for some deletion mutants, we also showed that the presence of the PKR protein was an essential feature for this phenotype. In particular, the Dicer N1 variant, which was shown to be capable of RNAi activity in cells that did not express PKR (Kennedy et al., 2015) was in our hands antiviral only in the presence of PKR, and remained antiviral when rendered catalytically inactive. A link between Dicer and PKR was also proposed in mouse embryonic stem cells where Dicer appears to prevent the PKR-induced IFN-I response (Gurung *et al*, 2021). However, no mechanism was proposed, and the authors hypothesized that it might be linked to miRNA production. Our data seem to indicate that the PKR-mediated antiviral effect observed in cells expressing helicase-truncated Dicer proteins is dominant over the RNAi-mediated effect. One would expect that RNAi would be more potent when PKR is not expressed since it should compete with Dicer for dsRNA binding. The fact that it is not the case during the antiviral response raises interesting perspectives.

PKR is a key effector protein involved in pathways such as apoptosis, autophagy, cell cycle control and immunity (Williams, 1999). Besides its well-known role in translation control *via* phosphorylation of the eIF2α factor (Donnelly *et al*, 2013) it also plays key roles in modulating IFN-I signaling pathways and can negatively regulate STAT1 and STAT3

transcriptional activity in a kinase-dependent manner (Raven *et al*, 2006). It has also been involved in the NF-kB pathway, but in this case it can do so both in a catalytic-dependent (Gil *et al*, 2001) and independent way, via the IKK kinase (Bonnet *et al*, 2000; Ishii *et al*, 2001). Here, we showed that Dicer N1 expressing cells had a different transcriptome from Dicer WT expressing cells and that the differentially expressed genes are mostly involved in the interferon alpha/gamma and inflammatory/NF-kB pathways. Specifically, we could identify among those a substantial fraction of targets of key immune transcription factors such as STAT2 and NF-kB. We retrieved and validated the differential expression levels for known antiviral effectors such as PTGS2, APOBEC3B or OAS3 (Jiang *et al*, 2008; Lehman *et al*, 2022; Manjunath *et al*, 2023; Ryman *et al*, 2002). This observation is reminiscent of other studies that showed that Dicer could be involved in non-RNAi related signaling pathways. For instance, *Drosophila* Dicer-2 can induce the expression of a small antiviral peptide, Vago, in a tissue- and virus-specific manner (Deddouche *et al*, 2008). More recently, plant DCL2 was involved in auto-immunity activation upon *DCL4* loss and in the activation of defense gene expression such as nucleotide-binding domain/leucine-rich repeat immune receptors (Nielsen *et al*, 2023). We showed that by treating Dicer N1 expressing cells with an NF-kB inhibitor, we could abrogate their antiviral phenotype. We thus partially validated our hypothesis that the transcriptional deregulation of key genes involved in the innate immune response was responsible for the observed effect on virus infection. Furthermore, the fact that Dicer N1 cells were not protected against SARS-CoV-2 infection is also in favor of an involvement of NF-kB or STAT1/2 signaling pathways. Indeed, SARS-CoV-2 is known to benefit from the upregulation of the inflammatory response, mainly through the NF-kB pathway, which is essential for the replication and propagation of the virus (Nilsson-Payant *et al*, 2021).

Our study reinforces the non-canonical roles of Dicer in immune signaling pathways and its interplay with the IFN-I response. Dicer helicase domain sequesters PKR away from its

505 unconventional signaling function. We showed that Dicer N1 antiviral activity only depends on
506 the presence of PKR but not on its dimerization or catalytic activity. Even though we cannot at
507 this stage formally conclude on the mechanism at play, we can speculate that PKR cofactors
508 TRBP and/or PACT might be involved. Indeed, PKR can be activated by PACT upon stress
509 (Farabaugh *et al*, 2020; Ito *et al*, 1999). Conversely, TRBP can inhibit PKR directly or sequester
510 PACT away from PKR (Chukwurah & Patel, 2018; Daher *et al*, 2009). Since both proteins are
511 also interacting with Dicer, *via* its helicase domain, and thus cannot interact with it anymore in
512 the Dicer N1 cells, they are therefore expected to preferentially interact with other partners such
513 as PKR in the Dicer N1 background and they could limit or change its canonical function. This
514 could in theory explain the activation of the NF-kB pathway in a PKR-dependent manner in the
515 presence of a helicase-truncated Dicer. Interestingly, it was previously shown that the NF-kB
516 pathway could promote SINV infection, but only in mature non-dividing neurons (Yeh *et al*,
517 2019). In the proliferating cell line that we used, we rather showed that the basal activation
518 level of NF-kB in Dicer N1 cells is antiviral. In agreement with this observation, inhibiting NF-
519 kB in Dicer WT cells has no effect on SINV, which is similar to what has been reported in the
520 Yeh et al. study. Our results therefore indicate that in actively dividing cells, the NF-kB status
521 dictates the fate of SINV infection, and this can be in part controlled by the Dicer isoform
522 expressed. This also means that in cells that naturally express isoforms of helicase-truncated
523 Dicer, *i.e.* oocytes and stem cells, it would be important to check whether signaling pathways
524 are deregulated and whether this contributes to the antiviral effect that has been reported for the
525 AviD isoform (Poirier *et al*, 2021).

526 Overall, our study reinforces the idea of a crosstalk between IFN-I and RNAi highlighting
527 a non-canonical function of human Dicer upon infection. We showed that Dicer helicase
528 domain is linked to the prevention of the immune signaling pathway, and can therefore prevent
529 basal activation of this pathway. PKR, free from its interaction with human Dicer, displays an

antiviral IFN-I-triggering role against alphaviruses and an enterovirus that is independent from Dicer activity.

MATERIAL & METHODS

Plasmids, cloning and mutagenesis

N1 DICER, N1-CM DICER, ΔHEL1 DICER and ΔHEL1-CM DICER were generated by PCR mutagenesis from pDONR-DICER described in (Girardi *et al*, 2015). ΔHEL2i and ΔHEL2 DICER and their catalytic mutants (CM) were generated by InFusion mutagenesis (Takara Bio) on pDONR-DICER and pDONR-DICER catalytic mutant vectors. pLenti Flag-HA-V5 vector was modified from pLenti6-V5 gateway vector (Thermo Fisher scientific V49610) by Gibson cloning. WT, N1, N1-CM, ΔHEL1, ΔHEL2i, ΔHEL2, ΔHEL1-CM, ΔHEL2i-CM and ΔHEL2-CM DICER from pDONR plasmids were cloned in pLenti flag-HA-V5 by Gateway recombination.

pLenti MYC:PKR and pLenti human ACE2 vectors were purchased from VectorBuilder. pLenti MYC:CTRL vector was modified from pLenti MYC:PKR by InFusion cloning (Tanaka Bio). PKR K296R and PKR T451A were obtained by InFusion mutagenesis (Takara Bio) on pLenti MYC:PKR vector.

All primers used are listed in Supplementary Table 1.

Cell lines

HEK293T, HEK293T/NoDice (2.20), HEK293T/NoDiceΔPKR cell lines were a gift from Pr. Bryan Cullen (Duke University, Durham NC, USA) and described in (Bogerd *et al*, 2014; Kennedy *et al*, 2015). Vero E6 cells were bought at ATCC (CRL-1586).

Cell culture and transfection

Cells were maintained in Dulbecco's modified Eagle medium (DMEM, Gibco, Life Technologies) supplemented with 10% fetal bovine serum (FBS, Clontech) in a humidified

atmosphere with 5% CO_2 at 37°C. Transfections were performed using Lipofectamine 2000 (Invitrogen, Fisher Scientific) according to the manufacturer's instructions.

BAY 11-7082 treatment

NoDice FHA:DICER WT #4 and N1 #6 cells were treated with BAY 11-7082 (Merck) by replacing the culture medium with a medium containing the indicated BAY 11-082 concentrations at 1µM or 5µM or the corresponding volume of DMSO only in the control conditions. Treatment was maintained for 1h and media was changed with the infection media with SINV-GFP at an MOI of 0.02 for 24h. Proteins, RNA and supernatants were then collected and analyzed.

Lentivirus production and generation of stable cell lines

The lentiviral supernatant from single transfer vector was produced by transfecting HEK293T cells with 1.7µg of the transfer vector (either pLenti6 FHA-V5 or pLenti MYC), 0.33 µg of the pVSV envelope plasmid (Addgene #8454) and 1.33µg of pSPAX2 packaging plasmid (Addgene #12260) using Lipofectamine 2000 (Invitrogen, Fisher Scientific) reagent according to the manufacturer's protocol. HEK293T were maintained in DMEM (Gibco, Life Technologies) medium supplemented with 10% Fetal bovine serum (FBS, Clontech). One well from a 6-well-plate at 70% confluency was used for the transfection. The medium was replaced 6 hours post-transfection. After 48 hours, the medium containing viral particles was collected and filtered through a 0.45µm PES filter. Different cell lines were transduced: NoDice (for N1, N1-CM, ΔHEL1, ΔHEL1-CM, ΔHEL2i, ΔHEL2i-CM, ΔHEL2 and ΔHEL2-CM), NoDiceΔPKR (for WT, NA, ΔHEL1, ΔHEL1-CM, ΔHEL2i, ΔHEL2i-CM, ΔHEL2 and ΔHEL2-CM), NoDiceΔPKR FHA:CTL or FHA:DICER WT #2 or FHA:DICER N1 #6 (for CTRL, PKR, K296R, T451A), NoDice:FHA DICER WT #4 or N1 #6 (for ACE2). One well of

a 6-well-plate was transduced using 500µL of filtered lentiviral supernatant either expressing DICER or PKR or ACE2 constructs, 500µL of DMEM supplemented with 10% FBS and 4µg/mL polybrene (Merck, Sigma Aldrich) for 6 hours. Then, the medium was changed with DMEM supplemented with 10% FBS for 24 hours and the resistant cell clones were selected with the right antibiotic and subsequently maintained under the selection. For NoDice, the selection lasted for 2 weeks with blasticidin at 15µg/mL (Invivogen). For NoDiceΔPKR, the selection lasted for 2 weeks with blasticidin at 10µg/mL (Invivogen). For NoDiceΔPKR FHA:CTL or DICER WT #2, the selection lasted 11 days with hygromycin at 100µg/mL and for NoDiceΔPKR FHA:DICER N1 #6 it was the same but with hygromycin at 150µg/mL (Invivogen). Lastly, the ACE2-tranduced cells were selected for 10 days with zeocin at 15µg/mL (Invivogen).

Viral stocks, virus infection

Viral stocks of SINV WT, SINV-2A-GFP and SINV-GFP were produced as described in (Girardi *et al*, 2015). SINV-2A-GFP was described in (Thomas *et al*, 2003). Cells were infected with SINV (strain AR339), SINV-2A-GFP and SINV-GFP at an MOI of 0.02 or for SINV-GFP at an MOI of 2 and samples were collected at the different indicated time points.

Viral stocks of SFV were propagated in Vero E6 cells from the initial stock (strain UVE/SFV/UNK/XX1745; EVAg 001V-02468). Cells were infected at an MOI of 1.10^{-4} for 24 hours.

Viral stocks of EV71 were produced by one passage in BHK21 cells from the initial stock (ATCC VR-1432). Cells were infected at an MOI of 0.1 for 24 hours.

Viral stocks of VSV-GFP were propagated in BHK21 cells from the initial stock (strain Indiana isolate PI10; described in (Mueller *et al*, 2010)). Cells were infected at an MOI of 1.10^{-5} for 24 hours.

Viral stocks of SARS-CoV-2 were produced by two passages in Vero E6 cells from the initial stock (strain human/DEU/HH-1/2020; EVAg 002V-03991). Cells were infected at an MOI of 0.01 or 0.001 for 24 or 48 hours.

Analysis of viral titer by plaque assay

For SINV, SINV-2A-GFP and SINV-GFP, Vero E6 cells were seeded in 96-well plates and infected with 10-fold serial dilutions of infection supernatants for 1 hour. The inoculum was removed and cells were covered with 2.5% carboxymethyl cellulose and cultured for 72 hours at 37°C in a humidified atmosphere of 5% CO_2. Plaques were counted manually under the microscope and viral titer was calculated according to the formula: *PFU/mL = #plaques/ (Dilution*Volume of inoculum).*

For SFV and VSV-GFP, Vero E6 cells were seeded in 24-well plates format and were infected with 10-fold serial dilutions of infection supernatants for 1 hour. The inoculum was removed and cells were covered with 2.5% carboxymethyl cellulose and cultured for 48 hours at 37°C in a humidified atmosphere with 5% CO_2. For plaques visualization, the carboxymethyl cellulose was removed. Cells were fixed with 4% formaldehyde (Merck, Sigma Aldrich) in PBS (phosphate buffered saline, Gibco) for 20 minutes at room temperature (RT). Cells were then stained with a 1X crystal violet solution for 20 minutes at RT (2% crystal violet, Sigma; 20% ethanol; 4% formaldehyde, Merck). Plates were washed with clear water and plaques were counted manually. The viral titer was calculated according to the formula: *PFU/mL = #plaques/ (Dilution*Volume of inoculum).*

Analysis of viral titer by TCID50

For EV71 and SARS-CoV-2, Vero E6 cells were seeded in 96-well plates already containing 10-fold serial dilutions of infection supernatants. Cells were maintained three to four days at

631 37°C in a humidified atmosphere with 5% CO_2. Wells containing dead cells were counted
632 manually under the microscope and viral titer was calculated according the Spearman-Kaerber
633 50% lethal dose formula described in (Wilham *et al*, 2010; Wulff *et al*, 2012).
634
635 **Western blot analysis**
636 Proteins were extracted and homogenized in the appropriate volume of ice-cold lysis buffer
637 (50mM Tris-HCl pH 7.5, 5mM EDTA, 150mM NaCl, 0.05% SDS, 1% Triton X-100 and
638 protease inhibitor cocktail (complete Mini, Merck)). Proteins were quantified using the
639 Bradford method (Bio-Rad) and 30µg of total protein extract were loaded on 10% acrylamide-
640 bis-acrylamide gels or 4-20% Mini-PROTEAN TGX Precast Gels (Bio-Rad). Proteins were
641 separated by migration at 135V in 1X Tris-Glycine-SDS buffer (Euromedex). Proteins were
642 electro-transferred on a nitrocellulose membrane in 1X Tris-Glycine buffer supplemented with
643 20% ethanol. Equal loading was verified by Ponceau S staining (Merck). Membranes were
644 blocked for 1 hour at RT under stirring in 5% milk (Roth) diluted in PBS-Tween 0.2% (PBS-
645 T). Membranes were probed with the following antibodies overnight at 4°C under stirring: anti-
646 hDICER (1:1000, A301-937A, Euromedex, Bethyl), anti-PKR (1:1000, ab32506 Abcam), anti-
647 PKR (1:1000, #12297 Cell signaling), anti-p-PKR (1:1000, ab 81303 Abcam), anti-PACT
648 (1:500, ab75749 Abcam), anti-TARBP2 (1:500, sc-514124, Cliniscience, Santa Cruz), anti-
649 HA-HRP (1:10000, 12013819001 Merck, Sigma Aldrich), anti-c-Myc (1:1000, ab32072
650 Abcam), anti-p-eIF2α (1:1000, #9721 Cell signaling), anti-α-Tubulin-HRP (1:10000, 1E4C11
651 Fisher Scientific), anti-SINV capsid (1:5000, kind gift from Dr. Diane Griffin, Johns Hopkins
652 University School of Medicine, Baltimore, MD), anti-GFP (1:1000, 11814460001 Merck,
653 Sigma Aldrich), anti-GAPDH-HRP (1:10000, G9545 Merck, Sigma Aldrich), anti-SARS-CoV-
654 2 Nucleocapsid (1:1000, ab273167 Abcam), anti-AGO2 (1:250, kind gift from Pr. Gunter
655 Meister, University of Regensburg), anti-ACE2 (1:1000, AF933 Bio-Techne), anti-NF-kB/p65

(1:1000, #8242 Cell signaling), anti-p-NF-kB/p65 (1:1000, #3033 Cell signaling) and anti-IkBα (1:1000, #4812 Cell signaling). The detection was performed using a specific secondary antibody coupled to the horseradish peroxidase (HRP): anti-mouse-HRP (1:4000, A4416 Merck, Sigma Aldrich), anti-rabbit-HRP (1:10000, #31460 Fisher Scientific), anti-rat-HRP (1:10000, #31470 Fisher Scientific) and anti-goat-HRP (1:10000, #A15999 Invitrogen). Detection was done using Chemiluminescent Substrate or SuperSignal West Femto maximum sensitivity substrate (Pierce, Fisher Scientific) and visualized with a Fusion FX imaging system (Vilber).

RNA extraction

Total RNA was extracted using TRI Reagent solution (Invitrogen, Fisher Scientific) according to the manufacturer's instructions.

Northern blot analysis

5 micrograms of total RNA were loaded on a 17.5% acrylamide-urea 4M gel and resolved in 1X Tris-Borate-EDTA buffer. Small RNAs were electro-transferred onto a nylon Hybond-NX membrane (GE Healthcare) in 0.5X Tris-Borate-EDTA buffer. RNAs were chemically cross-linked to the membrane for 90 minutes at 65°C using 1-ethyl-3-[3-dimethylaminopropyl]carbodiimide hydrochloride (EDC) (Merck, Sigma Aldrich). The membrane was pre-hybridized for 30 minutes in Perfect Hyb plus (Merck, Sigma Aldrich) at 50°C in rotation. Oligodeoxyribonucleotide probes (see Supp. Table 1) were labeled at the 5'-end with 25 µCi of [γ-32P]dATP using T4 polynucleotide kinase (Fischer Scientific). The unbound [γ-32P]dATP was removed with MicroSpin G-25 column (GE Healthcare) and the probe was incubated overnight at 50°C with the membrane in rotation. The membrane was washed twice with 5X SSC (Saline-Sodium citrate buffer, Euromedex), 0.1% SDS for 15

minutes at 50°C and once with 1X SSC (Euromedex), 0.1% SDS for 5 minutes at 50°C. The membrane was exposed on a phosphorimaging plate in a cassette and the signal was recorded using a Typhoon FLA-7000 laser scanner (GE Healthcare).

RT-qPCR analysis

DNaseI treatment was performed on 1µg of extracted RNAs (Invitrogen). DNase treated RNAs were then retro-transcribed using a random nonameric primers with the SuperScript IV (SSIV) reverse transcriptase according to the manufacturer's instructions (Invitrogen, Fisher Scientific). Real-time quantitative PCR was performed on 1/10 dilution of cDNA using SYBR green PCR master mix (Fisher Scientific) and the primers listed in Supp. Table 1.

Strand-specific semi-quantitative RT-PCR on SINV antigenome

Negative-strand-specific reverse transcription was performed using a primer specific to the 5' region of the SINV plus-strand genome (nucleotides 1 to 42 – Supp. Table 1). 100 ng of RNA, 1µL of 2µM specific primer, 1µL of 10mM dNTPs and water up to 13µL final volume were mixed and incubated at 65°C for 5 min. 4µL of 5X SSIV Buffer (Invitrogen), 1µL of 0.1M DTT (dithiothreitol), 1µL of RNase inhibitor (Ribolock, Fisher Scientific) and 1µL of SSIV reverse transcriptase (Invitrogen) were added and the mix was incubated at 55°C for 10 min then 80°C for 10 min. 1/20 of the cDNA was amplified by PCR using the GoTaq DNA polymerase mix (Promega) with specific antigenome primers (Supp. Table 1). PCR products were loaded on a 1% agarose gel and gel pictures were taken with a Fusion FX imaging system (Vilber).

Immunoprecipitation

Immunoprecipitations were done on tagged proteins. Cells were harvested, infected at the corresponding MOI and time and washed once with ice-cold PBS (Gibco, Life Technologies) and resuspended in 600µL of ice-cold lysis buffer (50mM Tris-HCl pH 7.5, 140 mM NaCl, 1.5 mM $MgCl_2$, 0.1% NP-40 and protease inhibitor cocktail (complete Mini, Merck, Sigma Aldrich). Cells were lysed for 10 min incubation on ice and lysates were cleared with a 15 min centrifugation at 12 000g and 4°C. 25µL of the lysates were kept as protein INPUT. Then, samples were divided in two and 40µL of magnetic beads coated with monoclonal anti-HA or anti-MYC antibodies were added (MACS purification system, Miltenyi Biotech). The samples were incubated for 1 hour at 4°C under rotation. Samples were sequentially loaded onto µColumns (MACS purification system, Miltenyi Biotech). The columns were washed 4 times with 200µL of lysis buffer. The elution was done with 95°C-pre-heated 2X Laemmli buffer (20% glycerol, 4% SDS, 125mM Tris-HCl pH 6.8, 10% (v/v) 2-β-mercaptoethanol, 0.004% Bromophenol Blue). Proteins were analyzed by western blot.

Immunostaining

Cells were plated on Millicell EZ 8-well slide (Merck Millipore) and infected with the different viruses at the corresponding MOI and infection time. Then, cells were fixed for 10 minutes at RT with 4% formaldehyde (Merck, Sigma Aldrich) diluted in PBS 1X (Gibco). Cells were incubated with a blocking solution (5% normal goat serum, 0.1% Triton X-100, PBS 1X) for 1h at RT. Primary J2 antibody diluted in blocking solution was added at 1:1000 dilution for 3h at RT. Cells were washed three times with PBS 1X-0.1% Triton X-100 (Phosphate buffered saline- Triton, PBS-T) and incubated 1h at RT in the dark with a secondary antibody solution containing goat anti-mouse Alexa 594 (A11032, Invitrogen, Fisher Scientific) fluorescent-coupled antibody diluted to 1:1000 in PBS-T solution. After three washes with PBS-T, cell nuclei were stained with DAPI diluted to 1:5000 in PBS 1X for 2 minutes at RT in the dark

(Life technologies, Fischer Scientific). Slides were finally mounted on coverslips and the Fluoromount-G mounting media (Southern Biotech). Images were acquired using an epifluorescence BX51 (Olympus) microscope with a mercury source illuminator (U-RFL-T, Olympus) and with x40 immersion oil objective.

Small RNA cloning and sequencing

NoDice FHA:DICER WT #4 or N1 #6 cells were plated in P150mm petri dishes at 25 000 000 cells per dish and infected the following day with SINV-GFP at an MOI of 0.02 for 24h. Cells were collected in 1.3mL of ice-cold lysis buffer (50mM Tris-HCl pH 7.5, 150 mM NaCl, 5mM EDTA, 1% NP-40, 0,5mM DTT, 0,1U/mL of RNase inhibitor and protease inhibitor cocktail (complete Mini, Merck, Sigma Aldrich)). Cells were lysed by putting the extract on ice for 15min. First, human AGO proteins were immunoprecipitated from whole extract to enrich for loaded small-RNAs. AGO-IP was done following the protocol described in (Hauptmann *et al*, 2015). Briefly, 50µL of magnetic Dynabeads coupled to G protein (Invitrogen, Fisher Scientific) were coupled to anti-Flag M2 antibody (F1804, Merck, Sigma Aldrich) overnight at 4°C under rotation. The day after, Flag-TNRC6B WT or mutant (with Tryptophans mutated to Alanines; called TNRC6B Ala) peptides were incubated with the coupled beads for 3h at 4°C under rotation. Meanwhile, lysates were cleared with a centrifugation step at 10 000g for 10min at 4°C and 100µL were kept as INPUT (20µL for proteins and 80µL for RNAs). Then, lysates were divided in two and put on the beads coupled to the peptides and incubated at 4°C for 3h under rotation. After 4 washing steps with 300µL of ice-cold washing buffer, beads were split: 280µL were eluted with 1mL of TRI Reagent solution (Invitrogen, Fisher Scientific) and RNAs were isolated according to the manufacturer's instructions; 20µL were kept for proteins analysis of IP efficiency by western blot and 20µL of 95°C-pre-heated 2X Laemmli buffer were added

(20% glycerol, 4% SDS, 125mM Tris-HCl pH 6.8, 10% (v/v) 2-β-mercaptoethanol, 0.004% Bromophenol Blue).

For small RNA libraries preparation, Illumina TruSeq small RNA library preparation kit was used according to the manufacturer's protocol (RS-200-0012, Illumina).

Samples were analyzed with a Bioanalyzer device, and only AGO-IPs with TNRC6B wild-type peptide in infected conditions in triplicates were analyzed for both cell lines, while only one AGO-IP TNRC6B Ala control was analyzed for each cell line.

Libraries were sequenced on an Illumina HiSeq 4000 sequencer as single-end 50 base reads at the GenomEast platform at the Institute of Genetics and Molecular and Cellular Biology (Illkirch, France). Image analysis and base calling were performed using RTA version 2.7.7 and bcl2fastq version 2.20.0.422.

mRNA sequencing

NoDice FHA:DICER WT #4 or N1 #6 cells were plated in P100mm petri dishes at 5 000 000 cells per dish and infected the following day with SINV-GFP at an MOI of 2 for 12h or 0.02 for 24h. Cells were collected in Trizol reagent (Invitrogen, Thermo Fisher Scientific) and RNAs were isolated according to the manufacturer's instructions.

Library preparation and sequencing were performed at the GenomEast platform at the Institute of Genetics and Molecular and Cellular Biology (Illkirch, France). RNA-Seq libraries were generated according to the manufacturer's instructions from 250 ng of total RNA using the Illumina Stranded mRNA Prep, Ligation kit (Reference Guide - PN 1000000124518) and IDT for Illumina RNA UD Indexes Ligation (Illumina, San Diego, USA). Briefly, Oligo(dT) magnetic beads were used to purify and capture the mRNA molecules containing polyA tails.The purified mRNA were then fragmented at 94°C for 2 min and copied into first strand complementary DNA (cDNA) using reverse transcriptase and random primers. Second strand

cDNA synthesis further generated blunt-ended double-stranded cDNA and incorporated dUTP in place of dTTP to achieve strand specificity by quenching the second strand during amplification. Following A-tailing of DNA fragments and ligation of pre-index anchors, PCR amplification was used to add indexes and primer sequences and to enrich DNA libraries (30 sec at 98°C; [10 sec at 98°C, 30 sec at 60°C, 30 sec at 72°C] x 12 cycles; 5 min at 72°C). Surplus PCR primers were further removed by purification using SPRIselect beads (Beckman-Coulter, Villepinte, France) and the final libraries were checked for quality and quantified using capillary electrophoresis.

Libraries were sequenced on an Illumina HiSeq 4000 sequencer as paired-end 100 base reads. Image analysis and base calling were performed using RTA version 2.7.7 and bcl2fastq version 2.20.0.422.

Bioinformatics analysis of small RNA sequencing data

Sequencing reads of sRNA-seq libraries were processed and analyzed with the following workflow. Cutadapt v1.16 (Martin, 2011) was first run to trim the 3' adapter (command: cutadapt -a TGGAATTCTCGGGTGCCAAGG -e 0.1 --no-indels -O 6 -m 18 --discard-untrimmed -o <name>-cutadapt.fastq <name>.fastq) and an additional filter was applied to only keep 18- to 32-nt long trimmed reads for further analyses. Sample quality checks were performed before and after these preprocessing steps using FastQC v0.11.8 (https://www.bioinformatics.babraham.ac.uk/projects/fastqc/). Preprocessed reads were then mapped simultaneously to the human (GENCODE Human (GRCh38.p13) release 41) and SINV-GFP (private sequence derived from NC_001547.1 – RefSeq database) genomes, using Bowtie v1.3.1 (Langmead *et al*, 2009) (command: bowtie -q --phred33-quals -v 2 -y -a --best --strata -m 30 -x hg38coreGencodeSINVGFP <name>-preprocessed.fastq <name>-hg38coreGencodeSINVGFP.bwtmap). Only alignments from the lowest mismatch stratum

with at most 2 mismatches were reported for each read, provided that their number was not exceeding 30. For each library, small RNA reads deriving solely from SINV-GFP were computationally extracted and further characterized. Representations of their length distribution and localisation along the viral genome were both made in R with the ggplot2 and Bioconductor Gviz (Hahne & Ivanek, 2016) packages respectively.

Bioinformatics analysis of mRNA sequencing data

RNA-seq data were processed and analyzed using the following workflow. The first 5'-end base of each read, a T-overhang added during the library preparation with the Illumina Stranded mRNA protocol, was first trimmed, before using Skewer v0.2.2 (Jiang *et al*, 2014) in paired-end mode for average quality read filtering and adapter trimming (command: skewer -Q 25 -x CTGTCTCTTATACACATCT -y CTGTCTCTTATACACATCT -l 31 -m pe -t 2 -o <name> --quiet <name>_R1.fq <name>_R2.fq). Sample quality checks were performed before and after these preprocessing steps using FastQC v0.11.8 (https://www.bioinformatics.babraham.ac.uk/projects/fastqc/). Then, human full-length protein-coding transcripts (GENCODE Human (GRCh38.p13) release 41) and SINV-GFP both genomic and subgenomic transcripts (private sequence derived from NC_001547.1 – RefSeq database) were quantified using Salmon v1.10.0 (Patro *et al*, 2017) in mapping-based mode with the selective alignment algorithm and a decoy-aware transcriptome (command: salmon quant -p 6 -i index/gencode41.hg38.sinv.decoys_index --libType A --seqBias --gcBias --numBootstraps 30 -1 data/<name>_preprocessed_R1.fq.gz -2 data/<name>_preprocessed_R2.fq.gz -o salmon-quants/<name>). Transcript-level abundance and count estimates thus obtained were next imported into R and further analyzed with the tximport (Soneson *et al*, 2016) and DESeq2 (Love *et al*, 2014) packages. Briefly, original transcript-level counts were summarized to gene-level estimated counts and an offset was

produced from transcript-level abundance estimates to correct for changes to the average transcript length across samples. Differential expression analyses between tested conditions were then conducted at the gene-level, and statistical significance was defined with an adjusted p-value < 0.05 and an absolute log2 fold change > 1 thresholds. Finally, gene set enrichment analysis (GSEA) studies were performed using the GSEA_4.3.2 Mac application, as made available by the Broad Institute and the University of California, San Diego (https://www.gsea-msigdb.org/gsea/index.jsp) (Mootha *et al*, 2003; Subramanian *et al*, 2005). These analyses were conducted on the DESeq2 normalized counts of each comparison dataset against the Hallmark Gene Sets (v2023.1) provided by the Molecular Signatures Database (MSigDB), and by using the Human_Ensembl_Gene_ID_MSigDB.v2023.1.Hs.chip annotation file and all other parameters by default, except the permutation type which was set to gene_set.

Heatmaps and volcano plots of RNA-seq differential expression data were generated in R using respectively the pheatmap package and a custom Shiny application based on the ggplot2 and ggrepel packages, while the global gene set enrichment dot plot was adapted from VisualizeRNAseq (https://github.com/GryderArt/VisualizeRNAseq).

Analysis of transcription factor enrichment

Lists of NF-kB/p65, STAT1, STAT2, IRF2 and IRF3 regulated genes were downloaded from Harmonizome (Rouillard *et al*, 2016). Genes from these lists that were differentially expressed between the indicated RNAseq experimental conditions were selected, and their mRNA expression log2 fold change was plotted as cumulative distribution histograms. The two-sample Kolmogorov-Smirnov test was used to assess whether each distribution was statistically different from the distribution of WT DICER cells infected with SINV vs. mock infected. p-values are indicated on each histogram.

Statistical analysis

All the plaque assay statistical analysis was done with PRISM 9 (GraphPad) using One-way ANOVA with a p-value threshold at $p<0.05$ on the logarithmic values.

All the qPCR statistical analysis was done with PRISM 9 (GraphPad) using One-way ANOVA with a p-value threshold at $p<0.05$ on the log2 values or unpaired t-test on the log2 values.

Detailed statistical analysis for each figure can be found in Supplementary Table 2.

Data availibility

The sequencing data discussed in this publication have been deposited in NCBI's Gene Expression Omnibus (Edgar *et al*, 2002) and are accessible through GEO Series accession numbers XXX and YYY (attribution pending).

SUPPLEMENTARY DATA

Supplementary data accompany this manuscript, they consist of Supplementary Figures and Tables Legends, six Supplementary Figures and two Supplementary Tables.

FUNDING INFORMATION

This work of the Interdisciplinary Thematic Institute IMCbio+, as part of the ITI 2021-2028 program of the University of Strasbourg, CNRS and Inserm, was supported by IdEx Unistra (ANR-10-IDEX-0002), by SFRI-STRAT'US project (ANR-20-SFRI-0012), EUR IMCBio (IMCBio ANR-17-EURE-0023) and Equipex Insectarium ANR-11-EQPX-0022 under the framework of the French Investments for the Future Program. Sequencing was performed by the GenomEast platform, a member of the 'France Génomique' consortium (ANR-10-INBS-0009). MB is funded by a doctoral fellowship from the Ministère de l'enseignement supérieur, de la recherche et de l'innovation and from the Fondation pour la Recherche Médicale (grant

879 number FDT202204014935). LG is funded by a postdoctoral fellowship from the Fondation
880 pour la Recherche Médicale (funding number SPF202209015746). SP also received funding
881 from the European Research Council (ERC-CoG-647455 RegulRNA).
882

883 **ACKNOWLEDGEMENTS**

884 We would like to thank members of the laboratory for fruitful discussions, as well as Pr. Petr
885 Svoboda (Institute of Molecular Genetics of the Czech Academy of Sciences, Prag) for sharing
886 unpublished data and exchanging ideas.
887

REFERENCES

Ahmad S & Hur S (2015) Helicases in Antiviral Immunity: Dual Properties as Sensors and Effectors. *Trends in Biochemical Sciences* 40: 576–585

Akhrymuk I, Frolov I & Frolova EI (2018) Sindbis Virus Infection Causes Cell Death by nsP2-Induced Transcriptional Shutoff or by nsP3-Dependent Translational Shutoff. *J Virol* 92: e01388-18

Baldaccini M & Pfeffer S (2021) Untangling the roles of RNA helicases in antiviral innate immunity. *PLOS Pathogens* 17: e1010072

Berlanga JJ, Ventoso I, Harding HP, Deng J, Ron D, Sonenberg N, Carrasco L & de Haro C (2006) Antiviral effect of the mammalian translation initiation factor 2alpha kinase GCN2 against RNA viruses. *EMBO J* 25: 1730–1740

Bogerd HP, Whisnant AW, Kennedy EM, Flores O & Cullen BR (2014) Derivation and characterization of Dicer- and microRNA-deficient human cells. *RNA* 20: 923–937

Bonnet MC, Weil R, Dam E, Hovanessian AG & Meurs EF (2000) PKR stimulates NF-kappaB irrespective of its kinase function by interacting with the IkappaB kinase complex. *Mol Cell Biol* 20: 4532–4542

Christian F, Smith EL & Carmody RJ (2016) The Regulation of NF-κB Subunits by Phosphorylation. *Cells* 5: 12

Chukwurah E & Patel RC (2018) Stress-induced TRBP phosphorylation enhances its interaction with PKR to regulate cellular survival. *Sci Rep* 8

Daher A, Laraki G, Singh M, Melendez-Peña CE, Bannwarth S, Peters AHFM, Meurs EF, Braun RE, Patel RC & Gatignol A (2009) TRBP Control of PACT-Induced Phosphorylation of Protein Kinase R Is Reversed by Stress. *Molecular and Cellular Biology* 29: 254–265

Deddouche S, Matt N, Budd A, Mueller S, Kemp C, Galiana-Arnoux D, Dostert C, Antoniewski C, Hoffmann JA & Imler J-L (2008) The DExD/H-box helicase Dicer-2 mediates the induction of antiviral activity in drosophila. *Nat Immunol* 9: 1425–1432

Dey M, Cao C, Dar AC, Tamura T, Ozato K, Sicheri F & Dever TE (2005) Mechanistic Link between PKR Dimerization, Autophosphorylation, and eIF2α Substrate Recognition. *Cell* 122: 901–913

Donnelly N, Gorman AM, Gupta S & Samali A (2013) The eIF2α kinases: their structures and functions. *Cell Mol Life Sci* 70: 3493–3511

Edgar R, Domrachev M & Lash AE (2002) Gene Expression Omnibus: NCBI gene expression and hybridization array data repository. *Nucleic Acids Res* 30: 207–210

Farabaugh KT, Krokowski D, Guan B-J, Gao Z, Gao X-H, Wu J, Jobava R, Ray G, de Jesus TJ, Bianchi MG, *et al* (2020) PACT-mediated PKR activation acts as a hyperosmotic stress intensity sensor weakening osmoadaptation and enhancing inflammation. *eLife* 9: e52241

Flemr M, Malik R, Franke V, Nejepinska J, Sedlacek R, Vlahovicek K & Svoboda P (2013) A Retrotransposon-Driven Dicer Isoform Directs Endogenous Small Interfering RNA Production in Mouse Oocytes. *Cell* 155: 807–816

Gibbings D, Mostowy S, Jay F, Schwab Y, Cossart P & Voinnet O (2012) Selective autophagy degrades DICER and AGO2 and regulates miRNA activity. *Nat Cell Biol* 14: 1314–1321

Gil J, Rullas J, García MA, Alcamí J & Esteban M (2001) The catalytic activity of dsRNA-dependent protein kinase, PKR, is required for NF-κB activation. *Oncogene* 20: 385–394

Girardi E, Lefèvre M, Chane-Woon-Ming B, Paro S, Claydon B, Imler J-L, Meignin C & Pfeffer S (2015) Cross-species comparative analysis of Dicer proteins during Sindbis virus infection. *Sci Rep* 5: 10693

Guo Z, Li Y & Ding S-W (2019) Small RNA-based antimicrobial immunity. *Nat Rev Immunol* 19: 31–44

Gurung C, Fendereski M, Sapkota K, Guo J, Huang F & Guo Y-L (2021) Dicer represses the interferon response and the double-stranded RNA-activated protein kinase pathway in mouse embryonic stem cells. *Journal of Biological Chemistry* 296: 100264

Hahne F & Ivanek R (2016) Visualizing Genomic Data Using Gviz and Bioconductor. *Methods Mol Biol* 1418: 335–351

Hauptmann J, Schraivogel D, Bruckmann A, Manickavel S, Jakob L, Eichner N, Pfaff J, Urban M, Sprunck S, Hafner M, *et al* (2015) Biochemical isolation of Argonaute protein complexes by Ago-APP. *Proc Natl Acad Sci U S A* 112: 11841–11845

Hoffmann M, Kleine-Weber H, Schroeder S, Krüger N, Herrler T, Erichsen S, Schiergens TS, Herrler G, Wu N-H, Nitsche A, *et al* (2020) SARS-CoV-2 Cell Entry Depends on ACE2 and TMPRSS2 and Is Blocked by a Clinically Proven Protease Inhibitor. *Cell* 181: 271-280.e8

Ishii T, Kwon H, Hiscott J, Mosialos G & Koromilas AE (2001) Activation of the IκBα kinase (IKK) complex by double-stranded RNA-binding defective and catalytic inactive mutants of the interferon-inducible protein kinase PKR. *Oncogene* 20: 1900–1912

Ito T, Yang M & May WS (1999) RAX, a Cellular Activator for Double-stranded RNA-dependent Protein Kinase during Stress Signaling *. *Journal of Biological Chemistry* 274: 15427–15432

Ivashkiv LB & Donlin LT (2014) Regulation of type I interferon responses. *Nature Reviews Immunology* 14: 36–49

Jiang D, Guo H, Xu C, Chang J, Gu B, Wang L, Block TM & Guo J-T (2008) Identification of Three Interferon-Inducible Cellular Enzymes That Inhibit the Replication of Hepatitis C Virus. *Journal of Virology* 82: 1665–1678

Jiang H, Lei R, Ding S-W & Zhu S (2014) Skewer: a fast and accurate adapter trimmer for next-generation sequencing paired-end reads. *BMC Bioinformatics* 15: 182

Jm T, Wb K, Kd R & Hw H (2003) Sindbis virus vectors designed to express a foreign protein as a cleavable component of the viral structural polyprotein. *Journal of virology* 77

Kanarek N & Ben-Neriah Y (2012) Regulation of NF-κB by ubiquitination and degradation of the IκBs. *Immunol Rev* 246: 77–94

Kennedy EM, Whisnant AW, Kornepati AVR, Marshall JB, Bogerd HP & Cullen BR (2015) Production of functional small interfering RNAs by an amino-terminal deletion mutant of human Dicer. *Proc Natl Acad Sci USA* 112: E6945-6954

Kong J, Bie Y, Ji W, Xu J, Lyu B, Xiong X, Qiu Y & Zhou X (2023) Alphavirus infection triggers antiviral RNAi immunity in mammals. *Cell Rep* 42: 112441

Langmead B, Trapnell C, Pop M & Salzberg SL (2009) Ultrafast and memory-efficient alignment of short DNA sequences to the human genome. *Genome Biol* 10: R25

Lehman CW, Smith A, Kelly J, Jacobs JL, Dinman JD & Kehn-Hall K (2022) EGR1

Upregulation during Encephalitic Viral Infections Contributes to Inflammation and Cell Death. *Viruses* 14: 1210

Love MI, Huber W & Anders S (2014) Moderated estimation of fold change and dispersion for RNA-seq data with DESeq2. *Genome Biol* 15: 550

Ma E, MacRae IJ, Kirsch JF & Doudna JA (2008) Autoinhibition of Human Dicer by Its Internal Helicase Domain. *Journal of Molecular Biology* 380: 237–243

Maillard PV, Ciaudo C, Marchais A, Li Y, Jay F, Ding SW & Voinnet O (2013) Antiviral RNA interference in mammalian cells. *Science* 342: 235–238

Maillard PV, Van der Veen AG, Deddouche-Grass S, Rogers NC, Merits A & Reis e Sousa C (2016) Inactivation of the type I interferon pathway reveals long double-stranded RNA-mediated RNA interference in mammalian cells. *EMBO J* 35: 2505–2518

Manjunath L, Oh S, Ortega P, Bouin A, Bournique E, Sanchez A, Martensen PM, Auerbach AA, Becker JT, Seldin M, *et al* (2023) APOBEC3B drives PKR-mediated translation shutdown and protects stress granules in response to viral infection. *Nat Commun* 14: 820

Martin M (2011) Cutadapt removes adapter sequences from high-throughput sequencing reads. *EMBnet.journal* 17: 10–12

Meister G & Tuschl T (2004) Mechanisms of gene silencing by double-stranded RNA. *Nature* 431: 343–9

Montavon TC, Baldaccini M, Lefèvre M, Girardi E, Chane-Woon-Ming B, Messmer M, Hammann P, Chicher J & Pfeffer S (2021) Human DICER helicase domain recruits PKR and modulates its antiviral activity. *PLoS Pathog* 17: e1009549

Mootha VK, Lindgren CM, Eriksson K-F, Subramanian A, Sihag S, Lehar J, Puigserver P, Carlsson E, Ridderstråle M, Laurila E, *et al* (2003) PGC-1alpha-responsive genes involved in oxidative phosphorylation are coordinately downregulated in human diabetes. *Nat Genet* 34: 267–273

Mueller S, Gausson V, Vodovar N, Deddouche S, Troxler L, Perot J, Pfeffer S, Hoffmann JA, Saleh M-C & Imler J-L (2010) RNAi-mediated immunity provides strong protection against the negative-strand RNA vesicular stomatitis virus in Drosophila. *Proceedings of the National Academy of Sciences* 107: 19390–19395

Nielsen CPS, Han L, Arribas-Hernández L, Karelina D, Petersen M & Brodersen P (2023) Sensing of viral RNA in plants via a DICER-LIKE Ribonuclease. 2023.01.10.523395 doi:10.1101/2023.01.10.523395 [PREPRINT]

Nilsson-Payant BE, Uhl S, Grimont A, Doane AS, Cohen P, Patel RS, Higgins CA, Acklin JA, Bram Y, Chandar V, *et al* (2021) The NF-κB Transcriptional Footprint Is Essential for SARS-CoV-2 Replication. *Journal of Virology* 95: 10.1128/jvi.01257-21

Patro R, Duggal G, Love MI, Irizarry RA & Kingsford C (2017) Salmon provides fast and bias-aware quantification of transcript expression. *Nat Methods* 14: 417–419

Pichlmair A & Reis e Sousa C (2007) Innate recognition of viruses. *Immunity* 27: 370–383

Pierce JW, Schoenleber R, Jesmok G, Best J, Moore SA, Collins T & Gerritsen ME (1997) Novel inhibitors of cytokine-induced IkappaBalpha phosphorylation and endothelial cell adhesion molecule expression show anti-inflammatory effects in vivo. *J Biol Chem* 272: 21096–21103

Poirier EZ, Buck MD, Chakravarty P, Carvalho J, Frederico B, Cardoso A, Healy L, Ulferts R, Beale R & Reis e Sousa C (2021) An isoform of Dicer protects mammalian stem cells

against multiple RNA viruses. *Science* 373: 231–236

Raven JF, Wang S, Kazemi S, Baltzis D, Hatzoglou M, Tremblay ML & Koromilas AE (2006) The eIF2α kinase PKR is a negative regulator of Stat1 and Stat3. *The FASEB Journal* 20: A496–A496

Richardson SJ, Willcox A, Hilton DA, Tauriainen S, Hyoty H, Bone AJ, Foulis AK & Morgan NG (2010) Use of antisera directed against dsRNA to detect viral infections in formalin-fixed paraffin-embedded tissue. *J Clin Virol* 49: 180–185

Rouillard AD, Gundersen GW, Fernandez NF, Wang Z, Monteiro CD, McDermott MG & Ma'ayan A (2016) The harmonizome: a collection of processed datasets gathered to serve and mine knowledge about genes and proteins. *Database* 2016: baw100

Ryman KD, White LJ, Johnston RE & Klimstra WB (2002) Effects of PKR/RNase L-Dependent and Alternative Antiviral Pathways on Alphavirus Replication and Pathogenesis. *Viral Immunology* 15: 53–76

Soneson C, Love M & Robinson M (2016) Differential analyses for RNA-seq: transcript-level estimates improve gene-level inference. doi:10.12688/f1000research.7563.2 [PREPRINT]

Subramanian A, Tamayo P, Mootha VK, Mukherjee S, Ebert BL, Gillette MA, Paulovich A, Pomeroy SL, Golub TR, Lander ES, *et al* (2005) Gene set enrichment analysis: a knowledge-based approach for interpreting genome-wide expression profiles. *Proc Natl Acad Sci U S A* 102: 15545–15550

Takahashi T, Nakano Y, Onomoto K, Murakami F, Komori C, Suzuki Y, Yoneyama M & Ui-Tei K (2018a) LGP2 virus sensor regulates gene expression network mediated by TRBP-bound microRNAs. *Nucleic Acids Res* 46: 9134–9147

Takahashi T, Nakano Y, Onomoto K, Yoneyama M & Ui-Tei K (2018b) Virus Sensor RIG-I Represses RNA Interference by Interacting with TRBP through LGP2 in Mammalian Cells. *Genes (Basel)* 9

Taylor DR, Tian B, Romano PR, Hinnebusch AG, Lai MMC & Mathews MB (2001) Hepatitis C Virus Envelope Protein E2 Does Not Inhibit PKR by Simple Competition with Autophosphorylation Sites in the RNA-Binding Domain. *Journal of Virology* 75: 1265–1273

tenOever BR (2016) The Evolution of Antiviral Defense Systems. *Cell Host & Microbe* 19: 142–149

Thomas JM, Klimstra WB, Ryman KD & Heidner HW (2003) Sindbis virus vectors designed to express a foreign protein as a cleavable component of the viral structural polyprotein. *J Virol* 77: 5598–5606

van der Veen AG, Maillard PV, Schmidt JM, Lee SA, Deddouche-Grass S, Borg A, Kjær S, Snijders AP & Reis e Sousa C (2018) The RIG-I-like receptor LGP2 inhibits Dicer-dependent processing of long double-stranded RNA and blocks RNA interference in mammalian cells. *EMBO J* 37

Weber F, Wagner V, Rasmussen SB, Hartmann R & Paludan SR (2006) Double-Stranded RNA Is Produced by Positive-Strand RNA Viruses and DNA Viruses but Not in Detectable Amounts by Negative-Strand RNA Viruses. *J Virol* 80: 5059–5064

Wilham JM, Orrú CD, Bessen RA, Atarashi R, Sano K, Race B, Meade-White KD, Taubner LM, Timmes A & Caughey B (2010) Rapid End-Point Quantitation of Prion Seeding

1064 Activity with Sensitivity Comparable to Bioassays. *PLOS Pathogens* 6: e1001217
1065 Williams BR (1999) PKR; a sentinel kinase for cellular stress. *Oncogene* 18: 6112–6120
1066 Wulff NH, Tzatzaris M & Young PJ (2012) Monte Carlo simulation of the Spearman-Kaerber
1067 TCID50. *Journal of Clinical Bioinformatics* 2: 5
1068 Yeh JX, Park E, Schultz KLW & Griffin DE (2019) NF-κB Activation Promotes Alphavirus
1069 Replication in Mature Neurons. *Journal of Virology* 93: e01071-19
1070 Zapletal D, Taborska E, Pasulka J, Malik R, Kubicek K, Zanova M, Much C, Sebesta M,
1071 Buccheri V, Horvat F, *et al* (2022) Structural and functional basis of mammalian
1072 microRNA biogenesis by Dicer. *Molecular Cell* 82: 4064-4079.e13
1073 Zhang Y, Xu Y, Dai Y, Li Z, Wang J, Ye Z, Ren Y, Wang H, Li W, Lu J, *et al* (2021) Efficient
1074 Dicer processing of virus-derived double-stranded RNAs and its modulation by RIG-I-
1075 like receptor LGP2. *PLOS Pathogens* 17: e1009790
1076

FIGURE LEGENDS

Figure 1. Analysis of Dicer N1 effect on SINV replication

A, Mean (+/- SEM) of SINV, SINV-GFP and SINV-2A-GFP viral titers in NoDice FHA:DICER WT #4 and N1 #6 infected at an MOI ranging from 0.001 to 1 for 24h (n = 3) from plaque assay quantification. Ordinary two-way ANOVA test with Bonferroni correction. ***: $p < 0.001$; ****: $p < 0.0001$. **B,** Western blot analysis of DICER, p-PKR, PKR, CAPSID and GFP expression in SINV, SINV-GFP and SINV-2A-GFP infected NoDice FHA:DICER WT #4 and N1 #6 cells at an MOI of 0.02 for 24h. Gamma-Tubulin was used as loading control. **C,** Immunofluorescence analysis on NoDice FHA:DICER WT #4 and N1 #6 cells in mock, SINV, SINV-GFP and SINV-2A-GFP infected cells at an MOI of 0.02 for 24h. J2 antibody (red) was used to detect dsRNA upon infection. DAPI was used to stain the nuclei (blue). Magnification 40X; scale bar = 100 µm. **D,** RT-qPCR on SINV genome in NoDice FHA:DICER WT #4 and N1 #6 cells infected with SINV-GFP at an MOI of 0.02 for 24h. Mean (+/- SEM); n = 3. Unpaired t-test. ****: $p < 0.0001$.

Figure 2. Dicer N1 activity against several viruses

A, (Top) Mean (+/- SEM) of SFV viral titers in NoDice FHA:DICER WT #4 and N1 #6 infected at an MOI of 1.10^{-4} for 24h (n = 3) from plaque assay quantification. Unpaired t-test. *: $p < 0.05$. (Bottom) Immunofluorescence analysis on NoDice FHA:DICER WT #4 and N1 #6 cells in SFV infected cells. J2 antibody (red) was used to detect dsRNA upon infection. DAPI was used to stain the nuclei (blue). Magnification 40X; scale bar = 100 µm. **B,** (Top) Mean (+/- SEM) of EV71 viral titers in NoDice FHA:DICER WT #4 and N1 #6 infected at an MOI of 0.1 for 24h (n = 3) from TCID50 quantification. Unpaired t-test. *: $p < 0.05$. (Bottom) Immunofluorescence analysis on NoDice FHA:DICER WT #4 and N1 #6 cells in EV71 infected cells. J2 antibody (red) was used to detect dsRNA upon infection. DAPI was used to

stain the nuclei (blue). Magnification 40X; scale bar = 100 µm. **C,** (Top) Mean (+/- SEM) of VSV-GFP viral titers in NoDice FHA:DICER WT #4 and N1 #6 infected at an MOI of 1.10^{-5} for 24h (n = 3) from plaque assay quantification. Unpaired t-test. ns: non-significant. (Bottom) Immunofluorescence analysis on NoDice FHA:DICER WT #4 and N1 #6 cells in VSV-GFP infected cells. J2 antibody (red) was used to detect dsRNA upon infection. DAPI was used to stain the nuclei (blue). Magnification 40X; scale bar = 100 µm. **D,** Western blot analysis of human ACE2 expression in NoDice FHA:DICER WT #4 and N1 #6. Gamma-Tubulin was used as a loading control. **E,** Western blot analysis of DICER, p-PKR, PKR and NUCLEOCAPSID expression in SARS-CoV-2 infected NoDice FHA:DICER WT #4 and N1 #6 cells at an MOI of 0.001 for 48h. GAPDH was used as loading control. **F,** Mean (+/- SEM) of SARS-CoV-2 viral titers in NoDice FHA:DICER WT #4 and N1 #6 infected at an MOI of 0.001 for 48h (n = 3) from TCID50 quantification. Unpaired t-test. *: $p < 0.05$. **G,** Immunofluorescence analysis on NoDice FHA:DICER WT #4 and N1 #6 cells in SARS-CoV-2 infected cells at an MOI of 0.001 for 48h. J2 antibody (red) was used to detect dsRNA upon infection. DAPI was used to stain the nuclei (blue). Magnification 40X; scale bar = 100 µm. **H,** RT-qPCR on SARS-CoV-2 genome (ORF1A and SPIKE) in NoDice FHA:DICER WT #4 and N1 #6 cells infected with SARS-CoV-2 at an MOI of 0.001 for 48h. Mean (+/- SEM); n = 3. Unpaired t-test. *: $p < 0.05$; ns: non-significant.

Figure 3. Analysis of the importance of Dicer N1 catalytic activity in its antiviral phenotype

A, Representative histograms of the distribution of viral reads (in percent) per RNA length upon small RNA sequencing in NoDice FHA:DICER WT #4 (left) and N1 #6 (left) cells infected with SINV-GFP at an MOI of 0.02 for 24h. Blue: positive strand; red: negative strand. **B,** Representative graphs of the mapping of 22-nt-reads on SINV-GFP genome in NoDice

FHA:DICER WT #4 (left) and N1 #6 (right) cells. On the bottom: magnification of the mapping for the first 1000nt. Blue: positive strand; red: negative strand. **C,** Schematic representation of two Dicer mutants, N1 and N1-CM (catalytic mutant). In N1-CM, the two catalytic mutations are highlighted in red. **D,** Western blot analysis of DICER, HA, AGO2, PKR and TRBP expression in the monoclonal cell lines NoDice FHA:DICER WT #4, N1 #6 and N1-CM #2.17. Gamma-Tubulin was used as a loading control. **E,** Northern blot analysis of mirR-16 expression in the same samples as in D. Expression of snRNA U6 was used as a loading control. **F,** Western blot analysis of DICER, p-PKR, PKR, p-eIF2α and CAPSID expression in SINV-GFP infected cells at an MOI of 0.02 for 24h. Gamma-Tubulin was used as loading control. **G,** Mean (+/- SEM) of SINV-GFP viral titers in the same samples as in D, infected at an MOI of 0.02 for 24h (n = 3) from plaque assay quantification. Ordinary one-way ANOVA test with Bonferroni correction. **: $p < 0.01$.

Figure 4. Analysis of the importance of the helicase sub-domains for Dicer antiviral activity

A, Schematic representation of the different Dicer helicase subdomain mutants. **B,** Western blot analysis of HA (for Dicer) and CAPSID expression in SINV-GFP infected cells at an MOI of 0.02 for 24h. Monoclonal NoDice FHA:DICER helicase mutant and their respective catalytic mutant cells are represented: WT #4, ΔHEL1 #15, ΔHEL1-CM #1, ΔHEL2 #9, ΔHEL2-CM #21, ΔHEL2i #27 and ΔHEL2i-CM #21. Gamma-Tubulin was used as loading control. **C,** Mean (+/- SEM) of SINV-GFP viral titers in the same samples as in B, infected at an MOI of 0.02 for 24h (n = 3) from plaque assay quantification. Ordinary one-way ANOVA test with Bonferroni correction. ***: $p < 0.001$; ****: $p < 0.0001$; ns: non-significant. **D,** Western blot analysis of HA (for Dicer) and CAPSID expression in SINV-GFP infected cells at an MOI of 0.02 for 24h. Polyclonal NoDice FHA:DICER (left) and NoDiceΔPKR FHA:DICER (right) helicase mutant

cells are represented. Gamma-Tubulin was used as loading control. **E,** Mean (+/- SEM) of SINV-GFP viral titers in the same samples as in D, infected at an MOI of 0.02 for 24h (n = 3) from plaque assay quantification. Ordinary one-way ANOVA test with Dunnett correction. *: $p < 0.05$; **: $p < 0.01$; ***: $p < 0.001$; ns: non-significant.

Figure 5. Importance of PKR dimerization and/or catalytic activities in Dicer N1 antiviral activity

A, Schematic representation of PKR and its two point mutants: K296R and T451A. **B,** Western blot analysis of DICER, p-PKR, PKR, p-eIF2α and CAPSID expression in SINV-GFP infected NoDiceΔPKR FHA:DICER WT #2 with a MYC:EMPTY CTRL vector, MYC:PKR, MYC K296R or MYC:T451A cells at an MOI of 0.02 for 24h. Gamma-Tubulin was used as loading control. **C,** Mean (+/- SEM) of SINV-GFP viral titers in the same samples as in B, infected at an MOI of 0.02 for 24h (n = 3) from plaque assay quantification. Ordinary one-way ANOVA test with Dunnett correction. ns: non-significant. **D,** Western blot analysis of DICER, p-PKR, PKR, p-eIF2α and CAPSID expression in SINV-GFP infected NoDiceΔPKR FHA:DICER N1 #6 with a MYC:EMPTY CTRL vector, MYC:PKR, MYC K296R or MYC:T451A cells at an MOI of 0.02 for 24h. Gamma-Tubulin was used as loading control. **E,** Mean (+/- SEM) of SINV-GFP viral titers in the same samples as in D, infected at an MOI of 0.02 for 24h (n = 3) from plaque assay quantification. Ordinary one-way ANOVA test with Dunnett correction. *: $p < 0.05$.

Figure 6. Transcriptomic analysis of Dicer N1 and WT cells

A, Z-score hierarchical clustering heatmap of genes identified by RNA sequencing analysis as differentially expressed between WT vs. N1 cells, either mock or SINV-infected cells (MOI 2 12 hpi or MOI 0.02 24 hpi). Gene clusters are delimited with black brackets and numbered from

I to V. **B-D**, Volcano plot for differentially expressed genes (DEGs) between SINV-infected (MOI of 0.02 for 24h) and mock NoDice FHA:DICER WT #4 cells (B); SINV-infected and mock NoDice FHA:DICER N1 #6 cells (C); mock NoDice FHA:DICER WT #4 and mock NoDice FHA:DICER N1 #6 cells (D). Each gene is marked as a dot (red: upregulated ≥ 2-fold, blue: downregulated ≤ 2-fold, grey: unchanged). The horizontal line denotes an adjusted p-value of 0.05 and the vertical ones the Log2 fold change cut-off (-1 and 1). **E,** Biological states and processes associated terms enrichment performed with GSEA using the hallmark gene sets. Colors indicate NES (normalized enrichment score) that are either positive (red) or negative (blue). Dot size corresponds to -log10(FDR q-val) of enrichment.

Figure 7. Analysis of the transcription factors involvement in Dicer N1 and WT cells transcriptomic changes

A-B, Histograms representing the cumulative probability of differentially expressed genes controlled by the transcription factors NF-kB/p65 (A) or STAT2 (B), plotted according to their Log2 fold change. The vertical lines stand for the Log2 fold change cut-off (-1 and 1). The two-sample Kolmogorov-Smirnov test was used to assess whether each distribution was statistically different from the distribution of NoDice FHA:DICER WT #4 cells infected with SINV vs. mock. p-values are indicated on each histogram. Red: WT SINV-002-24h vs WT MOCK; blue: N1 SINV-002-24h vs N1 MOCK; black: N1 MOCK vs WT MOCK. **C-D,** Z-score hierarchical clustering heatmap of genes identified by RNA sequencing analysis as differentially expressed between WT vs. N1 cells, either mock or SINV-infected cells (MOI 2 12 hpi or MOI 0.02 24 hpi). Each heatmap represents differentially expressed genes controlled by one transcription factor: NF-kB/p65 (C) or STAT2 (D). **E,** RT-qPCR on upregulated genes in the N1 MOCK vs WT MOCK condition and controlled by either NF-kB/p65 or STAT2. Mean (+/- SEM); n = 3. Unpaired t-test. **: $p < 0.01$; ***: $p < 0.001$; ****: $p < 0.0001$.

Figure 8. NF-kB/p65 involvement in Dicer N1 antiviral phenotype

A, Western blot analysis of DICER, p-p65 and p65 (left) and DICER, p-PKR, p-eIF2α and CAPSID (right) expression in SINV-GFP infected NoDice FHA:DICER WT #4 and N1 #6 cells at an MOI of 0.02 between 3 and 24h. Gamma-Tubulin was used as loading control. **B,** Western blot analysis of DICER, p-p65, p65 and CAPSID (top) and DICER and IkBα (bottom) expression in SINV-GFP infected NoDice FHA:DICER N1 #6 cells at an MOI of 0.02 for 24h. Before infection, cells were treated with the NF-kB/p65 inhibitor, BAY 11-7082 or the vehicle (DMSO) at the indicated concentrations for 1 h. Gamma-Tubulin was used as loading control. **C,** RT-qPCR on PTGS2 (NF-kB/p65 target) in NoDice FHA:DICER N1 #6 mock cells treated with BAY 11-7082 or the vehicle (DMSO) at the indicated concentrations for 1h. Mean (+/- SEM), n = 3. Ordinary one-way ANOVA with Sidak correction. **: $p < 0.01$; ns: non-significant. **D,** Mean (+/- SEM) of SINV-GFP viral titers in the same samples as in C, infected at an MOI of 0.02 for 24h (n = 3) from plaque assay quantification. Ordinary one-way ANOVA test with Dunnett correction. **: $p < 0.01$; ns: non-significant.

Figure 1

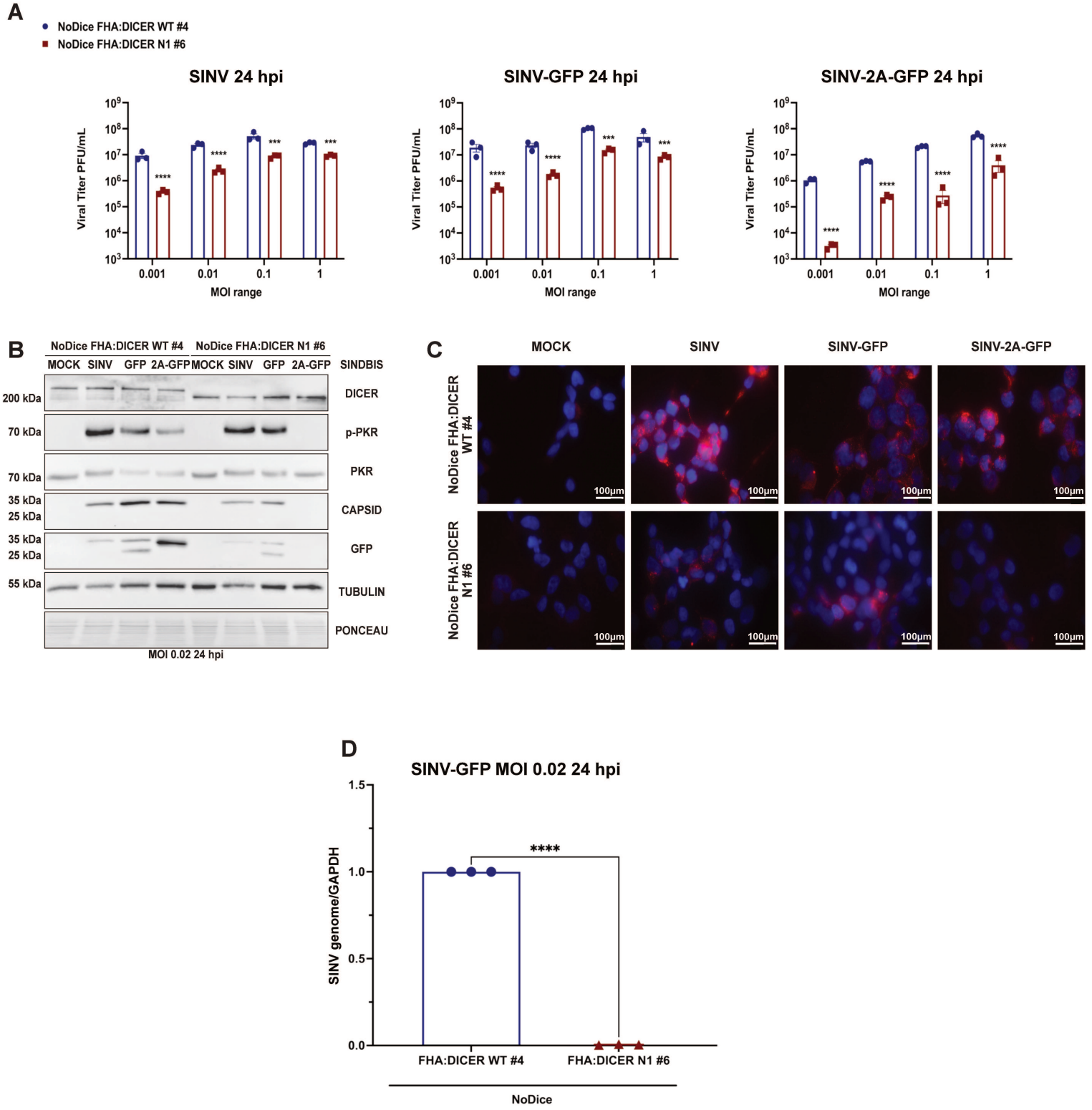
A
NoDice FHA:DICER WT #4
NoDice FHA:DICER N1 #6
SINV 24 hpi
SINV-GFP 24 hpi
SINV-2A-GFP 24 hpi
Viral Titer PFU/mL
MOI range
0.001
0.01
0.1
1
B
NoDice FHA:DICER WT #4
NoDice FHA:DICER N1 #6
MOCK SINV GFP 2A-GFP MOCK SINV GFP 2A-GFP SINDBIS
200 kDa
DICER
70 kDa
p-PKR
70 kDa
PKR
35 kDa
25 kDa
CAPSID
35 kDa
25 kDa
GFP
55 kDa
TUBULIN
PONCEAU
MOI 0.02 24 hpi
C
MOCK
SINV
SINV-GFP
SINV-2A-GFP
NoDice FHA:DICER WT #4
NoDice FHA:DICER N1 #6
100µm
D
SINV-GFP MOI 0.02 24 hpi
SINV genome/GAPDH
FHA:DICER WT #4
FHA:DICER N1 #6
NoDice

Figure 2

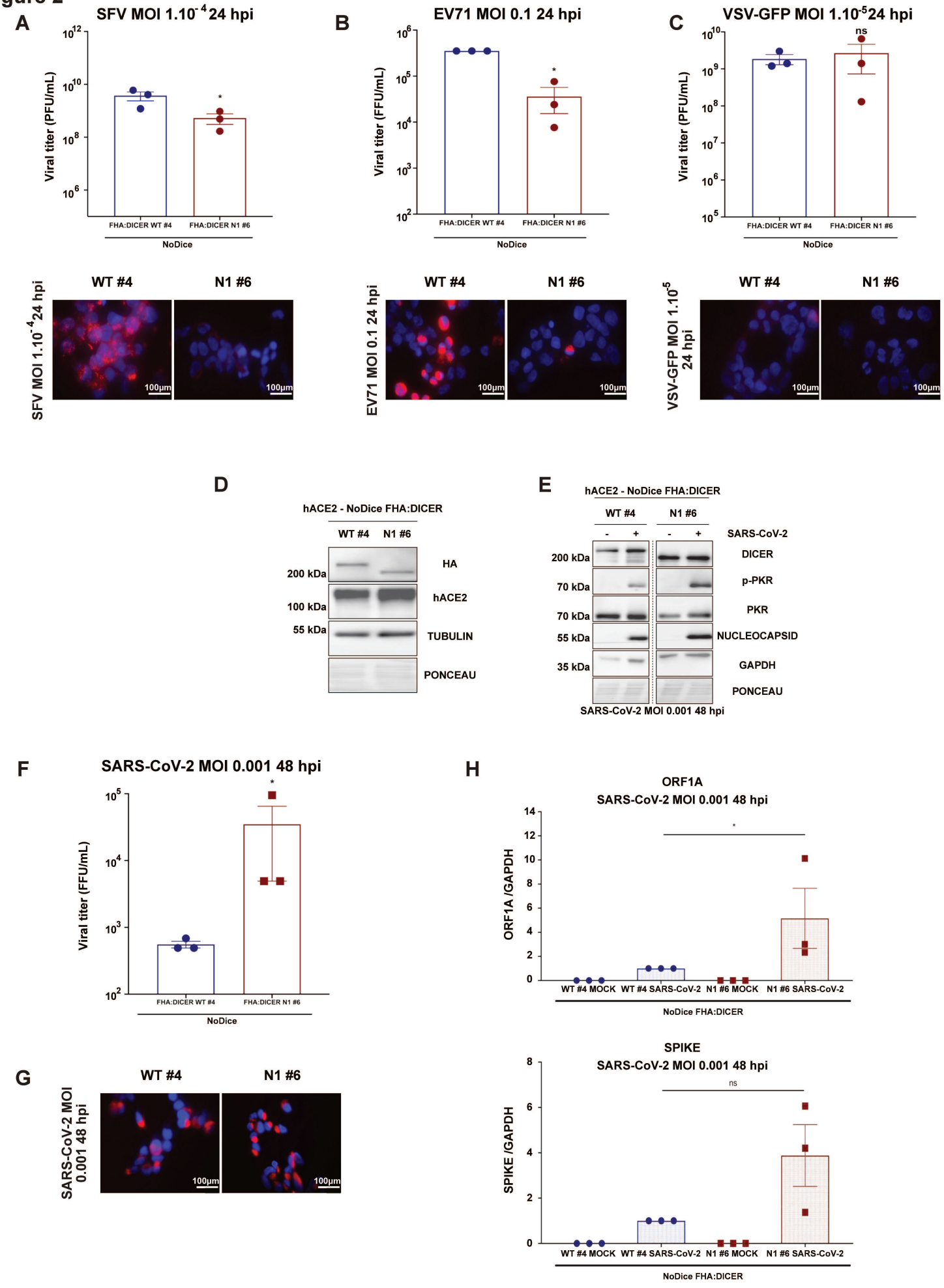
A
SFV MOI 1.10-4 24 hpi
Viral titer (PFU/mL)
FHA:DICER WT #4
FHA:DICER N1 #6
NoDice
B
EV71 MOI 0.1 24 hpi
Viral titer (FFU/mL)
C
VSV-GFP MOI 1.10-5 24 hpi
ns
WT #4
N1 #6
100µm
D
hACE2 - NoDice FHA:DICER
200 kDa
100 kDa
55 kDa
HA
hACE2
TUBULIN
PONCEAU
E
hACE2 - NoDice FHA:DICER
SARS-CoV-2
200 kDa
70 kDa
35 kDa
DICER
p-PKR
PKR
NUCLEOCAPSID
GAPDH
PONCEAU
SARS-CoV-2 MOI 0.001 48 hpi
F
SARS-CoV-2 MOI 0.001 48 hpi
G
H
ORF1A
ORF1A /GAPDH
WT #4 MOCK
WT #4 SARS-CoV-2
N1 #6 MOCK
N1 #6 SARS-CoV-2
NoDice FHA:DICER
SPIKE
SPIKE /GAPDH

Figure 3

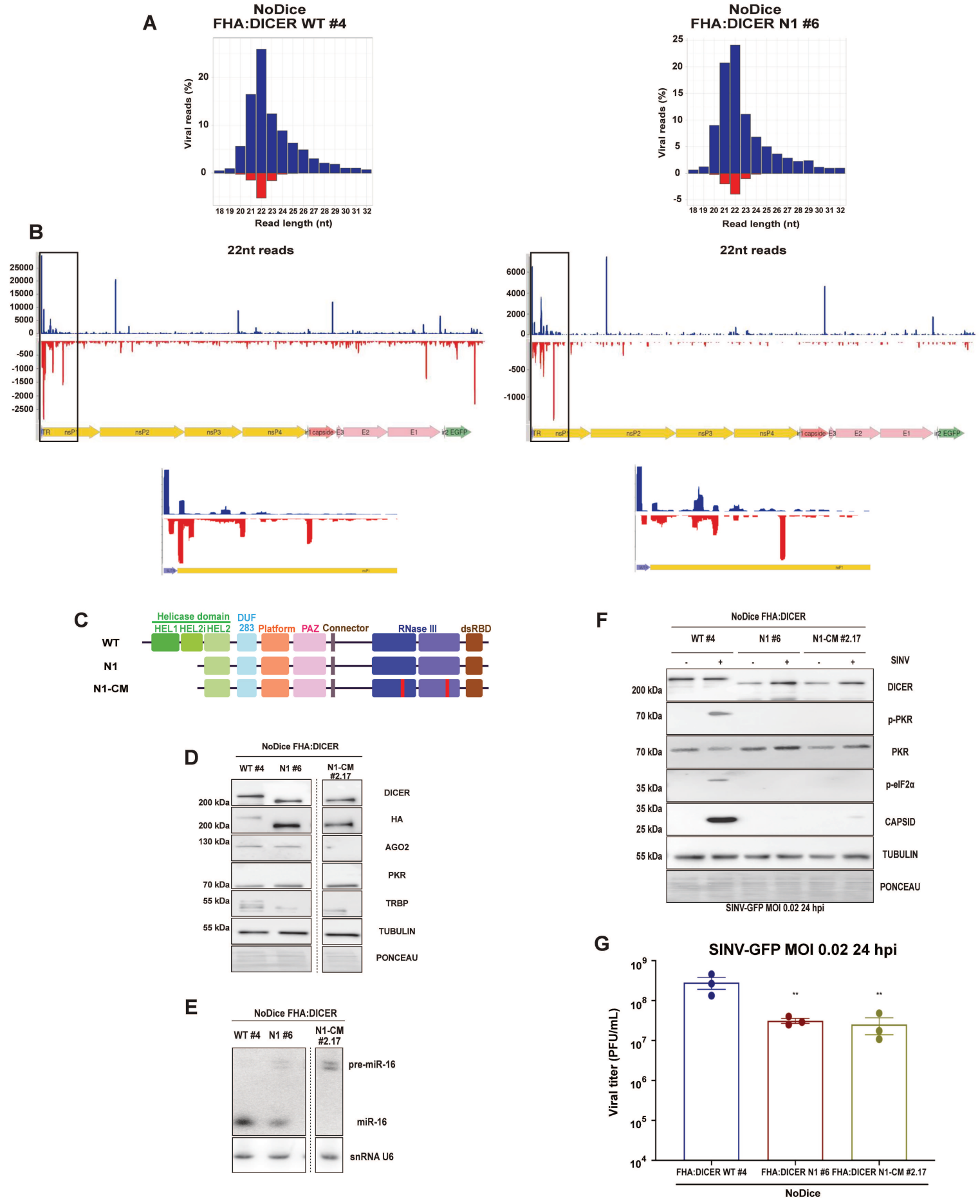
A
NoDice
FHA:DICER WT #4
Viral reads (%)
Read length (nt)
NoDice
FHA:DICER N1 #6
Viral reads (%)
Read length (nt)
B
22nt reads
22nt reads
C
Helicase domain
HEL1 HEL2i HEL2
DUF
283
Platform
PAZ
Connector
RNase III
dsRBD
WT
N1
N1-CM
D
NoDice FHA:DICER
WT #4
N1 #6
N1-CM #2.17
200 kDa
DICER
200 kDa
HA
130 kDa
AGO2
70 kDa
PKR
55 kDa
TRBP
55 kDa
TUBULIN
PONCEAU
E
NoDice FHA:DICER
WT #4
N1 #6
N1-CM #2.17
pre-miR-16
miR-16
snRNA U6
F
NoDice FHA:DICER
WT #4
N1 #6
N1-CM #2.17
SINV
200 kDa
DICER
70 kDa
p-PKR
70 kDa
PKR
35 kDa
p-eIF2α
35 kDa
25 kDa
CAPSID
55 kDa
TUBULIN
PONCEAU
SINV-GFP MOI 0.02 24 hpi
G
SINV-GFP MOI 0.02 24 hpi
Viral titer (PFU/mL)
FHA:DICER WT #4
FHA:DICER N1 #6
FHA:DICER N1-CM #2.17
NoDice

Figure 4

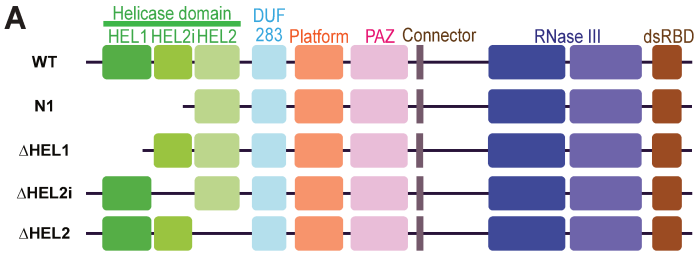
A
Helicase domain
HEL1 HEL2i HEL2
DUF 283
Platform
PAZ
Connector
RNase III
dsRBD
WT
N1
ΔHEL1
ΔHEL2i
ΔHEL2

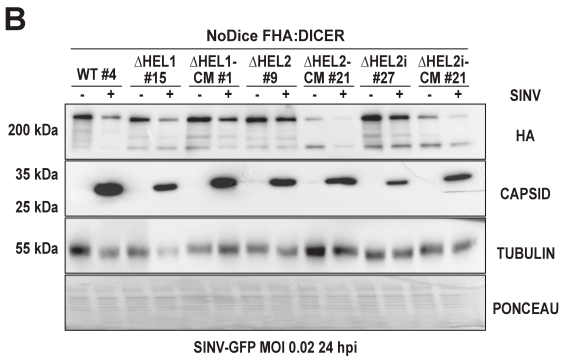
B
NoDice FHA:DICER
WT #4
ΔHEL1 #15
ΔHEL1-CM #1
ΔHEL2 #9
ΔHEL2-CM #21
ΔHEL2i #27
ΔHEL2i-CM #21
SINV
HA
CAPSID
TUBULIN
PONCEAU
200 kDa
35 kDa
25 kDa
55 kDa
SINV-GFP MOI 0.02 24 hpi

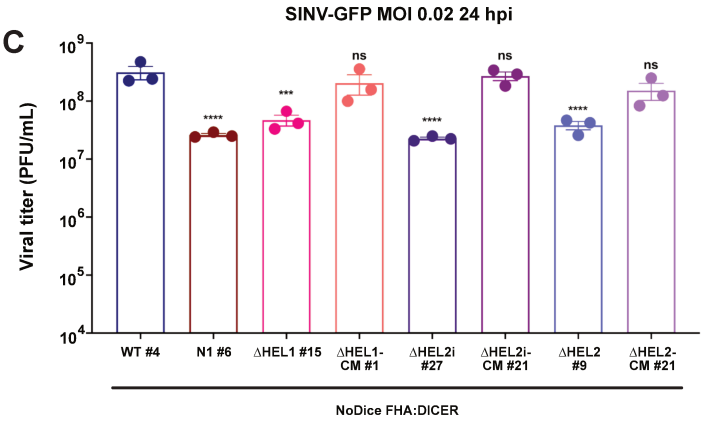
C
SINV-GFP MOI 0.02 24 hpi
Viral titer (PFU/mL)
WT #4
N1 #6
ΔHEL1 #15
ΔHEL1-CM #1
ΔHEL2i #27
ΔHEL2i-CM #21
ΔHEL2 #9
ΔHEL2-CM #21
NoDice FHA:DICER

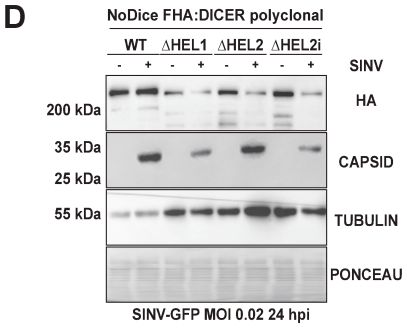
D
NoDice FHA:DICER polyclonal
WT
ΔHEL1
ΔHEL2
ΔHEL2i
SINV
HA
CAPSID
TUBULIN
PONCEAU
200 kDa
35 kDa
25 kDa
55 kDa
SINV-GFP MOI 0.02 24 hpi

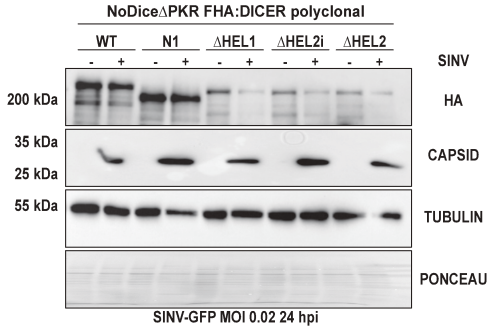
NoDiceΔPKR FHA:DICER polyclonal
WT
N1
ΔHEL1
ΔHEL2i
ΔHEL2
SINV
HA
CAPSID
TUBULIN
PONCEAU
200 kDa
35 kDa
25 kDa
55 kDa
SINV-GFP MOI 0.02 24 hpi

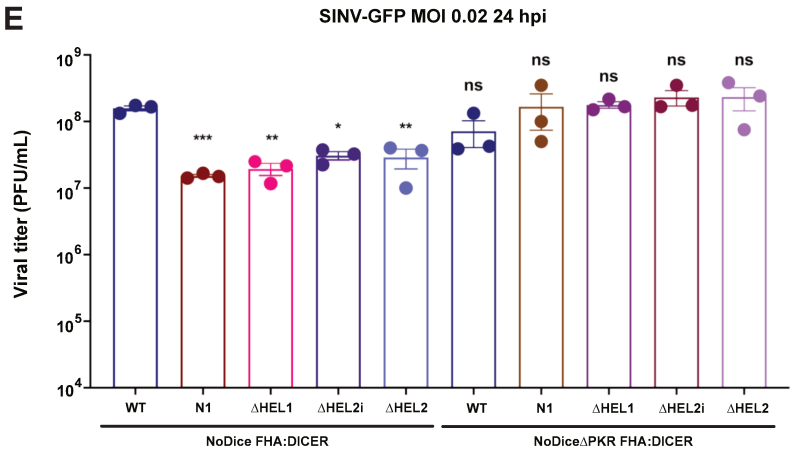
E
SINV-GFP MOI 0.02 24 hpi
Viral titer (PFU/mL)
WT
N1
ΔHEL1
ΔHEL2i
ΔHEL2
NoDice FHA:DICER
NoDiceΔPKR FHA:DICER

Figure 5

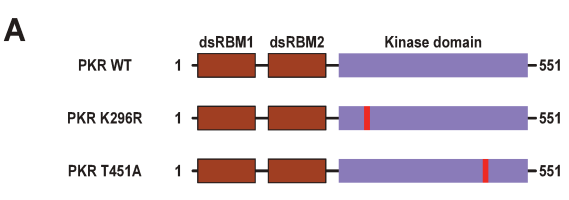

Properties	References
Dimeric kinase	Lemaire et al., 2008
Loss of activity Monomeric	Dey et al., 2005
Loss of activity Dimeric	Taylor et al., 2001

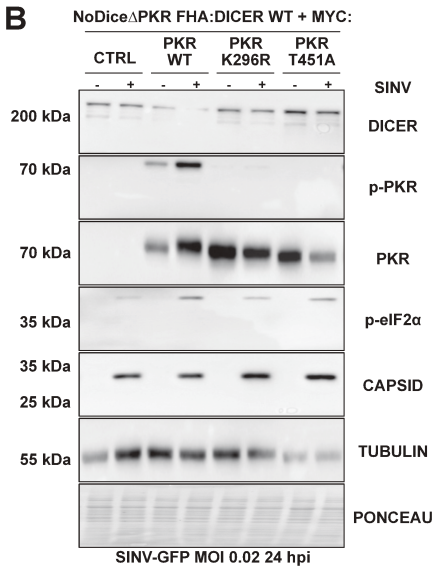

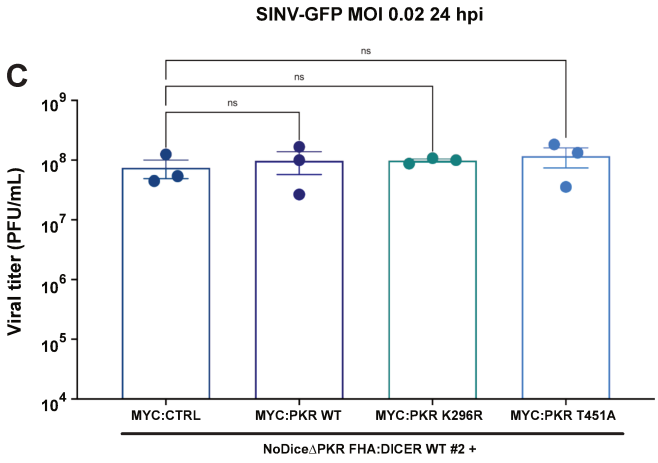

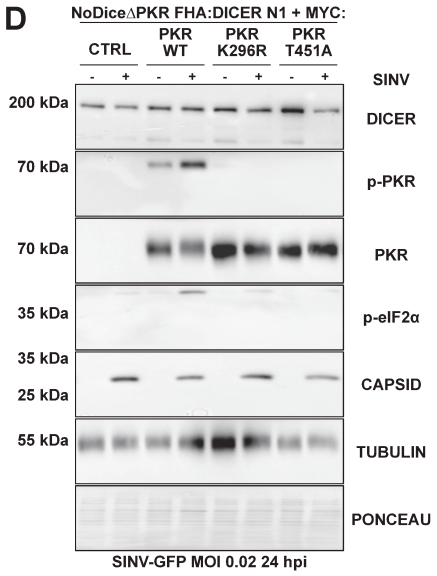

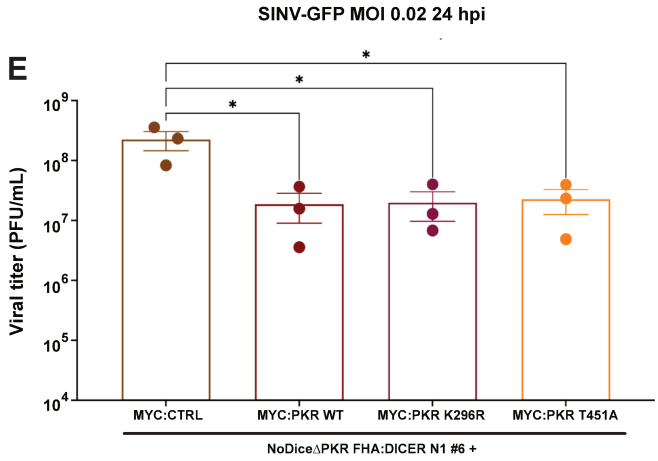

Figure 6

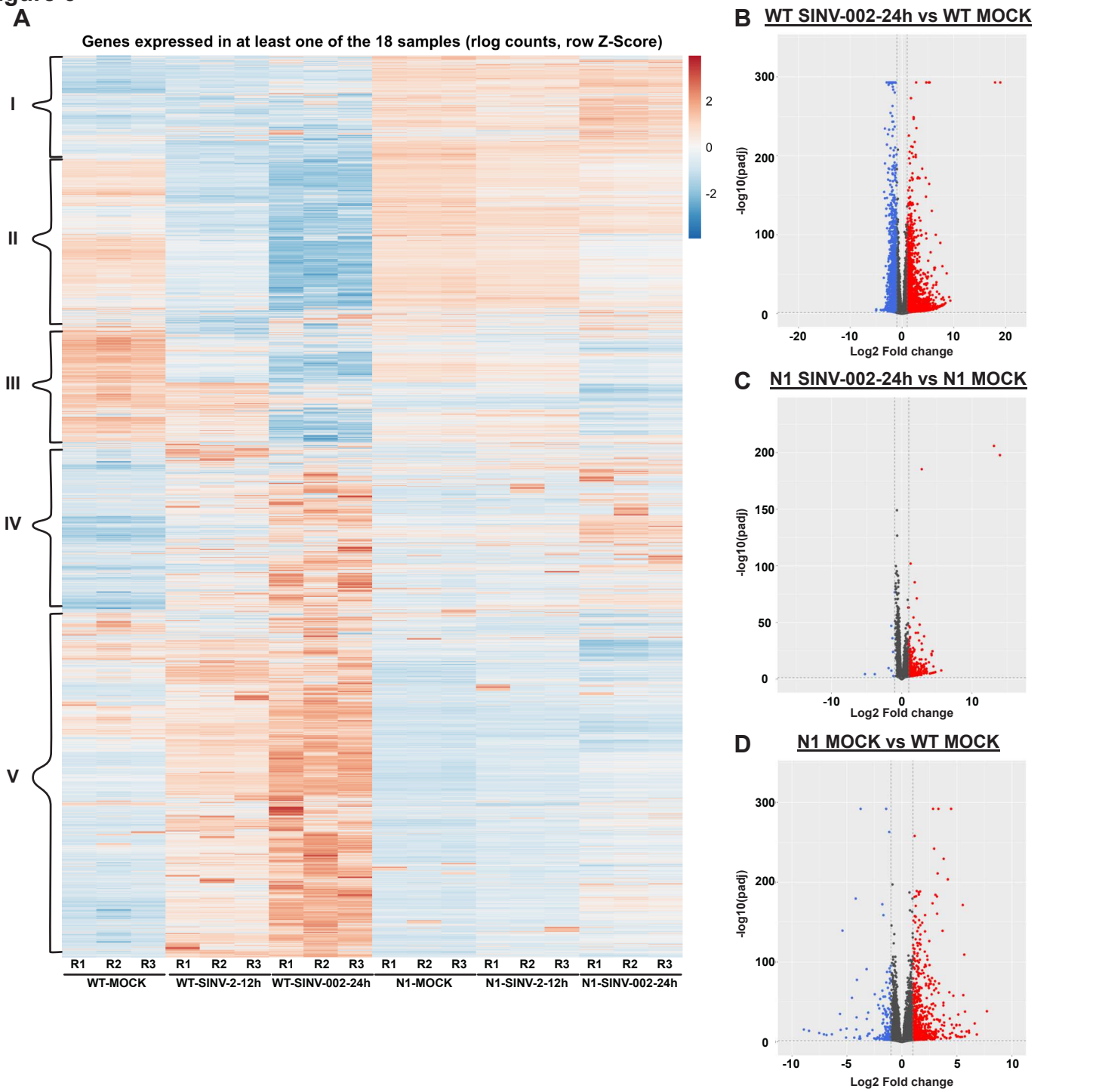
A
Genes expressed in at least one of the 18 samples (rlog counts, row Z-Score)
I
II
III
IV
V
2
0
-2
R1 R2 R3 R1 R2 R3 R1 R2 R3 R1 R2 R3 R1 R2 R3 R1 R2 R3
WT-MOCK
WT-SINV-2-12h
WT-SINV-002-24h
N1-MOCK
N1-SINV-2-12h
N1-SINV-002-24h
B
WT SINV-002-24h vs WT MOCK
-log10(padj)
Log2 Fold change
C
N1 SINV-002-24h vs N1 MOCK
-log10(padj)
Log2 Fold change
D
N1 MOCK vs WT MOCK
-log10(padj)
Log2 Fold change

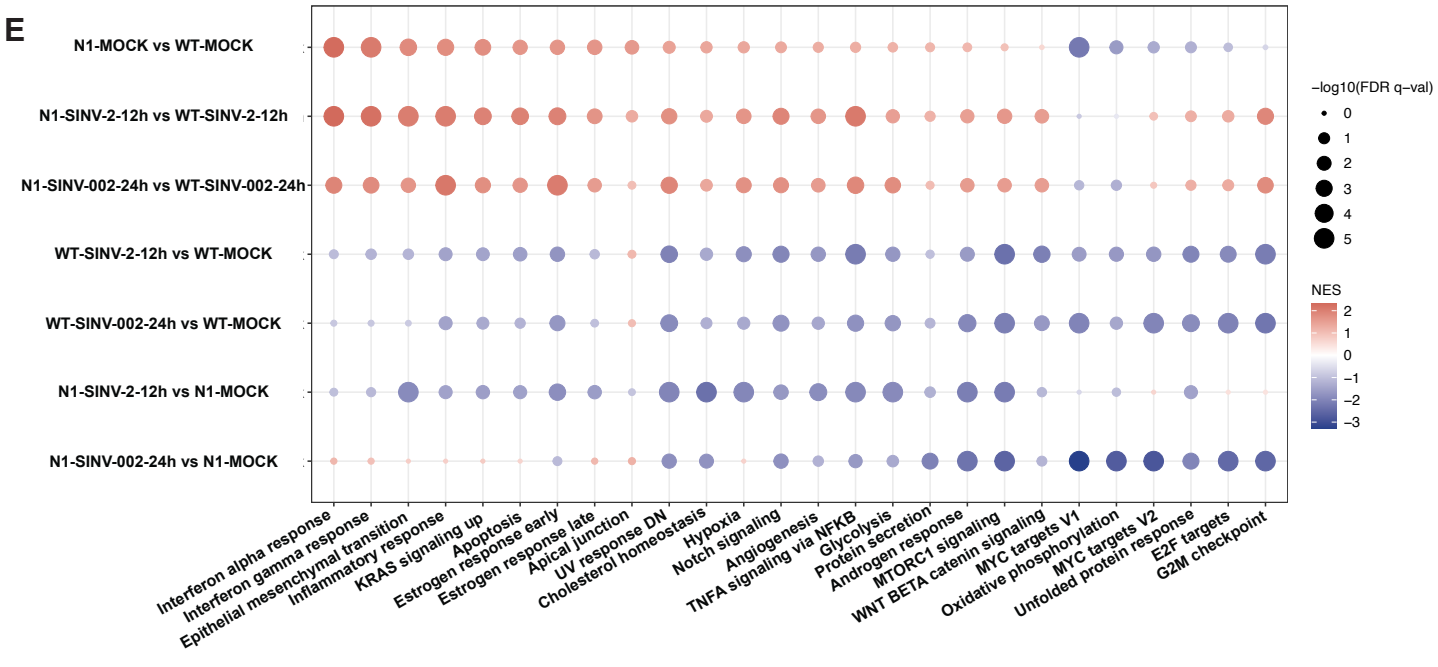
E
N1-MOCK vs WT-MOCK
N1-SINV-2-12h vs WT-SINV-2-12h
N1-SINV-002-24h vs WT-SINV-002-24h
WT-SINV-2-12h vs WT-MOCK
WT-SINV-002-24h vs WT-MOCK
N1-SINV-2-12h vs N1-MOCK
N1-SINV-002-24h vs N1-MOCK
Interferon alpha response
Interferon gamma response
Epithelial mesenchymal transition
Inflammatory response
KRAS signaling up
Apoptosis
Estrogen response early
Estrogen response late
Apical junction
UV response DN
Cholesterol homeostasis
Hypoxia
Notch signaling
Angiogenesis
TNFA signaling via NFKB
Glycolysis
Protein secretion
Androgen response
MTORC1 signaling
WNT BETA catenin signaling
MYC targets V1
Oxidative phosphorylation
MYC targets V2
Unfolded protein response
E2F targets
G2M checkpoint
−log10(FDR q−val)
NES

Figure 7

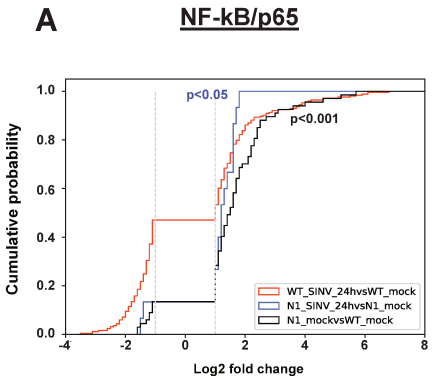
A
NF-kB/p65
p<0.05
p<0.001
Cumulative probability
Log2 fold change
WT_SINV_24hvsWT_mock
N1_SINV_24hvsN1_mock
N1_mockvsWT_mock

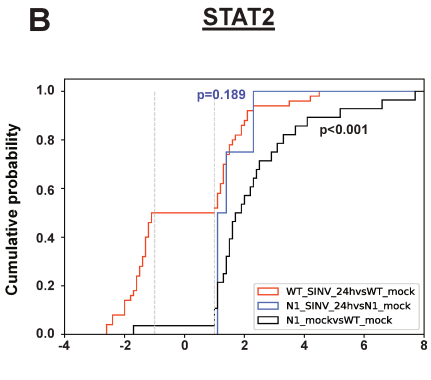
B
STAT2
p=0.189
p<0.001
Cumulative probability
WT_SINV_24hvsWT_mock
N1_SINV_24hvsN1_mock
N1_mockvsWT_mock

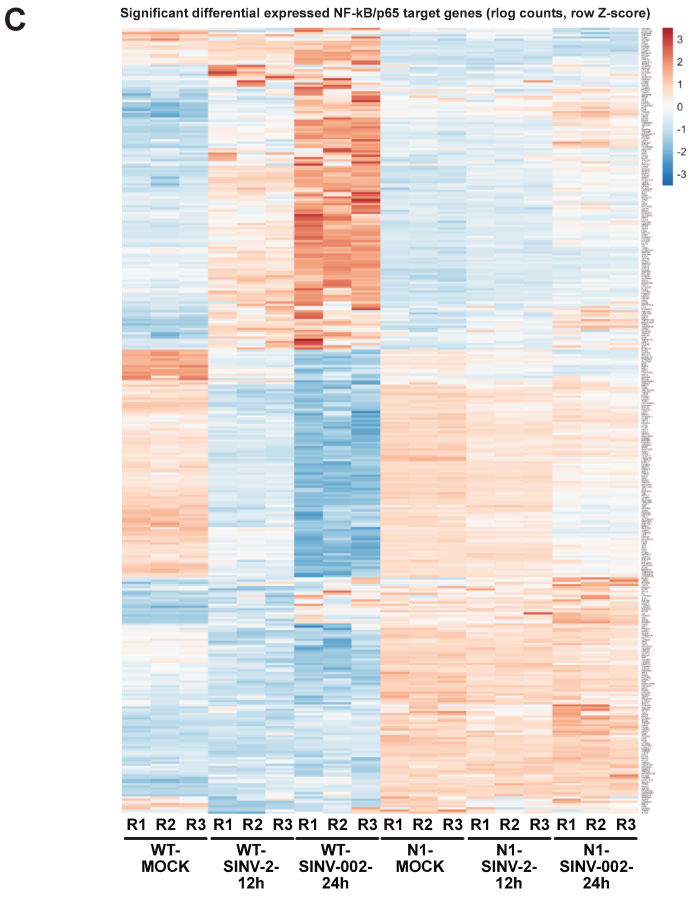
C
Significant differential expressed NF-kB/p65 target genes (rlog counts, row Z-score)
R1 R2 R3
WT-MOCK
WT-SINV-2-12h
WT-SINV-002-24h
N1-MOCK
N1-SINV-2-12h
N1-SINV-002-24h

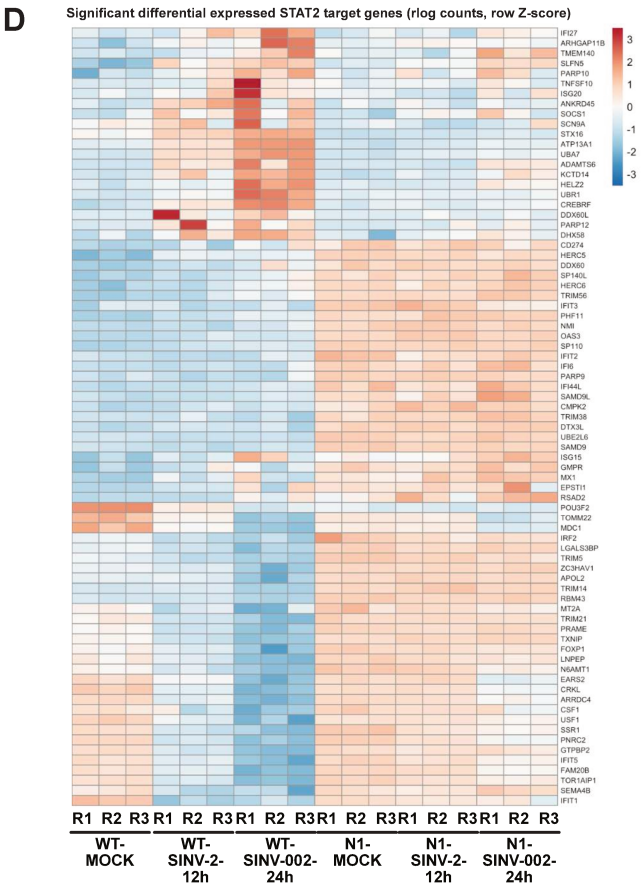
D
Significant differential expressed STAT2 target genes (rlog counts, row Z-score)
R1 R2 R3
WT-MOCK
WT-SINV-2-12h
WT-SINV-002-24h
N1-MOCK
N1-SINV-2-12h
N1-SINV-002-24h

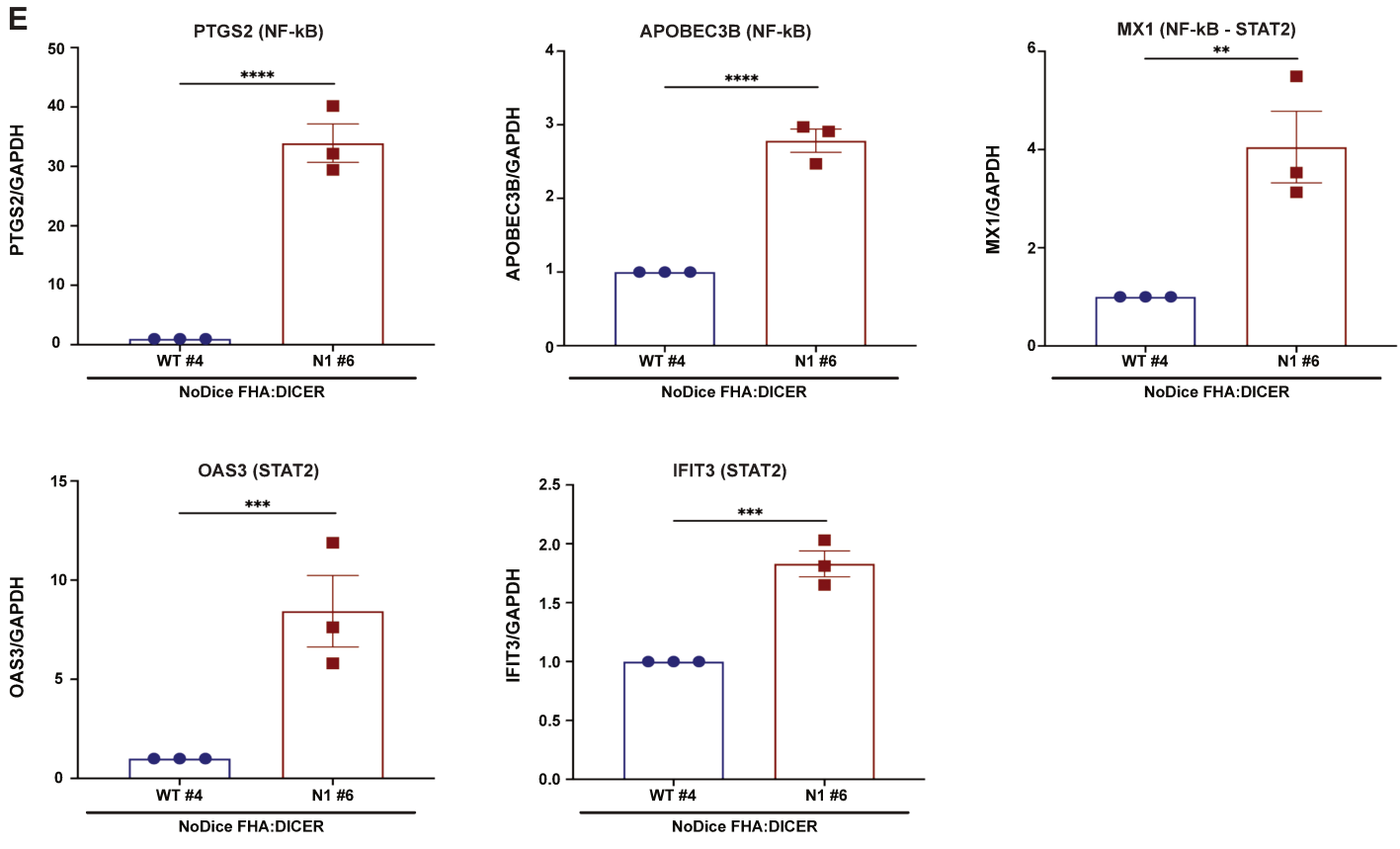
E
PTGS2 (NF-kB)
PTGS2/GAPDH
APOBEC3B (NF-kB)
APOBEC3B/GAPDH
MX1 (NF-kB - STAT2)
MX1/GAPDH
OAS3 (STAT2)
OAS3/GAPDH
IFIT3 (STAT2)
IFIT3/GAPDH
WT #4
N1 #6
NoDice FHA:DICER

Figure 8

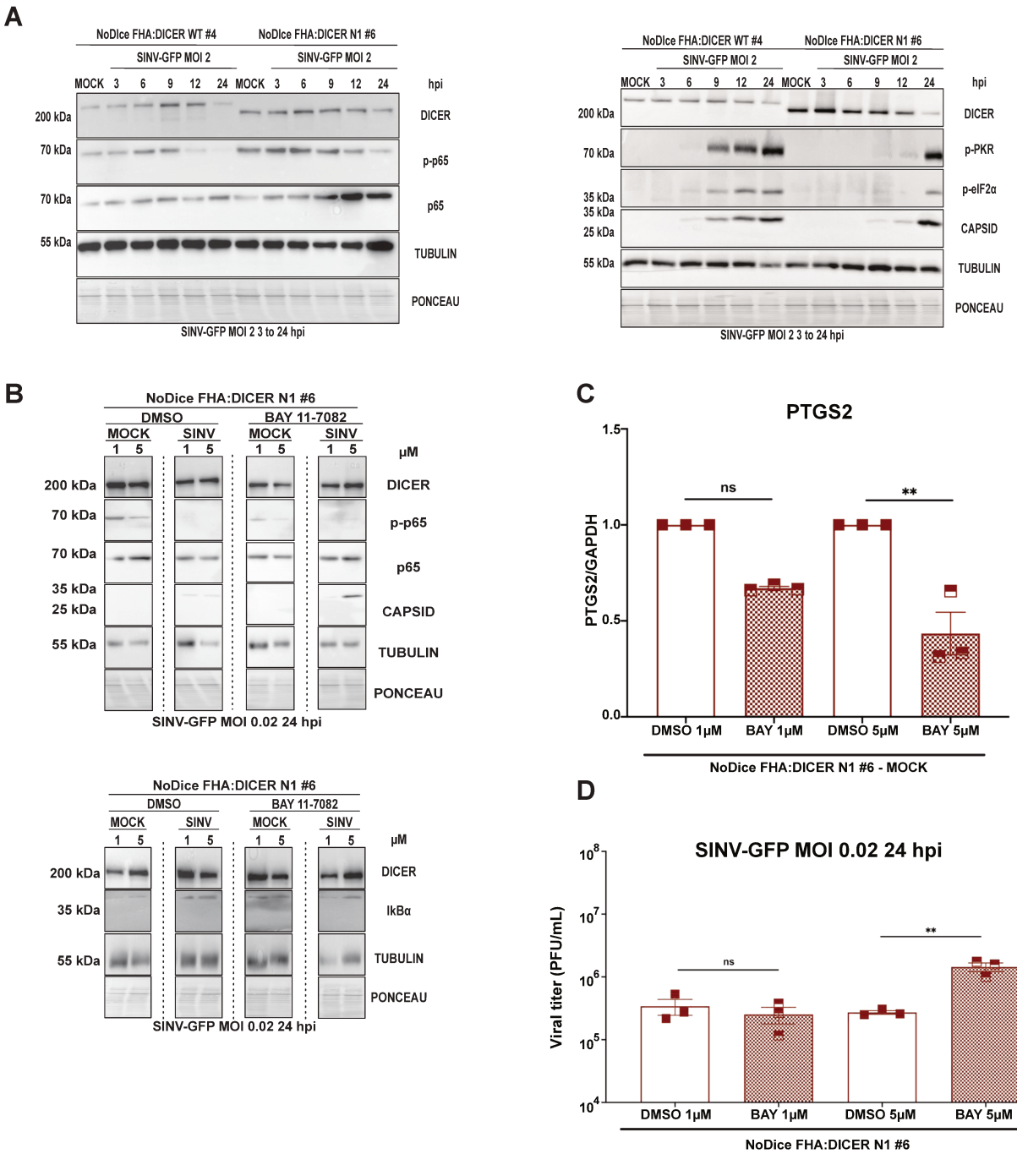
A
NoDIce FHA:DICER WT #4
NoDIce FHA:DICER N1 #6
SINV-GFP MOI 2
MOCK 3 6 9 12 24 MOCK 3 6 9 12 24 hpi
200 kDa DICER
70 kDa p-p65
70 kDa p65
55 kDa TUBULIN
PONCEAU
SINV-GFP MOI 2 3 to 24 hpi
NoDIce FHA:DICER WT #4
NoDIce FHA:DICER N1 #6
SINV-GFP MOI 2
MOCK 3 6 9 12 24 MOCK 3 6 9 12 24 hpi
200 kDa DICER
70 kDa p-PKR
35 kDa p-eIF2α
35 kDa
25 kDa CAPSID
55 kDa TUBULIN
PONCEAU
SINV-GFP MOI 2 3 to 24 hpi
B
NoDice FHA:DICER N1 #6
DMSO
BAY 11-7082
MOCK SINV MOCK SINV
1 5 1 5 1 5 1 5 µM
200 kDa DICER
70 kDa p-p65
70 kDa p65
35 kDa
25 kDa CAPSID
55 kDa TUBULIN
PONCEAU
SINV-GFP MOI 0.02 24 hpi
NoDice FHA:DICER N1 #6
DMSO
BAY 11-7082
MOCK SINV MOCK SINV
1 5 1 5 1 5 1 5 µM
200 kDa DICER
35 kDa IkBα
55 kDa TUBULIN
PONCEAU
SINV-GFP MOI 0.02 24 hpi
C
PTGS2
PTGS2/GAPDH
1.5
1.0
0.5
0.0
ns
**
DMSO 1µM
BAY 1µM
DMSO 5µM
BAY 5µM
NoDice FHA:DICER N1 #6 - MOCK
D
SINV-GFP MOI 0.02 24 hpi
Viral titer (PFU/mL)
10^8
10^7
10^6
10^5
10^4
ns
**
DMSO 1µM
BAY 1µM
DMSO 5µM
BAY 5µM
NoDice FHA:DICER N1 #6

SUPPLEMENTARY DATA

Canonical and non-canonical contributions of human Dicer helicase domain in antiviral defense

Morgane Baldaccini, Léa Gaucherand, Béatrice Chane-Woon-Ming, Mélanie Messmer, Floriane Gucciardi, Sébastien Pfeffer*

SUPPLEMENTARY FIGURES AND TABLES LEGENDS

Supplementary Figure 1. Analysis of Dicer N1 effect on SINV replication

A, Schematic representation of SINV-GFP and SINV-2A-GFP genome organization and representative fluorescent pictures of GFP expressed by the two viruses upon infection of NoDice FHA:DICER WT #4 cells at an MOI of 2 for 12h. Scale bar = 50µm, magnification 20X. ORF: Open reading frame, nsP: non-structural proteins, C: capsid, E1 to E3: envelope proteins. **B,** Agarose gel of RT-PCR on SINV antigenome in SINV-GFP infected NoDice FHA:DICER WT #4 and N1 #6 cells at an MOI of 0.02 for 24h.

Supplementary Figure 2. Analysis of the importance of Dicer N1 catalytic activity for its antiviral phenotype

A, Representation of small RNA reads distribution (in percent) upon AGO-IP in the three replicates for NoDice FHA:DICER WT #4 and N1 #6. Green: only human; Red: only viral; grey: both human and viral. **B,** Representative histograms of distribution of viral reads per length (in percent) upon small RNA sequencing for replicates 2 and 3 in NoDice FHA:DICER WT #4 (Top) and N1 #6 (Bottom) cells infected with SINV-GFP at an MOI of 0.02 for 24h. Blue: positive strand; red: negative strand. **C,** Representative graphs of the mapping of 22-nt-

reads on SINV-GFP genome for replicates 2 and 3 in NoDice FHA:DICER WT #4 (Top) and N1 #6 (Bottom) cells. **D,** Western blot analysis of DICER, p-PKR, PKR, p-eIF2α and CAPSID expression in SINV-GFP infected polyclonal NoDice FHA:DICER WT, N1 and N1-CM cells at an MOI of 0.02 for 24h. Gamma-Tubulin was used as loading control. **E,** Mean (+/- SEM) of SINV-GFP viral titers in the same samples as in D, infected at an MOI of 0.02 for 24h (n = 3) from plaque assay quantification. Ordinary one-way ANOVA test with Bonferroni correction. ****: $p < 0.0001$. **F,** Western blot analysis of Dicer interacting partners upon HA-IP in NoDice FHA:DICER WT #4, N1 #6 and N1-CM #2.17 cells, in mock (left) or SINV-GFP infected (right) conditions at an MOI of 2 for 6h. Anti-HA antibodies were used to validate the immunoprecipitation and Ponceau was used as a loading control.

Supplementary Figure 3. Analysis of the importance of the helicase sub-domains for Dicer antiviral activity

A, Western blot analysis of DICER, HA, AGO2, PKR, TRBP and PACT expression in the monoclonal cell lines NoDice FHA:DICER WT #4, N1 #6, ΔHEL1 #15, ΔHEL2i #27 and ΔHEL2 #9 (left) and ΔHEL1-CM #1, ΔHEL2i-CM #21 and ΔHEL2-CM #21 (right). Gamma-Tubulin was used as a loading control. **B,** Northern blot analysis of mirR-16 expression in the same samples as in A. Expression of snRNA U6 was used as a loading control. **C,** Western blot analysis of DICER, HA, AGO2, PKR, TRBP and PACT expression in the monoclonal cell lines NoDiceΔPKR FHA:DICER WT, N1, ΔHEL1, ΔHEL2i and ΔHEL2. Gamma-Tubulin was used as a loading control. **D,** Northern blot analysis of mirR-16 expression in the same samples as in C. Expression of snRNA U6 was used as a loading control.

Supplementary Figure 4. Transcriptomic analysis of Dicer N1 cells

A, Histograms representing SINV-GFP genomic and subgenomic distribution detected by RNA-sequencing analysis in NoDice FHA:DICER WT #4 or N1 #6 cells uninfected (NI, grey) or infected at an MOI of 2 for 12h (orange) or 0.02 for 24h (purple). Here is represented the percentage of viral reads compared to the total mapped reads in each condition. TPM: transcripts per million. Ordinary two-way ANOVA test with Bonferroni correction. ****: $p < 0.0001$; ns: non-significant. **B,** Volcano plot showing for each gene the log2 fold change and adjusted p value between SINV-infected (MOI of 2 for 12h) and mock NoDice FHA:DICER WT #4 cells (right), or SINV-infected and mock NoDice FHA:DICER N1 #6 cells (left). Each gene is marked as a dot (red: upregulated, blue: downregulated, grey: unchanged). The horizontal line denotes an adjusted p-value of 0.05 and the vertical ones the Log2 fold change cut-off (-1 and 1). **C-D,** GSEA enrichment plots for selected biological states and processes linked to inflammatory and antiviral pathways for mock NoDice FHA:DICER N1#6 mock vs mock NoDice FHA:DICER WT #4 (C) vs. SINV-infected (MOI of 0.02 for 24h) vs. mock NoDice FHA:DICER WT #4 cells (D).

Supplementary Figure 5. Analysis of the transcription factors involved in Dicer N1 cells mRNAs deregulation

A-C, Histograms representing the cumulative probability of differentially expressed genes controlled by the transcription factors IRF2 (A), IRF3 (B) or STAT1 (C), plotted according to their Log2 fold change. The vertical lines stand for the Log2 fold change cut-offs (-1 and 1). The two-sample Kolmogorov-Smirnov test was used to assess whether each distribution was statistically different from the distribution of NoDice FHA:DICER WT #4 cells infected with SINV vs. mock. p-values are indicated on each histogram. Red: WT SINV-002-24h vs WT MOCK; blue: N1 SINV-002-24h vs N1 MOCK; black: N1 MOCK vs WT MOCK. **D-E,** Volcano plot for differentially expressed genes (DEGs) under the control of NF-kB/p65 (D) or

STAT2 (E). Each gene is marked as a dot and plotted based on its log2 fold change and adjusted p values comparing SINV-infected (MOI of 0.02 for 24h) vs mock NoDice FHA:DICER WT #4 cells (left), or mock NoDice FHA:DICER WT #4 vs mock NoDice FHA:DICER N1 #6 cells (right). The horizontal line denotes an adjusted p-value of 0.05 and the vertical ones the Log2 fold change cut-offs (-1 and 1). **F,** RT-qPCR on selected differentially expressed genes (DEGs) controlled by either NF-kB/p65 or STAT2 in NoDice FHA:DICER WT #4 and N1#6 cells inefected or not with SINV-GFP at an MOI of 0.02 for 24h and controlled by either NF-kB/p65 or STAT2. Mean (+/- SEM); n = 3. Ordinary one-way ANOVA with Dunnett correction. *: $p < 0.05$; **: $p < 0.01$; ****: $p < 0.0001$; ns: non-significant.

Supplementary Figure 6. NF-kB/p65 involvement in Dicer N1 antiviral phenotype

A, Western blot analysis of DICER, p-p65, p65 ad CAPSID (left) and DICER and IkBα (right) expression in SINV-GFP infected NoDice FHA:DICER WT #4 cells at an MOI of 0.02 for 24h. Before infection, cells were treated with the NF-kB/p65 inhibitor, BAY 11-7082 or the vehicle (DMSO) at the indicated concentrations for 1 h. Gamma-Tubulin was used as loading control. **B,** Mean (+/- SEM) of SINV-GFP viral titers in the same samples as in 1, infected at an MOI of 0.02 for 24h (n = 3) from plaque assay quantification. Ordinary one-way ANOVA test with Dunnett correction. ns: non-significant.

Supplementary Table 1. List of primers

Supplementary Table 2. Summary of statistical analysis in RT-qPCR and plaque assay experiments

Supplementary figure 1

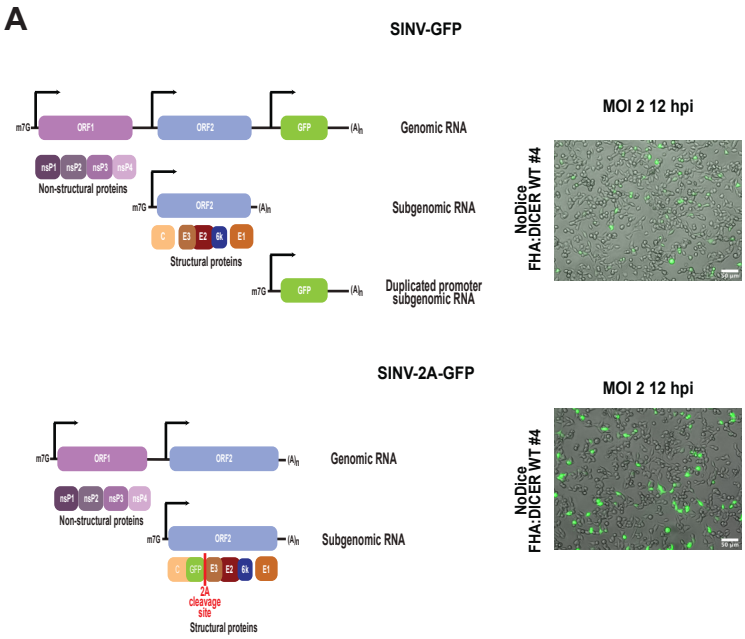

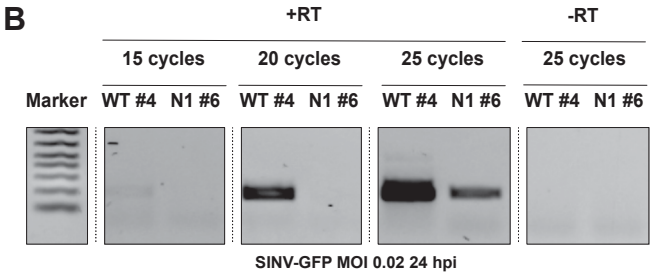

Supplementary Figure 2

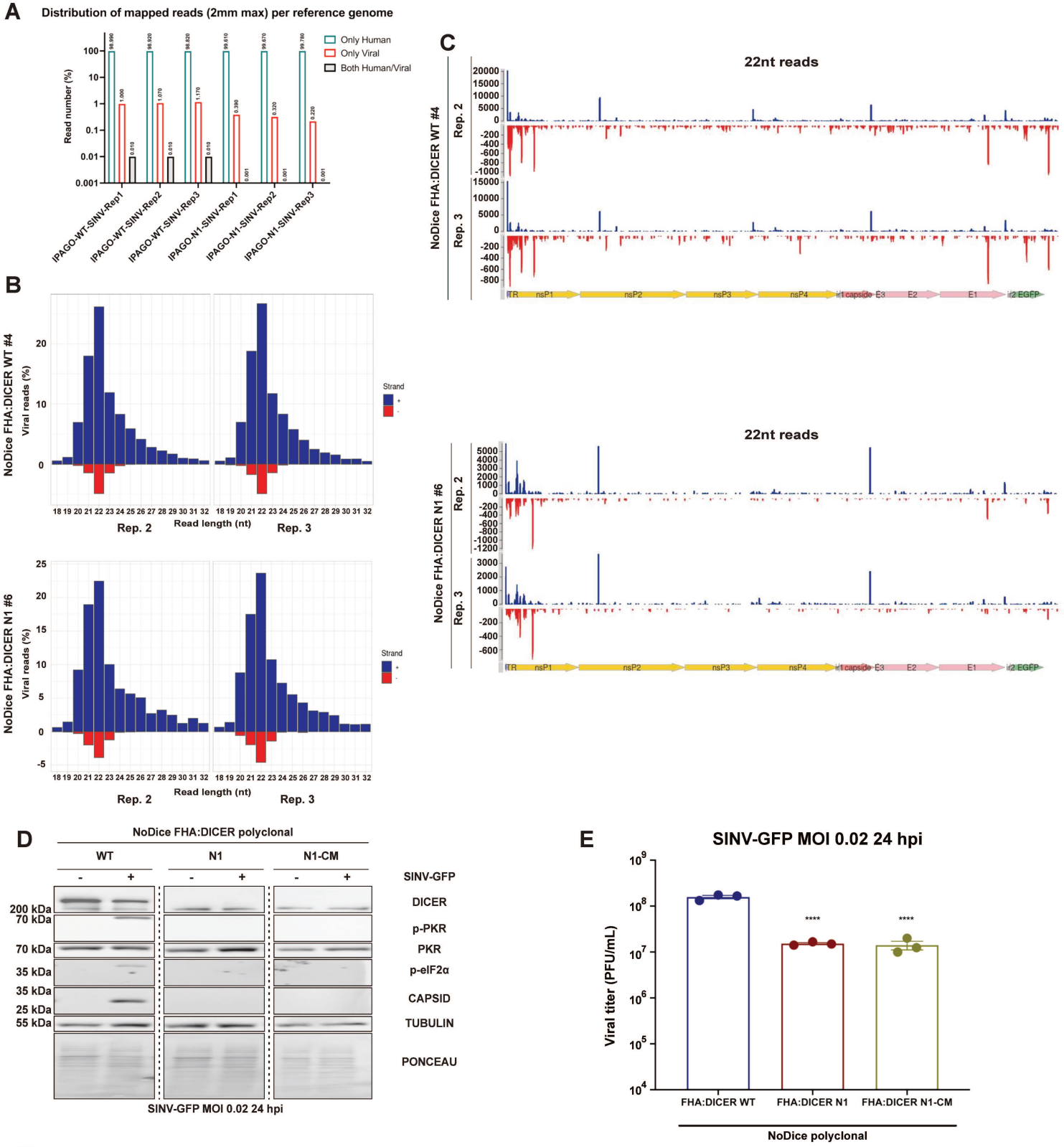

Supplementary Figure 3

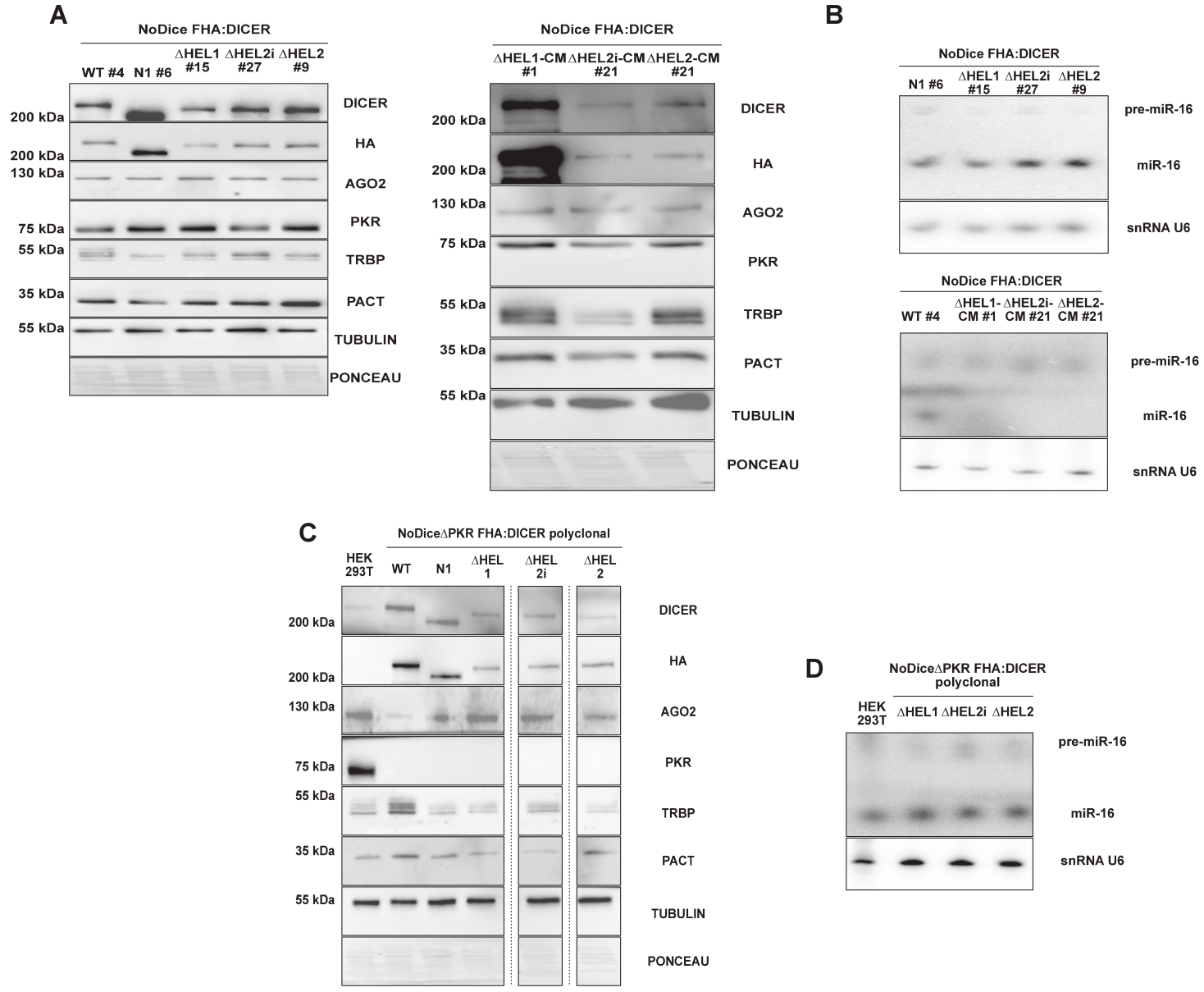

Supplementary Figure 4

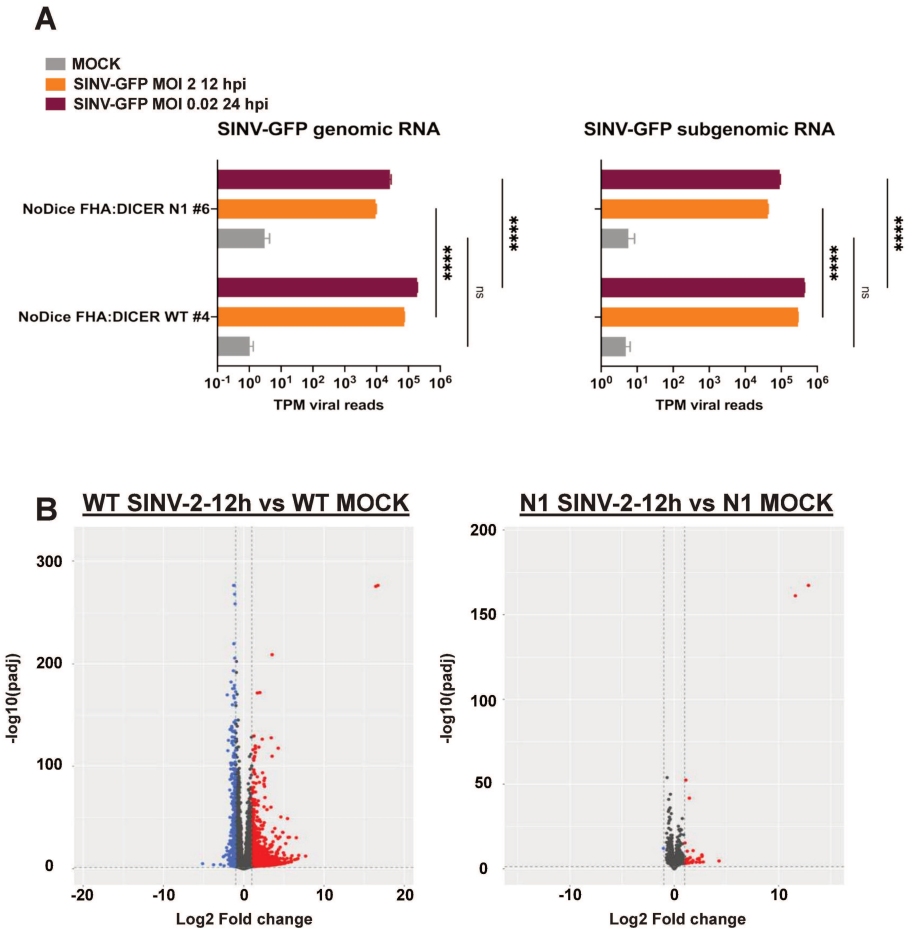

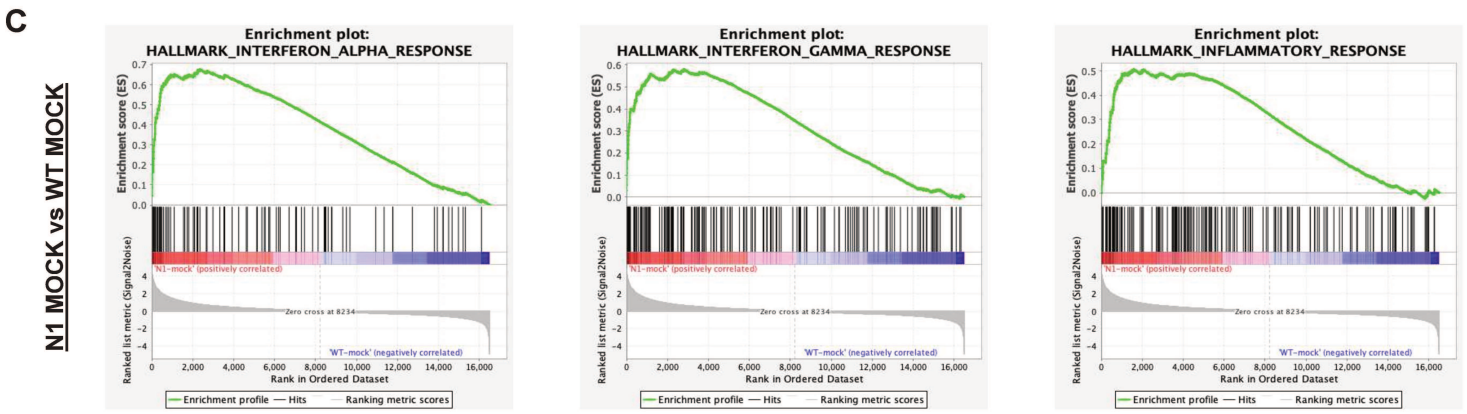

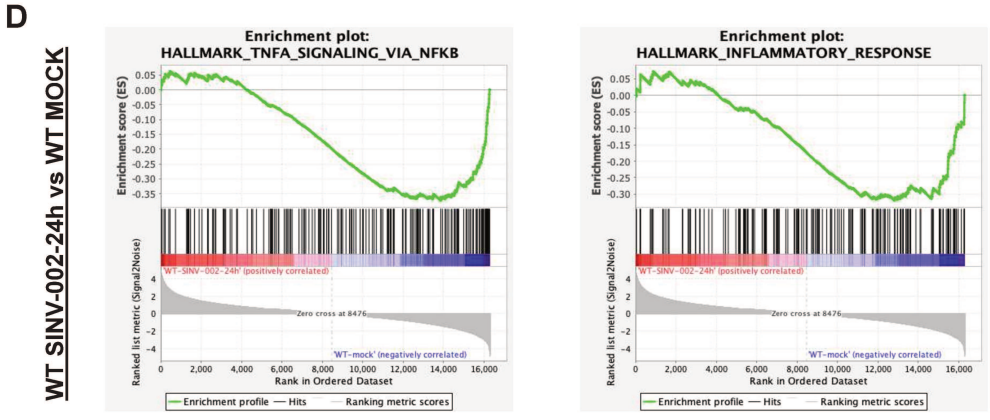

Supplementary Figure 5

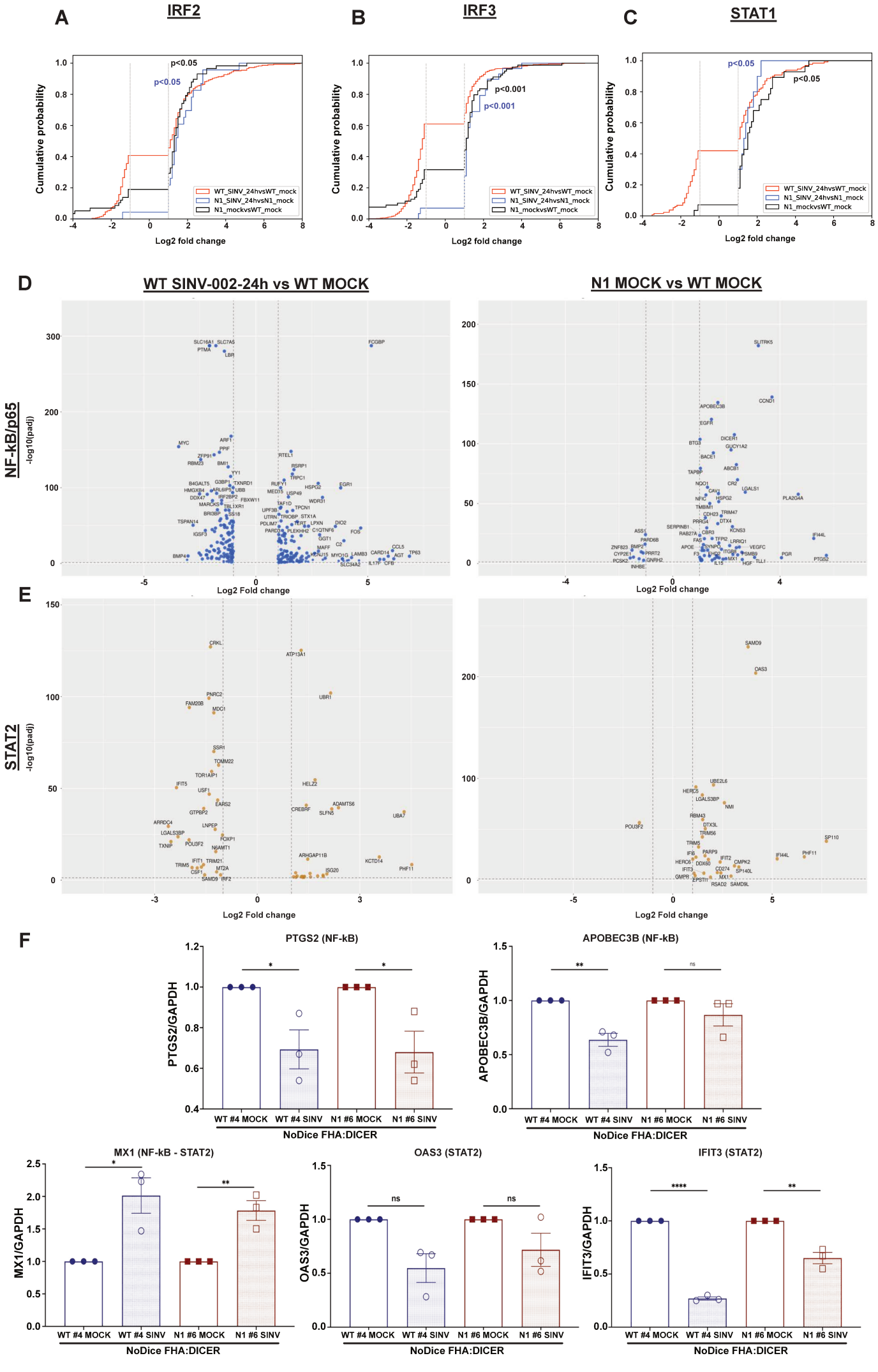

Supplementary Figure 6

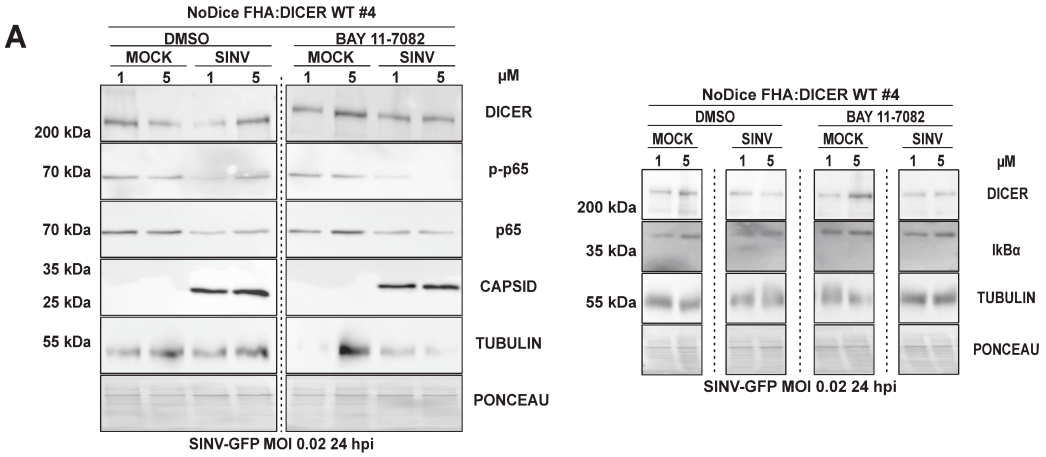

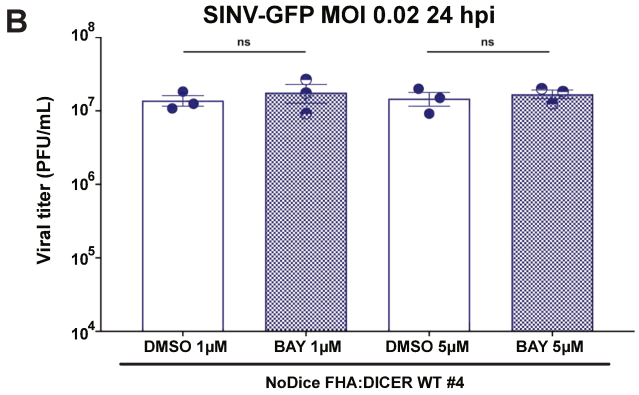

Type	Target	Fw	
PCR primers for mutagenesis	PKR K296R	CGTTATTAGACGTGTTAAATATAATAACGAGAAGG	A
	PKR T451A	TAAGGGAGCATTGCGATACATGAGCCCAGAAC	CGC
	MYC EMPTY	AGGATCTGACCCAGCTTTCTTGTACAAAGTGG	GCT
	N1-CM	ACCAATTCAGTCGACATGGAAGCAGAATTC	GA
	ΔHEL1	CGCCAAGAAAATATCAGGTTAGTAATGCTGAAACTGC	GTTGC
	ΔHEL2i	TTAGACAGAAATTTTCCTTCTCCTTTTACCAAC	AA
	ΔHEL2	CAGAGACACCTGTCATGGATGATGATCACG	TGA
RT-PCR primers	RT specific SINV	ATTGACGGCGTAGTACACACTATTGAATCAAACAGCCGACCA	
	PCR SINV antigenome	TAGACGTAGACCCCCAGAGTC	
qPCR primers	SINV genome	CCACTACGCAAGCAGAGACG	
	GAPDH	CTTTGGTATCGTGGAAGGACT	
	OAS3	TGCTGCCAGCCTTTGACGCC	
	PTGS2	ACCCACTCCAAACACAGTGC	
	APOBEC3B	GACCCTTTGGTCCTTCGAC	
	MX1	AAGCTGATCCGCCTCCACTT	
	IFIT3	ATGAGTGAGGTCACCAAGAATTCCC	
Northern blot probes	miR-16	CGCCAATATTTACGTGCTGCTA	
	U6	GCAGGGGCCATGCTAATCTTCTCTGTATCG	

Discussion/Perspectives

In light of the recent COVID-19 pandemic, the need to precisely understand the host-virus dynamics became a major issue to rapidly develop vaccines and antiviral treatments. Besides SARS-CoV-2, many viruses remain a constant health threat. Among those, alphaviruses are responsible for hundreds of deaths per year worldwide. These viruses besides being maintained in vertebrate wild animals can sometimes spill over into human hosts. In both wild animals and humans, viruses, as obligatory intracellular parasites depending on the host cellular machinery, face the innate immune system that relies mainly on the IFN-I response in mammals. In addition, because they also replicate in invertebrate vectors, alphaviruses have to face the arthropod immune system that mostly relies on the antiviral RNAi pathway.

These two immune responses ultimately allow to control the infection and clear the organism of viruses, which would make them redundant in a given system and it has therefore been proposed that they were mutually exclusive. Hence, RNAi relying on the type III endoribonuclease Dicer-2 was described as the main immune response against viruses in mosquitoes (Campbell et al., 2008; Myles et al., 2008). In mammals, IFN-I was deeply studied for its localized, but also global, viral infection suppression since this cytokine-based system allows the signaling through the whole body in addition of acting in the infected cell itself (Carpentier and Morrison, 2018; Schoggins et al., 2011).

However, in mosquitoes, a fine-tuned balance between RNAi and other immune signaling pathways triggered by the Toll-Imd system exists (Lee et al., 2019). The question remains whether mammals can also sustain the existence of these two pathways. Interestingly, the main conserved function of Dicer is in the miRNA biogenesis pathway. As opposed to insects, mammals only express one Dicer gene, which is dedicated to miRNA cleavage, and do not express a second RNAi-dedicated Dicer (Aderounmu et al., 2023). The immune-related role of mammalian Dicer has been a subject of intense debate for many years. There have been several studies, even recently, which proposed that an efficient antiviral RNAi response could be detected in mouse and human somatic cells, also upon infection with alphaviruses such as SFV (Adiliaghdam et al., 2020; Kong et al., 2023; Li et al., 2013; Yang Li et al., 2016). Other groups failed to detect Dicer-related antiviral activities in somatic cells,

except in some cases in the absence of a functional IFN-I pathway(Girardi et al., 2013; Maillard et al., 2016, 2013; Schuster et al., 2019).

The thesis project presented here focuses on this interplay that could modulate the role played by human Dicer upon viral infection. Dicer is already described as an interaction hub between the RNAi and IFN-I. We hypothesized that these interactions could have a negative impact on Dicer functionality in the antiviral defence. Thus, by performing the study of Dicer interactome upon SINV infection, we discovered Dicer co-factors that were specifically enriched upon infection. The same partners were also retrieved with another alphavirus, SFV. Interestingly, many of them were already linked to the immune response: the kinase PKR, the deaminase ADAR1, the helicase DHX9 and the dsRBP PACT. These interactions were confirmed in two cell types, the human embryonic kidney HEK293T cells and the human colorectal carcinoma HCT116 cells. To go further, I developed the bimolecular Venus-based fluorescence complementation assay (BiFC) to visualize the exact interaction localization in cells, which allowed to confirm that all the interactions involving Dicer are localized in the cytoplasm.

As Dicer helicase domain is essential both to directly modulate its processivity and as a platform for the interactions with its known co-factors, I wondered whether this domain was also involved in mediating these interactions. Even though many of them were partly RNA-dependent, I could also show that two helicase-truncated mutant N1 and N3, deleted respectively from the two first part and the whole helicase domain, were completely losing the interactions upon infection. Conversely, the helicase domain alone was still able to interact with all the tested partners. Thus, Dicer helicase domain is important to maintain many interactions with partners that are involved in the IFN-I response in human cells upon SINV infection.

Then, we looked further in the functionality of the helicase domain. In Dicer N1- and N3- expressing cells, we observed a strong antiviral phenotype against alphaviruses SINV and SFV. This was correlated with a strong decrease in both antigenomic and genomic SINV RNAs, indicating a defect in viral replication in these cells. On the contrary, cells expressing only the helicase domain were infected as well, if not better, than cells expressing Dicer WT.

I decided to deepen our research on Dicer helicase domain functionality, focusing on Dicer N1 antiviral activity. Dicer N1 was already described to be more processive against synthetic dsRNAs (Kennedy et al., 2015). Besides, some papers described that deleting a part of Dicer helicase domain is sufficient to induce a RNAi-dependent phenotype, which can be antiviral in human (Flemr et al., 2013; Poirier et al., 2021). Using three different methods, I was able to rule out any RNAi involvement in the antiviral phenotype. Indeed, in the absence of AGO2 or when rendering Dicer N1 catalytically inactive, we still observe a decrease in SINV infection in Dicer N1 cells. In addition, small RNA sequencing revealed that there was no increased accumulation of SINV-specific siRNAs in Dicer N1 cells compared to WT cells. However, when we looked at the other helicase mutants, deleted from individual helicase subdomains, we observed that the phenotype was dependent on Dicer catalytic activity.

Besides being functionally different, the helicase mutants could also present a difference in interacting partners. Hence, the HEL2i domain is already known to be involved in mediating the interactions with TRBP and PACT (Daniels et al., 2009; Yoontae Lee et al., 2006). As stated before, Dicer N1 no longer interacts with PKR, the top hit interacting partner in infected cells. I thus decided to look into the functionality of this interaction by using NoDiceΔPKR cells complemented with the different helicase mutants. PKR presence in cells was necessary to maintain the antiviral phenotype in all the cases. Indeed, even for the RNAi-dependent mutants, when PKR was knocked-out, the antiviral phenotype was not seen anymore. One hypothesis concerning the helicase mutants could be that PKR is somehow involved in dsRNA binding by Dicer and/or cleavage upon infection either because of its direct binding or because PKR could also bring and/or sequester other proteins that could modulate Dicer activity. What we should take into account as well is the infection kinetics and the fact that the timeframe of the response might be different between the two cellular responses (RNAi and IFN-I). We can imagine that since they both depend on the same signal molecule, dsRNA, they might compete for its binding. However, one major difference between them is that all the RNAi components are already expressed and ready to detect and act against dsRNA, whereas the transcriptional response induced by IFN-I might take longer to kick into action. Therefore, upon 24h of infection, IFN has time to set up whereas in the early time points (6h), RNAi could display some antiviral mechanism. But what about the role played by PKR in that scenario? PKR can detect dsRNA early upon infection and block cellular translation.

In addition, SINV is mostly insensitive to its translation inhibition since it can use alternative mechanisms of initiation (Ventoso et al., 2006). This means that PKR might be involved in a different pathway than its canonical eIF2α-phosphorylation role.

In Dicer N1 cells, as PKR is free, I was wondering whether it can increase its kinase activity. However, it does not seem to be the case since by blotting the phosphorylated PKR active form I saw a decrease in PKR activation. This could be due to a less efficient infection with less dsRNA accumulation. I further confirmed that the canonical PKR dimerization of kinase activity was not necessary for the observed antiviral activity of Dicer N1, by stably co-expressing PKR mutants and Dicer N1. Both the wild type and the mutant forms of PKR could complement the absence of PKR and restore the antiviral effect of Dicer N1 against SINV.

The other means for PKR to play an antiviral role is a signaling activity. PKR was linked to the induction of IFN-I pathway allowing IRFs, STATs or NF-kB activation upon viral infections (Marion C. Bonnet et al., 2000; Pflugheber et al., 2002; A. H. Wong et al., 1997). Besides, in Dicer N1 cells, as RNAi was not the reason for SINV infection drop, the main other antiviral pathway left was IFN-I. So, I performed total RNA sequencing in Dicer WT and N1 cells infected or not with SINV. As expected upon SINV infection in WT cells, a transcriptional shut-off was observed. Conversely, that kind of shut-off was not detected in N1 cells. By looking at the N1 mock cells, we could identify differentially expressed genes (DEGs) compared to WT mock cells. Several DEGs in N1 mock or SINV-infected cells were found linked to the GO terms “Interferon response” and “Inflammatory response”. This suggested that in N1 mock cells, immune-related genes were already expressed at a basal level then allowing N1 cells to better face the infection. Interestingly, they were controlled by immune-related transcription factors. Among them, NF-kB and STAT2 regulated genes were highly represented in Dicer N1 cells compared to WT cells. That kind of gene expression enrichment could be explained by two mechanisms. The first one is a post-transcriptional regulation by miRNAs. For instance, miRNAs are well-known to control the expression of many NF-kB pathway related factors. That cannot be ruled out considering the fact that Dicer N1 does not interact anymore with both TRBP and PACT that are partially responsible for pre-miRNA cleavage accuracy (Kok et al., 2007). Moreover, recent Dicer structures reinforce the fact that helicase domain is essential for the good fit and the accurate cleavage of pre-miRNAs (Zapletal et al., 2022). N1 Dicer is then more prone to generate mirtrons that would not be able to recognize efficiently their

targets leading to an expression dysregulation. Unfortunately, analysis of mirtrons accumulation in N1 cells was not performed yet. This could be informative for further studies on the effect of the helicase deletion on miRNA processing in N1 cells. The second regulation mechanism is by a transcriptional control of the immune targets. IFN-I is a highly regulated pathway with multiple layers of regulation but the main one is the phosphorylation and translocation of immune-related transcription factors. Dicer was already linked in plants and insects to the induction of an immune transcriptional response (Deddouche et al., 2008; Nielsen et al., 2023). In those cases, the helicase domain was not directly involved and the need for other factors in the activation cascade was raised, although they were not identified. We can also hypothesize that a nuclear role of Dicer could be involved, as it was described in the case of the reduction of deleterious endogenous dsRNA (Burger et al., 2017). But no transcriptional activator role was described.

Since we showed that PKR kinase activity was shown to be dispensable to Dicer N1 activity, and it is known that this is also the case for its role in NF-kB activation (Marion C. Bonnet et al., 2000), I decided finally to study in more details the involvement of this pathway. Surprisingly, blocking the NF-kB pathway with a specific drug, BAY 11-7082, in Dicer WT cells did not change the infection outcome. However, doing the same thing in Dicer N1 cells reverted the antiviral effect showing a strong correlation between NF-kB activation and the antiviral phenotype. Unfortunately, I observed that BAY 11-7082 was rapidly inducing apoptosis in treated cells, preventing us from increasing the drug concentration to observe a complete blocking of NF-kB activity. Thus, we should consider performing knock-down or knock-out of NF-kB to confirm its involvement. Besides, I did not test the dependency to other factors such as STAT1, STAT2 or IRF3 in Dicer N1 antiviral phenotype. Indeed, these transcription factors' targets were significantly enriched in N1 mock cells, letting us thinking that there might be multiple layers of regulation involved. In particular, among STAT2 targets, some ISGylation pathway members were strongly enriched, such as for instance ISG15 and OAS3. Both of them are known to play a strong antiviral role against alphaviruses and are therefore good candidates to explain its antiviral activity against SINV (Bréhin et al., 2009; Lenschow et al., 2007; Yize Li et al., 2016). To further understand the underlying mechanism, one could imagine to perform a small-scale inactivation screen since we now have candidate target genes that are up-regulated in Dicer N1 cells.

PKR is the central actor in the immune transcriptional activation. However, the way PKR is linked to the transcriptional activation remains to be determined. There is still in a gap in the knowledge concerning PKR partners upon stresses or viral infections. In specific cases, such as NF-kB induction, PKR was shown to interact directly with IKK kinases complex (Bonnet et al., 2006). We can hypothesize that in Dicer N1 cells, PKR has specific partners that allow transcriptional activation of downstream genes. To go further, we could carry out the study on PKR partners in Dicer WT or N1 cells in mock and virus-infected conditions to correlate the differences in partners with the transcriptional activation. We can also propose that the release of specific partners by the deletion of Dicer helicase domain might modulate PKR interactome and so, its function. Two dsRBPs, known cofactors of PKR and Dicer, are of prime interest: TRBP and PACT. They have antagonist properties on PKR function. Indeed, whereas PACT is a PKR activator by direct binding, TRBP behaves as a PKR inhibitor either by direct binding or by PACT sequestration (Chukwurah and Patel, 2018; Farabaugh et al., 2020; Gupta et al., 2003). The link between free TRBP, PACT and PKR and Dicer N1 antiviral activity should be studied in the light of these interactions.

Unfortunately, I did not have time to go deeper into the functionality of the whole Dicer interactome upon infection. Some of its partners upon infection such as ADAR1, PACT or DHX9 are also linked to the miRNA pathway, blurring again the frontier between miRNA and IFN-I response. Since we also observed that Dicer N1 could no longer interact with those, we could envision that they might play a role in the differential immune response of Dicer N1 expressing cells. To study these partners, we should also take into account their potential role in miRNA and siRNA pathways. For instance, ADAR1 can block the potential antiviral pathway by its editing activity on miRNA (Uhl et al., 2023). Besides, ADAR1 is also linked to the limitation of the inflammatory response mainly by editing either exogenous or endogenous dsRNAs thereby preventing their recognition by PKR or MDA5 (Chung et al., 2018; Pujantell et al., 2017). It would be of interest to see whether in Dicer N1 cells, ADAR1 functionality is deregulated. I mentioned the role played by DHX9 in the miRNA pathway, but it is also well-known for its potential nuclear localization that is linked to the activation of STAT1 or NF-kB (S. Liu et al., 2021; Ren et al., 2023). Finally, PACT, also known to regulate Dicer accuracy in pre-miRNA loading and cleavage, is by itself linked to immune signaling as a potential RIG-I activator upon viral infection (Kok et al., 2011). Overall, it is clear that Dicer helicase domain

gathers all of these potential pro- or anti-viral partners, maintaining an inflammatory equilibrium. Precise localization studies of PACT and DHX9 in Dicer N1 cells could also shed light on the cellular mechanism at play.

The question remains how Dicer helicase is physically linked to the immune response and to all of these partners. By having a look at other Dicer partners, I found EDC4 (part of the de-capping complex) and WDR48 (part of the deubiquitylation complex) often found in P-bodies and stress granules, and linked to mRNA and protein stability respectively. Dicer localization should be explored regarding its specific interaction with these two components. Dicer was already linked to a potential localization to P-Bodies (Much et al., 2016). Further studies have to focus on the effect of the helicase deletion to re-localize Dicer into other compartments because of the loss of localization partners. On the other hand, we should again look at the potential role of EDC4 or WDR48 to sequester the whole Dicer complex into granules, reinforcing our hypothesis of a blocking of Dicer potential antiviral RNAi activity by protein partners. Of note, EDC4 and WDR48 are also involved into the regulation of immune signaling pathways, linking again Dicer with the regulation of the IFN-I response (Han et al., 2021; Mikuda et al., 2018; Xing et al., 2023).

Finally, by looking at other viruses I hoped to get insights into Dicer N1 antiviral mechanism. I could generalize the phenotype to other +ssRNA viruses like SFV or EV71 but not to -ssRNA such as VSV. It therefore seems that an accessible dsRNA molecule (which is not the case in VSV-infected cells) is need to allow Dicer N1 antiviral effect. Surprisingly, the antiviral phenotype could not be observed upon SARS-CoV-2 infection. Yet, AviD Dicer (ΔHEL2i) displayed an antiviral effect against this virus in an RNAi-dependent manner (Poirier et al., 2021). In our case, Dicer N1 does not seem to display antiviral RNAi but rather an immune-related response. By making the link between all these observations, I hypothesize that the pro-inflammatory response in Dicer N1 cells may turn pro-viral in the case of SARS-CoV-2 infection. Indeed, NF-kB pathway was extensively shown to be important for SARS-CoV-2 to create a pro-inflammatory environment in order to better infect human cells, this being used now as an infection marker for diagnosis (W. Li et al., 2021; Nilsson-Payant et al., 2021; Su et al., 2021). This might explain the inverted phenotype. We should therefore look at the infection outcome when we block the NF-kB pathway with the BAY inhibitor. It has already

been reported that in other cell types, this had a positive effect on SARS-CoV-2 infection (Nilsson-Payant et al., 2021).

Altogether, the thesis work presented here allows the addition of a new piece in the puzzle that is the cross-talk between RNAi and IFN-I in human cells, emphasizing the role of Dicer helicase domain in the maintenance of a lower immune state. The complex partners network around the helicase domain displays a crucial role in the modulation of the immune response against alphaviruses and enteroviruses. Moreover, I could highlight a new non-canonical role of Dicer helicase domain in the blocking of the immune transcriptional response induced by its main partner upon infection, PKR. This work is giving insights into the mutual exclusivity between two evolutionary conserved immune pathways in human cells.

REFERENCES

Aderounmu, A.M., Aruscavage, P.J., Kolaczkowski, B., Bass, B.L., 2023a. Ancestral protein reconstruction reveals evolutionary events governing variation in Dicer helicase function. eLife 12, e85120. https://doi.org/10.7554/eLife.85120

Adiliaghdam, F., Basavappa, M., Saunders, T.L., Harjanto, D., Prior, J.T., Cronkite, D.A., Papavasiliou, N., Jeffrey, K.L., 2020. A Requirement for Argonaute 4 in Mammalian Antiviral Defense. Cell Rep 30, 1690-1701.e4. https://doi.org/10.1016/j.celrep.2020.01.021

Aguilar, P.V., Leung, L.W., Wang, E., Weaver, S.C., Basler, C.F., 2008. A Five-Amino-Acid Deletion of the Eastern Equine Encephalitis Virus Capsid Protein Attenuates Replication in Mammalian Systems but Not in Mosquito Cells. Journal of Virology 82, 6972–6983. https://doi.org/10.1128/JVI.01283-07

Ahola, T., Karlin, D.G., 2015. Sequence analysis reveals a conserved extension in the capping enzyme of the alphavirus supergroup, and a homologous domain in nodaviruses. Biol Direct 10, 16. https://doi.org/10.1186/s13062-015-0050-0

Akhrymuk, I., Frolov, I., Frolova, E.I., 2018. Sindbis Virus Infection Causes Cell Death by nsP2-Induced Transcriptional Shutoff or by nsP3-Dependent Translational Shutoff. J Virol 92, e01388-18. https://doi.org/10.1128/JVI.01388-18

Akhrymuk, I., Frolov, I., Frolova, E.I., 2016. Both RIG-I and MDA5 detect alphavirus replication in concentration-dependent mode. Virology 487, 230–241. https://doi.org/10.1016/j.virol.2015.09.023

Akhrymuk, I., Kulemzin, S.V., Frolova, E.I., 2012. Evasion of the Innate Immune Response: the Old World Alphavirus nsP2 Protein Induces Rapid Degradation of Rpb1, a Catalytic Subunit of RNA Polymerase II. J Virol 86, 7180–7191. https://doi.org/10.1128/JVI.00541-12

Angelini, P., Macini, P., Finarelli, A.C., Pol, C., Venturelli, C., Bellini, R., Dottori, M., 2008. Chikungunya epidemic outbreak in Emilia-Romagna (Italy) during summer 2007. Parassitologia 50, 97–98.

Arnaud, N., Dabo, S., Maillard, P., Budkowska, A., Kalliampakou, K.I., Mavromara, P.,

Garcin, D., Hugon, J., Gatignol, A., Akazawa, D., Wakita, T., Meurs, E.F., 2010. Hepatitis C virus controls interferon production through PKR activation. PLoS One 5, e10575. https://doi.org/10.1371/journal.pone.0010575

Arya, R., Kumari, S., Pandey, B., Mistry, H., Bihani, S.C., Das, A., Prashar, V., Gupta, G.D., Panicker, L., Kumar, M., 2021. Structural insights into SARS-CoV-2 proteins. J Mol Biol 433, 166725. https://doi.org/10.1016/j.jmb.2020.11.024

Awasthi, N., Liongue, C., Ward, A.C., 2021. STAT proteins: a kaleidoscope of canonical and non-canonical functions in immunity and cancer. Journal of Hematology & Oncology 14, 198. https://doi.org/10.1186/s13045-021-01214-y

Backes, S., Langlois, R.A., Schmid, S., Varble, A., Shim, J.V., Sachs, D., tenOever, B.R., 2014. The mammalian response to virus infection is independent of small RNA silencing. Cell Rep 8, 114–125. https://doi.org/10.1016/j.celrep.2014.05.038

Baggen, J., Thibaut, H.J., Strating, J.R.P.M., van Kuppeveld, F.J.M., 2018. The life cycle of non-polio enteroviruses and how to target it. Nat Rev Microbiol 16, 368–381. https://doi.org/10.1038/s41579-018-0005-4

Balachandran, S., Roberts, P.C., Brown, L.E., Truong, H., Pattnaik, A.K., Archer, D.R., Barber, G.N., 2000. Essential Role for the dsRNA-Dependent Protein Kinase PKR in Innate Immunity to Viral Infection. Immunity 13, 129–141. https://doi.org/10.1016/S1074-7613(00)00014-5

Banerjee, A.D., Abraham, G., Colonno, R.J., 1977. Vesicular stomatitis virus: mode of transcription. J Gen Virol 34, 1–8. https://doi.org/10.1099/0022-1317-34-1-1

Barrangou, R., Fremaux, C., Deveau, H., Richards, M., Boyaval, P., Moineau, S., Romero, D.A., Horvath, P., 2007. CRISPR provides acquired resistance against viruses in prokaryotes. Science 315, 1709–1712. https://doi.org/10.1126/science.1138140

Barry, G., Breakwell, L., Fragkoudis, R., Attarzadeh-Yazdi, G., Rodriguez-Andres, J., Kohl, A., Fazakerley, J.K., 2009. PKR acts early in infection to suppress Semliki Forest virus production and strongly enhances the type I interferon response. J Gen Virol 90, 1382–1391. https://doi.org/10.1099/vir.0.007336-0

Bartholomeeusen, K., Daniel, M., LaBeaud, D.A., Gasque, P., Peeling, R.W., Stephenson, K.E.,

Ng, L.F.P., Ariën, K.K., 2023. Chikungunya fever. Nat Rev Dis Primers 9, 1–21. https://doi.org/10.1038/s41572-023-00429-2

Baxter, V.K., Heise, M.T., 2020b. Chapter Nine - Immunopathogenesis of alphaviruses, in: Carr, J.P., Roossinck, M.J. (Eds.), Advances in Virus Research, Immunopathology. Academic Press, pp. 315–382. https://doi.org/10.1016/bs.aivir.2020.06.002

Benkirane, M., Neuveut, C., Chun, R.F., Smith, S.M., Samuel, C.E., Gatignol, A., Jeang, K.-T., 1997. Oncogenic potential of TAR RNA binding protein TRBP and its regulatory interaction with RNA-dependent protein kinase PKR. The EMBO Journal 16, 611–624. https://doi.org/10.1093/emboj/16.3.611

Berlanga, J.J., Ventoso, I., Harding, H.P., Deng, J., Ron, D., Sonenberg, N., Carrasco, L., de Haro, C., 2006. Antiviral effect of the mammalian translation initiation factor 2alpha kinase GCN2 against RNA viruses. EMBO J 25, 1730–1740. https://doi.org/10.1038/sj.emboj.7601073

Bernstein, E., Caudy, A.A., Hammond, S.M., Hannon, G.J., 2001. Role for a bidentate ribonuclease in the initiation step of RNA interference. Nature 409, 363–366. https://doi.org/10.1038/35053110

Birbach, A., Gold, P., Binder, B.R., Hofer, E., Martin, R. de, Schmid, J.A., 2002. Signaling Molecules of the NF-κB Pathway Shuttle Constitutively between Cytoplasm and Nucleus *. Journal of Biological Chemistry 277, 10842–10851. https://doi.org/10.1074/jbc.M112475200

Bogerd, H.P., Skalsky, R.L., Kennedy, E.M., Furuse, Y., Whisnant, A.W., Flores, O., Schultz, K.L.W., Putnam, N., Barrows, N.J., Sherry, B., Scholle, F., Garcia-Blanco, M.A., Griffin, D.E., Cullen, B.R., 2014. Replication of many human viruses is refractory to inhibition by endogenous cellular microRNAs. J. Virol. 88, 8065–8076. https://doi.org/10.1128/JVI.00985-14

Bonnet, M.C., Daurat, C., Ottone, C., Meurs, E.F., 2006. The N-terminus of PKR is responsible for the activation of the NF-kappaB signaling pathway by interacting with the IKK complex. Cell Signal 18, 1865–1875. https://doi.org/10.1016/j.cellsig.2006.02.010

Bonnet, M. C., Weil, R., Dam, E., Hovanessian, A.G., Meurs, E.F., 2000. PKR stimulates NF-kappaB irrespective of its kinase function by interacting with the IkappaB kinase complex. Mol

Cell Biol 20, 4532–4542. https://doi.org/10.1128/mcb.20.13.4532-4542.2000

Bortolotti, D., Gentili, V., Rizzo, S., Schiuma, G., Beltrami, S., Strazzabosco, G., Fernandez, M., Caccuri, F., Caruso, A., Rizzo, R., 2021. TLR3 and TLR7 RNA Sensor Activation during SARS-CoV-2 Infection. Microorganisms 9, 1820. https://doi.org/10.3390/microorganisms9091820

Breakwell, L., Dosenovic, P., Karlsson Hedestam, G.B., D'Amato, M., Liljeström, P., Fazakerley, J., McInerney, G.M., 2007. Semliki Forest virus nonstructural protein 2 is involved in suppression of the type I interferon response. J Virol 81, 8677–8684. https://doi.org/10.1128/JVI.02411-06

Bréhin, A.-C., Casadémont, I., Frenkiel, M.-P., Julier, C., Sakuntabhai, A., Desprès, P., 2009. The large form of human 2',5'-Oligoadenylate Synthetase (OAS3) exerts antiviral effect against Chikungunya virus. Virology 384, 216–222. https://doi.org/10.1016/j.virol.2008.10.021

Brown, D.M., Zhang, Y., Scheuermann, R.H., 2020. Epidemiology and Sequence-Based Evolutionary Analysis of Circulating Non-Polio Enteroviruses. Microorganisms 8, 1856. https://doi.org/10.3390/microorganisms8121856

Brown, R.S., Anastasakis, D.G., Hafner, M., Kielian, M., 2020. Multiple capsid protein binding sites mediate selective packaging of the alphavirus genomic RNA. Nat Commun 11, 4693. https://doi.org/10.1038/s41467-020-18447-z

Brummer-Korvenkontio, M., Vapalahti, O., Kuusisto, P., Saikku, P., Manni, T., Koskela, P., Nygren, T., Brummer-Korvenkontio, H., Vaheri, A., 2002. Epidemiology of Sindbis virus infections in Finland 1981-96: possible factors explaining a peculiar disease pattern. Epidemiol Infect 129, 335–345. https://doi.org/10.1017/s0950268802007409

Bukreyev, A., Skiadopoulos, M.H., Murphy, B.R., Collins, P.L., 2006. Nonsegmented Negative-Strand Viruses as Vaccine Vectors. J Virol 80, 10293–10306. https://doi.org/10.1128/JVI.00919-06

Burger, K., Schlackow, M., Potts, M., Hester, S., Mohammed, S., Gullerova, M., 2017. Nuclear phosphorylated Dicer processes double-stranded RNA in response to DNA damage. J Cell Biol 216, 2373–2389. https://doi.org/10.1083/jcb.201612131

Byrnes, A.P., Griffin, D.E., 1998. Binding of Sindbis Virus to Cell Surface Heparan Sulfate. Journal of Virology 72, 7349–7356. https://doi.org/10.1128/JVI.72.9.7349-7356.1998

Campbell, C.L., Keene, K.M., Brackney, D.E., Olson, K.E., Blair, C.D., Wilusz, J., Foy, B.D., 2008. Aedes aegyptiuses RNA interference in defense against Sindbis virus infection. BMC Microbiology 8, 47. https://doi.org/10.1186/1471-2180-8-47

Carpentier, K.S., Morrison, T.E., 2018. Innate immune control of alphavirus infection. Curr Opin Virol 28, 53–60. https://doi.org/10.1016/j.coviro.2017.11.006

Carrasco, L., Sanz, M.A., González-Almela, E., 2018. The Regulation of Translation in Alphavirus-Infected Cells. Viruses 10, 70. https://doi.org/10.3390/v10020070

Cesaro, T., Michiels, T., 2021. Inhibition of PKR by Viruses. Frontiers in Microbiology 12.

Chang, Y.-H., Lau, K.S., Kuo, R.-L., Horng, J.-T., 2017. dsRNA Binding Domain of PKR Is Proteolytically Released by Enterovirus A71 to Facilitate Viral Replication. Front Cell Infect Microbiol 7, 284. https://doi.org/10.3389/fcimb.2017.00284

Chen, J., Li, Z., Guo, J., Xu, S., Zhou, J., Chen, Q., Tong, X., Wang, D., Peng, G., Fang, L., Xiao, S., 2022. SARS-CoV-2 nsp5 Exhibits Stronger Catalytic Activity and Interferon Antagonism than Its SARS-CoV Ortholog. Journal of Virology 96, e00037-22. https://doi.org/10.1128/jvi.00037-22

Chen, K.-R., Yu, C.-K., Kung, S.-H., Chen, S.-H., Chang, C.-F., Ho, T.-C., Lee, Y.-P., Chang, H.-C., Huang, L.-Y., Lo, S.-Y., Chang, J.-C., Ling, P., 2018. Toll-Like Receptor 3 Is Involved in Detection of Enterovirus A71 Infection and Targeted by Viral 2A Protease. Viruses 10, 689. https://doi.org/10.3390/v10120689

Chen, R., Wang, E., Tsetsarkin, K.A., Weaver, S.C., 2013. Chikungunya Virus 3′ Untranslated Region: Adaptation to Mosquitoes and a Population Bottleneck as Major Evolutionary Forces. PLOS Pathogens 9, e1003591. https://doi.org/10.1371/journal.ppat.1003591

Chen, W., Foo, S.-S., Zaid, A., Teng, T.-S., Herrero, L.J., Wolf, S., Tharmarajah, K., Vu, L.D., van Vreden, C., Taylor, A., Freitas, J.R., Li, R.W., Woodruff, T.M., Gordon, R., Ojcius, D.M., Nakaya, H.I., Kanneganti, T.-D., O'Neill, L.A.J., Robertson, A.A.B., King, N.J., Suhrbier, A., Cooper, M.A., Ng, L.F.P., Mahalingam, S., 2017. Specific inhibition of NLRP3 in chikungunya

disease reveals a role for inflammasomes in alphavirus-induced inflammation. Nat Microbiol 2, 1435–1445. https://doi.org/10.1038/s41564-017-0015-4

Chendrimada, T.P., Gregory, R.I., Kumaraswamy, E., Norman, J., Cooch, N., Nishikura, K., Shiekhattar, R., 2005. TRBP recruits the Dicer complex to Ago2 for microRNA processing and gene silencing. Nature 436, 740–744. https://doi.org/10.1038/nature03868

Choi, U.Y., Kang, J.-S., Hwang, Y.S., Kim, Y.-J., 2015. Oligoadenylate synthase-like (OASL) proteins: dual functions and associations with diseases. Exp Mol Med 47, e144–e144. https://doi.org/10.1038/emm.2014.110

Chong, P., Hsieh, S.-Y., Liu, C.-C., Chou, A.-H., Chang, J.-Y., Wu, S.-C., Liu, S.-J., Chow, Y.-H., Su, I.-J., Klein, M., 2012. Production of EV71 vaccine candidates. Hum Vaccin Immunother 8, 1775–1783. https://doi.org/10.4161/hv.21739

Chukwurah, E., Patel, R.C., 2018a. Stress-induced TRBP phosphorylation enhances its interaction with PKR to regulate cellular survival. Sci Rep 8. https://doi.org/10.1038/s41598-018-19360-8

Chung, H., Calis, J.J.A., Wu, X., Sun, T., Yu, Y., Sarbanes, S.L., Dao Thi, V.L., Shilvock, A.R., Hoffmann, H.-H., Rosenberg, B.R., Rice, C.M., 2018. Human ADAR1 prevents endogenous RNA from triggering translational shutdown. Cell 172, 811-824.e14. https://doi.org/10.1016/j.cell.2017.12.038

Cieslak, T.J., Christopher, G.W., Kortepeter, M.G., Rowe, J.R., Pavlin, J.A., Culpepper, R.C., Eitzen, E.M., 2000. Immunization against potential biological warfare agents. Clin Infect Dis 30, 843–850. https://doi.org/10.1086/313812

Clark, L.E., Clark, S.A., Lin, C., Liu, J., Coscia, A., Nabel, K.G., Yang, P., Neel, D.V., Lee, H., Brusic, V., Stryapunina, I., Plante, K.S., Ahmed, A.A., Catteruccia, F., Young-Pearse, T.L., Chiu, I.M., Llopis, P.M., Weaver, S.C., Abraham, J., 2022. VLDLR and ApoER2 are receptors for multiple alphaviruses. Nature 602, 475–480. https://doi.org/10.1038/s41586-021-04326-0

Clerzius, G., Gélinas, J.-F., Daher, A., Bonnet, M., Meurs, E.F., Gatignol, A., 2009. ADAR1 interacts with PKR during human immunodeficiency virus infection of lymphocytes and contributes to viral replication. J Virol 83, 10119–10128. https://doi.org/10.1128/JVI.02457-08

Clerzius, G., Gélinas, J.-F., Gatignol, A., 2011. Multiple levels of PKR inhibition during HIV-1 replication. Reviews in Medical Virology 21, 42–53. https://doi.org/10.1002/rmv.674

Clerzius, G., Shaw, E., Daher, A., Burugu, S., Gélinas, J.-F., Ear, T., Sinck, L., Routy, J.-P., Mouland, A.J., Patel, R.C., Gatignol, A., 2013. The PKR activator, PACT, becomes a PKR inhibitor during HIV-1 replication. Retrovirology 10, 96. https://doi.org/10.1186/1742-4690-10-96

Correa-Giron, P., Calisher, C.H., Baer, G.M., 1972. Epidemic Strain of Venezuelan Equine Encephalomyelitis Virus from a Vampire Bat Captured in Oaxaca, Mexico, 1970. Science 175, 546–547. https://doi.org/10.1126/science.175.4021.546

Cruz, C.C., Suthar, M.S., Montgomery, S.A., Shabman, R., Simmons, J., Johnston, R.E., Morrison, T.E., Heise, M.T., 2010. Modulation of type I IFN induction by a virulence determinant within the alphavirus nsP1 protein. Virology 399, 1–10. https://doi.org/10.1016/j.virol.2009.12.031

Cuddihy, A.R., Wong, A.H., Tam, N.W., Li, S., Koromilas, A.E., 1999. The double-stranded RNA activated protein kinase PKR physically associates with the tumor suppressor p53 protein and phosphorylates human p53 on serine 392 in vitro. Oncogene 18, 2690–2702. https://doi.org/10.1038/sj.onc.1202620

Daher, A., Laraki, G., Singh, M., Melendez-Peña, C.E., Bannwarth, S., Peters, A.H.F.M., Meurs, E.F., Braun, R.E., Patel, R.C., Gatignol, A., 2009. TRBP Control of PACT-Induced Phosphorylation of Protein Kinase R Is Reversed by Stress. Molecular and Cellular Biology 29, 254–265. https://doi.org/10.1128/MCB.01030-08

Daniels, S.M., Melendez-Peña, C.E., Scarborough, R.J., Daher, A., Christensen, H.S., El Far, M., Purcell, D.F., Lainé, S., Gatignol, A., 2009a. Characterization of the TRBP domain required for Dicer interaction and function in RNA interference. BMC Mol Biol 10, 38. https://doi.org/10.1186/1471-2199-10-38

Dar, A.C., Dever, T.E., Sicheri, F., 2005. Higher-Order Substrate Recognition of eIF2α by the RNA-Dependent Protein Kinase PKR. Cell 122, 887–900. https://doi.org/10.1016/j.cell.2005.06.044

De Cock, A., Michiels, T., 2016. Cellular microRNAs Repress Vesicular Stomatitis Virus but

Not Theiler's Virus Replication. Viruses 8, 75. https://doi.org/10.3390/v8030075

de Groot, R.J., Hardy, W.R., Shirako, Y., Strauss, J.H., 1990. Cleavage-site preferences of Sindbis virus polyproteins containing the non-structural proteinase. Evidence for temporal regulation of polyprotein processing in vivo. EMBO J 9, 2631–2638.

de Oliveira, E.C., Fonseca, V., Xavier, J., Adelino, T., Morales Claro, I., Fabri, A., Marques Macario, E., Viniski, A.E., Campos Souza, C.L., Gomes da Costa, E.S., Soares de Sousa, C., Guimarães Dias Duarte, F., Correia de Medeiros, A., Campelo de Albuquerque, C.F., Venancio Cunha, R., Oliveira De Moura, N.F., Bispo de Filippis, A.M., Oliveira, T. de, Lourenço, J., de Abreu, A.L., Alcantara, L.C.J., Giovanetti, M., 2021. Short report: Introduction of chikungunya virus ECSA genotype into the Brazilian Midwest and its dispersion through the Americas. PLoS Negl Trop Dis 15, e0009290. https://doi.org/10.1371/journal.pntd.0009290

Deddouche, S., Matt, N., Budd, A., Mueller, S., Kemp, C., Galiana-Arnoux, D., Dostert, C., Antoniewski, C., Hoffmann, J.A., Imler, J.-L., 2008. The DExD/H-box helicase Dicer-2 mediates the induction of antiviral activity in drosophila. Nat. Immunol. 9, 1425–1432. https://doi.org/10.1038/ni.1664

Delisle, E., Rousseau, C., Broche, B., Leparc-Goffart, I., L'Ambert, G., Cochet, A., Prat, C., Foulongne, V., Ferre, J.B., Catelinois, O., Flusin, O., Tchernonog, E., Moussion, I.E., Wiegandt, A., Septfons, A., Mendy, A., Moyano, M.B., Laporte, L., Maurel, J., Jourdain, F., Reynes, J., Paty, M.C., Golliot, F., 2015. Chikungunya outbreak in Montpellier, France, September to October 2014. Euro Surveill 20, 21108. https://doi.org/10.2807/1560-7917.es2015.20.17.21108

Demarchi, F., Gutierrez, M.I., Giacca, M., 1999. Human Immunodeficiency Virus Type 1 Tat Protein Activates Transcription Factor NF-κB through the Cellular Interferon-Inducible, Double-Stranded RNA-Dependent Protein Kinase, PKR. J Virol 73, 7080–7086.

Deperasińska, I., Schulz, P., Siwicki, A.K., 2018. Salmonid Alphavirus (SAV). J Vet Res 62, 1–6. https://doi.org/10.2478/jvetres-2018-0001

Deresiewicz, R.L., Thaler, S.J., Hsu, L., Zamani, A.A., 1997. Clinical and neuroradiographic manifestations of eastern equine encephalitis. N Engl J Med 336, 1867–1874. https://doi.org/10.1056/NEJM199706263362604

Dey, D., Siddiqui, S.I., Mamidi, P., Ghosh, Sukanya, Kumar, C.S., Chattopadhyay, S., Ghosh, Subhendu, Banerjee, M., 2019. The effect of amantadine on an ion channel protein from Chikungunya virus. PLoS Negl Trop Dis 13, e0007548. https://doi.org/10.1371/journal.pntd.0007548

Dey, M., Cao, C., Dar, A.C., Tamura, T., Ozato, K., Sicheri, F., Dever, T.E., 2005. Mechanistic Link between PKR Dimerization, Autophosphorylation, and eIF2α Substrate Recognition. Cell 122, 901–913. https://doi.org/10.1016/j.cell.2005.06.041

Dey, M., Mann, B.R., Anshu, A., Mannan, M.A., 2014. Activation of Protein Kinase PKR Requires Dimerization-induced cis-Phosphorylation within the Activation Loop*. Journal of Biological Chemistry 289, 5747–5757. https://doi.org/10.1074/jbc.M113.527796

Donaszi-Ivanov, A., Mohorianu, I., Dalmay, T., Powell, P.P., 2013. Small RNA analysis in Sindbis virus infected human HEK293 cells. PLoS One 8, e84070. https://doi.org/10.1371/journal.pone.0084070

Donzé, O., Abbas-Terki, T., Picard, D., 2001. The Hsp90 chaperone complex is both a facilitator and a repressor of the dsRNA-dependent kinase PKR. The EMBO Journal 20, 3771–3780. https://doi.org/10.1093/emboj/20.14.3771

Du, H., Yin, P., Yang, X., Zhang, L., Jin, Q., Zhu, G., 2015. Enterovirus 71 2C Protein Inhibits NF-κB Activation by Binding to RelA(p65). Sci Rep 5, 14302. https://doi.org/10.1038/srep14302

Duff, M.F., 1968. Hand-foot-and-mouth syndrome in humans: coxackie A10 infections in New Zealand. Br Med J 2, 661–664.

Durbin, J.E., Hackenmiller, R., Simon, M.C., Levy, D.E., 1996. Targeted Disruption of the Mouse Stat1 Gene Results in Compromised Innate Immunity to Viral Disease. Cell 84, 443–450. https://doi.org/10.1016/S0092-8674(00)81289-1

Durbin, R.K., Mertz, S.E., Koromilas, A.E., Durbin, J.E., 2002. PKR protection against intranasal vesicular stomatitis virus infection is mouse strain dependent. Viral Immunol 15, 41–51. https://doi.org/10.1089/088282402317340224

Esen, N., Blakely, P.K., Rainey-Barger, E.K., Irani, D.N., 2012. Complexity of the microglial

activation pathways that drive innate host responses during lethal alphavirus encephalitis in mice. ASN Neuro 4, 207–221. https://doi.org/10.1042/AN20120016

Estola, T., 1970. Coronaviruses, a New Group of Animal RNA Viruses. Avian Diseases 14, 330–336. https://doi.org/10.2307/1588476

Facts about Sindbis fever [WWW Document], 2017. URL https://www.ecdc.europa.eu/en/sindbis-fever/facts (accessed 4.25.23).

Fairman-Williams, M.E., Guenther, U.-P., Jankowsky, E., 2010. SF1 and SF2 helicases: family matters. Curr. Opin. Struct. Biol. 20, 313–324. https://doi.org/10.1016/j.sbi.2010.03.011

Farabaugh, K.T., Krokowski, D., Guan, B.-J., Gao, Z., Gao, X.-H., Wu, J., Jobava, R., Ray, G., de Jesus, T.J., Bianchi, M.G., Chukwurah, E., Bussolati, O., Kilberg, M., Buchner, D.A., Sen, G.C., Cotton, C., McDonald, C., Longworth, M., Ramakrishnan, P., Hatzoglou, M., 2020a. PACT-mediated PKR activation acts as a hyperosmotic stress intensity sensor weakening osmoadaptation and enhancing inflammation. eLife 9, e52241. https://doi.org/10.7554/eLife.52241

Farabaugh, K.T., Majumder, M., Guan, B.-J., Jobava, R., Wu, J., Krokowski, D., Gao, X.-H., Schuster, A., Longworth, M., Chan, E.D., Bianchi, M., Dey, M., Koromilas, A.E., Ramakrishnan, P., Hatzoglou, M., 2017. Protein Kinase R Mediates the Inflammatory Response Induced by Hyperosmotic Stress. Mol Cell Biol 37, e00521-16. https://doi.org/10.1128/MCB.00521-16

Fareh, M., Yeom, K.-H., Haagsma, A.C., Chauhan, S., Heo, I., Joo, C., 2016. TRBP ensures efficient Dicer processing of precursor microRNA in RNA-crowded environments. Nat Commun 7, 13694. https://doi.org/10.1038/ncomms13694

Feng, Q., Langereis, M.A., Lork, M., Nguyen, M., Hato, S.V., Lanke, K., Emdad, L., Bhoopathi, P., Fisher, P.B., Lloyd, R.E., van Kuppeveld, F.J.M., 2014. Enterovirus 2Apro Targets MDA5 and MAVS in Infected Cells. Journal of Virology 88, 3369–3378. https://doi.org/10.1128/JVI.02712-13

Ferran, M.C., Lucas-Lenard, J.M., 1997. The vesicular stomatitis virus matrix protein inhibits transcription from the human beta interferon promoter. J Virol 71, 371–377.

Firth, A.E., Chung, B.Y., Fleeton, M.N., Atkins, J.F., 2008. Discovery of frameshifting in Alphavirus 6K resolves a 20-year enigma. Virol J 5, 108. https://doi.org/10.1186/1743-422X-5-108

Fish, L., Navickas, A., Culbertson, B., Xu, Y., Nguyen, H.C.B., Zhang, S., Hochman, M., Okimoto, R., Dill, B.D., Molina, H., Najafabadi, H.S., Alarcón, C., Ruggero, D., Goodarzi, H., 2019. Nuclear TARBP2 drives oncogenic dysregulation of RNA splicing and decay. Mol Cell 75, 967-981.e9. https://doi.org/10.1016/j.molcel.2019.06.001

Fitzgerald, K.D., Semler, B.L., 2009. Bridging IRES elements in mRNAs to the eukaryotic translation apparatus. Biochim Biophys Acta 1789, 518–528. https://doi.org/10.1016/j.bbagrm.2009.07.004

Flemr, M., Malik, R., Franke, V., Nejepinska, J., Sedlacek, R., Vlahovicek, K., Svoboda, P., 2013. A Retrotransposon-Driven Dicer Isoform Directs Endogenous Small Interfering RNA Production in Mouse Oocytes. Cell 155, 807–816. https://doi.org/10.1016/j.cell.2013.10.001

Forrester, N.L., Palacios, G., Tesh, R.B., Savji, N., Guzman, H., Sherman, M., Weaver, S.C., Lipkin, W.I., 2012. Genome-scale phylogeny of the alphavirus genus suggests a marine origin. J Virol 86, 2729–2738. https://doi.org/10.1128/JVI.05591-11

Fossat, N., Lundsgaard, E.A., Costa, R., Rivera-Rangel, L.R., Nielsen, L., Mikkelsen, L.S., Ramirez, S., Bukh, J., Scheel, T.K.H., 2023. Identification of the viral and cellular microRNA interactomes during SARS-CoV-2 infection. Cell Reports 42. https://doi.org/10.1016/j.celrep.2023.112282

Frolov, I., Hardy, R., Rice, C.M., 2001. Cis-acting RNA elements at the 5’ end of Sindbis virus genome RNA regulate minus- and plus-strand RNA synthesis. RNA 7, 1638–1651.

Fros, J.J., Domeradzka, N.E., Baggen, J., Geertsema, C., Flipse, J., Vlak, J.M., Pijlman, G.P., 2012. Chikungunya virus nsP3 blocks stress granule assembly by recruitment of G3BP into cytoplasmic foci. J Virol 86, 10873–10879. https://doi.org/10.1128/JVI.01506-12

Fros, J.J., Liu, W.J., Prow, N.A., Geertsema, C., Ligtenberg, M., Vanlandingham, D.L., Schnettler, E., Vlak, J.M., Suhrbier, A., Khromykh, A.A., Pijlman, G.P., 2010. Chikungunya virus nonstructural protein 2 inhibits type I/II interferon-stimulated JAK-STAT signaling. J Virol 84, 10877–10887. https://doi.org/10.1128/JVI.00949-10

Fros, J.J., Major, L.D., Scholte, F.E.M., Gardner, J., van Hemert, M.J., Suhrbier, A., Pijlman, G.P., 2015. Chikungunya virus non-structural protein 2-mediated host shut-off disables the unfolded protein response. J Gen Virol 96, 580–589. https://doi.org/10.1099/vir.0.071845-0

Fros, J.J., Pijlman, G.P., 2016. Alphavirus Infection: Host Cell Shut-Off and Inhibition of Antiviral Responses. Viruses 8, 166. https://doi.org/10.3390/v8060166

Fung, S.-Y., Siu, K.-L., Lin, H., Chan, C.-P., Yeung, M.L., Jin, D.-Y., 2022. SARS-CoV-2 NSP13 helicase suppresses interferon signaling by perturbing JAK1 phosphorylation of STAT1. Cell & Bioscience 12, 36. https://doi.org/10.1186/s13578-022-00770-1

Furr, S.R., Chauhan, V.S., Sterka, D., Grdzelishvili, V., Marriott, I., 2008. Characterization of retinoic acid–inducible gene-I expression in primary murine glia following exposure to vesicular stomatitis virus. J Neurovirol 14, 10.1080/13550280802337217. https://doi.org/10.1080/13550280802337217

Gaedigk-Nitschko, K., Schlesinger, M.J., 1991. Site-directed mutations in Sindbis virus E2 glycoprotein's cytoplasmic domain and the 6K protein lead to similar defects in virus assembly and budding. Virology 183, 206–214. https://doi.org/10.1016/0042-6822(91)90133-v

Galabru, J., Hovanessian, A., 1987. Autophosphorylation of the protein kinase dependent on double-stranded RNA. Journal of Biological Chemistry 262, 15538–15544. https://doi.org/10.1016/S0021-9258(18)47759-9

Gao, Y., Goonawardane, N., Ward, J., Tuplin, A., Harris, M., 2019. Multiple roles of the non-structural protein 3 (nsP3) alphavirus unique domain (AUD) during Chikungunya virus genome replication and transcription. PLoS Pathog 15, e1007239. https://doi.org/10.1371/journal.ppat.1007239

Gao, Z., Chiao, P., Zhang, Xia, Zhang, Xiaohong, Lazar, M.A., Seto, E., Young, H.A., Ye, J., 2005. Coactivators and corepressors of NF-kappaB in IkappaB alpha gene promoter. J Biol Chem 280, 21091–21098. https://doi.org/10.1074/jbc.M500754200

Gardner, C.L., Ebel, G.D., Ryman, K.D., Klimstra, W.B., 2011. Heparan sulfate binding by natural eastern equine encephalitis viruses promotes neurovirulence. Proceedings of the National Academy of Sciences 108, 16026–16031. https://doi.org/10.1073/pnas.1110617108

Garoff, H., Simons, K., Dobberstein, B., 1978. Assembly of the Semliki Forest virus membrane glycoproteins in the membrane of the endoplasmic reticulum in vitro. J Mol Biol 124, 587–600. https://doi.org/10.1016/0022-2836(78)90173-0

Ge, P., Tsao, J., Schein, S., Green, T.J., Luo, M., Zhou, Z.H., 2010. CryoEM Model of the Bullet-Shaped Vesicular Stomatitis Virus. Science 327, 689–693. https://doi.org/10.1126/science.1181766

Georgel, P., Jiang, Z., Kunz, S., Janssen, E., Mols, J., Hoebe, K., Bahram, S., Oldstone, M.B.A., Beutler, B., 2007. Vesicular stomatitis virus glycoprotein G activates a specific antiviral Toll-like receptor 4-dependent pathway. Virology 362, 304–313. https://doi.org/10.1016/j.virol.2006.12.032

Gil, J., Alcamí, J., Esteban, M., 2000. Activation of NF-κB by the dsRNA-dependent protein kinase, PKR involves the IκB kinase complex. Oncogene 19, 1369–1378. https://doi.org/10.1038/sj.onc.1203448

Gil, J., Alcamí, J., Esteban, M., 1999. Induction of apoptosis by double-stranded-RNA-dependent protein kinase (PKR) involves the alpha subunit of eukaryotic translation initiation factor 2 and NF-kappaB. Mol Cell Biol 19, 4653–4663. https://doi.org/10.1128/MCB.19.7.4653

Girardi, E., Chane-Woon-Ming, B., Messmer, M., Kaukinen, P., Pfeffer, S., 2013. Identification of RNase L-dependent, 3'-end-modified, viral small RNAs in Sindbis virus-infected mammalian cells. mBio 4, e00698-00613. https://doi.org/10.1128/mBio.00698-13

Girardi, E., López, P., Pfeffer, S., 2018. On the Importance of Host MicroRNAs During Viral Infection. Front Genet 9, 439. https://doi.org/10.3389/fgene.2018.00439

Gomez de Cedrón, M., Ehsani, N., Mikkola, M.L., García, J.A., Kääriäinen, L., 1999. RNA helicase activity of Semliki Forest virus replicase protein NSP2. FEBS Lett 448, 19–22. https://doi.org/10.1016/s0014-5793(99)00321-x

Gorchakov, R., Frolova, E., Williams, B.R.G., Rice, C.M., Frolov, I., 2004. PKR-Dependent and -Independent Mechanisms Are Involved in Translational Shutoff during Sindbis Virus Infection. J Virol 78, 8455–8467. https://doi.org/10.1128/JVI.78.16.8455-8467.2004

Gorchakov, R., Garmashova, N., Frolova, E., Frolov, I., 2008. Different Types of nsP3-Containing Protein Complexes in Sindbis Virus-Infected Cells. J Virol 82, 10088–10101. https://doi.org/10.1128/JVI.01011-08

Gresíková, M., Sekeyová, M., Tempera, G., Guglielmino, S., Castro, A., 1978. Identification of a Sindbis virus strain isolated from Hyaloma marginatum ticks in Sicily. Acta Virol 22, 231–232.

Gunnery, S., Rice, A.P., Robertson, H.D., Mathews, M.B., 1990. Tat-responsive region RNA of human immunodeficiency virus 1 can prevent activation of the double-stranded-RNA-activated protein kinase. Proc Natl Acad Sci U S A 87, 8687–8691. https://doi.org/10.1073/pnas.87.22.8687

Gupta, V., Huang, X., Patel, R.C., 2003a. The carboxy-terminal, M3 motifs of PACT and TRBP have opposite effects on PKR activity. Virology 315, 283–291. https://doi.org/10.1016/s0042-6822(03)00589-0

Guzmán, C., Calderón, A., Mattar, S., Tadeu-Figuereido, L., Salazar-Bravo, J., Alvis-Guzmán, N., Martinez, E.Z., González, M., 2020. Chapter 6 - Ecoepidemiology of Alphaviruses and Flaviviruses, in: Ennaji, M.M. (Ed.), Emerging and Reemerging Viral Pathogens. Academic Press, pp. 101–125. https://doi.org/10.1016/B978-0-12-819400-3.00006-5

Guzmán-Terán, C., Calderón-Rangel, A., Rodriguez-Morales, A., Mattar, S., 2020. Venezuelan equine encephalitis virus: the problem is not over for tropical America. Ann Clin Microbiol Antimicrob 19, 19. https://doi.org/10.1186/s12941-020-00360-4

Haac, M.E., Anderson, M.A.E., Eggleston, H., Myles, K.M., Adelman, Z.N., 2015. The hub protein loquacious connects the microRNA and short interfering RNA pathways in mosquitoes. Nucleic Acids Res 43, 3688–3700. https://doi.org/10.1093/nar/gkv152

Haase, A.D., Jaskiewicz, L., Zhang, H., Laine, S., Sack, R., Gatignol, A., Filipowicz, W., 2005. TRBP, a regulator of cellular PKR and HIV-1 virus expression, interacts with Dicer and functions in RNA silencing. EMBO Rep 6, 961–7.

Hahn, Y.S., Grakoui, A., Rice, C.M., Strauss, E.G., Strauss, J.H., 1989. Mapping of RNA-temperature-sensitive mutants of Sindbis virus: complementation group F mutants have lesions in nsP4. J Virol 63, 1194–1202.

Hale, V.L., Dennis, P.M., McBride, D.S., Nolting, J.M., Madden, C., Huey, D., Ehrlich, M., Grieser, J., Winston, J., Lombardi, D., Gibson, S., Saif, L., Killian, M.L., Lantz, K., Tell, R.M., Torchetti, M., Robbe-Austerman, S., Nelson, M.I., Faith, S.A., Bowman, A.S., 2022. SARS-CoV-2 infection in free-ranging white-tailed deer. Nature 602, 481–486. https://doi.org/10.1038/s41586-021-04353-x

Hammond, S.M., Boettcher, S., Caudy, A.A., Kobayashi, R., Hannon, G.J., 2001. Argonaute2, a link between genetic and biochemical analyses of RNAi. Science 293, 1146–1150. https://doi.org/10.1126/science.1064023

Hamre, D., Procknow, J.J., 1966. A New Virus Isolated from the Human Respiratory Tract. Proceedings of the Society for Experimental Biology and Medicine 121, 190–193. https://doi.org/10.3181/00379727-121-30734

Han, A.-P., Yu, C., Lu, L., Fujiwara, Y., Browne, C., Chin, G., Fleming, M., Leboulch, P., Orkin, S.H., Chen, J.-J., 2001. Heme-regulated eIF2α kinase (HRI) is required for translational regulation and survival of erythroid precursors in iron deficiency. The EMBO Journal 20, 6909–6918. https://doi.org/10.1093/emboj/20.23.6909

Han, D., Wang, L., Chen, B., Zhao, W., Liang, Y., Li, Y., Zhang, H., Liu, Y., Wang, X., Chen, T., Li, C., Song, X., Luo, D., Li, Z., Yang, Q., 2021. USP1-WDR48 deubiquitinase complex enhances TGF-β induced epithelial-mesenchymal transition of TNBC cells via stabilizing TAK1. Cell Cycle 20, 320–331. https://doi.org/10.1080/15384101.2021.1874695

Harding, H.P., Zeng, H., Zhang, Y., Jungries, R., Chung, P., Plesken, H., Sabatini, D.D., Ron, D., 2001. Diabetes mellitus and exocrine pancreatic dysfunction in perk-/- mice reveals a role for translational control in secretory cell survival. Mol Cell 7, 1153–1163. https://doi.org/10.1016/s1097-2765(01)00264-7

Hastie, E., Grdzelishvili, V.Z., 2012. Vesicular stomatitis virus as a flexible platform for oncolytic virotherapy against cancer. J Gen Virol 93, 2529–2545. https://doi.org/10.1099/vir.0.046672-0

Henrik Gad, H., Paulous, S., Belarbi, E., Diancourt, L., Drosten, C., Kümmerer, B.M., Plate, A.E., Caro, V., Desprès, P., 2012. The E2-E166K substitution restores Chikungunya virus growth in OAS3 expressing cells by acting on viral entry. Virology 434, 27–37. https://doi.org/10.1016/j.virol.2012.07.019

Her, L.S., Lund, E., Dahlberg, J.E., 1997. Inhibition of Ran guanosine triphosphatase-dependent nuclear transport by the matrix protein of vesicular stomatitis virus. Science 276, 1845–1848. https://doi.org/10.1126/science.276.5320.1845

Her, Z., Teng, T.-S., Tan, J.J.L., Teo, T.-H., Kam, Y.-W., Lum, F.-M., Lee, W.W.L., Gabriel, C., Melchiotti, R., Andiappan, A.K., Lulla, V., Lulla, A., Win, M.K., Chow, A., Biswas, S.K., Leo, Y.-S., Lecuit, M., Merits, A., Rénia, L., Ng, L.F.P., 2015. Loss of TLR3 aggravates CHIKV replication and pathology due to an altered virus-specific neutralizing antibody response. EMBO Mol Med 7, 24–41. https://doi.org/10.15252/emmm.201404459

Hinnebusch, A.G., 1993. Gene-specific translational control of the yeast GCN4 gene by phosphorylation of eukaryotic initiation factor 2. Mol Microbiol 10, 215–223. https://doi.org/10.1111/j.1365-2958.1993.tb01947.x

Ho, B.-C., Yu, I.-S., Lu, L.-F., Rudensky, A., Chen, H.-Y., Tsai, C.-W., Chang, Y.-L., Wu, C.-T., Chang, L.-Y., Shih, S.-R., Lin, S.-W., Lee, C.-N., Yang, P.-C., Yu, S.-L., 2014. Inhibition of miR-146a prevents enterovirus-induced death by restoring the production of type I interferon. Nat Commun 5, 3344. https://doi.org/10.1038/ncomms4344

Honda, K., Taniguchi, T., 2006. IRFs: master regulators of signalling by Toll-like receptors and cytosolic pattern-recognition receptors. Nat Rev Immunol 6, 644–658. https://doi.org/10.1038/nri1900

Huang, T.T., Kudo, N., Yoshida, M., Miyamoto, S., 2000. A nuclear export signal in the N-terminal regulatory domain of IκBα controls cytoplasmic localization of inactive NF-κB/IκBα complexes. Proceedings of the National Academy of Sciences 97, 1014–1019. https://doi.org/10.1073/pnas.97.3.1014

Hyde, J.L., Chen, R., Trobaugh, D.W., Diamond, M.S., Weaver, S.C., Klimstra, W.B., Wilusz, J., 2015. The 5′ and 3′ ends of alphavirus RNAs – Non-coding is not non-functional. Virus Research, Special Issue: Functions of the ends of positive strand RNA virus genomes 206, 99–107. https://doi.org/10.1016/j.virusres.2015.01.016

Isaacs, A., Lindenmann, J., 1957. Virus interference. I. The interferon. Proc R Soc Lond B Biol Sci 147, 258–267. https://doi.org/10.1098/rspb.1957.0048

Ishii, T., Kwon, H., Hiscott, J., Mosialos, G., Koromilas, A.E., 2001. Activation of the IκBα

kinase (IKK) complex by double-stranded RNA-binding defective and catalytic inactive mutants of the interferon-inducible protein kinase PKR. Oncogene 20, 1900–1912. https://doi.org/10.1038/sj.onc.1204267

Ito, T., Yang, M., May, W.S., 1999. RAX, a Cellular Activator for Double-stranded RNA-dependent Protein Kinase during Stress Signaling *. Journal of Biological Chemistry 274, 15427–15432. https://doi.org/10.1074/jbc.274.22.15427

Ivashkiv, L.B., Donlin, L.T., 2014. Regulation of type I interferon responses. Nature Reviews Immunology 14, 36–49. https://doi.org/10.1038/nri3581

Iwasaki, S., Kobayashi, M., Yoda, M., Sakaguchi, Y., Katsuma, S., Suzuki, T., Tomari, Y., 2010. Hsc70/Hsp90 chaperone machinery mediates ATP-dependent RISC loading of small RNA duplexes. Mol Cell 39, 292–299. https://doi.org/10.1016/j.molcel.2010.05.015

Jackson, L.A., Anderson, E.J., Rouphael, N.G., Roberts, P.C., Makhene, M., Coler, R.N., McCullough, M.P., Chappell, J.D., Denison, M.R., Stevens, L.J., Pruijssers, A.J., McDermott, A., Flach, B., Doria-Rose, N.A., Corbett, K.S., Morabito, K.M., O'Dell, S., Schmidt, S.D., Swanson, P.A., Padilla, M., Mascola, J.R., Neuzil, K.M., Bennett, H., Sun, W., Peters, E., Makowski, M., Albert, J., Cross, K., Buchanan, W., Pikaart-Tautges, R., Ledgerwood, J.E., Graham, B.S., Beigel, J.H., 2020. An mRNA Vaccine against SARS-CoV-2 — Preliminary Report. N Engl J Med NEJMoa2022483. https://doi.org/10.1056/NEJMoa2022483

Jacquet, S., Culbertson, M., Zhang, C., El Filali, A., De La Myre Mory, C., Pons, J.-B., Filippi-Codaccioni, O., Lauterbur, M.E., Ngoubangoye, B., Duhayer, J., Verez, C., Park, C., Dahoui, C., Carey, C.M., Brennan, G., Enard, D., Cimarelli, A., Rothenburg, S., Elde, N.C., Pontier, D., Etienne, L., 2022. Adaptive duplication and genetic diversification of protein kinase R contribute to the specificity of bat-virus interactions. Science Advances 8, eadd7540. https://doi.org/10.1126/sciadv.add7540

Jairak, W., Chamsai, E., Udom, K., Charoenkul, K., Chaiyawong, S., Techakriengkrai, N., Tangwangvivat, R., Suwannakarn, K., Amonsin, A., 2022. SARS-CoV-2 delta variant infection in domestic dogs and cats, Thailand. Sci Rep 12, 8403. https://doi.org/10.1038/s41598-022-12468-y

Jinek, M., Chylinski, K., Fonfara, I., Hauer, M., Doudna, J.A., Charpentier, E., 2012. A programmable dual-RNA-guided DNA endonuclease in adaptive bacterial immunity. Science

337, 816–821. https://doi.org/10.1126/science.1225829

Johnson, K.M., Martin, D.H., 1974. Venezuelan equine encephalitis. Adv Vet Sci Comp Med 18, 79–116.

Karin, M., Ben-Neriah, Y., 2000. Phosphorylation Meets Ubiquitination: The Control of NF-κB Activity. Annual Review of Immunology 18, 621–663. https://doi.org/10.1146/annurev.immunol.18.1.621

Kariuki Njenga, M., Nderitu, L., Ledermann, J.P., Ndirangu, A., Logue, C.H., Kelly, C.H.L., Sang, R., Sergon, K., Breiman, R., Powers, A.M., 2008. Tracking epidemic Chikungunya virus into the Indian Ocean from East Africa. J Gen Virol 89, 2754–2760. https://doi.org/10.1099/vir.0.2008/005413-0

Kato, H., Sato, S., Yoneyama, M., Yamamoto, M., Uematsu, S., Matsui, K., Tsujimura, T., Takeda, K., Fujita, T., Takeuchi, O., Akira, S., 2005. Cell Type-Specific Involvement of RIG-I in Antiviral Response. Immunity 23, 19–28. https://doi.org/10.1016/j.immuni.2005.04.010

Kato, H., Takeuchi, O., Sato, S., Yoneyama, M., Yamamoto, M., Matsui, K., Uematsu, S., Jung, A., Kawai, T., Ishii, K.J., Yamaguchi, O., Otsu, K., Tsujimura, T., Koh, C.-S., Reis e Sousa, C., Matsuura, Y., Fujita, T., Akira, S., 2006. Differential roles of MDA5 and RIG-I helicases in the recognition of RNA viruses. Nature 441, 101–105. https://doi.org/10.1038/nature04734

Katze, M.G., Wambach, M., Wong, M.L., Garfinkel, M., Meurs, E., Chong, K., Williams, B.R., Hovanessian, A.G., Barber, G.N., 1991. Functional expression and RNA binding analysis of the interferon-induced, double-stranded RNA-activated, 68,000-Mr protein kinase in a cell-free system. Mol Cell Biol 11, 5497–5505.

Kawagishi-Kobayashi, M., Silverman, J.B., Ung, T.L., Dever, T.E., 1997. Regulation of the protein kinase PKR by the vaccinia virus pseudosubstrate inhibitor K3L is dependent on residues conserved between the K3L protein and the PKR substrate eIF2alpha. Molecular and Cellular Biology 17, 4146–4158. https://doi.org/10.1128/MCB.17.7.4146

Kawahara, Y., Zinshteyn, B., Chendrimada, T.P., Shiekhattar, R., Nishikura, K., 2007a. RNA editing of the microRNA-151 precursor blocks cleavage by the Dicer–TRBP complex. EMBO reports 8, 763–769. https://doi.org/10.1038/sj.embor.7401011

Kennedy, E.M., Whisnant, A.W., Kornepati, A.V.R., Marshall, J.B., Bogerd, H.P., Cullen, B.R., 2015. Production of functional small interfering RNAs by an amino-terminal deletion mutant of human Dicer. PNAS 112, E6945–E6954. https://doi.org/10.1073/pnas.1513421112

Kim, A.S., Diamond, M.S., 2022. A molecular understanding of alphavirus entry and antibody protection. Nat Rev Microbiol 1–12. https://doi.org/10.1038/s41579-022-00825-7

Kim, D.Y., Firth, A.E., Atasheva, S., Frolova, E.I., Frolov, I., 2011. Conservation of a packaging signal and the viral genome RNA packaging mechanism in alphavirus evolution. J Virol 85, 8022–8036. https://doi.org/10.1128/JVI.00644-11

Kim, Y., Lee, J.H., Park, J.-E., Cho, J., Yi, H., Kim, V.N., 2014a. PKR is activated by cellular dsRNAs during mitosis and acts as a mitotic regulator. Genes Dev. 28, 1310–1322. https://doi.org/10.1101/gad.242644.114

Kim, Y., Park, J., Kim, S., Kim, M., Kang, M.-G., Kwak, C., Kang, M., Kim, B., Rhee, H.-W., Kim, V.N., 2018. PKR Senses Nuclear and Mitochondrial Signals by Interacting with Endogenous Double-Stranded RNAs. Molecular Cell 71, 1051-1063.e6. https://doi.org/10.1016/j.molcel.2018.07.029

Kim, Y., Yeo, J., Lee, J.H., Cho, J., Seo, D., Kim, J.-S., Kim, V.N., 2014b. Deletion of human tarbp2 reveals cellular microRNA targets and cell-cycle function of TRBP. Cell Rep 9, 1061–1074. https://doi.org/10.1016/j.celrep.2014.09.039

Kirchhoff, S., Wilhelm, D., Angel, P., Hauser, H., 1999. NFkappaB activation is required for interferon regulatory factor-1-mediated interferon beta induction. Eur J Biochem 261, 546–554. https://doi.org/10.1046/j.1432-1327.1999.00308.x

Kirui, J., Abidine, Y., Lenman, A., Islam, K., Gwon, Y.-D., Lasswitz, L., Evander, M., Bally, M., Gerold, G., 2021. The Phosphatidylserine Receptor TIM-1 Enhances Authentic Chikungunya Virus Cell Entry. Cells 10, 1828. https://doi.org/10.3390/cells10071828

Klimstra, W.B., Nangle, E.M., Smith, M.S., Yurochko, A.D., Ryman, K.D., 2003. DC-SIGN and L-SIGN Can Act as Attachment Receptors for Alphaviruses and Distinguish between Mosquito Cell- and Mammalian Cell-Derived Viruses. Journal of Virology 77, 12022–12032. https://doi.org/10.1128/JVI.77.22.12022-12032.2003

Knipe, D., Howley, P.M., 2013. Fields virology, Philadelphia. ed, PA: Wolters Kluwer/Lippincott Williams & Wilkins Health.

Kok, K.-H., Lui, P.-Y., Ng, M.-H.J., Siu, K.-L., Au, S.W.N., Jin, D.-Y., 2011. The double-stranded RNA-binding protein PACT functions as a cellular activator of RIG-I to facilitate innate antiviral response. Cell Host Microbe 9, 299–309. https://doi.org/10.1016/j.chom.2011.03.007

Kok, K.H., Ng, M.-H.J., Ching, Y.-P., Jin, D.-Y., 2007a. Human TRBP and PACT Directly Interact with Each Other and Associate with Dicer to Facilitate the Production of Small Interfering RNA. J. Biol. Chem. 282, 17649–17657. https://doi.org/10.1074/jbc.M611768200

Kong, J., Bie, Y., Ji, W., Xu, J., Lyu, B., Xiong, X., Qiu, Y., Zhou, X., 2023. Alphavirus infection triggers antiviral RNAi immunity in mammals. Cell Rep 42, 112441. https://doi.org/10.1016/j.celrep.2023.112441

Kozak, C.A., Gatignol, A., Graham, K., Jeang, K.T., Mcbride, O.W., 1995. Genetic mapping in human and mouse of the locus encoding TRBP, a protein that binds the TAR region of the human immunodeficiency virus (HIV-1). Genomics 25, 66–72. https://doi.org/10.1016/0888-7543(95)80110-8

Krishnamoorthy, T., Pavitt, G.D., Zhang, F., Dever, T.E., Hinnebusch, A.G., 2001. Tight Binding of the Phosphorylated α Subunit of Initiation Factor 2 (eIF2α) to the Regulatory Subunits of Guanine Nucleotide Exchange Factor eIF2B Is Required for Inhibition of Translation Initiation. Molecular and Cellular Biology 21, 5018–5030. https://doi.org/10.1128/MCB.21.15.5018-5030.2001

Krupovic, M., Koonin, E.V., 2015. Polintons: a hotbed of eukaryotic virus, transposon and plasmid evolution. Nat Rev Microbiol 13, 105–115. https://doi.org/10.1038/nrmicro3389

Kumar, A., Haque, J., Lacoste, J., Hiscott, J., Williams, B.R., 1994. Double-stranded RNA-dependent protein kinase activates transcription factor NF-kappa B by phosphorylating I kappa B. Proc Natl Acad Sci U S A 91, 6288–6292.

Kumar, A., Ishida, R., Strilets, T., Cole, J., Lopez-Orozco, J., Fayad, N., Felix-Lopez, A., Elaish, M., Evseev, D., Magor, K.E., Mahal, L.K., Nagata, L.P., Evans, D.H., Hobman, T.C., 2021. SARS-CoV-2 Nonstructural Protein 1 Inhibits the Interferon Response by Causing

Depletion of Key Host Signaling Factors. Journal of Virology 95, e00266-21. https://doi.org/10.1128/JVI.00266-21

Kumar, K.U., Srivastava, S.P., Kaufman, R.J., 1999. Double-stranded RNA-activated protein kinase (PKR) is negatively regulated by 60S ribosomal subunit protein L18. Mol Cell Biol 19, 1116–1125. https://doi.org/10.1128/MCB.19.2.1116

Kuo, R.-L., Chen, C.-J., Wang, R.Y.L., Huang, H.-I., Lin, Y.-H., Tam, E.-H., Tu, W.-J., Wu, S.-E., Shih, S.-R., 2019. Role of Enteroviral RNA-Dependent RNA Polymerase in Regulation of MDA5-Mediated Beta Interferon Activation. J Virol 93, e00132-19. https://doi.org/10.1128/JVI.00132-19

Kuo, R.-L., Kao, L.-T., Lin, S.-J., Wang, R.Y.-L., Shih, S.-R., 2013. MDA5 Plays a Crucial Role in Enterovirus 71 RNA-Mediated IRF3 Activation. PLOS ONE 8, e63431. https://doi.org/10.1371/journal.pone.0063431

Laakkonen, P., Ahola, T., Kääriäinen, L., 1996. The effects of palmitoylation on membrane association of Semliki forest virus RNA capping enzyme. J Biol Chem 271, 28567–28571. https://doi.org/10.1074/jbc.271.45.28567

Labadie, K., Larcher, T., Joubert, C., Mannioui, A., Delache, B., Brochard, P., Guigand, L., Dubreil, L., Lebon, P., Verrier, B., de Lamballerie, X., Suhrbier, A., Cherel, Y., Le Grand, R., Roques, P., 2010. Chikungunya disease in nonhuman primates involves long-term viral persistence in macrophages. J Clin Invest 120, 894–906. https://doi.org/10.1172/JCI40104

Laine, M., Luukkainen, R., Toivanen, A., 2004. Sindbis viruses and other alphaviruses as cause of human arthritic disease. Journal of Internal Medicine 256, 457–471. https://doi.org/10.1111/j.1365-2796.2004.01413.x

Lampio, A., Kilpeläinen, I., Pesonen, S., Karhi, K., Auvinen, P., Somerharju, P., Kääriäinen, L., 2000. Membrane binding mechanism of an RNA virus-capping enzyme. J Biol Chem 275, 37853–37859. https://doi.org/10.1074/jbc.M004865200

Lan, J., Ge, J., Yu, J., Shan, S., Zhou, H., Fan, S., Zhang, Q., Shi, X., Wang, Q., Zhang, L., Wang, X., 2020. Structure of the SARS-CoV-2 spike receptor-binding domain bound to the ACE2 receptor. Nature 581, 215–220. https://doi.org/10.1038/s41586-020-2180-5

Landers, V.D., Wilkey, D.W., Merchant, M.L., Mitchell, T.C., Sokoloski, K.J., 2021. The Alphaviral Capsid Protein Inhibits IRAK1-Dependent TLR Signaling. Viruses 13, 377. https://doi.org/10.3390/v13030377

LaStarza, M.W., Lemm, J.A., Rice, C.M., 1994. Genetic analysis of the nsP3 region of Sindbis virus: evidence for roles in minus-strand and subgenomic RNA synthesis. J Virol 68, 5781–5791.

Lau, N.C., Lim, L.P., Weinstein, E.G., Bartel, D.P., 2001. An abundant class of tiny RNAs with probable regulatory roles in Caenorhabditis elegans. Science 294, 858–862. https://doi.org/10.1126/science.1065062

Lee, D., Le Pen, J., Yatim, A., Dong, B., Aquino, Y., Ogishi, M., Pescarmona, R., Talouarn, E., Rinchai, D., Zhang, P., Perret, M., Liu, Z., Jordan, I., Elmas Bozdemir, S., Bayhan, G.I., Beaufils, C., Bizien, L., Bisiaux, A., Lei, W., Hasan, M., Chen, J., Gaughan, C., Asthana, A., Libri, V., Luna, J.M., Jaffré, F., Hoffmann, H.-H., Michailidis, E., Moreews, M., Seeleuthner, Y., Bilguvar, K., Mane, S., Flores, C., Zhang, Y., Arias, A.A., Bailey, R., Schlüter, A., Milisavljevic, B., Bigio, B., Le Voyer, T., Materna, M., Gervais, A., Moncada-Velez, M., Pala, F., Lazarov, T., Levy, R., Neehus, A.-L., Rosain, J., Peel, J., Chan, Y.-H., Morin, M.-P., Pino-Ramirez, R.M., Belkaya, S., Lorenzo, L., Anton, J., Delafontaine, S., Toubiana, J., Bajolle, F., Fumadó, V., DeDiego, M.L., Fidouh, N., Rozenberg, F., Pérez-Tur, J., Chen, S., Evans, T., Geissmann, F., Lebon, P., Weiss, S.R., Bonnet, D., Duval, X., CoV-Contact Cohort, COVID Human Genetic Effort, Pan-Hammarström, Q., Planas, A.M., Meyts, I., Haerynck, F., Pujol, A., Sancho-Shimizu, V., Dalgard, C.L., Bustamante, J., Puel, A., Boisson-Dupuis, S., Boisson, B., Maniatis, T., Zhang, Q., Bastard, P., Notarangelo, L., Béziat, V., Perez de Diego, R., Rodriguez-Gallego, C., Su, H.C., Lifton, R.P., Jouanguy, E., Cobat, A., Alsina, L., Keles, S., Haddad, E., Abel, L., Belot, A., Quintana-Murci, L., Rice, C.M., Silverman, R.H., Zhang, S.-Y., Casanova, J.-L., 2022. Inborn errors of OAS–RNase L in SARS-CoV-2–related multisystem inflammatory syndrome in children. Science 379, eabo3627. https://doi.org/10.1126/science.abo3627

Lee, H.Y., Zhou, K., Smith, A.M., Noland, C.L., Doudna, J.A., 2013. Differential roles of human Dicer-binding proteins TRBP and PACT in small RNA processing. Nucleic Acids Res 41, 6568–6576. https://doi.org/10.1093/nar/gkt361

Lee, J.Y., Moon, H.J., Lee, W.K., Chun, H.J., Han, C.W., Jeon, Y.-W., Lim, Y., Kim, Y.H.,

Yao, T.-P., Lee, K.-H., Jun, T.-Y., Rha, H.K., Kang, J.-K., 2006. Merlin facilitates ubiquitination and degradation of transactivation-responsive RNA-binding protein. Oncogene 25, 1143–1152. https://doi.org/10.1038/sj.onc.1209150

Lee, R.C., Ambros, V., 2001. An extensive class of small RNAs in Caenorhabditis elegans. Science 294, 862–864. https://doi.org/10.1126/science.1065329

Lee, R.C., Feinbaum, R.L., Ambros, V., 1993. The C. elegans heterochronic gene lin-4 encodes small RNAs with antisense complementarity to lin-14. Cell 75, 843–854. https://doi.org/10.1016/0092-8674(93)90529-y

Lee, S., Channappanavar, R., Kanneganti, T.-D., 2020. Coronaviruses: Innate Immunity, Inflammasome Activation, Inflammatory Cell Death, and Cytokines. Trends Immunol 41, 1083–1099. https://doi.org/10.1016/j.it.2020.10.005

Lee, W.-S., Webster, J.A., Madzokere, E.T., Stephenson, E.B., Herrero, L.J., 2019. Mosquito antiviral defense mechanisms: a delicate balance between innate immunity and persistent viral infection. Parasit Vectors 12, 165. https://doi.org/10.1186/s13071-019-3433-8

Lee, Y., Ahn, C., Han, J., Choi, H., Kim, J., Yim, J., Lee, J., Provost, P., Rådmark, O., Kim, S., Kim, V.N., 2003. The nuclear RNase III Drosha initiates microRNA processing. Nature 425, 415–419. https://doi.org/10.1038/nature01957

Lee, Y., Hur, I., Park, S.Y., Kim, Y.K., Suh, M.R., Kim, V.N., 2006. The role of PACT in the RNA silencing pathway. Embo J 25, 522–32.

Lee, Yoontae, Hur, I., Park, S.-Y., Kim, Y.-K., Suh, M.R., Kim, V.N., 2006. The role of PACT in the RNA silencing pathway. EMBO J 25, 522–532. https://doi.org/10.1038/sj.emboj.7600942

Lee, Y., Kim, M., Han, J., Yeom, K.-H., Lee, S., Baek, S.H., Kim, V.N., 2004. MicroRNA genes are transcribed by RNA polymerase II. The EMBO Journal 23, 4051–4060. https://doi.org/10.1038/sj.emboj.7600385

Lei, X., Han, N., Xiao, X., Jin, Q., He, B., Wang, J., 2014. Enterovirus 71 3C Inhibits Cytokine Expression through Cleavage of the TAK1/TAB1/TAB2/TAB3 Complex. Journal of Virology 88, 9830–9841. https://doi.org/10.1128/JVI.01425-14

Lei, X., Xiao, X., Xue, Q., Jin, Q., He, B., Wang, J., 2013. Cleavage of Interferon Regulatory Factor 7 by Enterovirus 71 3C Suppresses Cellular Responses. Journal of Virology 87, 1690–1698. https://doi.org/10.1128/JVI.01855-12

Lello, L.S., Bartholomeeusen, K., Wang, S., Coppens, S., Fragkoudis, R., Alphey, L., Ariën, K.K., Merits, A., Utt, A., 2021. nsP4 Is a Major Determinant of Alphavirus Replicase Activity and Template Selectivity. Journal of Virology 95, e00355-21. https://doi.org/10.1128/JVI.00355-21

Lemaire, P.A., Anderson, E., Lary, J., Cole, J.L., 2008. Mechanism of PKR Activation by dsRNA. Journal of Molecular Biology 381, 351–360. https://doi.org/10.1016/j.jmb.2008.05.056

Lenschow, D.J., Lai, C., Frias-Staheli, N., Giannakopoulos, N.V., Lutz, A., Wolff, T., Osiak, A., Levine, B., Schmidt, R.E., García-Sastre, A., Leib, D.A., Pekosz, A., Knobeloch, K.-P., Horak, I., Virgin, H.W., 2007. IFN-stimulated gene 15 functions as a critical antiviral molecule against influenza, herpes, and Sindbis viruses. Proceedings of the National Academy of Sciences 104, 1371–1376. https://doi.org/10.1073/pnas.0607038104

Letchworth, G.J., Rodriguez, L.L., Del cbarrera, J., 1999. Vesicular stomatitis. Vet J 157, 239–260. https://doi.org/10.1053/tvjl.1998.0303

Leung, J.Y.-S., Ng, M.M.-L., Chu, J.J.H., 2011. Replication of Alphaviruses: A Review on the Entry Process of Alphaviruses into Cells [WWW Document]. Advances in Virology. https://doi.org/10.1155/2011/249640

Levis, R., Schlesinger, S., Huang, H.V., 1990. Promoter for Sindbis virus RNA-dependent subgenomic RNA transcription. J Virol 64, 1726–1733. https://doi.org/10.1128/JVI.64.4.1726-1733.1990

Li, C., Zhu, Z., Du, X., Cao, W., Yang, F., Zhang, X., Feng, H., Li, D., Zhang, K., Liu, X., Zheng, H., 2017. Foot-and-mouth disease virus induces lysosomal degradation of host protein kinase PKR by 3C proteinase to facilitate virus replication. Virology 509, 222–231. https://doi.org/10.1016/j.virol.2017.06.023

Li, M., Shillinglaw, W., Henzel, W.J., Beg, A.A., 2001. The Rela(p65) subunit of NF-kappaB is essential for inhibiting double-stranded RNA-induced cytotoxicity. J Biol Chem 276, 1185–

1194. https://doi.org/10.1074/jbc.M006647200

Li, Q., Verma, I.M., 2002. NF-κB regulation in the immune system. Nat Rev Immunol 2, 725–734. https://doi.org/10.1038/nri910

Li, S., Peters, G.A., Ding, K., Zhang, X., Qin, J., Sen, G.C., 2006. Molecular basis for PKR activation by PACT or dsRNA. PNAS 103, 10005–10010. https://doi.org/10.1073/pnas.0602317103

Li, T., Kenney, A.D., Liu, H., Fiches, G.N., Zhou, D., Biswas, A., Que, J., Santoso, N., Yount, J.S., Zhu, J., 2021. SARS-CoV-2 Nsp14 activates NF-κB signaling and induces IL-8 upregulation. bioRxiv 2021.05.26.445787. https://doi.org/10.1101/2021.05.26.445787

Li, W., Qiao, J., You, Q., Zong, S., Peng, Q., Liu, Y., Hu, S., Liu, W., Li, S., Shu, X., Sun, B., 2021. SARS-CoV-2 Nsp5 Activates NF-κB Pathway by Upregulating SUMOylation of MAVS. Front Immunol 12, 750969. https://doi.org/10.3389/fimmu.2021.750969

Li, Yize, Banerjee, S., Wang, Y., Goldstein, S.A., Dong, B., Gaughan, C., Silverman, R.H., Weiss, S.R., 2016. Activation of RNase L is dependent on OAS3 expression during infection with diverse human viruses. Proc Natl Acad Sci U S A 113, 2241–2246. https://doi.org/10.1073/pnas.1519657113

Li, Yang, Basavappa, M., Lu, J., Dong, S., Cronkite, D.A., Prior, J.T., Reinecker, H.-C., Hertzog, P., Han, Y., Li, W.-X., Cheloufi, S., Karginov, F.V., Ding, S.-W., Jeffrey, K.L., 2016. Induction and suppression of antiviral RNA interference by influenza A virus in mammalian cells. Nat Microbiol 2, 16250. https://doi.org/10.1038/nmicrobiol.2016.250

Li, Y., Lu, J., Han, Y., Fan, X., Ding, S.-W., 2013. RNA interference functions as an antiviral immunity mechanism in mammals. Science 342, 231–234. https://doi.org/10.1126/science.1241911

Li, Y., Renner, D.M., Comar, C.E., Whelan, J.N., Reyes, H.M., Cardenas-Diaz, F.L., Truitt, R., Tan, L.H., Dong, B., Alysandratos, K.D., Huang, J., Palmer, J.N., Adappa, N.D., Kohanski, M.A., Kotton, D.N., Silverman, R.H., Yang, W., Morrisey, E.E., Cohen, N.A., Weiss, S.R., 2021. SARS-CoV-2 induces double-stranded RNA-mediated innate immune responses in respiratory epithelial-derived cells and cardiomyocytes. Proceedings of the National Academy of Sciences 118, e2022643118. https://doi.org/10.1073/pnas.2022643118

Li, Z., Wolff, K.C., Samuel, C.E., 2010. RNA adenosine deaminase ADAR1 deficiency leads to increased activation of protein kinase PKR and reduced vesicular stomatitis virus growth following interferon treatment. Virology 396, 316–322. https://doi.org/10.1016/j.virol.2009.10.026

Lin, R.-J., Yu, H.-P., Chang, B.-L., Tang, W.-C., Liao, C.-L., Lin, Y.-L., 2009. Distinct Antiviral Roles for Human 2′,5′-Oligoadenylate Synthetase Family Members against Dengue Virus Infection1. The Journal of Immunology 183, 8035–8043. https://doi.org/10.4049/jimmunol.0902728

Linder, A., Bothe, V., Linder, N., Schwarzlmueller, P., Dahlström, F., Bartenhagen, C., Dugas, M., Pandey, D., Thorn-Seshold, J., Boehmer, D.F.R., Koenig, L.M., Kobold, S., Schnurr, M., Raedler, J., Spielmann, G., Karimzadeh, H., Schmidt, A., Endres, S., Rothenfusser, S., 2021. Defective Interfering Genomes and the Full-Length Viral Genome Trigger RIG-I After Infection With Vesicular Stomatitis Virus in a Replication Dependent Manner. Frontiers in Immunology 12.

Liu, G., Cao, W., Salawudeen, A., Zhu, W., Emeterio, K., Safronetz, D., Banadyga, L., 2021. Vesicular Stomatitis Virus: From Agricultural Pathogen to Vaccine Vector. Pathogens 10, 1092. https://doi.org/10.3390/pathogens10091092

Liu, J., Li, Y., Liu, Q., Yao, Q., Wang, X., Zhang, H., Chen, R., Ren, L., Min, J., Deng, F., Yan, B., Liu, L., Hu, Z., Wang, M., Zhou, Y., 2021. SARS-CoV-2 cell tropism and multiorgan infection. Cell Discov 7, 1–4. https://doi.org/10.1038/s41421-021-00249-2

Liu, S., He, L., Wu, J., Wu, X., Xie, L., Dai, W., Chen, L., Xie, F., Liu, Z., 2021. DHX9 contributes to the malignant phenotypes of colorectal cancer via activating NF-κB signaling pathway. Cell Mol Life Sci 78, 8261–8281. https://doi.org/10.1007/s00018-021-04013-3

Liu, T., Zhang, L., Joo, D., Sun, S.-C., 2017. NF-κB signaling in inflammation. Sig Transduct Target Ther 2, 1–9. https://doi.org/10.1038/sigtrans.2017.23

Liu, Y., Qin, C., Rao, Y., Ngo, C., Feng, J.J., Zhao, J., Zhang, S., Wang, T.-Y., Carriere, J., Savas, A.C., Zarinfar, M., Rice, S., Yang, H., Yuan, W., Camarero, J.A., Yu, J., Chen, X.S., Zhang, C., Feng, P., 2021. SARS-CoV-2 Nsp5 Demonstrates Two Distinct Mechanisms Targeting RIG-I and MAVS To Evade the Innate Immune Response. mBio 12, e02335-21. https://doi.org/10.1128/mBio.02335-21

Liu, Yuanzhi, Wang, M., Cheng, A., Yang, Q., Wu, Y., Jia, R., Liu, M., Zhu, D., Chen, S., Zhang, S., Zhao, X.-X., Huang, J., Mao, S., Ou, X., Gao, Q., Wang, Y., Xu, Z., Chen, Z., Zhu, L., Luo, Q., Liu, Yunya, Yu, Y., Zhang, L., Tian, B., Pan, L., Rehman, M.U., Chen, X., 2020. The role of host eIF2α in viral infection. Virology Journal 17, 112. https://doi.org/10.1186/s12985-020-01362-6

Lobigs, M., Zhao, H.X., Garoff, H., 1990. Function of Semliki Forest virus E3 peptide in virus assembly: replacement of E3 with an artificial signal peptide abolishes spike heterodimerization and surface expression of E1. J Virol 64, 4346–4355.

López, P., Girardi, E., Mounce, B.C., Weiss, A., Chane-Woon-Ming, B., Messmer, M., Kaukinen, P., Kopp, A., Bortolamiol-Becet, D., Fendri, A., Vignuzzi, M., Brino, L., Pfeffer, S., 2020. High-Throughput Fluorescence-Based Screen Identifies the Neuronal MicroRNA miR-124 as a Positive Regulator of Alphavirus Infection. Journal of Virology 94, e02145-19. https://doi.org/10.1128/JVI.02145-19

Lopez, S., Yao, J.S., Kuhn, R.J., Strauss, E.G., Strauss, J.H., 1994. Nucleocapsid-glycoprotein interactions required for assembly of alphaviruses. J Virol 68, 1316–1323.

Lu, J., Yi, L., Zhao, J., Yu, J., Chen, Y., Lin, M.C., Kung, H.-F., He, M.-L., 2012. Enterovirus 71 Disrupts Interferon Signaling by Reducing the Level of Interferon Receptor 1. Journal of Virology 86, 3767–3776. https://doi.org/10.1128/JVI.06687-11

Lulla, A., Lulla, V., Tints, K., Ahola, T., Merits, A., 2006. Molecular Determinants of Substrate Specificity for Semliki Forest Virus Nonstructural Protease. J Virol 80, 5413–5422. https://doi.org/10.1128/JVI.00229-06

Lund, J.M., Alexopoulou, L., Sato, A., Karow, M., Adams, N.C., Gale, N.W., Iwasaki, A., Flavell, R.A., 2004. Recognition of single-stranded RNA viruses by Toll-like receptor 7. Proc Natl Acad Sci U S A 101, 5598–5603. https://doi.org/10.1073/pnas.0400937101

Luo, Z., Ge, M., Chen, J., Geng, Q., Tian, M., Qiao, Z., Bai, L., Zhang, Q., Zhu, C., Xiong, Y., Wu, K., Liu, F., Liu, Y., Wu, J., 2017. HRS plays an important role for TLR7 signaling to orchestrate inflammation and innate immunity upon EV71 infection. PLOS Pathogens 13, e1006585. https://doi.org/10.1371/journal.ppat.1006585

Lyles, D.S., 2000. Cytopathogenesis and Inhibition of Host Gene Expression by RNA Viruses.

Microbiol Mol Biol Rev 64, 709–724.

Ma, E., MacRae, I.J., Kirsch, J.F., Doudna, J.A., 2008. Autoinhibition of Human Dicer by Its Internal Helicase Domain. Journal of Molecular Biology 380, 237–243. https://doi.org/10.1016/j.jmb.2008.05.005

Maggi, L.B., Heitmeier, M.R., Scheuner, D., Kaufman, R.J., Buller, R.M., Corbett, J.A., 2000. Potential role of PKR in double-stranded RNA-induced macrophage activation. EMBO J 19, 3630–3638. https://doi.org/10.1093/emboj/19.14.3630

Maillard, P.V., Ciaudo, C., Marchais, A., Li, Y., Jay, F., Ding, S.W., Voinnet, O., 2013. Antiviral RNA interference in mammalian cells. Science 342, 235–238. https://doi.org/10.1126/science.1241930

Maillard, P.V., Veen, A.G.V. der, Deddouche-Grass, S., Rogers, N.C., Merits, A., Sousa, C.R. e, 2016. Inactivation of the type I interferon pathway reveals long double-stranded RNA-mediated RNA interference in mammalian cells. The EMBO Journal 35, 2505–2518. https://doi.org/10.15252/embj.201695086

Marques, J., Anwar, J., Eskildsen-Larsen, S., Rebouillat, D., Paludan, S.R., Sen, G., Williams, B.R.G., Hartmann, R., 2008. The p59 oligoadenylate synthetase-like protein possesses antiviral activity that requires the C-terminal ubiquitin-like domain. Journal of General Virology 89, 2767–2772. https://doi.org/10.1099/vir.0.2008/003558-0

Mathiot, C.C., Grimaud, G., Garry, P., Bouquety, J.C., Mada, A., Daguisy, A.M., Georges, A.J., 1990. An outbreak of human Semliki Forest virus infections in Central African Republic. Am J Trop Med Hyg 42, 386–393. https://doi.org/10.4269/ajtmh.1990.42.386

McAllister, C.S., Taghavi, N., Samuel, C.E., 2012. Protein kinase PKR amplification of interferon β induction occurs through initiation factor eIF-2α-mediated translational control. J Biol Chem 287, 36384–36392. https://doi.org/10.1074/jbc.M112.390039

McNab, F., Mayer-Barber, K., Sher, A., Wack, A., O'Garra, A., 2015. Type I interferons in infectious disease. Nat Rev Immunol 15, 87–103. https://doi.org/10.1038/nri3787

Meister, G., Landthaler, M., Peters, L., Chen, P.Y., Urlaub, H., Lührmann, R., Tuschl, T., 2005. Identification of Novel Argonaute-Associated Proteins. Current Biology 15, 2149–2155.

https://doi.org/10.1016/j.cub.2005.10.048

Meurs, E.F., Watanabe, Y., Kadereit, S., Barber, G.N., Katze, M.G., Chong, K., Williams, B.R., Hovanessian, A.G., 1992. Constitutive expression of human double-stranded RNA-activated p68 kinase in murine cells mediates phosphorylation of eukaryotic initiation factor 2 and partial resistance to encephalomyocarditis virus growth. J Virol 66, 5805–5814.

Mikuda, N., Kolesnichenko, M., Beaudette, P., Popp, O., Uyar, B., Sun, W., Tufan, A.B., Perder, B., Akalin, A., Chen, W., Mertins, P., Dittmar, G., Hinz, M., Scheidereit, C., 2018. The IκB kinase complex is a regulator of mRNA stability. EMBO J 37, e98658. https://doi.org/10.15252/embj.201798658

Miller, W.A., Koev, G., 2000. Synthesis of Subgenomic RNAs by Positive-Strand RNA Viruses. Virology 273, 1–8. https://doi.org/10.1006/viro.2000.0421

Minkoff, J.M., tenOever, B., 2023. Innate immune evasion strategies of SARS-CoV-2. Nat Rev Microbiol 21, 178–194. https://doi.org/10.1038/s41579-022-00839-1

Mishra, A.R., Byrareddy, S.N., Nayak, D., 2020. IFN-I Independent Antiviral Immune Response to Vesicular Stomatitis Virus Challenge in Mouse Brain. Vaccines (Basel) 8, 326. https://doi.org/10.3390/vaccines8020326

Mogensen, T.H., 2019. IRF and STAT Transcription Factors - From Basic Biology to Roles in Infection, Protective Immunity, and Primary Immunodeficiencies. Front Immunol 9, 3047. https://doi.org/10.3389/fimmu.2018.03047

Moreira Marrero, L., Botto Nuñez, G., Frabasile, S., Delfraro, A., 2022. Alphavirus Identification in Neotropical Bats. Viruses 14, 269. https://doi.org/10.3390/v14020269

Moustaqil, M., Ollivier, E., Chiu, H.-P., Van Tol, S., Rudolffi-Soto, P., Stevens, C., Bhumkar, A., Hunter, D.J.B., Freiberg, A.N., Jacques, D., Lee, B., Sierecki, E., Gambin, Y., 2021. SARS-CoV-2 proteases PLpro and 3CLpro cleave IRF3 and critical modulators of inflammatory pathways (NLRP12 and TAB1): implications for disease presentation across species. Emerging Microbes & Infections 10, 178–195. https://doi.org/10.1080/22221751.2020.1870414

Much, C., Auchynnikava, T., Pavlinic, D., Buness, A., Rappsilber, J., Benes, V., Allshire, R., O'Carroll, D., 2016. Endogenous Mouse Dicer Is an Exclusively Cytoplasmic Protein. PLOS

Genetics 12, e1006095. https://doi.org/10.1371/journal.pgen.1006095

Mueller, S., Gausson, V., Vodovar, N., Deddouche, S., Troxler, L., Perot, J., Pfeffer, S., Hoffmann, J.A., Saleh, M.-C., Imler, J.-L., 2010. RNAi-mediated immunity provides strong protection against the negative-strand RNA vesicular stomatitis virus in Drosophila. Proceedings of the National Academy of Sciences 107, 19390–19395. https://doi.org/10.1073/pnas.1014378107

Murphy, A.K., Clennon, J.A., Vazquez-Prokopec, G., Jansen, C.C., Frentiu, F.D., Hafner, L.M., Hu, W., Devine, G.J., 2020. Spatial and temporal patterns of Ross River virus in south east Queensland, Australia: identification of hot spots at the rural-urban interface. BMC Infectious Diseases 20, 722. https://doi.org/10.1186/s12879-020-05411-x

Myles, K.M., Kelly, C.L.H., Ledermann, J.P., Powers, A.M., 2006. Effects of an Opal Termination Codon Preceding the nsP4 Gene Sequence in the O'Nyong-Nyong Virus Genome on Anopheles gambiae Infectivity. Journal of Virology 80, 4992–4997. https://doi.org/10.1128/JVI.80.10.4992-4997.2006

Myles, K.M., Wiley, M.R., Morazzani, E.M., Adelman, Z.N., 2008. Alphavirus-derived small RNAs modulate pathogenesis in disease vector mosquitoes. Proceedings of the National Academy of Sciences 105, 19938–19943. https://doi.org/10.1073/pnas.0803408105

Nakamura, T., Kunz, R.C., Zhang, C., Kimura, T., Yuan, C.L., Baccaro, B., Namiki, Y., Gygi, S.P., Hotamisligil, G.S., 2015. A critical role for PKR complexes with TRBP in Immunometabolic regulation and eIF2α phosphorylation in obesity. Cell Rep 11, 295–307. https://doi.org/10.1016/j.celrep.2015.03.021

Nasar, F., Palacios, G., Gorchakov, R.V., Guzman, H., Da Rosa, A.P.T., Savji, N., Popov, V.L., Sherman, M.B., Lipkin, W.I., Tesh, R.B., Weaver, S.C., 2012. Eilat virus, a unique alphavirus with host range restricted to insects by RNA replication. Proc Natl Acad Sci U S A 109, 14622–14627. https://doi.org/10.1073/pnas.1204787109

Nayak, G., Bhuyan, S.K., Bhuyan, R., Sahu, A., Kar, D., Kuanar, A., 2022. Global emergence of Enterovirus 71: a systematic review. Beni Suef Univ J Basic Appl Sci 11, 78. https://doi.org/10.1186/s43088-022-00258-4

Nie, Y., Hammond, G.L., Yang, J.-H., 2007. Double-stranded RNA deaminase ADAR1

increases host susceptibility to virus infection. J Virol 81, 917–923. https://doi.org/10.1128/JVI.01527-06

Nielsen, C.P.S., Arribas-Hernández, L., Han, L., Andersen, S.U., Pumplin, N., Brodersen, P., 2023. Evidence for an RNAi-independent role of DICER-LIKE2 in conferring growth inhibition and basal antiviral resistance. https://doi.org/10.1101/2023.01.10.523401

Nilsson-Payant, B.E., Uhl, S., Grimont, A., Doane, A.S., Cohen, P., Patel, R.S., Higgins, C.A., Acklin, J.A., Bram, Y., Chandar, V., Blanco-Melo, D., Panis, M., Lim, J.K., Elemento, O., Schwartz, R.E., Rosenberg, B.R., Chandwani, R., tenOever, B.R., 2021. The NF-κB Transcriptional Footprint Is Essential for SARS-CoV-2 Replication. Journal of Virology 95, 10.1128/jvi.01257-21. https://doi.org/10.1128/jvi.01257-21

Norder, H., Lundström, J.O., Kozuch, O., Magnius, L.O., 1996. Genetic relatedness of Sindbis virus strains from Europe, Middle East, and Africa. Virology 222, 440–445. https://doi.org/10.1006/viro.1996.0441

Nowee, G., Bakker, J.W., Geertsema, C., Ros, V.I.D., Göertz, G.P., Fros, J.J., Pijlman, G.P., 2021. A Tale of 20 Alphaviruses; Inter-species Diversity and Conserved Interactions Between Viral Non-structural Protein 3 and Stress Granule Proteins. Frontiers in Cell and Developmental Biology 9.

Oeckinghaus, A., Ghosh, S., 2009. The NF-κB Family of Transcription Factors and Its Regulation. Cold Spring Harb Perspect Biol 1, a000034. https://doi.org/10.1101/cshperspect.a000034

Olajide, O.A., Iwuanyanwu, V.U., Adegbola, O.D., Al-Hindawi, A.A., 2022. SARS-CoV-2 Spike Glycoprotein S1 Induces Neuroinflammation in BV-2 Microglia. Mol Neurobiol 59, 445–458. https://doi.org/10.1007/s12035-021-02593-6

Olsen, P.H., Ambros, V., 1999. The lin-4 regulatory RNA controls developmental timing in Caenorhabditis elegans by blocking LIN-14 protein synthesis after the initiation of translation. Dev Biol 216, 671–680. https://doi.org/10.1006/dbio.1999.9523

Omaña-Cepeda, C., Martínez-Valverde, A., del Mar Sabater- Recolons, M., Jané-Salas, E., Marí-Roig, A., López-López, J., 2016. A literature review and case report of hand, foot and mouth disease in an immunocompetent adult. BMC Res Notes 9, 165.

https://doi.org/10.1186/s13104-016-1973-y

Ong, K.C., Badmanathan, M., Devi, S., Leong, K.L., Cardosa, M.J., Wong, K.T., 2008. Pathologic characterization of a murine model of human enterovirus 71 encephalomyelitis. J Neuropathol Exp Neurol 67, 532–542. https://doi.org/10.1097/NEN.0b013e31817713e7

Onomoto, K., Jogi, M., Yoo, J.-S., Narita, R., Morimoto, S., Takemura, A., Sambhara, S., Kawaguchi, A., Osari, S., Nagata, K., Matsumiya, T., Namiki, H., Yoneyama, M., Fujita, T., 2012. Critical Role of an Antiviral Stress Granule Containing RIG-I and PKR in Viral Detection and Innate Immunity. PLoS One 7, e43031. https://doi.org/10.1371/journal.pone.0043031

Onomoto, K., Yoneyama, M., Fung, G., Kato, H., Fujita, T., 2014. Antiviral innate immunity and stress granule responses. Trends Immunol 35, 420–428. https://doi.org/10.1016/j.it.2014.07.006

Ota, H., Sakurai, M., Gupta, R., Valente, L., Wulff, B.-E., Ariyoshi, K., Iizasa, H., Davuluri, R.V., Nishikura, K., 2013. ADAR1 forms a complex with Dicer to promote microRNA processing and RNA-induced gene silencing. Cell 153, 575–589. https://doi.org/10.1016/j.cell.2013.03.024

Otsuka, M., Jing, Q., Georgel, P., New, L., Chen, J., Mols, J., Kang, Y.J., Jiang, Z., Du, X., Cook, R., Das, S.C., Pattnaik, A.K., Beutler, B., Han, J., 2007. Hypersusceptibility to Vesicular Stomatitis Virus Infection in Dicer1-Deficient Mice Is Due to Impaired miR24 and miR93 Expression. Immunity 27, 123–134. https://doi.org/10.1016/j.immuni.2007.05.014

Park, M.S., Phan, H.-D., Busch, F., Hinckley, S.H., Brackbill, J.A., Wysocki, V.H., Nakanishi, K., 2017. Human Argonaute3 has slicer activity. Nucleic Acids Res 45, 11867–11877. https://doi.org/10.1093/nar/gkx916

Parrott, M.M., Sitarski, S.A., Arnold, R.J., Picton, L.K., Hill, R.B., Mukhopadhyay, S., 2009. Role of Conserved Cysteines in the Alphavirus E3 Protein. J Virol 83, 2584–2591. https://doi.org/10.1128/JVI.02158-08

Patel, C.V., Handy, I., Goldsmith, T., Patel, R.C., 2000. PACT, a Stress-modulated Cellular Activator of Interferon-induced Double-stranded RNA-activated Protein Kinase, PKR. J. Biol. Chem. 275, 37993–37998. https://doi.org/10.1074/jbc.M004762200

Patel, R.C., Sen, G.C., 1998. PACT, a protein activator of the interferon-induced protein kinase, PKR. The EMBO Journal 17, 4379–4390. https://doi.org/10.1093/emboj/17.15.4379

Pawlica, P., Yario, T.A., White, S., Wang, J., Moss, W.N., Hui, P., Vinetz, J.M., Steitz, J.A., 2021. SARS-CoV-2 expresses a microRNA-like small RNA able to selectively repress host genes. Proceedings of the National Academy of Sciences 118, e2116668118. https://doi.org/10.1073/pnas.2116668118

Peters, G.A., Hartmann, R., Qin, J., Sen, G.C., 2001. Modular Structure of PACT: Distinct Domains for Binding and Activating PKR. Molecular and Cellular Biology 21, 1908–1920. https://doi.org/10.1128/MCB.21.6.1908-1920.2001

Peters, G.A., Li, S., Sen, G.C., 2006. Phosphorylation of Specific Serine Residues in the PKR Activation Domain of PACT Is Essential for Its Ability to Mediate Apoptosis*. Journal of Biological Chemistry 281, 35129–35136. https://doi.org/10.1074/jbc.M607714200

Pfaller, C.K., Li, Z., George, C.X., Samuel, C.E., 2011. Protein kinase PKR and RNA adenosine deaminase ADAR1: new roles for old players as modulators of the interferon response. Current Opinion in Immunology, Special section: Cytokines/Immunogenetics and transplantation 23, 573–582. https://doi.org/10.1016/j.coi.2011.08.009

Pflugheber, J., Fredericksen, B., Sumpter, R., Wang, C., Ware, F., Sodora, D.L., Gale, M., 2002. Regulation of PKR and IRF-1 during hepatitis C virus RNA replication. Proceedings of the National Academy of Sciences 99, 4650–4655. https://doi.org/10.1073/pnas.062055699

Pham, A.M., Maria, F.G.S., Lahiri, T., Friedman, E., Marié, I.J., Levy, D.E., 2016. PKR Transduces MDA5-Dependent Signals for Type I IFN Induction. PLOS Pathogens 12, e1005489. https://doi.org/10.1371/journal.ppat.1005489

Phillips, A.T., Rico, A.B., Stauft, C.B., Hammond, S.L., Aboellail, T.A., Tjalkens, R.B., Olson, K.E., 2016. Entry Sites of Venezuelan and Western Equine Encephalitis Viruses in the Mouse Central Nervous System following Peripheral Infection. J Virol 90, 5785–5796. https://doi.org/10.1128/JVI.03219-15

Pietilä, M.K., van Hemert, M.J., Ahola, T., 2018. Purification of Highly Active Alphavirus Replication Complexes Demonstrates Altered Fractionation of Multiple Cellular Membranes. J Virol 92, e01852-17. https://doi.org/10.1128/JVI.01852-17

Pittman, P.R., Makuch, R.S., Mangiafico, J.A., Cannon, T.L., Gibbs, P.H., Peters, C.J., 1996. Long-term duration of detectable neutralizing antibodies after administration of live-attenuated VEE vaccine and following booster vaccination with inactivated VEE vaccine. Vaccine 14, 337–343. https://doi.org/10.1016/0264-410x(95)00168-z

Poirier, E.Z., Buck, M.D., Chakravarty, P., Carvalho, J., Frederico, B., Cardoso, A., Healy, L., Ulferts, R., Beale, R., Reis e Sousa, C., 2021. An isoform of Dicer protects mammalian stem cells against multiple RNA viruses. Science 373, 231–236. https://doi.org/10.1126/science.abg2264

Ponia, S.S., Robertson, S.J., McNally, K.L., Subramanian, G., Sturdevant, G.L., Lewis, M., Jessop, F., Kendall, C., Gallegos, D., Hay, A., Schwartz, C., Rosenke, R., Saturday, G., Bosio, C.M., Martens, C., Best, S.M., 2021. Mitophagy antagonism by ZIKV reveals Ajuba as a regulator of PINK1 signaling, PKR-dependent inflammation, and viral invasion of tissues. Cell Reports 37, 109888. https://doi.org/10.1016/j.celrep.2021.109888

Powers, A.M., Brault, A.C., Shirako, Y., Strauss, E.G., Kang, W., Strauss, J.H., Weaver, S.C., 2001. Evolutionary relationships and systematics of the alphaviruses. J Virol 75, 10118–10131. https://doi.org/10.1128/JVI.75.21.10118-10131.2001

Powers, A.M., Logue, C.H., 2007. Changing patterns of chikungunya virus: re-emergence of a zoonotic arbovirus. J Gen Virol 88, 2363–2377. https://doi.org/10.1099/vir.0.82858-0

Pujantell, M., Riveira-Muñoz, E., Badia, R., Castellví, M., Garcia-Vidal, E., Sirera, G., Puig, T., Ramirez, C., Clotet, B., Esté, J.A., Ballana, E., 2017. RNA editing by ADAR1 regulates innate and antiviral immune functions in primary macrophages. Sci Rep 7, 13339. https://doi.org/10.1038/s41598-017-13580-0

Qian, Q., Zhou, H., Shu, T., Mu, J., Fang, Y., Xu, J., Li, T., Kong, J., Qiu, Y., Zhou, X., 2020. The Capsid Protein of Semliki Forest Virus Antagonizes RNA Interference in Mammalian Cells. J Virol 94, e01233-19. https://doi.org/10.1128/JVI.01233-19

Qiu, Y., Xu, Y., Zhang, Y., Zhou, H., Deng, Y.-Q., Li, X.-F., Miao, M., Zhang, Q., Zhong, B., Hu, Y., Zhang, F.-C., Wu, L., Qin, C.-F., Zhou, X., 2017. Human Virus-Derived Small RNAs Can Confer Antiviral Immunity in Mammals. Immunity 46, 992-1004.e5. https://doi.org/10.1016/j.immuni.2017.05.006

Quiroz, E., Moreno, N., Peralta, P.H., Tesh, R.B., 1988. A human case of encephalitis associated with vesicular stomatitis virus (Indiana serotype) infection. Am J Trop Med Hyg 39, 312–314. https://doi.org/10.4269/ajtmh.1988.39.312

Ramsey, J., Mukhopadhyay, S., 2017. Disentangling the Frames, the State of Research on the Alphavirus 6K and TF Proteins. Viruses 9, 228. https://doi.org/10.3390/v9080228

Reeves, W.C., Hutson, G.A., Bellamy, R.E., Scrivani, R.P., 1958. Chronic latent infections of birds with Western equine encephalomyelitis virus. Proc Soc Exp Biol Med 97, 733–736. https://doi.org/10.3181/00379727-97-23862

Reineke, L.C., Lloyd, R.E., 2014. The Stress Granule Protein G3BP1 Recruits Protein Kinase R To Promote Multiple Innate Immune Antiviral Responses. J Virol 89, 2575–2589. https://doi.org/10.1128/JVI.02791-14

Reinhart, B.J., Slack, F.J., Basson, M., Pasquinelli, A.E., Bettinger, J.C., Rougvie, A.E., Horvitz, H.R., Ruvkun, G., 2000. The 21-nucleotide let-7 RNA regulates developmental timing in Caenorhabditis elegans. Nature 403, 901–906. https://doi.org/10.1038/35002607

Ren, X., Wang, D., Zhang, G., Zhou, T., Wei, Z., Yang, Y., Zheng, Y., Lei, X., Tao, W., Wang, A., Li, M., Flavell, R.A., Zhu, S., 2023. Nucleic DHX9 cooperates with STAT1 to transcribe interferon-stimulated genes. Science Advances 9, eadd5005. https://doi.org/10.1126/sciadv.add5005

Robb, G.B., Rana, T.M., 2007. RNA helicase A interacts with RISC in human cells and functions in RISC loading. Mol. Cell 26, 523–537. https://doi.org/10.1016/j.molcel.2007.04.016

Rodríguez, L.L., 2002. Emergence and re-emergence of vesicular stomatitis in the United States. Virus Res 85, 211–219. https://doi.org/10.1016/s0168-1702(02)00026-6

Rogers, KJ., Jones-Burrage, S., Maury, W., Mukhopadhyay, S., 2020. TF protein of Sindbis virus antagonizes host type I interferon responses in a palmitoylation-dependent manner. Virology 542, 63–70. https://doi.org/10.1016/j.virol.2020.01.001

Romano, P.R., Garcia-Barrio, M.T., Zhang, X., Wang, Q., Taylor, D.R., Zhang, F., Herring, C., Mathews, M.B., Qin, J., Hinnebusch, A.G., 1998. Autophosphorylation in the Activation Loop

Is Required for Full Kinase Activity In Vivo of Human and Yeast Eukaryotic Initiation Factor 2α Kinases PKR and GCN2. Molecular and Cellular Biology 18, 2282–2297. https://doi.org/10.1128/MCB.18.4.2282

Roques, P., Fritzer, A., Dereuddre-Bosquet, N., Wressnigg, N., Hochreiter, R., Bossevot, L., Pascal, Q., Guehenneux, F., Bitzer, A., Ramljak, I.C., Grand, R.L., Lundberg, U., Meinke, A., 2022. Effectiveness of CHIKV vaccine VLA1553 demonstrated by passive transfer of human sera. JCI Insight 7. https://doi.org/10.1172/jci.insight.160173

Rothenburg, S., Seo, E.J., Gibbs, J.S., Dever, T.E., Dittmar, K., 2009. Rapid evolution of protein kinase PKR alters sensitivity to viral inhibitors. Nat Struct Mol Biol 16, 63–70. https://doi.org/10.1038/nsmb.1529

Rozo-Lopez, P., Drolet, B.S., Londoño-Renteria, B., 2018. Vesicular Stomatitis Virus Transmission: A Comparison of Incriminated Vectors. Insects 9, 190. https://doi.org/10.3390/insects9040190

Rusch, L., Zhou, A., Silverman, R.H., 2000. Caspase-dependent apoptosis by 2',5'-oligoadenylate activation of RNase L is enhanced by IFN-beta. J Interferon Cytokine Res 20, 1091–1100. https://doi.org/10.1089/107999000750053762

Ruvolo, P.P., Gao, F., Blalock, W.L., Deng, X., May, W.S., 2001. Ceramide Regulates Protein Synthesis by a Novel Mechanism Involving the Cellular PKR Activator RAX *. Journal of Biological Chemistry 276, 11754–11758. https://doi.org/10.1074/jbc.M011400200

Ryan, C., Ivanova, L., Schlesinger, M.J., 1998. Effects of site-directed mutations of transmembrane cysteines in sindbis virus E1 and E2 glycoproteins on palmitylation and virus replication. Virology 249, 62–67. https://doi.org/10.1006/viro.1998.9281

Ryman, K.D., Klimstra, W.B., Nguyen, K.B., Biron, C.A., Johnston, R.E., 2000. Alpha/Beta Interferon Protects Adult Mice from Fatal Sindbis Virus Infection and Is an Important Determinant of Cell and Tissue Tropism. J Virol 74, 3366–3378.

Sadler, A.J., Latchoumanin, O., Hawkes, D., Mak, J., Williams, B.R.G., 2009. An Antiviral Response Directed by PKR Phosphorylation of the RNA Helicase A. PLOS Pathogens 5, e1000311. https://doi.org/10.1371/journal.ppat.1000311

Sadler, A.J., Williams, B.R.G., 2007. Structure and Function of the Protein Kinase R, in: Pitha, P.M. (Ed.), Interferon: The 50th Anniversary, Current Topics in Microbiology and Immunology. Springer, Berlin, Heidelberg, pp. 253–292. https://doi.org/10.1007/978-3-540-71329-6_13

Sakurai, H., Chiba, H., Miyoshi, H., Sugita, T., Toriumi, W., 1999. IκB Kinases Phosphorylate NF-κB p65 Subunit on Serine 536 in the Transactivation Domain *. Journal of Biological Chemistry 274, 30353–30356. https://doi.org/10.1074/jbc.274.43.30353

Samuel, C.E., 1979. Mechanism of interferon action: phosphorylation of protein synthesis initiation factor eIF-2 in interferon-treated human cells by a ribosome-associated kinase processing site specificity similar to hemin-regulated rabbit reticulocyte kinase. Proc Natl Acad Sci U S A 76, 600–604. https://doi.org/10.1073/pnas.76.2.600

Samuel, C.E., Duncan, R., Knutson, G.S., Hershey, J.W., 1984. Mechanism of interferon action. Increased phosphorylation of protein synthesis initiation factor eIF-2 alpha in interferon-treated, reovirus-infected mouse L929 fibroblasts in vitro and in vivo. J Biol Chem 259, 13451–13457.

Santoro, M.G., Rossi, A., Amici, C., 2003. NF-κB and virus infection: who controls whom. The EMBO Journal 22, 2552–2560. https://doi.org/10.1093/emboj/cdg267

Sanz, M.A., García-Moreno, M., Carrasco, L., 2015. Inhibition of host protein synthesis by Sindbis virus: correlation with viral RNA replication and release of nuclear proteins to the cytoplasm. Cellular Microbiology 17, 520–541. https://doi.org/10.1111/cmi.12381

Schäfer, A., Brooke, C.B., Whitmore, A.C., Johnston, R.E., 2011. The role of the blood-brain barrier during Venezuelan equine encephalitis virus infection. J Virol 85, 10682–10690. https://doi.org/10.1128/JVI.05032-11

Schilte, C., Couderc, T., Chretien, F., Sourisseau, M., Gangneux, N., Guivel-Benhassine, F., Kraxner, A., Tschopp, J., Higgs, S., Michault, A., Arenzana-Seisdedos, F., Colonna, M., Peduto, L., Schwartz, O., Lecuit, M., Albert, M.L., 2010. Type I IFN controls chikungunya virus via its action on nonhematopoietic cells. J Exp Med 207, 429–442. https://doi.org/10.1084/jem.20090851

Schoggins, J.W., Wilson, S.J., Panis, M., Murphy, M.Y., Jones, C.T., Bieniasz, P., Rice, C.M.,

2011. A diverse range of gene products are effectors of the type I interferon antiviral response. Nature 472, 481–485. https://doi.org/10.1038/nature09907

Scholte, F.E.M., Tas, A., Albulescu, I.C., Žusinaite, E., Merits, A., Snijder, E.J., van Hemert, M.J., 2015. Stress granule components G3BP1 and G3BP2 play a proviral role early in Chikungunya virus replication. J Virol 89, 4457–4469. https://doi.org/10.1128/JVI.03612-14

Schulz, O., Pichlmair, A., Rehwinkel, J., Rogers, N.C., Scheuner, D., Kato, H., Takeuchi, O., Akira, S., Kaufman, R.J., Reis e Sousa, C., 2010. Protein kinase R contributes to immunity against specific viruses by regulating interferon mRNA integrity. Cell Host Microbe 7, 354–361. https://doi.org/10.1016/j.chom.2010.04.007

Schuster, S., Overheul, G.J., Bauer, L., van Kuppeveld, F.J.M., van Rij, R.P., 2019. No evidence for viral small RNA production and antiviral function of Argonaute 2 in human cells. Sci Rep 9, 13752. https://doi.org/10.1038/s41598-019-50287-w

Segev, Y., Barrera, I., Ounallah-Saad, H., Wibrand, K., Sporild, I., Livne, A., Rosenberg, T., David, O., Mints, M., Bramham, C.R., Rosenblum, K., 2015. PKR Inhibition Rescues Memory Deficit and ATF4 Overexpression in ApoE ε4 Human Replacement Mice. J. Neurosci. 35, 12986–12993. https://doi.org/10.1523/JNEUROSCI.5241-14.2015

Silva, L.A., Khomandiak, S., Ashbrook, A.W., Weller, R., Heise, M.T., Morrison, T.E., Dermody, T.S., 2014. A Single-Amino-Acid Polymorphism in Chikungunya Virus E2 Glycoprotein Influences Glycosaminoglycan Utilization. Journal of Virology 88, 2385–2397. https://doi.org/10.1128/JVI.03116-13

Singh, D., Yi, S.V., 2021. On the origin and evolution of SARS-CoV-2. Exp Mol Med 53, 537–547. https://doi.org/10.1038/s12276-021-00604-z

Singh, M., Castillo, D., Patel, C.V., Patel, R.C., 2011. Stress-Induced Phosphorylation of PACT Reduces Its Interaction with TRBP and Leads to PKR Activation. Biochemistry 50, 4550–4560. https://doi.org/10.1021/bi200104h

Singh, M., Chazal, M., Quarato, P., Bourdon, L., Malabat, C., Vallet, T., Vignuzzi, M., van der Werf, S., Behillil, S., Donati, F., Sauvonnet, N., Nigro, G., Bourgine, M., Jouvenet, N., Cecere, G., 2022. A virus-derived microRNA targets immune response genes during SARS-CoV-2 infection. EMBO reports 23, e54341. https://doi.org/10.15252/embr.202154341

Singh, M., Fowlkes, V., Handy, I., Patel, C.V., Patel, R.C., 2009. Essential Role of PACT-Mediated PKR Activation in Tunicamycin-induced Apoptosis. J Mol Biol 385, 457–468. https://doi.org/10.1016/j.jmb.2008.10.068

Singh, M., Patel, R.C., 2012. Increased interaction between PACT molecules in response to stress signals is required for PKR activation. Journal of Cellular Biochemistry 113, 2754–2764. https://doi.org/10.1002/jcb.24152

Singh, S.K., Unni, S.K., 2011. Chikungunya virus: host pathogen interaction. Reviews in Medical Virology 21, 78–88. https://doi.org/10.1002/rmv.681

Smithburn, K.C., Haddow, A.J., 1944. Semliki Forest Virus: I. Isolation and Pathogenic Properties. The Journal of Immunology 49, 141–157. https://doi.org/10.4049/jimmunol.49.3.141

Staples, J.E., Breiman, R.F., Powers, A.M., 2009. Chikungunya Fever: An Epidemiological Review of a Re-Emerging Infectious Disease. CLIN INFECT DIS 49, 942–948. https://doi.org/10.1086/605496

Stojdl, D.F., Abraham, N., Knowles, S., Marius, R., Brasey, A., Lichty, B.D., Brown, E.G., Sonenberg, N., Bell, J.C., 2000. The murine double-stranded RNA-dependent protein kinase PKR is required for resistance to vesicular stomatitis virus. J Virol 74, 9580–9585. https://doi.org/10.1128/jvi.74.20.9580-9585.2000

Stojdl, D.F., Lichty, B.D., tenOever, B.R., Paterson, J.M., Power, A.T., Knowles, S., Marius, R., Reynard, J., Poliquin, L., Atkins, H., Brown, E.G., Durbin, R.K., Durbin, J.E., Hiscott, J., Bell, J.C., 2003. VSV strains with defects in their ability to shutdown innate immunity are potent systemic anti-cancer agents. Cancer Cell 4, 263–275. https://doi.org/10.1016/S1535-6108(03)00241-1

Strauss, E.G., Rice, C.M., Strauss, J.H., 1983. Sequence coding for the alphavirus nonstructural proteins is interrupted by an opal termination codon. Proc Natl Acad Sci U S A 80, 5271–5275.

Strauss, J.H., Strauss, E.G., 1994. The alphaviruses: gene expression, replication, and evolution. Microbiol Rev 58, 491–562.

Stromberg, Z.R., Fischer, W., Bradfute, S.B., Kubicek-Sutherland, J.Z., Hraber, P., 2020.

Vaccine Advances against Venezuelan, Eastern, and Western Equine Encephalitis Viruses. Vaccines (Basel) 8, 273. https://doi.org/10.3390/vaccines8020273

Su, C.-M., Wang, L., Yoo, D., 2021. Activation of NF-κB and induction of proinflammatory cytokine expressions mediated by ORF7a protein of SARS-CoV-2. Sci Rep 11, 13464. https://doi.org/10.1038/s41598-021-92941-2

Suhrbier, A., 2019. Rheumatic manifestations of chikungunya: emerging concepts and interventions. Nat Rev Rheumatol 15, 597–611. https://doi.org/10.1038/s41584-019-0276-9

Suhrbier, A., Jaffar-Bandjee, M.-C., Gasque, P., 2012. Arthritogenic alphaviruses—an overview. Nat Rev Rheumatol 8, 420–429. https://doi.org/10.1038/nrrheum.2012.64

Suopanki, J., Sawicki, D.L., Sawicki, S.G., Kääriäinen, L., 1998. Regulation of alphavirus 26S mRNA transcription by replicase component nsP2. J Gen Virol 79 (Pt 2), 309–319. https://doi.org/10.1099/0022-1317-79-2-309

Suthar, M.S., Shabman, R., Madric, K., Lambeth, C., Heise, M.T., 2005. Identification of adult mouse neurovirulence determinants of the Sindbis virus strain AR86. J Virol 79, 4219–4228. https://doi.org/10.1128/JVI.79.7.4219-4228.2005

Taghavi, N., Samuel, C.E., 2012. Protein kinase PKR catalytic activity is required for the PKR-dependent activation of mitogen-activated protein kinases and amplification of interferon beta induction following virus infection. Virology 427, 208–216. https://doi.org/10.1016/j.virol.2012.01.029

Takahashi, T., Miyakawa, T., Zenno, S., Nishi, K., Tanokura, M., Ui-Tei, K., 2013. Distinguishable in vitro binding mode of monomeric TRBP and dimeric PACT with siRNA. PLoS One 8, e63434. https://doi.org/10.1371/journal.pone.0063434

Tandale, B.V., Sathe, P.S., Arankalle, V.A., Wadia, R.S., Kulkarni, R., Shah, S.V., Shah, S.K., Sheth, J.K., Sudeep, A.B., Tripathy, A.S., Mishra, A.C., 2009. Systemic involvements and fatalities during Chikungunya epidemic in India, 2006. Journal of Clinical Virology 46, 145–149. https://doi.org/10.1016/j.jcv.2009.06.027

tenOever, B.R., 2016. The Evolution of Antiviral Defense Systems. Cell Host & Microbe 19, 142–149. https://doi.org/10.1016/j.chom.2016.01.006

TESH, R.B., PERALTA, P.H., JOHNSON, K.M., 1969. ECOLOGIC STUDIES OF VESICULAR STOMATITIS VIRUS: I. PREVALENCE OF INFECTION AMONG ANIMALS AND HUMANS LIVING IN AN AREA OF ENDEMIC VSV ACTIVITY1. American Journal of Epidemiology 90, 255–261. https://doi.org/10.1093/oxfordjournals.aje.a121068

Thoms, M., Buschauer, R., Ameismeier, M., Koepke, L., Denk, T., Hirschenberger, M., Kratzat, H., Hayn, M., Mackens-Kiani, T., Cheng, J., Straub, J.H., Stürzel, C.M., Fröhlich, T., Berninghausen, O., Becker, T., Kirchhoff, F., Sparrer, K.M.J., Beckmann, R., 2020. Structural basis for translational shutdown and immune evasion by the Nsp1 protein of SARS-CoV-2. Science 369, 1249–1255. https://doi.org/10.1126/science.abc8665

Trottier, M.D., Palian, B.M., Shoshkes Reiss, C., 2005. VSV replication in neurons is inhibited by type I IFN at multiple stages of infection. Virology 333, 215–225. https://doi.org/10.1016/j.virol.2005.01.009

Tyrrell, D. a. J., Bynoe, M.L., 1965. Cultivation of a Novel Type of Common-cold Virus in Organ Cultures. Br Med J 1, 1467–1470. https://doi.org/10.1136/bmj.1.5448.1467

Uhl, S., Jang, C., Frere, J.J., Jordan, T.X., Simon, A.E., tenOever, B.R., 2023. ADAR1 Biology Can Hinder Effective Antiviral RNA Interference. Journal of Virology 97, e00245-23. https://doi.org/10.1128/jvi.00245-23

Utt, A., Das, P.K., Varjak, M., Lulla, V., Lulla, A., Merits, A., 2014. Mutations Conferring a Noncytotoxic Phenotype on Chikungunya Virus Replicons Compromise Enzymatic Properties of Nonstructural Protein 2. J Virol 89, 3145–3162. https://doi.org/10.1128/JVI.03213-14

Valdmanis, P.N., Gu, S., Schüermann, N., Sethupathy, P., Grimm, D., Kay, M.A., 2012. Expression determinants of mammalian argonaute proteins in mediating gene silencing. Nucleic Acids Research 40, 3704–3713. https://doi.org/10.1093/nar/gkr1274

Van Bortel, W., Dorleans, F., Rosine, J., Blateau, A., Rousset, D., Matheus, S., Leparc-Goffart, I., Flusin, O., Prat, C., Cesaire, R., Najioullah, F., Ardillon, V., Balleydier, E., Carvalho, L., Lemaître, A., Noel, H., Servas, V., Six, C., Zurbaran, M., Leon, L., Guinard, A., van den Kerkhof, J., Henry, M., Fanoy, E., Braks, M., Reimerink, J., Swaan, C., Georges, R., Brooks, L., Freedman, J., Sudre, B., Zeller, H., 2014. Chikungunya outbreak in the Caribbean region, December 2013 to March 2014, and the significance for Europe. Euro Surveill 19, 20759.

https://doi.org/10.2807/1560-7917.es2014.19.13.20759

Varble, A.J., Ried, C.D., Hammond, W.J., Marquis, K.A., Woodruff, M.C., Ferran, M.C., 2016. The vesicular stomatitis virus matrix protein inhibits NF-κB activation in Mouse L929 cells. Virology 499, 99–104. https://doi.org/10.1016/j.virol.2016.09.009

Vasiljeva, L., Merits, A., Auvinen, P., Kääriäinen, L., 2000. Identification of a novel function of the alphavirus capping apparatus. RNA 5'-triphosphatase activity of Nsp2. J Biol Chem 275, 17281–17287. https://doi.org/10.1074/jbc.M910340199

Vazquez, C., Swanson, S.E., Negatu, S.G., Dittmar, M., Miller, J., Ramage, H.R., Cherry, S., Jurado, K.A., 2021. SARS-CoV-2 viral proteins NSP1 and NSP13 inhibit interferon activation through distinct mechanisms. PLOS ONE 16, e0253089. https://doi.org/10.1371/journal.pone.0253089

Ventoso, I., 2012. Adaptive Changes in Alphavirus mRNA Translation Allowed Colonization of Vertebrate Hosts. Journal of Virology 86, 9484–9494. https://doi.org/10.1128/JVI.01114-12

Ventoso, I., Sanz, M.A., Molina, S., Berlanga, J.J., Carrasco, L., Esteban, M., 2006a. Translational resistance of late alphavirus mRNA to eIF2alpha phosphorylation: a strategy to overcome the antiviral effect of protein kinase PKR. Genes Dev 20, 87–100. https://doi.org/10.1101/gad.357006

Wang, C., Sun, M., Yuan, X., Ji, L., Jin, Y., Cardona, C.J., Xing, Z., 2017. Enterovirus 71 suppresses interferon responses by blocking Janus kinase (JAK)/signal transducer and activator of transcription (STAT) signaling through inducing karyopherin-α1 degradation. Journal of Biological Chemistry 292, 10262–10274. https://doi.org/10.1074/jbc.M116.745729

Wang, D., Westerheide, S.D., Hanson, J.L., Baldwin, A.S., 2000. Tumor Necrosis Factor α-induced Phosphorylation of RelA/p65 on Ser529 Is Controlled by Casein Kinase II *. Journal of Biological Chemistry 275, 32592–32597. https://doi.org/10.1074/jbc.M001358200

Wang, X., Wang, H., Li, Y., Jin, Y., Chu, Y., Su, A., Wu, Z., 2015. TIA-1 and TIAR interact with 5'-UTR of enterovirus 71 genome and facilitate viral replication. Biochem Biophys Res Commun 466, 254–259. https://doi.org/10.1016/j.bbrc.2015.09.020

Webb, L.G., Veloz, J., Pintado-Silva, J., Zhu, T., Rangel, M.V., Mutetwa, T., Zhang, L., Bernal-

Rubio, D., Figueroa, D., Carrau, L., Fenutria, R., Potla, U., Reid, S.P., Yount, J.S., Stapleford, K.A., Aguirre, S., Fernandez-Sesma, A., 2020. Chikungunya virus antagonizes cGAS-STING mediated type-I interferon responses by degrading cGAS. PLoS Pathog 16, e1008999. https://doi.org/10.1371/journal.ppat.1008999

Wen, X., Huang, X., Mok, B.W.-Y., Chen, Y., Zheng, M., Lau, S.-Y., Wang, P., Song, W., Jin, D.-Y., Yuen, K.-Y., Chen, H., 2014. NF90 Exerts Antiviral Activity through Regulation of PKR Phosphorylation and Stress Granules in Infected Cells. The Journal of Immunology 192, 3753–3764. https://doi.org/10.4049/jimmunol.1302813

Werneke, S.W., Schilte, C., Rohatgi, A., Monte, K.J., Michault, A., Arenzana-Seisdedos, F., Vanlandingham, D.L., Higgs, S., Fontanet, A., Albert, M.L., Lenschow, D.J., 2011. ISG15 Is Critical in the Control of Chikungunya Virus Infection Independent of UbE1L Mediated Conjugation. PLoS Pathog 7, e1002322. https://doi.org/10.1371/journal.ppat.1002322

Whelan, S.P.J., 2008. Vesicular Stomatitis Virus, in: Mahy, B.W.J., Van Regenmortel, M.H.V. (Eds.), Encyclopedia of Virology (Third Edition). Academic Press, Oxford, pp. 291–299. https://doi.org/10.1016/B978-012374410-4.00529-X

White, J.P., Lloyd, R.E., 2012. Regulation of stress granules in virus systems. Trends Microbiol 20, 175–183. https://doi.org/10.1016/j.tim.2012.02.001

White, L.K., Sali, T., Alvarado, D., Gatti, E., Pierre, P., Streblow, D., Defilippis, V.R., 2011. Chikungunya virus induces IPS-1-dependent innate immune activation and protein kinase R-independent translational shutoff. J Virol 85, 606–620. https://doi.org/10.1128/JVI.00767-10

WHO, 2023a. Chikungunya WHO report [WWW Document]. URL https://www.who.int/news-room/fact-sheets/detail/chikungunya (accessed 4.25.23).

WHO, 2023b. Enterovirus 71 WHO report [WWW Document]. URL https://www.who.int/teams/health-product-policy-and-standards/standards-and-specifications/vaccine-standardization/enterovirus-71 (accessed 4.26.23).

WHO, 2023c. WHO Coronavirus (COVID-19) Dashboard [WWW Document]. URL https://covid19.who.int (accessed 4.28.23).

Wickenhagen, A., Sugrue, E., Lytras, S., Kuchi, S., Noerenberg, M., Turnbull, M.L., Loney,

C., Herder, V., Allan, J., Jarmson, I., Cameron-Ruiz, N., Varjak, M., Pinto, R.M., Lee, J.Y., Iselin, L., Palmalux, N., Stewart, D.G., Swingler, S., Greenwood, E.J.D., Crozier, T.W.M., Gu, Q., Davies, E.L., Clohisey, S., Wang, B., Trindade Maranhão Costa, F., Freire Santana, M., de Lima Ferreira, L.C., Murphy, L., Fawkes, A., Meynert, A., Grimes, G., ISARIC4C Investigators, Da Silva Filho, J.L., Marti, M., Hughes, J., Stanton, R.J., Wang, E.C.Y., Ho, A., Davis, I., Jarrett, R.F., Castello, A., Robertson, D.L., Semple, M.G., Openshaw, P.J.M., Palmarini, M., Lehner, P.J., Baillie, J.K., Rihn, S.J., Wilson, S.J., 2021. A prenylated dsRNA sensor protects against severe COVID-19. Science 374, eabj3624. https://doi.org/10.1126/science.abj3624

Wilson, R.C., Tambe, A., Kidwell, M.A., Noland, C.L., Schneider, C.P., Doudna, J.A., 2015. Dicer-TRBP Complex Formation Ensures Accurate Mammalian MicroRNA Biogenesis. Molecular Cell 57, 397–407. https://doi.org/10.1016/j.molcel.2014.11.030

Wong, A.H., Tam, N.W., Yang, Y.L., Cuddihy, A.R., Li, S., Kirchhoff, S., Hauser, H., Decker, T., Koromilas, A.E., 1997. Physical association between STAT1 and the interferon-inducible protein kinase PKR and implications for interferon and double-stranded RNA signaling pathways. EMBO J 16, 1291–1304. https://doi.org/10.1093/emboj/16.6.1291

Wong, A.H.-T., Tam, N.W.N., Yang, Y.-L., Cuddihy, A.R., Li, S., Kirchhoff, S., Hauser, H., Decker, T., Koromilas, A.E., 1997. Physical association between STAT1 and the interferon-inducible protein kinase PKR and implications for interferon and double-stranded RNA signaling pathways. The EMBO Journal 16, 1291–1304. https://doi.org/10.1093/emboj/16.6.1291

Woo, P.C.Y., Wang, M., Lau, S.K.P., Xu, H., Poon, R.W.S., Guo, R., Wong, B.H.L., Gao, K., Tsoi, H., Huang, Y., Li, K.S.M., Lam, C.S.F., Chan, K., Zheng, B., Yuen, K., 2007. Comparative Analysis of Twelve Genomes of Three Novel Group 2c and Group 2d Coronaviruses Reveals Unique Group and Subgroup Features. J Virol 81, 1574–1585. https://doi.org/10.1128/JVI.02182-06

Xing, J., Hu, C., Che, S., Lan, Y., Huang, L., Liu, L., Yin, Y., Li, H., Liao, M., Qi, W., 2023. USP1-Associated Factor 1 Modulates Japanese Encephalitis Virus Replication by Governing Autophagy and Interferon-Stimulated Genes. Microbiol Spectr 11, e0318622. https://doi.org/10.1128/spectrum.03186-22

Yakub, I., Lillibridge, K.M., Moran, A., Gonzalez, O.Y., Belmont, J., Gibbs, R.A., Tweardy, D.J., 2005. Single Nucleotide Polymorphisms in Genes for 2′-5′-Oligoadenylate Synthetase and RNase L in Patients Hospitalized with West Nile Virus Infection. The Journal of Infectious Diseases 192, 1741–1748. https://doi.org/10.1086/497340

Yamashita, S., Nagata, T., Kawazoe, M., Takemoto, C., Kigawa, T., Güntert, P., Kobayashi, N., Terada, T., Shirouzu, M., Wakiyama, M., Muto, Y., Yokoyama, S., 2011. Structures of the first and second double-stranded RNA-binding domains of human TAR RNA-binding protein. Protein Sci 20, 118–130. https://doi.org/10.1002/pro.543

Yao, H., Song, Y., Chen, Y., Wu, N., Xu, J., Sun, C., Zhang, J., Weng, T., Zhang, Z., Wu, Z., Cheng, L., Shi, D., Lu, X., Lei, J., Crispin, M., Shi, Y., Li, L., Li, S., 2020. Molecular Architecture of the SARS-CoV-2 Virus. Cell 183, 730-738.e13. https://doi.org/10.1016/j.cell.2020.09.018

Yekta, S., Shih, I., Bartel, D.P., 2004. MicroRNA-Directed Cleavage of HOXB8 mRNA. Science 304, 594–596. https://doi.org/10.1126/science.1097434

Yi, L., He, Y., Chen, Y., Kung, H.-F., He, M.-L., 2011. Potent Inhibition of Human Enterovirus 71 Replication by Type I Interferon Subtypes. Antiviral Therapy 16, 51–58. https://doi.org/10.3851/IMP1720

Yi, R., Qin, Y., Macara, I.G., Cullen, B.R., 2003. Exportin-5 mediates the nuclear export of pre-microRNAs and short hairpin RNAs. Genes Dev 17, 3011–3016. https://doi.org/10.1101/gad.1158803

Yin, L., Zeng, Y., Zeng, R., Chen, Y., Wang, T.-L., Rodabaugh, K.J., Yu, F., Natarajan, A., Karpf, A.R., Dong, J., 2021. Protein kinase RNA-activated controls mitotic progression and determines paclitaxel chemosensitivity through B-cell lymphoma 2 in ovarian cancer. Oncogene 40, 6772–6785. https://doi.org/10.1038/s41388-021-02117-5

Yoon, C.-H., Lee, E.-S., Lim, D.-S., Bae, Y.-S., 2009. PKR, a p53 target gene, plays a crucial role in the tumor-suppressor function of p53. Proc Natl Acad Sci U S A 106, 7852–7857. https://doi.org/10.1073/pnas.0812148106

Zacks, M.A., Paessler, S., 2010. Encephalitic alphaviruses. Vet Microbiol 140, 281–286. https://doi.org/10.1016/j.vetmic.2009.08.023

Zapletal, D., Taborska, E., Pasulka, J., Malik, R., Kubicek, K., Zanova, M., Much, C., Sebesta, M., Buccheri, V., Horvat, F., Jenickova, I., Prochazkova, M., Prochazka, J., Pinkas, M., Novacek, J., Joseph, D.F., Sedlacek, R., Bernecky, C., O'Carroll, D., Stefl, R., Svoboda, P., 2022. Structural and functional basis of mammalian microRNA biogenesis by Dicer. Molecular Cell 82, 4064-4079.e13. https://doi.org/10.1016/j.molcel.2022.10.010

Zhang, D., Guo, R., Lei, L., Liu, H., Wang, Yawen, Wang, Yili, Qian, H., Dai, T., Zhang, T., Lai, Y., Wang, J., Liu, Z., Chen, T., He, A., O'Dwyer, M., Hu, J., 2021. Frontline Science: COVID-19 infection induces readily detectable morphologic and inflammation-related phenotypic changes in peripheral blood monocytes. Journal of Leukocyte Biology 109, 13–22. https://doi.org/10.1002/JLB.4HI0720-470R

Zhang, H., Kolb, F.A., Brondani, V., Billy, E., Filipowicz, W., 2002. Human Dicer preferentially cleaves dsRNAs at their termini without a requirement for ATP. Embo J 21, 5875–5885.

Zhang, K., Matsui, Y., Hadaschik, B.A., Lee, C., Jia, W., Bell, J.C., Fazli, L., So, A.I., Rennie, P.S., 2010. Down-regulation of type I interferon receptor sensitizes bladder cancer cells to vesicular stomatitis virus-induced cell death. International Journal of Cancer 127, 830–838. https://doi.org/10.1002/ijc.25088

Zhang, P., Samuel, C.E., 2008. Induction of Protein Kinase PKR-dependent Activation of Interferon Regulatory Factor 3 by Vaccinia Virus Occurs through Adapter IPS-1 Signaling*. Journal of Biological Chemistry 283, 34580–34587. https://doi.org/10.1074/jbc.M807029200

Zhang, Peifen, Li, Y., Xia, J., He, J., Pu, J., Xie, J., Wu, S., Feng, L., Huang, X., Zhang, Ping, 2014. IPS-1 plays an essential role in dsRNA-induced stress granule formation by interacting with PKR and promoting its activation. Journal of Cell Science 127, 2471–2482. https://doi.org/10.1242/jcs.139626

Zhang, X., Fugère, M., Day, R., Kielian, M., 2003. Furin Processing and Proteolytic Activation of Semliki Forest Virus. J Virol 77, 2981–2989. https://doi.org/10.1128/JVI.77.5.2981-2989.2003

Zhang, Y., Xu, Y., Dai, Y., Li, Z., Wang, J., Ye, Z., Ren, Y., Wang, H., Li, W., Lu, J., Ding, S.-W., Li, Y., 2021. Efficient Dicer processing of virus-derived double-stranded RNAs and its modulation by RIG-I-like receptor LGP2. PLOS Pathogens 17, e1009790.

https://doi.org/10.1371/journal.ppat.1009790

Zhong, H., Voll, R.E., Ghosh, S., 1998. Phosphorylation of NF-κB p65 by PKA Stimulates Transcriptional Activity by Promoting a Novel Bivalent Interaction with the Coactivator CBP/p300. Molecular Cell 1, 661–671. https://doi.org/10.1016/S1097-2765(00)80066-0

Zhong, J., Peters, A.H., Lee, K., Braun, R.E., 1999. A double-stranded RNA binding protein required for activation of repressed messages in mammalian germ cells. Nat Genet 22, 171–174. https://doi.org/10.1038/9684

Zhu, J., Zhang, Y., Ghosh, A., Cuevas, R.A., Forero, A., Dhar, J., Ibsen, M.S., Schmid-Burgk, J.L., Schmidt, T., Ganapathiraju, M.K., Fujita, T., Hartmann, R., Barik, S., Hornung, V., Coyne, C.B., Sarkar, S.N., 2014. Antiviral Activity of Human OASL Protein Is Mediated by Enhancing Signaling of the RIG-I RNA Sensor. Immunity 40, 936–948. https://doi.org/10.1016/j.immuni.2014.05.007

Zhu, Y., Wang, B., Huang, H., Zhao, Z., 2016. Enterovirus 71 induces anti-viral stress granule-like structures in RD cells. Biochem Biophys Res Commun 476, 212–217. https://doi.org/10.1016/j.bbrc.2016.05.094

Zhu, Z., Liu, P., Yuan, L., Lian, Z., Hu, D., Yao, X., Li, X., 2021. Induction of UPR Promotes Interferon Response to Inhibit PRRSV Replication via PKR and NF-κB Pathway. Front Microbiol 12, 757690. https://doi.org/10.3389/fmicb.2021.757690

Zimmerman, O., Holmes, A.C., Kafai, N.M., Adams, L.J., Diamond, M.S., 2023. Entry receptors — the gateway to alphavirus infection. J Clin Invest 133, e165307. https://doi.org/10.1172/JCI165307

Žusinaite, E., Tints, K., Kiiver, K., Spuul, P., Karo-Astover, L., Merits, A., Sarand, I., 2007. Mutations at the palmitoylation site of non-structural protein nsP1 of Semliki Forest virus attenuate virus replication and cause accumulation of compensatory mutations. J Gen Virol 88, 1977–1985. https://doi.org/10.1099/vir.0.82865-0

Annexes

Annex 1: RACK1 Associates with RNA-Binding Proteins Vigilin and SERBP1 to Facilitate Dengue Virus Replication

The following annex describes a collaborative work with Ali Amara's team in Paris where they focused on the role of RACK1 and its interacting partners upon Dengue virus (DENV) infection. They described RACK1 association with SERBP1 and Vigilin facilitating DENV translation and replication. I participated in this work by performing high molecular weight northern blot analysis on DENV genomic RNA stability upon treatment of either HAP1 WT or KO SERBP1 or KO SERBP1 of KO Vigilin cells with MK0608 replication inhibitor (Fig. 6). This allowed to rule out any involvement of the candidates in DENV genomic RNA stability while they keep to promote DENV replication.

AMERICAN SOCIETY FOR MICROBIOLOGY | Journal of Virology®

VIRUS-CELL INTERACTIONS

RACK1 Associates with RNA-Binding Proteins Vigilin and SERBP1 to Facilitate Dengue Virus Replication

Alexis Brugier,[a] Mohamed Lamine Hafirrassou,[a] Marie Pourcelot,[a] Morgane Baldaccini,[b] Vasiliya Kril,[a] Laurine Couture,[a] Beate M. Kümmerer,[c] Sarah Gallois-Montbrun,[d] Lucie Bonnet-Madin,[a] Pierre-Olivier Vidalain,[e] Constance Delaugerre,[a,f] Sébastien Pfeffer,[b] Laurent Meertens,[a] Ali Amara[a]

[a]Université de Paris, INSERM U944, CNRS 7212, Biology of Emerging Viruses Team, Institut de Recherche Saint-Louis, Hôpital Saint-Louis, Paris, France
[b]Université de Strasbourg, Architecture et Réactivité de l'ARN, Institut de Biologie Moléculaire et Cellulaire du CNRS, Strasbourg, France
[c]Institute of Virology, Medical Faculty, University of Bonn, Bonn, Germany
[d]Université de Paris, Institut Cochin, INSERM U1016, CNRS UMR8104, Paris, France
[e]Centre International de Recherche en Infectiologie, Team Viral Infection, Metabolism and Immunity, INSERM U1111, CNRS UMR5308, ENS de Lyon, Université Claude Bernard Lyon 1, Lyon, France
[f]Laboratoire de Virologie et Département des Maladies Infectieuses, Hôpital Saint-Louis, Assistance Publique–Hôpitaux de Paris, Paris, France

Alexis Brugier and Mohamed Lamine Hafirrassou contributed equally to this article. Author order was determined by the corresponding author after negotiation.

ABSTRACT Dengue virus (DENV) is a mosquito-borne flavivirus responsible for dengue disease, a major human health concern for which no effective treatment is available. DENV relies heavily on the host cellular machinery for productive infection. Here, we show that the scaffold protein RACK1, which is part of the DENV replication complex, mediates infection by binding to the 40S ribosomal subunit. Mass spectrometry analysis of RACK1 partners coupled to an RNA interference screen-identified Vigilin and SERBP1 as DENV host-dependency factors. Both are RNA-binding proteins that interact with the DENV genome. Genetic ablation of Vigilin or SERBP1 rendered cells poorly susceptible to DENV, as well as related flaviviruses, by hampering the translation and replication steps. Finally, we established that a Vigilin or SERBP1 mutant lacking RACK1 binding but still interacting with the viral RNA is unable to mediate DENV infection. We propose that RACK1 recruits Vigilin and SERBP1, linking the DENV genome to the translation machinery for efficient infection.

IMPORTANCE We recently identified the scaffolding RACK1 protein as an important host-dependency factor for dengue virus (DENV), a positive-stranded RNA virus responsible for the most prevalent mosquito-borne viral disease worldwide. Here, we have performed the first RACK1 interactome in human cells and identified Vigilin and SERBP1 as DENV host-dependency factors. Both are RNA-binding proteins that interact with the DENV RNA to regulate viral replication. Importantly, Vigilin and SERBP1 interact with RACK1 and the DENV viral RNA (vRNA) to mediate viral replication. Overall, our results suggest that RACK1 acts as a binding platform at the surface of the 40S ribosomal subunit to recruit Vigilin and SERBP1, which may therefore function as linkers between the viral RNA and the translation machinery to facilitate infection.

KEYWORDS dengue virus, host factors, RACK1, RNA-binding proteins, SERBP1, Vigilin

Dengue virus (DENV) belongs to the genus *Flavivirus* of the family *Flaviviridae*, which includes important emerging and reemerging viruses such as West Nile virus (WNV), yellow fever virus (YFV), Zika virus (ZIKV), and tick-borne encephalitis virus (TBEV) (1). DENV is transmitted to humans by an *Aedes* mosquito bite and may lead to a variety of diseases ranging from mild fever to lethal dengue hemorrhagic fever and dengue shock syndrome (2). Recent estimations indicate that half of the world's

Editor Anice C. Lowen, Emory University School of Medicine

Address correspondence to Ali Amara, ali.amara@inserm.fr.

The authors declare no conflict of interest.

Received 16 November 2021
Accepted 24 January 2022
Published 10 March 2022

population lives in areas where dengue fever is endemic (3), with 100 million symptomatic infections, including 500,000 cases of severe manifestations of the disease per year (4). There are currently no approved antiviral therapies against DENV, although a promising inhibitor targeting the viral NS3-NS4B interaction was recently described (5). Conversely, the recently approved tetravalent live attenuated vaccine showed disappointing efficacy (6, 7).

DENV is an enveloped virus containing a positive-stranded RNA genome of ~11 kb. Upon entry into the host cell, the viral genome is released in the cytoplasm and translated by the host machinery into a large polyprotein precursor that is processed by host and viral proteases. Co- and posttranslational processing gives rise to three structural proteins: the C (core), prM (precursor of the M protein), and E (envelope) glycoproteins, which form the viral particle and seven nonstructural proteins (NS) called NS1, NS2A, NS2B, NS3, NS4A, NS4B, and NS5 (8) that play central roles in viral genome replication, assembly, and modulation of innate immune responses (9). Like other flaviviruses, DENV genome replication takes place within virus-induced vesicles (Ve) derived from invaginations of the endoplasmic reticulum (ER) membrane (10, 11). These structures consist of 90-nm-wide vesicles containing a ±11-nm pore that allows exchanges between the Ve lumen and the cytosol (11). Within the Ve, viral NS proteins, viral RNA (vRNA), and some host factors assemble to form the viral replication complex (RC) that is essential for viral RNA synthesis. We have recently purified the DENV RC in human cells, using a tagged DENV subgenomic replicon, and determined its composition by mass spectrometry (12). Our study provided an unprecedented mapping of the DENV RC host interactome and identified cellular modules exploited by DENV during active replication. By combining these proteomics data with gene silencing experiments, we identified a set of host-dependency factors (HDFs) that have a critical impact on DENV infection and established an important role for RACK1 (receptor for activated C kinase 1) in DENV vRNA amplification (12), which was recently confirmed by others (13).

RACK1 is a core component of the 40S ribosomal subunit (14, 15), containing seven WD40 domains that mediate protein-protein interactions (16, 17). RACK1 is a scaffold protein (18, 19) described to interact with many cellular pathways such as Sarcoma (Src) tyrosine kinase (20, 21), cAMP/protein kinase A (PKA) (22), or receptor tyrosine kinase (23). Ribosomal RACK1 has also been shown to be involved in the association of mRNAs with polysomes (24), in the recruitment and phosphorylation of translational initiation factors (25–27), and in quality control during translation (28). The nonribosomal form of RACK1 is involved in innate immunity, by recruiting the PP2A phosphatase (29) or by targeting the VISA/TRAF complexes (30), and participates in the assembly and activation of the NLRP3 inflammasome (31). To date, only one proteomic study aiming to identify RACK1 cofactors has been performed in *Drosophila* S2 cells (32). RACK1 cellular partners in human cells are largely unknown.

Several viruses depend on RACK1 to complete their infectious cycle[31–35]. For instance, RACK1 is involved in internal ribosome entry site (IRES)-mediated translation of viruses possessing a type I IRES such as cricket paralysis virus or hepatitis C virus (33). RACK1 also contributes to poxvirus infection through a ribosome customization mechanism. Indeed, poxviruses trigger the phosphorylation of the serine 278 of RACK1 (34) to promote the selective translation of viral RNAs.

In this work, we have investigated the function of RACK1 during DENV life cycle. We performed the first interactome of RACK1 in human cells. Functional studies revealed that RACK1 interacts with the RNA-binding proteins Vigilin and SERBP1 to facilitate DENV replication.

RESULTS AND DISCUSSION

RACK1 interaction with the 40S ribosomal subunit is required for DENV infection. To confirm the role of RACK1 in DENV infection, we challenged parental and RACK1 knockout (RACK1^{KO}) HAP1 cells with DENV2-16681 particles at different multiplicities of infection (MOIs) and measured viral infection by quantifying the percentage of cells

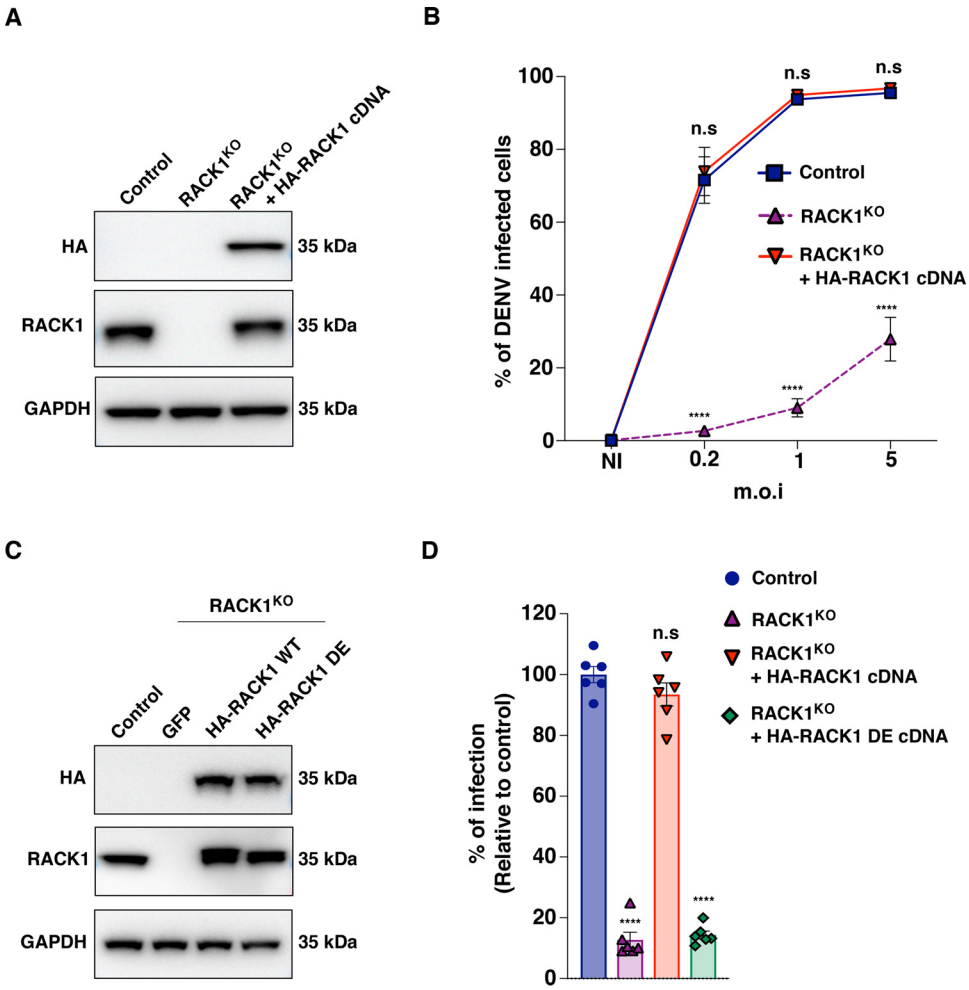

FIG 1 The interaction between RACK1 and the 40S ribosome is required for dengue virus (DENV) infection. (A) Western blot analysis of RACK1 expression in control, RACK1^{KO}, and RACK1^{KO} HAP1 cells transcomplemented with a hemagglutinin (HA)-RACK1 cDNA. Cell lysates were probed with the indicated antibodies. Shown is a representative Western blot of $n = 3$ technically independent experiments. (B) Role of RACK1 in DENV infection. Control, RACK1^{KO}, or RACK1^{KO} cells transcomplemented with a cDNA encoding wild-type (WT) HA-RACK1 were infected at different multiplicities of infection (m.o.i) with DENV2-16681. Levels of infection were determined by flow cytometry using the 2H2 prM monoclonal antibody (MAb) at 48 h postinfection (hpi). The data shown are the means ± stardard error of the mean (SEM) of four independent experiments performed in duplicate. Significance was calculated using two-way analysis of variance (ANOVA) with Dunnett's multiple-comparison test. (C) Western blot analysis of RACK1 expression in RACK1^{KO} HAP1 transcomplemented with cDNA encoding WT HA-RACK1 or the HA-RACK1 D/E mutant (HA-RACK1 DE cDNA). Cell lysates were probed with the indicated antibodies. Shown is a representative Western blot of three independent experiments. (D) Impact of RACK1 association to the 40S subunit of the ribosome in DENV infection. Control, RACK1^{KO}, and RACK1^{KO} HAP1 cells transcomplemented with cDNA encoding WT HA-RACK1 or the HA-RACK1 DE mutant were infected at MOI 1 with DENV2-16681 and harvested at 48 hpi. Levels of infection were determined by flow cytometry as described above. The data shown are the means ± SEM of three independent experiments performed in duplicate. Significance was calculated using one-way ANOVA with Dunnett's multiple-comparison test. ****, $P < 0.0001$; n.s, not significant; GAPDH, glyceraldehyde-3-phosphate dehydrogenase; GFP, green fluorescent protein; NI, not infected.

expressing the DENV antigen PrM. In agreement with our previous studies (12), DENV infection was severely impaired in HAP1 cells lacking RACK1 (Fig. 1A and B). Importantly, transcomplementation of the HAP1 RACK1^{KO} cells with a plasmid encoding human RACK1 rescued cell susceptibility to DENV infection (Fig. 1A and B), ruling out CRISPR-Cas9-mediated off-target effects and demonstrating that RACK1 is an important host factor for DENV.

RACK1 is a component of the 40S subunit of the ribosome and is located near the mRNA exit channel (17). To test whether DENV infection requires RACK1 association

with the 40S ribosome, we transcomplemented RACK1^{KO} cells with a RACK1 mutant defective for ribosome-binding (RACK1R36D/K38E, DE mutant) (34, 35). The RACK1 DE mutant, which displayed a wild-type (WT) expression level and was unable to associated with polysomes (data not shown and Ref. 36), failed to rescue DENV2-16681 infection (Fig. 1C and D). These results indicate that the interaction with the 40S ribosomal subunit is important for RACK1 proviral function.

Mapping the RACK1 interactome. Because RACK1 is a scaffold protein, we hypothesized that its proviral activity may rely on its ability to recruit host proteins near the ribosome for optimal translation. To characterize the RACK1 interactome in mammalian cells, we transfected 293T cells with a plasmid encoding an hemagglutinin (HA)-tagged version of human RACK1. We pulled down RACK1 and its binding partners using HA beads and eluted purified proteins with HA peptide according to the experimental procedures that we recently described (12). Immunoprecipitated proteins were separated by SDS-PAGE, visualized by silver staining, and subjected to mass spectrometry (MS) analysis (Fig. 2A). By analyzing the raw affinity purification-mass spectrometry (AP-MS) data set with SAINT express and MiST softwares (37), we identified 135 high-confidence host factors that copurified with RACK1 and showed a SAINT express score greater than 0.8 (supplemental material). Next, we analyzed the list of 135 high-confidence interactors with DAVID 6.8 to identify statistical enrichments for specific Gene Ontology (GO) terms from the "cellular component" (CC) annotation (38, 39) (Fig. 2B) and built the corresponding interaction network using Cytoscape 3.4.0 (40) (Fig. 2C). The 135 RACK1-interacting proteins were clustered into functional modules using enriched GO terms as a guideline and literature mining (Fig. 2C). As expected, the RACK1 interactome was significantly enriched in proteins associated with ribosome/polysome and mRNA translation (Rps3, eIF3, eIF4G, and eIF4J), stress granules (G3BP2 and LARP1), P-Bodies (Ago1 and 2), and RNA splicing factors (HNRNPA2B1 and U2AF2) (Fig. 2C). Interestingly, several proteins found in our study, such as Ago2, LARP1 and 2, and eIF3A, were also identified in a RACK1 interactome done in *Drosophila* S2 cells (32).

Vigilin, SERBP1, and ZNF598 are DENV host-dependency factors. To pinpoint the function of the RACK1 binding partners during DENV infection, we silenced by RNA interference (RNAi) the expression of the 49 highest ranked hits with an average peptide count of more than 28 and determined the consequences on viral infection (Fig. 3A; supplemental material). Four proteins, namely HNRNPA2B1, Vigilin, SERBP1, and ZNF598, whose silencing decreased infection by at least 50% without affecting cell viability in the two cell lines were considered for further investigation (Fig. 3A; supplemental material). These factors are RNA-binding proteins (RBP) involved in RNA splicing (HNRNPA2B1) (41) or translation regulation (Vigilin, SERBP1, and ZNF598) (28, 42, 43). HNRNPA2B1 was already described to interact with the 3′-untranslated region (UTR) part of the virus (44). Because HNRNPA2B1 is a nuclear protein (45), it was not further considered in our study. Vigilin is a multiple K-homology (KH) domain protein implicated in translation regulation and lipidic metabolism (24, 43, 46). This protein was recently described to bind the DENV RNA and, in association with the ribosomal-binding protein 1 (RRBP1), to facilitate viral RNA translation and replication (47). However, how this protein interacts with RACK1 to regulate DENV infection is still unknown. SERBP1 is a RACK1 cofactor (48) that is located at the entry channel of ribosomes (49) and enhances translation by promoting the association of mRNAs with polysomes (42). SERBP1 was also described to interact with DENV RNA. However, its role in DENV replication remains unclear (50). Finally, ZNF598 is an E3 ubiquitin-protein ligase known to interact with RACK1 and playing a key role in the ribosome quality control (28). ZNF598 was also described to play a role in innate immunity (51). However, its role in DENV infection is unknown.

We first confirmed that endogenous Vigilin, ZNF598, and SERBP1 proteins coimmunoprecipitated with HA-RACK1 ectopically expressed in 293T cells (Fig. 3B). Next, we validated the requirement of Vigilin, SERBP1, and ZNF598 using two approaches. On one hand, we found that knocking down by RNA interference Vigilin, SERBP1, or ZNF598 (Fig. 3C) significantly impaired DENV infection but not viability of primary human fibroblasts, which are DENV target cells (Fig. 3D and E). On the other hand, we

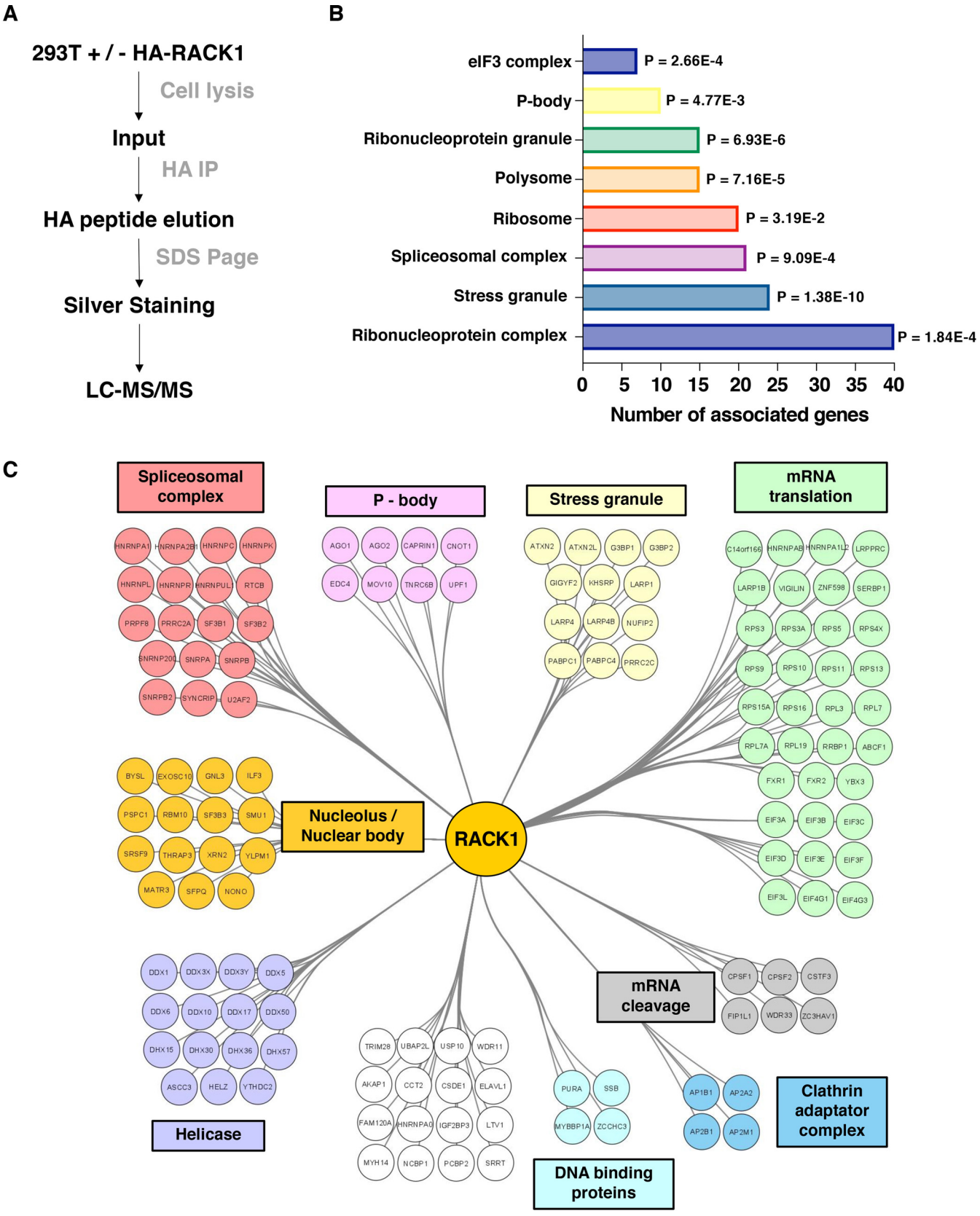

FIG 2 Global map of the RACK1 interactome in human cells. (A) Experimental scheme of our RACK1 immunoprecipitation approach. 293T cells expressing RACK1 or HA-RACK1 were lysed, and extracts were purified with anti-HA-coated beads before SDS-PAGE and mass spectrometry (MS) analysis. (B) Histogram indicating statistical enrichment for specific biological processes and cellular components, determined by Gene Ontology (GO) analysis.

(Continued on next page)

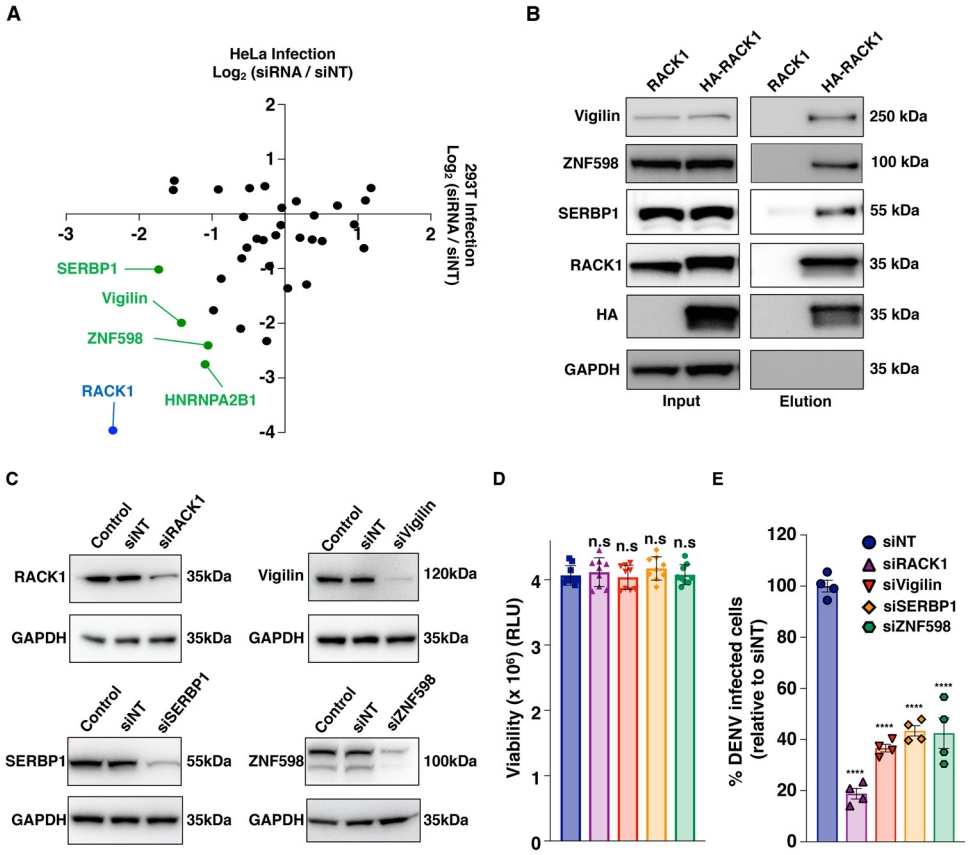

FIG 3 RNA interference (RNAi) screen-identified Vigilin, SERBP1, and ZNF598 are DENV host-dependency factors. (A) Host-dependency factors (HDFs) found in our RNAi screen. The data shown are representative of three independent experiments. Host-dependency factors are marked in green. The positive control (small interfering RNA [siRNA] pool targeting RACK1) is highlighted in blue. (B) Validation of the interaction between RACK1 and endogenous Vigilin or SERBP1 in 293T cells by immunoprecipitation. Cell extracts from 293T cells expressing RACK1 or HA-RACK1 were subjected to affinity purification using anti-HA beads, and interacting proteins were revealed by Western blotting. The data shown are representative of three independent experiments. (C) Human primary fibroblasts were transfected with the indicated siRNA pools. RACK1, Vigilin, SERBP1, and ZNF598 expression in siRNA transfected cells was assessed by Western blot analysis 48 h posttransfection. (D) The viability of siRNA transfected fibroblasts described in B was monitored by cell titer glow analysis. The data shown are the means ± SEM of three independent experiments performed in triplicate. Significance was calculated using two-way ANOVA with Dunnett's multiple-comparison test. (E) siRNA transfected fibroblasts described for panel B were challenged with DENV2-16681 at MOI 1. At 48 h posttransfection, the levels of infection were determined by flow cytometry using 2H2 MAb at 48 hpi. The data shown are the means ± SEM of three independent experiments performed in duplicate. Significance was calculated using one-way ANOVA with Dunnett's multiple-comparison test. RLU, relative light units; siNT, nontargeting siRNA.

used the CRISPR-Cas9 technology to edit the corresponding genes in HAP1 cells (Vigilin ^{KO}, SERBP1 ^{KO}, and ZNF598 ^{KO}) (Fig. 4). Gene editing and knockout generation were confirmed by genomic DNA sequencing (Fig. 4A) and Western blot analysis (Fig. 4B), respectively. In agreement with our previous findings, lack of RACK1, Vigilin, SERBP1, and ZNF598 expression had no impact on cell growth and viability as assessed by quantification of ATP levels in culture wells at different time points (Fig. 4C). HAP1 cells lacking Vigilin, SERBP1, or ZNF598 expression were poorly permissive to DENV infection as shown by the quantification of viral progeny in supernatants of infected cells (Fig. 4D), Western blot analysis of the DENV protein expression (NS3, E, and PrM)

FIG 2 Legend (Continued)
(C) Interaction network of RACK1-associated proteins identified by MS in 293T cells. Proteins were clustered into functional modules using enriched GO terms as a guideline and manual mining of literature. This panel is a representative network of $n = 3$ independent experiments showing similar results. LC-MS/MS, liquid chromatography-tandem MS.

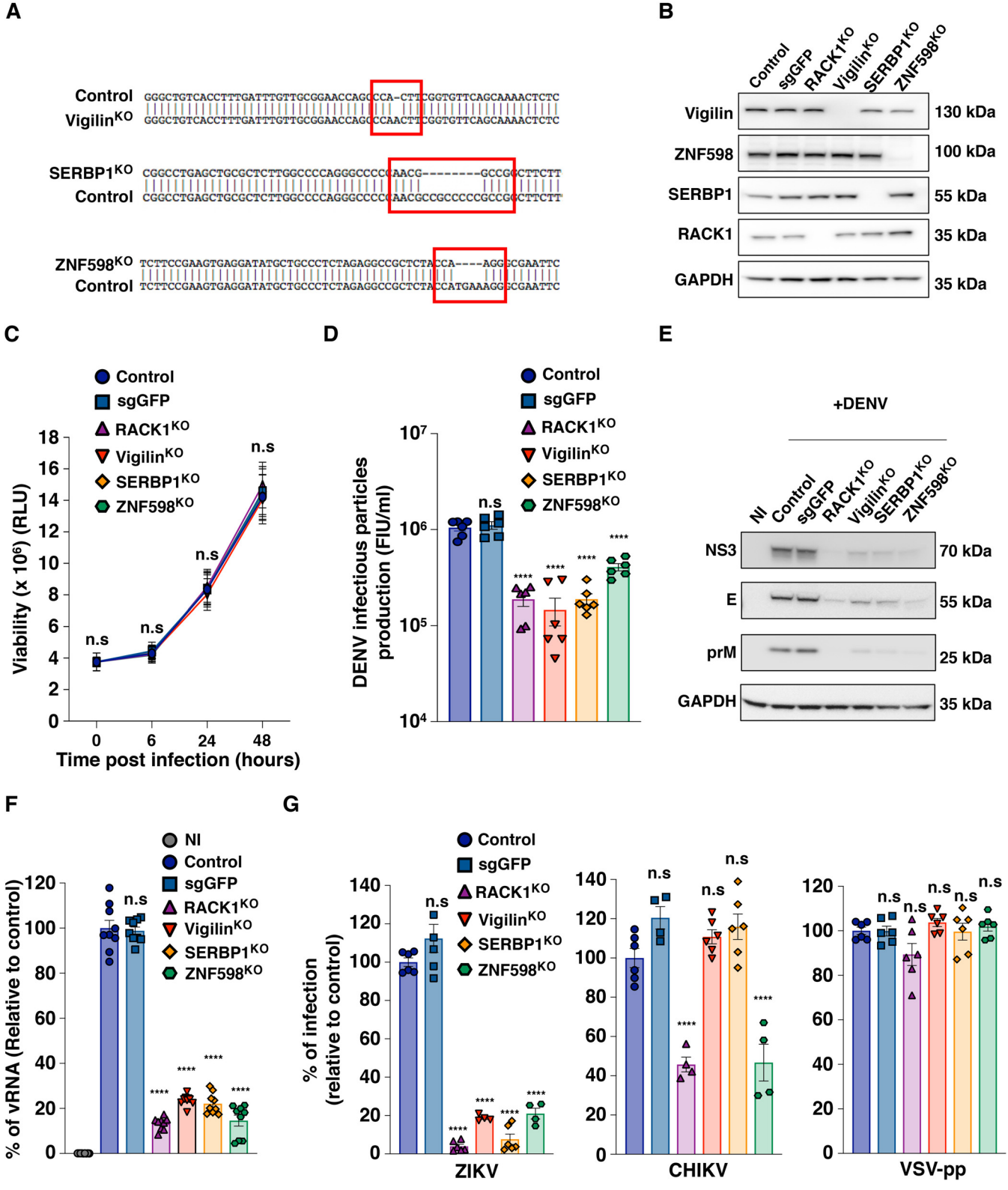

FIG 4 Impact of RACK1, Vigilin, SERBP1, and ZNF598 gene editing on infection by DENV and other enveloped viruses. (A) Sanger sequencing of *VIGILIN*, *SERBP1*, and *ZNF598* in control and Vigilin^{KO}, SERBP1^{KO}, or ZNF598^{KO} HAP1 cells, respectively. (B) Validation of Vigilin, SERBP1, and ZNF598 gene editing by Western blot analysis. Shown is a representative Western blot of three independent experiments. (C) Impact of RACK1, Vigilin, SERBP1, and ZNF598 gene editing on cell viability in HAP1 cells by cell titer glow analysis. The data shown are the means ± SEM of three independent experiments performed in duplicate. Significance was calculated using two-way ANOVA with Dunnett's multiple-comparison test. (D to G) Impact of RACK1/Vigilin/SERBP1/ZNF598 gene editing on DENV infectious cycle. The indicated cells were infected for 48 h at MOI 1 with DENV2-16681. (D) Supernatants from infected cells were

(Continued on next page)

(Fig. 4E), and quantification of the viral RNA (Fig. 4F). Parental (control) and HAP1 cells transfected with a nonspecific single guide RNA (targeting the green fluorescent protein [GFP]) were used as negative controls (Fig. 4), while RACK1^{KO} HAP1 cells were used as positive controls (Fig. 4). We then investigated whether these phenotypes were specific to DENV2-16681 or could be observed with other flaviviruses. We found that Vigilin, SERBP1, and ZNF598 mediate infection by other DENV serotypes (data not shown), as well as by Zika virus (ZIKV), a related flavivirus (Fig. 4G). In contrast, infections by the *Alphavirus* chikungunya virus (CHIKV) or the vesicular stomatitis virus G protein (VSV-G)-pseudotyped human immunodeficiency virus (VSVpp) were unaffected in Viligin^{KO} and SERBP1^{KO} cells (Fig. 4G). CHIKV infection but not VSVpp was significantly reduced in RACK1^{KO} and ZNF598^{KO} cells (Fig. 4G). Altogether, our data indicate that Vigilin, SERBP1, and ZNF598 are important host factors for DENV. ZNF598 is required for DENV and CHIKV infection, while Vigilin and SERBP1 are exclusively exploited by DENV and other related flaviviruses.

Vigilin and SERBP1 regulate DENV translation and replication. To determine whether Vigilin and SERBP1 impact initial vRNA translation or amplification, Vigilin^{KO} and SERPB1^{KO} cells were challenged with DENV2 *Renilla* luciferase (Luc) reporter virus (DV-R2A) through a time-course experiment to monitor the kinetic of viral infection (Fig. 5A). RACK1 ^{KO} cells were used as a positive control. A weak Luc activity was detected at 6 h postinfection, reflecting the initial translation of the incoming vRNA. This was followed by a marked increase in Luc activity caused by a combination of translation and replication of the viral genome (Fig. 5A). Depletion of RACK1, Vigilin, and SERBP1 had no impact on initial translation step but strongly impaired DENV translation and replication at later time points (Fig. 5A). Importantly, viral genome replication was completely restored in KO cells transduced with RACK1, SERBP1, or Vigilin cDNAs (Fig. 5A). CHIKV expressing the *Gaussia* luciferase replicated as efficiently in Vigilin or SERBP1 ^{KO} cells as in control cells, while its replication in RACK1^{KO} was impaired (Fig. 5B). To assess further the effect of Vigilin and SERBP1 on DENV vRNA replication, we used a *Renilla* luciferase (Rluc) reporter subgenomic replicon (sgDVR2A), which is a self-replicating DENV RNA containing a large in-frame deletion in the structural genes and represents a useful tool to exclusively monitor DENV translation and RNA amplification. Control, Vigilin^{KO}, SERBP1^{KO}, and RACK1^{KO} HAP1 cells were transfected with the *in vitro* transcribed DENVR2A subgenomic RNA, and vRNA replication was monitored over time by quantifying the Rluc activity in infected cell lysates (Fig. 5C). Depletion of RACK1, Vigilin, or SERBP1 had no impact during the early phase of DENV RNA translation. At 12 h posttransfection, the RLuc signal increased over time in control cells, while a strong reduction was observed (more than 10-fold reduction at 48 h postinfection [hpi]) in Vigilin^{KO} and SERBP1^{KO} cells (Fig. 5C). The RLuc signal was restored in Vigilin^{KO} or SERBP1^{KO} transcomplemented with their corresponding cDNAs (Fig. 5C).

Vigilin has been previously shown to mediate, in association with the host factor RRBP1, the stability of DENV vRNA (47). Since SERBP1 also binds the DENV RNA (50), we reasoned that it might play a similar role. To assess this hypothesis, RACK1^{KO}, Vigilin^{KO}, or SERBP1^{KO} HAP1 cells were challenged with DENV followed by treatment with MK0608 to inhibit viral replication (47). Then, we monitored the decay of the vRNA overtime by Northern blotting analysis using a probe that targets the DENV 3′-UTR (Fig. 6). We observed that the levels of the DENV genomic RNA were similar in control,

FIG 4 Legend (Continued)
harvested, and then the titer was determined by flow cytometry on Vero cells and expressed as fluorescence-activated cell sorter infectious unit (FIU)/mL. (E) Infection was assessed by immunoblot using anti-NS3, anti-prM, and anti-E DENV MAbs. The data shown are representative of three independent experiments. (F) Levels of infection were assessed by quantification of DENV viral RNA (vRNA) by quantitative reverse transcription-PCR using NS3 primers. The data shown are the means ± SEM of three independent experiments performed in duplicate. Significance was calculated using one-way ANOVA. (G) The indicated cells were infected with Zika virus (ZIKV) HD78 at MOI 2 (left), chikungunya virus (CHIKV) 21 at MOI 2 (middle), and vesicular stomatitis virus G protein-pseudotyped human immunodeficiency virus (VSV-pp) at MOI 2 (right). Levels of infection were determined by flow cytometry at 48 hpi. The data shown are the means ± SEM of at least two independent experiments performed in duplicate. Significance was calculated using one-way ANOVA with Dunnett's multiple-comparison test. n.s, not significant; ****, $P < 0.0001$.

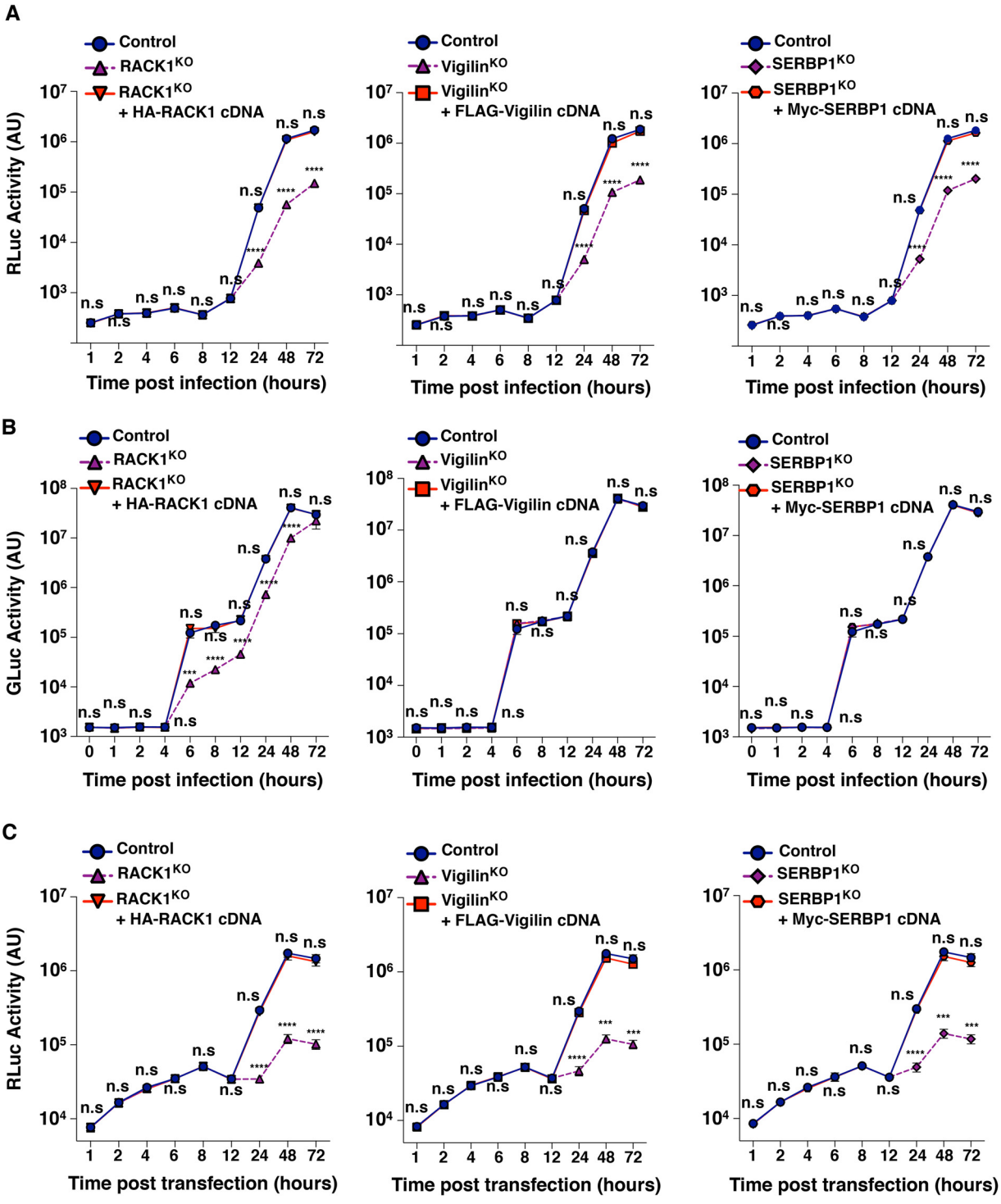

FIG 5 Vigilin and SERBP1 regulate DENV translation and replication. (A) The indicated cells were infected at MOI 1 with DENV-Luc. At the indicated time points, *Renilla* luciferase activity reflecting RNA translation (1 to 8 hpi) and replication (12 to 72 hpi) was measured. The data shown are the means ± SEM of three independent experiments performed in triplicate. Significance was calculated using two-way ANOVA with Dunnett's multiple-comparison test. (B) The indicated cells were infected at MOI 1 with CHIKV-Luc. *Gaussia* luciferase activity was monitored at the indicated time points. The data shown are the means ± SEM of three independent experiments performed in triplicate. Significance was calculated using two-way ANOVA with Dunnett's multiple-comparison test. (C) Impact of RACK1/Vigilin/SERBP1 KO on DENV life cycle in HAP1 cells transfected with a DENV replicon RNA expressing *Renilla* luciferase. *Renilla* luciferase activity was monitored at the indicated time point. The data shown are the means ± SEM of three independent experiments performed in triplicate. Significance was calculated using two-way ANOVA with Dunnett's multiple-comparison test. n.s, not significant; ****, $P < 0.0001$; AU, arbitrary units; Gluc, *Gaussia* luciferase; Rluc, *Renilla* luciferase.

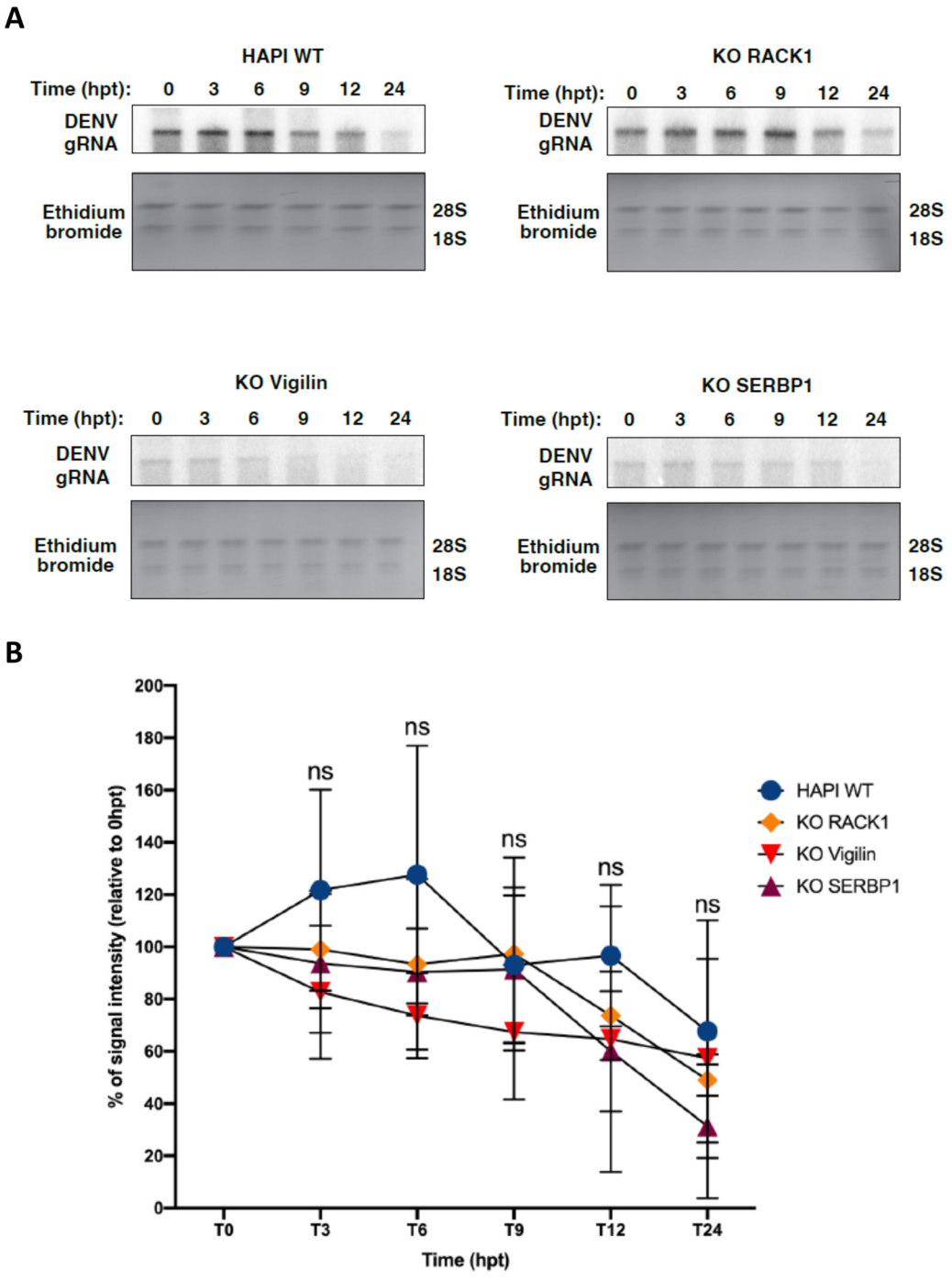

FIG 6 Northern blot analysis of the impact of RACK1, Vigilin, and SERBP1 knockout on DENV genomic RNA (gRNA) stability. (A) Indicated cells were infected at an MOI of 1 with DENV2-16681. Total RNA was extracted 48 h.p.i. at the indicated time after treatment with MK0608 replication inhibitor. The data shown are the means ± SEM of three independent experiments performed in triplicate. (B) vRNA stability is expressed as a percentage relative to the signal monitored at time point 0 h after MK0608 treatment. Ethidium bromide serves as a loading control, showing 28S and 18S rRNA. Statistics were performed using two-way ANOVA. hpt, h posttransfection; ns, nonsignificant.

RACK1^{KO}, and SERBP1^{KO} HAP1 cells up to 24 h after MK0608 treatment (Fig. 6). Surprisingly, a lack of Vigilin expression had a very mild effect on DENV RNA stability (Fig. 6). Together, these results show that RACK1, Vigilin, and SERBP1 promote viral replication without a major impact on the stability of DENV vRNA.

Vigilin and SERBP1 interactions with RACK1 are important for DENV infection. Scp160p and Asc1p, the yeast homologs of Vigilin and RACK1, respectively, have

been shown to interact each other (24). This interaction is thought to promote translation of specific mRNAs linked to Scp160p by mediating their association with polysomes (24). Because Vigilin is very well-conserved among different species, a similar interaction with RACK1 might occur in mammalian cells. Having established that Vigilin and SERBP1 do not have a major influence on the stability of the vRNA, we hypothesized that their proviral effect might be linked to their interaction with RACK1. Previous studies showed that Scp160p interacts with Asc1p via the KH 13 and 14 domains located in its C-terminal region (24, 52), while SERBP1 interacts directly with RACK1 through a motif (amino acids [aa] 354 to 474) that contains the RGG domain (48) (Fig. 7A). On the basis of these observations, we generated the corresponding deletion mutants of FLAG-tagged Vigilin (FLAG-Vigilin Mut) and Myc-tagged SERBP1 (Myc-SERPB1 Mut) (Fig. 7A) and tested their ability to interact with RACK1 (Fig. 7B). Pulldown experiments showed that RACK1 binds both WT FLAG Vigilin or WT Myc SERBP1 ectopically expressed in HEK-293T cells (Fig. 7B). In contrast, RACK1 failed to associate with mutant forms of Vigilin and SERBP1 (Fig. 7B). We next assessed the ability of the mutant forms to interact with DENV vRNA by performing an RNA immunoprecipitation (IP) assay after UV irradiation (Fig. 7C). For both RNA-binding proteins, the WT and mutant forms were able to specifically enrich the vRNA (at least 10-fold more than actin enrichment). Furthermore, we did not observe any significant differences in vRNA enrichment between the mutant and WT forms of the RBPs. These data demonstrate that Vigilin Mut and SERBP1 Mut bind the DENV vRNA to the same extent as their WT counterparts.

Finally, we investigated whether Vigilin and SERBP1 binding to RACK1 impacts DENV infection. For this, we stably expressed Mut Vigilin or Mut SERBP1 in Vigilin ^{KO} or SERBP1 ^{KO} cells, respectively (Fig. 8A). Infection studies showed that expression of Mut Vigilin or Mut SERBP1 in Vigilin ^{KO} or SERBP1 ^{KO} cells did not restore DENV2-16681 infection in contrast to their WT counterparts (Fig. 8B). Together, these data indicate that Vigilin and SERBP1 interaction with RACK1 is important for DENV infection

Conclusions. Our results provide new insights into the molecular mechanisms of DENV replication. We performed the first RACK1 interactome in human cells and identified Vigilin and SERBP1 as host factors for DENV infection. Both are RNA-binding proteins that interact with the DENV RNA and regulate viral replication. Importantly, our data suggest that the interaction of Vigilin and SERBP1 with RACK1 are important for DENV infection. The proviral function of RACK1 depends on its association with the 40S ribosomal subunit. Furthermore, mutants of SERBP1 or Vigilin that lost their ability to interact with RACK1 were unable to support infection. We propose a model in which RACK1 acts as a binding platform at the surface of the 40S ribosomal subunit to recruit Vigilin and SERBP1, which may therefore function as linkers between the viral RNA and the translation machinery to facilitate DENV infection. Strategies that interfere with RACK1-ribosome association or disturb the RACK1-Vigilin-SERBP1 complex may represent new ways to combat DENV-induced disease.

MATERIALS AND METHODS

Cell lines. HAP1 cells (Horizon Discovery) and HAP1 RACK1^{KO} (provided by Gabriele Fuchs, University at Albany) were cultured in Iscove's modified Dulbecco's medium (IMDM) supplemented with 10% fetal bovine serum (FBS), 1% penicillin-streptomycin, 1% GlutaMAX, and 25 mM HEPES. HEK293T (ATCC), Vero E6 (ATCC), BHK-21 (ATCC), and HeLa (ATCC) cells were cultured in Dulbecco's modified Eagle's medium (DMEM) supplemented with 10% FBS, 1% penicillin-streptomycin, 1% GlutaMAX, and 25 mM HEPES. Fibroblast BJ-5ta cells (ATCC) were cultured according to the manufacturer's instructions. A final concentration of 50 μM MK0608 was used in this study. All of the cell lines were cultured at 37°C and 5% CO_2.

Virus strains and replicons. DENV1-KDH0026A (gift from L. Lambrechts, Pasteur Institute, Paris, France), DENV2-16681 (Thailand/16681/84), DENV4 (H241), and ZIKV HD78788 were propagated in mosquito AP61 cell monolayers with limited cell passages. DENV2 Rluc reporter virus (DVR2A) was provided by Ralf Bartenschlager (University of Heidelberg). The CHIKV Luc reporter virus was described previously (53).To generate infectious virus, capped viral RNAs were generated from the NotI-linearized plasmids using a mMessage mMachine T7 transcription kit (Thermo Fisher Scientific) according to the manufacturer's instructions. RNAs were purified (see RNA IP protocol), resuspended in DNase/RNase-free water, aliquoted, and stored at −80°C until used. 30 μg of purified RNAs were transfected in BHK21 cells using Lipofectamine 3000 reagent. Supernatants were collected 72 h later and used for viral propagation on

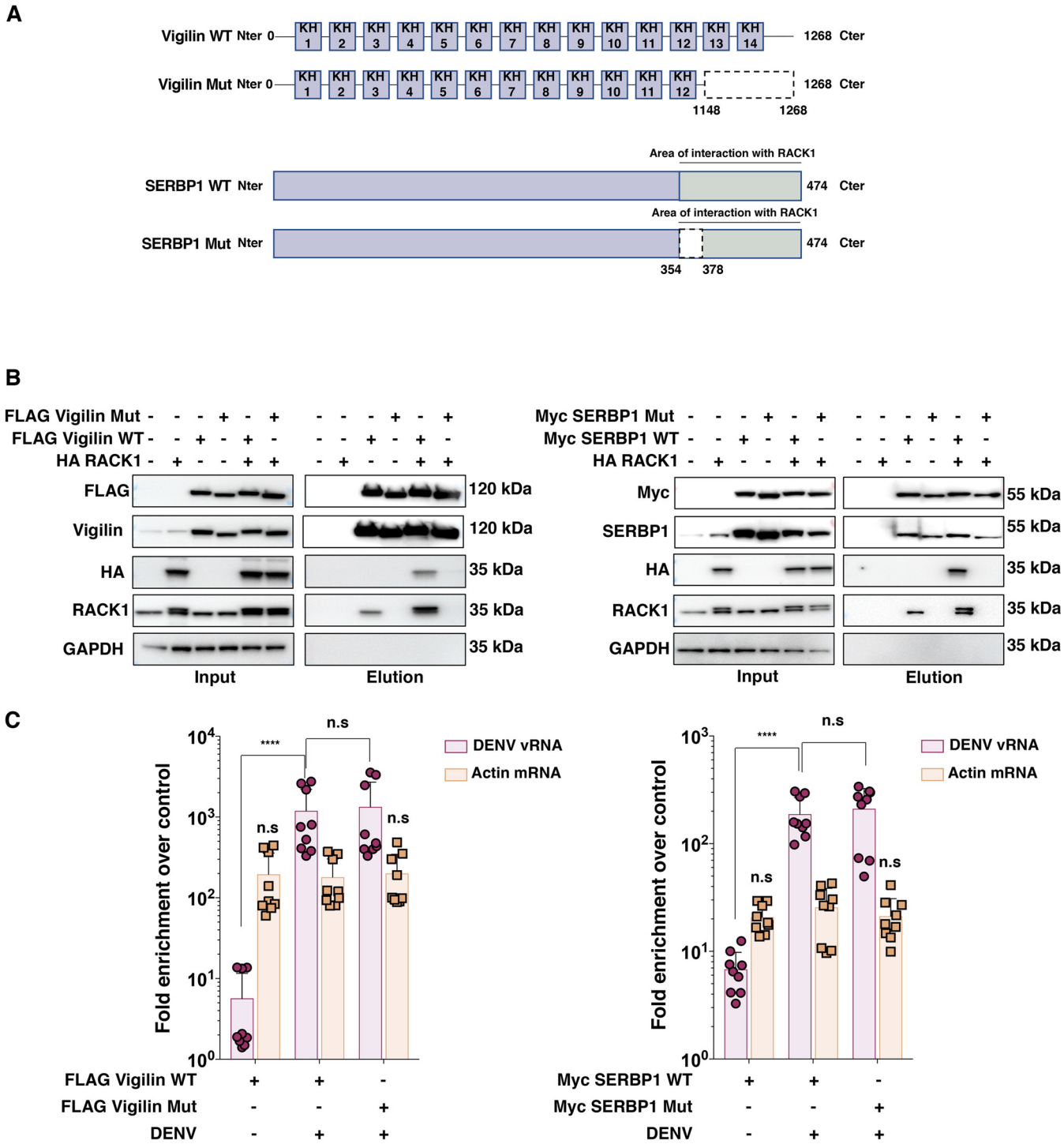

FIG 7 Characterization of Vigilin and SERBP1 mutants (Mut) deficient for RACK1 binding. (A) Schematic representations of Vigilin mutant (upper diagram) and SERBP1 mutant (lower diagram) constructs. (B) Evaluation of FLAG-Vigilin mutant (left) or Myc-SERBP1 mutant (right) interaction with RACK1. Cell extracts from 293T expressing the WT or mutated forms of Vigilin and SERBP1 were subjected to affinity purification using anti-FLAG- or -Myc-coated beads, respectively. Input and eluates were resolved by SDS-PAGE, and interacting proteins were revealed by Western blotting using corresponding antibodies. Shown is a representative Western blot of three independent experiments. (C) Analysis of Vigilin (WT and Mut) and SERBP1 (WT and Mut) interactions with the DENV RNA by RNA immunoprecipitation assay (RIP). The cells were infected at MOI 1 by DENV2-16681 and harvested 48 hpi. Tagged proteins were immunoprecipitated after UV cross-link at 254 nm using anti-FLAG- or -Myc-coated beads. The enrichment of DENV RNA or Actin RNA over the negative-control condition were determined by quantitative reverse transcription-PCR using specific primers and quantified using the ΔΔCt method. The data shown are the means ± SEM of three independent experiments performed in triplicate. Significance was calculated using a two-way ANOVA with Dunnett's multiple-comparison test. Cter, C terminus; Nter, N terminus; n.s, not significant; ****, $P < 0.0001$.

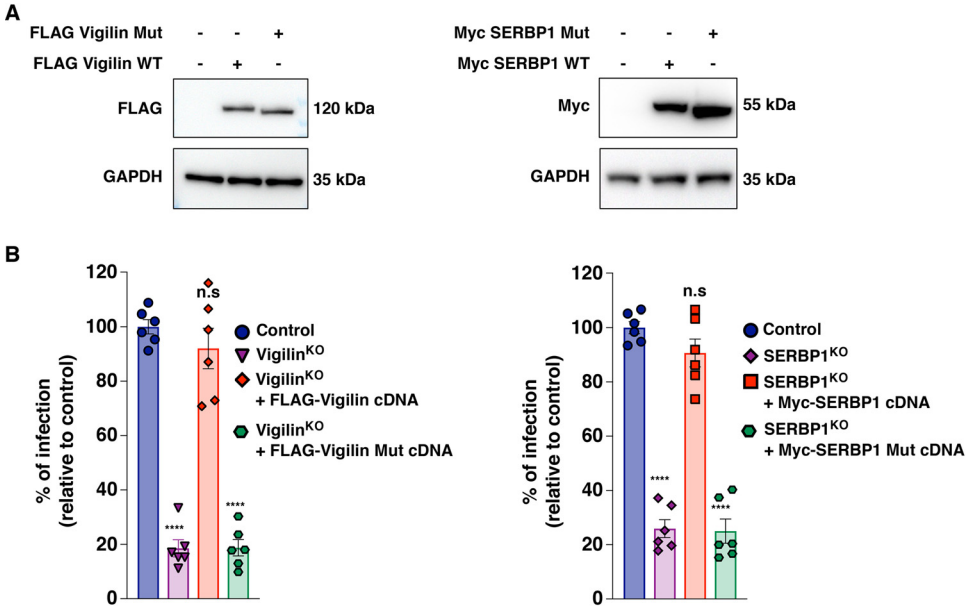

FIG 8 Vigilin and SERBP1 interaction with RACK1 is important in DENV infection. (A) Stable expression of Vigilin WT or Mut and SERBP1 WT or Mut in Vigilin ^{KO} or SERBP1 ^{KO} HAP1 cells, respectively. Western blot analysis of Vigilin or SERBP1 expression is shown. The data shown are representative of three independent experiments. (B) The indicated cells were infected at MOI 1 with DENV2-16681. Levels of infection were determined by flow cytometry at 48 hpi using the 2H2 MAb. The data shown are the means ± SEM of three technically independent experiments performed in duplicate. Significance was calculated using one-way ANOVA with Dunnett's multiple-comparison test. n.s, not significant; ****, $P < 0.0001$.

Vero E6 cells. For all of the viral stocks used in flow cytometry experiments, the viruses were purified through a 20% sucrose cushion by ultracentrifugation at 80,000 × *g* for 2 h at 4°C. The pellets were resuspended in HNE1X pH 7.4 (5 mM HEPES, 150 mM NaCl, 0.1 mM EDTA), aliquoted, and stored at −80°C. Viral stock titers were determined on Vero E6 cells by plaque-forming assay and were expressed as PFU/mL. Virus stocks were also determined by flow cytometry as described (54). Vero E6 cells were incubated 1 h with 100 μL of 10-fold serial dilutions of viral stocks. The inoculum was then replaced with 500 μL of culture medium, and the percentage of infected cells was quantified by flow cytometry using the 2H2 anti-PrM monoclonal antibody (MAb) at 8 h after infection. Viral titers were calculated and expressed as the number of fluorescence-activated cell sorter infectious units (FIU)/mL: titer = (average percentage of infection) × (number of cells in well) × (dilution factor)/(mL of inoculum added to cells).

To establish a DENV replicon plasmid, based on the infectious DENV2-16681 cDNA clone, the region encoding the structural proteins was mostly deleted and replaced by a cassette encoding ubiquitin-*Renilla* luciferase-foot-and-mouth disease virus (FMDV) 2A. DENV replicon RNA was generated as previously described (12). Infection or replication was determined by measuring the luciferase activity using TriStar LB942 microplate reader (Berthold Technologies). Red fluorescent protein (RFP)-expressing lentiviral vector pseudotyped with vesicular stomatitis virus glycoprotein G (VSV-G) were generated by transfecting HEK293FT cells with pNL4.3 Luc RFP ΔEnv, psPAX2, and pVSV-G (4:3:1 ratio) using Lipofectamine 3000. The ;Supernatants were harvested 48 h after transfection, cleared by centrifugation, filtered, and frozen at –80°C.

Polysome profiling. A total of 2 × 10^8 of indicated cells were incubated with 100 μg/mL of cycloheximide (CHX) for 10 min at 37°C and washed twice with cold phosphate-buffered saline (PBS) + 100 μg/mL CHX. The cells were pelleted by centrifugation at 4°C at 300 × *g* for 10 min and washed once with cold PBS + 100 μg/mL CHX. The pellet was resuspended in 2 mL lysis buffer (10 mM Tris-HCl, pH 7.5, 100 mM KCl, 10 mM magnesium acetate, 1% Triton X-100, 2 mM dithiothreitol [DTT]) containing 100 μg/mL CHX. The cells were pulverized by adding glass beads and vortexed for 5 min at 4°C. Cells debris were removed by centrifugation at 4°C at 3,000 × rpm for 10 min, and the supernatant was transferred to a 2 mL cryovial. The determination of polysome concentration was done by spectrophotometric estimation, based on the fact that ribosomes are ribonucleoprotein particles. Supernatant was quickly flash-frozen in liquid nitrogen and stored in a −80°C freezer. The supernatant was loaded on a 10 to 50% sucrose gradient (31% sucrose, 50 mM Tris-acetate, pH 7.6, 50 mM NH_4Cl, 12 mM $MgCl_2$, 1 mM DTT) and spun for 3 h at 39,000 rpm at 4°C in an SW41 swing-out rotor. The gradient was fractionated by hand and analyzed by immunoblotting.

Mass spectrometry analysis. HAP1 cells (5 × 10^8), expressing either the WT or the HA-tagged RACK1 proteins, were lysed in Pierce IP lysis buffer (Thermo Scientific) in the presence of Halt protease inhibitor cocktail (Thermo Scientific) for 30 min at 4°C and then cleared by centrifugation for 30 min at 6,000 × *g*. The supernatants were incubated overnight at 4°C with anti-HA magnetic beads. The beads

were washed three times with B015 buffer (20 mM Tris-HCl, pH 7.4, 150 mM NaCl, 5 mM $MgCl_2$, 10% glycerol, 0.5 mM EDTA, 0.05% Triton, 0.1% Tween 20), and the immune complexes were eluted twice with HA peptide (400 mg/mL) for 30 min at room temperature (RT). The eluates were concentrated on a Pierce concentrator (PES 10K) and stored at −20°C until used. A total of three coaffinity purifications and MS analysis experiments were performed with the HA-tagged RACK1 protein or the untagged RACK1 protein as a control in 293T cells. The samples were analyzed at Taplin Biological Mass Spectrometry Facility (Harvard Medical School). Briefly, concentrated eluates issued from immunopurification of endogenous and RACK1-HA-tagged protein were separated on 10% Tris-glycine SDS-PAGE gels (Invitrogen) and stained with Imperial Protein Stain (Thermo Fisher). Individual regions of the gel were cut into 1-mm^3 pieces and subjected to a modified in-gel trypsin digestion procedure (55). The peptides were desalted and subjected to a nanoscale reverse-phase high-performance liquid chromatography (HPLC) (56). Eluted peptides were then subjected to electrospray ionization and then tandem mass spectrometry (MS/MS) analysis into an LTQ Orbitrap Velos Pro ion-trap mass spectrometer (Thermo Fisher Scientific, Waltham, MA). The peptides were detected, isolated, and fragmented to produce a tandem mass spectrum of specific fragment ions for each peptide. The peptide sequences were determined by matching protein databases with the acquired fragmentation pattern by the Sequest software program (Thermo Fisher Scientific, Waltham, MA) (57). All databases include a reversed version of all the sequences, and the data were filtered to less than 2% peptide false discovery rate.

Network analysis. The AP-MS data set was analyzed with SAINTexpress and MIST software (37). Of the 1,671 proteins selected in our pipeline, 193 of 1,671 showed a probability score greater than 0.80 with SAINTexpress, and 135 of 193 showed an average peptide count greater than 10. This list of 135 host proteins was analyzed with DAVID 6.8 to identify statistical enrichments for specific GO terms from the cellular component (CC) annotation (38, 39). The interaction network was built using Cytoscape 3.4.0 (40), and the proteins were clustered into functional modules using enriched GO terms as a guideline and manual curation of literature.

Small interfering RNA (siRNA) screen assay. An arrayed ON-TARGETplus SMARTpool siRNA library targeting 49 of 135 proteins of our RACK1 network, which had an average peptide count great than 28, was purchased from Horizon Discovery. To this end, HeLa or 293T cells were transfected with a 30 nM final concentration of siRNA using the Lipofectamine RNAiMax (Life Technologies). 48 h posttransfection, the cells were infected with DENV2-16681 at MOI 5. Infection was quantified 48 h postinfection by flow cytometry and viability by CellTiter-Glo 2.0 assay (Promega). Two siRNA controls were included in the screen: a nontargeting siRNA used as a reference (siNT) and a siRNA targeting RACK1 (siRACK1) as a positive control for host-dependency factors (HDFs) (12). HDFs were defined as factors whose inhibition in both cell types decreases infection by at least 50% compared to siNT and viability by at most 20% of the siNT.

Gene editing and transcomplementation experiments. Single guide RNA (sgRNA) targeting Vigilin, SERBP1, and ZNF598 were designed using the CRISPOR software (58). Sequences for all the sgRNAs are listed in Table 1. The sgRNAs were cloned into the plasmid lentiCRISPR v2 (Addgene) according to the recommendations provided by the members of the Zhang's laboratory (Broad Institute, Cambridge, MA). HAP1 cells were transiently transfected with the plasmid expressing sgRNAs and selected with puromycin until all mock-transfected cells died. Clonal cell lines were isolated by limiting dilution and assessed by DNA sequencing and immunoblot for gene editing. The human HA-RACK1 WT and HA-RACK1 DE mutant plasmids were provided by Catherine Schuster (University of Strasbourg), the FLAG-tagged Vigilin cDNA was purchased from Genscript (clone OHu17734), and the Myc-tagged SERBP1 cDNA was purchased from Genscript (clone OHu26811C). After PCR, amplification products were cloned into a SpeI-NotI-digested (RACK1), NotI-XhoI-digested (Vigilin), or EcoRI-BamHI-digested (SERBP1) pLVX-IRES-ZsGreen1 vector. SERBP1 mutant and Vigilin mutant were obtained using the Q5 site-directed mutagenesis kit (E0554) (NEB) with deletion primers using the WT cDNA in pLVX as the template. All of the primers are listed in Table 1. Lentivirus-like particles for transduction were prepared in 293T cells by cotransfecting the plasmid of interest with psPAX2 (from N. Manel's lab, Curie Institute, Paris, France) and pCMV-VSV-G at a ratio of 4:3:1 with Lipofectamine 3000 (Thermo Fisher Scientific). The supernatants were collected 48 h after transfection, centrifuged (750 × *g*, 10 min), filtered using a 0.45-μm filter, and purified through a 20% sucrose cushion by ultracentrifugation (80,000 × *g* for 2 h at 4°C). The pellets were resuspended in HNE1X, pH 7.4, aliquoted, and stored at −80°C. Cells of interest were transduced by spinoculation (750 × *g* for 2 h at 32°C) and sorted for GFP-positive cells by flow cytometry if necessary.

Flow cytometry analysis. The indicated cells were plated in 24-well plates and infected. At indicated times, the cells were trypsinized and fixed with 2% paraformaldehyde (PFA) diluted in PBS for 15 min at room temperature. The cells were incubated for 1 h at 4°C with 1 μg/mL of 3E4 anti-E2 monoclonal antibody (CHIKV), 2H2 anti-prM monoclonal antibody (MAb) (DENV), or the anti-E protein MAb 4G2 (ZIKV). Antibodies were diluted in permeabilization flow cytometry buffer (PBS supplemented with 5% FBS, 0.5% saponin, 0.1% sodium azide). After washing, the cells were incubated with 1 μg/mL of Alexa Fluor 488- or 647-conjugated goat anti-mouse IgG diluted in permeabilization flow cytometry buffer for 30 min at 4°C. Acquisition was performed with an Attune NxT flow cytometer (Thermo Fisher Scientific), and the data were analyzed by FlowJo software (TreeStar).

Infectious virus yield assay. To assess the release of infectious particles during infection, the indicated cells were inoculated for 3 h with DENV2-16681, washed once with PBS, and maintained in the culture medium for 48 h. At the indicated time points, the supernatants were collected and kept at −80°C. Vero E6 cells were incubated with 3-fold serial dilutions of supernatant for 24 h, and prM expression was quantified by flow cytometry as previously described (54).

TABLE 1 Antibodies and reagents[a]

Reagent or resource	Source or sequence	Identifier
Antibodies		
Mouse anti-RACK1 (B-3)	Santa Cruz Biotechnology	sc-17754
Rabbit anti-HA tag (C29F4)	Cell Signaling	3724S
Mouse anti-β-tubulin (D-10)	Santa Cruz Biotechnology	sc-5274
Rabbit anti-Vigilin	Bethyl	A303-971A
Mouse anti-Vigilin (H-3)	Santa Cruz Biotechnology	sc-271523
Rabbit anti-ZNF598	Bethyl	A305-108A
Mouse anti-SERBP1 (1B9)	Santa Cruz Biotechnology	sc-100800
Rabbit anti-RPS3	Bethyl	A303-841A
Mouse anti-GAPDH (0411)	Santa Cruz Biotechnology	sc-47724
Mouse anti-dengue virus NS3 protein antibody	GeneTex	GTX629477
Rabbit anti-dengue virus envelope protein antibody	GeneTex	GTX127277
Rabbit anti-dengue virus prM protein antibody	GeneTex	GTX128093
Mouse anti-FLAG (M2)	Sigma-Aldrich	F1804
Mouse anti-Myc tag (9B11)	Cell Signaling	2276S
Polyclonal rabbit anti-mouse immunoglobulins/HRP	Agilent Technologies	P0260
Peroxidase AffiniPure donkey anti-rabbit IgG (H + L)	Jackson ImmunoResearch	711-035-152
Chemicals and reagents		
DMEM	Gibco	12440-053
IMDM	Gibco	41966-029
Paraformaldehyde (32%) aqueous solution	Electron Microscopy Sciences	15714
Lipofectamine RNAiMAX	Invitrogen	13778150
Lipofectamine 3000 transfection kit	Invitrogen	L3000-015
Halt protease and phosphatase inhibitor cocktail	Thermo Scientific	1861281
Bolt 4 to 12% Bis-Tris Plus gels	Invitrogen	NW04120BOX
Bolt 10% Bis-Tris Plus gel	Invitrogen	NW00100BOX
Tampon RIPA Pierce lysis buffer	Thermo Scientific	89900
20$\times$ Bolt MOPS SDS running buffer	Invitrogen	B0001
Pierce 1-Step transfer buffer	Thermo Scientific	84731
SuperSignal West Dura extended duration substrate	Thermo Scientific	34076
Maxima first-strand cDNA synthesis kit for reverse transcription-qPCR	Thermo Scientific	K1671
RNase H, recombinant	New England BioLabs	M0297S
TRIzol LS reagent	Ambion	10296010
RNeasy minikit	Qiagen	74106
Tampon RIPA Pierce lysis buffer	Thermo Scientific	87788
Q5 site-directed mutagenesis kit	NEB	E0554S
7-Deaza-2′-C-methyladenosine (MK0608, 50 μM final concn)	Biosynth Carbosynth	ND08351
Power SYBR Green PCR master mix	Life Technologies, Inc.	4367659
Critical commercial assay		
Pierce *Gaussia* luciferase glow assay kit	Thermo Scientific	16160
Renilla luciferase assay system	Promega	E2810
CellTiter-Glo 2.0 assay	Promega	G9242
Protein assay reagent A	Bio-Rad	500-0113
Protein assay reagent B	Bio-Rad	500-0114
Protein assay reagent S	Bio-Rad	500-0115
gRNA for CRISPR/Cas9 KO		
Control	GAGCTGGACGGCGACGTAAA	
Vigilin	GTTTTGCTGAACACCGAAGTGGGGGG	
SERBP1	AAGCCGGCGGGGGCGGCGTTGGG	
ZNF598	GGGGGCCGGATCCCGGACCATGG	
Plasmids		
pLentiCRISPRv2	Addgene	98290
pLentiCRISPRv2 sgRNA Vigilin	This paper	NA
pLentiCRISPRv2 sgRNA SERBP1	This paper	NA
pLentiCRISPRv2 sgRNA ZNF598	This paper	NA
pLVX-IRES-ZsGreen1	Takara	632187
pLVX-IRES-ZsGreen1 HA-RACK1 WT	This paper	NA
pLVX-IRES-ZsGreen1 HA-RACK1 D/E	This paper	NA
pLVX-IRES-ZsGreen1 FLAG-Vigilin	This paper	NA

(Continued on next page)

TABLE 1 (Continued)

Reagent or resource	Source or sequence	Identifier
pLVX-IRES-ZsGreen1 FLAG-Vigilin Mut	This paper	NA
pLVX-IRES-ZsGreen1 Myc-SERBP1	This paper	NA
pLVX-IRES-ZsGreen1 Myc-SERBP1 Mut	This paper	NA
Primers for site-directed mutagenesis		
Vigilin Mut forward	TAAGCGGCCGCGGATCCC	
Vigilin Mut reverse	TTCGTCCATGATTTTGCGAATGGCTTTG	
SERBP1 Mut forward	GGTGCTGATGGGCAGTGG	
SERBP1 Mut reverse	CTCTTTTGGACCCTCCTCTTTTAC	
qPCR primers		
DENV2 NS3 forward	TGTGCACACTGGAAAGAAGC	
DENV2 NS3 reverse	TGCGTAGTTGATGCCTTCAC	
Hs_GAPDH_2_SG QuantiTect primer assay	Qiagen	QT01192646

[a]DMEM, Dulbecco's modified Eagle's medium; GAPDH, glyceraldehyde-3-phosphate dehydrogenase; gRNA, genomic RNA; HA, hemagglutinin; HRP, horseradish peroxidase; IMDM, Iscove's modified Dulbecco's medium; MOPS, morpholinepropanesulfonic acid; Mut, mutant; qPCR, quantitative PCR; RIPA, radio immunoprecipitation assay; sgRNA, specific gRNA.

Immunoblots. The cell pellets were lysed in Pierce IP lysis buffer (Thermo Fisher Scientific) containing Halt protease and phosphatase inhibitor cocktails (Thermo Fisher Scientific) for 30 min at 4°C. Equal amounts of protein, determined by DC protein assay (Bio-Rad), were prepared in 4× LDS sample buffer (Pierce) containing 25 mM dithiothreitol (DTT) and heated at 95°C for 5 min. The samples were separated on Bolt 4 to 12% Bis-Tris gels in Bolt morpholinepropanesulfonic acid (MOPS) SDS running buffer (Thermo Scientific), and the proteins were transferred onto a polyvinylidene difluoride (PVDF) membrane (Bio-Rad) using the Power Blotter system (Thermo Fisher Scientific). The membranes were blocked with PBS containing 0.1% Tween 20 and 5% nonfat dry milk and incubated overnight at 4°C with primary antibodies (HA 1/5,000, RACK1 1/4,000, glyceraldehyde-3-phosphate dehydrogenase [GAPDH] 1/5,000, Vigilin 1/500, SERBP1 1/2,000, NS3 DENV 1/4,000, 2H2 prM DENV 1/4,000, E DENV 1/5,000, FLAG 1/2,000, Myc 1/1,000, tubulin 1/500, ZNF598 1/10,000, anti-mouse horseradish peroxidase [HRP] 1/5,000, anti-rabbit HRP 1/10,000). Staining was revealed with corresponding HRP-coupled secondary antibodies and developed using Super Signal West Dura extended duration substrate (Thermo Fisher Scientific) following the manufacturer's instructions. The signals were acquired with a Fusion Fx camera (VILBERT Lourmat).

Coimmunoprecipitation assay. The indicated cells were plated in 10-cm dishes (5×10^6) After 24 h, the cells were transfected with a total of 15 μg DNA expression plasmids (7.5 μg of each plasmid in cotransfection assays) using Lipofectamine 3000 (Thermo Fisher Scientific). After 24 h of transfection, the cells were washed once with PBS, collected, and centrifuged (400 × *g* for 5 min). The cell pellets were lysed in Pierce IP lysis buffer (Thermo Fisher Scientific) containing Halt protease and phosphatase inhibitor cocktails (Thermo Fisher Scientific) for 30 min at 4°C. Equal amounts of protein, determined by DC protein assay (Bio-Rad), were incubated overnight at 4°C, with either anti-FLAG magnetic beads, anti-HA magnetic beads, or anti-Myc magnetic beads. The beads were washed three times with BO15 buffer (20 mM Tris-HCl, pH 7.4, 150 mM NaCl, 5 mM $MgCl_2$, 10% glycerol, 0.5 mM EDTA, 0.05% Triton X-100, 0.1% Tween 20) before incubation. The retained complexes were eluted twice with either 3× FLAG peptide (200 μg/mL, Sigma-Aldrich), HA peptide (400 μg/mL, Roche), or cMyc peptide (200 μg/mL, Sigma-Aldrich) for 30 min at RT. The samples were prepared and immunoblotted as described above. For input, 1% of whole-cell lysates was loaded on the gel.

RNA immunoprecipitation. Indicated cells (2×10^6) were plated in 10-cm dishes, transfected for 48 h with the corresponding plasmids using Lipofectamine 3000, and then infected with DENV2-16681 at MOI 2. The culture medium was removed 48 h postinfection, and the cells were washed twice with cold PBS. The cells transfected with an empty plasmid and infected with DENV2-16681 were used as negative control to assess the experiment background. Before UV cross-link, 10 mL of cold PBS were added on the cell (2,000 mJ/cm^2). The cells were collected and spun 5 min at 4°C at 2,000 rpm. The cell pellets were lysed in 1 mL of Pierce IP lysis buffer (Thermo Fisher Scientific) containing Halt protease and phosphatase inhibitor cocktails (Thermo Fisher Scientific) + 250 U of RNasin (Promega) for 30 min at 4°C. Lysates were incubated with 250 U of turbo DNAse for 30 min at 37°C, then centrifugated for 15 min at 15,000 rpm. The supernatant was then collected. The protein of interest was immunoprecipitated and eluted (see the coimmunoprecipitation assay section). 100 μl of input and elution were incubated with 150 μL of proteinase K buffer (117 μl NT-2, 15 μL SDS 10%, and 18 μL of proteinase K) 1 h at 56°C, and then 750 μl of TRIzol reagent was added. RNA was extracted by phenol chloroform precipitation; 0.2 mL of chloroform per 1 mL of TRIzol reagent was added. The samples were vortexed vigorously for 15 s, incubated at room temperature for 3 min, and then centrifuged at 12,000 × *g* for 15 min at 4°C. Following centrifugation, the upper aqueous phase was transferred carefully without disturbing the interphase into fresh tube. The RNA from the aqueous phase was precipitated by mixing with 0.5 mL of isopropyl alcohol per 1 mL of TRIzol reagent used for the initial homogenization. The samples were incubated at RT for 10 min and centrifuged at 12,000 × *g* for 10 min at 2 to 4°C. The supernatant was removed completely, and the RNA pellet was washed twice with 1 mL of 75% ethanol per 1 mL of TRIzol

reagent used for the initial homogenization. The samples were mixed by vortexing and centrifuged at 7,500 × *g* for 5 min at 2 to 8°C. The RNA pellet was air dried for 5 to 10 min and then dissolved in RNase-free water.

RNA preparation and quantitative reverse transcription-PCR. Total RNA extraction from the indicated cells was performed using the RNeasy Plus minikit (Qiagen). RNA was quantified using a Nanodrop One (Thermo Fisher Scientific) before cDNA amplification. cDNA was prepared from 100 ng total RNA with Maxima first-strand synthesis kit (Thermo Fisher Scientific) including an additional step of RNase H treatment after reverse transcription. Quantitative PCR (qPCR) was performed using Power SYBR green PCR master Mix (Thermo Fisher Scientific) on a Light Cycler 480 (Roche). Quantification was based on the comparative threshold cycle (Ct) method, using GAPDH as endogenous reference control. For RNA immunoprecipitation assays (RIPs), cDNA amplification was performed on 2 μl of immunoprecipitated and input RNA. To assess for vRNA and actin enrichment, the ΔΔCt values were calculated as previously described (59). Briefly, we normalized each RIP fractions' Ct to the corresponding input fraction Ct average for the same qPCR assay (ΔCt [normalized RIP]) to account for sample preparation differences. Then, we adjusted the normalized RIP fraction Ct value for the normalized WT Ct value (ΔΔCt = ΔCt[normalized RIP] − ΔCt[normalized negative control]). Finally, we performed a linear conversion of the ΔΔCt (2^[−ΔΔCt]) to calculate the fold change over the negative-control condition.

Cell viability assay. Cell viability and proliferation were assessed using CellTiter-Glo 2.0 assay (Promega) according to the manufacturer's protocol. The cells (3×10^4) were plated in 48-well plates. At the indicated times, 100 μL of CellTiter-Glo reagent were added to each well. After 10 min of incubation, 200 μL from each well was transferred in an opaque 96-well plate (Cellstar, Greiner Bio-One), and luminescence was measured on a TriStar2 LB 942 (Berthold) with a 0.1-s integration time.

RNA stability measurement by high-molecular-weight Northern blot analysis. The indicated cells (1×10^6) were plated on a 60-mm dish and infected with DENV2-16681. At 48 h postinfection, medium was replaced by MK0608 (50 μM final concentration) containing medium to block viral replication. At the indicated time posttreatment, the cells were washed twice with cold PBS and harvested in TRIzol (Thermo Fisher Scientific). Total RNA extraction was performed as previously described in RIP protocol. The DENV2-specific probe was obtained after PCR amplification of the 3′-UTR of the DENV2-16681 infectious clone (from 10,205 to 10,704). The probes were then labeled with [α-^{32}P]dCTP using the Prime-a-gene kit (Promega). For high-molecular-weight Northern blot analysis to detect DENV2 genomic RNA, 5 μg of total RNA were denatured for 5 min at 65°C in RNA sample buffer (32% deionized formamide, 4% formaldehyde, 1× MOPS, 1 μg/μL ethidium bromide). Then, RNA loading buffer (50% glycerol, 1 mM EDTA, 0.4% bromophenol blue) was added. RNAs were resolved in a 1% agarose gel containing 1× MOPS and 3.7% formaldehyde in 1× MOPS buffer, before being transferred overnight on a nylon Hybond N^+ membrane (Cytiva) in a 20 × SSC solution (Euromedex). RNAs were UV cross-linked (120 mJ) with Stratagene Stratalinker 1800 (LabX). The membrane was blocked and hybridized overnight at 42°C using PerfectHyb Plus hybridization buffer (Sigma) with the corresponding labeled probe. The day after, the membrane was washed using 2× SSC, 0.1% SDS solution twice at 42°C and 0.1× SSC, 0.1% SDS twice at 50°C before being exposed on an imaging plate (Fujifilm) for 24 h. The plate was revealed using Typhoon FLA 7,000 (GE Healthcare). Densitometry analysis of the bands was performed using Image Quant TL 8.1 software (GE Healthcare).

Graphics and statistical analyses. The number of independent experimental replications is indicated in the legends. Graphical representation and statistical analyses of mean and standard error of the mean (SEM) were performed using Prism 8 software (GraphPad Software) as well as analysis of variance (ANOVA).

Data availability. The mass spectrometry proteomics data have been deposited in the ProteomeXchange Consortium via the PRIDE partner repository with the data set identifier PXD030765 (https://www.ebi.ac.uk/pride/archive/projects/PXD030765).

SUPPLEMENTAL MATERIAL

Supplemental material is available online only.

SUPPLEMENTAL FILE 1, PDF file, 0.1 MB.

ACKNOWLEDGMENTS

We thank Karim Majzoub and Alessia Zamborlini for critical readings of the manuscript and helpful discussions. We are grateful to Ralf Bartenschalger (Heidelberg University, Heidelberg, Germany), Gabriele Fuchs (University at Albany, Albany, NY), and Catherine Schuster (University of Strasbourg, Strasbourg, France) for providing us with DENV R2A reporter virus, RACK1 knockout cells, and RACK1 plasmids, respectively.

A.A. dedicates this work to the memory of Jean-Louis Virelizier (Unité d'Immunologie Virale, Institut Pasteur, Paris, France) and Renaud Mahieux (Ecole Normale Supérieure, Lyon, France), who left us during the SARS-CoV-2 epidemic.

This study was supported by Fondation pour la Recherche Medicale grant FRM-EQU202003010193, the French government's Investissement d'Avenir program, Laboratoire d'Excellence Integrative Biology of Emerging Infectious Diseases grant

ANR-10-LABX-62-IBEID, and ZIKAHOST grant ANR-15-CE15-00029. A.B. was supported by a scholarship from the French Ministry of Research.

A.B., M.-L.H., and A.A. conceived the study. A.B., M.-L.H., M.P., L.C., L.B.-M., C.D., L.M., and A.A. designed the experiments. A.B. and M.-L.H. performed the RACK1 interactome and the RNAi screen. P.-O.V. provided help in the data analysis. M.P., L.C., L.B.-M., and V.K. generated the viruses used in this study and performed infection studies. B.M.K. generated the DENV replicon and provided expertise in viral RNA production. S.P. and M.B. performed the DENV RNA stability experiments. S.G.-M. participated in the RNA IP experiments. A.B. and A.A. wrote the initial manuscript draft, and the other authors contributed to its editing in its final form.

We declare no conflice of interest.

REFERENCES

1. Holbrook MR. 2017. Historical perspectives on flavivirus research. Viruses 9:97. https://doi.org/10.3390/v9050097.
2. Halstead SB. 2007. Dengue. Lancet 370:1644–1652. https://doi.org/10.1016/S0140-6736(07)61687-0.
3. Brady OJ, Gething PW, Bhatt S, Messina JP, Brownstein JS, Hoen AG, Moyes CL, Farlow AW, Scott TW, Hay SI. 2012. Refining the global spatial limits of dengue virus transmission by evidence-based consensus. PLoS Negl Trop Dis 6:e1760. https://doi.org/10.1371/journal.pntd.0001760.
4. Bhatt S, Gething PW, Brady OJ, Messina JP, Farlow AW, Moyes CL, Drake JM, Brownstein JS, Hoen AG, Sankoh O, Myers MF, George DB, Jaenisch T, Wint GRW, Simmons CP, Scott TW, Farrar JJ, Hay SI. 2013. The global distribution and burden of dengue. Nature 496:504–507. https://doi.org/10.1038/nature12060.
5. Kaptein SJF, Goethals O, Kiemel D, Marchand A, Kesteleyn B, Bonfanti J-F, Bardiot D, Stoops B, Jonckers THM, Dallmeier K, Geluykens P, Thys K, Crabbe M, Chatel-Chaix L, Münster M, Querat G, Touret F, de Lamballerie X, Raboisson P, Simmen K, Chaltin P, Bartenschlager R, Van Loock M, Neyts J. 2021. A pan-serotype dengue virus inhibitor targeting the NS3-NS4B interaction. Nature 598:504–509. https://doi.org/10.1038/s41586-021-03990-6.
6. Hadinegoro SR, Arredondo-García JL, Capeding MR, Deseda C, Chotpitayasunondh T, Dietze R, Hj Muhammad Ismail HI, Reynales H, Limkittikul K, Rivera-Medina DM, Tran HN, Bouckenooghe A, Chansinghakul D, Cortés M, Fanouillere K, Forrat R, Frago C, Gailhardou S, Jackson N, Noriega F, Plennevaux E, Wartel TA, Zambrano B, Saville M, CYD-TDV Dengue Vaccine Working Group. 2015. Efficacy and long-term safety of a dengue vaccine in regions of endemic disease. N Engl J Med 373:1195–1206. https://doi.org/10.1056/NEJMoa1506223.
7. Ferguson NM, Rodríguez-Barraquer I, Dorigatti I, Mier-y-Teran-Romero L, Laydon DJ, Cummings DAT. 2016. Benefits and risks of the Sanofi-Pasteur dengue vaccine: modeling optimal deployment. Science 353:1033–1036. https://doi.org/10.1126/science.aaf9590.
8. Acosta EG, Kumar A, Bartenschlager R. 2014. Revisiting dengue virus-host cell interaction: new insights into molecular and cellular virology. Adv Virus Res 88:1–109. https://doi.org/10.1016/B978-0-12-800098-4.00001-5.
9. Zeidler JD, Fernandes-Siqueira LO, Barbosa GM, Da Poian AT. 2017. Non-canonical roles of dengue virus non-structural proteins. Viruses 9:42. https://doi.org/10.3390/v9030042.
10. Miller S, Krijnse-Locker J. 2008. Modification of intracellular membrane structures for virus replication. Nat Rev Microbiol 6:363–374. https://doi.org/10.1038/nrmicro1890.
11. Welsch S, Miller S, Romero-Brey I, Merz A, Bleck CKE, Walther P, Fuller SD, Antony C, Krijnse-Locker J, Bartenschlager R. 2009. Composition and three-dimensional architecture of the dengue virus replication and assembly sites. Cell Host Microbe 5:365–375. https://doi.org/10.1016/j.chom.2009.03.007.
12. Hafirassou ML, Meertens L, Umaña-Diaz C, Labeau A, Dejarnac O, Bonnet-Madin L, Kümmerer BM, Delaugerre C, Roingeard P, Vidalain P-O, Amara A. 2017. A global interactome map of the dengue virus NS1 identifies virus restriction and dependency host factors. Cell Rep 21:3900–3913. https://doi.org/10.1016/j.celrep.2017.11.094.
13. Shue B, Chiramel AI, Cerikan B, To T-H, Frölich S, Pederson SM, Kirby EN, Eyre NS, Bartenschlager RFW, Best SM, Beard MR. 2021. Genome-wide CRISPR screen identifies RACK1 as a critical host factor for flavivirus replication. J Virol 95:e00596-21. https://doi.org/10.1128/JVI.00596-21.
14. Ben-Shem A, Garreau de Loubresse N, Melnikov S, Jenner L, Yusupova G, Yusupov M. 2011. The structure of the eukaryotic ribosome at 3.0 Å resolution. Science 334:1524–1529. https://doi.org/10.1126/science.1212642.
15. Sengupta J, Nilsson J, Gursky R, Spahn CMT, Nissen P, Frank J. 2004. Identification of the versatile scaffold protein RACK1 on the eukaryotic ribosome by cryo-EM. Nat Struct Mol Biol 11:957–962. https://doi.org/10.1038/nsmb822.
16. Xu C, Min J. 2011. Structure and function of WD40 domain proteins. Protein Cell 2:202–214. https://doi.org/10.1007/s13238-011-1018-1.
17. Nielsen MH, Flygaard RK, Jenner LB. 2017. Structural analysis of ribosomal RACK1 and its role in translational control. Cell Signal 35:272–281. https://doi.org/10.1016/j.cellsig.2017.01.026.
18. Adams DR, Ron D, Kiely PA. 2011. RACK1, a multifaceted scaffolding protein: structure and function. Cell Commun Signal 9:22. https://doi.org/10.1186/1478-811X-9-22.
19. Gandin V, Senft D, Topisirovic I, Ronai ZA. 2013. RACK1 function in cell motility and protein synthesis. Genes Cancer 4:369–377. https://doi.org/10.1177/1947601913486348.
20. Chang BY, Conroy KB, Machleder EM, Cartwright CA. 1998. RACK1, a receptor for activated C kinase and a homolog of the β subunit of G proteins, inhibits activity of Src tyrosine kinases and growth of NIH 3T3 cells. Mol Cell Biol 18:3245–3256. https://doi.org/10.1128/MCB.18.6.3245.
21. Chang BY, Harte RA, Cartwright CA. 2002. RACK1: a novel substrate for the Src protein-tyrosine kinase. Oncogene 21:7619–7629. https://doi.org/10.1038/sj.onc.1206002.
22. Yarwood SJ, Steele MR, Scotland G, Houslay MD, Bolger GB. 1999. The RACK1 signaling scaffold protein selectively interacts with the cAMP-specific phosphodiesterase PDE4D5 isoform. J Biol Chem 274:14909–14917. https://doi.org/10.1074/jbc.274.21.14909.
23. Kiely PA, Sant A, O'Connor R. 2002. RACK1 is an insulin-like growth factor 1 (IGF-1) receptor-interacting protein that can regulate IGF-1-mediated Akt activation and protection from cell death. J Biol Chem 277:22581–22589. https://doi.org/10.1074/jbc.M201758200.
24. Baum S, Bittins M, Frey S, Seedorf M. 2004. Asc1p, a WD40-domain containing adaptor protein, is required for the interaction of the RNA-binding protein Scp160p with polysomes. Biochem J 380:823–830. https://doi.org/10.1042/BJ20031962.
25. Ceci M, Gaviraghi C, Gorrini C, Sala LA, Offenhäuser N, Carlo Marchisio P, Biffo S. 2003. Release of eIF6 (p27BBP) from the 60S subunit allows 80S ribosome assembly. Nature 426:579–584. https://doi.org/10.1038/nature02160.
26. Joshi B, Cai A-L, Keiper BD, Minich WB, Mendez R, Beach CM, Stepinski J, Stolarski R, Darzynkiewicz E, Rhoads RE. 1995. Phosphorylation of eukaryotic protein synthesis initiation factor 4E at Ser-209. J Biol Chem 270:14597–14603. https://doi.org/10.1074/jbc.270.24.14597.
27. Whalen SG, Gingras A-C, Amankwa L, Mader S, Branton PE, Aebersold R, Sonenberg N. 1996. Phosphorylation of eIF-4E on serine 209 by protein kinase C is inhibited by the translational repressors, 4E-binding proteins. J Biol Chem 271:11831–11837. https://doi.org/10.1074/jbc.271.20.11831.
28. Sundaramoorthy E, Leonard M, Mak R, Liao J, Fulzele A, Bennett EJ. 2017. ZNF598 and RACK1 regulate mammalian ribosome-associated quality control function by mediating regulatory 40S ribosomal ubiquitylation. Mol Cell 65:751–760.e4. https://doi.org/10.1016/j.molcel.2016.12.026.
29. Long L, Deng Y, Yao F, Guan D, Feng Y, Jiang H, Li X, Hu P, Lu X, Wang H, Li J, Gao X, Xie D. 2014. Recruitment of phosphatase PP2A by RACK1 adaptor protein deactivates transcription factor IRF3 and limits type I

interferon signaling. Immunity 40:515–529. https://doi.org/10.1016/j.immuni.2014.01.015.
30. Xie T, Chen T, Li C, Wang W, Cao L, Rao H, Yang Q, Shu H-B, Xu L-G. 2019. RACK1 attenuates RLR antiviral signaling by targeting VISA-TRAF complexes. Biochem Biophys Res Commun 508:667–674. https://doi.org/10.1016/j.bbrc.2018.11.203.
31. Duan Y, Zhang L, Angosto-Bazarra D, Pelegrín P, Núñez G, He Y. 2020. RACK1 mediates NLRP3 inflammasome activation by promoting NLRP3 active conformation and inflammasome assembly. Cell Rep 33:108405. https://doi.org/10.1016/j.celrep.2020.108405.
32. Kuhn L, Majzoub K, Einhorn E, Chicher J, Pompon J, Imler J-L, Hammann P, Meignin C. 2017. Definition of a RACK1 interaction network in *Drosophila melanogaster* using SWATH-MS. G3 7:2249–2258. https://doi.org/10.1534/g3.117.042564.
33. Majzoub K, Hafirassou ML, Meignin C, Goto A, Marzi S, Fedorova A, Verdier Y, Vinh J, Hoffmann JA, Martin F, Baumert TF, Schuster C, Imler J-L. 2014. RACK1 controls IRES-mediated translation of viruses. Cell 159:1086–1095. https://doi.org/10.1016/j.cell.2014.10.041.
34. Jha S, Rollins MG, Fuchs G, Procter DJ, Hall EA, Cozzolino K, Sarnow P, Savas JN, Walsh D. 2017. Trans-kingdom mimicry underlies ribosome customization by a poxvirus kinase. Nature 546:651–655. https://doi.org/10.1038/nature22814.
35. Kim HD, Kong E, Kim Y, Chang J-S, Kim J. 2017. RACK1 depletion in the ribosome induces selective translation for non-canonical autophagy. Cell Death Dis 8:e2800. https://doi.org/10.1038/cddis.2017.204.
36. Gallo S, Ricciardi S, Manfrini N, Pesce E, Oliveto S, Calamita P, Mancino M, Maffioli E, Moro M, Crosti M, Berno V, Bombaci M, Tedeschi G, Biffo S. 2018. RACK1 specifically regulates translation through its binding to ribosomes. Mol Cell Biol 38:e00230-18. https://doi.org/10.1128/MCB.00230-18.
37. Teo G, Liu G, Zhang J, Nesvizhskii AI, Gingras A-C, Choi H. 2014. SAINTexpress: improvements and additional features in significance analysis of interactome software. J Proteomics 100:37–43. https://doi.org/10.1016/j.jprot.2013.10.023.
38. Huang DW, Sherman BT, Lempicki RA. 2009. Systematic and integrative analysis of large gene lists using DAVID bioinformatics resources. Nat Protoc 4:44–57. https://doi.org/10.1038/nprot.2008.211.
39. Huang DW, Sherman BT, Lempicki RA. 2009. Bioinformatics enrichment tools: paths toward the comprehensive functional analysis of large gene lists. Nucleic Acids Res 37:1–13. https://doi.org/10.1093/nar/gkn923.
40. Shannon P, Markiel A, Ozier O, Baliga NS, Wang JT, Ramage D, Amin N, Schwikowski B, Ideker T. 2003. Cytoscape: a software environment for integrated models of biomolecular interaction networks. Genome Res 13:2498–2504. https://doi.org/10.1101/gr.1239303.
41. Liu Y, Shi S-L. 2021. The roles of hnRNP A2/B1 in RNA biology and disease. Wiley Interdiscip Rev RNA 12:e1612. https://doi.org/10.1002/wrna.1612.
42. Ahn J-W, Kim S, Na W, Baek S-J, Kim J-H, Min K, Yeom J, Kwak H, Jeong S, Lee C, Kim S-Y, Choi CY. 2015. SERBP1 affects homologous recombination-mediated DNA repair by regulation of CtIP translation during S phase. Nucleic Acids Res 43:6321–6333. https://doi.org/10.1093/nar/gkv592.
43. Cheng MH, Jansen R-P. 2017. A jack of all trades: the RNA-binding protein Vigilin. Wiley Interdiscip Rev RNA 8:1448.
44. Paranjape SM, Harris E. 2007. Y box-binding protein-1 binds to the dengue virus 3′-untranslated region and mediates antiviral effects. J Biol Chem 282:30497–30508. https://doi.org/10.1074/jbc.M705755200.
45. Brunetti JE, Scolaro LA, Castilla V. 2015. The heterogeneous nuclear ribonucleoprotein K (hnRNP K) is a host factor required for dengue virus and Junín virus multiplication. Virus Res 203:84–91. https://doi.org/10.1016/j.virusres.2015.04.001.
46. Mobin MB, Gerstberger S, Teupser D, Campana B, Charisse K, Heim MH, Manoharan M, Tuschl T, Stoffel M. 2016. The RNA-binding protein Vigilin regulates VLDL secretion through modulation of Apob mRNA translation. Nat Commun 7:12848. https://doi.org/10.1038/ncomms12848.
47. Ooi YS, Majzoub K, Flynn RA, Mata MA, Diep J, Li JK, van Buuren N, Rumachik N, Johnson AG, Puschnik AS, Marceau CD, Mlera L, Grabowski JM, Kirkegaard K, Bloom ME, Sarnow P, Bertozzi CR, Carette JE. 2019. An RNA-centric dissection of host complexes controlling flavivirus infection. Nat Microbiol 4:2369–2382. https://doi.org/10.1038/s41564-019-0518-2.
48. Bolger GB. 2017. The RNA-binding protein SERBP1 interacts selectively with the signaling protein RACK1. Cell Signal 35:256–263. https://doi.org/10.1016/j.cellsig.2017.03.001.
49. Brown A, Baird MR, Yip MC, Murray J, Shao S. 2018. Structures of translationally inactive mammalian ribosomes. Elife 7:e40486. https://doi.org/10.7554/eLife.40486.
50. Phillips SL, Soderblom EJ, Bradrick SS, Garcia-Blanco MA. 2016. Identification of proteins bound to dengue viral RNA *in vivo* reveals new host proteins important for virus replication. mBio 7:e01865-15. https://doi.org/10.1128/mBio.01865-15.
51. Wang G, Kouwaki T, Okamoto M, Oshiumi H. 2019. Attenuation of the innate immune response against viral infection due to ZNF598-promoted binding of FAT10 to RIG-I. Cell Rep 28:1961–1970.e4. https://doi.org/10.1016/j.celrep.2019.07.081.
52. Li A, Vargas CA, Brykailo MA, Openo KK, Corbett AH, Fridovich-Keil JL. 2004. Both KH and non-KH domain sequences are required for polyribosome association of Scp160p in yeast. Nucleic Acids Res 32:4768–4775. https://doi.org/10.1093/nar/gkh812.
53. Meertens L, Hafirassou ML, Couderc T, Bonnet-Madin L, Kril V, Kümmerer BM, Labeau A, Brugier A, Simon-Loriere E, Burlaud-Gaillard J, Doyen C, Pezzi L, Goupil T, Rafasse S, Vidalain P-O, Bertrand-Legout A, Gueneau L, Juntas-Morales R, Ben Yaou R, Bonne G, de Lamballerie X, Benkirane M, Roingeard P, Delaugerre C, Lecuit M, Amara A. 2019. FHL1 is a major host factor for chikungunya virus infection. Nature 574:259–263. https://doi.org/10.1038/s41586-019-1578-4.
54. Meertens L, Carnec X, Lecoin MP, Ramdasi R, Guivel-Benhassine F, Lew E, Lemke G, Schwartz O, Amara A. 2012. The TIM and TAM families of phosphatidylserine receptors mediate dengue virus entry. Cell Host Microbe 12:544–557. https://doi.org/10.1016/j.chom.2012.08.009.
55. Shevchenko A, Wilm M, Vorm O, Mann M. 1996. Mass spectrometric sequencing of proteins silver-stained polyacrylamide gels. Anal Chem 68:850–858. https://doi.org/10.1021/ac950914h.
56. Peng J, Gygi SP. 2001. Proteomics: the move to mixtures. J Mass Spectrom 36:1083–1091. https://doi.org/10.1002/jms.229.
57. Eng JK, McCormack AL, Yates JR. 1994. An approach to correlate tandem mass spectral data of peptides with amino acid sequences in a protein database. J Am Soc Mass Spectrom 5:976–989. https://doi.org/10.1016/1044-0305(94)80016-2.
58. Concordet J-P, Haeussler M. 2018. CRISPOR: intuitive guide selection for CRISPR/Cas9 genome editing experiments and screens. Nucleic Acids Res 46:W242–W245. https://doi.org/10.1093/nar/gky354.
59. Marmisolle FE, García ML, Reyes CA. 2018. RNA-binding protein immunoprecipitation as a tool to investigate plant miRNA processing interference by regulatory proteins of diverse origin. Plant Methods 14:9. https://doi.org/10.1186/s13007-018-0276-9.

Morgane Baldaccini

Rôle du domaine hélicase de la protéine Dicer humaine lors de l'infection virale

Role of human Dicer helicase domain upon viral infection

Résumé

Les cellules eucaryotes font face aux infections virales grâce à deux réponses immunitaires : l'interférence à l'ARN (ARNi) chez les invertébrés et les plantes et la réponse interféron de type I (IFN-I) chez les mammifères. Chez ces derniers, le rôle de l'ARNi dans la réponse antivirale est débattu, malgré la présence d'une machinerie active. Dans le cadre de ce projet, j'ai étudié le rôle du domaine hélicase du Dicer humain lors de l'infection virale. Le domaine hélicase permet l'interaction avec de nombreux partenaires de la voie de l'IFN-I dont la kinase PKR, qui est alors régulée. De plus, un mutant de délétion de ce domaine, Dicer N1, est antiviral contre les alphavirus et les enterovirus et cela indépendamment de son activité catalytique. J'ai montré que la présence de PKR mais pas de son activité catalytique est nécessaire à l'activité antivirale de N1. De plus, dans les cellules N1 non infectées, un groupe de gènes liés à la réponse antivirale est sur-exprimé et sous contrôle de facteurs de transcription de l'immunité dont NF-kB. J'ai ainsi identifié un rôle non-canonique du domaine hélicase de Dicer qui renforce l'idée d'une connexion entre ARNi et IFN-I.

Mots-clés : Dicer, virus, ARNi, réponse interféron, PKR, NF-kB

Abstract

Eukaryotic cells face viral infections through two immune responses: RNA interference (RNAi) in invertebrates and plants, and the type I interferon (IFN-I) response in mammals. In mammals, the role of RNAi in the antiviral response is debated, despite the presence of an active machinery. In this project, I investigated the role of the helicase domain of human Dicer during viral infection. The helicase domain allows interaction with numerous IFN-I-derived partners, including the PKR kinase, which is thus regulated. In addition, a deletion mutant of this domain, Dicer N1, is antiviral against alphaviruses and enteroviruses, independently of its catalytic activity. I have shown that the presence of PKR but not its catalytic activity is necessary for the antiviral activity of N1. Furthermore, in uninfected N1 cells, a group of genes linked to antiviral defense is over-expressed and under the control of immune transcription factors including NF-kB. I have thus identified a non-canonical role for Dicer helicase domain, reinforcing the idea of a crosstalk between RNAi and IFN-I.

Keywords: Dicer, viruses, RNAi, interferon response, PKR, NF-kB